SD2009-05-A

South Dakota
Department of Transportation
Office of Research

U.S. Department
of Transportation
Federal Highway
Administration

Mitigation of Corrosion in Continuously Reinforced Concrete Pavement

Study SD2009-05
Final Report
Volume 1

Prepared by
Allen L. Jones and Nadim I. Wehbe
South Dakota State University
Department of Civil and Environmental Engineering

DISCLAIMER

The contents of this report reflect the views of the authors who are responsible for the facts and accuracy of the data presented herein. The contents do not necessarily reflect the official views or policies of interested or supporting agencies that include the South Dakota Department of Transportation, the State Transportation Commission, or the Federal Highway Administration. This report does not constitute a standard, specification, or regulation.

The South Dakota Department of Transportation provides services without regard to race, color, gender, religion, national origin, age or disability, according to the provisions contained in SDCL §20-13, Title VI of the Civil Rights Act of 1964, the Rehabilitation Act of 1973, as amended, the Americans with Disabilities Act of 1990 and Executive Order 12898, Federal Actions to Address Environmental Justice in Minority Populations and Low-Income Populations, 1994. Any person who has questions concerning this policy or who believes he or she has been discriminated against should contact the Department's Civil Rights Office at 605-773-3540.

Any use of trade, product, or firm names is for descriptive purposed only and does not imply endorsement by the U.S. Government.

ACKNOWLEDGEMENTS

This work was performed under the direction of the SD2008-01 Technical Panel:

Joe Feller ..... Materials & Surfacing
John Forman ..... Pierre Region
Steve Gramm ..... Project Development
Gill Hedman ..... Materials & Surfacing
Brett Hestdalen ..... Federal Highway Administration
Darin Hodges ..... Materials & Surfacing
David Huft ..... Research
Jason Humphrey ..... Operations Support
Dan Johnston ..... Research
Ken Marks ..... Transportation Inventory Mgt.
Daris Ormesher ..... Research
Brian Raecke ..... Materials & Surfacing
Larry Engbrecht ..... SDACPA

The work was initiated in cooperation between the South Dakota Department of Transportation (SDDOT) Office of Research and South Dakota State University (SDSU). An additional collaborating agency included the United States Department of Transportation through the Mountain-Plains Consortium (MPC) University Transportation Center.

TECHNICAL REPORT STANDARD TITLE PAGE

1.Report No. SD2009-05-A	2. Government Accession No.	`
4 Title & Subtitle Mitigation of Corrosion in Continuously Reinforced Concrete Pavement		5. Report Date April 2013 6. Performing Organization Code
7. Author(s) Allen L. Jones, Nadim I. Wehbe		
9. Performing Organization Name and Address South Dakota State University, Department of Civil and Environmental Engineering Box 2219 Brookings, SD		10. Work Unit No. 11. Contract or Grant No. 311106
12. Sponsoring Agency Name and Address South Dakota Department of Transportation Office of Research 700 East Broadway Avenue Pierre, SD 57501-2586		13. Type of Report and Period Covered Executive Summary; July 2010 to April 2013 14. Sponsoring Agency Code
15. Supplementary Notes		

16. Abstract

Between 1995 and 2009, the South Dakota Department of Transportation (SDDOT) replaced over 250 miles of two-lane interstate with continuously reinforced concrete pavement (CRCP). After being in service for less than 15 years, several of these pavement sections showed signs of distress, including Y-cracking, network cracking, and cluster cracking. A previous SDDOT study concluded that the impact on performance of these recently constructed CRCP interstates from progressing corrosion of the reinforcing steel due to deicing chemicals is uncertain. Therefore, a separate study was necessary to assess the extent of reinforcement corrosion in South Dakota CRCP interstates, which is the topic of this research.

Three main objectives were addressed: determine the character, extent, and severity of corrosion in CRCP constructed since 1995; identify factors that contribute to observed levels of corrosion; and investigate cost-effective maintenance and rehabilitation mitigation strategies so that the service life of the pavements may be achieved. Field work included general observations, crack mapping, dust sampling, core sampling, and half-cell potential measurements of exsisting CRC pavements. Field work also included evaluating corrosion mitigation products that were applied to pavement test sections. Laboratory work consisted of chloride ion analysis on core and dust samples, and SEM analyses on selected CRCP reinforcement. Laboratory work also consisted of casting reinforced concrete specimens that used mix designs similar to the pavements evaluated in the field. The half-cell potentials for each specimen were monitored during the duration of the research project. Four of the laboratory specimens were also tested using chloride ion analysis and SEM techniques.

General observations showed that there were areas of severe spalling, but severe corrosion was not observed. The vertical and lateral chloride profiles indicated that chloride concentrations were above the chloride threshold of 1.244 lbs./yd^3 in the top one inch of pavement, and were generally above the threshold within the first half inch of a crack. Testing of the laboratory specimens showed similar results. SEM analyses generally showed limited to no signs of corrosion. This research also showed a strong correlation between crack density and elevated half-cell potential measurements. The results of this study show that observed pavement distresses are likely not the effect of corroded reinforcement and that reinforcement at cracked locations is the main area that is susceptible to corrosion caused by deicing salts.

The field testing of the mitigation products did not show any conclusive evidence that they reduce the corrosion of CRCP. Portions of the laboratory testing did show an increase in half-cell potential (reduction in corrosion), in comparison to the control specimens, but for other types of specimens no significant difference between the control specimens and specimens tested with sealers and MCI's were found. The SEM analyses of each of the specimens tested showed small amounts of pitting corrosion, but no difference in corrosion from specimen to specimen was observed.

17. Keywords Continuously reinforced concrete, corrosion, assessment, mitigation, South Dakota		18. Distribution Statement No restrictions. This document is available to the public from the sponsoring agency.	
19. Security Classification (of this report) Unclassified	20. Security Classification (of this page) Unclassified	21. No. of Pages 174	22. Price

TABLE OF CONTENTS

Disclaimer ii

Acknowledgements ii

Technical Report Standard Title Page iii

Table of Contents iv

List of Tables vii

List of Figures ix

1 Executive Summary 14

1.1 Initial and Statewide CRC Assessments 14

1.2 Mitigation PRODUCTS Assessment 15

2 Problem Description 17

3 Research Objectives and Plan 19

3.1 Research Objectives 19

3.2 Research Plan 19

4 Literature Review 26

4.1 CRCP use in Various States 26

4.2 CRCP in South Dakota 26

4.3 Corrosion of Reinforcing Steel in Concrete 29

4.3.1 Corrosion Process 29

4.3.2 Diffusion of Chlorides through Concrete 30

4.3.3 Time to Corrosion 32

4.4 Testing for Corrosion in Reinforced Concrete 34

4.4.1 Half-Cell Potential Method 34

4.4.2 Chloride Ion Testing 38

4.4.3 Scanning Electron Microscopy 40

4.5 Corrosion Mitigation Techniques 42

4.5.1 Topically Applied Penetrating Sealers 42

4.5.2 Topically Applied Migrating Corrosion Inhibitors 42

5 Materials and Methods 44

5.1 Initial CRCP Evaluation 44

5.1.1 Sioux Falls Sites 44
5.1.2 Interstate 29 South of Brookings and Interstate 90 Repairs 51
5.2 Statewide Assessment of Eight CRC Sites 51
5.3 Mitigation Product Testing 56
5.3.1 Corrosion Mitigation Products Tested 57
5.3.2 Field Testing of Corrosion Mitigation Products 59
5.3.3 Laboratory Testing of COrrosion Mitigation Products 63
5.3.4 Product Application and Chloride Ponding 67
6 Results 73
6.1 Initial CRCP Evaluation 73
6.1.1 Site I-29N, North of Sioux Falls at MRM 87 73
6.1.2 Site I-29N, South of Sioux Falls at MRM 68 83
6.1.3 Site I-90W, East of Sioux Falls at MRM 411 86
6.1.4 Interstate 29 near Brookings 89
6.1.5 Interstate 90 Repairs 92
6.2 Statewide CRCP Evaluation 95
6.2.1 Site I-29S, South of Beresford at MRM 33 95
6.2.2 Site I-29S, South of Beresford at MRM 44 98
6.2.3 Site I-90E, West of Rapid City at MRM 25 99
6.2.4 Site I-90E, West of Rapid City at MRM 54 100
6.2.5 Site I-90E, East of Presho at MRM 222 102
6.2.6 Site I-90E, East of Kennebec at MRM 246 104
6.2.7 Site I-29N, South of Watertown at MRM 168NB 105
6.2.8 Site I-29S, South of Watertown at MRM 168SB 106
6.3 Mitigation Product Testing 108
6.3.1 Field Testing of Mitigation Products 108
6.3.2 Laboratory Testing of Mitigation Products 118
7 Analytical Study 141
7.1 Discussion of Results from Initial CRCP Evaluation and Statewide Evaluation 141
7.1.1 General Observations 141
7.1.2 Chloride Ion Results 142
7.1.3 SEM Results 142

7.1.4 Analyzing the Half-Cell Potential Using the Numeric Magnitude Technique 143
7.1.5 Analyzing the Half-Cell Potential Using the Potential Difference Technique 144
7.1.6 Further Half-Cell Potential Analysis 145
7.1.7 Evaluation of the Site Selection Matrix 152
7.2 Discussion of Testing Results from Mitigation Products 155
7.2.1 Field Testing Results 155
7.2.2 Half-Cell Potential Using the Numeric Magnitude Technique – Field Data 157
7.2.3 Half-Cell Potential Using the Potential Difference Technique – Field Data 158
7.2.4 Laboratory Testing Results for Mitigation Products 160
8 Conclusions and Recommendations 167
8.1 Conclusions 167
8.2 Recommendations and Implementation 169
9 References 171

LIST OF TABLES

Table 4-1: Suggested chloride threshold values (Browne 1980) 34
Table 4-2: Probability of corrosion based on copper-copper sulfate electrode (after ASTM 2009) 36
Table 5-1: Pavement design information for Sioux Falls sites 45
Table 5-2: Precipitation value assigned based on geographic region 52
Table 5-3: Summary of recommended CRCP sites for statewide evaluation 56
Table 5-4: Pavement design information for eight selected sites 56
Table 5-5: SDDOT approved products list 57
Table 5-6: Product information 57
Table 5-7: Schedule of field testing 60
Table 5-8: Product application 62
Table 5-9: Mix design for no salt in mix specimens 67
Table 5-10: Concrete batches and compressive strengths 67
Table 5-11: Laboratory specimen parameters 69
Table 6-1: Alternative potentiometric chloride ion results for Sioux Falls sites (values in lbs./yd^3) 74
Table 6-2: Chloride content at MRM 87 determined by the ICP-MS method 75
Table 6-3: Chloride ion concentration from core samples at Sioux Falls sites (lbs./yd^3) 76
Table 6-4: ASTM indication of half-cell measurements at MRM 87 79
Table 6-5: Chloride content at MRM 68 determined by ICP-MS method 83
Table 6-6: Indication of half-cell measurements at MRM 68 in fall 2010 84
Table 6-7: Chloride content at MRM 411 determined by the ICP-MS method 86
Table 6-8: ASTM indication of half-cell measurements at MRM 411 88
Table 6-9: Summary of crack mapping results of I-29 south of Brookings 92
Table 6-10: Indication of half-cell measurements at MRM 33 95
Table 6-11: Chloride ion results from dust samples obtained during statewide CRCP evaluation 97
Table 6-12: Indication of half-cell measurements at MRM 44 99
Table 6-13: Indication of half-cell measurements at MRM 25 100
Table 6-14: Indication of half-cell measurements at MRM 54 101
Table 6-15: Indication of half-cell measurements of MRM 222 103
Table 6-16: Indication of half-cell measurements at MRM 246 105
Table 6-17: Indication of half-cell measurements at MRM 168NB 106
Table 6-18: Indication of half-cell measurements at MRM 168SB 108

Table 6-19: Summary data for MCI-2018 109
Table 6-20: Summary data for Ferrogard 903 and Protectosil CIT 113
Table 6-21: Summary data for Protectosil CIT 114
Table 6-22: Summary data for Ferrogard 903 114
Table 6-23: Summary data for Duralprep 3020 115
Table 6-24: Summary data for Chemtrete 40 116
Table 6-25: Summary data for No Products 117
Table 7-1: Distance to crack from dust samples with high chloride contents 142
Table 7-2: Modified corrosion probability ranges for MRM 87 146
Table 7-3: Significance levels for parameter estimates 149
Table 7-4: Summary of half-cell and crack density results 149
Table 7-5: Statewide evaluation site selection matrix correlation results 153

LIST OF FIGURES

Figure 4-1: Network and Y-cracking (Johnston 2009) 27
Figure 4-2: Cluster cracking (Johnston 2009) 27
Figure 4-3: Corroded reinforcement exposed during CRCP removal 31
Figure 4-4: Corroded reinforcement removed from degraded CRCP 31
Figure 4-5: The relative volumes of iron and its reaction products (ACI 2001) 32
Figure 4-6: Corrosion process in a reinforced concrete structure (after Tutti 1977) 33
Figure 4-7: Typical half-cell potential record (Stratfull 1973) 35
Figure 4-8: Equipotential contour map of a bridge deck (Stratfull 1973) 35
Figure 4-9: Cumulative frequency distribution of multiple bridge decks (Elsener, et al. 2003) 36
Figure 4-10: Example of an SEM optical image 40
Figure 4-11: Example of a SEM BSE image 41
Figure 4-12: Examples of oxygen (O), iron (Fe), and chloride (Cl) element maps 41
Figure 4-13: Example of an x-ray spectrograph 42
Figure 5-1: Horizontal slices of cores 46
Figure 5-2: Filter collection device and vacuum 47
Figure 5-3: Filter collection device 47
Figure 5-4: Drilling holes for dust samples 48
Figure 5-5: Dust created during drilling process 48
Figure 5-6: Collecting dust from drilled holes 49
Figure 5-7: Electrical connection to the reinforcing bar 50
Figure 5-8: Collecting half-cell measurements 50
Figure 5-9: Regions for statewide evaluation (SDDOT 2010) 55
Figure 5-10: Test section layout 59
Figure 5-11: Product application 61
Figure 5-12: Test sections after product application 61
Figure 5-13: Laboratory specimen dimensions 63
Figure 5-14: Cracked specimen 64
Figure 5-15: Form and steel shim for a cracked specimen 65
Figure 5-16: Reinforcement prior to placement in the forms 66
Figure 5-17: Horizontal slice scheme for concrete specimen 71
Figure 5-18: Vertical slice scheme for concrete specimen 71

Figure 5-19: Polished specimen reinforcement for SEM testing 72
Figure 6-1: Cracking on Interstate 29 at MRM 87 73
Figure 6-2: Chloride concentration versus depth in dust samples collected near Sioux Falls 75
Figure 6-3: Lateral chloride concentration of core samples, depth of 0.5 inch, Sioux Falls sites....76
Figure 6-4: Lateral chloride concentration of core samples, depth of 1.5 inches, Sioux Falls sites 77
Figure 6-5: Lateral chloride concentration of core samples, depth of 2.5 inches, Sioux Falls sites 77
Figure 6-6: Lateral chloride concentration of core samples, depth of 3.5 inches, Sioux Falls sites 78
Figure 6-7: Lateral chloride concentration of core samples, depth of 4.5 inches, Sioux Falls sites 78
Figure 6-8: MRM 87 half-cell cumulative frequency distribution 79
Figure 6-9: MRM 87 equipotential contour map 80
Figure 6-10: Thin layer of rust or possible corrosion 81
Figure 6-11: Secondary electron image of possible corrosion zone....81
Figure 6-12: Steel bar section from core MRM 87-4 (uncracked concrete core)....82
Figure 6-13: Energy dispersive spectrum of reinforcement sample - no chlorine present 83
Figure 6-14: MRM 68 half-cell cumulative frequency distributions 84
Figure 6-15: Main crack intersecting reinforcement 85
Figure 6-16: Local delamination along reinforcement 85
Figure 6-17: MRM 411 Half-cell potential cumulative frequency distribution during fall 2010....87
Figure 6-18: MRM 411 half-cell potential cumulative frequency distribution 87
Figure 6-19: Corrosion at crack locations 88
Figure 6-20: Corroded area enlarged....89
Figure 6-21: Elemental maps of corroded area (scanning electron microscope image, iron map, oxygen map, chlorine map, and silicon map) 89
Figure 6-22: Patched pavement with exposed reinforcing steel....90
Figure 6-23: Localized corrosion found in the concrete rubble that was eventually removed....90
Figure 6-24: Spalled area with no signs of corrosion....91
Figure 6-25: Corroded longitudinal reinforcing bar 92
Figure 6-26: Spalling and transverse cracking close to a repaired section....93
Figure 6-27: Longitudinal cracking on I-90 93
Figure 6-28: Severe loss of cross-sectional area 94
Figure 6-29: Corrosion at transverse crack location....94
Figure 6-30: MRM 33 half-cell cumulative frequency distribution 95

Figure 6-31: Dust sample 2 at MRM 33 96
Figure 6-32: Vertical chloride distribution for statewide CRCP evaluation 97
Figure 6-33: Spalling observed in passing lane at MRM 44 98
Figure 6-34: MRM 44 half-cell cumulative frequency distribution 99
Figure 6-35: MRM 25 half-cell cumulative frequency distribution 100
Figure 6-36: MRM 54 half-cell cumulative frequency distribution 101
Figure 6-37: Wide crack exhibiting spalling at MRM 222 102
Figure 6-38: MRM 222 half-cell cumulative frequency distribution 103
Figure 6-39: Dust sample one at MRM 222 104
Figure 6-40: MRM 246 half-cell cumulative frequency distribution 105
Figure 6-41: MRM 168NB half-cell cumulative frequency distribution 106
Figure 6-42: Cracking observed at MRM 168SB 107
Figure 6-43: MRM 168SB half-cell cumulative frequency distribution 107
Figure 6-44: Cumulative frequency distribution for MCI-2018 109
Figure 6-45: Equipotential contour map for MCI-2018 (August 25, 2011) 110
Figure 6-46: Contour map, half-cell potential differences, August 25, 2011 to October 6, 2011, MCI-2018 111
Figure 6-47: Half-cell potential measurements for MCI-2018 (August 25, 2011) 112
Figure 6-48: Half-cell potential differences, August 25, 2011 to October 6, 2011, MCI-2018 112
Figure 6-49: Cumulative frequency distribution for Ferrogard 903 and Protectosil CIT 113
Figure 6-50: Cumulative frequency distribution for Protectosil CIT 114
Figure 6-51: Cumulative frequency distribution for Ferrogard 903 115
Figure 6-52: Cumulative frequency distribution for Duralprep 3020 116
Figure 6-53: Cumulative frequency distribution for Chemtrete 40 117
Figure 6-54: Cumulative frequency distribution for No Products 118
Figure 6-55: Half-cell potential measurements for MCI-2018, cracked specimens 119
Figure 6-56: Half-cell potential measurements, MCI-2018, uncracked, salt in mix specimen 119
Figure 6-57: Half-cell potential measurements, Ferrogard 903 & Protectosil CIT, cracked specimens 120
Figure 6-58: Half-cell potential measurements, Ferrogard 903 and Protectosil CIT, uncracked, salt in mix specimen 121
Figure 6-59: Chloride profiles for Ferrogard 903 and Protectosil CIT 121
Figure 6-60: Optical image for Ferrogard 903 and Protectosil CIT 122
Figure 6-61: BSE image and element Maps for Ferrogard 903 and Protectosil CIT 123

Figure 6-62: Optical image for Ferrogard 903 and Protectosil CIT 123
Figure 6-63: BSE image and element maps for Ferrogard 903 and Protectosil CIT 124
Figure 6-64: Half-cell potential measurements for Protectosil CIT, cracked specimens 125
Figure 6-65: Half-cell potential measurements for Protectosil CIT, uncracked, salt in mix specimen 126
Figure 6-66: Chloride profiles for Protectosil CIT 126
Figure 6-67: Optical image for Protectosil CIT 127
Figure 6-68: BSE image and element maps for Protectosil CIT 127
Figure 6-69: Energy dispersive x-ray spectroscopy results for Protectosil CIT 128
Figure 6-70: Half-cell potential measurements, Ferrogard 903, cracked specimens 129
Figure 6-71: Half-cell potential measurements, Ferrogard 903, uncracked, salt in mix specimen 129
Figure 6-72: Chloride profiles for Ferrogard 903 130
Figure 6-73: Optical image for Ferrogard 903 131
Figure 6-74: BSE image and element maps for Ferrogard 903 131
Figure 6-75: Energy dispersive x-ray spectroscopy results for Ferrogard 903 132
Figure 6-76: Half-cell potential measurements for Duralprep 3020, cracked specimens 133
Figure 6-77: Half-cell potential measurements for Duralprep 3020, uncracked, salt in mix specimen 133
Figure 6-78: Half-cell potential measurements for Chemtrete 40, cracked specimens 134
Figure 6-79: Half-cell potential measurements for Chemtrete 40, uncracked, salt in mix specimen 135
Figure 6-80: Half-cell potential measurements for cracked, control specimens 135
Figure 6-81: Half-cell potential measurements for uncracked, control specimens 136
Figure 6-82: Chloride profiles for wet, cracked control specimen 136
Figure 6-83: Optical image of wet, cracked control specimen 137
Figure 6-84: BSE and element maps for wet, cracked control specimen 137
Figure 6-85: Energy dispersive x-ray spectroscopy results for wet, cracked control 138
Figure 6-86: Saw cut along the crack of dry, cracked control specimen showing the reinforcement 139
Figure 6-87: Close-up of corrosion of dry, cracked control specimen 139
Figure 6-88: Saw Cut along the simulated crack of Specimen 16 140
Figure 6-89: Close-up of corrosion of Specimen 16 140
Figure 7-1: Influence of cover depth on half-cell potential measurements (after Elsener 2003) 144
Figure 7-2: Frequency distribution of half-cell measurements at MRM 87 146
Figure 7-3: Frequency distributions of half-cell measurements at MRM 44 147
Figure 7-4: Example of half-cell potential measurements plotted against crack density values 148

Figure 7-5: Correlation models for Sioux Falls sites.....150
Figure 7-6: Correlation models for sites south of Sioux Falls on Interstate 29.....150
Figure 7-7: Correlation models for sites near Rapid City on Interstate 90.....151
Figure 7-8: Correlation data for sites south of Watertown on Interstate 90.....151
Figure 7-9: Correlation data for sites between Wall and Chamberlain on Interstate 90.....152
Figure 7-10: Crack density versus deicer applied for all sites surveyed.....153
Figure 7-11: Crack density versus age of all sites surveyed.....154
Figure 7-12: Surface condition index versus deicer application rate (all sites).....154
Figure 7-13: Average half-cell measurements for each section vs. time.....155
Figure 7-14: Relative change in half-cell measurements vs. time.....156
Figure 7-15: Relative change in half-cell measurements vs. time, normalized to control section.....156
Figure 7-16: Relative change in half-cell measurements for each measurement event vs. time.....157
Figure 7-17: Expected change in cumulative frequency distribution for effective product.....159
Figure 7-18: Parallel cumulative frequency distributions.....160
Figure 7-19: Wet specimens – change in half-cell potential after initial product application.....161
Figure 7-20: dry Specimens – change in half-cell potential after initial product application.....162
Figure 7-21: Half-cell potential of uncracked specimens with salt in mix.....163
Figure 7-22: Half-cell potential of uncracked control specimens.....164
Figure 7-23: Salt crystals from the chloride solution migrating through the concrete.....166

1 EXECUTIVE SUMMARY

This report presents a research study regarding corrosion of steel reinforcement in continuously reinforced concrete pavement (CRCP) in South Dakota. The study was funded by the South Dakota Department of Transportation (SDDOT), the Mountain-Plains Consortium (MPC) University Transportation Center, and South Dakota State University (SDSU). Data collection and experimental work were performed at SDSU in Brookings, SD and on interstates in South Dakota.

1.1 INITIAL AND STATEWIDE CRC ASSESSMENTS

An initial evaluation of CRCP was conducted in order to determine the extent of possible corrosion of CRCP on selected interstates in South Dakota. A CRCP evaluation was also performed on selected CRCP sites statewide in order to assess corrosion of other interstate sites relative to the Sioux Falls sites. The results of this assessment were compared to the results of the initial evaluation of CRCP, and conclusions with respect to corrosion were formulated from these evaluations. A summary of the analysis of the data collected is also discussed in this section.

The initial CRCP evaluation was conducted in three geographic locations: the Sioux Falls area, Interstate 29 south of Brookings, and Interstate 90 in Lyman County. The field work conducted at the Sioux Falls sites included general observations, crack mapping, core sampling, dust sampling, half-cell potential measurements, and concrete cover sampling at three sites. Half-cell potential measurements were obtained in accordance with ASTM C876-09. The laboratory work performed on the samples collected at these sites included SEM analysis of reinforcement from four concrete core samples and potentiometric chloride testing of 12 composite vertical dust samples. Three cores were also tested for chlorides using the potentiometric method, as well as the ICP-MS method for validation purposes.

The statewide assessment included the evaluation of eight interstate sites throughout South Dakota – two sites from each of the following geographic regions: Interstate 29 south of Sioux Falls, Interstate 29 south of Watertown, Interstate 90 between Wall and Chamberlain, and Interstate 90 near Rapid City. Field work included general observations, half-cell potential measurements, crack mapping (without crack width measurements), and dust sampling. Dust samples were analyzed for chloride content using the alternative potentiometric method at the EMES at SDSM&T.

General observations showed that there were sections of severe and localized reinforcement corrosion at some crack locations. Corrosion was not observed on reinforcement at non-cracked or non-distressed locations of the pavement, except for when the longitudinal reinforcement was placed near the longitudinal pavement joint. There were also areas in which severe spalling had occurred, but corrosion was not observed.

Crack mapping showed that cracks were generally wider and more frequent in the Sioux Falls area compared to the sites observed during the statewide evaluation. The average crack density for the sites near Sioux Falls was 44 percent higher than the average crack density for the statewide sites. Also, the Sioux Falls sites exhibited longitudinal cracking, while the sites included in the statewide evaluation did not.

The results of the chloride tests were used to develop vertical and horizontal chloride profiles. Vertical chloride profiles were developed from the dust samples that showed the chloride distribution with respect to depth in the pavement section. Horizontal chloride profiles were developed from core sampling and testing which showed the chloride distribution in half inch increments laterally from a cracked location.

The vertical chloride profiles indicated that chloride concentrations were above the chloride threshold of 1.244 lbs./yd^3 in the top one inch of pavement, and decreased to below threshold at the depth of reinforcement in most cases. There were only 2 cases in which the chloride content was above the chloride threshold at the level of reinforcement, and in both of these cases the dust sample was obtained within 3 inches of a crack location. The horizontal chloride profiles showed that the chloride concentration was above the threshold within the first half inch of 11 of 13 samples tested. Also, in two of three cases the chloride concentration was above the threshold value within the entire first lateral inch of the crack, at the level of the reinforcement.

SEM analyses were conducted on four core samples, three of which were collected at a cracked section of CRCP. One of the three core samples obtained at a cracked location exhibited signs of chloride-induced corrosion; the other three samples analyzed using the SEM showed no signs of corrosion. All SEM analysis was completed at the EMES at SDSM&T.

Equipotential contour and crack maps were developed from the half-cell potential and crack data collected. These maps are presented in Appendix B. The ASTM C876 methods for analyzing the half-cell potential measurements were deemed inappropriate for this research study. The literature indicates that there are several unquantifiable factors that affect the test. Therefore, the half-cell potential measurements were analyzed with respect to crack density instead of being analyzed separately using the ASTM C876 analysis methods.

Half-cell potential measurements and crack density were investigated for correlations on all eleven sites surveyed. The 20 most negative half-cell potential measurements were considered elevated at these sites. A total of 104 half-cell potential measurements were collected at each site, and a crack density value based on the crack density in the surrounding pavement was also assigned at each point at which a half-cell potential measurement was obtained. The t distribution was used to test the relationship between crack density and half-cell potential for statistical significance. There was a significant positive correlation between elevated half-cell potential measurements and crack density at seven of the eleven sites surveyed.

1.2 MITIGATION PRODUCTS ASSESSMENT

The main objective addressed in this portion of the study was to determine if topically applied corrosion mitigation products, such as penetrating sealers and migrating corrosion inhibitors (MCI), were an effective method to reduce or arrest the rate of corrosion in CRCP. The testing was conducted both in the field testing and in the laboratory. The field testing consisted of evaluating the change in half-cell potential of the reinforcement before and after the corrosion mitigation products were applied to sections of an interstate highway. Contour maps and time history plots of the data were then created for each test section in the field. The laboratory testing consisted of casting reinforced concrete specimens that used mix designs similar to the pavements evaluated in the field. The specimens had shallow wells on top of them which were used for ponding the specimens with a chloride solution. The half-cell potentials for each specimen were monitored during the duration of the research project. Four of the laboratory specimens were also tested using chloride ion analysis and scanning electron microscopy (SEM) techniques.

The field testing did not show any conclusive evidence that the corrosion mitigation products reduce the corrosion of CRCP in the field. Portions of the laboratory testing did show an increase in half-cell potential (reduction in corrosion), in comparison to the control specimens, but for other types of

specimens no significant difference between the control specimens and specimens tested with sealers and MCI's were found. The chloride ion analysis showed the expected migration of chlorides. The SEM analyses of each of the specimens tested showed small amounts of pitting corrosion, but no difference in corrosion from specimen to specimen was observed.

2 PROBLEM DESCRIPTION

Both jointed plain concrete pavement (JPCP) and CRCP have been used for interstate highways in the upper Midwest. The main difference in these pavement types is the mode in which the pavement section will control distresses, namely the widening of cracks (Muench, et al. 2001). In contrast with JPCP where reinforcement is only present in the form of dowel bars placed at transverse joints, CRCP does not incorporate transverse joints but is reinforced with a mesh of longitudinal and transverse steel bars throughout the slab (Johnston 2009). In JCPC, dimensional change due to thermal effects is accommodated at the joints (Muench, et al. 2001). Engineers designate the spacing between these contraction joints such that the effects of temperature and moisture will not produce intermediate cracking within each slab. Slab lengths between joints range from 12 to 20 feet. In CRCP, the thermal effects cause frequent tight transverse cracks, typically spaced at intervals of 2 to 4 feet to develop in the slab. The amount of steel reinforcement is designed to control further widening of these cracks.

JPCP is generally less expensive than CRCP to construct. However, the contraction joints in JPCP result in annoying driving conditions due to the repetitive "thud" noise caused by the passage of the wheels over the joints. The "roughness" at the joint is aggravated by factors such as concrete dimensional changes due to temperature variation, heaving due to freeze-thaw conditions, and possibly moisture ingress through the joint. The joints in JPCP may cause early deterioration of the pavement. CRCP eliminates the need for the repetitive contraction joints, thereby resulting in smoother driving conditions. Some regions in the United States have experienced significant success with CRCP, while the use of CRCP in other regions has been discontinued due to poor performance.

Prior to the 1960's there were no CRCP projects constructed in South Dakota (Johnston 2009). Due to the lack of data on the performance of CRCP in the state, two test sections of CRCP were constructed in 1963 on Interstate 90 in South Dakota. The variation between the two sections was the depth of transverse reinforcement, with one section having 2.5 inches of depth to the center of the steel and the other having 3.69 inches. Both of these pavement sections were 8 inches thick and used #5 longitudinal bars spaced 6 inches center-to-center. After five years of monitoring, the SDDOT observed smaller average crack widths and less frequency of cracks in the section which had the depth of reinforcement of 2.5 inches. Furthermore, after 45 years of being in service, both sections of pavement did not require significant rehabilitation.

An analysis of performance and life-cycle costs of concrete pavements in South Dakota was conducted in the 1990s (Johnston 2009). Due to the favorable results exhibited by CRCP, the SDDOT adopted CRCP as a high-quality construction alternative to JPCP for interstate pavement. Between 1995 and 2009, the SDDOT replaced over 250 miles of two-lane interstate with CRCP. The goal of using CRCP was to create high-performance roadway sections that required limited maintenance. However, after being in service for less than 15 years, several of these pavement sections showed signs of undesired distress, including Y-cracking, network cracking, and cluster cracking. At some locations, the crack interval was as frequent as one foot or less with punchout failures observed on Interstate 29. It is thought that the punchout failures could become more frequent due to the cracking patterns that favor this type of failure. A description of the different types of CRCP distress based on the Distress Identification Manual (FHWA 2003) is presented in Appendix D.

Based on these observations, the SDDOT conducted a study entitled, "Impact, Cause, and Remedies for Excessive Cracking in CRC Pavement" (Johnston 2009). The purpose of the study was to identify

design, construction, and material alternatives that would optimize future CRCP construction. Subsequently, modifications to concrete gradation, steel content, centerline chair assembly, steel depth, aggregate preparation due to environmental factors, cement content, and curing compound application rate were incorporated into projects that were scheduled for the following construction season. These modifications are discussed in Chapter 4. Furthermore, the study concluded that the impact on performance from progressing corrosion of the reinforcing steel due to deicing chemicals is uncertain and, therefore, the service life estimates for in-place CRCP may have been too optimistic at the time. The study concluded that there was uncertainty of the effect of deicing chemical on the steel reinforcement in CRCP built in South Dakota between 1995 and 2009, and recommended that the extent of corrosion in CRCP in South Dakota interstates and potential corrosion mitigation strategies be evaluated.

Based on the SDDOT findings (Johnston 2009), this study was undertaken to assess the reinforcement corrosion extent and corrosion mitigation strategies in CRCP. This study was also tasked with testing topically applied corrosion mitigation products (corrosion inhibitors and sealants) as a method to stop or slow the corrosion process in existing CRCP sections. Various test section sites for corrosion mitigation products were proposed based on the results of the half-cell potential testing on various CRCP sections through the state as part of this project. Therefore, this study also tested the effectiveness of topically applied corrosion inhibitors.

3 RESEARCH OBJECTIVES AND PLAN

3.1 RESEARCH OBJECTIVES

Three main objectives are addressed in this study:

1. *Determine the character, extent, and severity of corrosion in CRCP constructed in South Dakota since 1995.*

The work was initiated with a thorough search of the available literature on CRCP pavement performance since 1995 relative to reinforcing steel corrosion. The literature review relied heavily on the work conducted as part of SD2004-07 (Johnston, 1997), additional publications aree included as appropriate. To supplement the work of SD2004-07, extensive field and laboratory testing was conducted as part of this research project. The testing was designed to determine the character, extent, and severity of corrosion in selected CRC pavements constructed in South Dakota. Details are contained within the research plan.

2. *Identify factors and interactions among factors that contribute to observed levels of corrosion.*

Parameters of particular interest identified during previous research include geographic distribution, age, traffic, precipitation, and deicing rates. Proposed field and laboratory testing were designed to verify these factors as well as identify any other factors that contribute to corrosion. Factors and their interactions were investigated in an effort to explain the observed levels of corrosion.

3. *Develop cost effective maintenance and rehabilitation mitigation strategies for treatment of CRC pavements with corrosion problems so that the service life of the pavements can be achieved.*

As part of the field and laboratory testing, evaluation of five commercial products and two combinations were conducted to determine if cost-effective maintenance and rehabilitation strategies for treating CRC pavements were viable. The primary objective was to determine if the products will be sufficiently effective such that the service life of the pavements can be achieved.

3.2 RESEARCH PLAN

The research plan in this study was designed to determine the extent of corrosion in CRC pavements at present and assess mitigation products that may assist in reducing or stopping corrosion. The main goal is to determine if significant reduction in service life of recent CRC pavement sections is expected. The process of developing the research plan identified 14 research tasks to address the research objectives. This research was a collaborative effort between South Dakota State University (SDSU) and the South Dakota School of Mines & Technology (SDSM&T) Engineering and Mining Experiment Station. The following section outlines each of the tasks that were performed for this research project.

Task 1: *Review literature pertaining to steel reinforcement corrosion in concrete, especially with regard to CRC pavements, with particular emphasis on mitigation techniques.*

This task was accomplished through direct search in the relevant literature, and contacts with SDDOT, FHWA, and other state departments of transportation that had experience with corrosion in CRC pavements. The literature review consisted of a survey of literature regarding the extent of deterioration of CRCP in South Dakota, and reviewing the history of CRCP in other states. The process of corrosion caused by deicing salts and the time required to begin this process were also surveyed in the literature. Various commercially available corrosion inhibitors and sealant products were also investigated in order to evaluate the benefits, cost, and advantages and disadvantages of each treatment method. Finally,

testing procedures to examine the extent of corrosion in reinforced concrete were investigated in the literature. The results of the literature search are presented in Chapter 4.

Task 2: *Collect information on CRC projects, including results from the prior study, and conduct interviews with appropriate SDDOT personnel on particular projects using a questionnaire.*

This task consisted of collecting information on CRCP projects in South Dakota by conducting interviews with SDDOT personnel. The information collected was focused towards factors and interactions that might affect CRC corrosion as well as discussion of products for corrosion mitigation. The effort was based on the literature review, the prior research study, and discussions with SDDOT research personnel. Results of this information are presented in Chapter 5.

Task 3: *Develop a work plan for CRC project evaluation selection*

Based on the literature review and information gained from SDDOT personnel, a work plan was developed that addresses implementation of field and laboratory testing. The work plan contained detailed sampling methods, safety procedures, anticipated laboratory testing, and evaluation methods to be used on results. The main elements of the work plan consisted of:

1. Initial field sampling and testing, and associated laboratory testing at three sites near Sioux Falls (Task 5),
2. Laboratory corrosion testing of cast concrete specimens and evaluation of mitigation strategies (Task 8),
3. Evaluation and testing of proposed mitigation strategies in the field using a test section near Sioux Falls (Task 10), and
4. Long term monitoring of the selected sites across the state (Task 11).

The Work Plan was devised to provide project elements that could be sequentially reviewed by the Technical Panel and approved prior to implementing subsequent elements of the Work Plan. This provided for a process of revision and improvement of the Work Plan during execution of the project. Details of the elements of the Work Plan follow in the remaining tasks.

Task 4: *Meet with the project's technical panel to discuss the project scope and work plan.*

This meeting was based on the Technical Panel's review of the Work Plan produced in Task 3 and set the framework for the project. The meeting was conducted on August 24, 2010 where the research team outlined the Work Plan for the main elements of the project and discussed assistance required from the SDDOT. Revisions were implemented as appropriate prior to implementing subsequent tasks of the proposed work.

Task 5: *Conduct an initial CRC evaluation near Sioux Falls (projects north, south and east) and develop a preliminary assessment of the level of corrosion observed and the probable extent of any problems. Crack mapping will also be conducted in CRC pavements near Brookings and qualitative observations will be made at selected sites on I-90 and I-25.*

Sites Near Sioux Falls

An initial CRC pavement corrosion evaluation was based on field sampling/testing and laboratory testing at three project sites near Sioux Falls conducted in accordance with the Work Plan developed as part of Task 3. Field samples were submitted to the Engineering and Mining Experiment Station (EMES) at the SDSM&T for analysis. Following analysis of the field and laboratory results, a preliminary assessment of observed corrosion and extent of corrosion persistence was performed. Specific field and laboratory testing based on discussions with the SDDOT Office of Research and SD2004-07 consisted of the following:

1) Initial field testing and sampling near Sioux Falls. The purpose of field sampling was to obtain samples for laboratory testing.
    a. Field sampling occurred at three sites near Sioux Falls: Interstate 29 North and South and I90 East.
        i. Concrete coring of existing cracks (3 core samples) and uncracked areas (1 core sample) per project site were obtained for chloride distribution testing in the laboratory.
        ii. Dust profile sampling at depths of 1, 2, 3, and 4 inches (4 composite samples per project) were obtained for chloride penetration testing in the laboratory.
    b. Half-cell potential measurements at the field testing sites using a standard copper-copper sulfate reference electrode were also performed.
    c. Crack mapping of the areas where sampling and measurements were obtained. A crack mapping protocol was devised. The crack width of the mapped cracks were measured and recorded. The results are summarized in terms of crack intensity (crack length per unit surface area) and crack width frequency distribution in Chapter 6. The crack data was used to determine correlation between pavement cracking and the extent of corrosion.
2) Laboratory Analytical testing was performed by EMES at SDSM&T. The purpose of the testing was to determine if corrosion was occurring on the reinforcing steel, and the persistence and penetration of chloride in the concrete section. Testing consisted of the following:
    a. Conventional analysis for chloride of three thin slices of the concrete profile using concrete cores at crack locations at each project site.
    b. Potentiometric testing of dust profiling samples for chloride content at each project site. This was based on 60 chloride content tests including:
        i. Four dust samples per profile applied to four profiles per project site for the three project sites, and
        ii. One pulverized composite sample from each core of each test site.
    c. Scanning electron microscope (SEM) of the sampled reinforcing from the thin slice cores at each project site.

    Chloride content was determined following the potentiometric method outlined by the Virginia Department of Transportation (Clemena and Apusen, 2002). SEM examination was carried out using a Zeiss Supra40 variable-pressure field-emission SEM equipped with an energy-dispersive X-ray spectrometer.

Once the field and laboratory testing was complete, an assessment of the results was performed. The results were focused towards determining the extent and severity of corrosion in the existing CRC pavement reinforcing and the effect of corrosion on pavement performance. The results are summarized in Chapter 6 and 7.

CRCP pavement Near Brookings

Crack width mapping and qualitative observations were also conducted on a CRC pavement section near Brookings. The intent of this work was to gather additional observations that supplemented the detailed data collected near Sioux Falls for gaining knowledge towards addressing the project goals. The CRCP pavement near Brookings was replaced the summer of 2010 and gathering this information was deemed useful for the project.

Crack width mapping consisted of two levels of mapping. The first consisted of detailed crack mapping of one CRCP roadway length and one consisted of crack width mapping at random locations along the section of CRCP roadway that was replaced. Qualitative measurements consisted of simple photography and field notes as appropriate.

Selected Sites along I-29 and I-90

The SDDOT also conducted repairs of CRCP pavement sections at selected sites along I-29 and I-90 during the summer of 2010. The repairs allowed for direct observation of the pavement section and reinforcing during the repair process. Effort for this task included simple photography and field notes at each observed site. No quantitative measurements were obtained.

Task 6: *Meet with the technical panel via videoconference to discuss preliminary results, any desirable work plan modifications and the necessity of completing further work based on the magnitude of the problem.*

Following review of the Task 5 summary, the Technical Panel convened with the research team to discuss the results of the project. This meeting occurred on February 11, 2011. The main goal of the meeting was to assess the project results relative to potential modifications to the Work Plan and assess further work tasks and additional evaluation sites (discussed in Task 12) based on the results completed to date.

Task 7: *Upon approval of the technical panel, resume CRC project evaluation statewide based on the final work plan.*

This task was essentially part of Task 6. At the completion of the Technical Panel meeting outlined in Task 6, the Technical Panel evaluated the results of the work completed to date. An evaluation of the quantitative results was presented and preliminary recommendations were provided. Ranges of expected trends were also reported to the Technical Panel as they related to observations collected during the project. This information is presented in Chapter 7.

The Work Plan outlined in Task 3 was evaluated to note if any revisions or modifications are appropriate. The Technical Panel approved the research team to proceed forward with Tasks 8 through 15 without change.

Task 8: *Conduct laboratory corrosion testing designed to demonstrate the effectiveness of various mitigation strategies including crack sealing, corrosion inhibitors and any other promising alternatives identified and develop a field test section matrix, including monitoring, for their application.*

This task consisted of performing additional laboratory testing of reinforced concrete specimens cast in the laboratory and subjecting the specimens to controlled corrosion. As part of this work, various corrosion mitigation products were investigated to test the effectiveness of the products for possible use in field evaluation. The selection of corrosion mitigation techniques was based on the literature review, input by the SDDOT, and previous research. Five different topically applied corrosion inhibitors and

sealers were chosen for testing and two of the corrosion inhibitors were tested together to investigate the combined effect. These corrosion mitigation products were tested both in the field and in the laboratory.

This task consisted of three distinct subtasks:

1) Casting reinforced concrete specimens in the laboratory and subjecting them to a corrosive environment to simulate existing field conditions,
2) Applying mitigation strategies in the laboratory and assessing their effectiveness to limit additional corrosion, and
3) Based on the results, producing a testing matrix that allowed for the application of the mitigation strategies in the field for evaluation.

Proposed specific testing consisted of the following:

1) Casting square beam specimens that were six inches by six inches in section by 20 inches in length that contained a single length of No. 3 reinforcing steel that was at a 4 inch depth. A wire was attached to the reinforcing prior to casting for the purposes half-cell potential testing. A simulated crack was cast into the specimens.
2) A magnesium chloride solution of 28% was introduced into the specimen crack to induce corrosion. A well was cast into the specimens to facilitate ponding of the chloride solution.
3) The specimens were cycled in and out of a moist room on one week intervals until the threshold corrosion was achieved. Threshold corrosion was determined as part of the literature search.
4) Once threshold corrosion was obtained, mitigation products were applied to test their effectiveness on the corroded specimens. Three corrosion inhibitors and two sealants were used in this research. Specific products were selected by the SDDOT based on input from the research team and the findings of the literature search.
5) For the purposes of comparison, control specimens were constructed to subject them to magnesium chloride and no corrosion. Based on the above, 14 specimens were constructed and tested (six products or combinations applied to two specimens each and two control specimens).
6) Continuous monitoring of the specimens in the laboratory were conducted using half-cell measurements.
7) Once the mitigation products are applied, the specimens were subjected to the corrosive simulation described above. The specimens were subjected to a combination of additional corrosion simulation dictated by the results of Tasks 1 through 7. Once sufficient corrosion was established, the specimens were sent to EMES at the SDSM&T for analysis. Various specimens were testing using SEM (4 tests), however, the control specimens were not tested by SEM as this information was not deemed useful. Two applications of the mitigation products were used on some of the specimens during the course of the research.

Once the testing was completed, the results were evaluated for effectiveness relative to corrosion of the reinforcing steel. Based on the evaluation, a matrix test plan was developed that allowed for systematic application of the products in the field. This effort is outlined in Task 10.

The results of this Task are presented in Chapters 6 and 7.

Task 9: *Meet with the technical panel to discuss interim results and finalize the field test sections.*

Upon completion and summarization of the results of Task 8, the Technical Panel convened on June 1, 2011 with the research team to discuss the interim results of the project and discuss implementation of the test matrix developed as part of Task 8. The Technical Panel approved of the products and combination, and field evaluation of the mitigation products were implemented as outlined in the next task.

Task 10: *Obtain baseline measurements including half-cell potentials on proposed test section locations and install test sections using SDDOT maintenance forces with appropriate instrumentation for long term monitoring.*

Once the testing matrix was finalized, the mitigation products were applied and tested in the field. The field testing of the products was conducted on Interstate-29 Northbound (N) at Mile Road Marker (MRM) 87. The test section consisted of a roadway section that was 400 feet long where each of the products was tested in 50-foot-long sections separated by a 20-foot-long untested area for separation. This resulted in six product test sections and one control section. The products were only applied on one travelling lane by SDSU using the appropriate Personal Protective Equipment (PPE). The manufacturer's guidelines for installation were used for application.

The research plan was designed such that visual observation and half-cell measurements were the basis for assessing the effectiveness of the products. Half-cell measurements were conducted as follows:

1) Half-cell measurements were obtained on scan lines at 1, 3, 5, 7, 9 and 11 feet from the roadway edge on a regularly spaced grid.
2) Prior to product application, baseline half-cell measurements were obtained to document the current condition of the reinforcing.
3) Following curing of the products, half-cell measurements were obtained at the same locations as the baseline measurements.
4) Half-cell measurements were obtained time increments after the time of application.

The results of this Task are presented in Chapter 6 and 7.

Task 11: *Evaluate the initial effectiveness of the mitigation strategies employed within six months after installation.*

After the six month measurements of the test section were obtained, the research term evaluated the measurements relative to the effectiveness of the treatments to inhibit corrosion. The half-cell measurements were compared to prior testing obtained in the research project in an effort to correlate effectiveness to identified interaction factors. This work is presented in Chapter 7.

Task 12: *Provide a statewide assessment of CRC corrosion condition and potential based on the results of the project evaluations.*

CRCP projects in South Dakota since 1995 were evaluated for use in assessing statewide condition of these CRCP. The research plan selected 8 of these projects based on condition, age, precipitation, maintenance activities, etc. for visual observation (photography and field notes), corrosion assessment using half-cell measurements and chloride profile testing. The condition of each site was summarized relative to the findings of this study. Two chloride profiles were obtained at each of the sites that consisted of 4 dust samples per profile for a total of 36 additional chloride tests for the project. No crack mapping or other field sampling or laboratory testing was conducted at these sites. The visual observations, half-cell measurements and chloride testing results were used to correlate to results obtained during the initial CRCP evaluation and the previous SDDOT study. These results are presented in Chapter 6 and 7.

Task 13: *Develop recommendations for a future CRC corrosion mitigation evaluation research project including an estimated timeframe allowing sufficient time to provide clear verification of a given treatment's effectiveness.*

Conclusions regarding the relationships of cracking on chloride ingress and half-cell potential are presented in Chapter 8 of this report. The general observations were also used to draw conclusions on the extent of corrosion in CRCP. Recommendations concerning further study, testing methods, and quality control during the construction of CRCP are also presented in Chapter 8. These recommendations also apprise the SDDOT regarding the effectiveness of mitigation products relative to reinforcement corrosion in CRCP.

Task 14: *Prepare a final report and executive summary of the research methodology, findings, conclusions, and recommendations.*

This final report was prepared that presents a comprehensive summary of the project. This task consists of documenting the project results including testing methods, findings, conclusions, and recommendations. Recommendations for ongoing testing and evaluation of pavements as a means to understand corrosion potential of CRC pavements over time are included. The final report was submitted to the SDDOT Technical Panel for review and comment, and was then revised to incorporate these comments.

Task 15: *Make an executive presentation to the SDDOT Research Review Board at the conclusion of the project.*

This task included an executive presentation that was given to the SDDOT Research Review Board in Pierre, South Dakota. The presentation was provided on February 13, 2013 and summarized the research activities that were accomplished in this project with conclusions and recommendations that resulted from the research.

4 LITERATURE REVIEW

This chapter presents the literature review that was conducted as part of this study. Several literature sources on the history of CRCP, corrosive effects of deicing salts in reinforced concrete, and corrosion testing for reinforced concrete were reviewed and are reported in this chapter. Also reported is detailed information regarding the corrosion process and the transport mechanism of chlorides through concrete. The three main corrosion evaluation methods presented are the half-cell potential technique, chloride ion testing, and scanning electron microscopy.

4.1 CRCP USE IN VARIOUS STATES

The first CRCP roadway was constructed in the United States as early as 1927; however, widespread use of CRCP did not occur until the early 1960s (Tayabi, et al. 1998). Many CRCP roadways were installed as part of the nationwide interstate system. Several states have used CRCP as an alternative to jointed concrete pavement, including Texas, Illinois, Minnesota, Wisconsin and South Dakota.

According to the 1998 CRCP performance report from the FHWA (Tayabi, et al.), CRCP is the most extensively used concrete pavement in the state of Texas. Thousands of miles of CRCP interstate were constructed in the 1950s and 1960s in Texas. The original CRCP has performed well in the state, and so have the CRCP overlays on top of asphalt concrete. Field tests that have been conducted in Texas have proved beneficial for understanding the effects of curing and crack-control methods.

Many test sections have been constructed in Illinois to determine the influence of pavement thickness on CRCP performance (CRSI 2001). The effectiveness of CRCP overlays on original CRCP has also been studied in Illinois. Pavements have performed well in the state, despite the fact that many of the trucks on these heavily-traveled roadways are over the legal weight limits. By 2001, the Illinois Department of Transportation was specifying CRCP on all of their heavily traveled roadways. However, one recent problem observed on some CRCP interstates in Illinois is the development of premature longitudinal cracking on roadways within ten years of construction (Roesler, et al. 2010). After a two year study, it was concluded that the cause of the problem was the use of a tube feeding technique to place the reinforcing steel in the concrete during CRCP construction. This construction technique results in the settlement of reinforcing steel relative to the stationary concrete during construction. The use of tube-fed steel in CRCP has ceased due to the findings of this study.

Although the states of Texas and Illinois have had success with CRCP, other states have not. For instance, Minnesota built 29 CRCP projects between 1964 and 1973. Pavement distresses, such as delamination of concrete at the top layer of steel and tension failure (steel rupture) have been observed in these pavements (Tayabi, et al. 1998). The required maintenance procedures for distressed sections have included full-depth patching, asphalt overlays, and reconstruction. This has led to the discontinuation of CRCP in Minnesota. Wisconsin has also experienced undesirable results with CRCP, with the most common distress being corrosion of the reinforcing steel. Corrosion has in turn caused further deterioration in the form of punchouts, spalling, wide transverse cracks, and delamination.

4.2 CRCP IN SOUTH DAKOTA

The first CRCP sections constructed in South Dakota date back to 1963, and performed well for 45 years (Johnston 2009). No considerable maintenance or reconstruction had to be performed on CRCP sections constructed in 1963. However, undesired cracking patterns such as Y-cracking (one crack separates into two cracks), network cracking (simultaneous fine cracks near transverse cracks), and cluster cracking

(multiple transverse cracks within a foot or less) have been observed in CRCP that was constructed within the past 15 years throughout the state. Examples of these distresses can be seen in Figure 4-1 and Figure 4-2.

Figure 4-1: Network and Y-cracking (Johnston 2009)

Figure 4-2: Cluster cracking (Johnston 2009)

Spalling is another distress that has been observed in recently constructed sections of CRCP in South Dakota (Johnston 2009). Spalling occurs when concrete degrades within close proximity to a crack or joint. Spall development of CRCP constructed in the last 15 years is estimated to have increased by a factor of 1.8 over that of the old CRCP. Spall development reflected excessive crack width and potential to trap water and deicing salts in Johnston's study.

The South Dakota Department of Transportation (SDDOT) study (Johnston 2009) concluded that concrete gradation, steel content, centerline chair assembly, steel depth, environment (temperature, wind velocity, etc.), cement content, and curing compound application rate are important design aspects that affect the distresses in CRCP. Based on these conclusions, the following design and material modifications were recommended:

1. Depth of concrete cover should be modified to 3.75 inches for all pavements greater than or equal to 9 inches thick.
2. The maximum steel ratio should be 0.6% using #5 bars.
3. At least 10% of the coarse aggregate should be retained on the 1" sieve.
4. Chair support of the reinforcing steel should be increased to prevent sagging of steel bars.
5. The application of curing compound should occur within 30 minutes, and the minimum rate of application should be 1.5 gallons/125ft^2.
6. Aggregate stockpiles should be wetted (for cooling purposes) when temperatures are anticipated to be greater than 80°F.
7. Prior to paving, the road base and steel reinforcing bars should be wetted in order to prevent water loss from concrete.
8. The cement content requirement should be 510 lbs./yd^3, and modified Class F fly ash should be added at 112 lbs./yd^3.
9. Performance curves resulting from the Pavement Management program should include CRCP pavements built since 1995 and exclude older CRCP sections.
10. Separate research should be performed in order to:
    a. Determine methods to mitigate deterioration of newer CRCP.
    b. Investigate effectiveness of topically applied corrosion inhibitors.
    c. Reassess CRCP sections in light of longitudinal cracking that was observed after the original distress surveys of this study

Furthermore, the study concluded that service life estimates for in-place CRCP may be too optimistic because the impact on performance from increasing corrosion due to deicing chemicals is uncertain (Johnston 2009). This SDDOT study noted that one attempt to alleviate further corrosion on a severely distressed section of Interstate 29 in Lincoln County involved applying a corrosion inhibitor, named Hycrete, to the shoulder. However, the product was deemed insufficient for use on pavement because it caused the pavement to be too slippery.

The Federal Highway Administration affirms several findings of the SDDOT study by stating that the key factors influencing crack propagation are environmental conditions at the time of construction, amount of steel, concrete strength, and restraint due to friction between the slab and the base (Tayabi, et al. 1998). Others recognize that coarse aggregate type and time of crack occurrence have an effect on crack width in

CRCP (Suy & McCullough 1994). The identification of these factors is beneficial for future construction of CRCP in South Dakota. However, the effect of steel reinforcement corrosion on pavement performance is still uncertain. The mechanism of corrosion in concrete is discussed in the following section.

4.3 CORROSION OF REINFORCING STEEL IN CONCRETE

Deterioration due to corrosion of steel in reinforced concrete has been the topic of many research studies in the past 50 years (ACI 2001; Stratfull 1973; Stark 1989; Virmani & Clemeña 1998). These studies recognized that a marine environment and the increased use of deicing salts on roads and bridges beginning in the late 1960s have caused significant corrosion in reinforced concrete infrastructure worldwide. The majority of previous literature has mainly looked into the effects of corrosion on reinforced concrete bridges and buildings. However, recent propagation of corrosion of the reinforcement in CRCP in South Dakota has prompted efforts to evaluate roadways for corrosion. This section presents a review of the general corrosion process in reinforced concrete.

4.3.1 CORROSION PROCESS

Reinforcing steel is derived from naturally occurring iron ore (Virmani & Clemeña 1998; Smith & Hashemi 2005). In order to produce steel, iron is extracted from the ore through the use of a blast furnace, in which a high amount of energy is used. Consequently, this energy is stored in the iron, which, through further processing, is made into steel. When the steel is exposed to the natural environment, it gets exposed to other chemicals from its surroundings. Accordingly, deterioration occurs because the steel has a tendency to return to its less energized state. This deterioration is called corrosion. The electrochemical reaction that causes this corrosion is classified as an oxidation reaction.

Concrete normally has high alkalinity, which means that it has a relatively high ability to neutralize acid (ACI 2001). When the high alkalinity concrete cures around the reinforcement, a passive film layer is formed on the reinforcement. If left undisturbed, this film has the ability to protect the steel reinforcement bars from corrosion. Thus, concrete is a highly effective protection system against corrosion for the reinforcing steel. However, if the concrete is introduced to high concentrations of chlorides from deicing salts, a marine environment, or contaminated aggregates, the passive film will begin to break down and the protection of the steel reinforcement bars is compromised. Although it is widely accepted that this process occurs, the exact mechanisms involved with breaking down the passive film is unknown since it happens at the atomic level.

Once the passive film is compromised, the steel reinforcement is no longer protected from moisture and oxygen (Virmani & Clemeña 1998). Thus, corrosion is allowed to occur on the surface of the steel reinforcement. The following reactions summarize the corrosion process in reinforced concrete:

In the presence of Oxygen:

1. Oxidation Reaction:

$$Fe \rightarrow Fe^{+2} + 2e^{-} \qquad \textbf{(Eqn. 2-1)}$$

2. Reduction reaction, which results in the formation of hydroxide ions:

$$½\, O_2 + H_2O + 2e^{-} \rightarrow 2\, OH^{-} \qquad \textbf{(Eqn. 2-2)}$$

3. The positively charged ferrous ions react with the negatively charged hydroxide ions, and then with water, to eventually form ferrous hydroxide, or rust:

$$Fe^{+2} + 2OH^{-} \rightarrow Fe(OH)_2 \quad \textbf{(Eqn. 2-3)}$$

$$4Fe(OH)_2 + 2H_2O + O_2 \rightarrow 4Fe(OH)_3 \quad \textbf{(Eqn. 2-4)}$$

$$2Fe(OH)_3 \rightarrow Fe_2O_3 + 3H_2O \quad \textbf{(Eqn. 2-5)}$$

In the absence of oxygen, the following process takes place:

1. Oxidation reaction and the subsequent reaction with water forms ferrous hydroxide:

$$Fe^{+2} + 4Cl^{-} \rightarrow (FeCl_4)^{-2} + 2e^{-} \quad \textbf{(Eqn. 2-6)}$$

$$(FeCl_4)^{-2} + 2H_2O \rightarrow Fe(OH)_2 + 2H^{+} + 4Cl^{-} \quad \textbf{(Eqn. 2-7)}$$

2. The reduction reaction results in the formation of hydrogen gas:

$$2H^{+} + 2e^{-} \rightarrow H_2 \quad \textbf{(Eqn. 2-8)}$$

Equations 2-1 through 2-8 summarize the flow of electrons from one site on the reinforcing steel to another. As the electrons are transferred, the electrode potential can be measured (Richardson 2002). This phenomenon is important to this research and will be discussed in a later section.

The corrosion in reinforced concrete can be caused by either macrocell or microcell corrosion. According to Jaggi, et al. (2001), macrocell corrosion is when there is a distinct anode (corroding area) and distinct cathode (non-corroding area) on the reinforcement. The cathodic area is much larger than the anode and this leads to pitting of the rebar or localized corrosion (Jaggi, et al. 2001). According to ACI (2001), "Reinforced concrete with significant gradients in chloride-ion content is vulnerable to macrocell corrosion." Macrocell corrosion is the most common type of corrosion caused by chloride ingress. According to Jaggi, et al. (2001), microcell corrosion is when anodic and cathodic reactions are contiguous, leading to uniform corrosion over the entire surface. Uniform corrosion is usually caused by very high chloride content at the bars or by carbonation (Jaggi, et al. 2001).

4.3.2 DIFFUSION OF CHLORIDES THROUGH CONCRETE

The most common method for chlorides to penetrate concrete is by diffusion, which is the movement of chloride ions under a concentration gradient (Stanish, et al. 1997). Concrete is heterogeneous in nature, therefore the diffusion rate depends on the diffusion coefficient through the pore solution, as well as the capillary pore structure. Also, as cracks widen in the pavement chlorides from deicing intrude more easily through the concrete toward the steel reinforcement. Thus, the time for the chlorides to reach the steel reinforcement in a cracked reinforced concrete specimen is significantly reduced compared to uncracked reinforced concrete.

Tests conducted by Arya and Ofori-Darko (1996) indicate that crack width, effective depth, frequency, orientation (whether a crack is transverse or longitudinal to the steel bar), and the ability to self-heal are all factors that contribute to corrosion. Others have concluded that wider cracks cause higher corrosion rates (Otieno, et al. 2006). In light of this research, corrosion may be an increasing problem in the recently constructed CRCP in South Dakota because some of these pavements exhibit wide cracks which are either transverse or longitudinal to the reinforcement. Examples of corrosion of reinforcement in

some CRCP sections in South Dakota are shown in Figure 4-3 and Figure 4-4. The reinforcement shown in these photographs are from CRCP which was constructed in 1968.

Figure 4-3: Corroded reinforcement exposed during CRCP removal

Figure 4-4: Corroded reinforcement removed from degraded CRCP

Furthermore, the oxidation products formed during the corrosion process can be several times greater in volume than the original steel (ACI 2001). The increased volume of the corroded steel places more stress on the surrounding concrete, which in turn leads to further deterioration, reduced structural capacity of the roadway, and eventually premature maintenance or reconstruction (Stark 1989). Figure 4-5 shows the volume of iron relative to its reaction products.

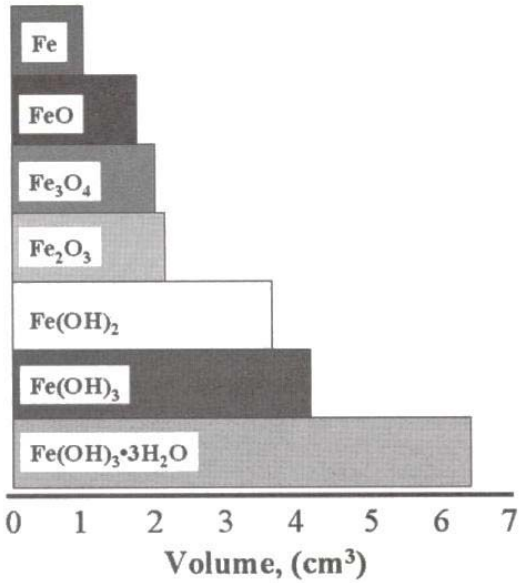

Figure 4-5: The relative volumes of iron and its reaction products (ACI 2001)

4.3.3 TIME TO CORROSION

According to Tutti (1977), the corrosion process has two phases in the service life of a reinforced concrete structure, as shown in Figure 4-6. The first phase, t_0, is the amount of time required for the chlorides to penetrate through the concrete and break down the protective passive film layer of the reinforcement. When the passive film is compromised, corrosion begins. Phase two of the corrosion process is denoted as t_1, and it is the length of time from t_0 required for the concrete to spall or delaminate, or for the reinforcement to lose its load-bearing capacity. It is at the end of this second phase that the concrete in a structure will fail. This includes spalling, delamination, and/or loss of bond capacity between the steel reinforcing bar and the concrete. Following is a description of the two phases.

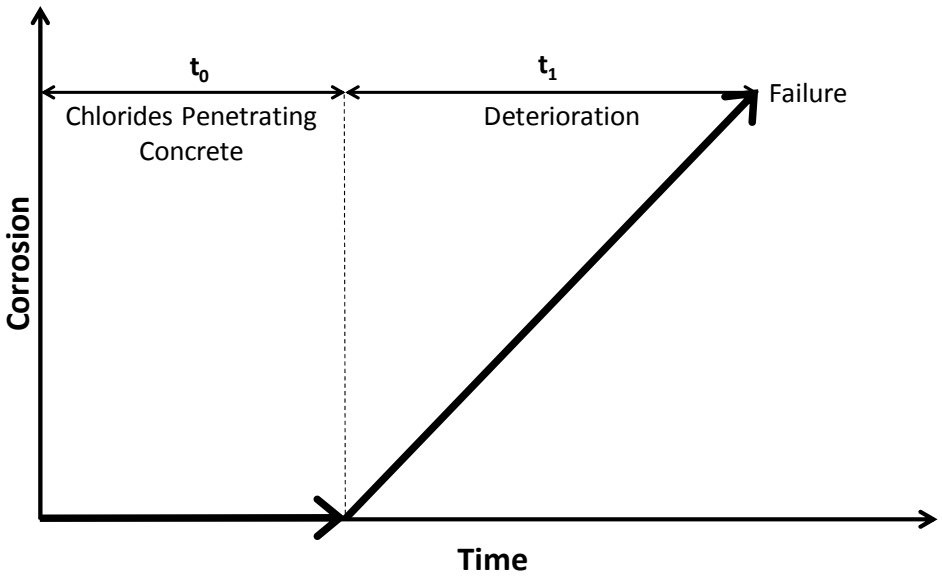

Figure 4-6: Corrosion process in a reinforced concrete structure (after Tutti 1977)

Phase 1 of the Corrosion Process

The critical factors that affect phase one are the chloride diffusion rate, the degree of chloride binding, and the chloride threshold value. In concrete, there are two states in which chlorides can exist: bound and free. Together, the two states make up the total chloride content (Liang, et al. 2010). As the chlorides penetrate, some chlorides are allowed to bind or be physically adsorbed by the concrete. These chlorides are referred to as "bound" chlorides. Therefore, they do not cause damage to the reinforcing steel. Fly ash and slag can be included as admixtures to the concrete in an effort to allow the chlorides to more easily bind in the concrete. In contrast, free chlorides in concrete have the ability to dissolve in water and adversely affect the protective passive layer of the reinforcement. Therefore, free chlorides are of concern when analyzing the corrosion of reinforced concrete.

The chloride threshold level is defined as the chloride content at the depth of the steel that will result in the breakdown of the passive film (Bohni 2005). Many studies have been conducted to determine the chloride threshold value, but no exact value is agreed upon in the literature due to the many factors that affect the threshold. Such factors include chloride ion binding, chloride ion mobility, oxidizing conditions, binder type, and pH of the concrete. Previous work done by the FHWA suggests that this value is 0.033 percent Cl^- by mass (0.78 kg/m^3) of concrete (Clear 1976). Bohni (2005) states that conservative threshold values range from 0.2 to 0.5 Cl^- percent by mass of cement. Others have suggested ranges of chloride that indicate the level of corrosion risk. Everett and Treadway (1980) explain that chloride contents of 0.4 percent Cl^- by mass of cement is low risk; 0.4 to 1.0 percent Cl^- by mass of cement is medium risk; and 1.0 percent Cl^- by mass of cement indicates high risk. Browne (1980) suggested less conservative ranges of corrosion risk, as shown in Table 4-1.

Table 4-1: Suggested chloride threshold values (Browne 1980)

Percent Cl^- by Mass Cement	Risk Level
Less than 0.4	Negligible
0.4 to 1.0	Possible
1.0 to 2.0	Probable
Greater than 2.0	Certain

Phase 2 of the Corrosion Process

Phase two is influenced by many factors, including the availability of oxygen, the electrical resistivity of concrete, the environment (relative humidity and temperature), the inherent strength of the concrete, the degree of cracking in the concrete, porosity, degree of saturation, and the pH of the pore solution (Hansson, et al. 1998). Although some of the factors affecting both phases of the corrosion process cannot be fully controlled, the use of corrosion inhibitors could be a potential method for mitigation of corrosion. This subject will be discussed later in this report.

4.4 TESTING FOR CORROSION IN REINFORCED CONCRETE

The three methods to investigate the corrosion of reinforced concrete pavement that will be discussed in this section are the half-cell potential method, chloride ion testing, and scanning electron microscopy. Several other corrosion monitoring methods exist (Böhni 2005), such as impedance spectroscopy, galvanostatic pulse measurement, and electrode resistivity measurement. However, those methods will not be discussed in this report they were not used during the experimental work for this study.

4.4.1 HALF-CELL POTENTIAL METHOD

As discussed in Section 4.3.1, the electrode potential can be measured for a piece of corroding steel reinforcement embedded in concrete (Richardson 2002). In the case of reinforced concrete, steel is the metal and the surrounding concrete is the electrolyte. The potential measurements indicate the ease of electron transfer between a corroding and non-corroding area on the steel reinforcement. The potential cannot be measured directly, but rather relative to a standard reference electrode. Common reference electrodes used to measure corrosion in reinforced concrete include copper-copper sulfate, silver-silver chloride, and saturated calomel electrodes. The copper-copper sulfate electrode is most commonly used (Ali 1990).

When measuring the half-cell potential against a standard reference electrode, data can be recorded over time to monitor the progression of the reinforced concrete toward corrosion initiation (Elsener & Böhni 1990). At the beginning of the corrosion process, a sudden negative change in potential is observed. This change becomes more gradual as time progresses, as shown in Figure 4-7. The potential difference between one half-cell (the corroding area on the steel bar) and the other half-cell (the reference electrode) can reach as high as 0.5 volts or more when referenced to a standard copper-copper sulfate electrode.

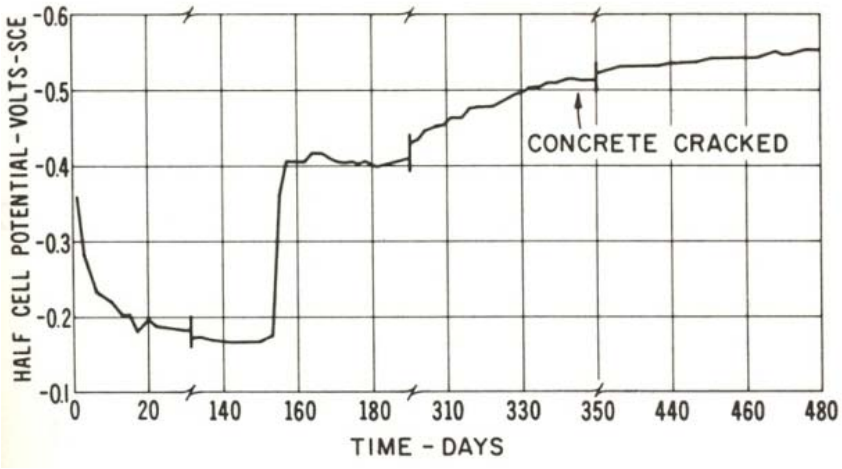

Figure 4-7: Typical half-cell potential record (Stratfull 1973)

The American Society for Testing Materials (ASTM) method C-876 (2009) entitled "Standard Test Method for Corrosion Potentials of Uncoated Reinforcing Steel in Concrete" can be utilized in the field and in the laboratory to obtain half-cell measurements. According to the ASTM procedure, potential can be measured using a reference electrode, electrical junction device, electrical contact solution, voltmeter, and electrical lead wires.

The data from these tests can be presented using an equipotential contour map and/or cumulative frequency distribution (ASTM 2009). The equipotential contour map allows for a visual representation of the potentials over the areas surveyed. An example of an equipotential contour map for a bridge deck is shown in Figure 4-8. The values of the half-cell potential values are in millivolts, and each grid square is 18 inches x 11 inches. The cumulative frequency distribution is a statistical data representation technique that shows the distribution of the potentials measured. Figure 4-9 shows an example of a cumulative frequency distribution from measurements obtained over different bridge decks.

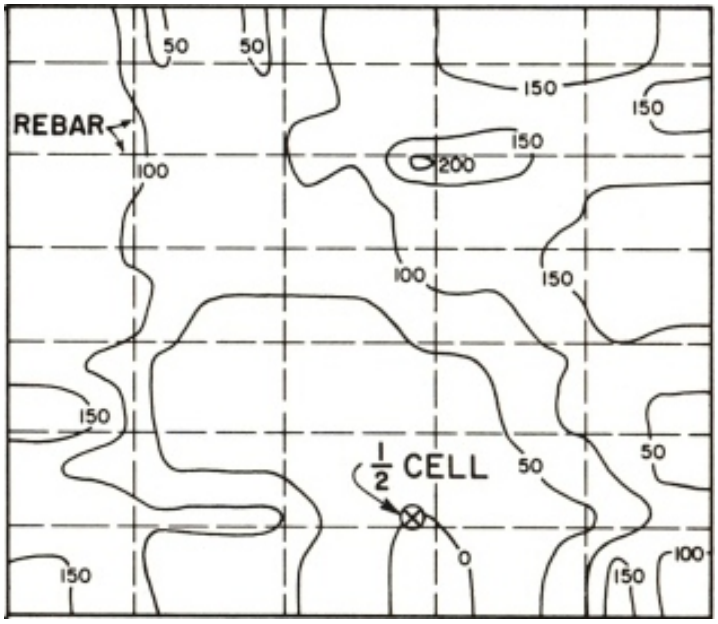

Figure 4-8: Equipotential contour map of a bridge deck (Stratfull 1973)

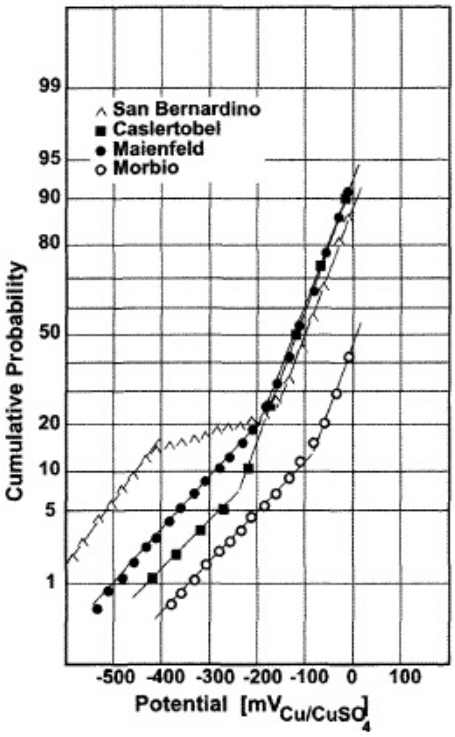

Figure 4-9: Cumulative frequency distribution of multiple bridge decks (Elsener, et al. 2003)

The half-cell potential values obtained can be analyzed using the Numeric Magnitude Technique (NMT) and the Potential Difference Technique (PDT) (ASTM 2009). The NMT assigns potential value ranges that indicate the degree of corrosion. This is shown in Table 4-2: Probability of corrosion based on copper-copper sulfate electrode (after ASTM 2009). where more negative half-cell potential values indicate a higher probability that the steel reinforcement is corroding. When the PDT is used, the high potential values are simply compared to low potential values. The locations in a section of reinforced concrete with low (or more negative) half-cell potential values would indicate areas where the probability of corrosion is higher than the areas with high (more positive) half-cell potential values. Equipotential contour maps, such as the one shown in Figure 4-8, are often used to graphically detect areas with high or low half-cell potential measurements.

Table 4-2: Probability of corrosion based on copper-copper sulfate electrode (after ASTM 2009)

Potential Measurement	Indication
> -200 mV	90% probability that no reinforcing steel is corroding
-200 mv to -350 mV	Corrosion activity is uncertain
< -350 mV	Greater than 90% probability steel is corroding

Half-cell potential is a quick non-destructive method to determine the amount of corrosion in reinforced concrete, but there are several factors that can affect the half-cell potential besides corrosion and this can make the results difficult to interpret. These include: electrical resistivity of the concrete due to humidity, the presence of ions in the pore solution; the presence of a high-resistance surface layer; polarization effects electrical discontinuity of the reinforcing steel, presence of stray currents, galvanized

coated reinforcing steel, chloride concentration, cover thickness of the concrete, presence of inhibitors, fresh concrete, and oxygen concentration (Elsener & Böhni 1990; Assouli, et. al. 2008; Elsener 2001). Relevant to this study, it is important to note that higher chloride ion concentrations result in more negative potential values and more severe corrosion (Gu & Beaudoin 1998).

Results from potential measurements must be carefully interpreted when corrosion inhibitors are applied to the surface of concrete. Elsener (2001) showed that uncertainties of half-cell measurements have been observed in tests involving inorganic surface applied corrosion inhibitors. Furthermore, Gu and Beaudoin (1998) report the effects on half-cell measurements when using specific types of corrosion inhibitors and sealants. These effects are summarized as follows:

1. Anodic corrosion inhibitors shift potential values towards positive. ASTM C-876 (2009) guidelines can be applied directly.
2. Cathodic corrosion inhibitors shift potential values towards negative. ASTM C-876 (2009) guidelines cannot be applied directly. The potential shift should be taken into account when interpreting results.
3. Mixed corrosion inhibitors may shift potential values towards either positive or negative. Manufacturers should be contacted in order to determine the effects of specific products and these effects should be taken into account when interpreting results.
4. Organic coatings and sealants shift potential values towards positive and the results may not be applicable when using the half-cell potential technique. Measurements can be obtained on areas where the organic coating is removed or damaged.

Another major influence on half-cell potential measurements is the moisture content on the surface layer of the concrete; the higher the moisture content the more negative the values can shift, but the potential gradients do not change (Elsener, et al. 2003). Also, dry concrete can make detection of passive bars more difficult due to the small area of polarization (Elsener, et. al. 2003). When the oxygen at the reinforcement level is depleted, the half-cell potential drops significantly to approximately -900 mV CSE even though the reinforcement is not corroding significantly (Elsener et al. 2003; Bohni 2005). However, based on research by Pour-Ghaz, et al. (2009), the oxygen availability is not a significant factor affecting half-cell potential unless the concrete is completely deprived of oxygen, such as in a completely submerged specimen. The type of corrosion can also have an impact on the half-cell potentials. Uniform corrosion has similar potentials at the surface of the concrete and at the level of the reinforcement, but local corrosion can have significantly lower potentials at the concrete surface than at the reinforcement, especially when the concrete cover is thick (Elsener, et al. 2003).

The many factors that can affect half-cell potentials make the measurements difficult to analyze, especially when measurements are obtained in the field versus in a laboratory. Therefore, Elsener (2001) does not recommend using the numeric magnitude technique to assess the potential for corrosion. This is because in the field, many environmental variables can lead to large swings in half-cell potential for the same pavement or structure over a short period of time. This change in half-cell potential is not be related to the rate of corrosion in the reinforcement. Pour-Ghas (2009) recommends that potential ranges be related to the resistivity of the system, however no standard relationship has yet been identified. Also, testing the effectiveness of penetrating corrosion inhibitors by measuring half-cell potential is difficult because the inhibitors may change the properties of the concrete such as resistivity, etc. (Elsener 2003).

Although the numeric magnitude technique is not recommended for field testing, the potential difference technique is less affected by environmental factors. If the measurements for the entire section are obtained over a short amount of time, it can be assumed that environmental factors affect the entire section in a similar manner. This implies that the profile of the spatial change should stay the same but the magnitudes of the values will change, and therefore the potential difference technique is valid even when environmental factors vary greatly from one set of measurements to the next set of measurements for a section.

Although the half-cell potential method can be used to indicate whether or not corrosion has initiated in reinforced concrete, the method cannot be used to determine the rate of corrosion (Malhotra & Carino 2004). Concrete resistivity and polarization resistance methods can be used to make corrosion rate measurements. It should also be noted that concrete resistivity and polarization resistance methods, as well as carbonation tests and chloride ion content values, were suggested by Malhotra & Carino to supplement half-cell potential data.

4.4.2 CHLORIDE ION TESTING

As mentioned in section 4.3.3, the chloride threshold level is an important factor that affects the rate of corrosion. Thus, it is beneficial to obtain the chloride ion content when examining reinforced concrete for potential corrosion issues. By compiling the chloride ion contents of multiple samples from different depths at the same location, a composite chloride profile can be formed. The data can then be used to determine the extent of chloride penetration in the concrete and whether the reinforcing steel is at risk of corrosion at the given chloride content. If the reinforcement is at risk, it may be necessary to repair or replace the reinforced concrete section.

One testing method that can be used for determining the chloride ion content in a ground concrete sample, or dust sample, is entitled "An Internal-Calibration Potentiometric Method for Determining the Chloride Ion Content in Ground Concrete Samples" (Clemeña & Apusen 2002). The Virginia Transportation Research Council (VTRC) proposed this method as an alternative to the standard test method AASHTO T-260 (AASHTO 2004), "Sampling and Testing for Chloride Ion in Concrete and Concrete Raw Materials", and its equivalent ASTM C-1152 (ASTM 2004). The purpose of the alternative method was to alleviate the costs from labor and reagents typically used with the standard test method (Clemeña & Apusen 2002). An additional benefit is that the alternative method takes significantly less time to perform than the other two methods. Other methods have been suggested to perform chloride ion testing at reduced time and cost, including one such method that involves prepackaged rapid test kits. Although the price and time of the test is reduced significantly with the prepackaged kits, there is a lack of consistency in the results.

The alternative method proposed by the VTRC is based on internal calibration and the concepts of the Nernst equation for electrical potential (Clemeña & Apusen 2002). By using internal calibration, the inconsistency problems associated with prepackaged rapid test kits is avoided. The simplified Nernst equation used in the VTRC report is as follows:

$$E_x = K + S \cdot log C_x \qquad \textbf{(Eqn. 2-9)}$$

Where:

E_x = Potential (mV);

K = Reference potential (mV);

S = Response slope of the electrode; and

C_x = Concentration of chloride ions in the concrete sample (g/mL)

$$C_x = \frac{W_x}{V_x} \quad \textbf{(Eqn. 2-10)}$$

Where:

W_x = Weight of the chloride ions in the concrete sample (g)

V_x = Volume of the concrete solution (mL)

Note that the concentration of chloride ions (C_x) is simply the ratio of the weight of chloride ions to the volume of a digested (ground) concrete sample. By adding a small amount of chloride solution with a known concentration and negligible volume compared to the concrete sample, a new potential measurement can be obtained which follows the relationship:

$$E_{x+S} = S \cdot log\left(\frac{W_x + W_s}{V_x}\right) = K + S \cdot logC'_x \quad \textbf{(Eqn. 2-11)}$$

Where:

W_x = Original weight of the concrete sample (g);

W_s = Weight of chloride solution (g);

V_x = Volume of concrete sample (mL); and

C'_x = Concentration of chloride ions in sample after addition of chloride solution (g/mL).

A second addition of chloride solution results in the following:

$$E_{x+2S} = K + S \cdot logC''_x \quad \textbf{(Eqn. 2-12)}$$

Where:

C''_x = Concentration of chloride ions in sample after second addition of chloride solution (g/mL).

By performing algebraic substitutions on the above three equations, the following relationship is generated:

$$\frac{E_x - E_{x+S}}{E_x - E_{x+2S}} = \frac{logC_x - logC'_x}{logC_x - logC''_x} \quad \textbf{(Eqn. 2-13)}$$

Although this equation cannot be solved directly for the desired value of C_x, the concentration of chloride ions in the concrete sample can be determined through iterations (Clemeña & Apusen 2002).

Determination of chloride ion contents using the inductively coupled plasma – mass spectrometry (ICP-MS) method was also investigated. However using this method in reinforced concrete is uncommon. When testing a sample using the ICP-MS method, an inductively coupled plasma source converts the atoms within the sample into ions (Wolf 2005). A mass spectrometer is then used to detect the ions. According to the United States Geological Survey, elements that prefer to form negative ions, including chlorine, are very difficult to detect with ICP-MS because ions formed by the ICP discharge are typically

positive. However, some researchers have reported using the ICP-MS method to detect stable chlorine in heavy concrete on the level of 0.01 ppm (Hou, et al. 2007).

4.4.3 SCANNING ELECTRON MICROSCOPY

In addition to half-cell potential measurements and chloride ion determination, a scanning electron microscope (SEM) can be used to analyze reinforced concrete specimens which may be experiencing corrosion (Duke 2010a). SEM tests can be conducted on the reinforcement as well as the concrete. Besides gaining high resolution images of specimens, depth and cross-sectional area measurements are also possible with SEM images. Therefore, it is possible to determine the degree of corrosion based on loss of cross-sectional area of the reinforcement. Also, if the chloride contents are high enough, SEM tests may be able to create a chemical profile of the sample. This will allow the determination of chloride concentration throughout the depth of the sample.

SEM provides high resolution optical images shown in Figure 4-10, as well as backscattered electron (BSE) images (Figure 4-11) which provide even higher resolution and detail. Depth and cross-sectional area can be measured with SEM images allowing the magnitude of the corrosion to be determined based on the cross section loss of the reinforcement.

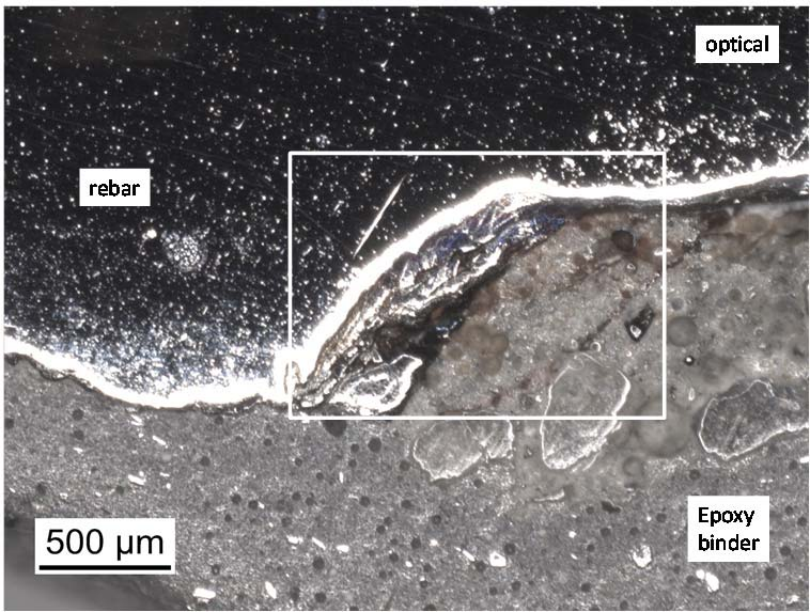

Figure 4-10: Example of an SEM optical image

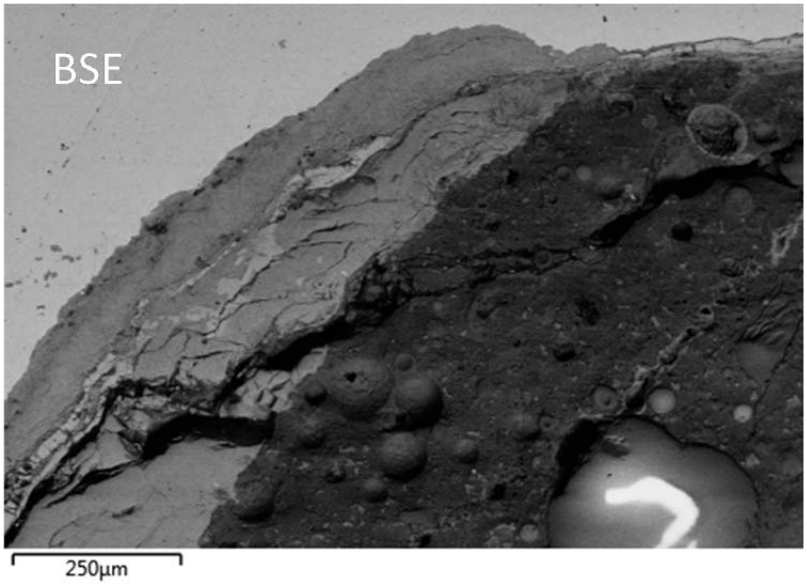

Figure 4-11: Example of a SEM BSE image

Furthermore, energy dispersive X-ray spectroscopy can be used in conjunction with SEM testing (MEE 2010). With this process, the elemental composition of the sample can be determined by measuring the amount of energy emitted by an x-ray during analysis and correlating the amount of energy to that which is characteristic to specific elements. The results from this method can be presented in elemental maps or x-ray spectrum graphs. An example of an elemental map and an X-ray spectrum graph are shown in Figure 4-12 and Figure 4-13. Energy dispersive X-ray spectroscopy can be used along with SEM testing to show which elements are present in the sample. The results from this energy dispersive method can be used to create either elemental maps that visually show the areas of high concentrations for a specific element or X-ray spectrum graphs. The three elements that are the most important for analyzing the corrosion of reinforcement in concrete are shown in the elemental maps in Figure 4-12. The non-corroded reinforcement is black in the oxygen (O) elemental map and bright red in the iron (Fe) elemental map. The corroded parts of the reinforcement show up as bright green in the oxygen elemental map and as dark red in the iron elemental map. The chloride (Cl) element map shows the areas with chloride ions present as blue. Figure 4-13 shows an example of an X-ray spectrum graph with the relative peaks of each element within the sample.

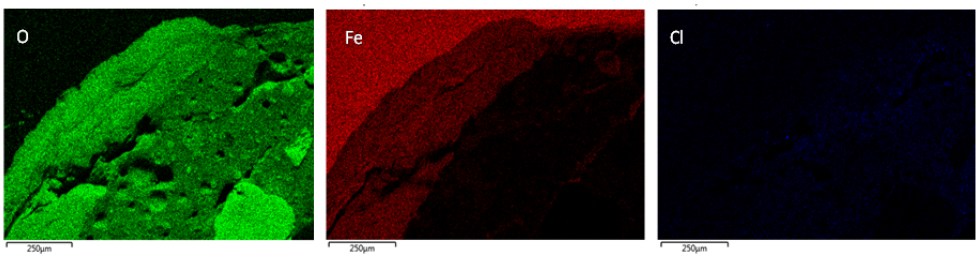

Figure 4-12: Examples of oxygen (O), iron (Fe), and chloride (Cl) element maps

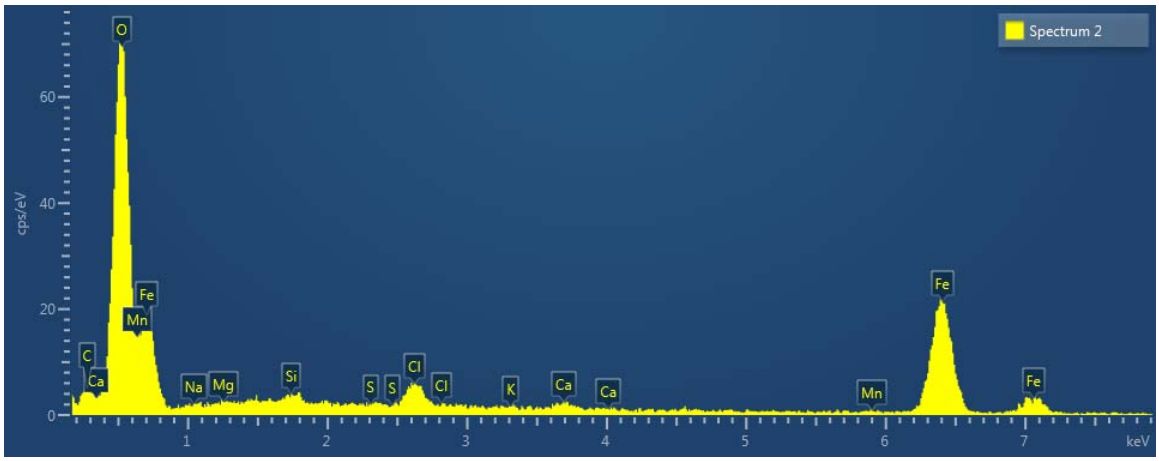

Figure 4-13: Example of an x-ray spectrograph

4.5 CORROSION MITIGATION TECHNIQUES

A corrosion inhibitor is a chemical compound which prevents, slows, or stops the corrosion process of reinforcement in concrete. Corrosion inhibitors prevent corrosion by reducing the rate of ingress of chlorides, increasing the chemical binding of chlorides, or raising the chloride threshold value for corrosion initiation. Some corrosion inhibitors can also reduce the rate of corrosion once it has been initiated (Hansson, et. al. 1998). The corrosion mitigation techniques discussed in this section are topically applied and include penetrating sealers and migrating corrosion inhibitors. These corrosion mitigation techniques are well suited for rehabilitating preexisting structures because they are relatively easy to apply and they penetrate into the concrete reducing the chance that they will wear off or wash away.

4.5.1 TOPICALLY APPLIED PENETRATING SEALERS

Penetrating sealants protect the concrete by sealing the pores in the concrete near the concrete's surface. This reduces the penetration of water into the concrete and indirectly protects the reinforcement. Reducing the amount of water that penetrates in to the concrete has a twofold benefit. The chloride ions that CRCP is exposed to are usually dissolved in water, therefore reducing the amount of water that penetrates into the concrete will reduce the amount of chlorides that can penetrate to the reinforcement. Reducing the amount of water that penetrates to the reinforcement can also slow the corrosion process, because the corrosion process requires water for corrosion to occur (ACI 2001).

The penetrating sealers used in this study were silane based. Silane sealers are currently used by many state DOT's for sealing bridge decks. The SDDOT currently uses 40 percent non-water based silane for bridges (Leibrock 2012). Silane sealers have also been shown to reduce chloride penetration in uncracked concrete, and to increase the half-cell potentials of reinforced concrete specimens in a laboratory setting (Ibrahim, et al. 1999).

4.5.2 TOPICALLY APPLIED MIGRATING CORROSION INHIBITORS

A MCI is a chemical compound which can be applied to the surface of the concrete after it has cured. The MCI penetrates to the level of the reinforcement in order to prevent the corrosion of embedded steel

reinforcement and are typically used in repair systems (Ormellese, el. al. 2011). This study focused on testing organic MCI's based on amino alcohols, amines, and other proprietary blends.

Organic MCI's protect the reinforcement by adsorbing to the passive steel surface and forming a monomolecular protective film (Ormellese, et al. 2011, Balzoni, et al. 2006). The protective film that the MCI's form around the reinforcement is designed to inhibit both anodic and cathodic processes; therefore organic MCI's are often classified as mixed inhibitors. Some MCI products use a combination of corrosion prevention techniques such as a silane penetrating sealer mixed with a proprietary MCI that migrates to the reinforcement (Cortec 2011). The silane helps to seal the concrete pores and reduce the amount of future chloride ingress; the MCI is designed to migrate to the reinforcement to reduce or stop the corrosion that has taken place (Cortec 2011).

The use of MCIs has been gaining interest as a way to extend the service life of structures and pavements and has led to an increase in independent research on the effectiveness of MCIs. El-Hacha, et al. (2011) showed that MCI's helped to slow and delay the corrosion process initially but did not completely stop the corrosion process. Also, research by Bolzoni, et al. (2006) showed that corrosion inhibitors delayed the initiation of corrosion if applied before corrosion initiated; however, the MCI's did not significantly reduce the corrosion rate in chloride contaminated concrete where corrosion had already initiated. Corrosion inhibitors were most effective at lower levels of chloride concentration up to approximately 0.5% by weight of cement (El-Hacha, et al. 2011). The overall conclusion from the literature review is that MCI's can be effective if the chloride concentration is only slightly higher than the chloride threshold. MCI's also work best if applied before the breakdown of the passive layer and the onset of corrosion.

5 MATERIALS AND METHODS

This chapter outlines the data collection and experimental work that was performed during this study in order to evaluate the condition and extent of corrosion of CRCP in South Dakota. Field work included general observations, crack mapping, dust sampling, core sampling, and half-cell potential measurements of CRCP sections in South Dakota. Laboratory work consisted of chloride ion analysis on core and dust samples, and SEM analyses on the reinforcement in core samples obtained from CRCP in South Dakota. The condition evaluation was performed in two stages: initial evaluation and statewide evaluation.

The initial CRCP evaluation allowed researchers to develop a preliminary assessment of the level of corrosion observed and the probable extent of any corrosion issues. This initial evaluation included an in-depth evaluation of sites that were in the Sioux Falls area, as well as less rigorous evaluations of two other sites. The severity and extent of corrosion on interstates throughout South Dakota were evaluated in order to determine the overall condition of CRCP in the state during the statewide CRCP evaluation. The results from the statewide CRCP evaluation were used in conjunction with the initial CRCP evaluation to determine the character, extent, and severity of corrosion in CRCP in South Dakota. Factors that contribute to observed levels of corrosion were then identified.

Additional field and laboratory testing were also performed to determine the effectiveness of different topically applied corrosion mitigation products. The field testing included applying five different products and one combination of products, which were applied to the field test site. A control section was also designated at this site. Assessing product effectiveness consisted of half-cell potential measurements of each test section and the control section. The laboratory testing included the same product and product combinations as the field testing, but the products were applied to specimens that were in a climate controlled environment.

5.1 INITIAL CRCP EVALUATION

Three CRCP sites in the Sioux Falls, South Dakota area were chosen for evaluation sites. The three sites underwent general observation (field notes and photography), crack mapping, core sampling, dust sampling, half-cell potential measurements, concrete cover measurements, chloride ion testing on cores and dust samples, and SEM analysis of the steel reinforcement in the core samples. In addition to the three sites near Sioux Falls, general observations of pavement and reinforcing steel conditions were made from inspecting CRCP sites that were undergoing maintenance along Interstate 90 and a reconstruction along Interstate 29.

5.1.1 SIOUX FALLS SITES

The three sites near Sioux Falls were chosen based on previous road condition surveys conducted by the SDDOT, as well as input from SDDOT personnel. The three sites chosen were determined to be the most critical in terms of pavement distress and possibility of corrosion. Considerable longitudinal cracking, Y-cracking, and wide transverse cracking had been observed on these sites compared to the other roads surveyed. The three sites selected were:

1. Interstate 29 Northbound, North of Sioux Falls at mile reference marker (MRM) 87
2. Interstate 29 Northbound, South of Sioux Falls at MRM 68
3. Interstate 90 Westbound, East of Sioux Falls at MRM 411

Pavement design information for these sites is presented in Table 5-1.

Table 5-1: Pavement design information for Sioux Falls sites

Site	MRM 87	MRM 68	MRM 411
Concrete Thickness (inches)	8	11	8
Longitudinal bar size	6	6	6
Design longitudinal bar spacing (inches)	8	6	8
Design Longitudinal bar depth (inches)	3.0	4	3
Transverse bar size	4	4	4
Design transvers bar spacing (inches)	36	48	36

Crack mapping consisted of laying out a grid on the pavement surface for a 100 foot long by 12 foot wide (traveling lane) section. Each grid square was four feet in width by four feet in length. Cracks were then sketched on a datasheet to create a crack map, and the widths of the cracks were measured using a crack width gauge. The crack maps were digitally recreated using AutoCAD® and the average crack width and crack density was determined for each site. The crack density is defined as:

$$Crack\ Density = \frac{\Sigma Crack\ lengths\ for\ entire\ pavement\ section}{Pavement\ surface\ area\ surveyed} \qquad \textbf{(Eqn. 3-1)}$$

Four core samples were collected from each of the three sites for the purpose of general observation, chloride ion testing, and SEM analysis. Three of the cores at each site were obtained at crack locations, and one core was obtained at a location with uncracked pavement. The cores were obtained by SDDOT personnel. Laboratory testing of the cores was conducted by Engineering and Mining Experiment Station personnel at the South Dakota School of Mines & Technology in Rapid City, SD. Two cores from site MRM 87, one core from site MRM 68, and one core from site MRM 411 underwent SEM analysis.

Each core that underwent laboratory testing was prepared for chloride ion analysis by initially slicing the core horizontally at one inch increments down to the level of the top of the reinforcement. The final horizontal slice of the core was made directly below the reinforcing bar. The horizontal slices were then cut vertically at 0.5 inch increments away from crack locations. Each of the resulting samples was subsequently pulverized for the purpose of chloride ion testing. Figure 5-1 shows the horizontal slices of one of the cores prior to sectioning it vertically. Chloride testing of these samples was performed in order to determine the distribution of the chlorides laterally from crack locations at one inch depth increments. All of the chloride test samples in this study were tested using the alternative potentiometric method.

Figure 5-1: Horizontal slices of cores

The Zeiss Supra40VP variable-pressure field-emission SEM was used to analyze the reinforcement in the core samples. The horizontal slice containing the reinforcement was saw-cut to make a small enough sample to be placed into the SEM. The resulting sample was polished prior to placing it in the SEM. Results from the SEM included secondary electron images, backscattered electron images, and X-ray element distribution maps. The results were used to determine elemental composition (presence or absence of chlorine) and extent of corrosion, if any, within each sample.

Four composite dust samples were collected near core sample locations at all three sites. A composite dust sample consisted of four individual dust samples collected at depths of one, two, three, and four inches from the pavement surface. At the location of the dust sample, three 0.5-inch diameter holes within six inches of each other were drilled using a hammer drill. The dust created by the drilled hole was gathered using a filter collection device and handheld vacuum cleaner (Figure 5-2). The filter collection device was made of PVC pipe, plastic tubing, and a high efficiency particulate air (HEPA) filter backed by a U.S. No. 200 sieve screen (Figure 5-3). Figure 5-4 through Figure 5-6 show members of the research team collecting dust samples.

Figure 5-2: Filter collection device and vacuum

Figure 5-3: Filter collection device

Figure 5-4: Drilling holes for dust samples

Figure 5-5: Dust created during drilling process

Figure 5-6: Collecting dust from drilled holes

All dust samples were tested for chloride using the alternative potentiometric method. ICP-MS testing was also conducted on dust samples during this study. The purpose of this additional chloride testing was to compare the results between the two methods. However, the ICP-MS did not have low enough detection limits to detect the amounts of chlorides deeper than 1 inch below the pavement surface. This made the development of chloride profiles using ICP-MS data impossible.

Half-cell potential measurements were obtained using the Elcometer® 331 Model SH Concrete Covermeter and Elcometer® Copper-Copper Sulfate Half-Cell probe kit. The probe in the probe kit attaches electronically to the Elcometer® Covermeter (a voltmeter device). The probe contains the reference electrode that was used in this study, which was a copper-copper sulfate reference electrode. This test apparatus is in accordance with ASTM C876-09 (ASTM 2009). One measurement was obtained at each of the intersections of the grid lines used for crack mapping. Prior to taking the measurements, an electrical connection was made to one reinforcing bar that was exposed at the edge of the pavement next to the shoulder. The connection was made using a steel screw, lug, and 14 gage wire (Figure 5-7). The connections were sealed with epoxy glue, and the concrete above the connections was patched with Sakrete®. Four connections of this type were made at each site for redundancy. The wires from the connections were embedded in the pavement and routed to the side of the shoulder where they were placed in a protective electrical box.

Figure 5-7: Electrical connection to the reinforcing bar

One lead wire from the Covermeter was connected to the half-cell probe, and the other was connected to the wire from the electrical box in order to take measurements in accordance with ASTM C876-09 (ASTM 2009). The concrete surface was wetted at the grid points using a spray bottle prior to taking the half-cell measurements. Measurements were obtained by placing the probe's tip on the concrete surface. The Covermeter electronically stored the measurements and the values were uploaded to a computer at a later date. Figure 5-8 shows members of the research team collecting measurements at one of the Sioux Falls sites.

Figure 5-8: Collecting half-cell measurements

5.1.2 INTERSTATE 29 SOUTH OF BROOKINGS AND INTERSTATE 90 REPAIRS

The location of the Interstate 29 site was the southbound lane from MRM 110 to MRM 123. The CRCP of this section was originally constructed in 1968, but was removed and reconstructed using JPCP during the summer and fall of 2010. The original CRCP was evaluated by the research team prior to its removal.

This section of interstate was evaluated using general observation (notes and photographs) and crack mapping. Four crack map surveys were completed: three surveys were obtained for 24 foot long sections and one survey was obtained for a 72 foot section to obtain results over a longer segment of pavement. All four surveys were performed over the entire 24 foot width of the pavement. The methods discussed in section 5.1.1 were used to perform the crack mapping. In addition to the general observation and crack mapping, SDDOT personnel used a ground-penetrating radar (GPR) device to determine the location of the transverse and longitudinal reinforcement.

Sections of CRCP on Interstate 90 were also undergoing repairs during the summer of 2010. The pavement undergoing repairs was originally constructed in 2000. The repair work included removal and replacement of full depth pavement at locations that exhibited severe deterioration. At MRM 222 in the eastbound lane, a total of six repair locations were open for observation on August 31, 2010. Reinforcement had been replaced at two of the locations, and the reinforcement was in the process of being replaced at the other four locations. Notes and photographs were obtained at all six locations, as well as at other locations near the repair sites in order to evaluate the condition of the reinforcement and pavement surface.

5.2 STATEWIDE ASSESSMENT OF EIGHT CRC SITES

Eight sites of the CRCP installed since 1995 in South Dakota were selected and evaluated for corrosion using general observation, half-cell potential measurements, and chloride ion analysis from concrete dust samples. Within each site, a 100 foot long by 12 foot wide traveling lane was examined. Half-cell potential measurements were obtained at the intersection points of a four foot by four foot grid, for a total of 104 total measurements. Two dust samples were collected from each site. The dust samples were obtained at gridline intersections with half-cell measurements that fell within the most negative ten percent of the measurement. The results were correlated to the data obtained in the initial field evaluation of the Sioux Falls sites.

Selection of the eight sites was based on the following criteria: pavement condition, pavement age, precipitation, pavement maintenance activities, and amount of deicer application. To compare the vulnerability to corrosion of the different CRCP sites, a rating system that reflected the selection criteria listed above was devised. For each site, each selection criterion was assigned a numeric value to indicate the effect of the criterion on the reinforcement to corrosion susceptibility. The values were subsequently weighted and applied in a rating formula to quantitatively rank CRCP projects and segments within projects for their susceptibility to corrosion. Based on this rating system a site selection matrix was generated that included all CRCP installed since 1995. A high numerical rating in the site selection matrix indicates a pavement section that is less vulnerable to corrosion. Location of the site was also considered as a final selection factor in order to ensure wide geographic representation of the CRCP projects. The following discussion provides the detail behind the rating method.

The 2010 Highway Needs and Project Analysis Report from the SDDOT (2010) was used in order to determine the pavement condition of the CRCP projects. The report lists the surface condition, roughness, D-cracking/alkali silica reaction (ASR), joint spalling, corner cracking, faulting, joint seal

damage, and punchouts indices for each pavement segment. Note that a pavement *segment* refers to a length of pavement as it is recorded in the 2010 Highway Needs and Project Analysis Report. A pavement *project* refers to a length of pavement that corresponds to a SDDOT project number. Since the surface condition index (SCI) is based on these individual indices, excluding the roughness index for urban areas, all CRCP segments built after 1995 were rated for condition according to this value. The highest SCI value a pavement segment can receive is 5.0. Therefore, a condition value was determined on a scale of 5 as follows:

$$CV = SCI / 5.0 \quad \textbf{(Eqn. 3-2)}$$

Where:

CV = Condition value, and

SCI = Surface condition index

Note that the condition value cannot exceed 1.0. The higher the condition value, the less susceptible the pavement segment is to corrosion.

The age rating was based on the year the CRCP segment was installed. The time span of interest for this study was the twelve year period from 1995 to 2007. The age value assigned to each CRCP segment was determined as follows:

$$AV = (YC - 1995) / 12 \quad \textbf{(Eqn. 3-3)}$$

Where:

AV = Age value, and

YC = Year constructed

The precipitation value was based on the broad geographical precipitation type at the various CRCP sites. Sites were assigned a rating of 1.0 or 0.5 for relative "dry" or relative "wet" precipitation, respectively. Three geographic locations were used to divide the state of South Dakota: west of the Missouri River; east of the Missouri River and north of Brookings; and east of the Missouri River and south of Brookings. To assess corrosion susceptibility, the steel reinforcement in a geographic location which receives less precipitation is considered to be less susceptible to corrosion, whereas steel reinforcement in a geographic location receiving more precipitation is more susceptible to corrosion. Table 5-2 displays the precipitation rating assigned to each geographic location:

Table 5-2: Precipitation value assigned based on geographic region

Geographic Location	Wet or Dry	Precipitation Rating
West of Missouri River	Dry	1.0
East of Missouri River and north of Brookings	Dry	1.0
East of Missouri River and south of Brookings	Wet	0.5

The three year average maintenance cost to the mainline (driving surface) was used to rate the CRCP segments with respect to maintenance activities. This value is the average yearly cost associated with the driving surface per mile over the previous three years. The highest maintenance cost reported in the 2010 Highway Needs and Project Analysis Report (SDDOT 2010) for constructed CRCP segments was $2,712. Therefore, this figure was used as the base for determining a maintenance activities value as follows:

$$MAV = (\$2712 - AMC) / \$2712 \quad \textbf{(Eqn. 3-4)}$$

Where:

MAV = Maintenance activities value, and

AMC = Three year average maintenance cost (dollars)

Deicer application amounts were determined by examining the SDDOT winter maintenance data from 2002 to 2010 (Leibrock 2011). For each deicing product type, the weight of deicing product applied was determined according to the reporting maintenance unit. The estimated deicer applied per mile was determined by summing the weight of all deicers used in a reporting maintenance unit and dividing that value by the total miles of interstate under the jurisdiction of the reporting maintenance unit. Boundary changes that took place for units 271 and 272 in 2005 were taken into account when determining the deicer application amounts. The largest estimated amount of deicer applied per mile was determined to be 487,828 pounds. This value was used as the base for determining the deicer application value as follows:

$$DAV = (487{,}828 - EDAM) / 487{,}828 \quad \textbf{(Eqn. 3-5)}$$

Where:

DAV = Deicer application value, and

EDAM = Estimated deicer applied per mile (lbs.)

A weighting factor was assigned to each of the categories based on its relative importance in considering corrosion. Condition, maintenance activities, and deicer application were assigned a weighting factor of 1.0, which is the highest weighting factor assigned to a pavement segment. The age value and the precipitation value were assigned weighting factors of 0.30 and 0.15, respectively. Each pavement segment was rated according to the following equation:

$$PSR = \sum CVal \times CWF \quad \textbf{(Eqn. 3-6)}$$

Where:

PSR = Pavement segment rating;

CVal = Category value; and

CWF = Category weighting factor

Based on Equation 3-6, the maximum pavement segment rating possible is 3.45. Once each pavement segment was rated, the CRCP projects were rated. Each project can have multiple segments with differing lengths. Therefore, the project rating was computed as the geometric average of the pavement segment ratings within the project by using the following formula:

$$PR = \sum_{1}^{\#\ of\ Segments\ in\ Project} \frac{PSR \times PSL}{TPL} \quad \textbf{(Eqn. 3-6)}$$

Where:

PR = Project rating;

PSR = Pavement segment rating;

PSL = Pavement segment length; and

TPL = Total project length

Site selection values and the computed ratings for projects and segments are shown in Table A-1 in Appendix A. The forty potential CRCP projects identified in this study are sorted in Table A-1 by project rating and are ranked between 1 and 40. A higher numerical ranking indicates lower susceptibility to corrosion.

Four regions outside of the Sioux Falls area were chosen to represent general geographic areas for the entire state of South Dakota. Two sites from each of these 4 regions were selected for the statewide CRCP evaluation. The geographic regions were Interstate 90 between Wall and Chamberlain; Interstate 90 near Rapid City; Interstate 29 south of Sioux Falls; and Interstate 29 south of Watertown as shown in Figure 5-9. One of the 2 sites selected within each geographic region received a relative high rating (low susceptibility to corrosion), and one received a relative low rating (high susceptibility to corrosion). A total of 8 sites were surveyed to compare half-cell potential and chloride ion results with the measurements obtained at the Sioux Falls study sites. The eight recommended sites that were subjected to additional evaluation are summarized in Table 5-3 and shown in bold in Table A-1. Note that since the project ranked 27 was inaccessible at the time of this study, the project ranked 25 was chosen as the higher ranking site for the region south of Sioux Falls. Pavement design information for the eight sites is presented in Table 5-4.

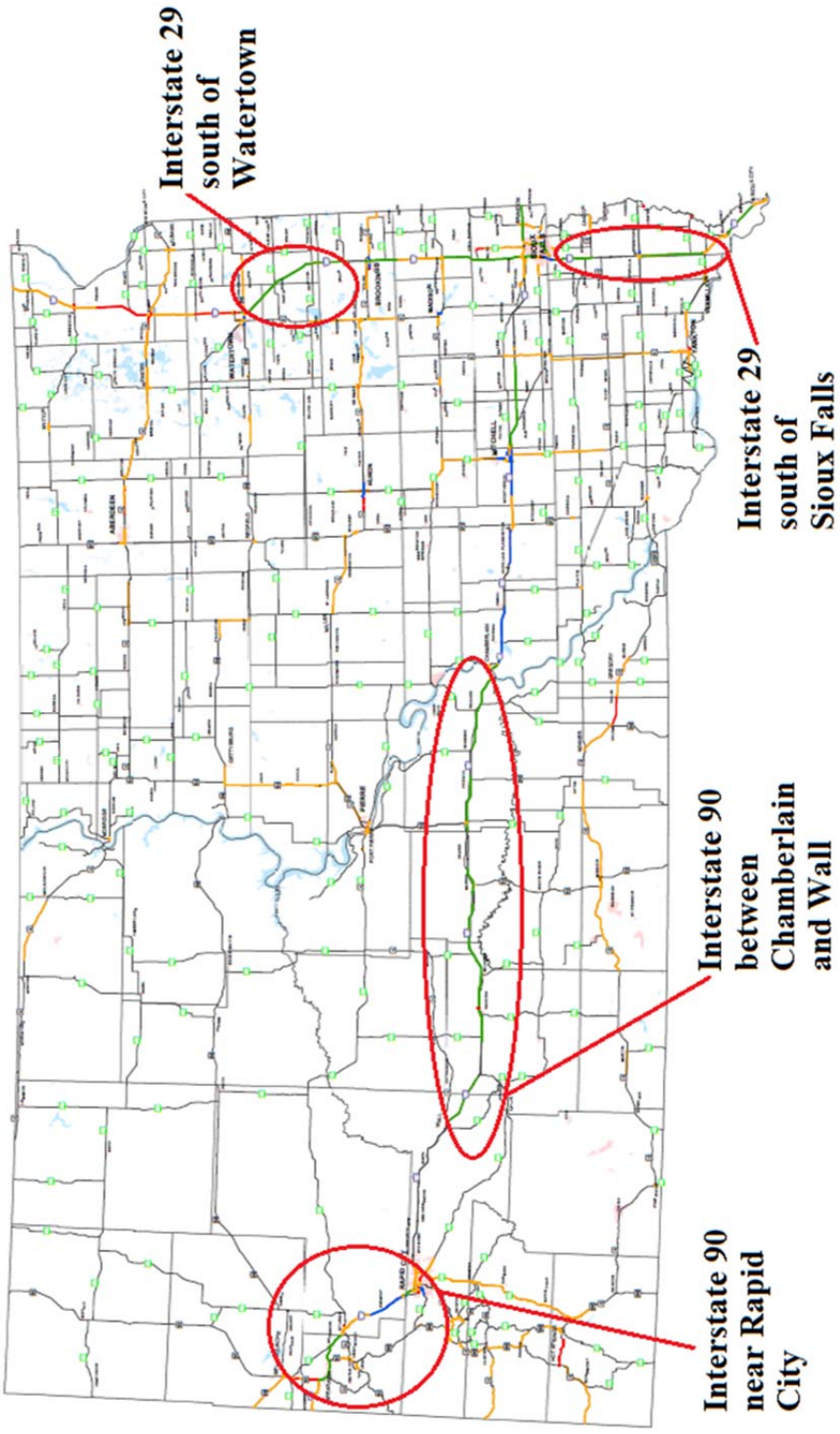

Figure 5-9: Regions for statewide evaluation (SDDOT 2010)

Table 5-3: Summary of recommended CRCP sites for statewide evaluation

Site	Project Rank	Project Rating	Segment Rank	Segment Rating	Begin MRM	End MRM	Length (miles)	Lane
I-90 between Chamberlain and Wall – High at MRM 246	33	2.916	67	2.907	247.0	251.6	4.60	EB
			68	2.912	246.0	247.0	1.00	EB
			70	2.921	236.0	246.0	10.00	EB
I-90 between Chamberlain and Wall – Low at MRM 222	14	2.526	40	2.526	213.1	226.7	13.58	EB
			41	2.533	226.7	227.0	0.32	EB
I-90 near Rapid City – High at MRM 54	38	3.120	76	3.079	52.4	56.0	3.56	EB
			79	3.161	52.4	56.0	3.56	WB
I-90 near Rapid City – Low at MRM 25	15	2.539	39	2.515	18.48	19.42	0.94	EB
			43	2.541	19.42	28.34	8.92	EB
I-29 South of Watertown – High at MRM 168	40	3.173	80	3.173	165.0	179.0	14.00	NB
I-29 South of Watertown – Low at MRM 168	35	2.967	74	2.967	165.0	179.0	14.00	SB
I-29 South of Sioux Falls – High at MRM 44	25	2.824	56	2.824	37.32	46.31	8.99	SB
I-29 South of Sioux Falls – Low at MRM 33	17	2.579	45	2.579	27.0	37.3	10.32	SB

Table 5-4: Pavement design information for eight selected sites

Site	MRM 33	MRM 44	MRM 25	MRM 54	MRM 222	MRM 246	MRM 168NB	MRM 168SB
Concrete Thickness (inches)	10	11.5	10	11.5	10	10	10	10
Longitudinal bar size	6	5	6	*	*	5	6	6
Design longitudinal bar spacing (inches)	6.5	4.5	48	*	*	4.75	6.25	6.25
Design Longitudinal bar depth (inches)	3.5	3.5	3.5	*	*	3.5	3.5	3.5
Transverse bar size	4	4	4	*	*	4	4	4
Design transverse bar spacing (inches)	48	42	48	*	*	42	42	42
Notes	*Information not available							

5.3 MITIGATION PRODUCT TESTING

This section outlines the data collection from both the field and laboratory testing that were performed during this study. The field and laboratory testing were performed to determine the effectiveness of different topically applied corrosion mitigation products. The field testing included applying five

different products and one combination of products, which were applied to the field test site. A control section was also designated at this site. Assessing product effectiveness consisted of half-cell potential measurements of each test section and the control section. The laboratory testing included the same product and product combinations as the field testing, but the products were applied to specimens that were in a controlled environment.

5.3.1 CORROSION MITIGATION PRODUCTS TESTED

The products chosen were penetrating sealers and MCI's. The products were selected using the following methodology (Leibrock 2012):

- First, available products were located through the SDDOT approved products list shown in Table 5-5, the literature search, and discussions with SDDOT personnel.
- Additional product information was obtained from MSDS sheets, product sheets, and by contacting company representatives.
- The product information was then organized by product chemical composition and method of mitigation, i.e. sealers serves MCIs. Product summary information is shown in Table 5-6, and discussed in more detail in the following sections.
- The method of product search and recommended products were presented and to the Technical Panel and approved.

Table 5-5: SDDOT approved products list

Product	Company
Baracade Silane 40	Euclid Chemical Co.
Enviroseal 40	BASF Building Systems
Hydrozo Silane 40	BASF Building Systems
Penetrating Sealer 40	BASF Building Systems
Protectosil Chem-Trete 40 VOC	Degussa Corporation
Sil-Act ATS-42	Advanced Chemical Technologies, Inc.
TK-590 Tri-Silane	T-K Products, a Division of Sierra Corp.
Weather Workers S-40 (J-29)	Dayton Superior Chemical Division

Table 5-6: Product information

Product	Type	Company	Cost ($/gallon)	Carrier of product
Protectosil CIT	MCI	Evonik Industries	67.00	100% silane w/ MCI
Ferrogard 903	MCI	Sika Corp	57.00	alcohol
DURALPREP 3020	MCI	The Euclid Chemical Company	120.00	water
MCI-2018	MCI	Cortec Corporation	Unknown	100% silane w/ MCI
Chemtrete 40 VOC	Silane	Evonik Industries	16.75	alcohol

5.3.1.1 MCI-2018

MCI-2018 is manufactured by Cortec Corporation. MCI-2018 is a silane concrete sealer, which also contains a proprietary MCI. It is a non-toxic blend that does not contain any nitrates, phosphates, or chromates. The manufacturer recommends using MCI-2018 for the protection and rehabilitation of

bridge decks, parking garages, tunnels, and reinforced concrete structures in marine environments (Cortec 2011).

Cortec (2011) recommends a total application rate of 125 to 175 ft^2 per gallon, per coat, with a minimum of two coats. Prior to application, the concrete surface should be free of all dust, dirt, and oil. The surface must also be dry prior to application. MCI-2018 can then be applied using a sprayer, squeegee, or a roller. The application of subsequent coats should be applied while the previous coat is still wet. After application, it is required to wait seven days before applying any coatings, such as other sealers or barriers, over the MCI-2018.

5.3.1.2 Protectosil CIT

Protectosil CIT is manufactured by the Evonik Degussa Corporation. Protectosil CIT is an "organofunctional" MCI that penetrates to the reinforcement and chemically bonds with the steel and the cement paste to inhibit the corrosion process. The manufacturer recommends using it on bridges exposed to corrosive conditions, parking garages, and steel reinforced concrete in a marine environment (Evonik 2012b).

Evonik (2012b) recommends an application rate of 175 to 225 ft^2 per gallon per coat, with a minimum of two coats. Prior to application, the concrete surface should be either ground down, pressure washed, sand blasted, or chemically cleaned to remove all dust, dirt, and oil from the concrete surface. The surface must also be dry prior to application. Protectosil CIT can then be applied using either a low pressure sprayer or a roller. The time between coat applications is 15 minutes. After application it is recommended to allow the product to cure for four hours before being exposed to rain.

5.3.1.3 Ferrogard 903

Ferrogard 903 is manufactured by the Sika Corporation. Ferrogard 903 is a corrosion inhibiting impregnation coating for hardened concrete surfaces (Sika 2011). It is a combination of amino alcohols, and organic and inorganic inhibitors. It is designed to form a layer around the reinforcement, displacing chloride ions at the steel surface and forming a physical barrier which protects both anodic and cathodic areas of the reinforcement. Recommended uses by the manufacturer include bridges and roadways exposed to corrosive conditions, parking garages, and steel reinforced concrete in a marine environment (Sika 2011).

For Ferrogard 903, Sika (2011) recommends an application rate of 200 ft^2 per gallon per coat, with a minimum of two coats. Prior to application, the concrete surface should be either steam cleaned, pressure washed, or sand blasted to remove all dust, dirt, and oil from the concrete surface. The surface must also be dry prior to application. Ferrogard 903 can then be applied using either an airless spray system, hand sprayer, or a roller. The required time between coat applications is one hour, and after application, it is required to wait at least one day before washing off any residue that remains.

5.3.1.4 Duralprep 3020

Duralprep 3020 is manufactured by the Euclid Chemical Company. It is a water-based, organic MCI that adsorbs to the reinforcement. The manufacturer recommended uses include bridges and highways exposed to corrosive conditions, parking garages, and steel reinforced concrete in a marine environment (The Euclid Chemical Company 2000).

The Euclid Chemical Company (2000) recommends a coverage rate of 200 to 400 ft^2 per gallon, per coat, with two coats recommended for dense substrates. Prior to application, the concrete surface should be either steam cleaned, pressure washed, or sand blasted to remove all dust, dirt, and oil from the concrete surface. The surface must also be dry prior to application. Duralprep 3020 can then be applied using either an airless spray system, hand sprayer, roller, or squeegee. The minimum time between coats is 7.5 hours; after application it is required to wait at least eight hours before washing off any of the residue, but traffic on the roadway may resume minutes after application if necessary.

5.3.1.5 Chemtrete 40

Chemtrete 40 VOC (referred to as Chemtrete 40) is manufactured by the Evonik Degussa Corporation. Chemtrete 40 is a silane concrete sealer in an alcohol carrier. The manufacturer recommended uses include highways, parking garages, airport runways, and also concrete and masonry buildings (Evonik 2011a).

Evonik (2011a) recommends an application rate of 150 to 250 ft^2 per gallon, per coat, with a minimum of two coats. Prior to application, the concrete surface should be either pressure washed, sand blasted, or chemically cleaned to remove all dust, dirt, and oil from the concrete surface. The surface must also be dry prior to application. Chemtrete 40 can then be applied using either a low pressure sprayer, or a roller. After application, it is recommended to allow the product to cure for two hours before being exposed to rain.

5.3.2 FIELD TESTING OF CORROSION MITIGATION PRODUCTS

The corrosion mitigation products were applied to 50-foot-long sections of the right hand lane on Interstate-29 Northbound at MRM 87 as shown in Figure 5-10. The sections were separated by 20-foot-long separation zones to eliminate overspray of the corrosion mitigation products and minimize effects between test sections. These test sections were prepared for half-cell potential testing by attaching 14 gauge wires with quadruple redundancy to the reinforcement. Table 5-7 shows the schedule of the field testing. Product application occurred on both August 31, 2011 and September 1, 2011. However, time from product application is calculated from August 31, 2011.

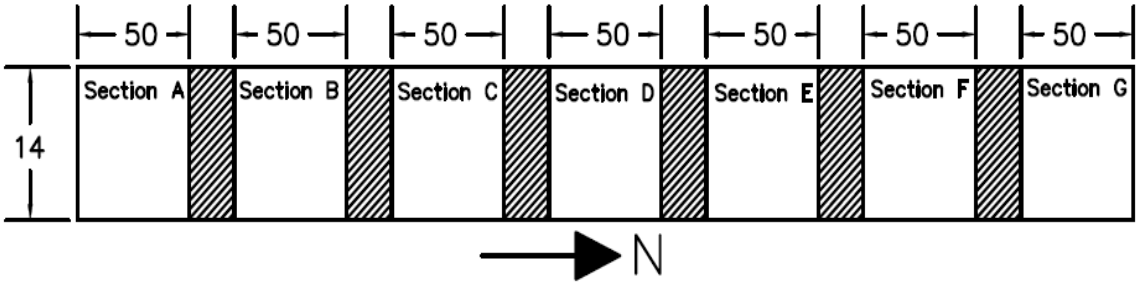

Figure 5-10: Test section layout

Table 5-7: Schedule of field testing

Date	Task Performed	Time From Product Application (Days)
August 25, 2011	Initial Half-Cell Potential Measurement	N/A
August 30, 2011	Power-washed Sections	N/A
August 31, 2011 to September 1, 2011	Products Applied	0
October 6, 2011	Half-Cell Potential Measurement	36
October 27, 2011	Half-Cell Potential Measurement	57
April 10, 2012	Half-Cell Potential Measurement	223
May 9, 2012	Half-Cell Potential Measurement	252

5.3.2.1 Product Application

Prior to product application, the north half of each section was power washed so that comparisons could be made between washed and unwashed pavements. After power washing, the test sections were allowed to dry for 24 hours prior to product application. Representatives from each product manufacturer were present during the product application. The products were applied using hand sprayers as shown in Figure 5-11. Figure 5-12 shows the test section after all products were appied. To obtain the target application rates, the sprayer nozzle was maintained at a distance of 9 to 12 inches from the surface of the pavement. Spraying was stopped when large trucks or continuous traffic drove past the site, in order to minimize drift of the spray. The product loss from the wind was estimated to be between 10 and 20 percent for all sections, by onsite research personnel.

Figure 5-11: Product application

Figure 5-12: Test sections after product application

The corrosion mitigation products were applied at the manufacturer's recommended rates. Table 5-8 summarizes the coats applied to each section as well as the target and actual average application rates. The actual average application rate per coat was determined by measuring volume of product that was applied to the test section in each coat and dividing this volume by area of the test section. The application rates for each coat were then averaged together for each test section as shown in Table 5-8.

Table 5-8: Product application

Product Section	Product	Coats	Target Application Rate per Coat (ft^2/gal)	Actual Average Application Rate per Coat (ft^2/gal)
A	MCI-2018	2	250	278
B	Ferrogard 903	1	300	308
	Protectosil CIT	2	200	200
C	Protectosil CIT	3	200	204
D	Ferrogard 903	3	300	300
E	Duralprep 3020	2	300	292
F	Chemtrete 40	2	200	200
G	No Product (Control Section)	---	---	---

The following list described product application procedures that differed from the project's planned procedure. This was due road closure time constraints and recommendations from manufacturer representatives that were on site:

- **Section A:** The entire section was power-washed prior to product application. The section was also power-washed after the application of MCI-2018. This was because the surface was slippery after product application and deemed unsafe for automobile travel.
- **Section B:** The entire section was power-washed prior to product application. The entire section was power-washed after the application of the Ferrogard 903. It was then allowed to dry before the application of Protectosil CIT.
- **Section D:** The entire section was power-washed after the application of the Ferrogard 903. This was because the surface was slippery after product application and deemed unsafe for automobile travel.
- **Section E:** The first coat of Duralprep 3020 was applied on August 31, 2011, the next morning, approximately three feet of Section E was mistakenly power-washed. Approximately 15 feet of Section E became wet from the power washing. This was allowed to dry and then the second coat was applied. Within a few hours of applying the second coat of Euclid Duralprep, the section was power-washed. This was because the surface was slippery after product application and deemed unsafe for automobile travel.

5.3.2.2 Half-Cell Potential

The half-cell potential was measured using a two foot by two foot grid for each section. This provided 182 measurements per test section per testing event. As shown in Table 5-7, half-cell measurements were taken before the products were applied and at intervals after the products were applied. Half-cell potential measurements were obtained when temperatures were consistently above freezing.

The half-cell potential measurements were obtained following the procedure outlined in ASTM C876-09, with the exception that plain tap water was used as the electrical contact solution instead of a dish soap and water mixture. Furthermore, a 15% percent of isopropyl or denatured alcohol by volume for cold weather applications was not added to the electrical contact solution when the temperature dropped below 50 degrees F. The concrete was pre-wetted by spraying it with water at the points where the half-cell potential was to be measured, and a wet sponge was used as the electrical contact between the reference electrode and the concrete as described in ASTM C876-09.

5.3.3 LABORATORY TESTING OF CORROSION MITIGATION PRODUCTS

The purpose of the laboratory testing was to compare the effectiveness of each product by minimizing variables that are apparent in field testing (weather, moisture, etc.). The laboratory setting allowed aspects of the environment to be controlled, such as temperature and the amount of chlorides that the specimens were exposed to. This section outlines the methods used cast and test the laboratory specimens. It also shows which products were applied to each specimen.

5.3.3.1 Specimens

The laboratory specimens were cast 12-inches long by 8-inches wide by 8-inches tall. The steel reinforcement in all specimens was a No. 4 rebar. All of the specimens were cast with a shallow well on top to allow the application/ponding of chlorides to the specimen. Figure 5-13 shows the dimensions and layout of the specimens and Figure 5-14 shows an example of a completed/cast specimen.

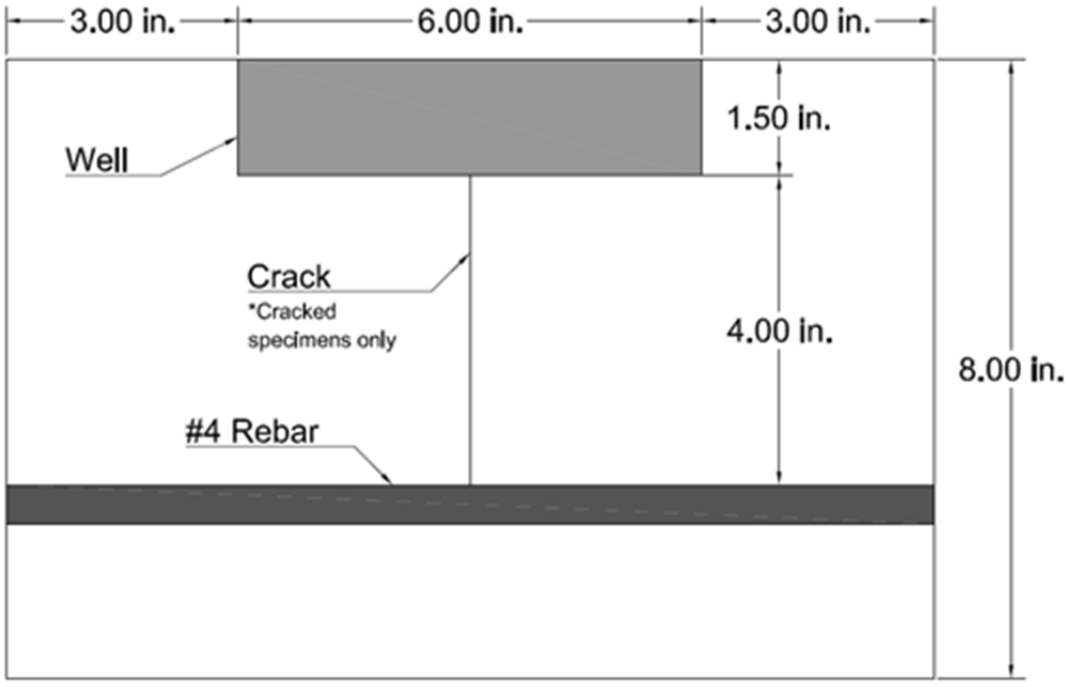

Figure 5-13: Laboratory specimen dimensions

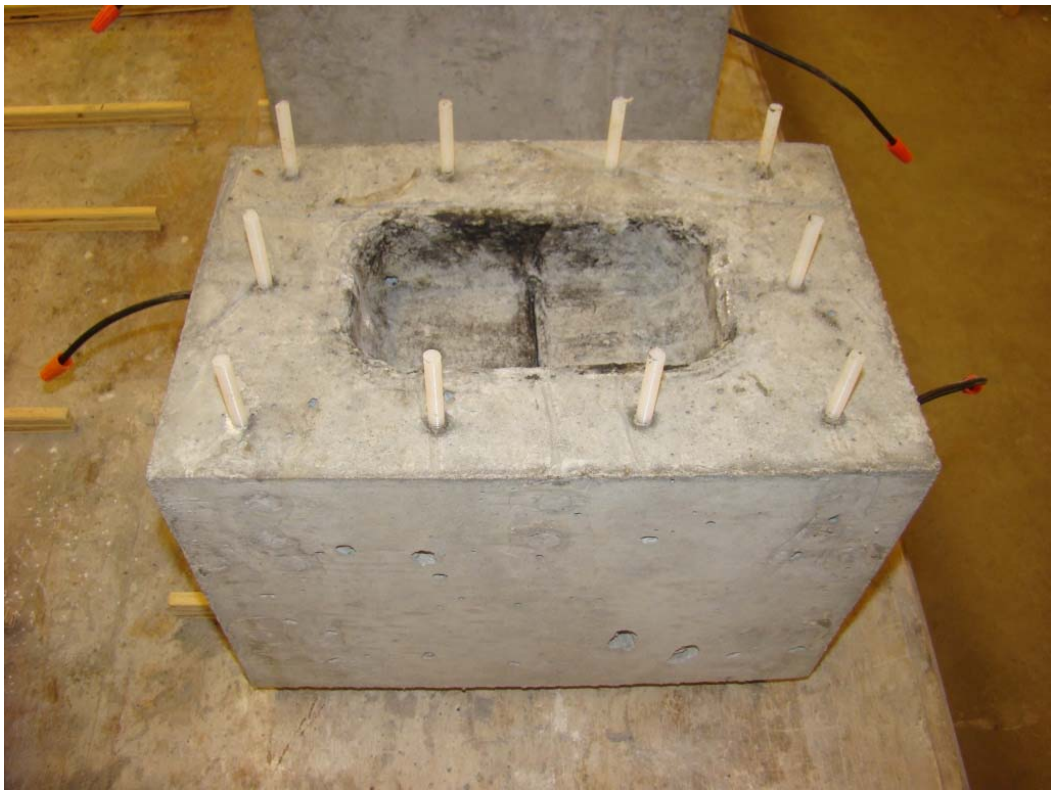

Figure 5-14: Cracked specimen

Figure 5-15 shows the form used to cast the specimens. The forms for the specimens were fabricated from plywood with the wells formed using a piece of a two inch thick by four inch wide board that had been cut and sanded to shape. This resulted in a well that was approximately three and a half inches wide by six inches long and one and a half inches deep. Some specimens were cast with a steel shim to simulate a crack; the simulated crack was introduced into the specimen by placing 0.01 inch-thick shim stock into the specimens between the well and reinforcing. The average crack thickness of cracks surveyed at the Sioux Falls Sites was 0.01 inch, therefore that was the thickness used to simulate cracks. The steel shim was cut so that it tapered from three inches long at the top to two and a half inches long at the level of the reinforcement. The steel shim extended four inches from the bottom of the well to the top of the reinforcement. After the specimens cured for 48 hours, the steel shims were removed from the specimens leaving a simulated crack. Uncracked specimens were also produced as part of the study.

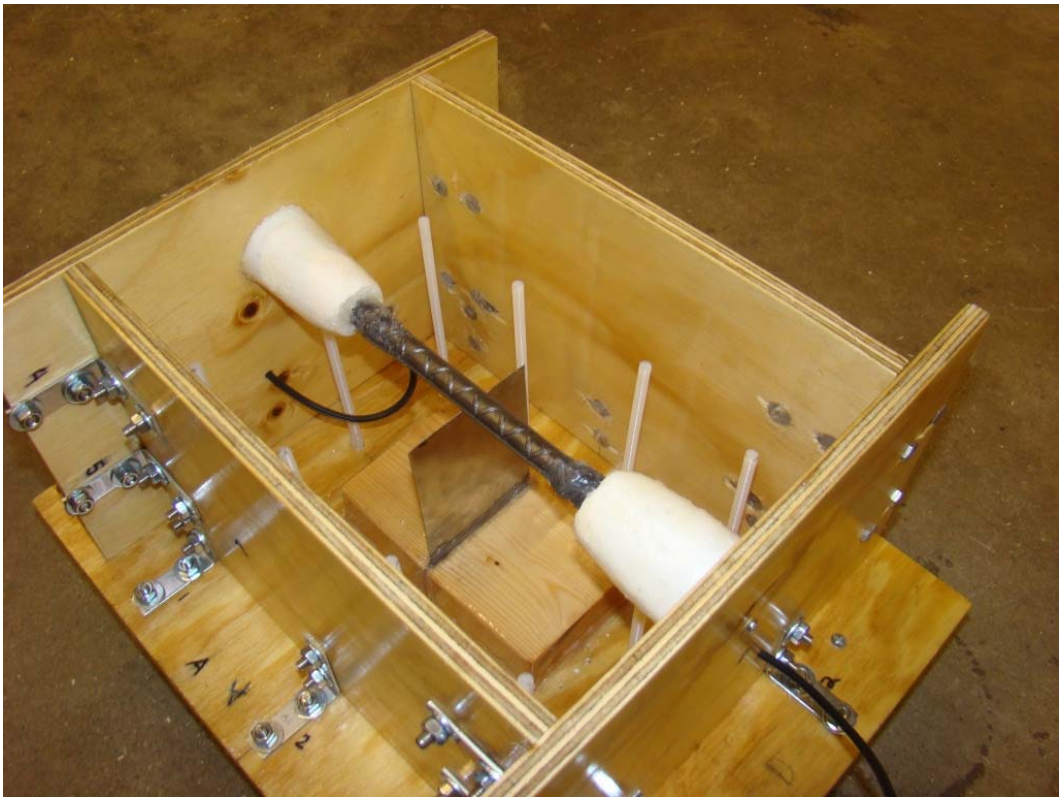

Figure 5-15: Form and steel shim for a cracked specimen

The steel reinforcement was wire brushed prior to casting the specimen to remove all corrosion and oil. The reinforcement was then connected to 14 gauge, insulated copper wires that extended out of the side of the specimen. These wires were used to obtain half-cell potential measurements. The wires were connected to the reinforcement by drilling a hole through the reinforcing and then attaching the wire with a screw and electrical lug. The connections were covered with butyl rubber which was then covered with silicone sealer as shown in Figure 5-16, to prevent the connections from corroding and affecting electrical connection. The reinforcement was held in place by Styrofoam inserts while the specimens were cast as shown in Figure 5-15. Once the specimens were cured, the Styrofoam was removed and the holes were patched with Quickcrete®.

Figure 5-16: Reinforcement prior to placement in the forms

Prior to casting, the forms and shims were lightly coated in oil to assist in form release. The concrete for the specimens was mixed using a portable mixes and the molds were filled in three lifts. The concrete was consolidated by rodding 25 times per lift with a tamping rod and tapping the sides of the mold with a rubber mallet 10-15 times per lift. After the mold was full, the top was smoothed off using the rod. After the specimens were cast, they were covered with plastic, and allowed to cure in the forms for approximately 24 hours. The forms were then removed and the specimens were cured in a moist curing room for 14 days before being dry cured for the remainder of the curing process.

Two different concrete mix designs were used for the laboratory specimens. One design used salt in the mixture to expedite the onset of corrosion, and the other did not use salt. The mix design with no salt in the mix followed the concrete mix design of the product test section on Interstate 29 as is shown in Table 5-9. The concrete materials consisted of the following:

- Fine Aggregate from Northern Concrete Aggregate, Luverne, MN;
- Coarse Aggregate from Concrete Materials, Sioux Falls;
- Portland Cement was Dacotah Type I-II from Rapid City;
- Fly Ash from Coal Creek, Underwood, ND;
- Air Entraining Agent (Daravair R) from WR Grace; and
- Water Reducer (WRDA 82) from WR Grace.

Table 5-9: Mix design for no salt in mix specimens

Constituent	Absolute Volume per Cubic Yard (Cubic Feet)	Specific Gravity	Mix/Cubic Yard (lbs.)
Cement	2.58	3.17	510.34
Fly Ash	0.71	2.53	112.09
Water	3.79	1.00	236.50
Sand	7.23	2.64	1191.04
Rock	10.93	2.62	1786.92
Air (6.5%)	1.76	0.00	0.00
		Total:	**3836.89**

The concrete mix design with salt in the mix was the same as the no salt mix design with the exception that the water was replaced with a 23 percent by weight sodium chloride solution. The sodium chloride solution was formed by dissolving 99.8 percent pure sodium chloride in the water of the concrete mix.

The no salt concrete mix design was used for the cracked specimens and two uncracked control specimens. The cracked specimens were cast from four batches of concrete. The first two batches were mixed on May 11, 2011 and used to cast Specimens 1-9. The third and fourth batches were mixed on May 17, 2011 and they were used to cast Specimens 10-16. Two, uncracked specimens were cast with no salt in the mix on July 19, 2011. Six-inch-diameter by twelve-inch-tall cylinders were also cast from each batch and tested for compressive strength after being moist cured for 28 days. The salt in the mix concrete design was used for uncracked specimens. Six, uncracked specimens were cast with salt in the mix on November 3, 2011. Table 5-10 shows the properties for each of the batches of concrete that were produced.

Table 5-10: Concrete batches and compressive strengths

Mix Design	Batch Number	Specimens Cast	Air Content (%)	Slump (inches)	Unit Weight ($lbs/ft^{3)}$	Average Compressive Strength (psi)
No Salt in Mix	1	1-9	6.3	2.25	145.1	4757
	2		7.3	1.75	142.8	4379
	3	10-16	6.6	1.75	144.2	5094
	4		6.4	2.25	144.6	5145
Salt in Mix	5	17-22	3.7	0.5	150.0	6554
No Salt in Mix	6	23,24	4.0	0.5	148.6	7,081

5.3.4 PRODUCT APPLICATION AND CHLORIDE PONDING

Once the specimens were cured, the specimens were subjected to the following:

1) Each product or product combination was applied to two cracked specimens and one uncracked specimen with salt in mix.
2) Each of the cracked specimens were ponded with a chloride solution, to initiate corrosion, before the products were applied. These were referred to as wet specimens. None of the uncracked specimens were ponded with a chloride solution.

3) The products were then applied to the bottom of the wells. The target product application rate for the specimens was the same as the target application rate for the field testing. The volume of products needed for each specimen was calculated based on the area of the bottom of the well. The required amount of product was then measured with a syringe and applied to the specimen using a spray bottle that had already been primed with the product.
4) Once the products were applied, one cracked specimen for each product and two of the cracked control specimens were left dry (referred to as dry specimens). The wet specimens were subsequently reponded.
5) Wet specimens had the products applied to them twice. The wet specimens were also reponded after the second product application.
6) Measurements of half-cell potential were obtained at various intervals.
7) There were also four cracked specimens and two uncracked specimens with no salt in the mix that did not have products applied to them; these were referred to as control specimens.

The products were initially applied on October 3-4, 2011 for all cracked specimens. For each product or product combination, one of the cracked specimens also had the products reapplied on February 17-18, 2012. The uncracked specimens with salt in the mix had products applied to them on December 20-21, 2011. The other cracked specimen for each product and two of the cracked control specimens were reponded with a chloride solution on December 5, 2011 (64 days after the products were applied). Table 5-11 lists the specimen types and the product combinations used for laboratory testing.

Table 5-11: Laboratory specimen parameters

Specimen Label	Specimen Type	Mix Type	Ponding Type	Product Applied
Specimen 1	Cracked	No Salt in Mix	Wet	MCI-2018
Specimen 2			Dry	MCI-2018
Specimen 3			Wet	Ferrogard 903 & Protectosil CIT
Specimen 4			Dry	Ferrogard 903 & Protectosil CIT
Specimen 5			Wet	Ferrogard 903
Specimen 6			Dry	Ferrogard 903
Specimen 7			Wet	Protectosil CIT
Specimen 8			Dry	Protectosil CIT
Specimen 9			Wet	Duralprep 3020
Specimen 10			Dry	Control
Specimen 11			Dry	Duralprep 3020
Specimen 12			Wet	Chemtrete 40
Specimen 13			Dry	Chemtrete 40
Specimen 14			Dry	Control
Specimen 15			Wet	Control
Specimen 16			Wet	Control
Specimen 17	Uncracked	Salt in Mix	No Ponding	MCI-2018
Specimen 18				Ferrogard 903 & Protectosil CIT
Specimen 19				Ferrogard 903
Specimen 20				Protectosil CIT
Specimen 21				Duralprep 3020
Specimen 22				Chemtrete 40
Specimen 23		No Salt in Mix	No Ponding	Control
Specimen 24				Control

5.3.4.1 Half-Cell Potential

The half-cell potential was measured similarly to field testing using a sealed copper-copper sulfate reference electrode. However, unlike the field testing, the specimens were only sprayed with water using a small handheld sprayer to pre-wet the concrete surface and no wet sponge was used as a contact between the reference electrode and the concrete. Prior to obtaining the half-cell potential measurement of a specimen, an electrical connection was made with reinforcement by attaching the Elcometer to one of the 14 gauge copper wires that had previously been attached to the reinforcement. Initial half-cell potential measurements were obtained on May 25, 2011, or 14 days after Specimens 1 through 9 were cast and 8 days after Specimens 10 through 18 were cast. Insert initial half-cell measurements dates of Specimens 19 through 24. Half-cell potential measurements were obtained approximately one to three times per week throughout the remainder of the study.

5.3.4.2 Chloride Ion Analysis and Scanning Electron Microscopy Testing

Four specimens were chosen for chloride ion analysis. Specimen choice was based on the following:

1) Half-cell potential measurements with time.
2) Whether the specimen was cracked or uncracked.
3) Wet verses dry specimens.

4) Specimen ponding.
5) Specimens with product applied verses control specimens.

The specimens chosen for testing were Specimen 3 (Ferrogard 903 & Protectosil CIT), Specimen 5 (Ferrogard 903), Specimen 7 (Protectosil CIT), and Specimen 15 (control). The un-cracked specimens were not considered for chloride potential testing because their variation of half-cell potential with time was minimal. Additionally, they were never subjected to a subsequent ponded chloride solution. The wet, cracked specimens were chosen for analysis because they had chlorides applied after product application. These specimens also had the products applied twice instead of once like the dry specimens. These more severe conditions were thought to allow the differences in effectiveness of the products to be more visible in the laboratory testing; therefore, SEM testing was only performed on wet, cracked specimens.

Specimens 3 and 5 were chosen because they had the largest increase in half-cell potential from product reapplication until several months into the study when compared to other wet specimens. Specimen 7 was chosen because the measured half-cell potential became more negative than other similar specimens once the products were applied. Specimen 15 was chosen because it was the wet, cracked control specimen that appeared to be representative of the other untreated specimens in the laboratory tests. The chloride and SEM results from Specimen 15 were intended to serve as a benchmark for comparison to the other results from the chloride ion concentration testing.

To perform the chloride ion analysis, the laboratory specimens were sliced using a vertical and horizontal scheme. The specimens were first cut into five horizontal slices below the well. The top three slices were one inch thick and the fourth slice, directly above the reinforcement, was approximately 3/4 inches thick as shown in Figure 5-17. The fourth horizontal slice was reduced to less than one inch thick due to cutting equipment limitations. The horizontal slices were then cut vertically at 1/2 inch increments away from the simulated crack location. Figure 5-18 shows the horizontal slices with the vertical cuts marked on them. Each of the resulting samples were then pulverized prior to chloride testing.

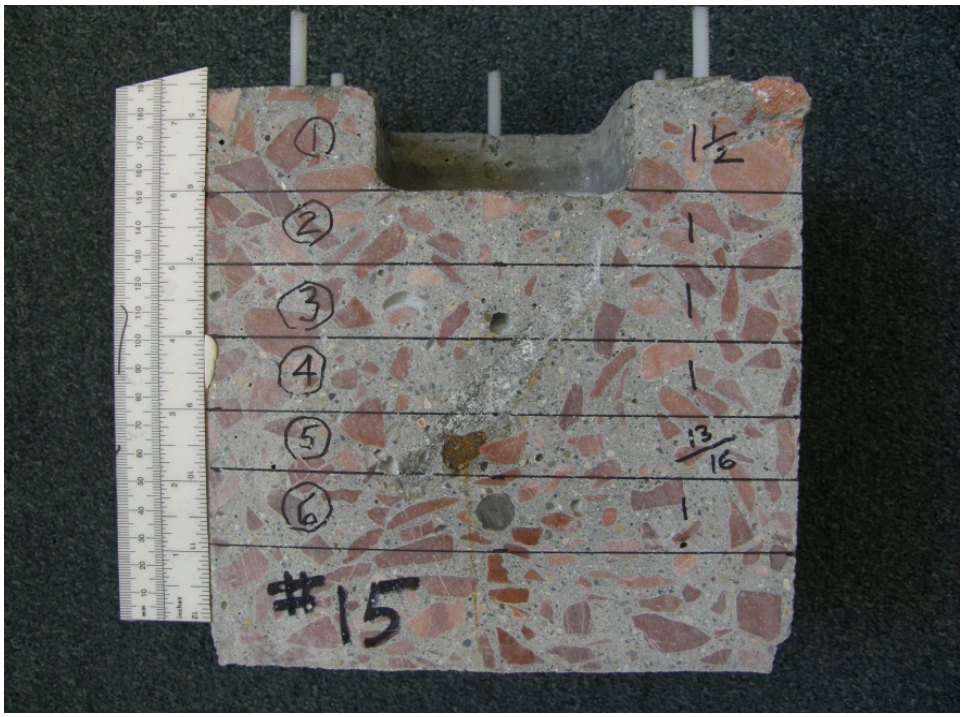

Figure 5-17: Horizontal slice scheme for concrete specimen

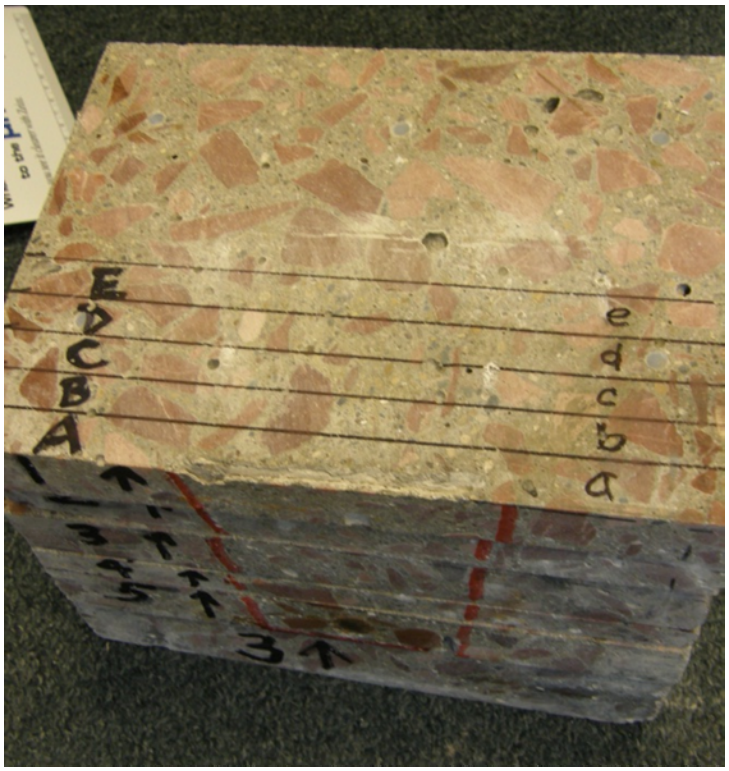

Figure 5-18: Vertical slice scheme for concrete specimen

The four specimens that were subjected to chloride testing were also selected for SEM testing. The horizontal slice containing the reinforcement was saw-cut to fit into the SEM device. The reinforcement was then covered with a layer of epoxy binder to prevent the corrosion around the edges of the reinforcement from flaking off during the polishing process as shown in Figure 5-19. The cut face of the reinforcement was polished prior to placing it into the SEM device. Results are presented in the next chapter (Chapter 6) and consist of secondary electron images, backscattered electron images, and X-ray element distribution maps. The background of the these methods were discussed in Chapter 4.

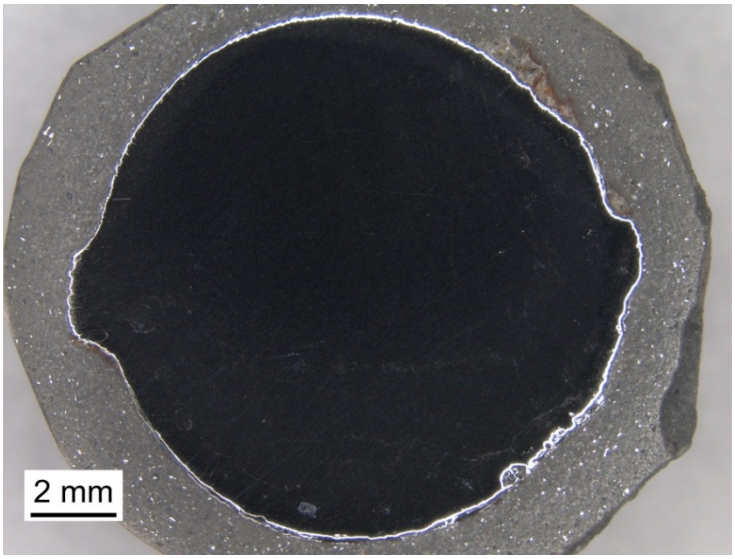

Figure 5-19: Polished specimen reinforcement for SEM testing

6 RESULTS

This chapter outlines the results obtained during this study. Results from half-cell potential measurements, chloride ion analysis, SEM testing, crack mapping, and general observations of the initial and statewide CRCP evaluations, and the product mitigation testing are presented.

6.1 INITIAL CRCP EVALUATION

The purpose of the initial CRCP evaluation was to develop a preliminary assessment of the level of corrosion observed and the effect of corrosion on pavement performance in pavement sections that were identified by SDDOT to be distressed. This section outlines the results obtained from the three CRCP sites near Sioux Falls, SD, the Interstate 29 reconstruction site near Brookings, SD, and Interstate 90 repairs.

6.1.1 SITE I-29N, NORTH OF SIOUX FALLS AT MRM 87

Crack mapping, dust sampling, and core sampling was completed for site MRM 87 on September 30, 2010. The first set of half-cell potential measurements was obtained on October 12, 2010. A second set of half-cell potential measurements was obtained on June 14, 2011 to determine the effect of one winter maintenance cycle on the half-cell measurements. Transverse, longitudinal, and Y-cracking were observed. The measured crack width at this site averaged 0.013 inches with minimum and maximum widths of approximately 0.006 inches and 0.033 inches, respectively. The crack density was 0.681 foot/square foot. Transverse crack spacing ranged from less than one to four feet apart. Figure 6-1 presents a picture of a section of this CRCP site.

Figure 6-1: Cracking on Interstate 29 at MRM 87

Five core samples were removed from the pavement section at MRM 87. Four of the cores were removed at cracked pavement locations with crack widths of 0.008, 0.033, 0.024, and 0.030 inches. The depth of the pavement section was approximately eight inches. The depth to pavement section reinforcement varied from 3.375 to 3.875 inches. The dust samples and cores were submitted to the Engineering and

Mining Experiment Station (EMES) at the South Dakota School of Mines & Technology (SDSM&T) for chloride and SEM analyses.

The chloride ion concentration in each of the dust samples was determined using the alternative potentiometric method. The results of all the potentiometric chloride testing for the Sioux Falls sites are presented in Table 6-1. This data was used to develop vertical chloride profiles, which show the chloride concentration versus the depth at which the dust sample was obtained. The chloride threshold value of 1.244 pounds of chloride per cubic yard of concrete was used to determine if the chloride content in the concrete would be a cause of concern with respect to corrosion. This threshold level equates to 0.2 percent chloride by mass of binder material, which is suggested by the FHWA (Clear 1976). A scatterplot of all the chloride profiles collected from the Sioux Falls sites is presented in Figure 6-2. The individual chloride profiles from the dust samples collected at MRM 87 are provide in Appendix C.

Table 6-1: Alternative potentiometric chloride ion results for Sioux Falls sites (values in lbs./yd^3)

		Sample Depth (inches)					
Site	**Sample**	***0.25***	***0.50***	***0.75***	***1.50***	***2.50***	***3.50***
MRM 87	1	14.88		0.88	0.29	0.25	0.46
	2		10.69		0.42	0.22	0.22
	3		10.85		0.4	0.47	0.64
	4		10.8		0.25	0.22	0.22
MRM 68	1		12.42		0.39	0.3	0.24
	2		13.59		0.39	0.3	0.24
	3		9.78		0.3	0.18	0.16
	4		13.01		0.47	0.3	0.27
MRM 411	1		10.79		0.32	0.34	0.38
	2		11.36		0.13	0.23	0.17
	3		9.49		0.4	0.37	0.35
	4		10.45		0.64	0.47	0.39
Minimum			9.49		0.13	0.18	0.16
Maximum			13.59		0.64	0.47	0.64
Average			11.2		0.37	0.3	0.31
Standard Deviation		---	1.293	---	0.13	0.09	0.14

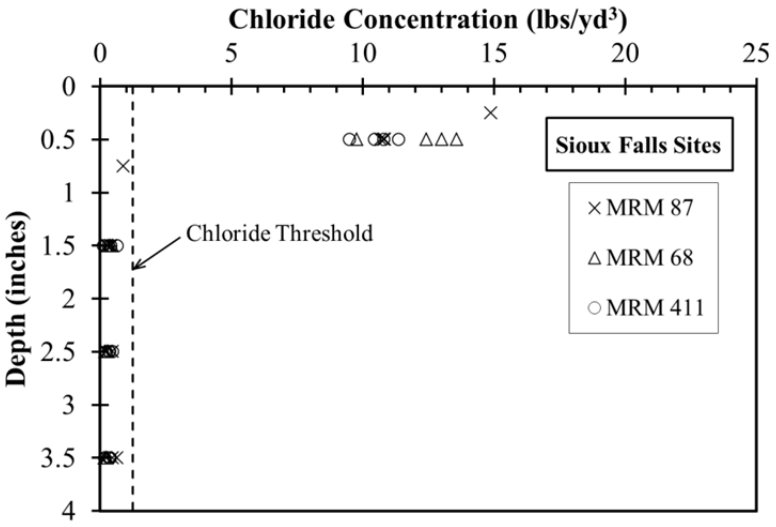

Figure 6-2: Chloride concentration versus depth in dust samples collected near Sioux Falls

Table 6-1 and Figure 6-2 show that the chloride ion concentration is typically above the threshold within the top one inch of the concrete. From depths of greater than 1 inch to 3.5 inches, the chloride concentrations are all below the threshold. The maximum chloride concentration obtained at 3.5 inches was 0.64 lbs./yd^3, which is approximately half of the chloride threshold.

The four composite dust samples obtained at site MRM 87 were also tested for chlorine using the ICP-MS method. The results are shown in Table 6-2. The detection limits of the ICP-MS procedure did not allow for the production of vertical chloride profiles. Only the chloride ion concentrations within the first one inch of the samples were high enough to be detected by the ICP-MS.

Table 6-2: Chloride content at MRM 87 determined by the ICP-MS method

Sample	Chloride Concentration of Top One Inch (lbs/yd^3)
MRM 87 Dust 1	14.53
MRM 87 Dust 2	10.50
MRM 87 Dust 3	11.30
MRM 87 Dust 4	7.67

One core sample from each of the Sioux Falls sites was also tested for chloride distribution away from the crack location at one inch depth increments and half inch lateral increments. This data is presented in Table 6-3 and Figure 6-3 through Figure 6-7. Note that chloride data for a depth of 4.5 inches is only available for MRM 68 because the reinforcement in the other two sites had cover depths that did not exceed 4 inches, whereas the cover depth at MRM 68 was 5.5 inches. All of the individual horizontal chloride profiles are also presented in Appendix C.

Table 6-3: Chloride ion concentration from core samples at Sioux Falls sites (lbs./yd^3)

	Depth of Core Slice	Distance Away from the Crack (inches)						
		0.00	***0.50***	***1.00***	***1.50***	***2.00***	***2.25***	***2.50***
MRM 87	0.5	16.2	15.1	12.1	10.72		9.49	
	1.5	8.12	4.11	0.92	0.25		0.3	
	2.5	5.24	2.63	0.46	0.35		0.24	
	3.5	7.26	5.11	2.7	0.78	0.74	0.715	0.69
MRM 68	0.5	12.86	11.58	16.74	12.07			
	1.5	7.18	3	0.88	0.71			
	2.5	5.29	3.05	0.79	0.34			
	3.5	5.65	2.71	0.35				
	4.5	5.58	4.11	1.8	0.54			
MRM 411	0.5	20.88	13.11	9.41				
	1.5	3.05	0.98	0.32				
	2.5	2.33	1.18	0.61				
	3.5	3.44	1.97					

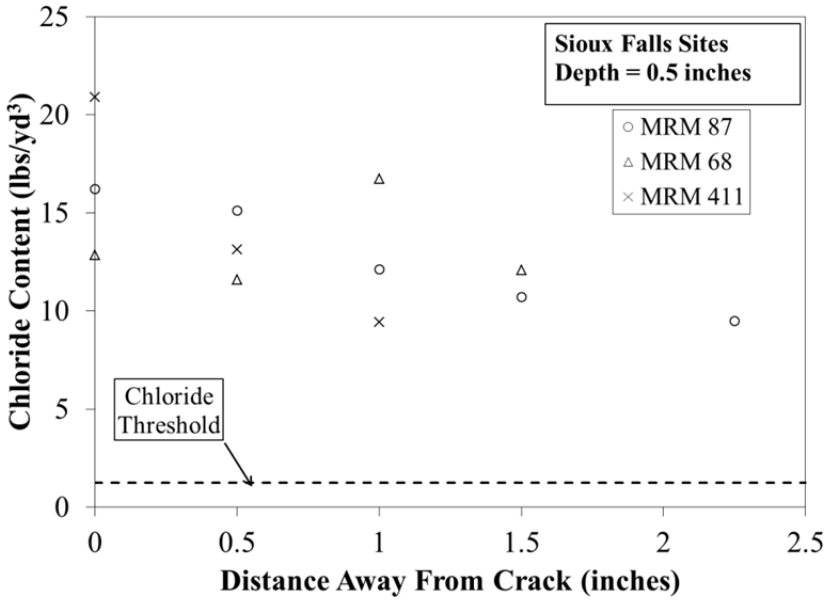

Figure 6-3: Lateral chloride concentration of core samples, depth of 0.5 inch, Sioux Falls sites

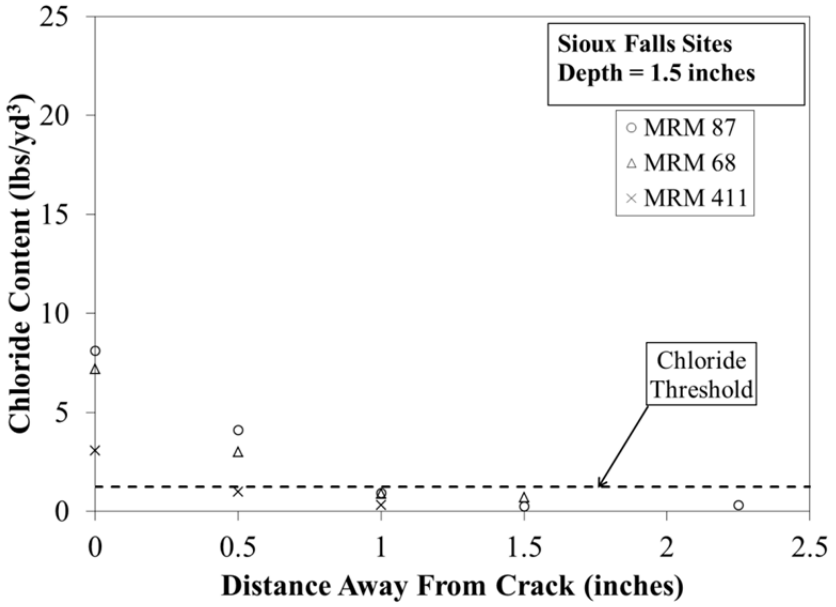

Figure 6-4: Lateral chloride concentration of core samples, depth of 1.5 inches, Sioux Falls sites

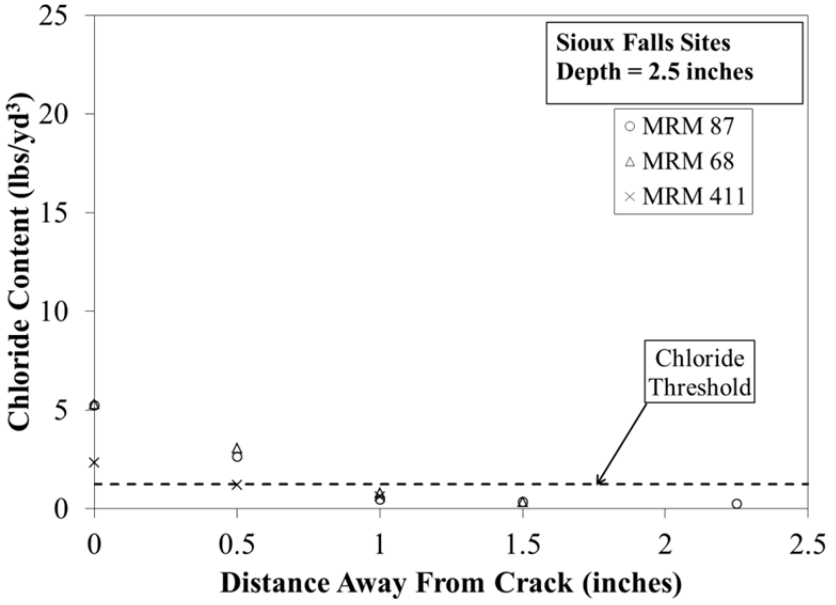

Figure 6-5: Lateral chloride concentration of core samples, depth of 2.5 inches, Sioux Falls sites

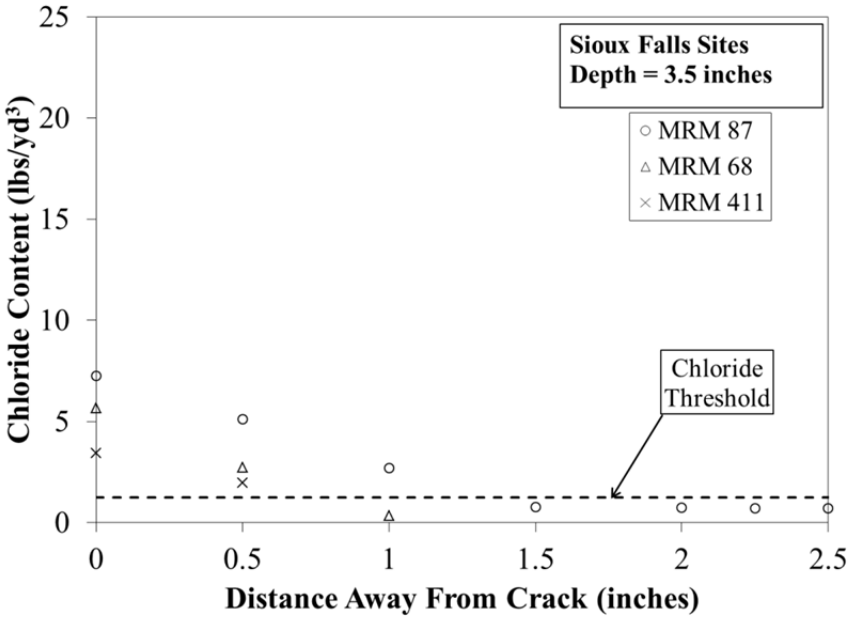

Figure 6-6: Lateral chloride concentration of core samples, depth of 3.5 inches, Sioux Falls sites

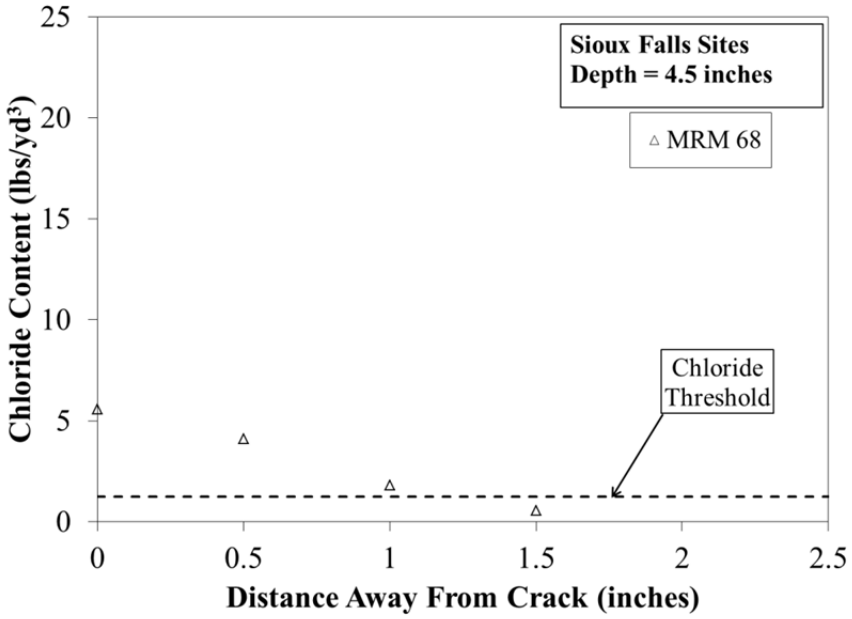

Figure 6-7: Lateral chloride concentration of core samples, depth of 4.5 inches, Sioux Falls sites

The data presented in the previous figures shows that the chloride concentrations are above the threshold within the top vertical inch of the pavement. Also, chloride concentrations are above the threshold within the first lateral half inch of a crack location. This is true even at depths of 3.5 and 4.5 inches.

Figure 6-8 presents the cumulative frequency distribution for half-cell potential at this site and Table 6-4 presents a summary of the data points that fall within ranges of the corrosion probabilities suggested in ASTM C876-09.

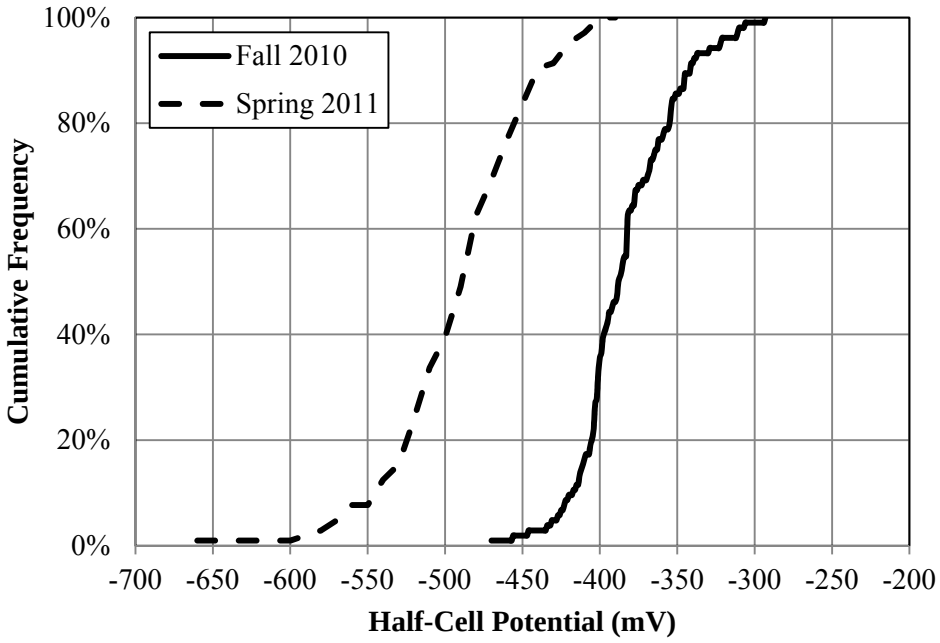

Figure 6-8: MRM 87 half-cell cumulative frequency distribution

Table 6-4: ASTM indication of half-cell measurements at MRM 87

Potential Measurement Range	Indication	Percent of Data Points in Range	
		Fall 2010	***Spring 2011***
> -200 mV	90% probability that no reinforcing steel is corroding	0.0%	0.0%
Between -200 mV and -350 mV	Corrosion activity is uncertain	14.4%	0.0%
< -350 mV	Greater than 90% probability steel is corroding	85.6%	100.0%

Equipotential contour maps were constructed using the half-cell data. The equipotential contour map for the spring measurements at MRM 87 is presented in Figure 6-9 along with its corresponding legend. Equipotential contour maps of both sets of half-cell potential measurements are presented in Appendix B.

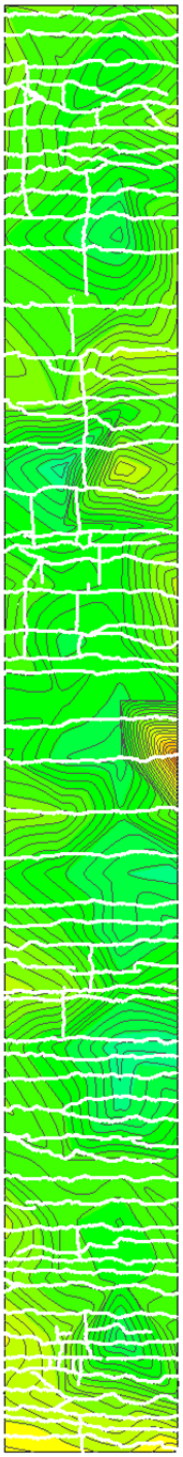

Minimum Reading (mV)	Maximum Reading (mV)	Color
−750.00	−720.00	
−720.00	−690.00	
−690.00	−660.00	
−660.00	−630.00	
−630.00	−600.00	
−600.00	−570.00	
−570.00	−540.00	
−540.00	−510.00	
−510.00	−480.00	
−480.00	−450.00	
−450.00	−420.00	
−420.00	−390.00	
−390.00	−360.00	
−360.00	−330.00	
−330.00	−300.00	
−300.00	−270.00	
−270.00	−240.00	
−240.00	−210.00	
−210.00	−180.00	
−180.00	−150.00	

Figure 6-9: MRM 87 equipotential contour map

The steel reinforcement of one of the cracked concrete core samples from site MRM 87 was analyzed using SEM. The core selected was core label MRM 87-3. The concrete cover to the reinforcement was 3.25 inches. The core had a vertical crack that was approximately 0.020 inches wide. After polishing the reinforcement, there was a thin layer of rust or possible corrosion observed on the outer edge of the rebar

using the optical microscope. This is shown in Figure 6-10. Figure 6-11 shows a secondary electron image of the possible corrosion zone.

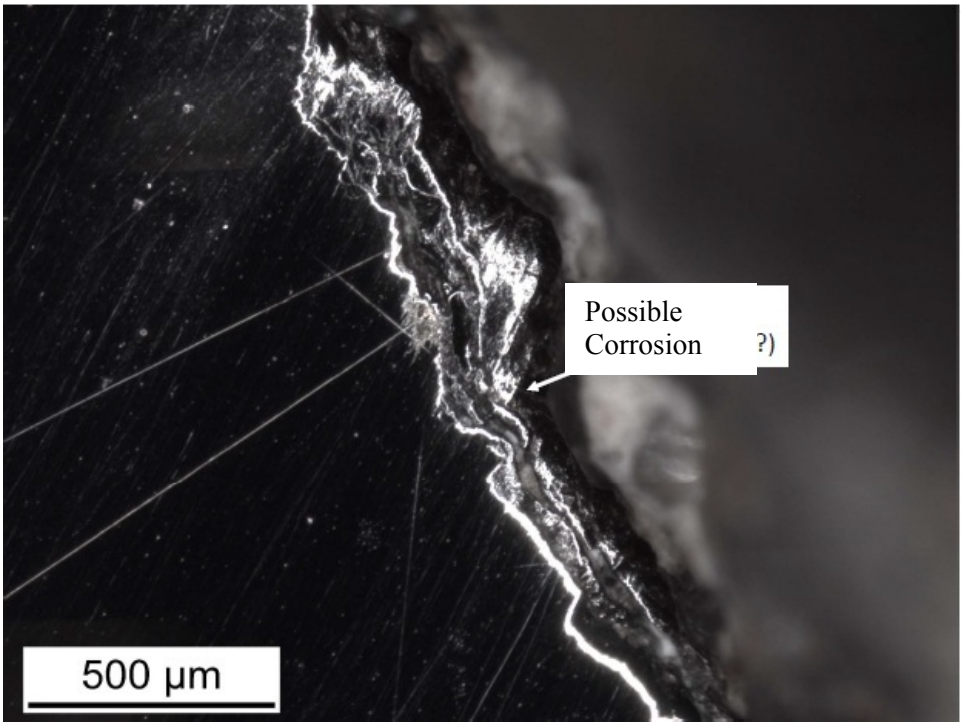

Figure 6-10: Thin layer of rust or possible corrosion

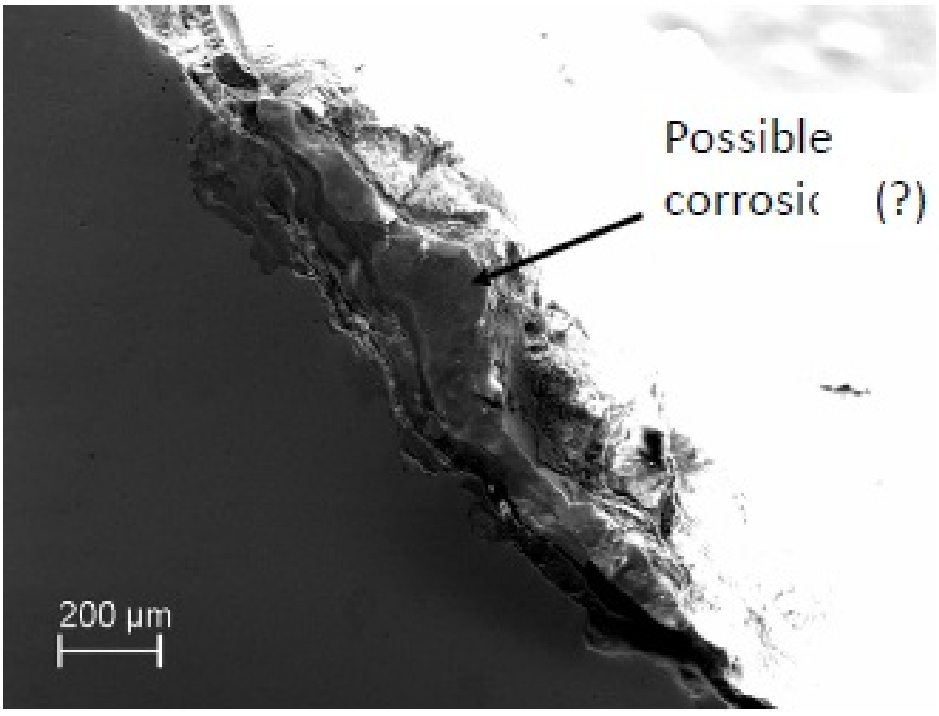

Figure 6-11: Secondary electron image of possible corrosion zone

Further examination of the SEM results showed that the layer consisted of iron oxides, silicon, calcium, aluminum, and manganese. Chlorine was generally low or absent. This led to the conclusion that the layer was probably an external layer of rust, and that the reinforcement was most likely not corroding. Also, since chlorine levels were low or absent, it is unlikely that deicers had any corrosive effects on the reinforcement at this location. In addition to the layer of rust, a thin layer of oxidized composition was detected around the entire perimeter of the bar cross-section. Based on this observation, it is not believed that this leads to corrosion.

The reinforcement in an uncracked concrete core from site MRM 87 was also analyzed to determine if corrosion was present in the reinforcement away from pavement cracks. The core was labeled MRM 87-4. A photograph of the polished section of reinforcement from this core is shown in Figure 6-12. The photograph shows that there are no signs of corrosion in the reinforcement. As with cracked core MRM 87-3, the intact core exhibited a thin oxidized layer around the entire perimeter of the steel bar. This layer was analyzed using SEM, and the results showed no signs of chlorine or corrosion. Figure 6-13 shows the energy dispersive spectrum of the sample. Only iron peaks are present.

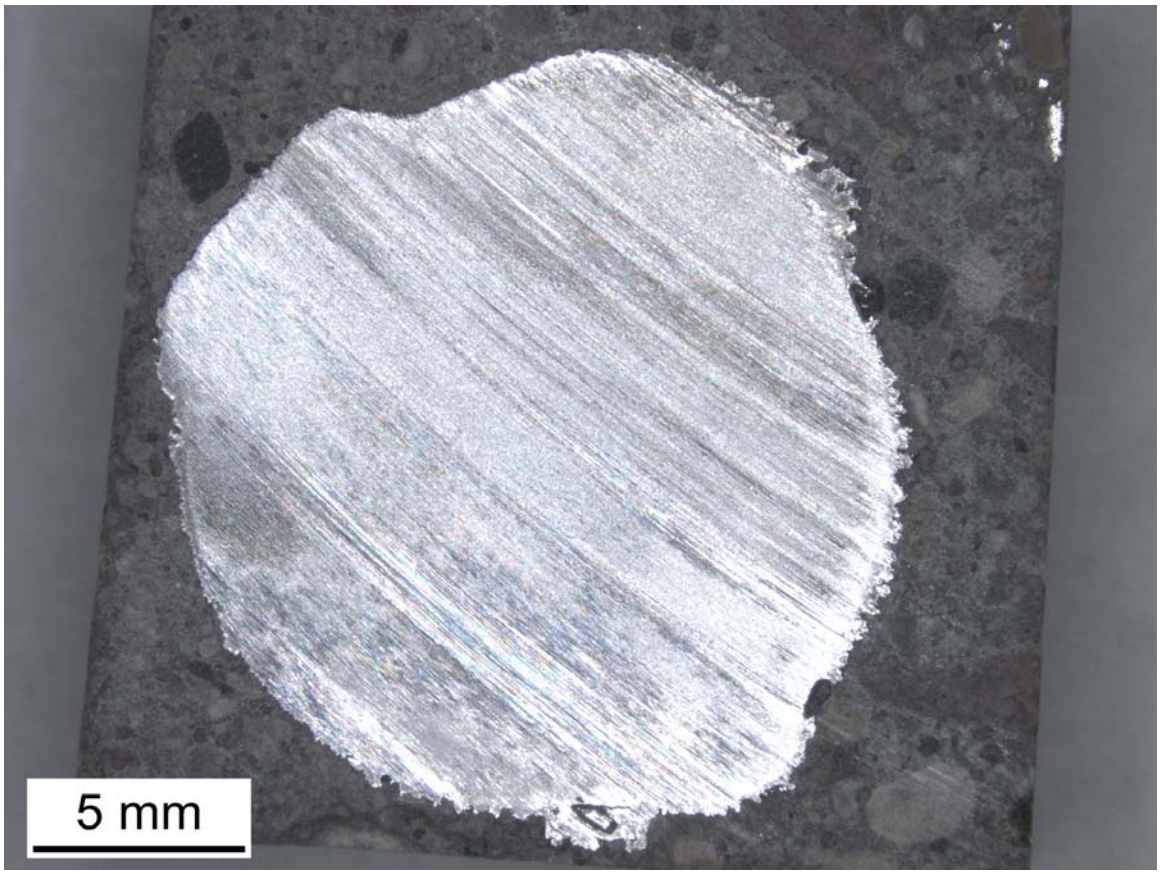

Figure 6-12: Steel bar section from core MRM 87-4 (uncracked concrete core)

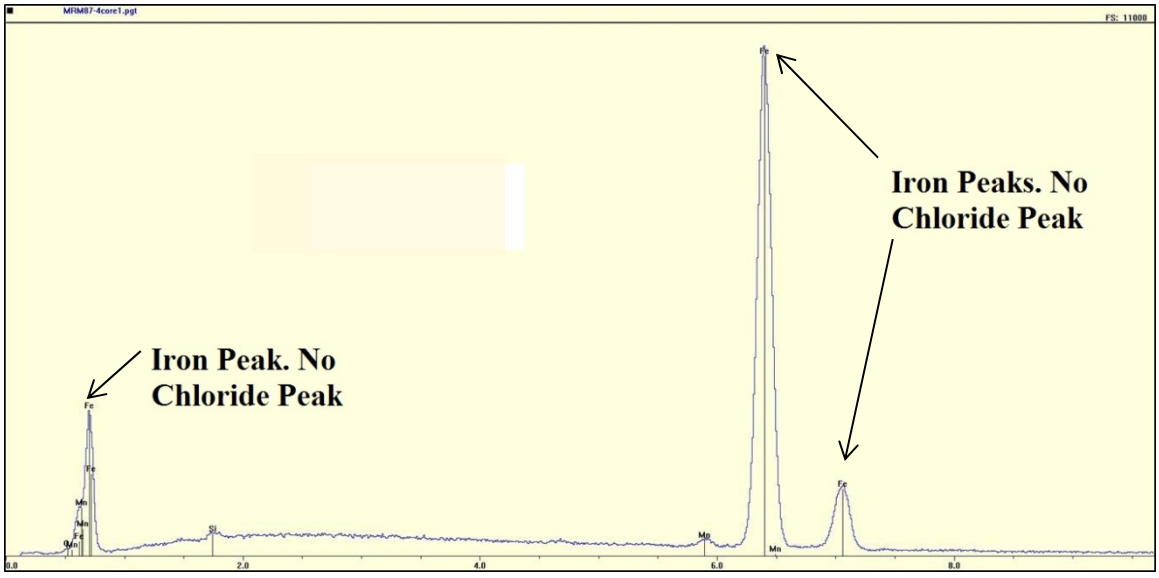

Figure 6-13: Energy dispersive spectrum of reinforcement sample - no chlorine present

6.1.2 SITE I-29N, SOUTH OF SIOUX FALLS AT MRM 68

Crack mapping, dust sampling, and core sampling was completed for site MRM 68 on September 30, 2010. The first set of half-cell potential measurements was recorded on October 12, 2010. A second set of half-cell potential measurements was obtained on June 14, 2011 in order to determine the effect of one winter maintenance cycle on the half-cell measurements. Transverse cracking and Y-cracking were observed at this site. Cracks averaged 0.014 inches in width with minimum and maximum widths of approximately 0.010 inches and 0.023 inches, respectively. The crack density was 0.331 foot/square foot. Generally, the transverse cracks were spaced 2 to 5 feet apart.

Four cores were removed from the pavement at this site. Three of the cores were removed at a crack location with widths of 0.012 inches, 0.039 inches, and 0.079 inches. The average depth to the center of the reinforcement at this site varied from 5.375 to 5.625 inches, which is deeper than the other two sites. Four composite dust samples were also obtained at this site. The cores and the dust samples were submitted to the EMES at SDSM&T for SEM and chloride ion analyses. Chloride concentrations from the dust samples were determined using the potentiometric method. The data from these tests are presented in Table 6-1 and Figure 6-2. The individual vertical chloride profiles are shown in Appendix C.

Two of the four composite dust samples obtained at site MRM 68 were also tested for chlorine using the ICP-MS method. The results are shown in Table 6-5. The detection limits of the ICP-MS procedure did not allow for the production of vertical chloride profiles. Only the chloride ion concentrations within the first one inch of the samples were high enough to be detected by the ICP-MS.

Table 6-5: Chloride content at MRM 68 determined by ICP-MS method

Sample	Chloride Concentration of Top One Inch (lbs/yd^3)
MRM 68 Dust 1	10.90
MRM 68 Dust 2	11.88

One core sample, core MRM 68-3, was also tested for chloride distribution away from the crack location at one inch depth increments and half inch lateral increments. The data from these analyses is presented

in Table 6-3 and Figure 6-3 through Figure 6-7. The individual lateral chloride profiles for this site are presented in Appendix C.

Figure 6-14 presents the cumulative frequency distribution for half-cell potential at this site and Table 6-6 presents a summary of the data points that fall within certain ranges of corrosion probability. The figure and the table show that all of the measurements obtained at this site indicate high probability of corrosion according to ASTM C876. Equipotential contour maps of both sets of half-cell potential measurements are presented in Appendix B.

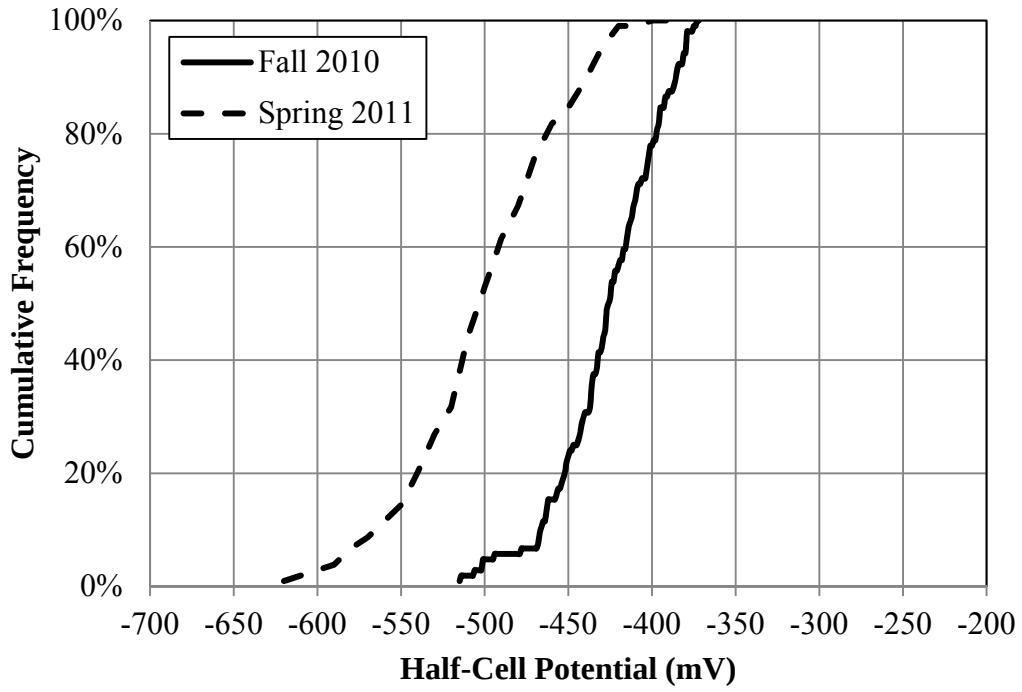

Figure 6-14: MRM 68 half-cell cumulative frequency distributions

Table 6-6: Indication of half-cell measurements at MRM 68 in fall 2010

Potential Measurement Range	Indication	Percent of Data Points in Range	
		Fall 2010	***Spring 2011***
> -200 mV	90% probability that no reinforcing steel is corroding	0.0%	0.0%
Between -200 mV and -350 mV	Corrosion activity is uncertain	0.0%	0.0%
< -350 mV	Greater than 90% probability steel is corroding	100.0%	100.0%

The steel reinforcement of one of the concrete core samples from this site was analyzed using SEM. The core selected was MRM 68-3. The concrete cover to the reinforcement was 5.25 inches. The core had a main vertical crack that was approximately 0.037 inches wide. Other minor cracks were observed that intersected the main crack. The main crack intersected the reinforcement in core MRM 68-3. However, corrosion was not evident (see Figure 6-15). After polishing the reinforcement and examining it with the

SEM, a thin oxidized layer (30-50 µm) was detected, consistent with that which was observed in core MRM 87-3. A backscattered electron image of a portion of the reinforcement is shown in Figure 6-16. There did not appear to be corrosion, even though there was local delamination evident along the reinforcement which could potentially allow the intrusion of chlorides.

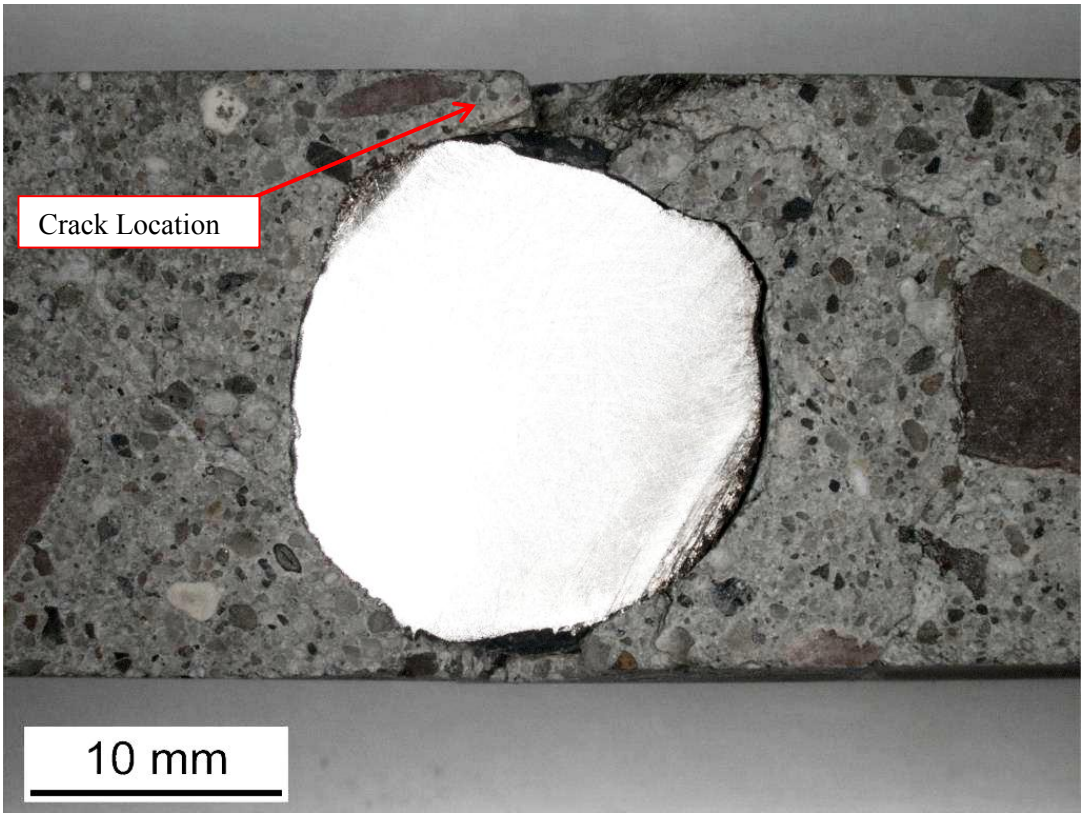

Figure 6-15: Main crack intersecting reinforcement

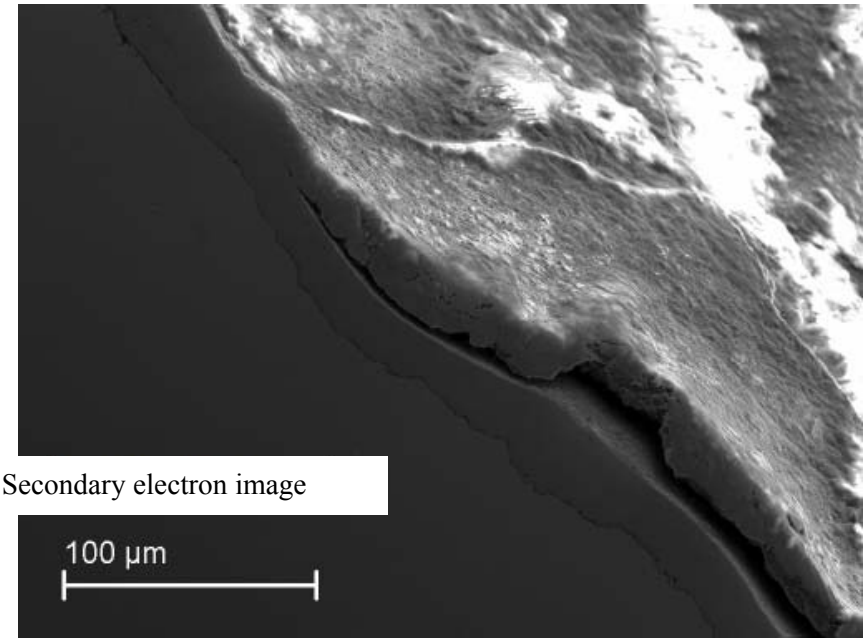

Figure 6-16: Local delamination along reinforcement

6.1.3 SITE I-90W, EAST OF SIOUX FALLS AT MRM 411

Crack mapping, dust sampling, core sampling, and half-cell potential measurements were completed at site MRM 411 on October 14, 2010. Follow-up half-cell potential measurements were obtained on November 3, 2010 for the purpose of validating the repeatability of measurements. A final set of half-cell potential measurements was obtained on June 14, 2011 to determine the effect of one winter maintenance on the half-cell potential measurements. Transverse cracks, longitudinal cracks, and Y-cracking were observed. Cracks at this site averaged 0.009 inches in width with minimum and maximum widths of 0.004 inches and 0.020 inches, respectively. The crack density was 0.814 foot/square foot. Transverse cracks were generally spaced 2 feet apart or less.

A total of four core samples were removed from the pavement section at site MRM 411. Three of the cores were removed at a crack location with widths of 0.033 inches, 0.024 inches, and 0.008 inches. The average depth to the center of reinforcement in the pavement section varied from 3.75 to 4.0 inches. Four dust samples were also obtained at this site. The cores and the dust samples were submitted to the EMES at SDSM&T for SEM and chloride ion analyses. The dust samples were tested for chloride using the alternative potentiometric method. The chloride profiles from the dust samples collected at MRM 411 are shown in Appendix C.

The four composite dust samples obtained at site MRM 411 were also tested for chlorine using the ICP-MS method. The results are shown in Table 6-7. Once again, the detection limits of the ICP-MS procedure did not allow for the production of vertical chloride profiles. Only the chloride ion concentrations within the first one inch of the samples were high enough to be detected by the ICP-MS.

Table 6-7: Chloride content at MRM 411 determined by the ICP-MS method

Sample	Chloride Concentration of Top One Inch (lbs/yd^3)
MRM 411 Dust 1	7.67
MRM 411 Dust 2	5.25
MRM 411 Dust 3	5.42
MRM 411 Dust 4	5.85

One core sample, core MRM 411-1, was also tested for chloride distribution away from the crack location at one inch depth increments and half inch lateral increments. These chloride profiles are also presented in Appendix C.

The initial and follow-up half-cell potential measurements obtained on October 14 and November 3, 2010, respectively, were compared to determine if there was a drift in the measurements. In general, the half-cell follow-up measurements were more negative than, but within 10 percent of, the initial measurements. The distributions from the two sets of measurements are presented in Figure 6-17.

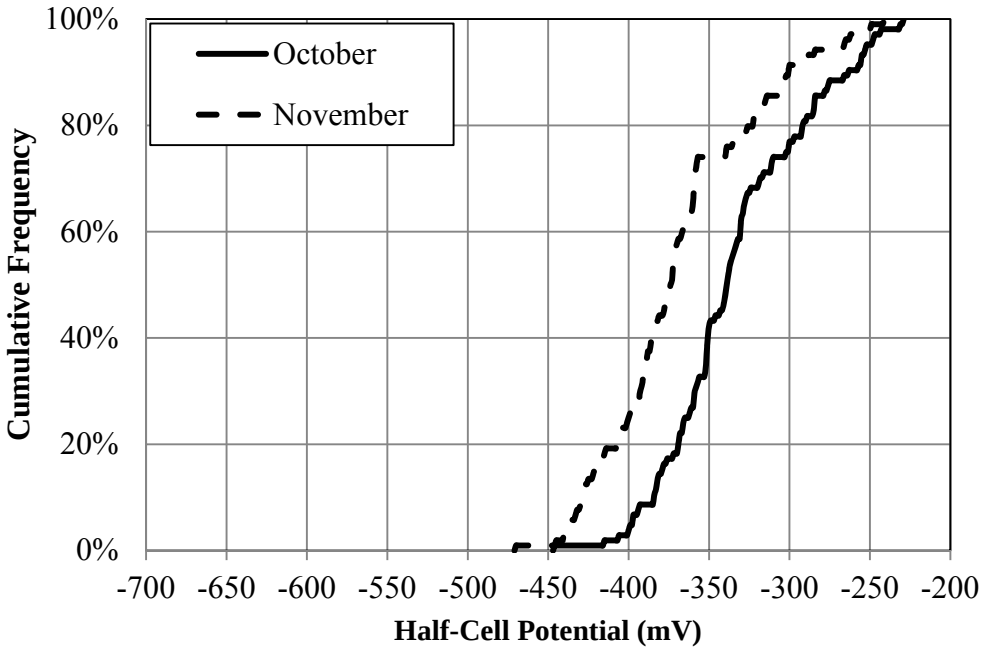

Figure 6-17: MRM 411 Half-cell potential cumulative frequency distribution during fall 2010

Figure 6-18 presents the cumulative frequency distribution for half-cell potential before and after one winter maintenance cycle. Table 6-8 presents a summary of the data points that fall within certain ranges of corrosion probability. Equipotential contour maps of both sets of half-cell potential measurements are presented in Appendix B.

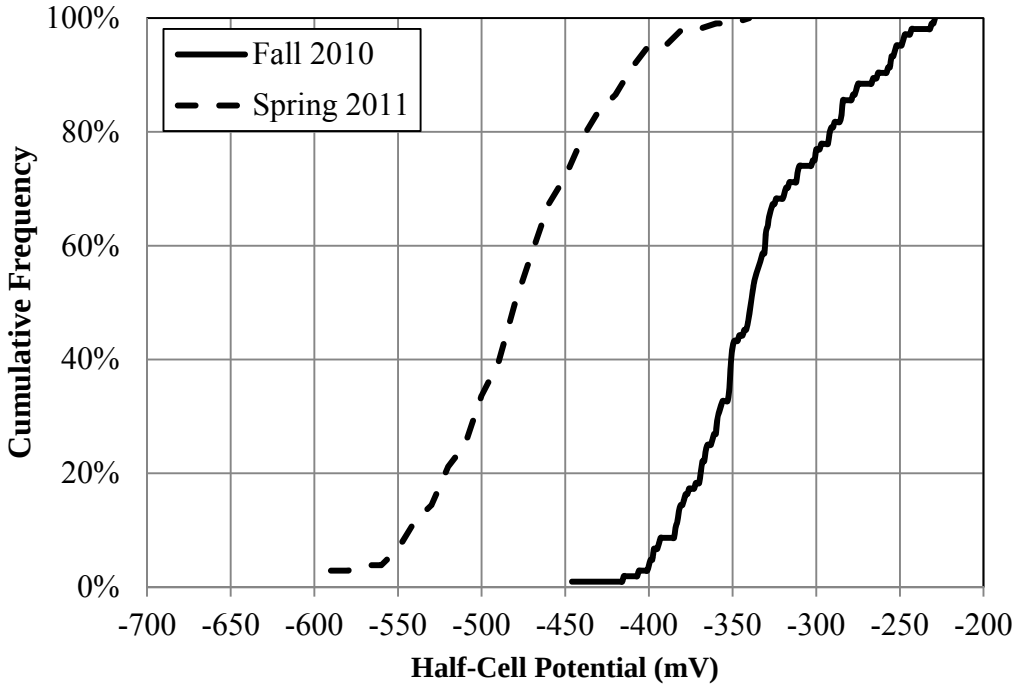

Figure 6-18: MRM 411 half-cell potential cumulative frequency distribution

Table 6-8: ASTM indication of half-cell measurements at MRM 411

Potential Measurement Range	Indication according to ASTM C-876	Percent of Data Points in Range	
		Fall 2010	*Spring 2011*
> -200 mV	90% probability that no reinforcing steel is corroding	0.0%	0.0%
Between -200 mV and -350 mV	Corrosion activity is uncertain	60.6%	1.9%
< -350 mV	Greater than 90% probability steel is corroding	39.4%	98.1%

The steel reinforcement of one of the concrete core samples from site MRM 411 was analyzed using SEM. The core selected was MRM 411-1. The concrete cover placed above the reinforcement was 3.5 inches, and a crack of width 0.012 inches was observed on the core. Figure 6-19 shows a core slice through the steel bar. It was observed that the steel bar intercepted several concrete cracks. Corrosion was detected at three locations around the bar perimeter. The corroded spots coincided with the locations of the cracks. The loss of cross-sectional area of the polished section of reinforcement due to corrosion was determined to be approximately 0.026in^2, or 6.0%.

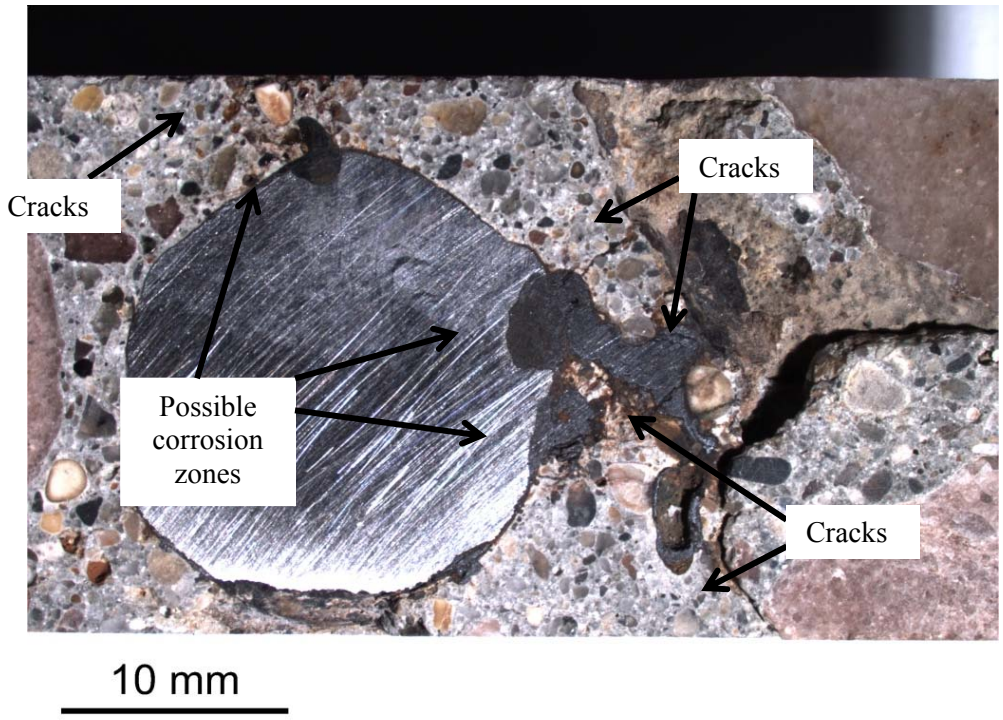

Figure 6-19: Corrosion at crack locations

The corroded area towards the top of Figure 6-19 was determined to be either minimal corrosion or surficial rusting based on energy dispersive analysis. There were also other areas along the exterior of the steel bar that were found to exhibit surficial rusting but not corrosion. Elemental mapping showed that the area on the right side of the reinforcement was corroded and the surrounding concrete contained

chlorine. Figure 6-20 shows an enlarged view of the corroded area and Figure 6-21 shows the elemental maps that correspond to the corroded area.

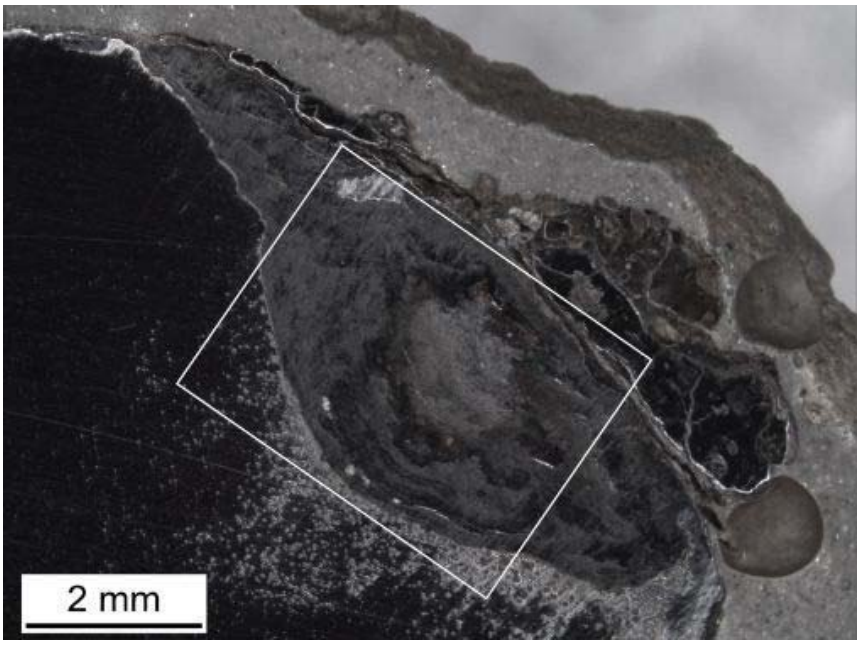

Figure 6-20: Corroded area enlarged

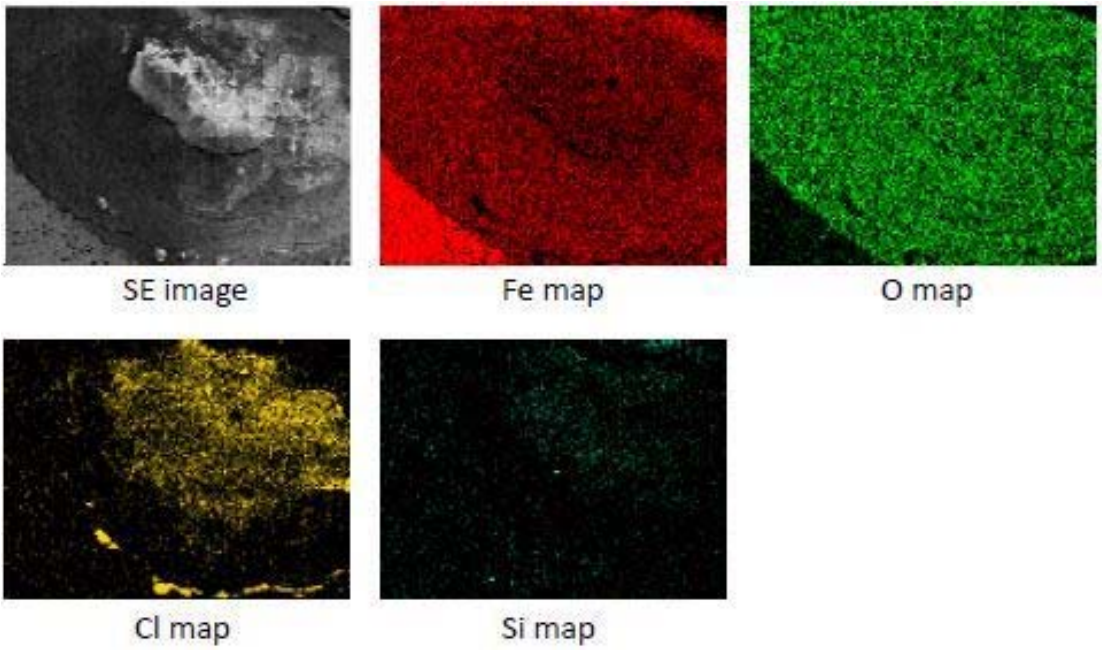

Figure 6-21: Elemental maps of corroded area (scanning electron microscope image, iron map, oxygen map, chlorine map, and silicon map)

6.1.4 INTERSTATE 29 NEAR BROOKINGS

The CRCP at this site was inspected by the researchers before it was removed as part of a 2010 Interstate 29 reconstruction project. General observation (notes and photographs) and crack mapping were

completed on July 1, 2010. Visual inspection revealed that several sections of pavement had been previously patched at this site. Most of these patches were filled with asphalt, while some were filled with concrete. The reinforcement steel in some of the patched locations showed signs of corrosion, as shown in Figure 6-22. It was uncertain if the corrosion in patched sections similar to that shown in Figure 6-22 was due to deicing salts, open exposure to precipitation, or a combination of both. However, within a patch, localized corrosion resulting in a noticeably reduced cross-sectional area of reinforcement was present, which could indicate that deicing salts or water intrusion played a role in the corrosion process. Localized corrosion was also observed on steel reinforcement from CRCP that had already been demolished by the time the research team had arrived at the site as shown in Figure 6-23.

Figure 6-22: Patched pavement with exposed reinforcing steel

Figure 6-23: Localized corrosion found in the concrete rubble that was eventually removed

Prior to inspection, ground penetrating radar was used to locate the longitudinal and transverse reinforcement bars embedded in the intact pavement. The ground penetrating radar instrument was provided and operated by SDDOT personnel. Transverse cracking was observed to have occurred directly above the transverse reinforcement bars throughout the site. The measured depth of the concrete cover over the reinforcing steel was inconsistent and ranged from less than 3 inches to 4 inches. Also, it was noted that some locations with a considerable amount of spalling did not show visible signs of corrosion. An example of one such location is presented in Figure 6-24. This indicates that corrosion may not necessarily have caused this type of pavement distress.

Figure 6-24: Spalled area with no signs of corrosion

The research team observed a longitudinal reinforcing bar that was severely corroded throughout its length as shown in Figure 6-25. This bar had been placed below the longitudinal center joint in the pavement section.

Figure 6-25: Corroded longitudinal reinforcing bar

Four pavement sections were randomly selected for crack mapping. Three of the sections were 24 foot long by 24 foot wide each, while the fourth section was 72 foot long by 24 foot wide. The short sections provided snapshots of the pavement condition at random locations, while the long section allowed for identification of repetitive distress patterns in the pavement. The results of the crack surveys are summarized in Table 6-9. The average crack width of each of the surveys was determined by taking the average of all cracks measured within the section. The average crack density and crack width of the four surveys was 0.605 foot/square foot and 0.030 inches, respectively. Random location 1 had the highest crack density, which was 23.5 percent greater than the average crack density. The crack density at random location 4 was 41.2 percent lower than the average crack density. The average crack widths for all of the sections surveyed were within 12 percent of the average.

Table 6-9: Summary of crack mapping results of I-29 south of Brookings

Survey	Location	Crack Density (ft/ft^2)	Average Crack Width (inches)
Random Location 1	964 feet north of mile marker 120	0.766	0.68
Random Location 2	Mile marker 119+00	0.702	0.83
Random Location 3	North of exit 114	0.553	0.71
Random Location 4 (longer section)	Mile marker 114	0.398	0.84

6.1.5 INTERSTATE 90 REPAIRS

The inspection of the CRCP repair sites and the surrounding intact pavement on Interstate 90 was performed and documented in the summer of 2010. The concrete surface of the existing pavement

showed several signs of distress, including longitudinal cracking, transverse cracking, and spalling. Figure 6-26 shows transverse cracking and spalling close to a newly repaired section of CRCP. Figure 6-27 shows a wide longitudinal crack next to the longitudinal joint in the pavement.

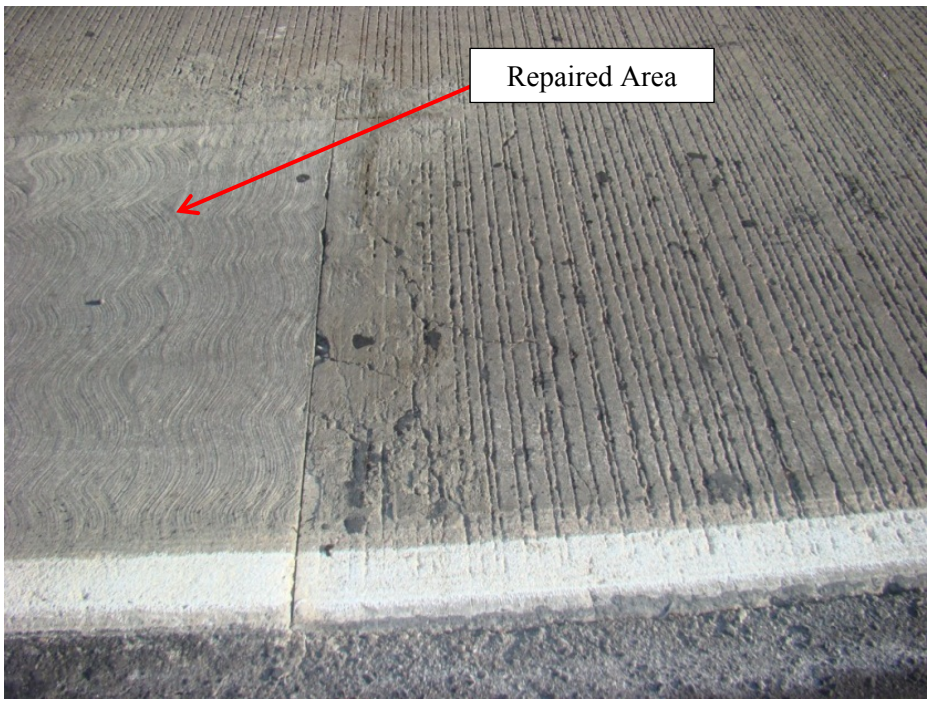

Figure 6-26: Spalling and transverse cracking close to a repaired section

Figure 6-27: Longitudinal cracking on I-90

In addition to the surface distress, noticeable loss of cross-section in the steel reinforcement was present at several locations within the sections that were cut for repair. At some locations, nearly half of the

cross-section had deteriorated as shown in Figure 6-28. Furthermore, most of the corrosion occurred at the intersections of the longitudinal bars with the transverse cracks. Figure 6-29 shows corrosion marks in exposed longitudinal bars. The red marks at the edge of the concrete cut in the photo represent crack locations. The corrosion marks in the successive bars can be seen to have occurred along the crack.

Figure 6-28: Severe loss of cross-sectional area

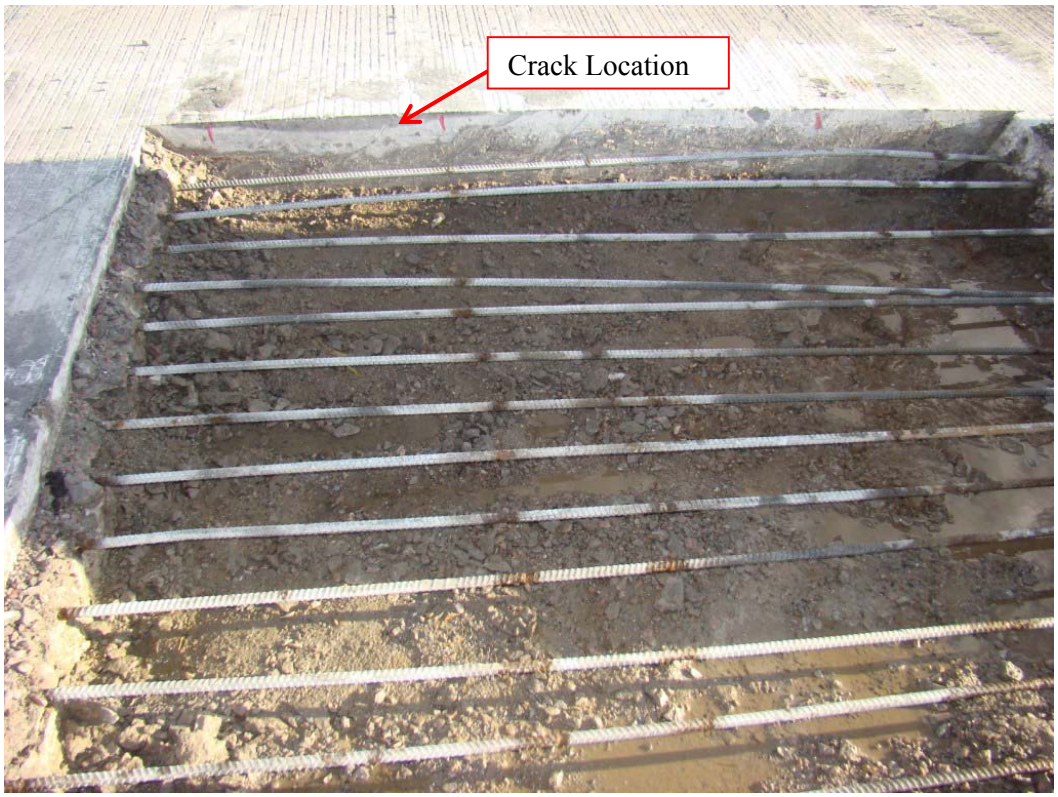

Figure 6-29: Corrosion at transverse crack location

6.2 STATEWIDE CRCP EVALUATION

The statewide CRCP evaluation consisted of obtaining general observations, half-cell measurements, crack mapping (excluding crack width measurements), and dust samples for the purpose of chloride ion analysis at eight sites throughout the state of South Dakota. The results obtained during the evaluation are discussed in this section.

6.2.1 SITE I-29S, SOUTH OF BERESFORD AT MRM 33

Evaluation of site MRM 33 occurred on July 21st, 2011. The crack density of the 100 foot section was determined to be 0.670 foot/square foot. Transverse and Y-cracking was observed. The transverse cracks were spaced at one to four feet. No longitudinal cracking was identified within the 100 foot section. The depth to the reinforcement was measured as 3.5 inches with a hand-held tape measure.

The results of the half-cell measurements were between a minimum of -525 mV and a maximum of -302 MV, with an average of -356 mV and standard deviation of 46.5 mV. The distribution of the half-cell measurements is presented in Figure 6-30. The equipotential contour maps are presented in Appendix B. The probability of corrosion activity based on the measured data, as suggested by ASTM C876, is presented in Table 6-10.

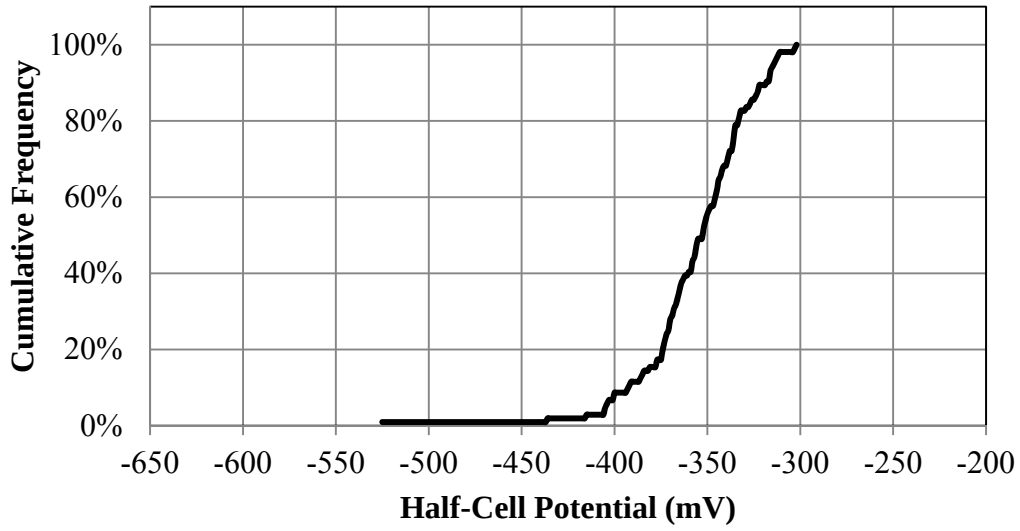

Figure 6-30: MRM 33 half-cell cumulative frequency distribution

Table 6-10: Indication of half-cell measurements at MRM 33

Potential Measurement Range	Indication according to ASTM C-876	Percent of Data Points in Range
> -200 mV	90% probability that no reinforcing steel is corroding	0.0%
Between -200 mV and -350 mV	Corrosion activity is uncertain	46.2%
< -350 mV	Greater than 90% probability steel is corroding	53.8%

Dust samples were obtained at the locations with the most elevated (most negative) measurements, unless the traffic on the passing lane imposed a safety concern for collecting a dust sample. The location of dust samples one and two had half-cell measurements of -436 mV and -525 mV, respectively. Cracks were observed within inches of both dust samples as shown in Figure 6-31.

Figure 6-31: Dust sample 2 at MRM 33

The results from the chloride analysis of the dust samples for all sites evaluated during the statewide CRCP evaluation are presented in Table 6-11 and Figure 6-32. The data shows that the chloride values are generally above the threshold within the top 1 inch of the pavement surface. The chloride levels are generally below the threshold at depths below 1 inch in the pavement. However, there are some cases in which the chloride ion concentration is above the threshold at a pavement depth of 3.75 inches. The reason for this will be discussed in Chapter 5. Individual vertical chloride profiles from this site are presented Appendix C.

Table 6-11: Chloride ion results from dust samples obtained during statewide CRCP evaluation

		Sample Depth (inches)							
Site	**Sample**	***0.25***	***0.75***	***1.25***	***1.75***	***2.25***	***2.75***	***3.25***	***3.75***
MRM 25	1	22.2	8.53	1.2	0.86	0.71	0.71	0.89	1.01
	2	22.33	3.94	0.91	0.61	0.54	0.54	0.99	0.91
MRM 33	1	10.91	2.43	0.52	0.34	0.39	0.27	0.29	0.37
	2	8.01	0.37	0.22	0.39	0.29	0.2	0.34	0.35
MRM 44	1	12.39	0.83	0.24	0.29	0.15	0.15	0.39	0.22
	2	14.61	2.9	0.37	0.24	0.22	0.22	0.32	0.39
MRM 54	1	13.23	1.53	0.39	0.44	0.46	0.47	0.49	0.52
	2	11.5	1.38	0.83	0.62	0.62	0.66	0.47	0.67
MRM 168NB	1	11.21	8.33	0.49	0.3	0.22	0.27	0.29	0.22
	2	9.64	0.88	0.49	0.27	0.37	0.72	1.01	1.15
MRM 168SB	1	12	1.33	0.32	0.51	0.29	0.54	0.34	0.34
	2	10.91	2.55	0.32	0.22	0.2	0.19	0.17	0.32
MRM 246	1	11.98	4.57	2.76	2.28	2.14	2.04	1.74	1.89
	2	6.78	3.64	1.2	1.3	1.01	1.53	1.79	1.87
MRM 222	1	11.55	9.98	2.04	0.15	0.12	0.08	0.13	0.05
	2	6.42	3.98	0.27	0.1	0.1	0.17	0.1	0.15
Minimum		6.42	0.37	0.22	0.1	0.1	0.08	0.1	0.05
Maximum		22.33	9.98	2.76	2.28	2.14	2.04	1.79	1.89
Average		12.229	3.573	0.786	0.558	0.489	0.548	0.609	0.652
Standard Deviation		4.4849	2.96	0.718	0.549	0.503	0.535	0.532	0.572

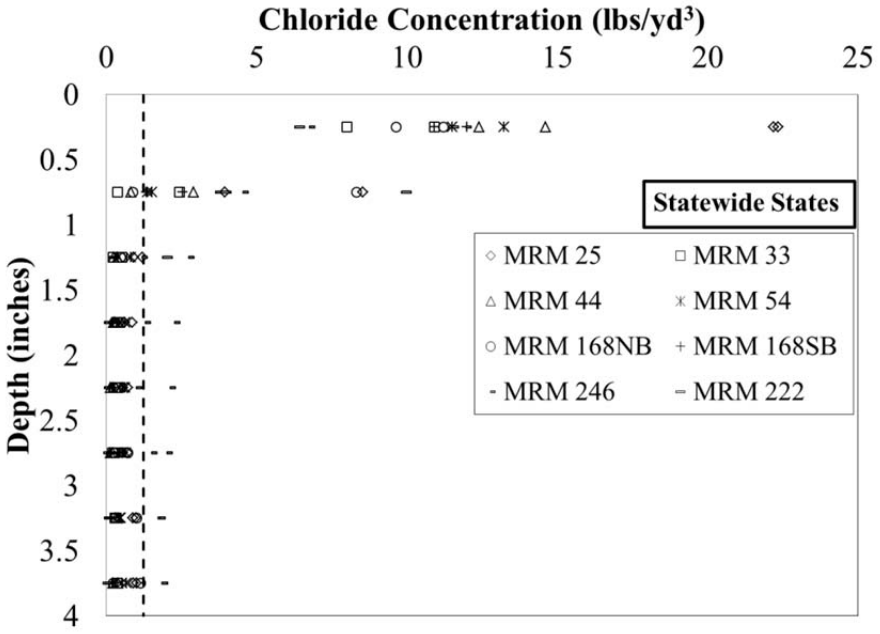

Figure 6-32: Vertical chloride distribution for statewide CRCP evaluation

6.2.2 SITE I-29S, SOUTH OF BERESFORD AT MRM 44

Evaluation of site MRM 44 occurred on July 20th, 2011. The crack density was 0.453 foot/square foot. Transverse, Y-cracking, and pop-outs were observed. The transverse cracks were spaced every one to four feet. No longitudinal cracking was identified within the 100 foot section. Spalling was observed in the passing lane, but not in the lane which was surveyed (see Figure 6-33). The depth to the reinforcement was measured as 3.5 inches with a hand-held tape measure.

Figure 6-33: Spalling observed in passing lane at MRM 44

The results of the half-cell measurements were between a minimum of -572 mV and a maximum of -396 mV, with an average of -481 mV and standard deviation of 63.4 mV. The distribution of the half-cell measurements is presented in Figure 6-34. The equipotential contour maps are presented in Appendix B. The probability of corrosion activity based on the measured data, as suggested by ASTM C876, is presented in Table 6-12.

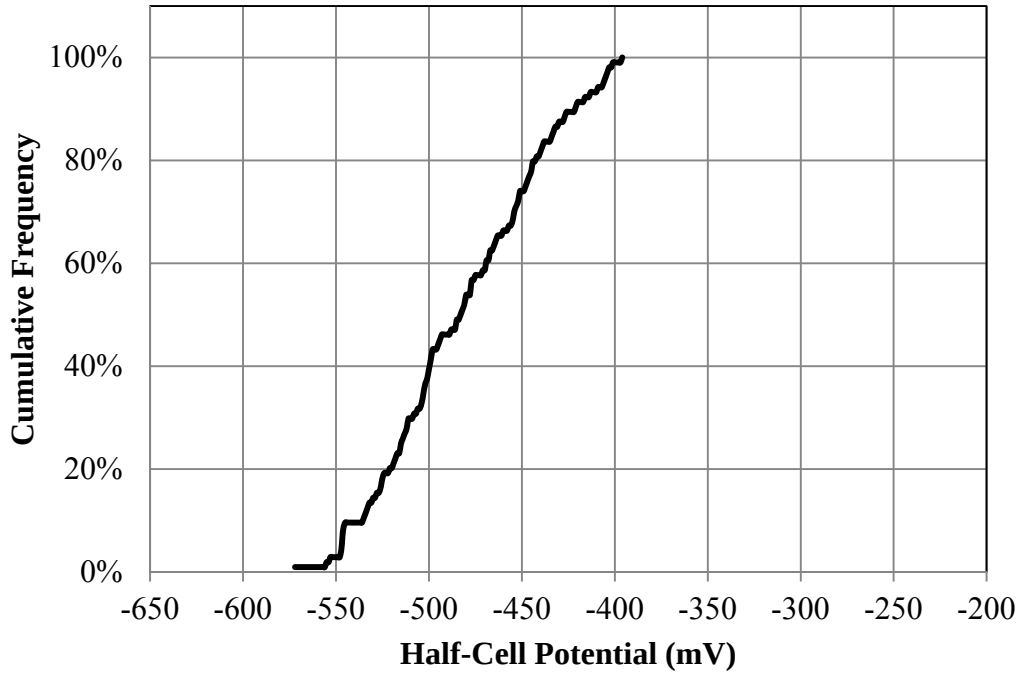

Figure 6-34: MRM 44 half-cell cumulative frequency distribution

Table 6-12: Indication of half-cell measurements at MRM 44

Potential Measurement Range	Indication according to ASTM C-876	Percent of Data Points in Range
> -200 mV	90% probability that no reinforcing steel is corroding	0.0%
Between -200 mV and -350 mV	Corrosion activity is uncertain	0%
< -350 mV	Greater than 90% probability steel is corroding	100%

The location of dust samples one and two had half-cell measurements of -555 mV and -572 mV, respectively. A crack was observed within four inches of both dust sample locations. Results from the chloride testing are presented in Figure 6-32 and Table 6-11. Individual vertical chloride profiles from this site are presented Appendix C.

6.2.3 SITE I-90E, WEST OF RAPID CITY AT MRM 25

Evaluation of site MRM 25 occurred on July 25th, 2011. The crack density for the 100 foot section was determined to be 0.383 foot/square foot. Transverse cracking and Y-cracking was observed. The transverse cracks were spaced approximately every four feet. No longitudinal cracking was identified within the 100 foot section. This site and site Interstate 90E at MRM 54 were constructed using limestone as the coarse aggregate in the mix design. The cracks at this site and MRM 54 were not as wide as those observed at the other sites in the statewide evaluation; however, the pavement surface was smoother due to tire wear. The depth to the reinforcement was measured as 4.125 inches using a hand-held tape measure.

The results of the half-cell measurements were between a minimum of -407 mV and a maximum of -268 mV, with an average of -318 mV and standard deviation of 42.2 mV. The distribution of the half-cell measurements is presented in Figure 6-35. The equipotential contour maps are presented in Appendix B. The probability of corrosion activity based on the measured data, as suggested by ASTM C876, is presented in Table 6-13.

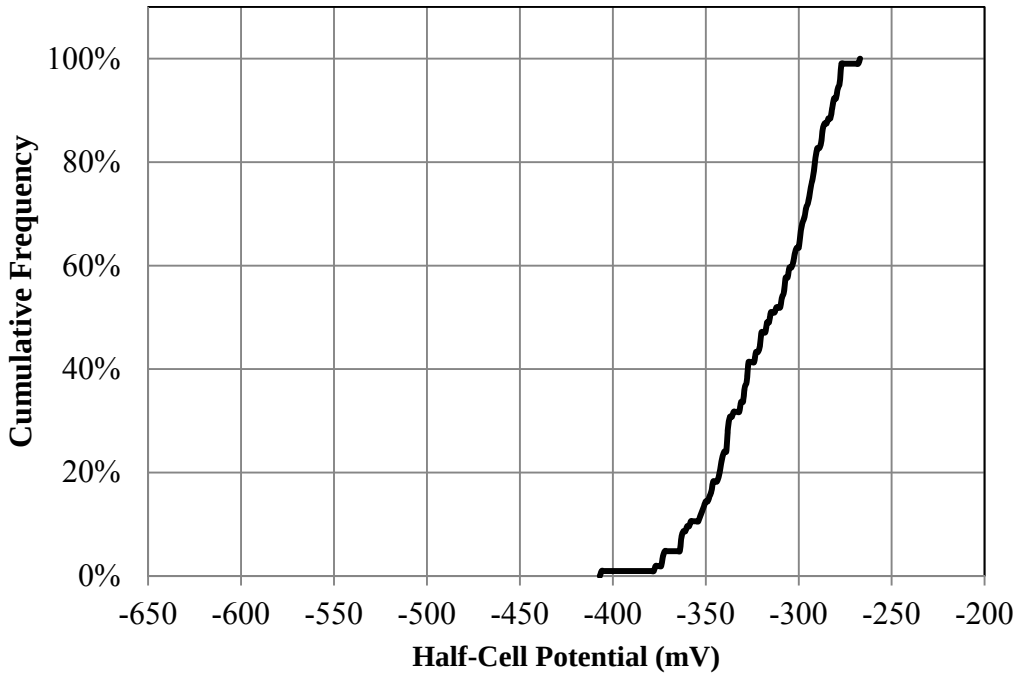

Figure 6-35: MRM 25 half-cell cumulative frequency distribution

Table 6-13: Indication of half-cell measurements at MRM 25

Potential Measurement Range	Indication according to ASTM C-876	Percent of Data Points in Range
> -200 mV	90% probability that no reinforcing steel is corroding	0.0%
Between -200 mV and -350 mV	Corrosion activity is uncertain	85.6%
< -350 mV	Greater than 90% probability steel is corroding	14.4%

The location of dust samples one and two had half-cell measurements of -407 mV and -364 mV, respectively. A crack was observed within three inches of both dust samples. Results from the chloride testing are presented in Figure 6-32 and Table 6-11. Individual vertical chloride profiles from this site are presented Appendix C.

6.2.4 SITE I-90E, WEST OF RAPID CITY AT MRM 54

Evaluation of site MRM 54 occurred on July 26th, 2011. The crack density for this site was 0.244 foot/square foot. Transverse cracking approximately every four feet was observed, with some exceptions.

Some transverse cracks had a wider spacing, up to 10 feet apart. One Y-crack was observed in the entire 100 foot section. No longitudinal cracking was identified within the 100 foot section. The depth to the reinforcement was measured as 4.125 inches with a hand-held tape measure.

The results of the half-cell measurements were between a minimum of -418 mV and a maximum of -221 mV, with an average of -290 mV and standard deviation of 51.5 mV. The distribution of the half-cell measurements is presented in Figure 6-36. The equipotential contour maps are presented in Appendix B. The probability of corrosion activity based on the measured data, as suggested by ASTM C876, is presented in Table 6-14.

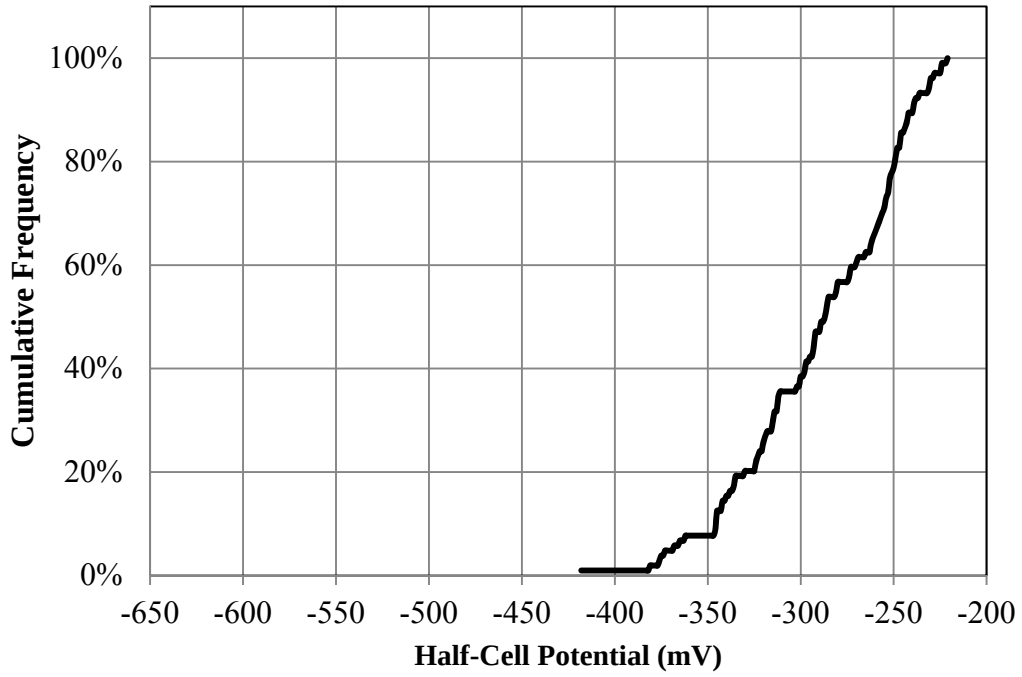

Figure 6-36: MRM 54 half-cell cumulative frequency distribution

Table 6-14: Indication of half-cell measurements at MRM 54

Potential Measurement Range	Indication according to ASTM C-876	Percent of Data Points in Range
> -200 mV	90% probability that no reinforcing steel is corroding	0.0%
Between -200 mV and -350 mV	Corrosion activity is uncertain	92.3%
< -350 mV	Greater than 90% probability steel is corroding	7.7%

The location of dust samples one and two had half-cell measurements of -418 mV and -375 mV, respectively. A crack was observed within six inches of both dust samples. Results from the chloride testing are presented in Figure 6-32 and Table 6-11. Individual vertical chloride profiles from this site are presented Appendix C.

6.2.5 SITE I-90E, EAST OF PRESHO AT MRM 222

Evaluation of site MRM 222 occurred on July 27th, 2011. The crack density of the surveyed section was 0.334 foot/square foot. Transverse and Y-cracking was observed. The transverse cracks were spaced approximately every two to four feet. 0 Several cracks were wide and exhibited spalling (Figure 6-37). No longitudinal cracking was identified within the 100 foot section. The depth to the reinforcement was measured as 5 inches with a hand-held tape measure.

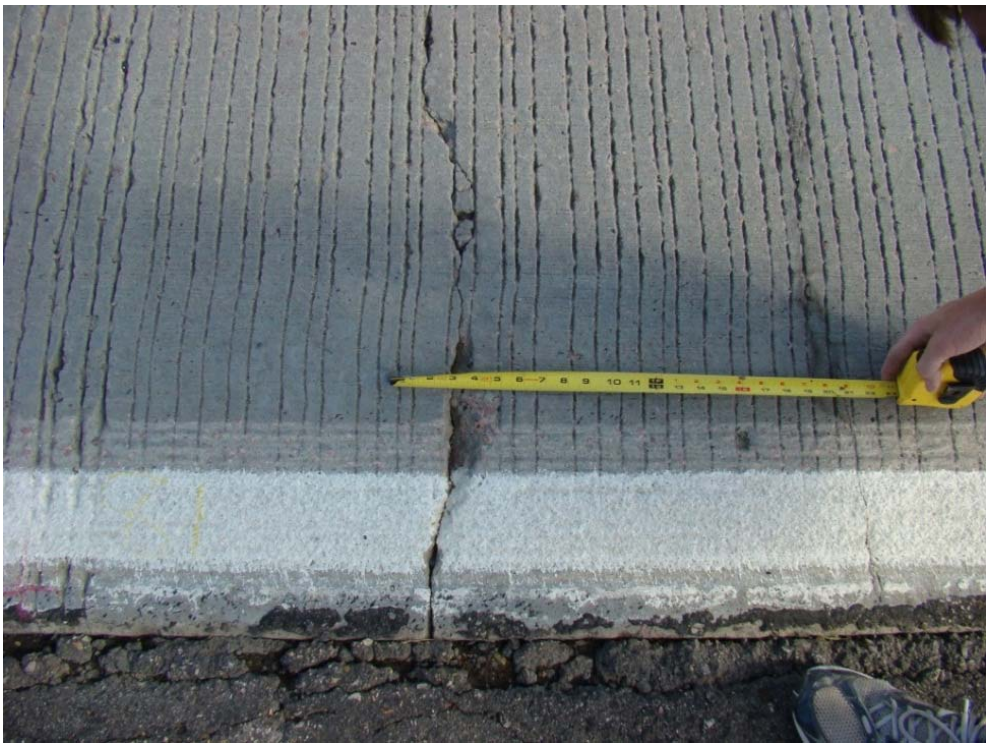

Figure 6-37: Wide crack exhibiting spalling at MRM 222

The results of the half-cell measurements were between a minimum of -626 mV and a maximum of -344 mV, with an average of -453 mV and standard deviation of 70.4 mV. The distribution of the half-cell measurements is presented in Figure 6-38. The equipotential contour maps are presented in Appendix B. The probability of corrosion activity based on the measured data, as suggested by ASTM C876, is presented in Table 4-16.

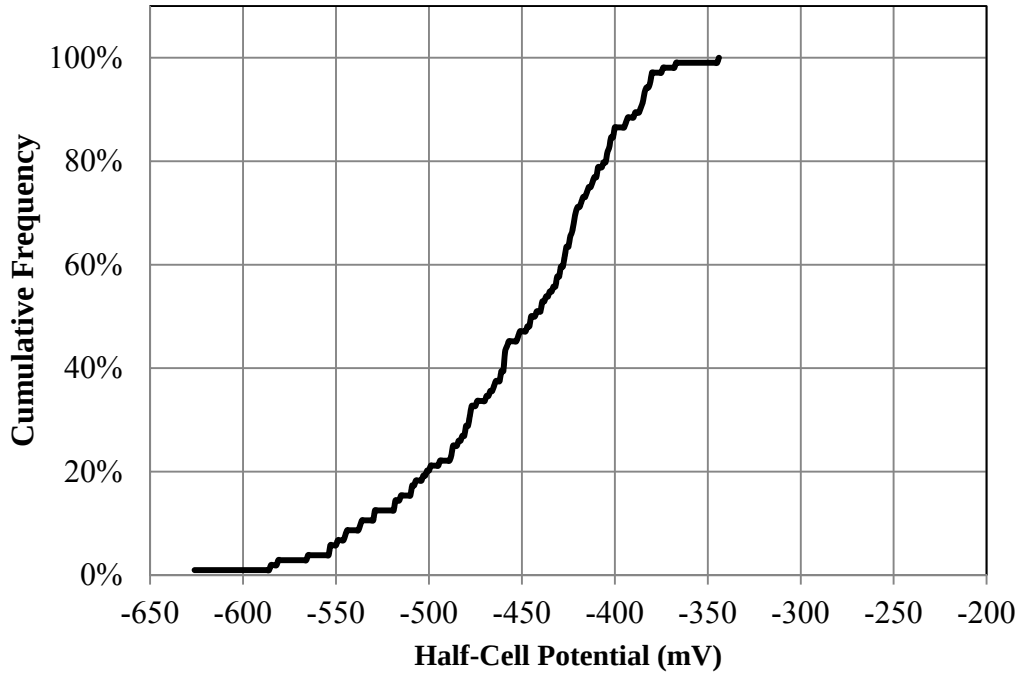

Figure 6-38: MRM 222 half-cell cumulative frequency distribution

Table 6-15: Indication of half-cell measurements of MRM 222

Potential Measurement Range	Indication according to ASTM C-876	Percent of Data Points in Range
> -200 mV	90% probability that no reinforcing steel is corroding	0.0%
Between -200 mV and -350 mV	Corrosion activity is uncertain	1.0%
< -350 mV	Greater than 90% probability steel is corroding	99.0%

The location of dust samples one and two had half-cell measurements of -626 mV and -585 mV, respectively. Dust sample one was obtained within three inches of a wide crack (see Figure 6-39), and dust sample two was obtained within eight inches of a crack. Results from the chloride testing are presented in Figure 6-32 and Table 6-11. Individual vertical chloride profiles from this site are presented Appendix C.

Figure 6-39: Dust sample one at MRM 222

6.2.6 SITE I-90E, EAST OF KENNEBEC AT MRM 246

Evaluation of site MRM 246 occurred on July 27th, 2011. The crack density for this site was calculated to be 0.290 foot/square foot. Transverse and Y-cracking was observed. The transvers cracks were spaced approximately every one to five feet. No longitudinal cracking was identified within the 100 foot section. The depth to the reinforcement was measured as 3.75 inches with a hand-held tape measure.

The results of the half-cell measurements were between a minimum of -559 mV and a maximum of -338 mV, with an average of -414 mV and standard deviation of 62.6 mV. The distribution of the half-cell measurements is presented in Figure 6-40. The equipotential contour maps are presented in Appendix B. The probability of corrosion activity based on the measured data, as suggested by ASTM C876, is presented in Table 6-16.

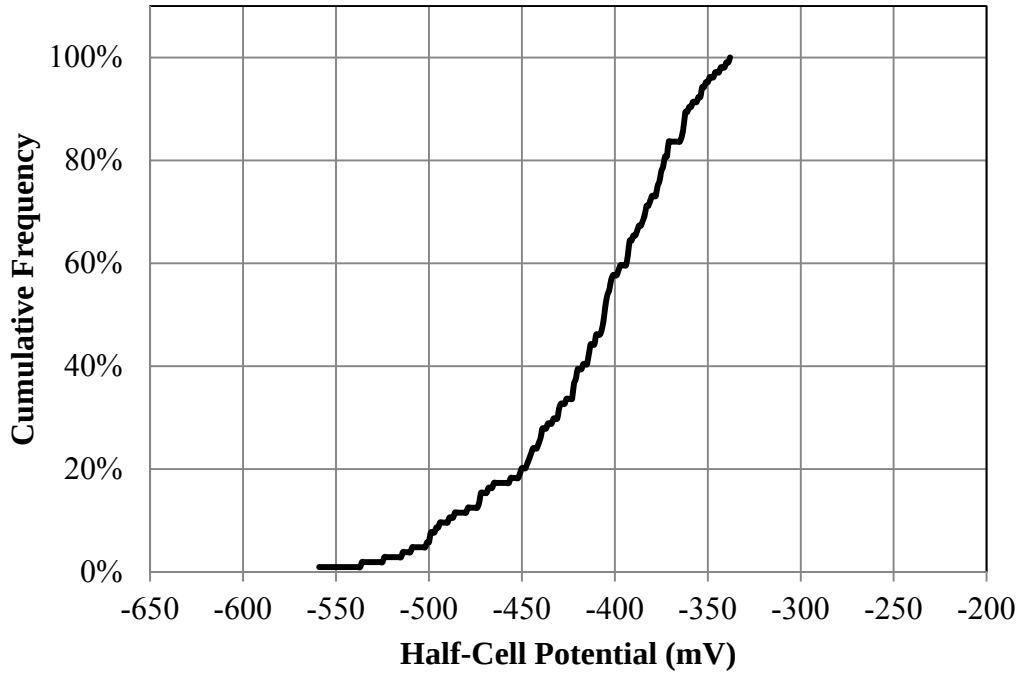

Figure 6-40: MRM 246 half-cell cumulative frequency distribution

Table 6-16: Indication of half-cell measurements at MRM 246

Potential Measurement Range	Indication according to ASTM C-876	Percent of Data Points in Range
> -200 mV	90% probability that no reinforcing steel is corroding	0.0%
Between -200 mV and -350 mV	Corrosion activity is uncertain	4.8%
< -350 mV	Greater than 90% probability steel is corroding	95.2%

The location of dust samples one and two had half-cell measurements of -559 mV and -536 mV, respectively. Dust sample one was obtained within three inches of a Y-crack, and dust sample two was obtained within an inch of a transverse crack. Results from the chloride testing are presented in Figure 6-32 and Table 6-11. Individual vertical chloride profiles from this site are presented Appendix C.

6.2.7 SITE I-29N, SOUTH OF WATERTOWN AT MRM 168NB

Evaluation of site MRM 168 northbound (NB) occurred on August 1st, 2011. The crack density was 0.371 foot/square foot on the section surveyed. Transverse and Y-cracking was observed. The transverse cracks were spaced approximately one to eight feet. No longitudinal cracking was identified within the 100 foot section. The depth to the reinforcement was measured as 4.0 inches with a hand-held measuring tape.

The results of the half-cell measurements were between a minimum of -545 mV and a maximum of -386 mV, with an average of -471 mV and standard deviation of 57.2 mV. The distribution of the half-cell

measurements is presented in Figure 6-41. The equipotential contour maps are presented in Appendix B. The probability of corrosion activity based on the measured data, as suggested by ASTM C876, is presented in Table 6-17.

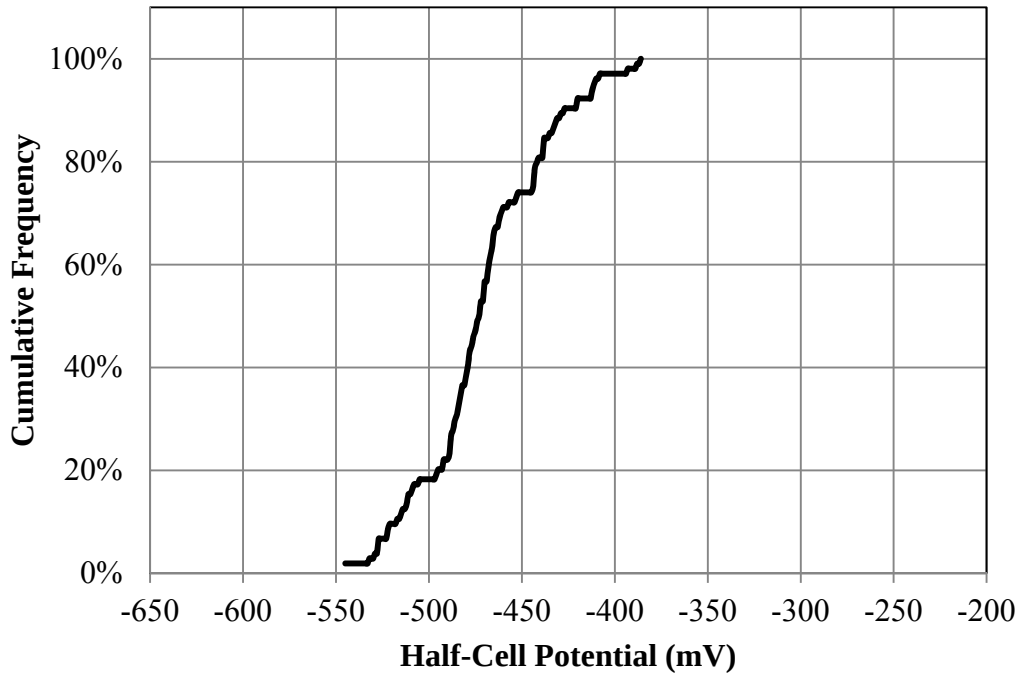

Figure 6-41: MRM 168NB half-cell cumulative frequency distribution

Table 6-17: Indication of half-cell measurements at MRM 168NB

Potential Measurement Range	Indication according to ASTM C-876	Percent of Data Points in Range
> -200 mV	90% probability that no reinforcing steel is corroding	0.0%
Between -200 mV and -350 mV	Corrosion activity is uncertain	0%
< -350 mV	Greater than 90% probability steel is corroding	100%

The location of dust samples one and two had half-cell measurements of -529 mV and -527 mV, respectively. Cracks were observed within five inches of both dust samples. Results from the chloride testing are presented in Figure 6-32 and Table 6-11. Individual vertical chloride profiles from this site are presented Appendix C.

6.2.8 SITE I-29S, SOUTH OF WATERTOWN AT MRM 168SB

Evaluation of site MRM 168 southbound (SB) occurred on August 1st, 2011. The crack density was calculated to be 0.322 foot/square foot. Transverse and Y-cracking was observed (see Figure 6-42). The transverse cracks were spaced from less than one foot to five feet apart. No longitudinal cracking was

identified within the 100 foot section. The depth to the reinforcement was measured as 4.25 inches with a hand-held tape measure.

Figure 6-42: Cracking observed at MRM 168SB

The results of the half-cell measurements were between a minimum of -529 mV and a maximum of -390 mV, with an average of -428 mV and standard deviation of 53.4 mV. The distribution of the half-cell measurements is presented in Figure 6-43. The equipotential contour maps are presented in Appendix B. The probability of corrosion activity based on the measured data, as suggested by ASTM C876, is presented in Table 6-18.

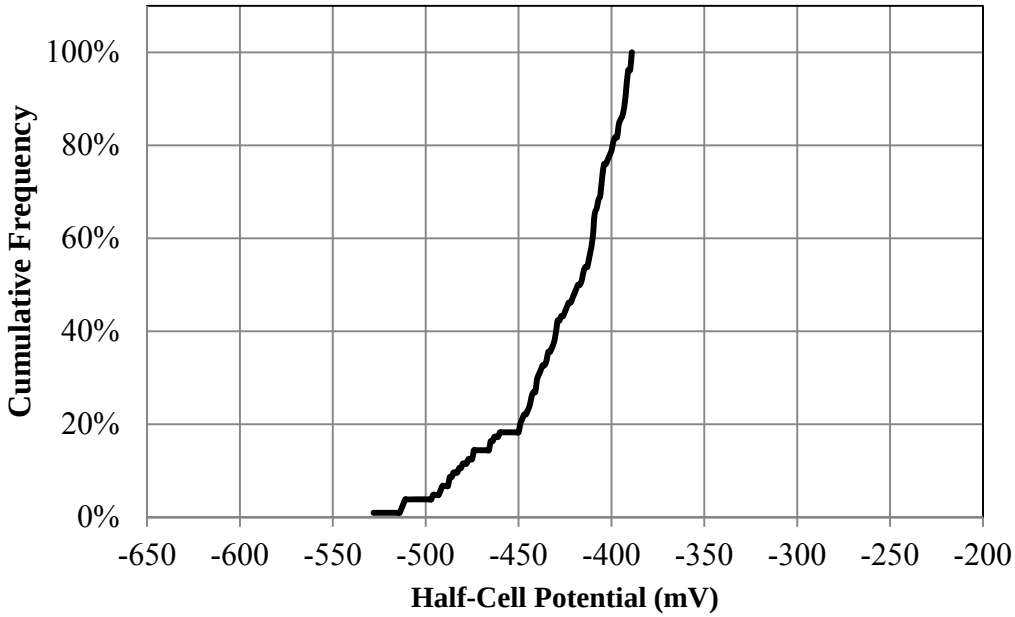

Figure 6-43: MRM 168SB half-cell cumulative frequency distribution

Table 6-18: Indication of half-cell measurements at MRM 168SB

Potential Measurement Range	Indication according to ASTM C-876	Percent of Data Points in Range
> -200 mV	90% probability that no reinforcing steel is corroding	0.0%
Between -200 mV and -350 mV	Corrosion activity is uncertain	0%
< -350 mV	Greater than 90% probability steel is corroding	100%

The location of dust samples one and two had half-cell measurements of -514 mV and -513 mV, respectively. Cracks were observed within three inches of both dust samples. Results from the chloride testing are presented in Figure 6-32 and Table 6-11. Individual vertical chloride profiles from this site are presented Appendix C.

6.3 MITIGATION PRODUCT TESTING

This section outlines the results of mitigation product testing during this study. Results are presented for the half-cell potential measurements, chloride ion analyses, and the SEM testing for both the test section in the field and the specimens from the laboratory testing.

6.3.1 FIELD TESTING OF MITIGATION PRODUCTS

The purpose of the field testing was to determine if topically applied corrosion mitigation products were effective in reducing corrosion in CRCP. This section outlines the results obtained from the CRCP test site located on Interstate 29.

The pavement at the test site was constructed in 1999. On September 30, 2010, the test site was crack mapped, and cores and dust samples were obtained. Concrete cover above the depth of the reinforcing was approximately 3.375 to 3.875 inches based on the measured depth of rebar in the cores obtained from the site. As previously discussed, the crack widths averaged 0.016 inches with minimum and maximum widths of 0.006 inches and 0.033 inches, respectively, with a crack density of 0.681 feet/square foot.

The products were applied to the test sections as shown in Table 5-8. The half-cell potential measurements were obtained once before product application, twice in the fall after the products had been applied, and also twice in the spring. The specific dates are listed in Table 5-7. The half-cell potential data from the field test section was used to create equipotential contour maps and cumulative frequency distributions. These were used to analyze the sections using the potential difference technique. Also, equipotential contour maps and plots of the magnitudes of the half-cell potential measurements can be used to show which areas are possibly corroding according to the numerical magnitude technique. Equipotential contour maps and plots of the half-cell potential measurements showing the difference in half-cell potential for each grid point from measurement to measurement were also created. These were used to illustrate change with time for each grid point.

6.3.1.1 MCI-2018

The mean, standard deviation, maximum and minimum for each date that the measurements were obtained from the MCI-2018 section are located in Table 6-19. The cumulative frequency distributions

for each of the five measurements obtained are shown in Figure 6-44. Figure 6-45 and Figure 6-46 show examples of the two different types of half-cell potential contour maps with their respective legends. Comprehensive contour maps for the MCI-2018 section are presented in Appendix E. Figure 6-47 and Figure 6-48 illustrate plots of the half-cell potential measurements and changes in half-cell potential measurements at the grid points of the MCI-2018 section, respectively. The remaining plots of the half-cell potential measurements and the changes in half-cell potential measurements are presented in Appendix F.

Table 6-19: Summary data for MCI-2018

Date	Mean (mV)	Standard Deviation (mV)	Minimum (mV)	Maximum (mV)
8/25/2011	-445.8	30.2	-563	-366
10/6/2011	-428.8	33.9	-548	-349
10/27/2011	-456.7	32.3	-556	-370
4/10/2012	-427.1	34.0	-507	-188
5/9/2012	-473.4	28.8	-570	-394

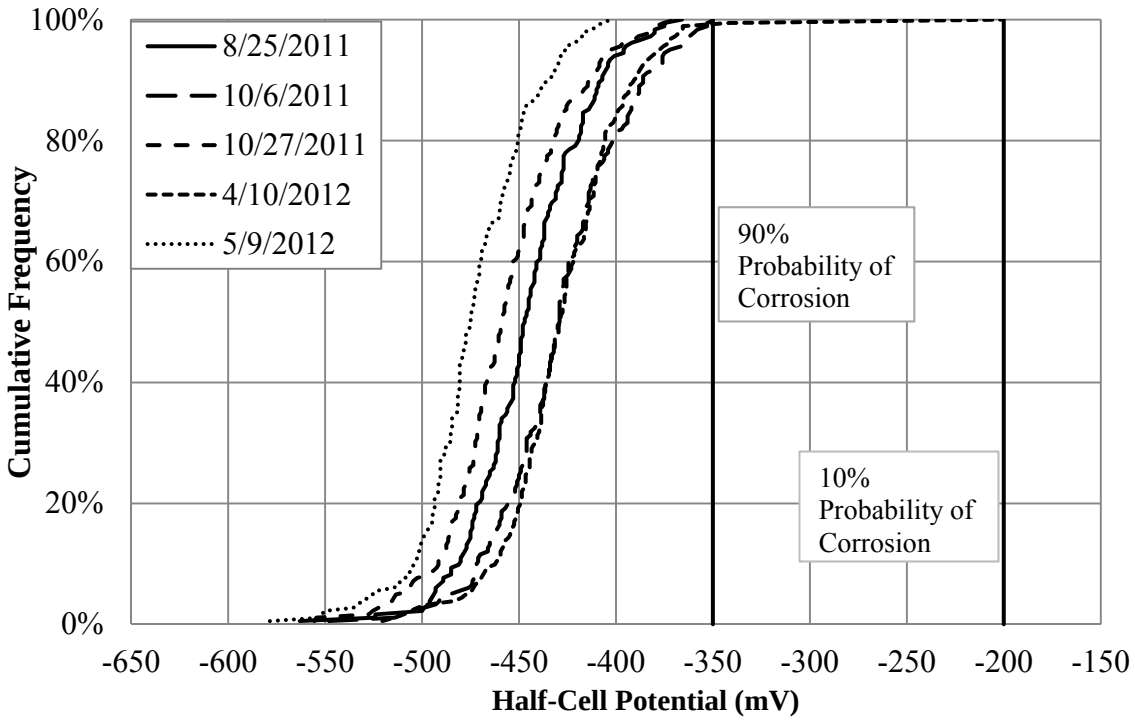

Figure 6-44: Cumulative frequency distribution for MCI-2018

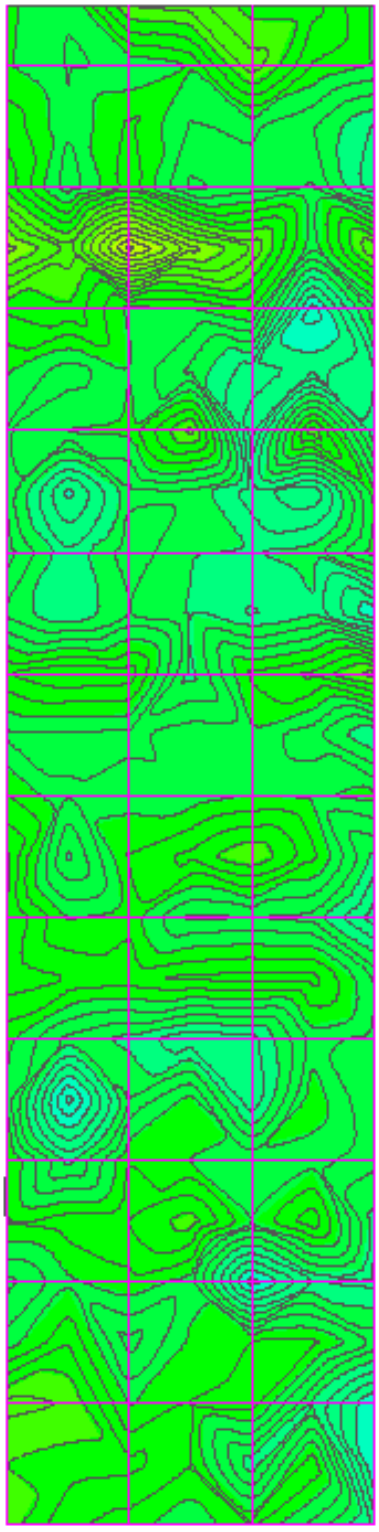

Minimum Reading (mV)	Maximum Reading (mV)	Color
−750.00	−720.00	
−720.00	−690.00	
−690.00	−660.00	
−660.00	−630.00	
−630.00	−600.00	
−600.00	−570.00	
−570.00	−540.00	
−540.00	−510.00	
−510.00	−480.00	
−480.00	−450.00	
−450.00	−420.00	
−420.00	−390.00	
−390.00	−360.00	
−360.00	−330.00	
−330.00	−300.00	
−300.00	−270.00	
−270.00	−240.00	
−240.00	−210.00	
−210.00	−180.00	
−180.00	−150.00	

Figure 6-45: Equipotential contour map for MCI-2018 (August 25, 2011)

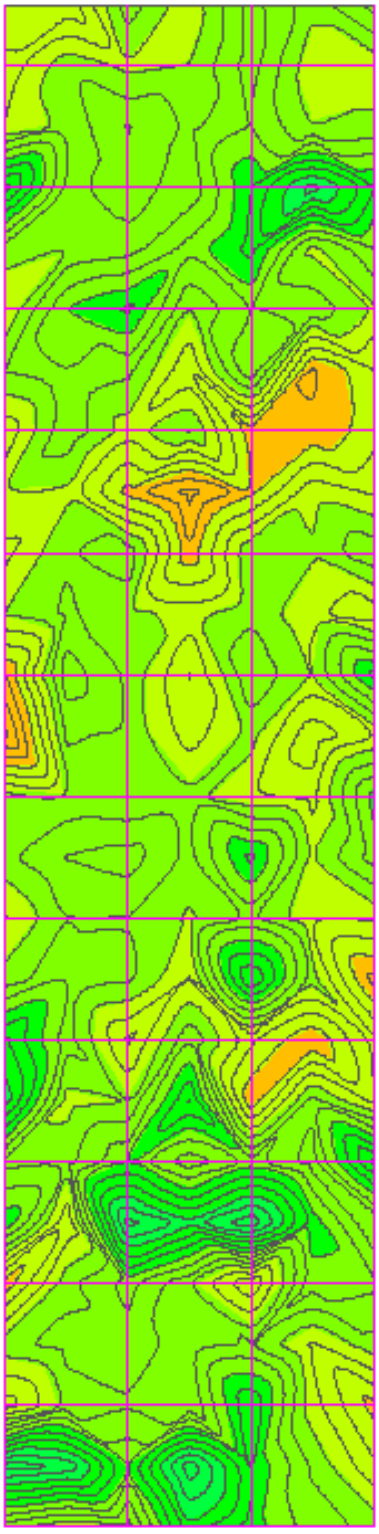

Minimum Elevation	Maximum Elevation	Color
−150.00	−120.00	
−120.00	−90.00	
−90.00	−60.00	
−60.00	−30.00	
−30.00	0.00	
0.00	30.00	
30.00	60.00	
60.00	90.00	
90.00	120.00	
120.00	150.00	
150.00	180.00	
180.00	210.00	
210.00	240.00	
240.00	270.00	

Figure 6-46: Contour map, half-cell potential differences, August 25, 2011 to October 6, 2011, MCI-2018

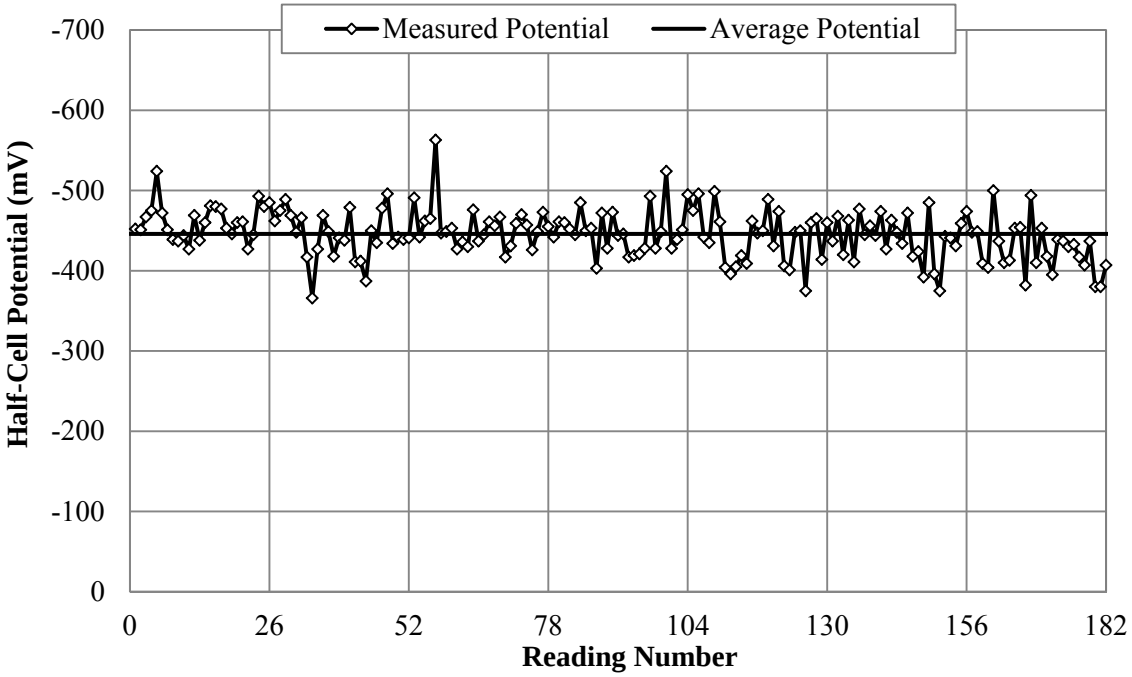

Figure 6-47: Half-cell potential measurements for MCI-2018 (August 25, 2011)

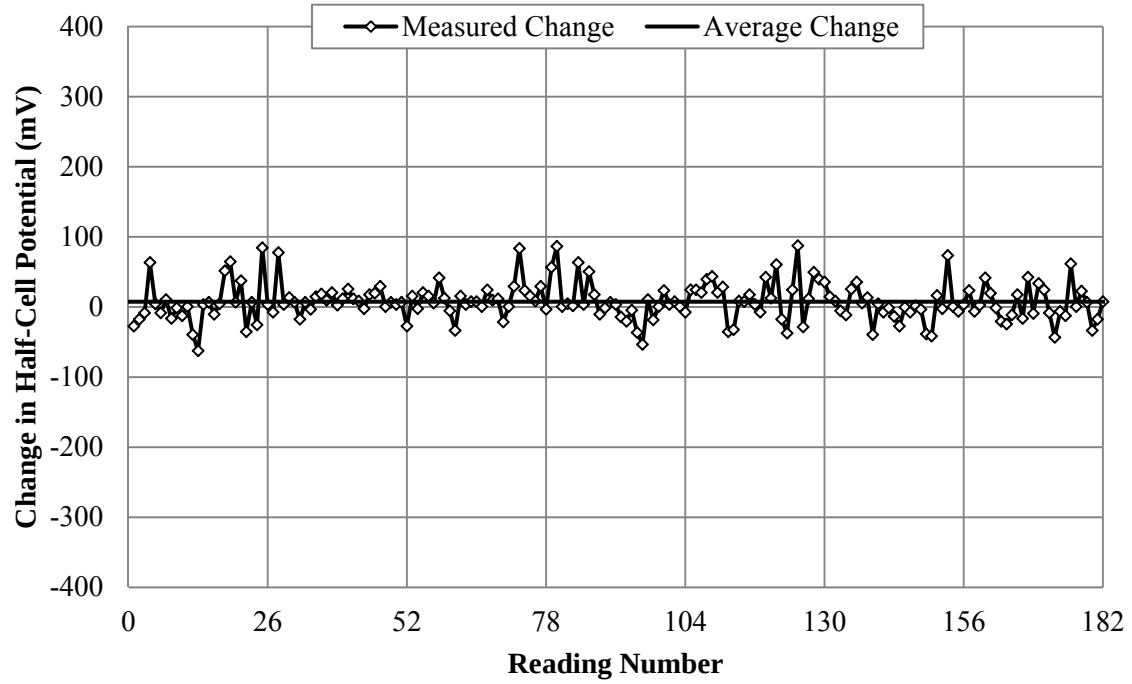

Figure 6-48: Half-cell potential differences, August 25, 2011 to October 6, 2011, MCI-2018

6.3.1.2 Ferrogard 903 and Protectosil CIT

The means, standard deviations, maximums and minimums for the half-cell potential data that was obtained from the Ferrogard 903 and Protectosil CIT section are located in Table 6-20. The cumulative frequency distributions of the half-cell potential measurements are shown in Figure 6-49. The contour maps for the Ferrogard 903 and Protectosil CIT section are shown in Appendix E, and the plots of the half-cell potential measurements and the plots of the changes in half-cell potential measurements are shown in Appendix F.

Table 6-20: Summary data for Ferrogard 903 and Protectosil CIT

Date	Mean (mV)	Standard Deviation (mV)	Minimum (mV)	Maximum (mV)
8/25/2011	-434.1	28.1	-529	-357
10/6/2011	-384.9	26.8	-482	-306
10/27/2011	-421.9	26.4	-489	-345
4/10/2012	-390.4	44.7	-454	-137
5/9/2012	-455.5	28.8	-537	-365

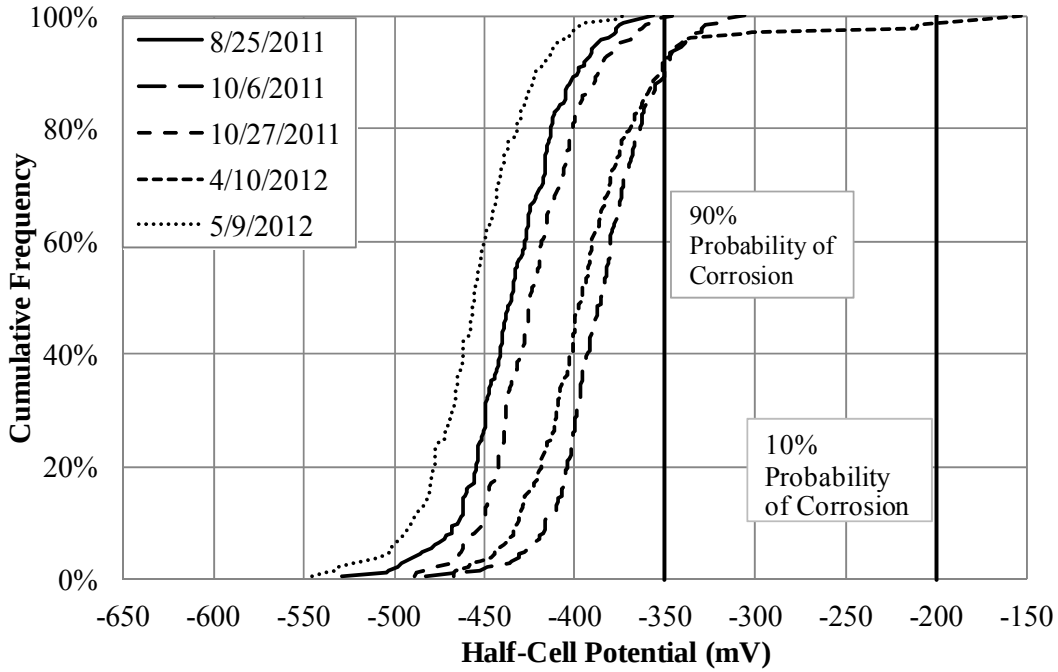

Figure 6-49: Cumulative frequency distribution for Ferrogard 903 and Protectosil CIT

6.3.1.3 Protectosil CIT

The means, standard deviations, maximums and minimums for the half-cell potential data that was obtained from the Protectosil CIT section are located in Table 6-21. The cumulative frequency distributions of the half-cell potential measurements are shown in Figure 6-50. The contour maps for the Protectosil CIT section are shown in Appendix E, and the half-cell potential measurement plots are shown in Appendix F.

Table 6-21: Summary data for Protectosil CIT

Date	Mean (mV)	Standard Deviation (mV)	Minimum (mV)	Maximum (mV)
8/25/2011	-459.2	29.8	-548	-368
10/6/2011	-433.7	30.7	-517	-321
10/27/2011	-461.5	31.9	-530	-381
4/10/2012	-432.8	36.5	-528	-242
5/9/2012	-485.4	31.0	-554	-396

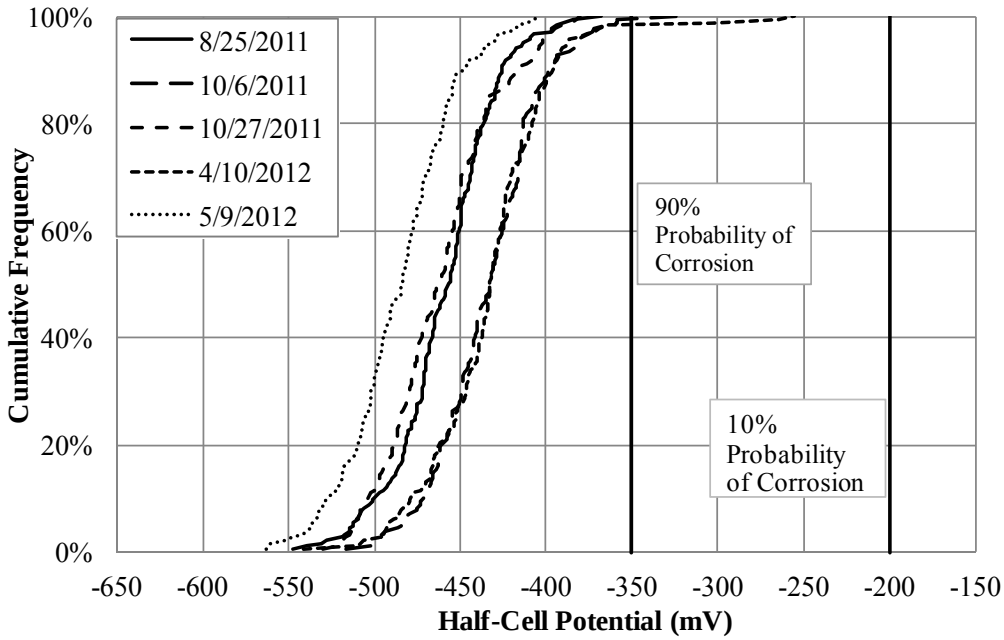

Figure 6-50: Cumulative frequency distribution for Protectosil CIT

6.3.1.4 Ferrogard 903

The means, standard deviations, maximums and minimums for the half-cell potential data that was obtained from the Ferrogard 903 section are located in Table 6-22. The cumulative frequency distributions of the half-cell potential measurements are shown in Figure 6-51. The contour maps for the Ferrogard 903 section are shown in Appendix E, and the half-cell potential measurement plots are shown in Appendix F.

Table 6-22: Summary data for Ferrogard 903

Date	Mean (mV)	Standard Deviation (mV)	Minimum (mV)	Maximum (mV)
8/25/2011	-437.5	34.2	-553	-342
10/6/2011	-382.5	32.6	-526	-303
10/27/2011	-416.0	32.1	-517	-328
4/10/2012	-397.2	40.7	-477	-205
5/9/2012	-467.4	34.2	-568	-373

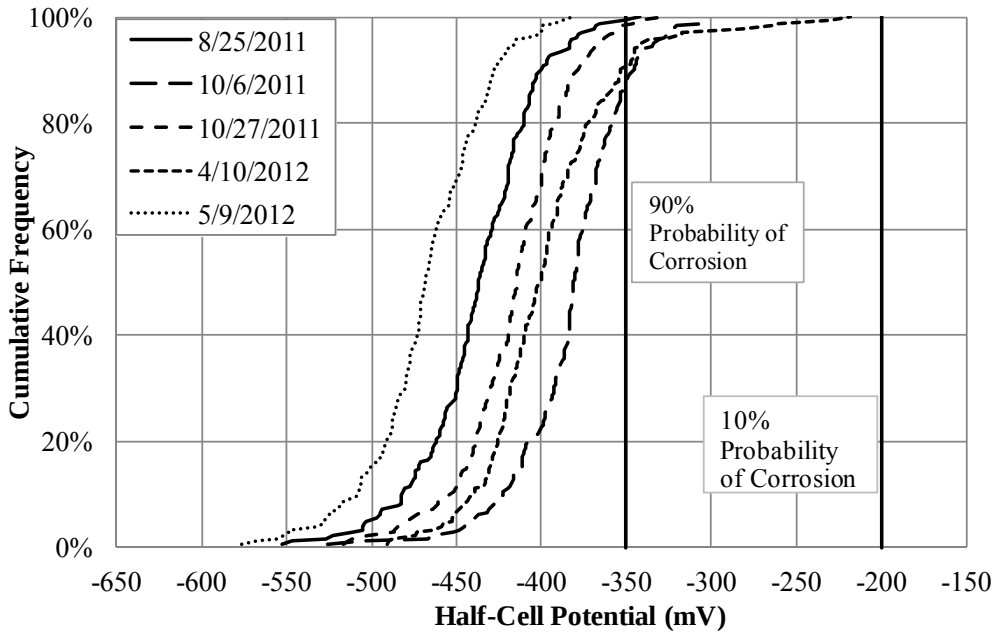

Figure 6-51: Cumulative frequency distribution for Ferrogard 903

6.3.1.5 Duralprep 3020

The means, standard deviations, maximums and minimums for the half-cell potential data that was obtained from the Duralprep 3020 section are located in Table 6-23. The cumulative frequency distributions of the half-cell potential measurements are shown in Figure 6-52. The contour maps for the Duralprep 3020 section are shown in Appendix E, and the half-cell potential measurement plots are shown in Appendix F.

Table 6-23: Summary data for Duralprep 3020

Date	Mean (mV)	Standard Deviation (mV)	Minimum (mV)	Maximum (mV)
8/25/2011	-436.2	33.0	-544	-367
10/6/2011	-402.0	37.6	-502	-209
10/27/2011	-424.4	35.9	-535	-357
4/10/2012	-406.9	38.2	-474	-219
5/9/2012	-474.4	36.5	-595	-377

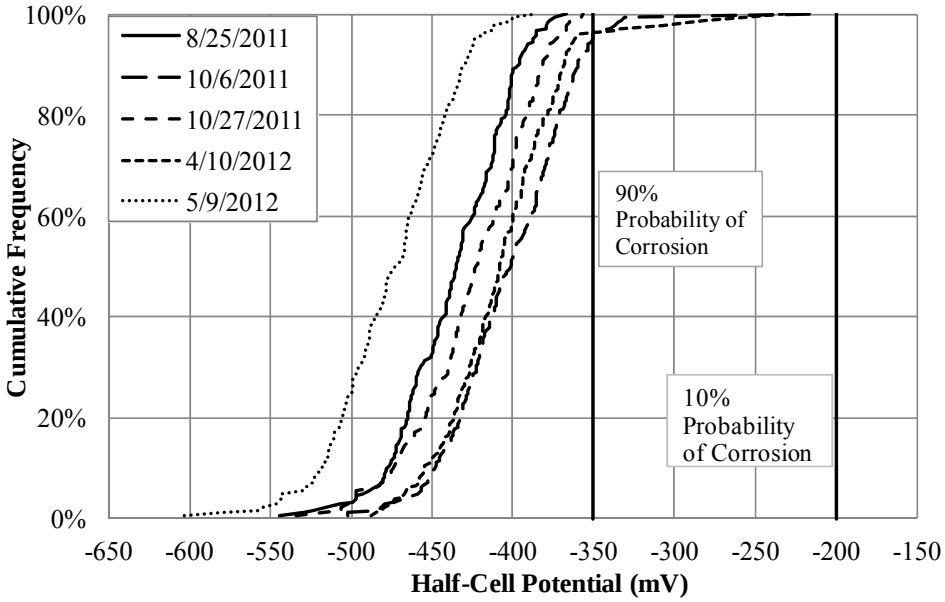

Figure 6-52: Cumulative frequency distribution for Duralprep 3020

6.3.1.6 Chemtrete 40

The means, standard deviations, maximums and minimums for the half-cell potential data that was obtained from the Chemtrete 40 section are located in Table 6-24. The cumulative frequency distributions of the half-cell potential measurements are shown in Figure 6-53. The contour maps for the Chemtrete 40 section are shown in Appendix E, and the half-cell potential measurement plots are shonw in Appendix F.

Table 6-24: Summary data for Chemtrete 40

Date	Mean (mV)	Standard Deviation (mV)	Minimum (mV)	Maximum (mV)
8/25/2011	-469.7	50.0	-629	-368
10/6/2011	-452.7	49.8	-628	-347
10/27/2011	-467.6	44.4	-615	-383
4/10/2012	-431.8	61.3	-604	-133
5/9/2012	-497.8	51.2	-673	-386

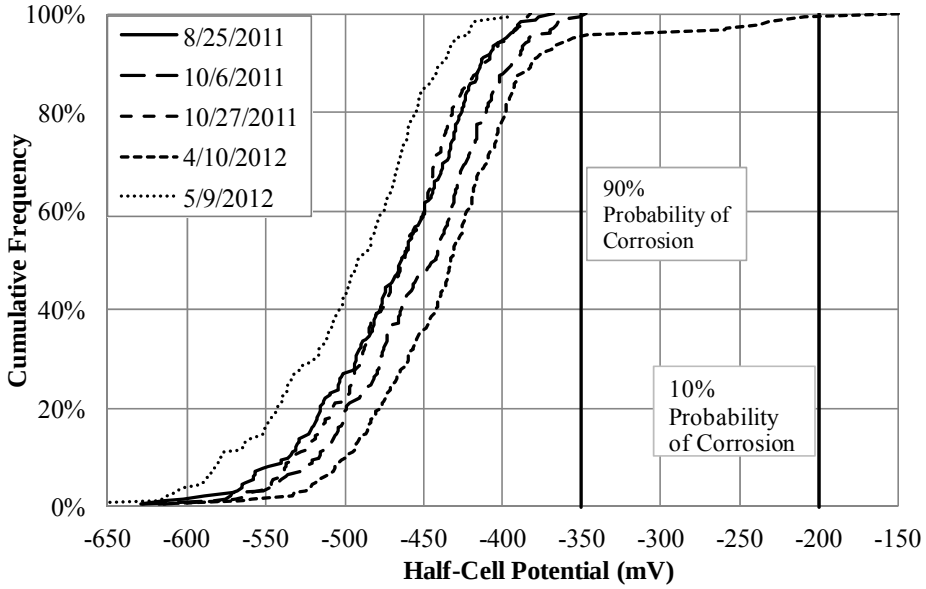

Figure 6-53: Cumulative frequency distribution for Chemtrete 40

6.3.1.7 Control (No Products)

The means, standard deviations, maximums and minimums for the half-cell potential data that was obtained from the control section are located in Table 6-25. The cumulative frequency distributions of the half-cell potential measurements are shown in Figure 6-54. The contour maps for the control section are shown in Appendix E, and the half-cell potential measurement plots are shown in Appendix F.

Table 6-25: Summary data for No Products

Date	Mean (mV)	Standard Deviation (mV)	Minimum (mV)	Maximum (mV)
8/25/2011	-447.8	34.6	-561	-366
10/6/2011	-429.3	34.7	-538	-249
10/27/2011	-447.9	31.7	-562	-363
4/10/2012	-435.4	38.6	-547	-121
5/9/2012	-496.9	34.2	-594	-410

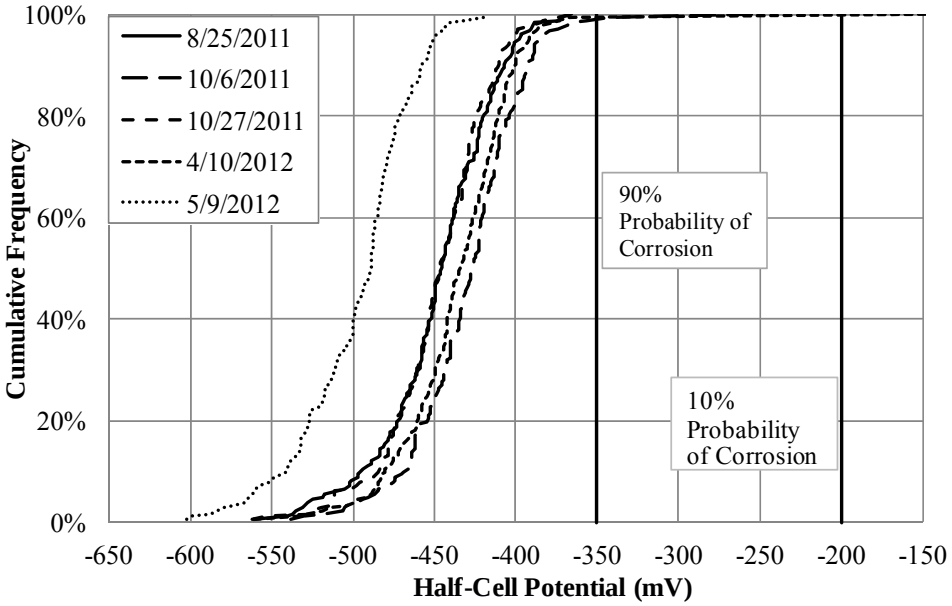

Figure 6-54: Cumulative frequency distribution for No Products

6.3.2 LABORATORY TESTING OF MITIGATION PRODUCTS

The purpose of the laboratory testing was to compare the effectiveness of each product in a controlled environment. The products were applied to various types of specimens, as described in Chapter 5. The half-cell potentials of all specimens were measured periodically during the testing period. Four wet, cracked specimens were also subjected to chloride ion testing and SEM testing, and two of the cracked, control specimens had the reinforcement removed for visual inspection after the half-cell potential testing was completed. This section outlines the results obtained from the laboratory specimens.

6.3.2.1 MCI-2018

Figure 6-55 shows the timeline of product and chloride introduction superimposed on the half-cell potential measurements for MCI-2018, applied to Specimens 1 and 2. Recall that Specimens 1 and 2 are wet and dry cracked specimens, respectively. The half-cell potential measurements for Specimen 17, an uncracked specimen with salt in the mix, are shown in Figure 6-56.

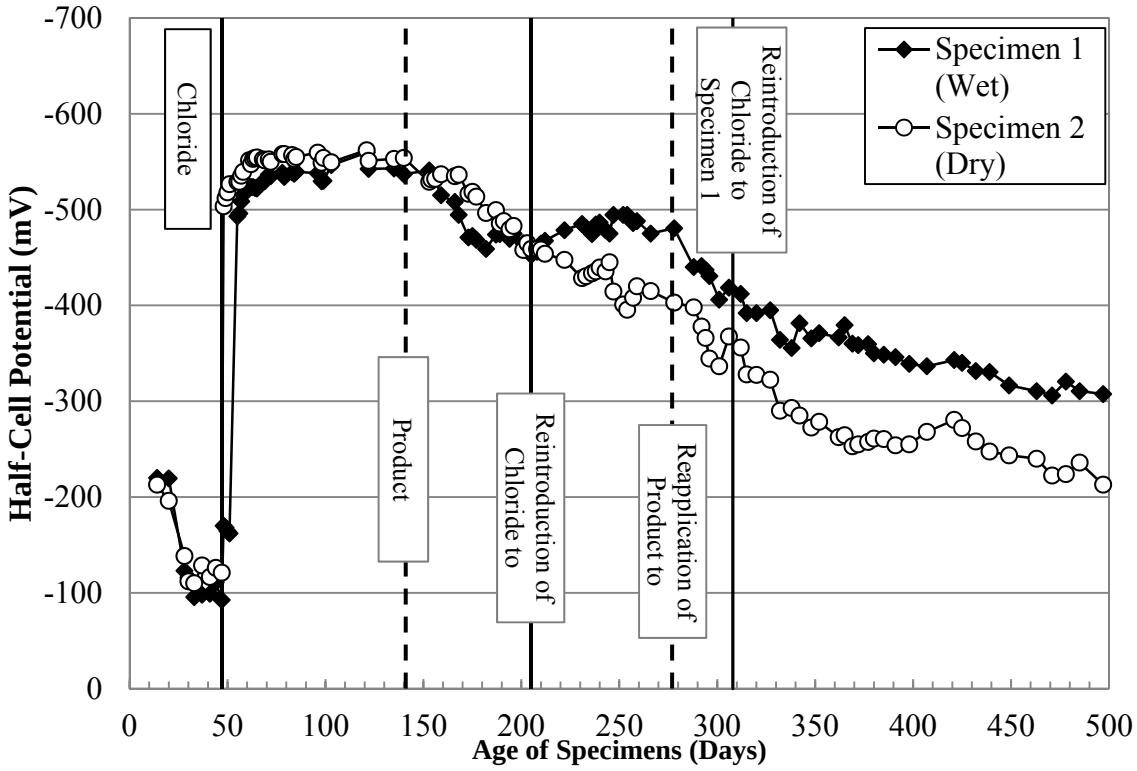

Figure 6-55: Half-cell potential measurements for MCI-2018, cracked specimens

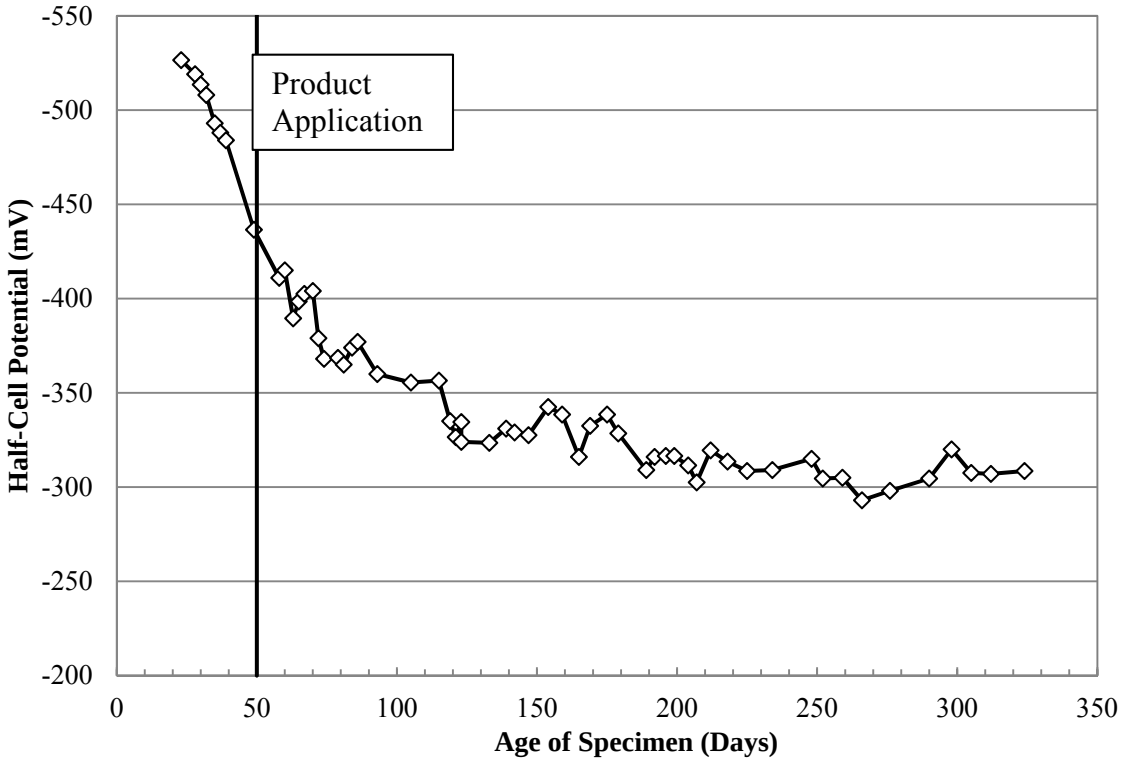

Figure 6-56: Half-cell potential measurements, MCI-2018, uncracked, salt in mix specimen

6.3.2.2 Ferrogard 903 and Protectosil CIT

Figure 6-57 shows the timeline of product and chloride introduction superimposed on the half-cell potential measurements for Ferrogard 903 and Protectosil CIT, applied to Specimens 3 and 4. Specimens 3 and 4 are wet and dry cracked specimens, respectively. The half-cell potential measurements for Specimen 18, an uncracked specimen with salt in the mix, are shown in Figure 6-58.

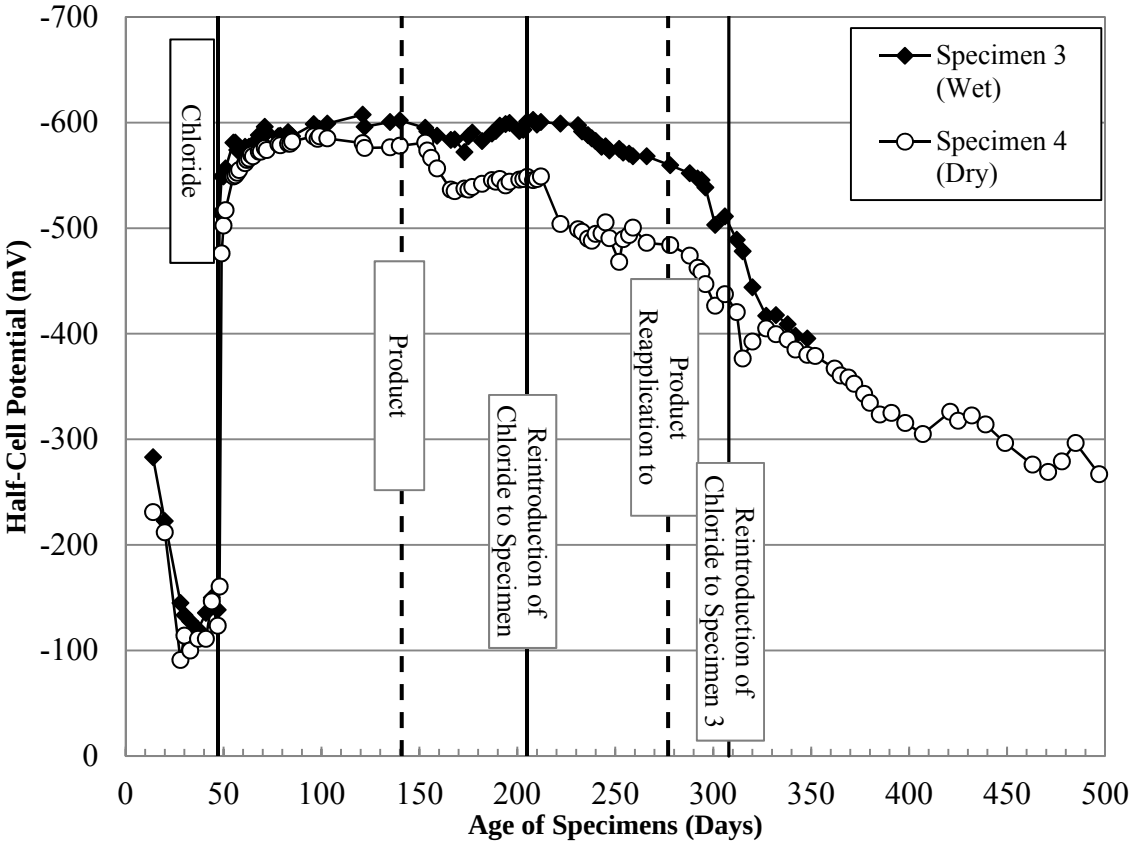

Figure 6-57: Half-cell potential measurements, Ferrogard 903 & Protectosil CIT, cracked specimens

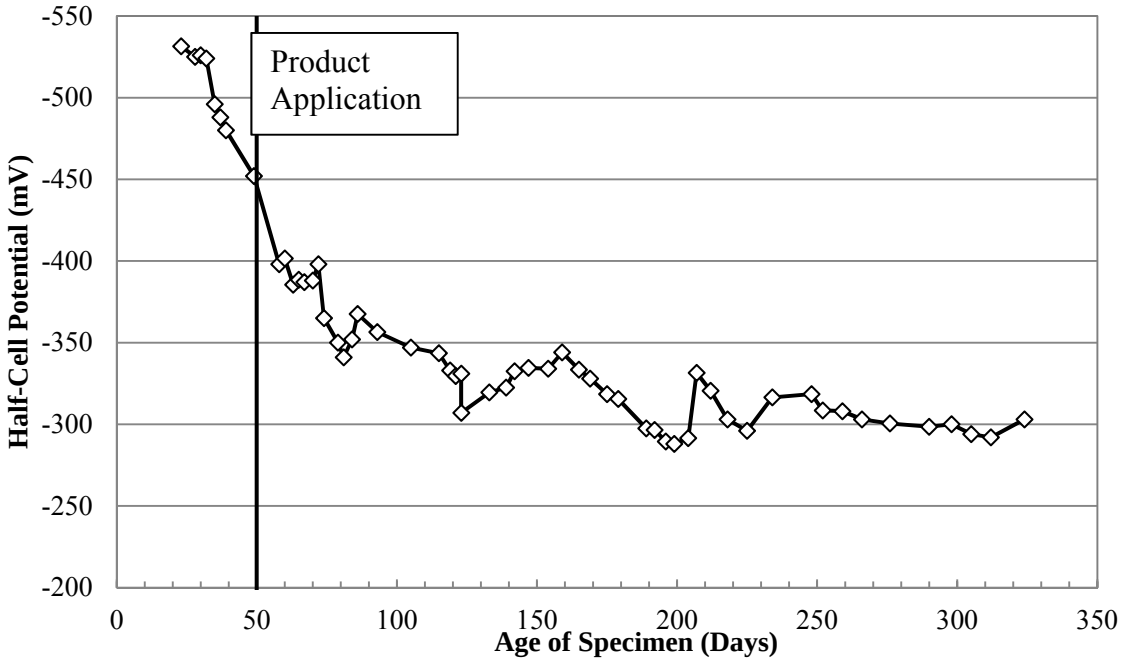

Figure 6-58: Half-cell potential measurements, Ferrogard 903 and Protectosil CIT, uncracked, salt in mix specimen

Specimen 3 was one of the four specimens subjected to chloride ion concentration and SEM testing. Figure 6-59 shows the chloride profiles for each horizontal slice of the specimen. The depth of each slice was measured from the bottom of the well.

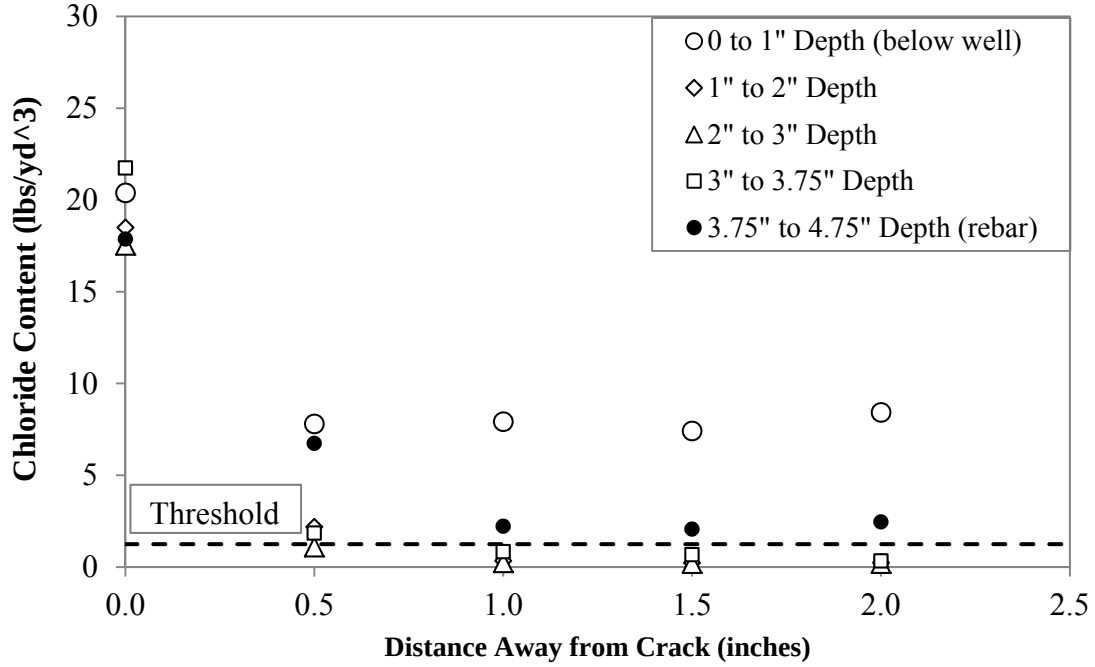

Figure 6-59: Chloride profiles for Ferrogard 903 and Protectosil CIT

Figure 6-60 through Figure 6-64 show the results of the SEM testing. Figure 6-60 is an optical image showing the thin ring of corrosion around the exterior of the reinforcement. The white rectangle shown in Figure 6-60 is the area that was further analyzed to produce the BSE image and elemental maps of oxygen (O), iron (Fe), and chloride (Cl) shown in Figure 6-61. The areas with concentrations of both iron (red) and oxygen (green) are the corroded areas. The thin layer of corrosion is clearly seen in the BSE image and shows up as brighter red than the rest of the corrosion on the iron element map. No significant concentrations of chlorides were detected in the chlorine element map as shown in Figure 6-61. Figure 6-62 and Figure 6-63 show similar results from another area of the reinforcement from Specimen 3. However, some small concentrations of chlorides are seen near the edges of the pitting corrosion shown in Figure 6-63. No X-ray spectrum graph was produced for Specimen 3.

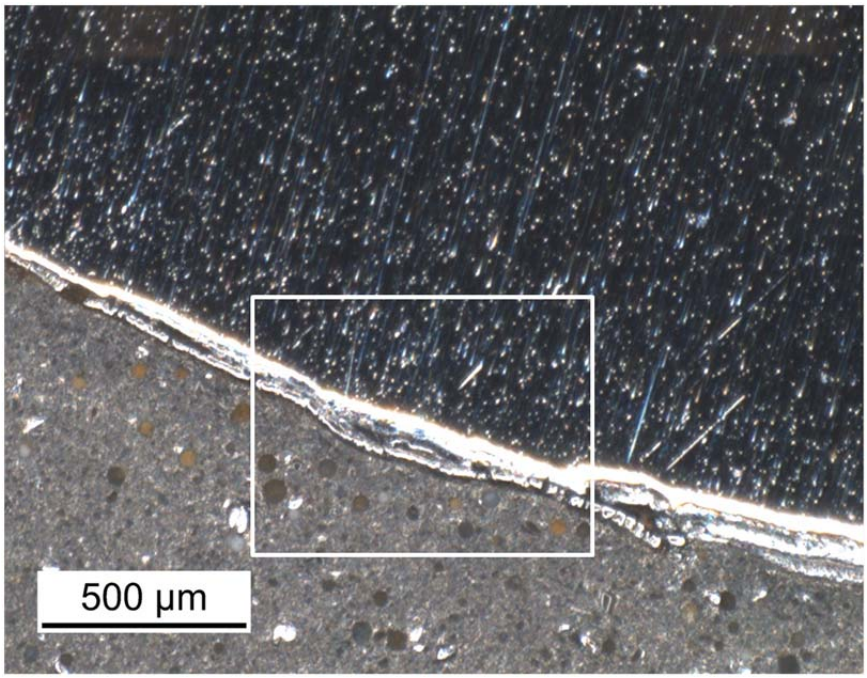

Figure 6-60: Optical image for Ferrogard 903 and Protectosil CIT

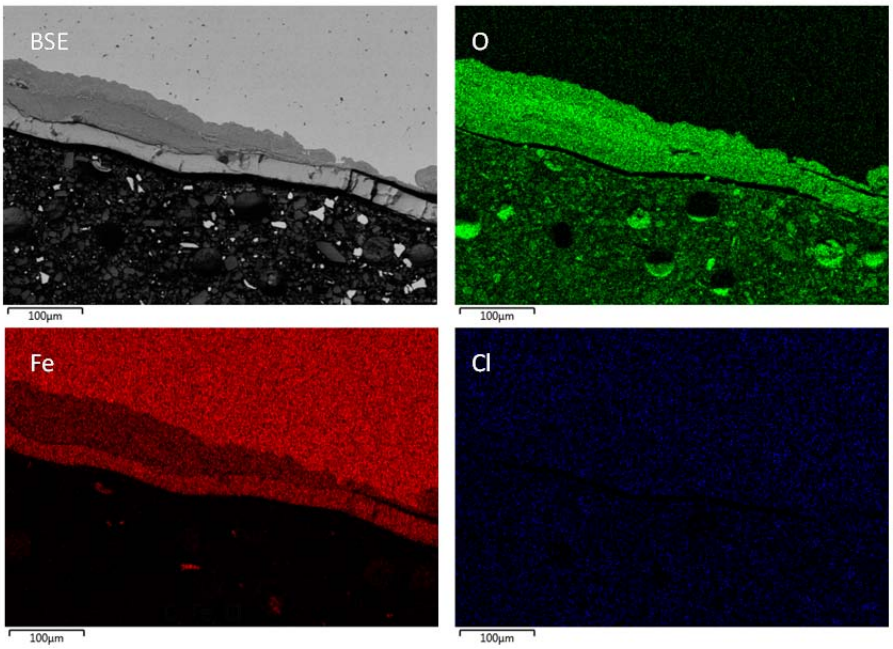

Figure 6-61: BSE image and element Maps for Ferrogard 903 and Protectosil CIT

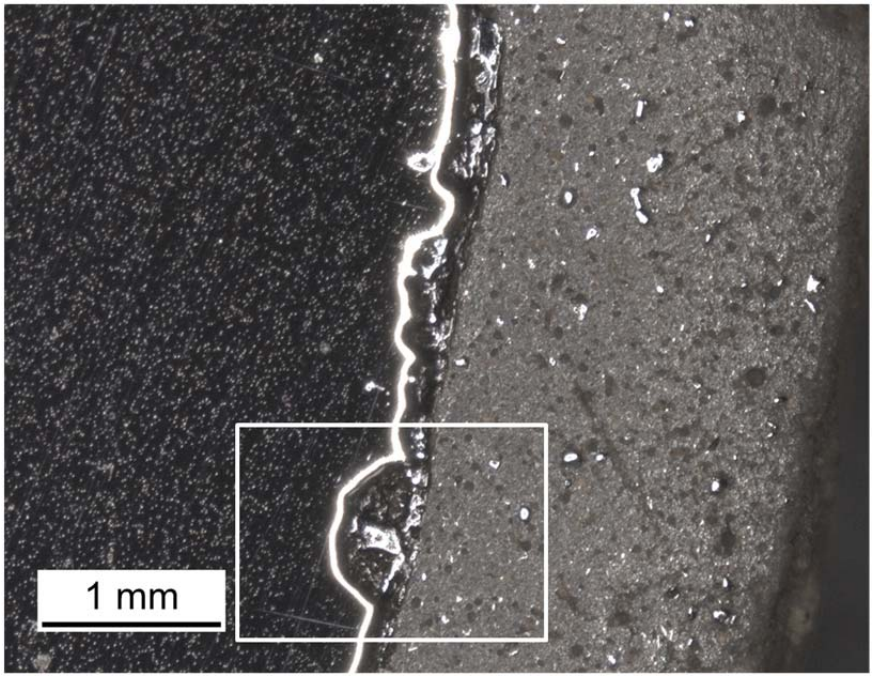

Figure 6-62: Optical image for Ferrogard 903 and Protectosil CIT

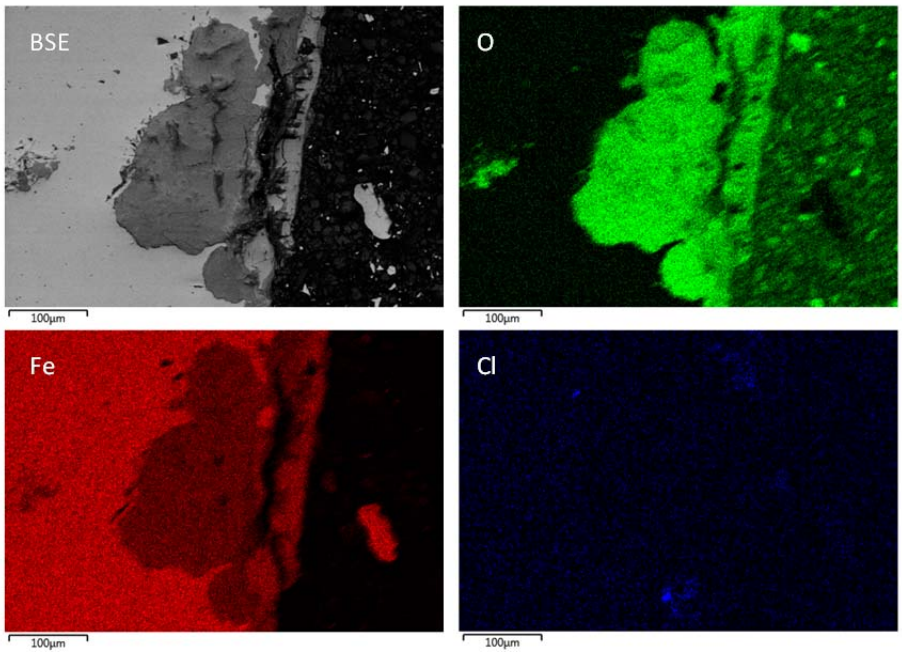

Figure 6-63: BSE image and element maps for Ferrogard 903 and Protectosil CIT

6.3.2.3 Protectosil CIT

Figure 6-64 shows the timeline of product and chloride introduction superimposed on the half-cell potential measurements for Protectosil CIT, applied to Specimens 5 and 6. Specimens 5 and 6 are wet and dry cracked specimens, respectively. The half-cell potential measurements for Specimen 19, an uncracked specimen with salt in the mix, are shown in Figure 6-65.

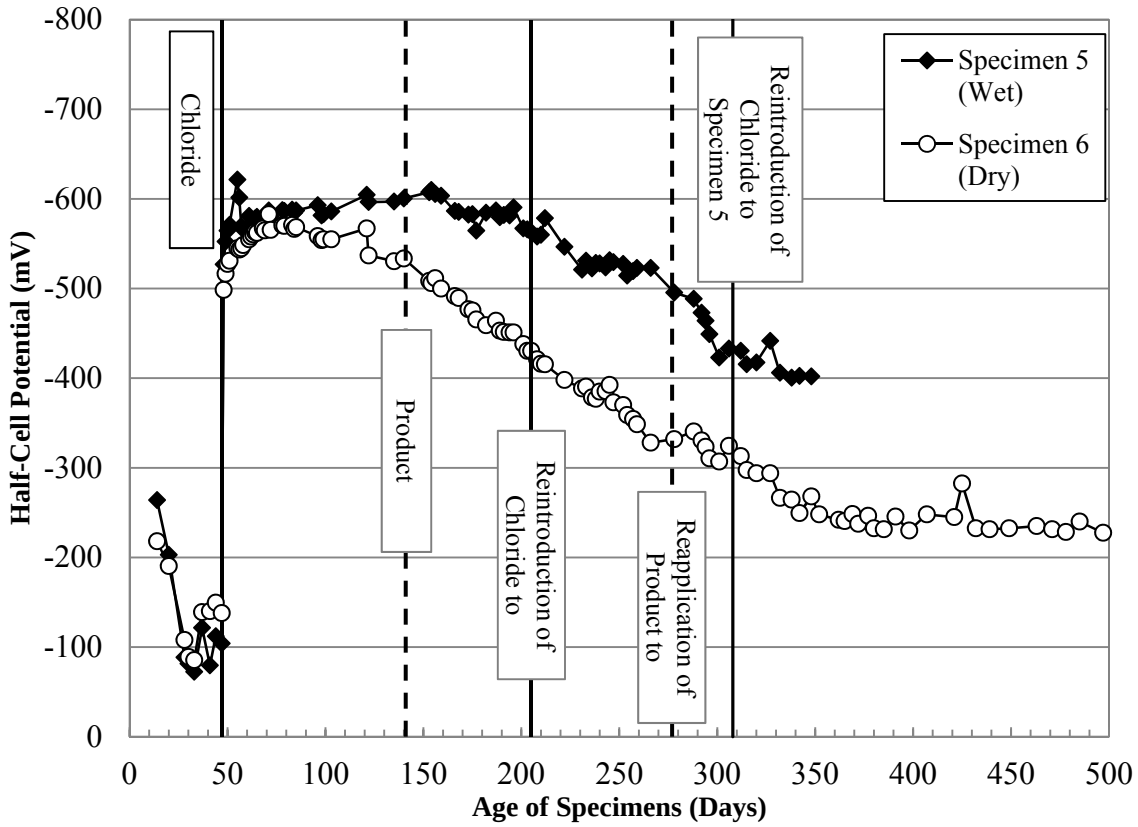

Figure 6-64: Half-cell potential measurements for Protectosil CIT, cracked specimens

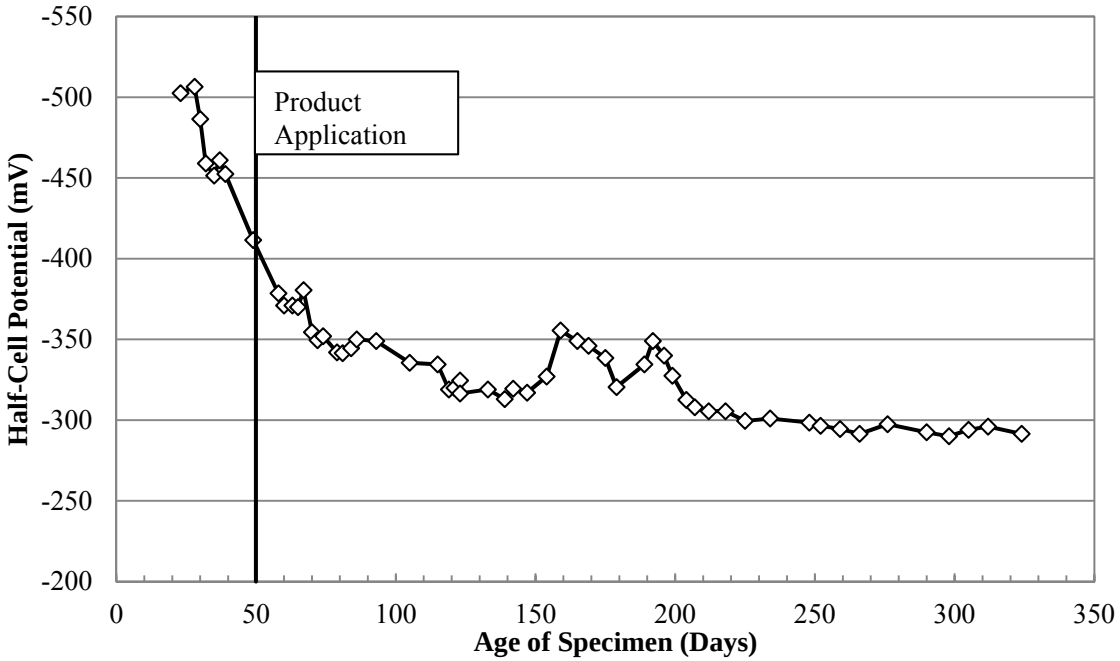

Figure 6-65: Half-cell potential measurements for Protectosil CIT, uncracked, salt in mix specimen

Specimen 5 was one of the four specimens subjected to chloride ion concentration and SEM testing. Figure 6-66 shows the chloride profiles for each horizontal slice of the specimen. The depth of each slice is measured from the bottom of the well.

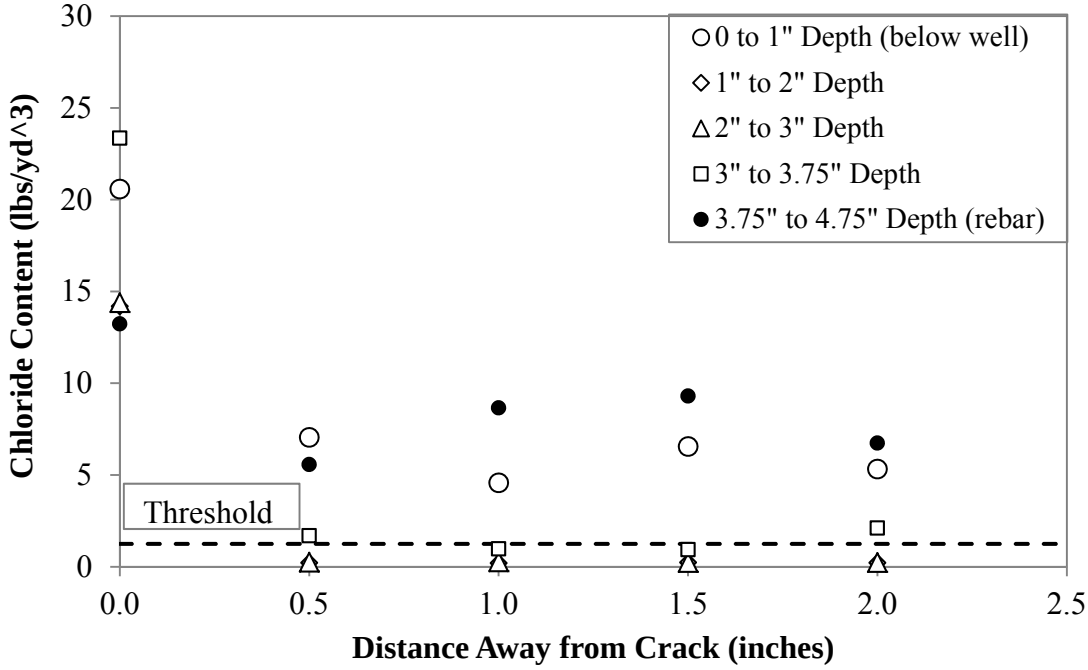

Figure 6-66: Chloride profiles for Protectosil CIT

Figure 6-67 through Figure 6-69 show the results for the SEM testing. Figure 6-67 is an optical image showing the thin ring of corrosion around the exterior of the reinforcement. The white rectangle shown in

Figure 6-67 is the area that was further analyzed to produce the BSE image and the elemental maps of oxygen, iron, and chloride shown in Figure 6-68. There was a thin layer of corrosion products around the entire reinforcement. A small concentration of chlorides can be seen near the edges of the pitting corrosion shown in Figure 6-68. Figure 6-69 shows the X-ray spectrum graph for Specimen 5 and the approximate element concentrations found at the indicated location of the reinforcement.

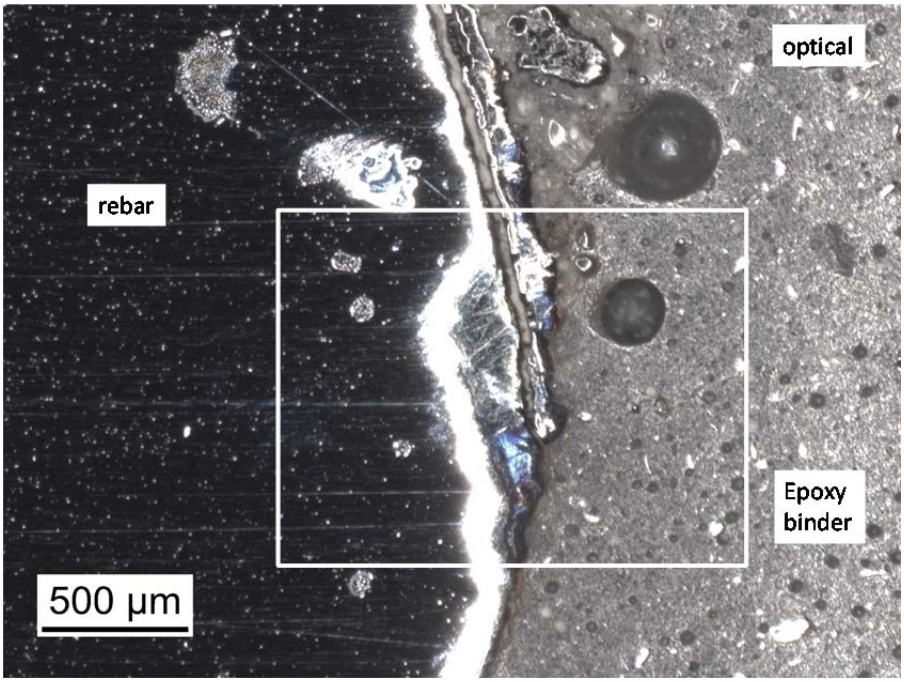

Figure 6-67: Optical image for Protectosil CIT

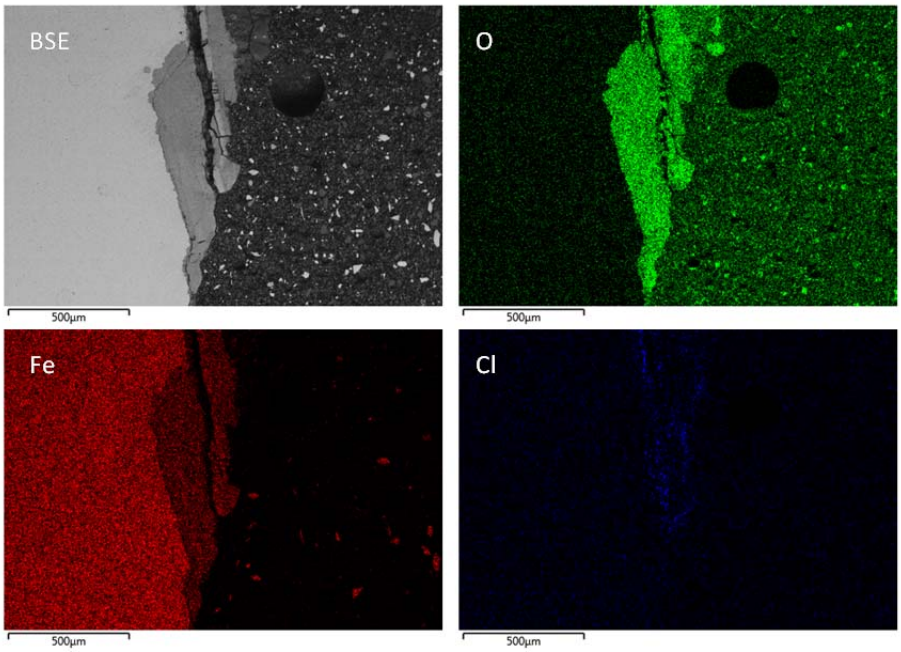

Figure 6-68: BSE image and element maps for Protectosil CIT

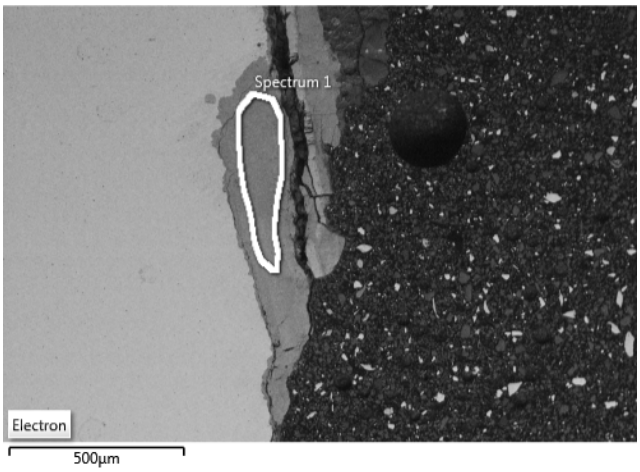

a. BSE Image of where the reinforcement was analyzed

Element	Wt%	Oxide	Oxide %
O	23.07		
Na	3.06	Na2O	4.13
Mg	0.00	MgO	0.00
Si	0.95	SiO2	2.03
S	0.09	SO3	0.22
Cl	0.43		0.00
K	0.00	K2O	0.00
Ca	0.43	CaO	0.61
Mn	0.52	MnO	0.68
Fe	71.43	FeO	91.90
Total:	100.00		99.57

b. Approximate element concentrations of the analyzed area

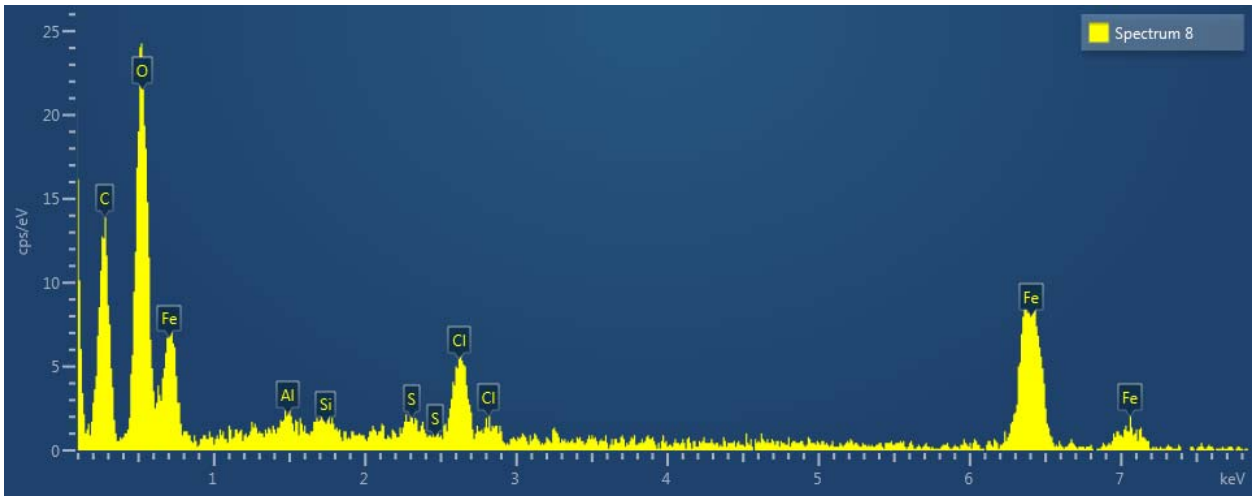

c. X-ray Spectrum Graph

Figure 6-69: Energy dispersive x-ray spectroscopy results for Protectosil CIT

6.3.2.4 Ferrogard 903

Figure 6-70 shows the timeline of product and chloride introduction superimposed on the half-cell measurements for Ferrogard 903, applied to Specimens 7 and 8. Specimens 7 and 8 were wet and dry cracked specimens, respectively. The half-cell potentials for Specimen 20, an uncracked specimen with salt in the mix, are shown in Figure 6-71.

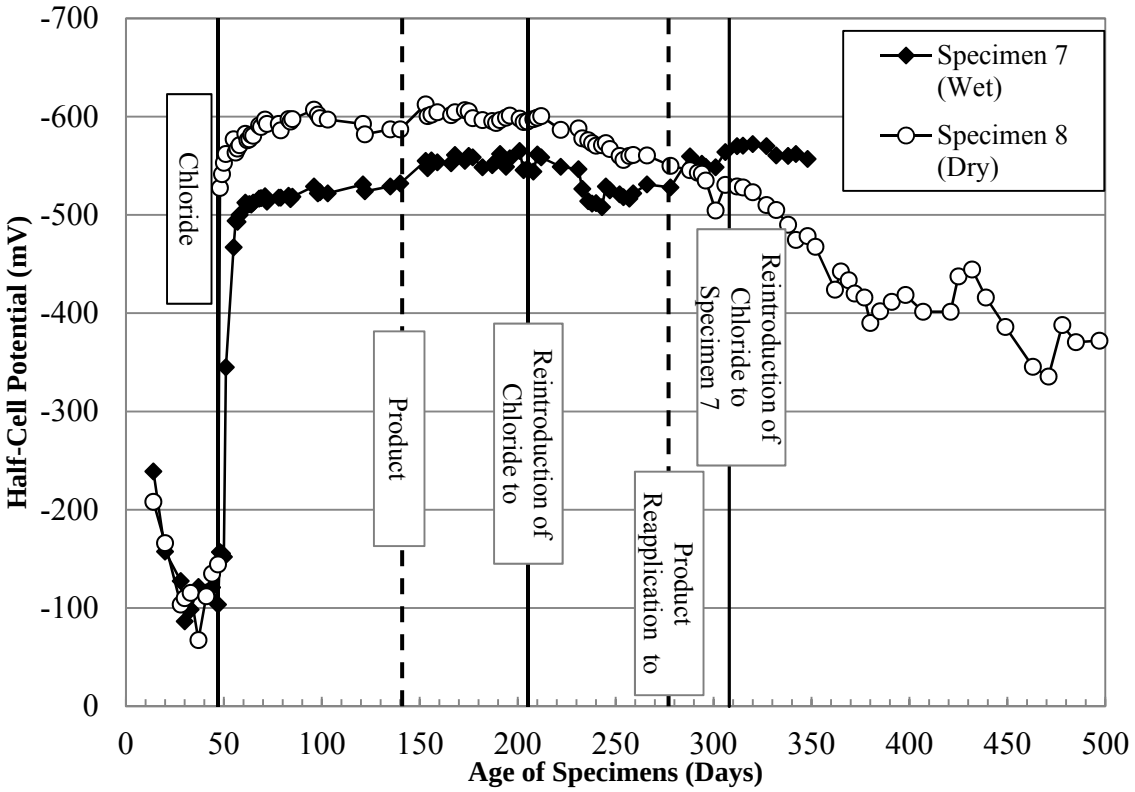

Figure 6-70: Half-cell potential measurements, Ferrogard 903, cracked specimens

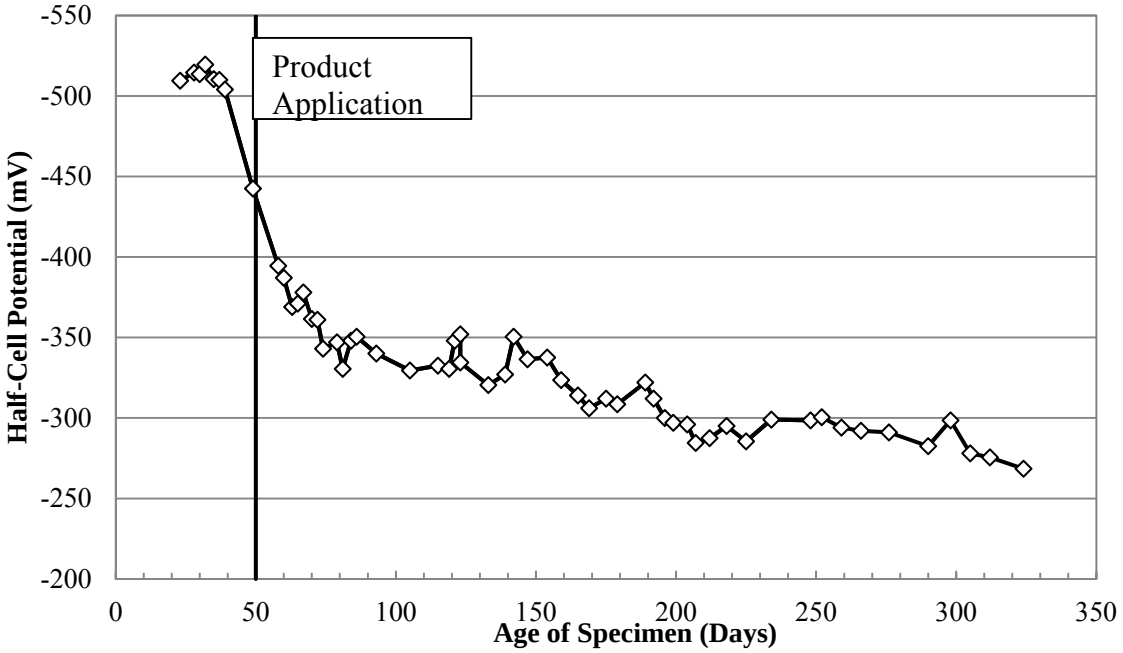

Figure 6-71: Half-cell potential measurements, Ferrogard 903, uncracked, salt in mix specimen

Specimen 7 was one of the four specimens subjected to chloride ion concentration and SEM testing. Figure 6-72 shows the chloride profiles for each horizontal slice of the specimen. The depth of each slice was measured from the bottom of the well.

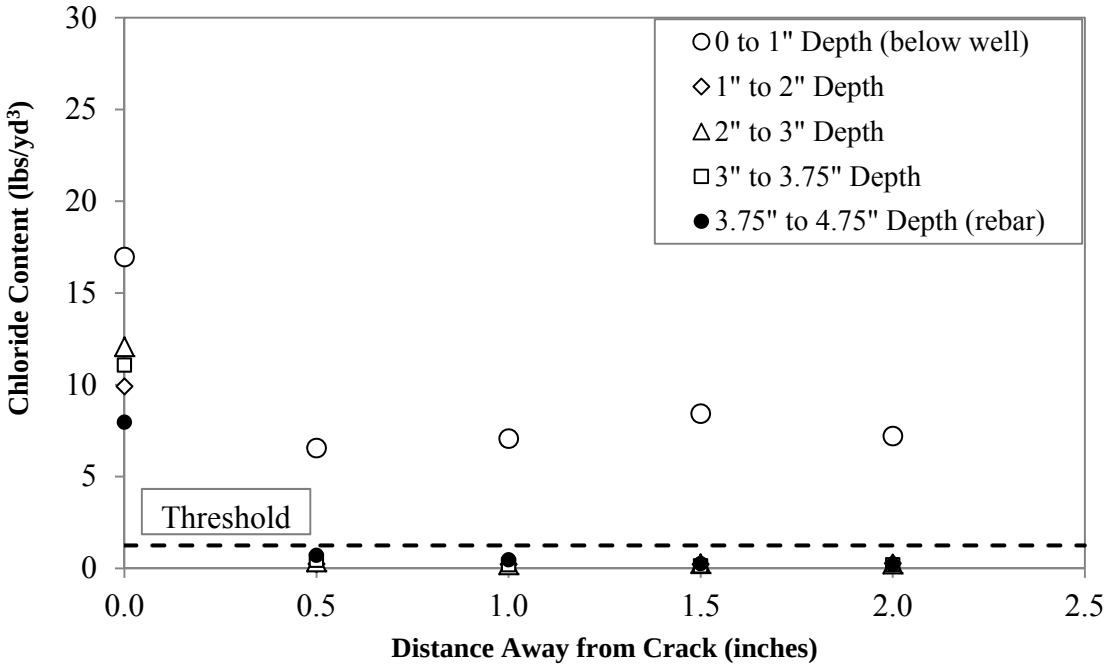

Figure 6-72: Chloride profiles for Ferrogard 903

Figure 6-73 through Figure 6-75 show the results for the SEM testing of Specimen 7. Figure 6-73 is an optical image showing localized corrosion. The white rectangle shown in Figure 6-73 is the area that was further analyzed to produce the BSE image and the elemental maps of oxygen, iron, and chloride shown in Figure 6-74. There was a thin layer of corrosion products around the entire reinforcement and some localized, pitting corrosion. A small concentration of chlorides can be seen near the edges of the pitting corrosion shown in Figure 6-74. Figure 6-75 shows the X-ray spectrum graph for Specimen 7 and the approximate element concentrations found at the indicated location of the reinforcement.

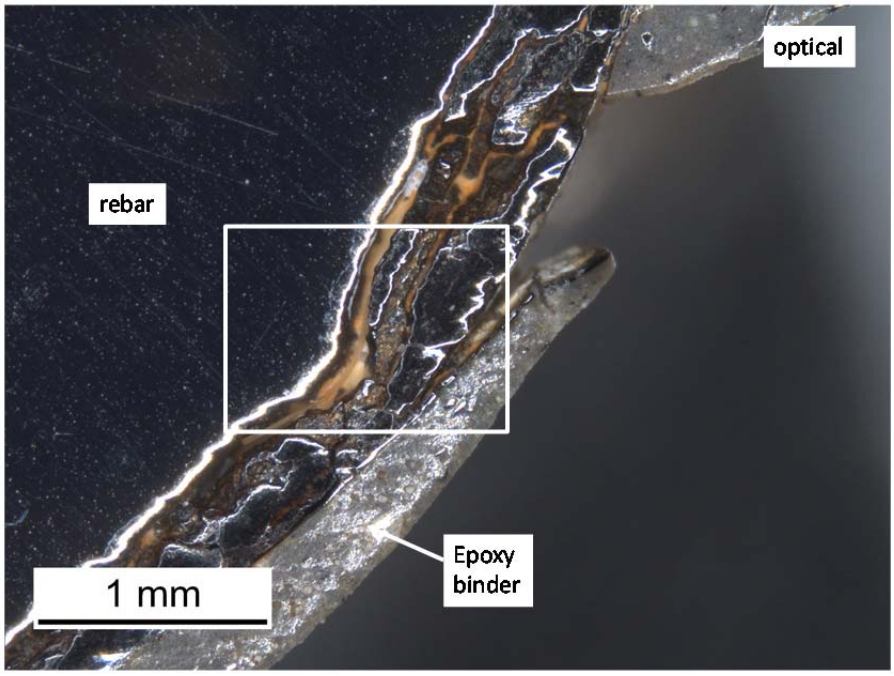

Figure 6-73: Optical image for Ferrogard 903

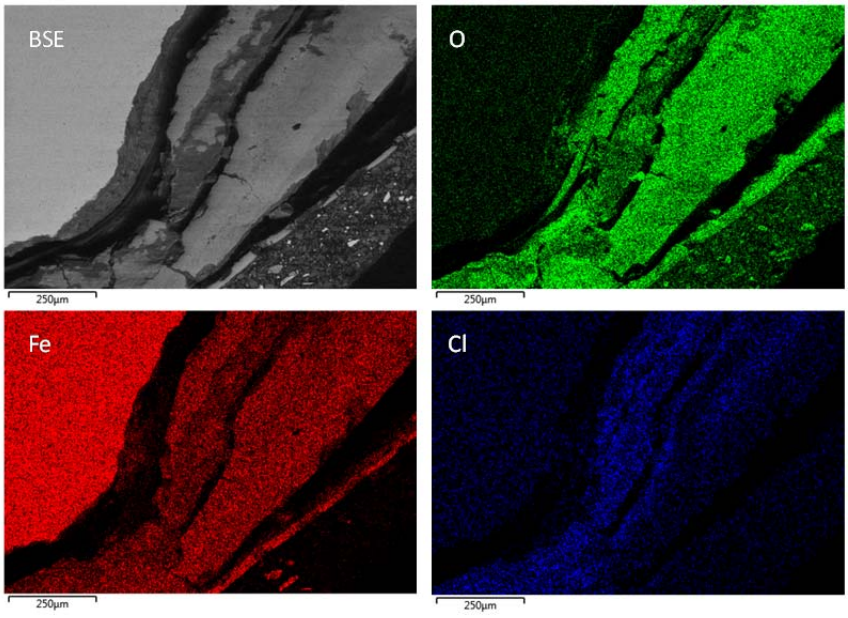

Figure 6-74: BSE image and element maps for Ferrogard 903

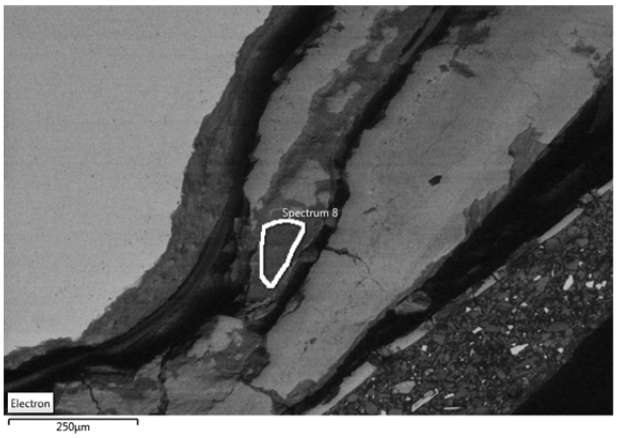

a. BSE image of where the reinforcement was analyzed

Element	Wt%	Oxide	Oxide %
O	25.84		
Na	0.00	Na2O	0.00
Mg	0.21	MgO	0.35
Al	5.08	Al2O3	9.60
Si	2.32	SiO2	4.97
S	0.12	SO3	0.29
Cl	2.50		0.00
K	0.00	K2O	0.00
Ca	0.43	CaO	0.60
Mn	0.27	MnO	0.34
Fe	63.24	FeO	81.35
Total:	100.00		97.50

b. Approximate element concentrations of the analyzed area

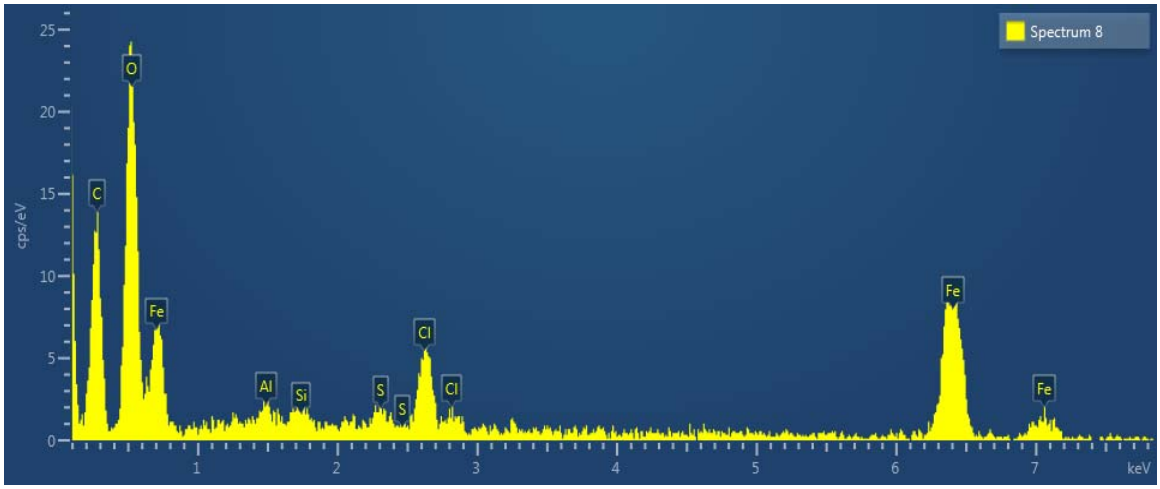

c. X-ray spectrum graph

Figure 6-75: Energy dispersive x-ray spectroscopy results for Ferrogard 903

6.3.2.5 Duralprep 3020

Figure 6-76 shows the timeline of product and chloride introduction superimposed on the half-cell potential measurements for Duralprep 3020, applied to Specimens 9 and 11. Specimens 9 and 11 were wet and dry cracked specimens, respectively. The half-cell potential measurements for Specimen 21, an uncracked specimen with salt in the mix, are shown in Figure 6-77.

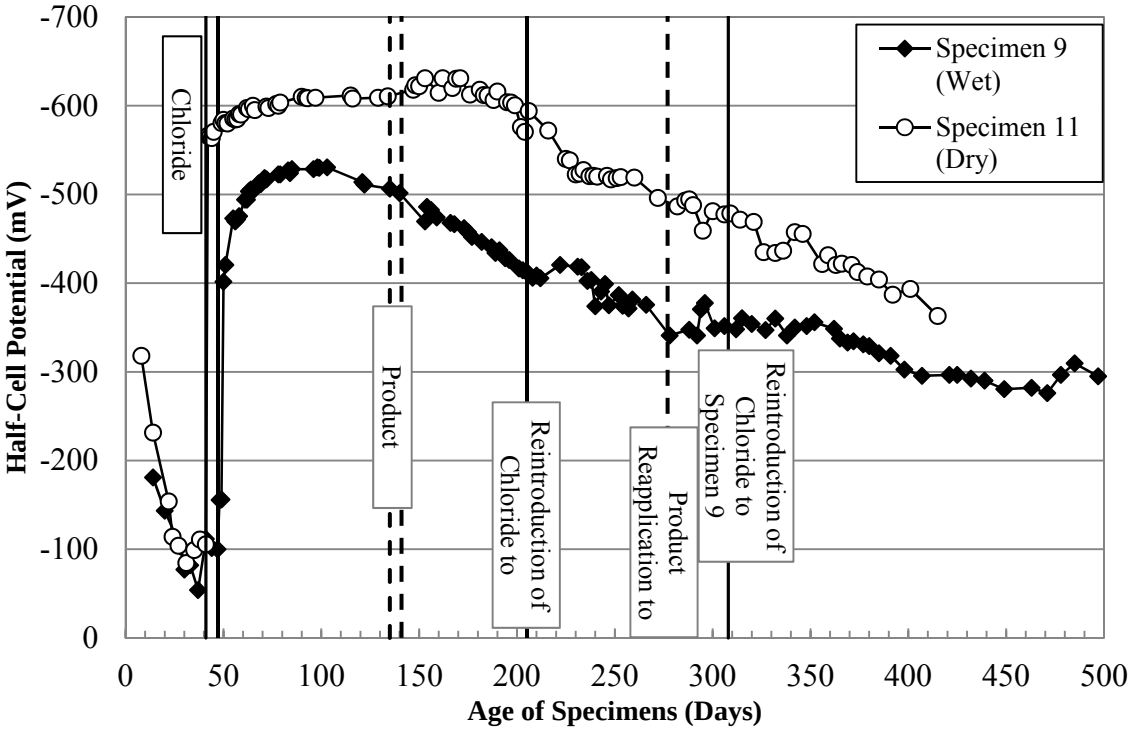

Figure 6-76: Half-cell potential measurements for Duralprep 3020, cracked specimens

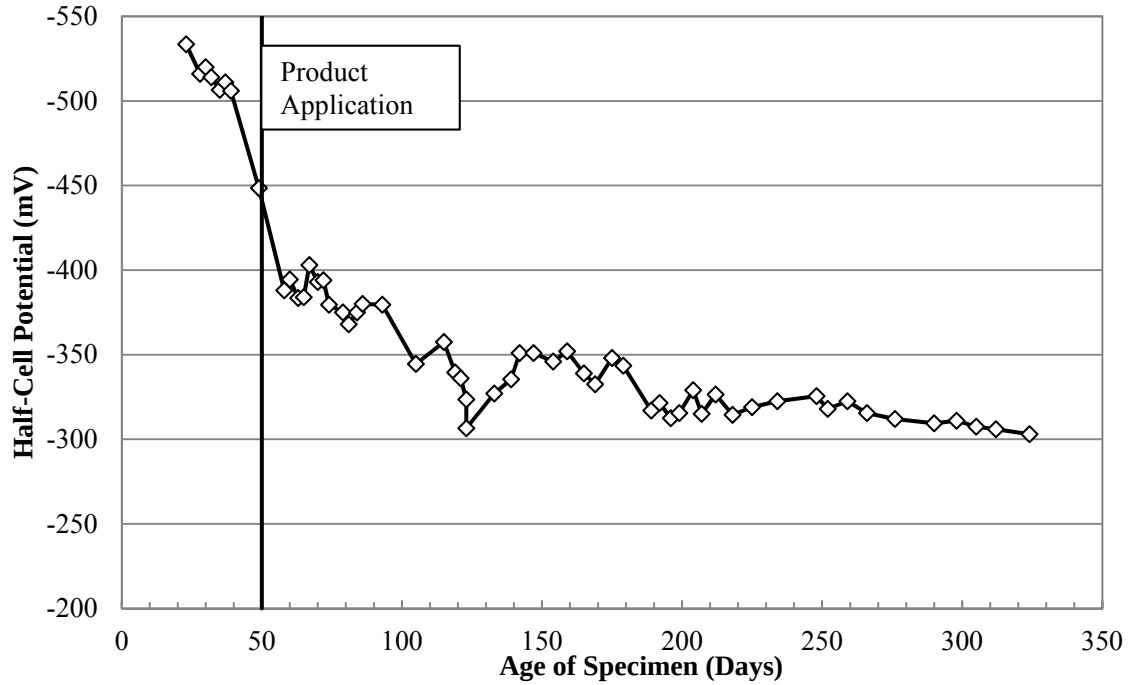

Figure 6-77: Half-cell potential measurements for Duralprep 3020, uncracked, salt in mix specimen

6.3.2.6 Chemtrete 40

Figure 6-78 shows the timeline of product and chloride introduction superimposed on the half-cell potential measurements for Chemtrete 40, applied to Specimens 12 and 13. Specimens 12 and 13 are wet and dry cracked specimens, respectively. The half-cell potential measurements for Specimen 22, an uncracked specimen with salt in the mix, are shown in Figure 6-79.

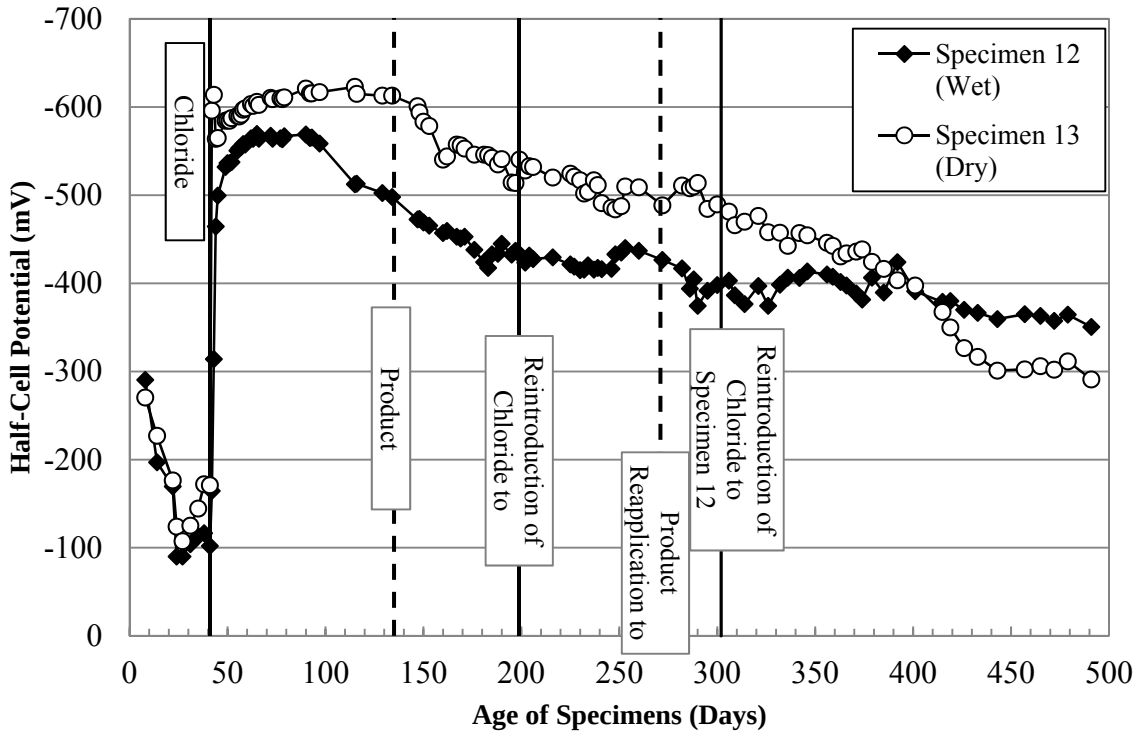

Figure 6-78: Half-cell potential measurements for Chemtrete 40, cracked specimens

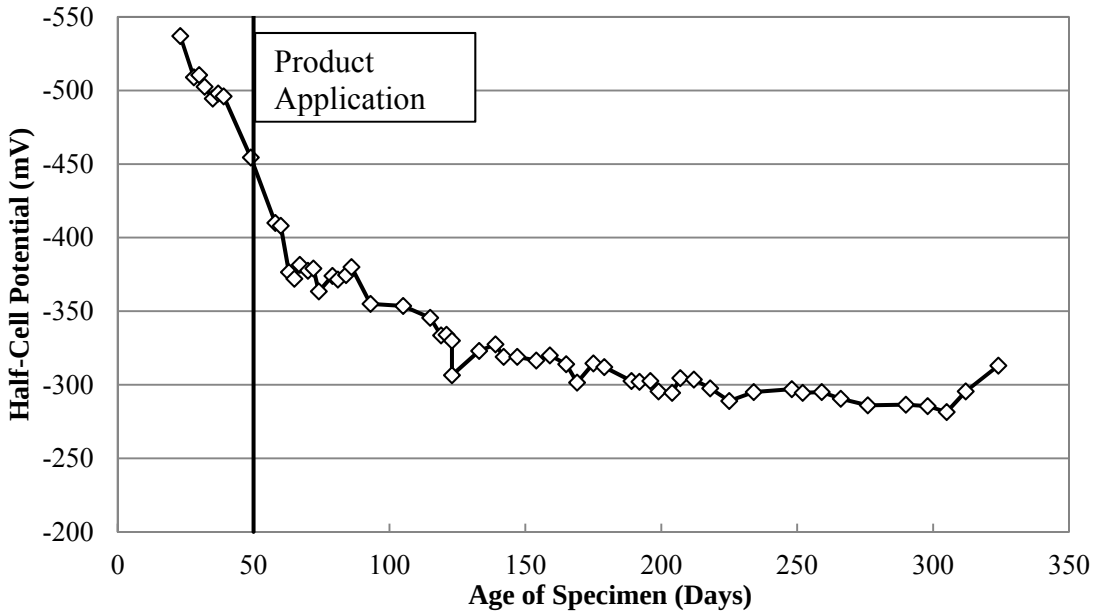

Figure 6-79: Half-cell potential measurements for Chemtrete 40, uncracked, salt in mix specimen

6.3.2.7 Control

The cracked control specimens with chlorides applied were Specimens 15 and 16 (wet) and Specimens 10 and 14 (dry). The half-cell potential measurements for those specimens are shown in Figure 6-80. The two uncracked control specimens without product application were Specimens 23 and 24. The half-cell potential measurements for these specimens are shown in Figure 6-81.

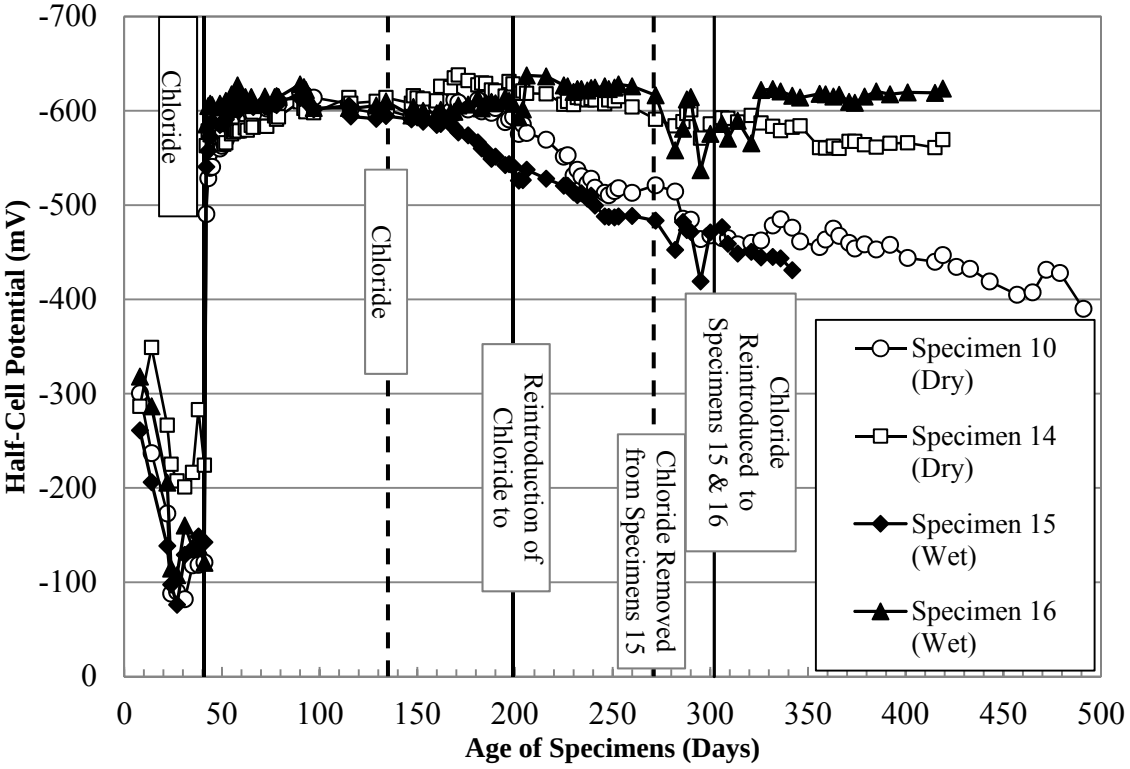

Figure 6-80: Half-cell potential measurements for cracked, control specimens

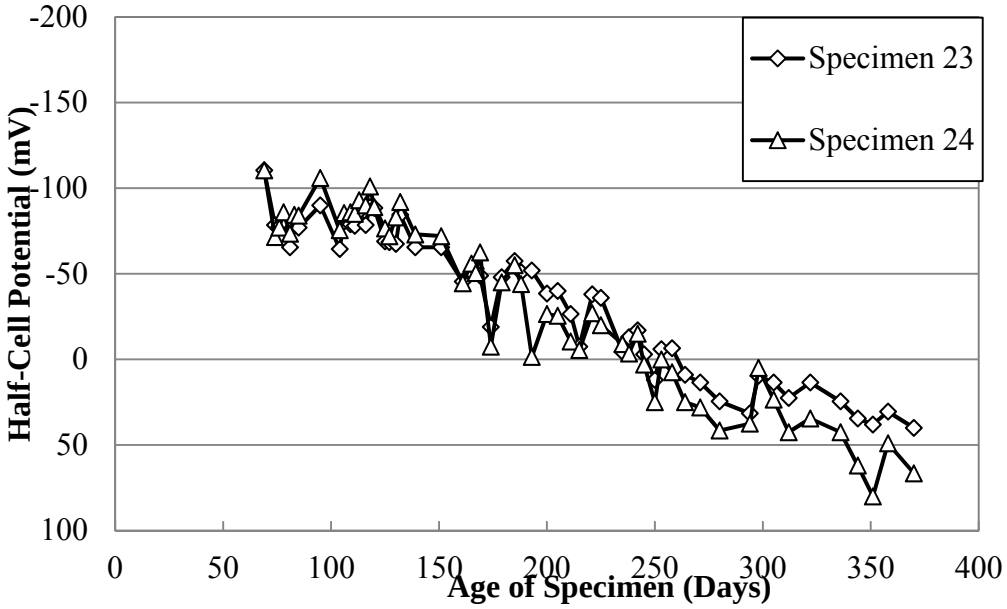

Figure 6-81: Half-cell potential measurements for uncracked, control specimens

Specimen 15 was one of the four specimens subjected to chloride ion concentration and SEM testing. Figure 6-82 shows the chloride profiles for each horizontal slice of the specimen. The depth of each slice was measured from the bottom of the well.

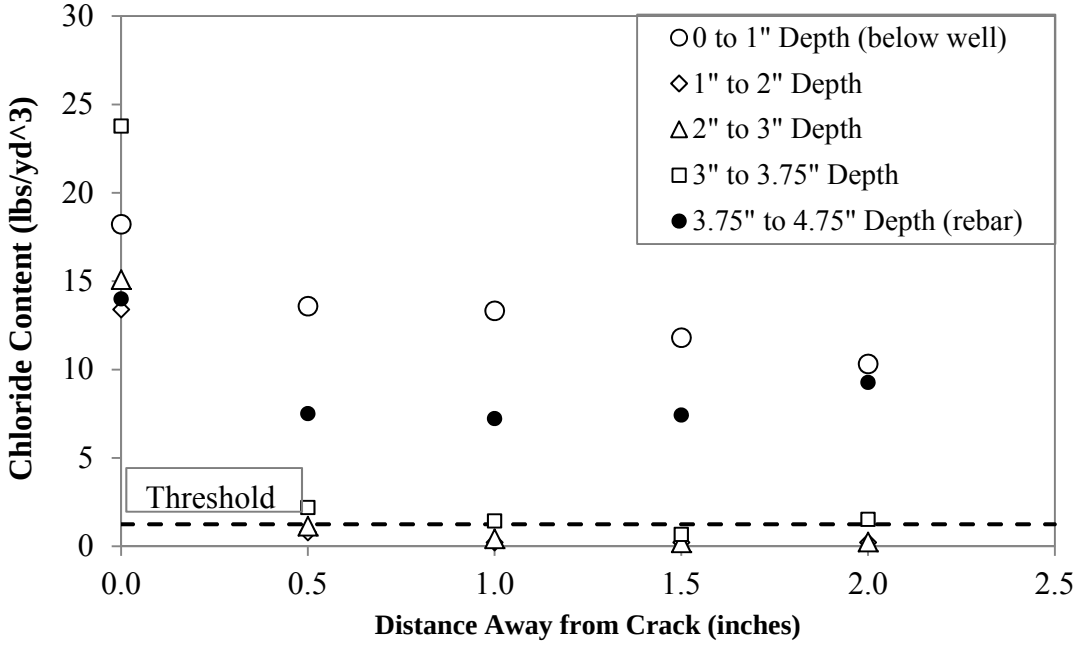

Figure 6-82: Chloride profiles for wet, cracked control specimen

Figure 6-83 through Figure 6-85 show the results for the SEM testing of Specimen 15. Figure 6-83 shows an optical image showing pitting corrosion. The white rectangle shown in Figure 6-83 is the area that was further analyzed to produce the BSE image and the elemental maps of oxygen, iron, and chloride shown in Figure 6-84. There was a thin layer of corrosion products around the entire reinforcement and some localized, pitting corrosion. A concentration of chlorides can be seen within the pitting corrosion shown

in Figure 6-84. Figure 6-85 shows the X-ray spectrum graph for Specimen 15 and the approximate element concentrations found at the indicated location of the reinforcement.

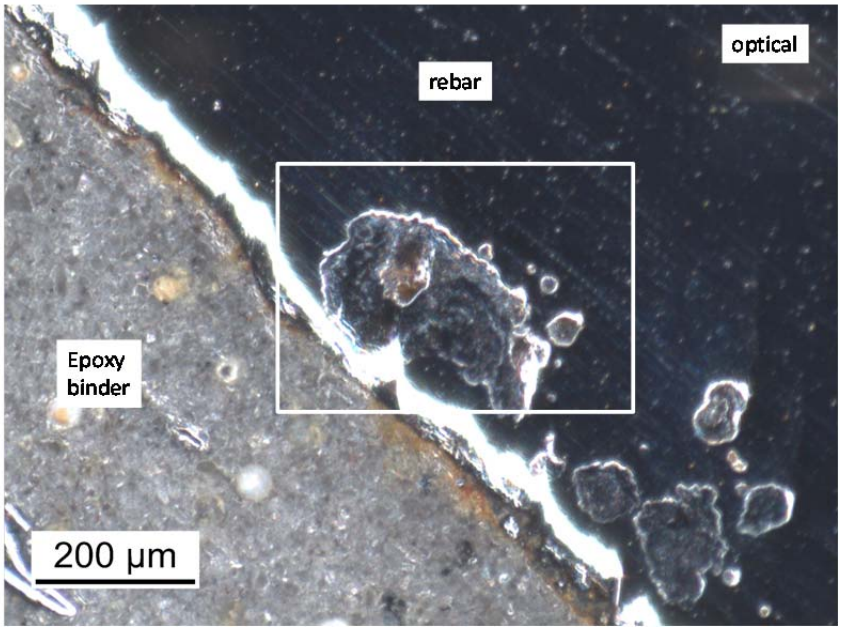

Figure 6-83: Optical image of wet, cracked control specimen

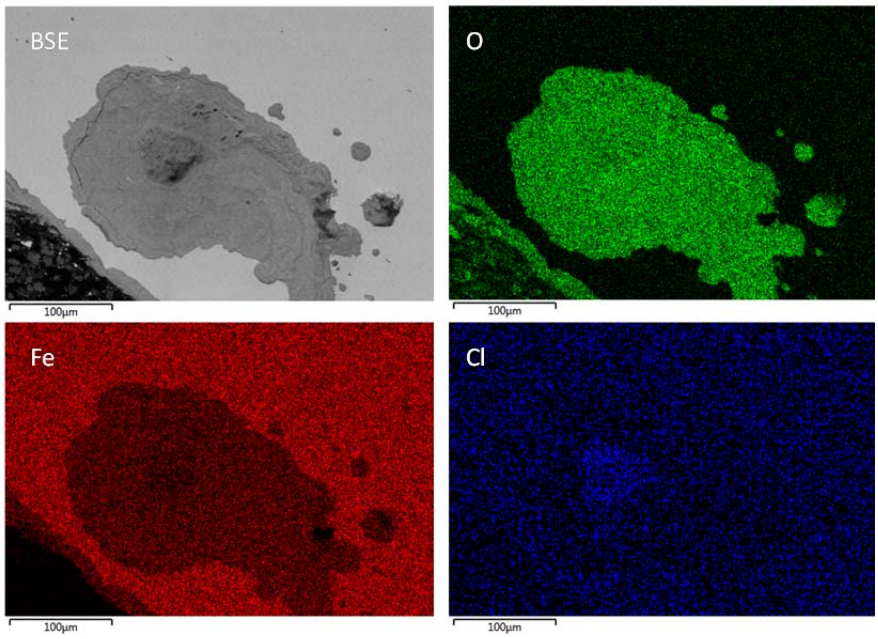

Figure 6-84: BSE and element maps for wet, cracked control specimen

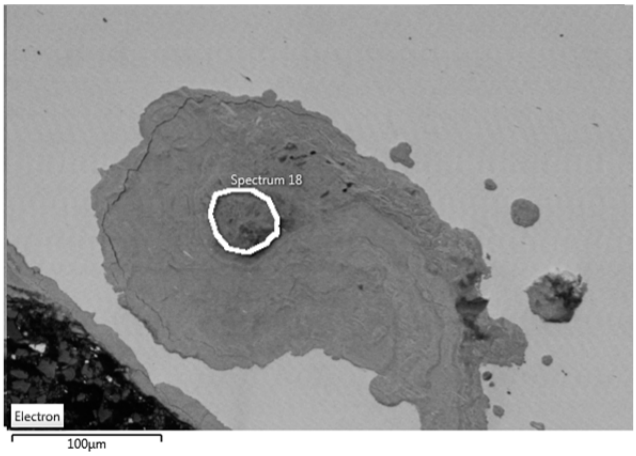

a. **BSE image of where the reinforcement was analyzed**

Element	Wt%	Oxide	Oxide %
O	25.84		
Na	0.00	Na2O	0.00
Mg	0.21	MgO	0.35
Al	5.08	Al2O3	9.60
Si	2.32	SiO2	4.97
S	0.12	SO3	0.29
Cl	2.50		0.00
K	0.00	K2O	0.00
Ca	0.43	CaO	0.60
Mn	0.27	MnO	0.34
Fe	63.24	FeO	81.35
Total:	100.00		97.50

b. **Approximate element concentrations of the analyzed area**

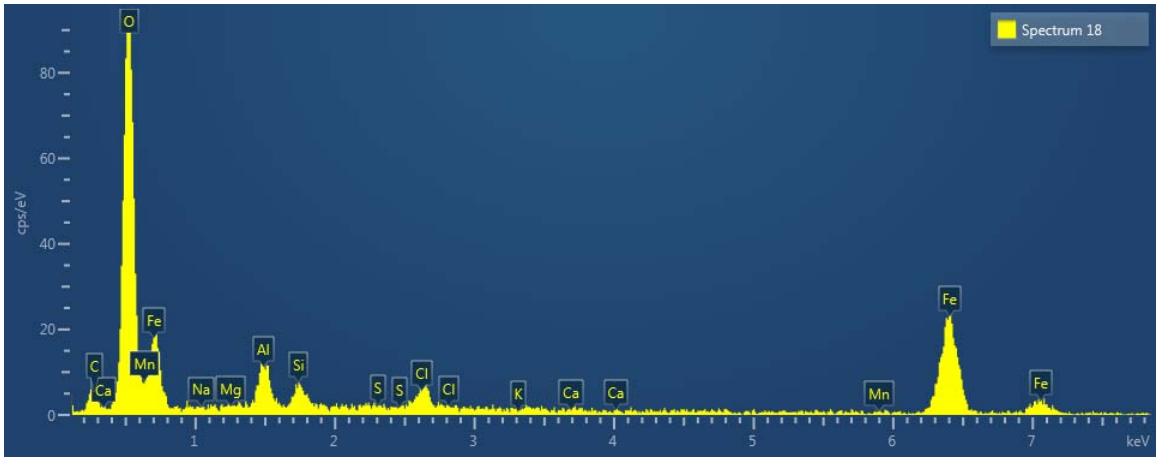

c. **X-ray spectrum graph**

Figure 6-85: Energy dispersive x-ray spectroscopy results for wet, cracked control

The reinforcement of Specimen 14 (dry, cracked specimen) and Specimen 16 (wet, cracked control specimen) was visually inspected after the half-cell potential testing was completed for these specimens. The purpose for the visual inspection was to determine if there was any visible difference between the observed levels of corrosion between the wet and the dry cracked specimens. It also allowed for an inspection of the reinforcement away from the simulated crack, and an inspection of the condition of the wire connections.

The specimen was cut in half along the simulated crack and the reinforcement from one of the halves was completely removed from the concrete. Figure 6-86 and Figure 6-87 show the reinforcement for Specimen 14. No corrosion was visible along the saw cut face, however the part of the reinforcement that was removed from the concrete did show slight surface oxidation (Figure 6-87). Also, no corrosion products were observed at the wire connection.

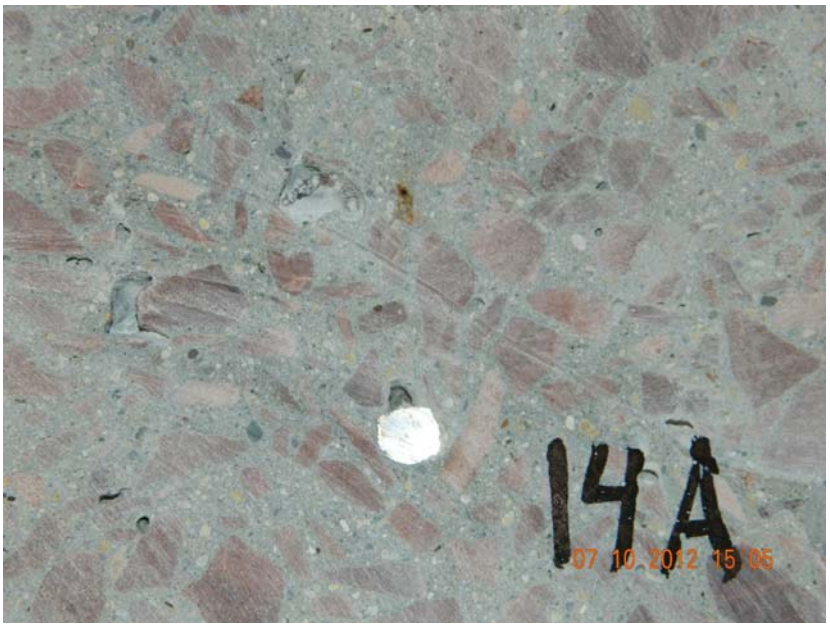

Figure 6-86: Saw cut along the crack of dry, cracked control specimen showing the reinforcement

Figure 6-87: Close-up of corrosion of dry, cracked control specimen

The reinforcement removed from Specimen 16 is shown in Figure 6-88 and Figure 6-89. Some staining of the concrete caused by corrosion was visible along the saw cut face, and an area of staining approximately one and a half inches long had formed near the crack as shown in Figure 6-89. This corrosion appears to have begun to deteriorate the ribs in the reinforcement, but the overall cross section loss of the bar was still negligible. A thin layer of corrosion products formed around the reinforcement near the wire connection, but there was no observable loss of material that would affect half-cell potential measurements.

Figure 6-88: Saw Cut along the simulated crack of Specimen 16

Figure 6-89: Close-up of corrosion of Specimen 16

7 ANALYTICAL STUDY

This chapter presents the discussion and analysis of the results obtained during this study. Analysis of the results from general observations, crack mapping, half-cell potential measurements, chloride ion analysis, and SEM testing of the initial CRCP evaluation, statewide evaluation of CRCP and mitigation product testing are discussed.

7.1 DISCUSSION OF RESULTS FROM INITIAL CRCP EVALUATION AND STATEWIDE EVALUATION

7.1.1 GENERAL OBSERVATIONS

Transverse and Y-cracking of CRCP was observed at the three test sites near Sioux Falls (I-29 MRM 68, I-29 MRM 87, and I-90 MRM 411). However, longitudinal cracking was observed at only two of the three sites (I-29 MRM 87 and I-29 MRM 411). The crack density at MRM 68 was also 68 percent and 83 percent lower than that which was recorded for sites MRM 87 and MRM 411, respectively. This likely results from MRM 68 being built in 2001, whereas MRM 87 was built in 1999 and MRM 411 was built in 1997. The newer pavement section has not been exposed to as much traffic or winter seasons as the other two sections. Also, the cover depth (5.5 inches) is greater than the other two sections (3.5 to 4.0 inches). This may have prevented additional cracking.

The cracks observed at the Sioux Falls sites were generally wider than those observed during the statewide evaluation. Also, two of the three sites near Sioux Falls had crack densities greater than 0.5 foot/square foot. Those same two sites exhibited longitudinal cracking. On the other hand, only one of the eight sites surveyed during the statewide evaluation had a crack density of greater than 0.5 foot/square foot, and no longitudinal cracks were observed in any of the sites included in the statewide evaluation. On average, the crack densities of the sites included in the statewide evaluation were 44 percent lower than the crack densities of the Sioux Falls sites. The increased crack densities observed on the Sioux Falls sites could make it easier for chlorides to reach the reinforcement. This could cause an increase in reinforcement corrosion.

The visual observations from Interstate 29 south of Brookings and the Interstate 90 repair site also showed signs of corrosion. Exposure of the embedded reinforcing bars revealed that corrosion occurred at crack locations or at locations of cold joints where patches were present in repaired CRCP. This type of corrosion was localized and varies in severity from rust stains to severe loss of the bar cross section. Recall that at some locations half of the cross section had been compromised. Away from the cracks and cold joints, no signs of localized corrosion were observed. Due to the corrosion observed, it is reasonable to conclude that cracks or other discontinuities in the concrete surface (i.e., patched locations) allowed chlorides to intrude at these locations and subsequently corrode the reinforcement.

The general observations imply that cracking is an issue when considering corrosion in the reinforcement of CRCP. Although it is theoretically possible for corrosion to instigate cracks in a reinforced concrete section, this is likely not the case in this study. Since no areas of localized corrosion were observed at non-distressed locations in the concrete, it is concluded that cracks preceded the corrosion that was visually observed.

7.1.2 CHLORIDE ION RESULTS

The chloride analysis of concrete cores and dust samples gives further evidence that a cracked section of CRCP is more susceptible to corrosion than an intact section. In general, the chloride content was above the chloride threshold within 1 inch of the surface of the pavement, and decreased to below the threshold below 1 inch in the pavement section. Analysis of the vertical chloride profiles of the dust samples showed that only 2 of the 28 composite dust samples had chloride ion concentration values above the threshold value of 1.244 lbs./yd^3 at a depth of three to four inches. Therefore, the reinforcement at these locations in the pavement was susceptible to corrosion initiation. The 2 chloride profiles that were at chloride ion concentrations above the chloride threshold were dust samples 1 and 2 at MRM 25. Table 7-1 displays the distance to the crack from these dust sample locations. It should be recognized that both of these chloride profiles show an increase in chloride content with depth. The main reason for this trend is that the dust sample was immediately adjacent to a crack below the pavement surface or intersected the crack.

Table 7-1: Distance to crack from dust samples with high chloride contents

Dust Sample	Distance to crack from dust sample (inches)	Chloride concentration (lbs./yd^3)	
		Depth=3.25 inches	Depth=3.75 inches
MRM 246 Dust Sample 1	3	1.74	1.89
MRM 246 Dust Sample 2	1	1.79	1.87

The lateral chloride profiles accomplished via core slicing showed another trend in the chloride data. The chloride content exceeded the threshold near a crack location and decreased away from the crack in all but one core slice tested. Also, the chloride concentration was above the threshold within the first 0.5 inch of the crack in all but two of the lateral chloride profiles. Furthermore, the core slice closest to the reinforcement of cores MRM 87 and MRM 68 (corresponding to core MRM 87-3 at 3.5 inches and core MRM 68-3 at 4.5 inches, respectively) showed chloride concentrations above the threshold for the first full inch away from the crack. This shows that the chloride concentration in the pavement section will only reach the threshold concentration deep in the section if it is near a crack, even though the concrete above this sample has not reached the chloride threshold.

7.1.3 SEM RESULTS

Corrosion was detected in one of the four reinforcement samples from the cores analyzed using SEM. The sample containing the corroded reinforcement, core MRM 411-1, exhibited corrosion at crack locations. Recall that approximately 6.0% of the cross-section had deteriorated. Since several cracks intersected this reinforcement location and corrosion was evident at these crack locations, it is likely that chlorides intruded through these cracks. The absence of corrosion in the reinforcement of the other two cracked cores that were tested indicates that a section of pavement can be cracked but the reinforcement may not be corroded.

Recall that the local delamination was observed in some of the cores. Chlorides could have penetrated in the delaminated surface and initiate the corrosion process. Also, the fact that no corrosion or chlorides were present in the reinforcement of the uncracked core samples indicates that chlorides did not penetrate

through the concrete matrix to reach the reinforcement and initiate corrosion. Finally, if corrosion of the reinforcement was caused by chlorides entering through the concrete matrix, one would have expected to find elevated chloride contents at the steel/concrete interface.

It was difficult to draw further, definite conclusions regarding the presence of corrosion in CRCP statewide from these analyses since only four reinforcement samples were tested using SEM methods. The limited SEM results showed that corrosion did not occur at every cracked location in the CRCP surface, but it was possible for chlorides to intrude through cracks and discontinuities in the pavement to cause corrosion.

7.1.4 ANALYZING THE HALF-CELL POTENTIAL USING THE NUMERIC MAGNITUDE TECHNIQUE

Recall from Chapter 2 that there are two methods used to interpret the results obtained from the half-cell test: numeric magnitude technique and potential difference technique. The numeric magnitude technique assigns potential value ranges to indicate the probability of corrosion, and these ranges were shown in Table 4-2. When the potential difference technique is used, the high potential values are simply compared to low potential values in order to determine areas that may be susceptible to corrosion.

The cumulative frequency distributions of the half-cell potential measurements of all sites surveyed were shown in the previous chapter, along with a table of percentage of measurements that fell within the different probability ranges suggested by ASTM C876. These results showed that the measurements obtained at all sites indicate a high probability of corrosion or that the corrosion activity is uncertain using the ASTM C876 numeric magnitude technique guidelines (ASTM 2009). These results caused the research team to question the validity of the corrosion probability ranges of the numeric magnitude technique. Therefore, a brief literature review was conducted in order to determine if the numeric magnitude technique was valid for this study. This review is presented subsequently.

There are several factors that influence half-cell potential measurements, including concrete resistance, moisture content, oxygen concentration at the steel interface, and concrete cover depth (Gu & Beaudoin 1998, Elsener 2003). First, the resistance of the concrete itself must be much lower than the internal resistor of the voltmeter being used in order to obtain accurate results with the half-cell test (Gu & Beaudoin 1998). The voltmeter was the Elcometer device in this study. The resistance of the concrete was effectively lowered and half-cell measurements stabilized by placing a presoaked sponge between the pavement surface and the probe's tip and spraying the concrete surface.

Elsener (2003) has shown that although water must be used to lower the resistivity of the concrete surface, it can cause a negative shift in half-cell potential values. For example, Elsener reported a negative shift of approximately 100 mV on the same bridge deck when measured after rainfall as opposed to before. Since there is a difference of only 150 mV between the range of high probability of corrosion and low probability of corrosion using the numeric magnitude technique, the interpretation technique should be used cautiously when water is used during the test. Also, the results in this study showed a negative shift in half-cell potential values between the fall and spring measurements. The cause of this shift may have been the weather conditions. It had rained within an hour of obtaining the spring half-cell potential measurements at all three Sioux Falls sites. However, the exact cause of this shift is unknown.

Low oxygen concentration at the steel interface may also cause the half-cell potential values to drop significantly (Gu & Beaudoin 1998). Low oxygen concentration can be caused by reinforcement under a dense concrete cover with low permeability. If the numeric magnitude technique is used when

interpreting half-cell data obtained from a site with low oxygen concentration, high negative half-cell values could be a misleading indicator that corrosion is occurring.

Elsener (2003) has also shown that with increasing concrete cover depths, the half-cell potential values can become more positive. Figure 7-1 shows that for varying cover depths, the half-cell potential measurements can vary significantly. Note that the difference between a cover depth of 10 mm and 20 mm (less than 1/2 in.) directly above a corroded bar, causes a potential shift of approximately 100 mV towards positive. This provides further evidence that the numeric magnitude technique should be used cautiously.

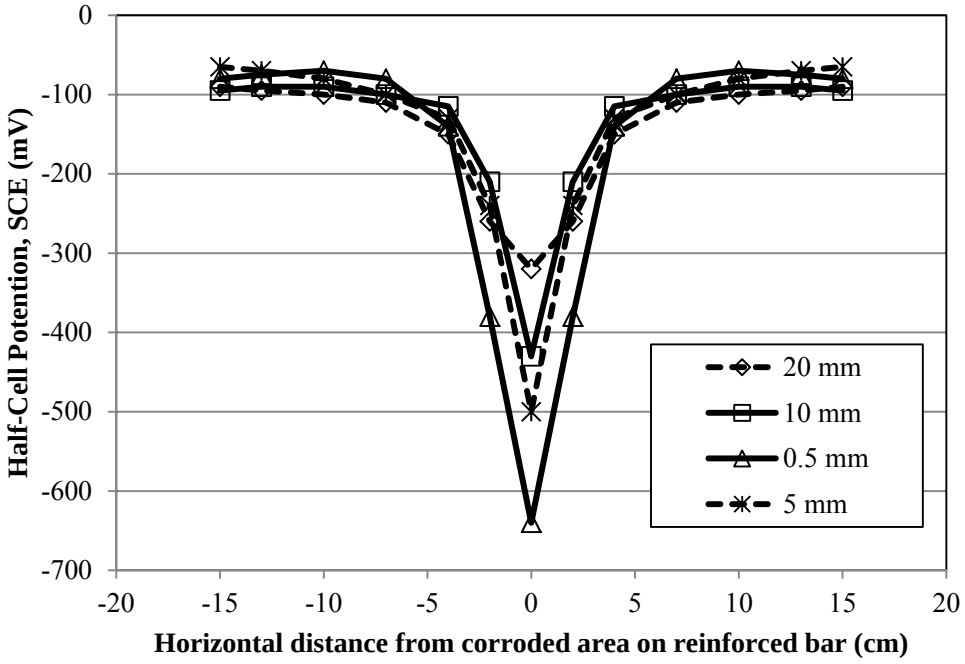

Figure 7-1: Influence of cover depth on half-cell potential measurements (after Elsener 2003)

It is also important to note that much of the research performed on the half-cell technique was based on results from structural surveys (bridge decks, bridge columns, and buildings). The ranges of values presented in ASTM C876 were based on laboratory and field research on these types of structures. It is not clear from the literature that this research also applies to reinforced pavement on a soil subgrade. This is important because the cover depths observed in this study ranged from three to over five inches, as opposed to buildings and bridges which have cover depths generally in the range of one to three inches.

7.1.5 ANALYZING THE HALF-CELL POTENTIAL USING THE POTENTIAL DIFFERENCE TECHNIQUE

Due to the inability to accurately quantify the effects of the factors previously discussed on the half-cell potential values, the numeric magnitude technique was regarded as an inappropriate method to evaluate the sites for corrosion. The analysis of the values using the potential difference technique was then considered. With this technique, the half-cell values are used to evaluate the relative difference between values to identify areas of elevated half-cell measurements. This was accomplished by constructing equipotential contour maps. Once the maps were created, areas of relative high and low half-cell potential could easily be identified. The areas with more negative half-cell potential values likely indicate

areas of higher potential of corrosion. Since concrete resistance, moisture content, oxygen concentration at the steel interface, and concrete cover depth were likely consistent over the length of pavement within the same site, these variables will have a reduced effect on the interpretation of the half-cell results. Therefore, it was deemed more appropriate to determine areas that have a high potential of corrosion.

Equipotential contour maps for all sites measured are presented in Appendix B. The most negative, or elevated, half-cell potential measurements indicate areas of high corrosion potential, and may be identified on the maps. This is helpful when determining areas within a site that could potentially be considered for repair work (such as a full-depth removal and patch). However, it is important to note that it is not possible to compare the extent of corrosion of one site to another using this method. Due to the findings in the literature and examination of the evaluation methods of ASTM C876, the half-cell measurements collected could not reliably be used to identify corrosion on their own. A more detailed analysis was necessary, and this is discussed subsequently.

7.1.6 FURTHER HALF-CELL POTENTIAL ANALYSIS

Although the numeric magnitude and potential difference techniques were not considered reliable for this study, the half-cell potential values were still used to draw conclusions about corrosion. Two additional analyses were considered to evaluate the half-cell potential data. These attempts included assigning modified ranges of half-cell potential values to indicate corrosion probability and correlating half-cell potential values to crack density.

7.1.6.1 Modified Ranges to Predict Corrosion Probability

The numeric magnitude technique assigns ranges of half-cell values that indicate a low, unknown, or high probability of corrosion. The goal of this first analysis was to determine appropriate values for those ranges for each site based on the half-cell potential data collected during this study. Half-cell potential measurements can decrease by approximately 150 mV or more at the onset of the corrosion process. Therefore, one could assume that the data points at which corrosion has initiated could be observed by evaluating the frequency distribution at a site. The points at which corrosion has initiated should be outliers towards the negative end of the distribution. For example, Figure 7-2 shows the frequency distribution of the half-cell measurements obtained at MRM 87. There is one value that is between -460 mV and -470 mV. This would be considered a negative outlier for this analysis. The values between -420 mV and -460 mV could also be considered negative outliers. Therefore, one could assign all data points with half-cell potential values between -420 mV and -470 mV to the “high probability of corrosion” range.

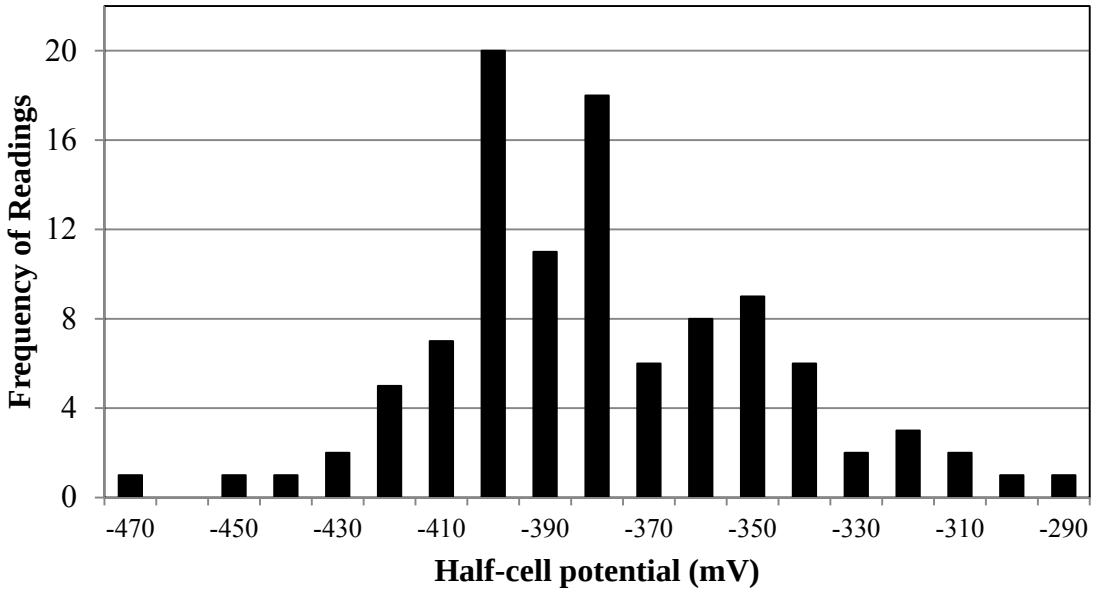

Figure 7-2: Frequency distribution of half-cell measurements at MRM 87

The same process could be completed with the "low probability of corrosion" range. The values more positive than -330 mV in Figure 7-2 could be considered to be outliers toward the positive end of the distribution. The data points that are more positive than -330 mV would therefore be considered to be in the "low probability of corrosion" range. Table 7-2 summarizes this initial analysis.

Table 7-2: Modified corrosion probability ranges for MRM 87

Potential Measurement Range	Indication according to ASTM C-876	Percent of Data Points in Range
> -330 mV	90% probability that no reinforcing steel is corroding	8.6%
Between -330 mV and -420 mV	Corrosion activity is uncertain	86.6%
< -420 mV	Greater than 90% probability steel is corroding	4.8%

This analysis could be completed for all of the sites surveyed. Subsequently, the percentage of points from each site that fell within each potential measurement range could be compared. The site with the highest percentage of points in the high probability range would be considered the site that is most probable to have the elevated levels of corrosion.

Although this method of analysis may be straightforward for this site, one significant flaw was observed: many sites have different distributions, and determining the outliers would be difficult. The distribution of MRM 44 as shown in Figure 7-3 displays this. One observer may assign all values more negative than -530 mV to the "high probability of corrosion range", while another may assign all values more negative than -550 to that same range. Therefore, this type of analysis is highly subjective to the researcher. Consequently, the method of assigning modified ranges of half-cell potential values to indicate corrosion probability was not used.

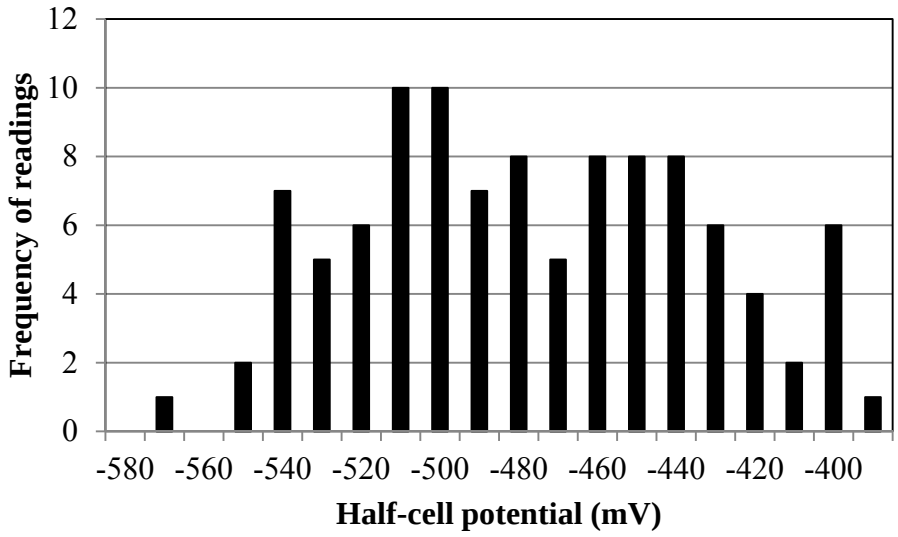

Figure 7-3: Frequency distributions of half-cell measurements at MRM 44

7.1.6.2 Correlating Half-Cell Potential Values to Crack Density

Since the previously discussed methods of evaluating half-cell potential measurements were considered unreliable for this study, correlations were made between the percentage of elevated half-cell measurements to the crack density of each individual pavement section surveyed. A percentage of the most negative half-cell measurements were considered to be elevated. In order to determine the percentage to be used in the final correlations, several values were tested, including 10, 20, and 30 percent of the most negative measurements at each site. After analyzing the data, the most negative 20 percent of the half-cell measurements recorded for each site were determined to have the most significant effect on crack density. Therefore, these values were considered elevated measurements.

Recall that the half-cell measurements were obtained at the gridline intersections of a four foot by four foot grid, and the cracks were mapped using this same grid resolution. A crack density value which corresponded to each (x, y) coordinate was determined by averaging the crack densities of the grid squares adjacent to the coordinate point at which the half-cell measurement was obtained.

By plotting the half-cell measurement against the crack density of each point for a specific site it was observed that there was a positive increase in the percentage of elevated half-cell measurements within a given crack density range as the crack density increased. This is shown in Figure 7-4 for site MRM 87.

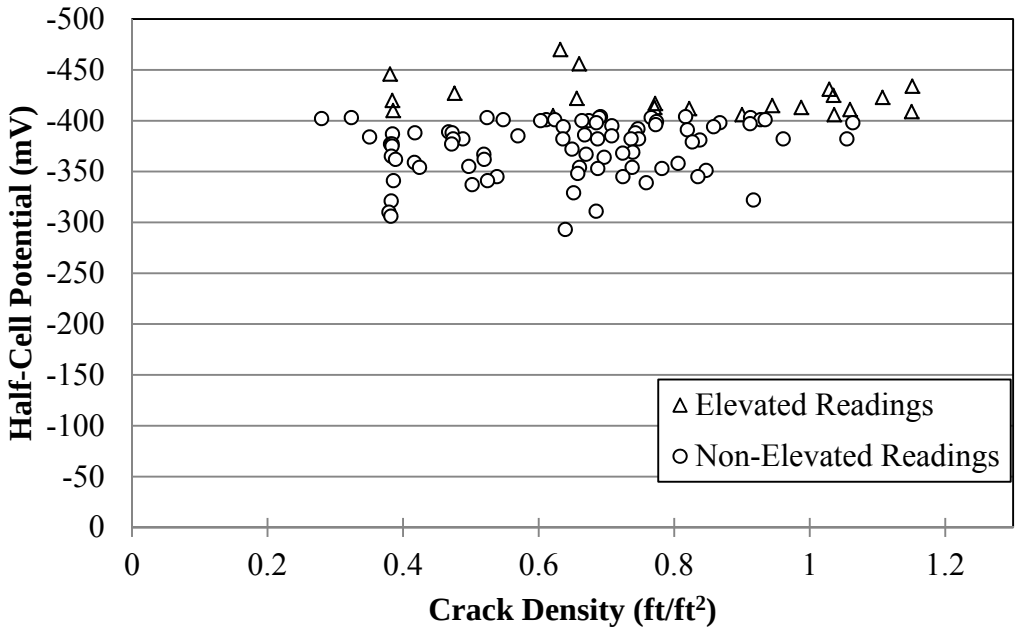

Figure 7-4: Example of half-cell potential measurements plotted against crack density values

Correlation models were established and tested in order to determine the significance of the relationship between crack density and half-cell potential measurements. The models were established by using the method of ordinary least squares. In this method, the sum of the squared distances between the actual data and the model estimate are minimized in order to determine the model that best fits the data. Correlation models were generated for each site using the general form of equation 5-1.

$$P = p_0 \times e^{rate \times cd} \quad \textbf{(Eqn. 7-1)}$$

Where:

P = Percent of elevated measurements

p_0 = Initial percent (parameter) of elevated measurements

rate = Rate of increase in percent of elevated measurements caused by crack density (parameter)

cd = Crack density

The null hypothesis, H_0, and alternative hypothesis, H_1, were as follows:

H_0: parameter (p_0 or rate) = 0

H_1: parameter (p_0 or rate) ≠ 0

The parameters of the established models were evaluated using the t-test statistic. Probability values (p-value) for each t-test statistic were determined based on the degrees of freedom. The significance ranges for this analysis is outlined in Table 7-3.

Table 7-3: Significance levels for parameter estimates

Significance Level	P-value
Very significant	<0.01
Moderately significant	0.01< p < 0.05
Significant	0.05 < p < 0.10
Insignificant	P > 0.10

The results of the correlations of the sites surveyed are summarized in Table 7-4. The table shows that all of the p-values indicate that the relationship between crack density and the p_0 parameter is insignificant. However, in this study the rate of the change in percent of elevated half-cell measurements (*rate*) was of more interest than the intercept of the equation (p_0) since the goal was to determine if there was a correlation, as opposed to determine a model equation to relate half-cell potential to crack density. The *rate* parameter was considered significant, moderately significant, or very significant at 8 of 11 CRCP sites surveyed. At 7 of these 8 sites, the correlation between crack density and elevated half-cell potential measurements was positive. This indicates that there was an increase in elevated half-cell measurements with an increase in crack density. Also, 6 of the 7 sites that had significant, moderately significant, and very significant positive correlations had R^2 values above 0.70. Figure 7-5 through Figure 7-9 show the original data and the corresponding correlations.

Table 7-4: Summary of half-cell and crack density results

Site	p_0			*rate*			R^2
	Estimate	P-value	Level of Significance	Estimate	P-value	Level of Significance	
MRM 87	0.003	0.32	Insignificant	5.199	< 0.01	Very Significant	0.92
MRM 68	0.054	0.40	Insignificant	3.527	0.17	Insignificant	0.31
MRM 411	0.006	0.52	Insignificant	3.890	0.02	Moderately Significant	0.76
MRM 33	0.003	0.50	Insignificant	5.361	0.01	Very Significant	0.85
MRM 44	0.174	0.43	Insignificant	0.624	0.69	Insignificant	0.03
MRM 25	1.184	0.20	Insignificant	-4.799	0.07	Significant	0.39
MRM 54	0.116	0.30	Insignificant	2.422	0.31	Insignificant	0.11
MRM 222	0.023	0.49	Insignificant	5.797	0.09	Significant	0.57
MRM 246	0.018	0.29	Insignificant	6.182	< 0.01	Very Significant	0.75
MRM 168NB	0.028	0.15	Insignificant	4.249	0.00	Very Significant	0.70
MRM 168SB	0.007	0.19	Insignificant	8.529	0.00	Very Significant	0.93

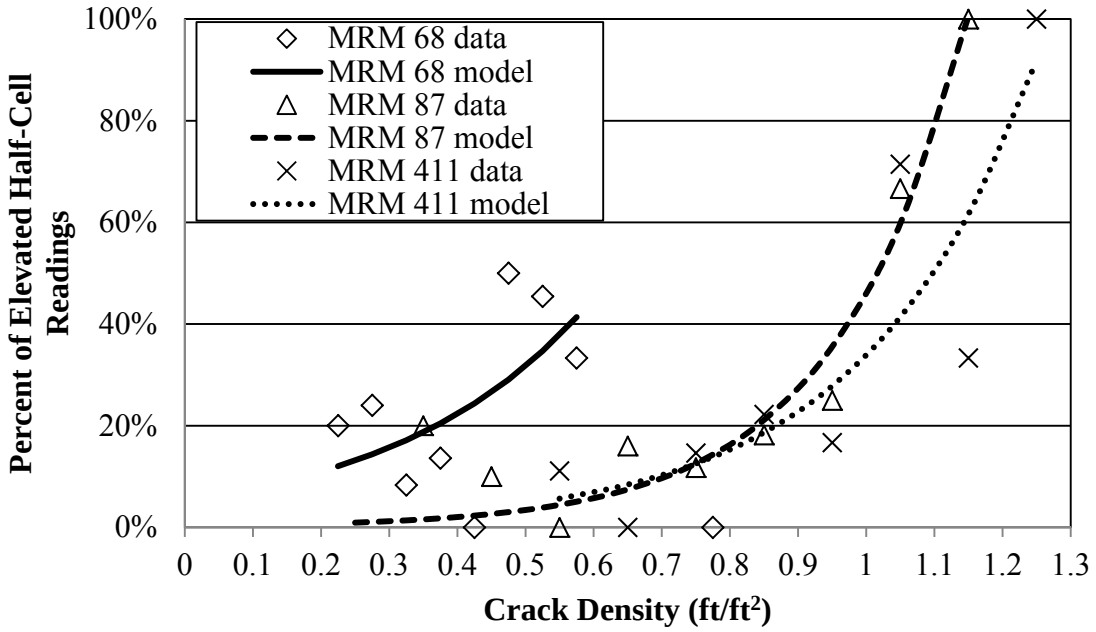

Figure 7-5: Correlation models for Sioux Falls sites

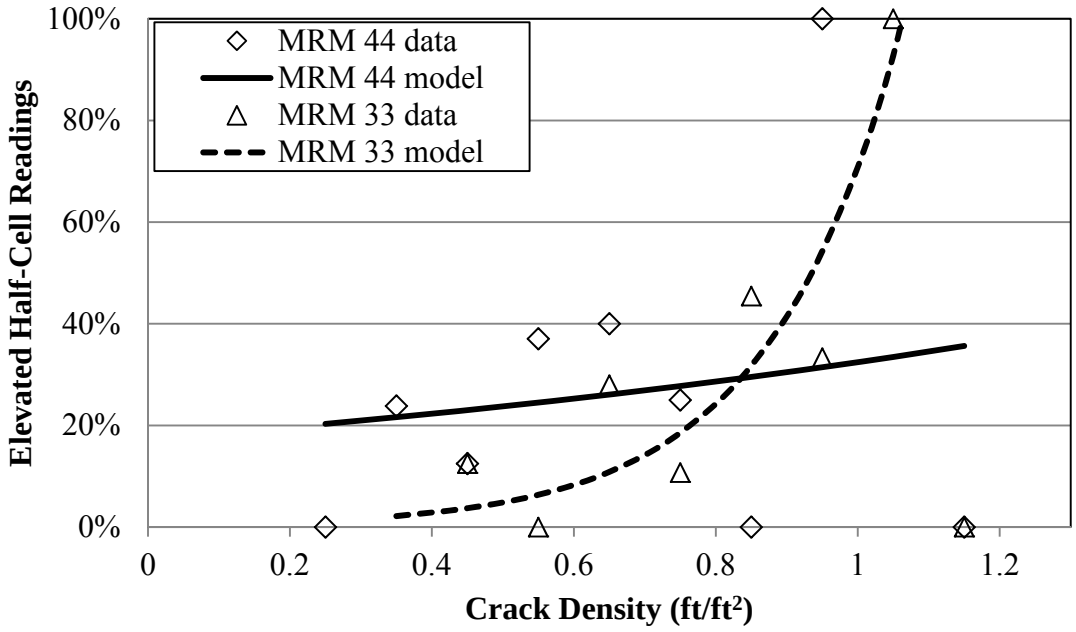

Figure 7-6: Correlation models for sites south of Sioux Falls on Interstate 29

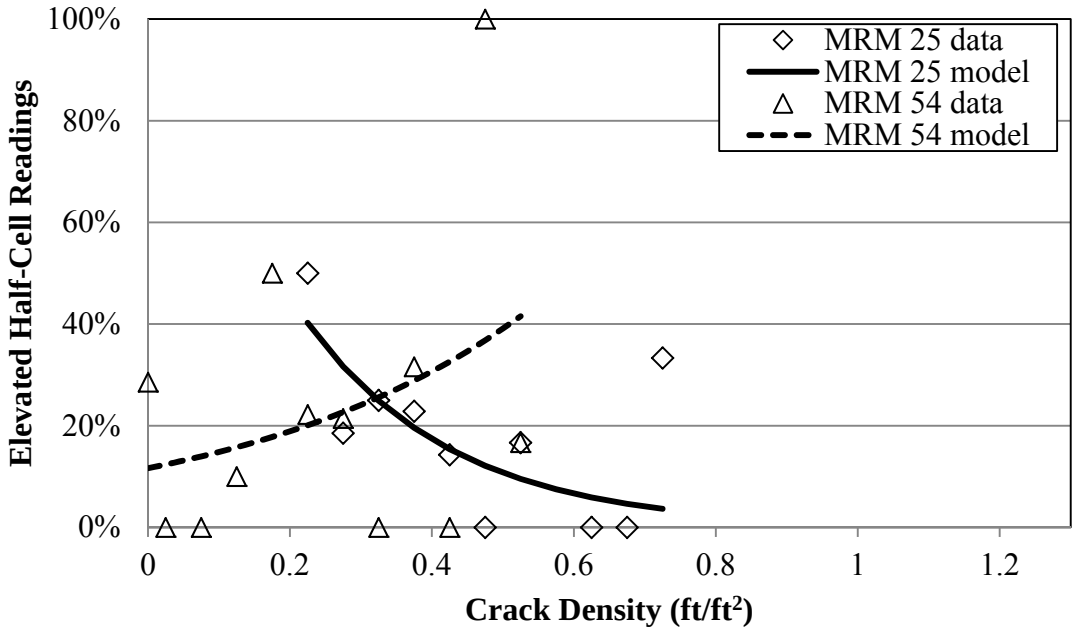

Figure 7-7: Correlation models for sites near Rapid City on Interstate 90

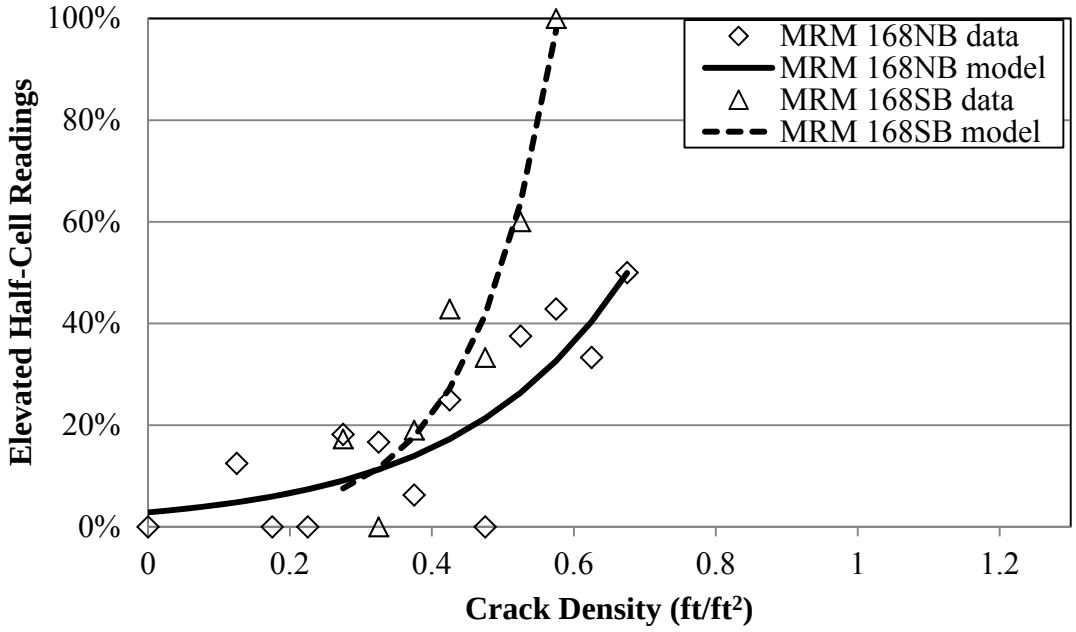

Figure 7-8: Correlation data for sites south of Watertown on Interstate 90

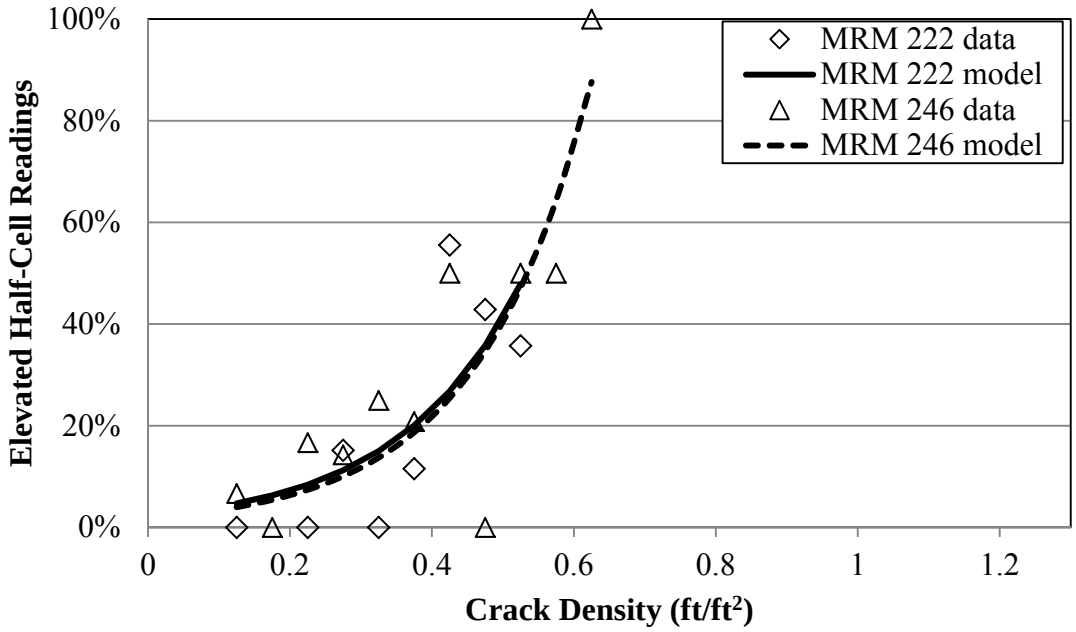

Figure 7-9: Correlation data for sites between Wall and Chamberlain on Interstate 90

7.1.7 EVALUATION OF THE SITE SELECTION MATRIX

Recall in section 5.2, a selection matrix was generated which ranked sites according to condition, age, precipitation, maintenance activities, and deicer application in order to select sites for the statewide evaluation. The complete matrix is shown in Appendix A. These factors were determined to have a direct impact on a CRCP section's susceptibility to corrosion. The matrix was evaluated to determine if it was a reliable tool to select eight CRCP sites for statewide evaluation. Three relationships were evaluated and will be discussed in this section: crack density versus deicer application amount, crack density versus age of pavement, and SCI versus deicer application rate. The data from all 11 sites surveyed were included in these analyses.

Polynomial, exponential, and linear models were evaluated for each relationship, and the model that best fit the data was determined. The best fit model for this study is defined as the model that had the highest p-values when correlating the dependent variable to the independent variable. The best fit model was linear for all relationships evaluated.

Table 7-5 presents the results from the three correlations evaluated. For the crack density versus deicer relationship, the deicer rate was defined as the rate at which the crack density increased as the deicer application amount increased. The age rate was defined as the rate at which the crack density increased as the age increased. For the SCI versus deicer relationship, the deicer rate was defined as the rate at which the SCI increased as the deicer amount increased.

Table 7-5: Statewide evaluation site selection matrix correlation results

Correlation Evaluated	Parameter Evaluated	Parameter Estimate	P-value	R^2
Crack density vs. deicer	*Deicer rate*	5.87×10^{-7}	0.08	0.30
Crack density vs. age	*Age rate*	0.0395	0.02	0.42
SCI vs. deicer	*Deicer rate*	-1.09×10^{-6}	0.07	0.32

The p-values were significant at the 0.10 significance level for the 3 relationships evaluated. The crack density increased significantly with an increase in deicer amount and age. The SCI decreased significantly with an increase in deicer amount. However, the coefficients of variation were below 0.50 in all cases. Therefore, the linear trends do not explain the variability in the data effectively. Figure 7-10 through Figure 7-12 present the data and model estimates.

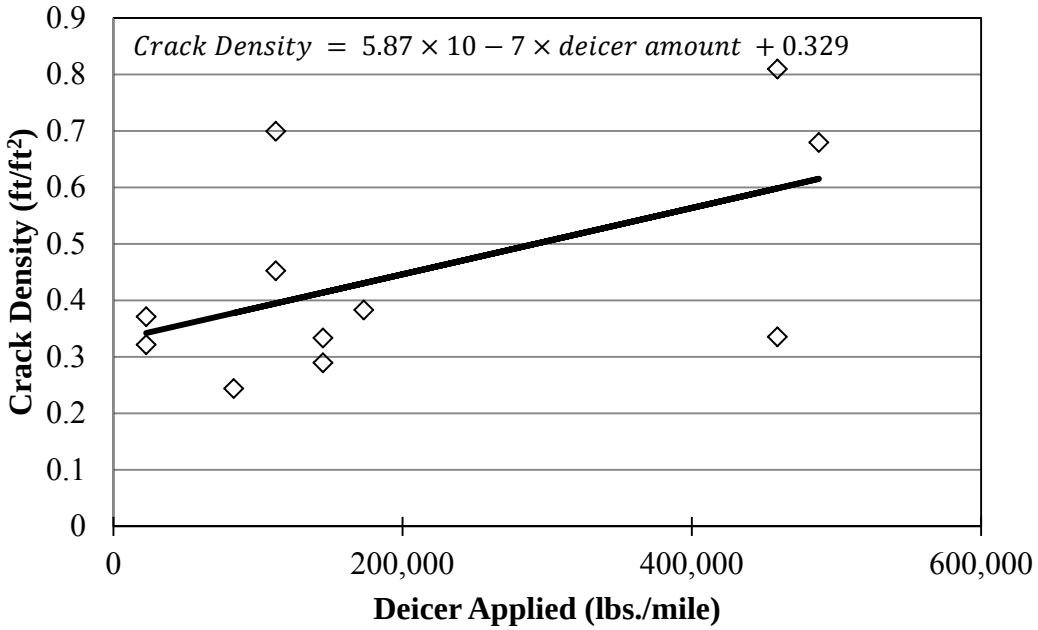

Figure 7-10: Crack density versus deicer applied for all sites surveyed

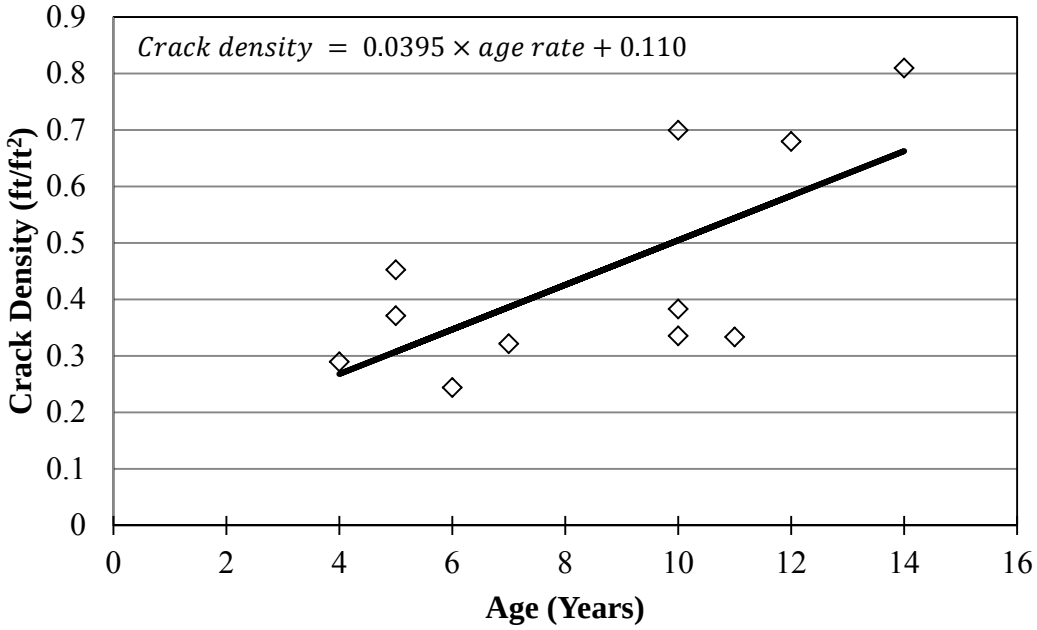

Figure 7-11: Crack density versus age of all sites surveyed

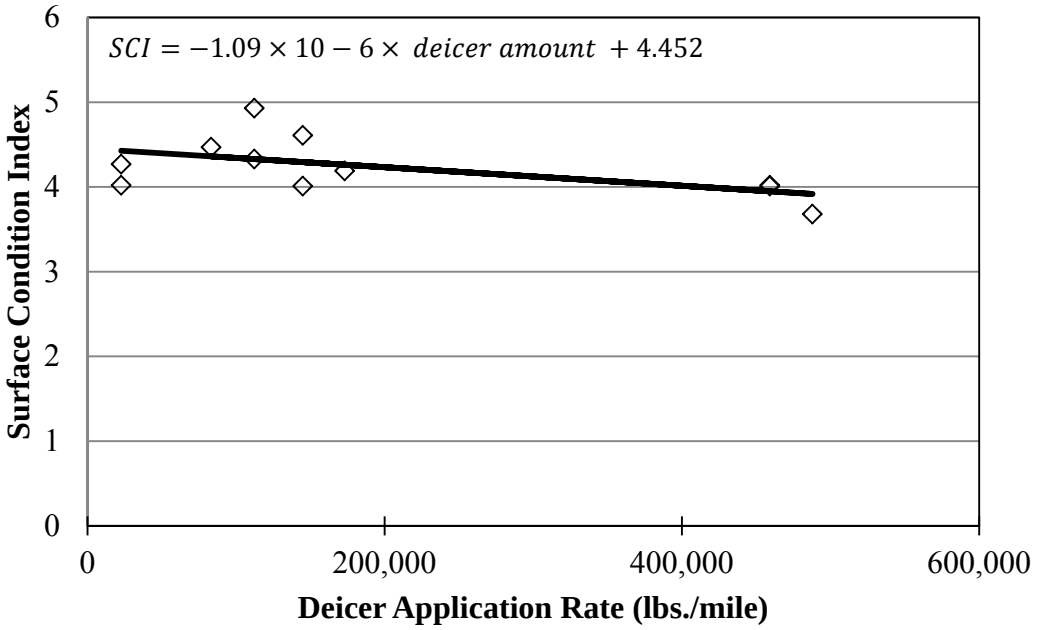

Figure 7-12: Surface condition index versus deicer application rate (all sites)

After analyzing crack density versus deicer application rate, crack density versus age, and SCI versus deicer application rate, the site selection matrix was deemed to be an appropriate means to select eight sites statewide for corrosion evaluation. Although the trend lines developed during the statistical analysis have low coefficient of determination values, the p-values showed that deicer application rates and age significantly affect the pavement condition (explained by crack density and SCI). Since the results presented earlier in this chapter have shown that qualitative pavement condition has a direct impact on the

level of corrosion in CRCP pavement, the site selection matrix was deemed appropriate to select the eight sites.

7.2 DISCUSSION OF TESTING RESULTS FROM MITIGATION PRODUCTS

7.2.1 FIELD TESTING RESULTS

Starting in the summer of 2011, the test site was evaluated and separated into test sections for the testing of topically applied corrosion mitigation products as discussed in Chapter 5. Figure 7-13 shows the average half-cell potentials for each of the test sections as a function of time. The set of average measurements on day zero on the graph, were obtained the day before the products were applied. The next two sets of measurements were obtained approximately one month apart after product application. The extended time interval with no measurements was during the winter months, and the final two sets of measurements were obtained one month apart after the temperatures were sufficiently warm to obtain measurements. The overall trend for every section was to alternate relatively more positive and more negative measurements. Figure 7-14 shows the overall change from the initial average measurements for each section from an initial normalized value of zero, and Figure 7-15 shows the overall change for each section from an initial normalized value of zero with the normalized control section measurements subtracted from each section. Figure 7-16 shows the difference in average half-cell potential from one measurement event to the next.

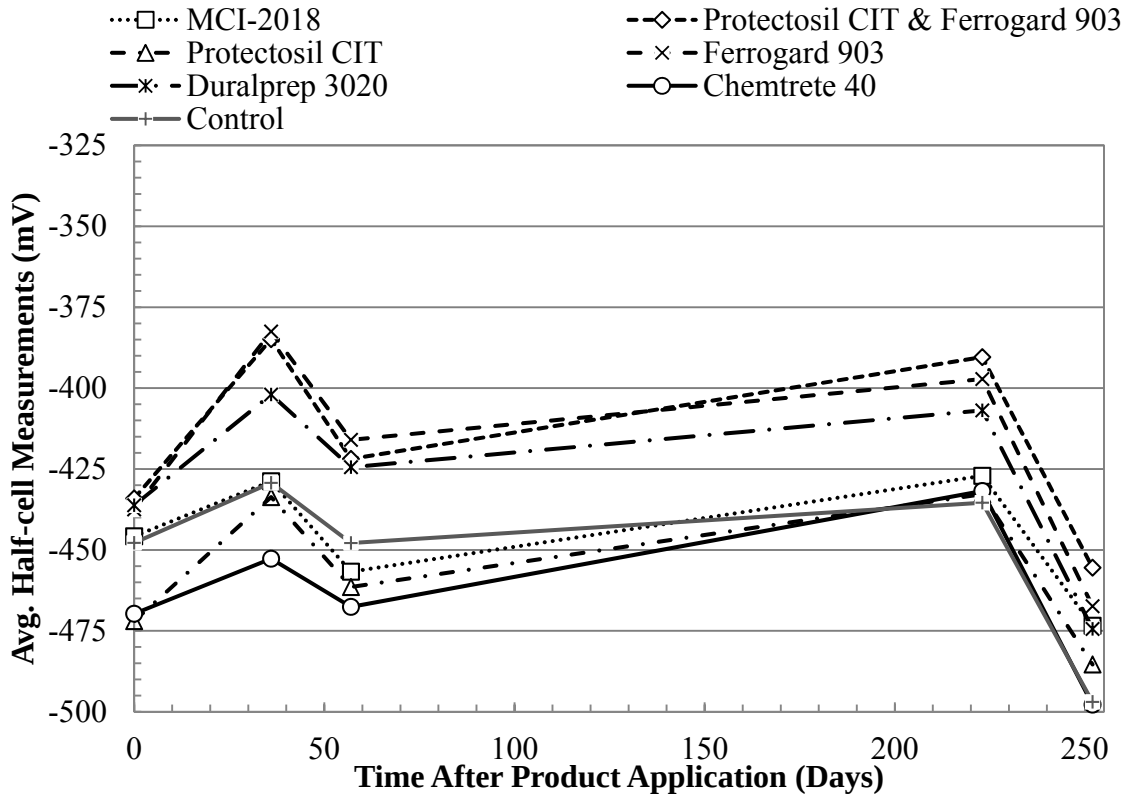

Figure 7-13: Average half-cell measurements for each section vs. time

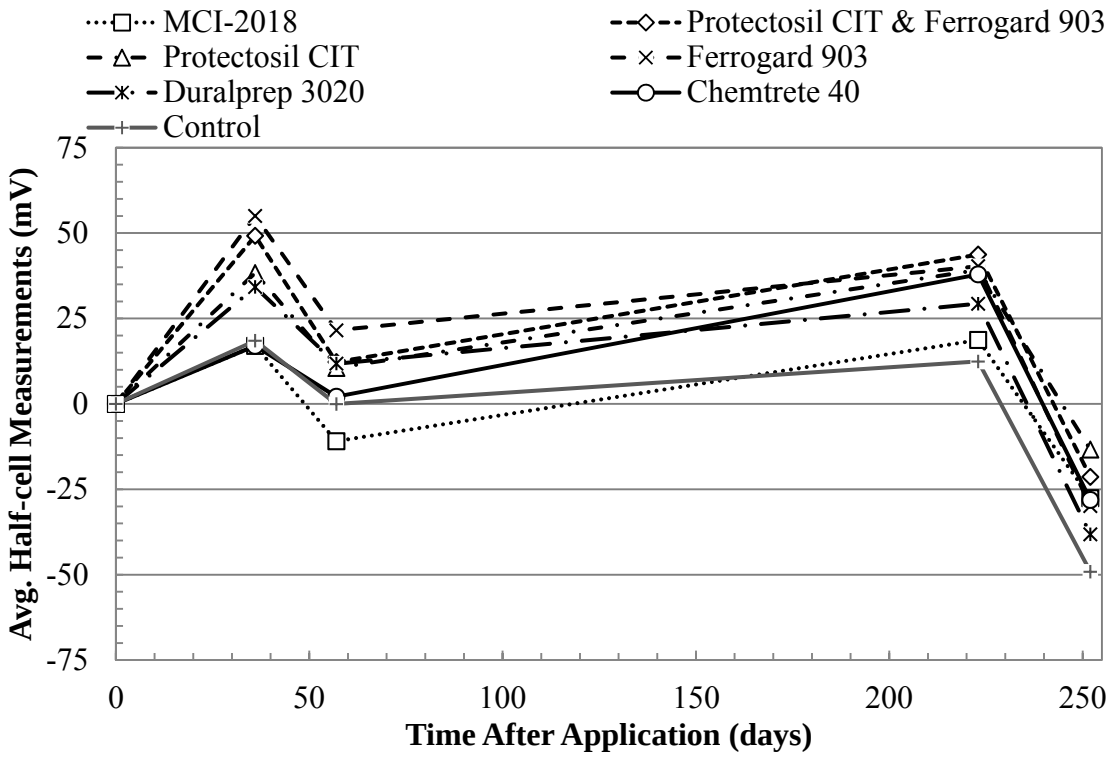

Figure 7-14: Relative change in half-cell measurements vs. time

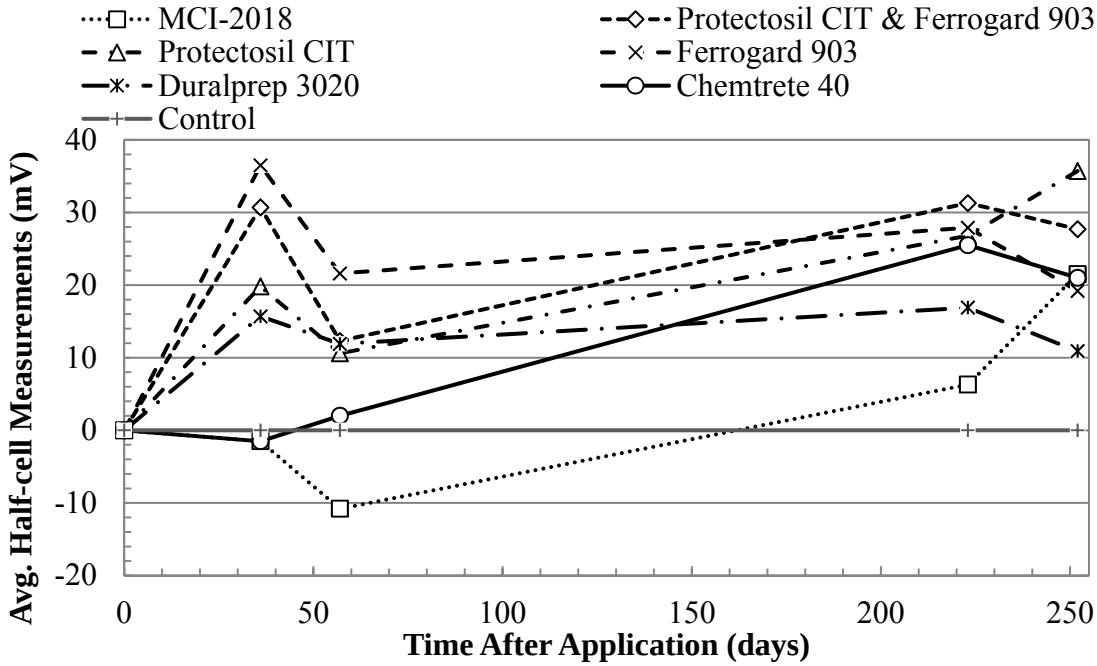

Figure 7-15: Relative change in half-cell measurements vs. time, normalized to control section

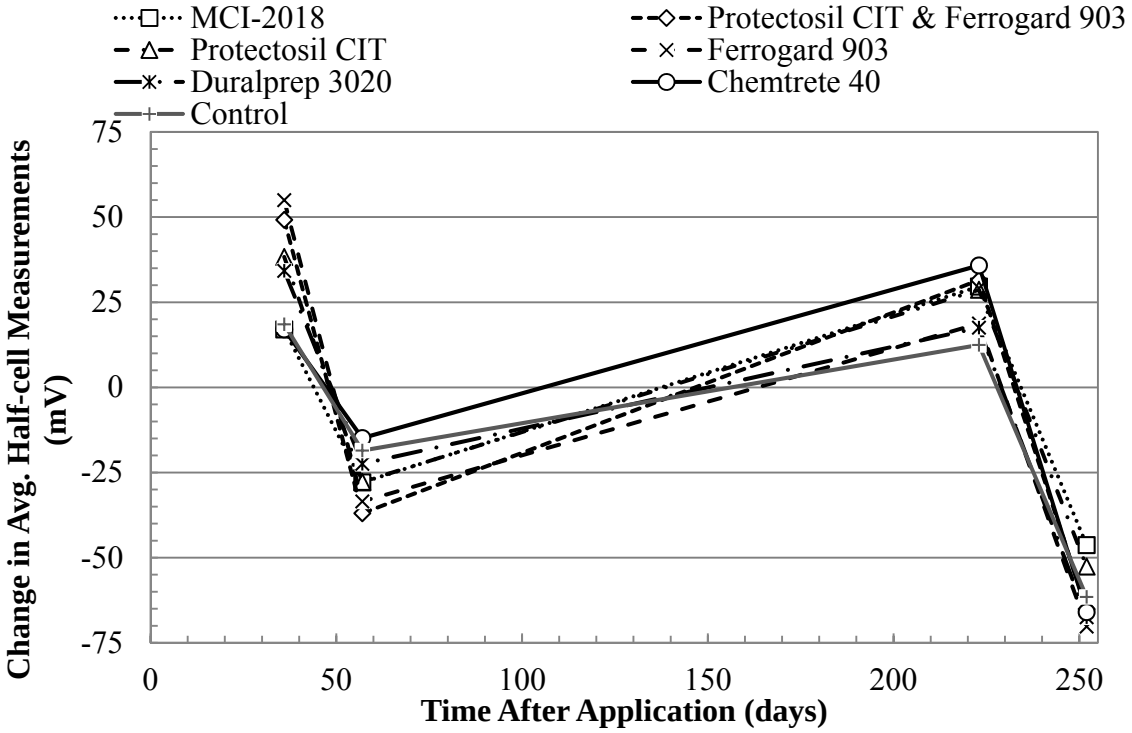

Figure 7-16: Relative change in half-cell measurements for each measurement event vs. time

7.2.2 HALF-CELL POTENTIAL USING THE NUMERIC MAGNITUDE TECHNIQUE – FIELD DATA

The average of each product section and the control section remained in the greater than 90 percent chance of corrosion range according to ASTM C876-09. Also, the majority of the points in each section remained in the high probability of corrosion range as shown by the cumulative distribution graphs in Figure 6-44 and Figure 6-49 through Figure 6-54, as well as the half-cell potential contour maps presented in Appendix E.

Figure 7-13, Figure 7-14, and Figure 7-16 show that average half-cell potential in the field tends to fluctuate up and down as a group. The control section also fluctuated in a similar manner as the product test sections, which shows that this fluctuation is not likely a primary effect of the corrosion mitigation products. According to Assouli, et al. (2008) and Elsener (2001 and 2003) these differences that occur throughout a section are due to differences in the environment such as the percent of moisture in the concrete, changes in temperature, or changes in chloride content. However, the temperature effect on the half-cell potential measurements was accounted for using the temperature correction coefficient from ASTM C876-09. The temperature coefficient of a copper-copper sulfate reference electrode is approximately 0.5 mV more negative per degree Fahrenheit for temperatures ranging from 32 to 120 degrees Fahrenheit (ASTM 2009). By using this coefficient, the bias caused by the differences in temperature was eliminated.

The environmental factor with the largest effect on half-cell potential is the moisture content of the concrete. The main factor affecting moisture content of the concrete in CRCP is rainfall. Elsener, et al. (2003) found that a bridge deck could experience a negative shift of up to 100 mV when comparing measurements obtained before a rainfall to measurements obtained after a rainfall. The negative shift in half-cell potential observed in this study may also have been caused by rainfall. During the week prior to

the last measurement obtained at the test site (May 9, 2012), the rainfall amounts were 0.3 inches on May 4, 2012, 0.02 inches on May 5, 2012, and 0.74 inches on May 6, 2012 (NOAA 2012). The weather was also cloudy and cool throughout the week prior to obtaining measurements which also potentially reduced the amount of evaporation which occurred after the rain. This rainfall likely resulted in increased moisture content in the concrete. The concrete also still appeared to be slightly damp along the cracks when the measurements were obtained. Because of the likely increased moisture content, the average half-cell potentials shifted to more negative values prior to the May 9, 2012 measurements than any of the previous measurements as shown in Figure 7-14. In comparison, no rain events occurred during the weeks prior to other field measurements.

As previously discussed, another factor that influences half-cell potential measurements is the depth of cover over the reinforcement. ASTM C876-09 states that concrete cover which is greater than three inches can result in the averaging of adjacent half-cell potentials. This can lead to more positive half-cell potential measurements at the location of the corrosion, but it also can cause larger areas to show slightly more negative half-cell measurements. This was shown previously in Figure 7-1. Because the cover for the tested pavement was greater than three inches, the deeper concrete cover may affect the magnitudes of the measured half-cell potentials.

Because of the fluctuations from measurement to measurement due to environmental changes, and also because the concrete cover is greater than three inches, the numeric magnitude method as specified by ASTM C876-09 does not appear to be valid for the analysis of the half-cell potential measurements obtained in the field.

7.2.3 HALF-CELL POTENTIAL USING THE POTENTIAL DIFFERENCE TECHNIQUE – FIELD DATA

The potential difference technique states that the most negative areas in each section are considered to be the corroding areas, and the magnitude of the variation indicates the probability of corrosion (ASTM 2009). The variations are shown by creating half-cell potential contour maps shown in Chapter 6 and Appendix E. Half-cell potential contour maps that show large variations in half-cell potential throughout the section indicate macrocell corrosion; this leads to localized corrosion at the location of the most negative locations on the map (ACI 2001). Analyzing the half-cell potentials with contour maps allows the areas of the CRCP with corrosion problems to be identified before the corrosion is evident at the surface. Also, the larger the differences in potentials are, the higher the probability of corrosion; however, no standard correlation between differences in half-cell potentials and the probability of corrosion has been established. Another negative aspect of the potential difference method is that it is not possible to determine the extent that corrosion has progressed but only to determine the areas with the highest probability of corrosion.

Because a half-cell potential contour map of a corroding pavement has large variances in half-cell potential, and a half-cell potential contour map of a non-corroding pavement has relatively small variations of half-cell potential throughout, a successful application of a corrosion mitigation product should either eliminate or greatly reduce the number of areas with more negative half-cell potentials. This would result in a more uniform contour map. This method of analysis was utilized by Elsener (2001), when analyzing bridge decks, and a reduction in areas with very negative potentials was observed with a corresponding positive shift in average half-cell potential after repairs. The contour maps, presented in Appendix E, did not have any observable reduction in variation after the products were applied. Based on this, none of the products tested where likely effective in the field.

Also, if the products were effective, a reduction in variation of the half-cell potentials throughout the test section would likely cause the tail at the negative end of the cumulative distribution plots to become much smaller. If the corrosion was completely stopped, the half-cell potentials should theoretically be uniform throughout the section and the cumulative frequency distribution would become a straight vertical line, but this is very unlikely due to variations in concrete properties and chloride concentrations throughout the section, and errors in the half-cell measurements. The greater the reduction in variation of half-cell potentials throughout the section the smaller the negative tail of the cumulative distribution will be. Therefore, a product would be considered effective if the negative tail of the cumulative frequency distribution is visibly reduced after the product was applied as shown in Figure 7-17, and for a very effective product the negative tail should be reduced to an almost straight line that extends from the approximately linear portion the cumulative frequency distribution.

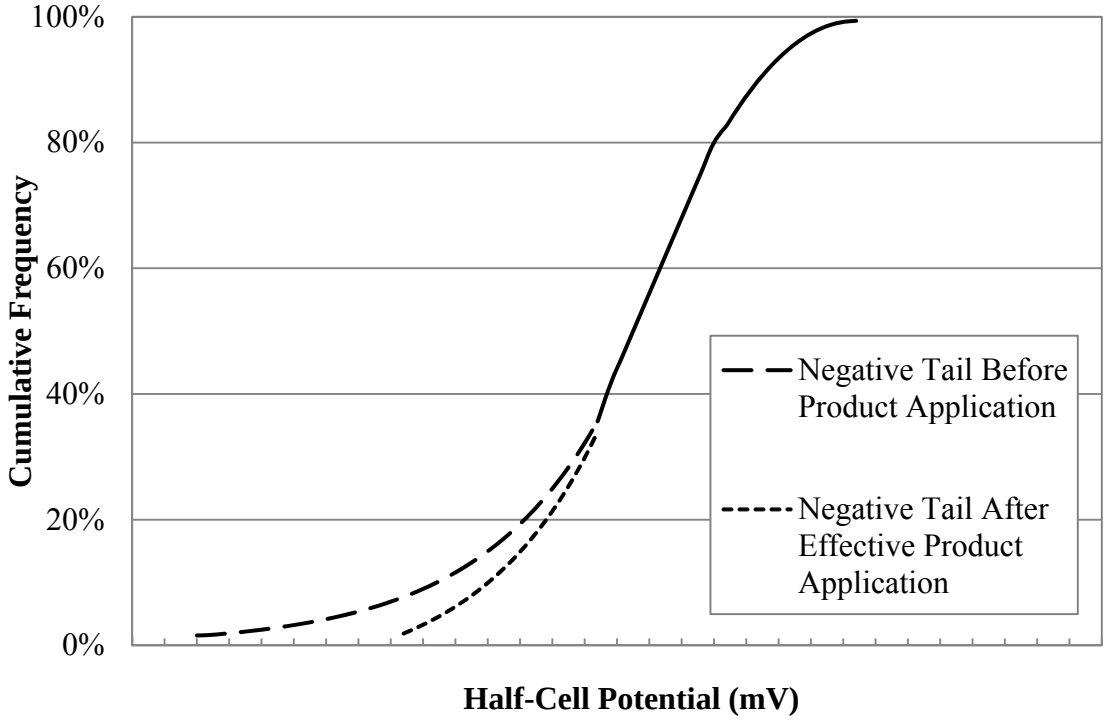

Figure 7-17: Expected change in cumulative frequency distribution for effective product

A reduction in variance would likely occur for an effective topically applied corrosion inhibitor; however, the change in magnitude of the half-cell potentials in a section can be affected by many other factors. Therefore changes may not have any relation to the effectiveness of the product at reducing corrosion. One important factor is that inhibitors can change the properties of the concrete such as its electrical resistance, which can change the magnitudes of the half-cell measurements without changing the corrosion rate of the reinforcement. This indicates that if the cumulative frequency distributions shift toward to either more positive or more negative values but the cumulative frequency distributions remain parallel, as shown if Figure 7-18, then no actual change in corrosion potential has occurred within the section. Therefore if the cumulative distribution curves remain parallel, then the corrosion mitigation product was ineffective.

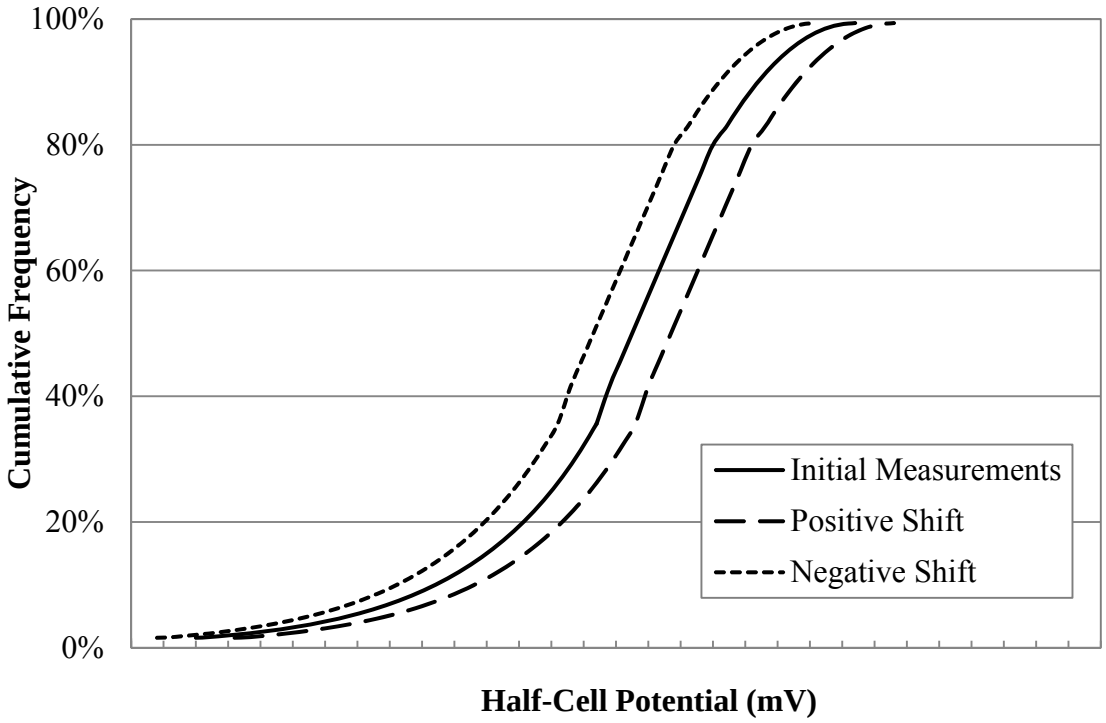

Figure 7-18: Parallel cumulative frequency distributions

None of the products visibly reduced the size of the tail for the cumulative distribution graphs as shown in Figure 6-44 and Figure 6-49 through Figure 6-54. For each product, the cumulative distribution graphs alternated from shifting to either a more positive measurement or a more negative measurement each time that the half-cell potential measurements were obtained, but the negative tails stayed approximately the same and the curves for each measurement were approximately parallel. This agrees with the analysis of the contour maps and indicates that none of the products were likely effective in the field.

7.2.4 LABORATORY TESTING RESULTS FOR MITIGATION PRODUCTS

Figure 7-19 shows the change in half-cell potential for each wet, cracked specimen from the time the products were initially applied. It has been split into two plots for ease of viewing. As shown in Figure 7-19, the Protectosil CIT & Ferrogard 903 and the Protectosil CIT specimens had the largest half-cell potential increases of any of the cracked, wet specimens. Therefore these specimens were chosen to be further analyzed with SEM and chloride ion concentration analysis. The Ferrogard 903 and one of the Control specimens were also further analyzed with SEM and chloride ion concentration analysis.

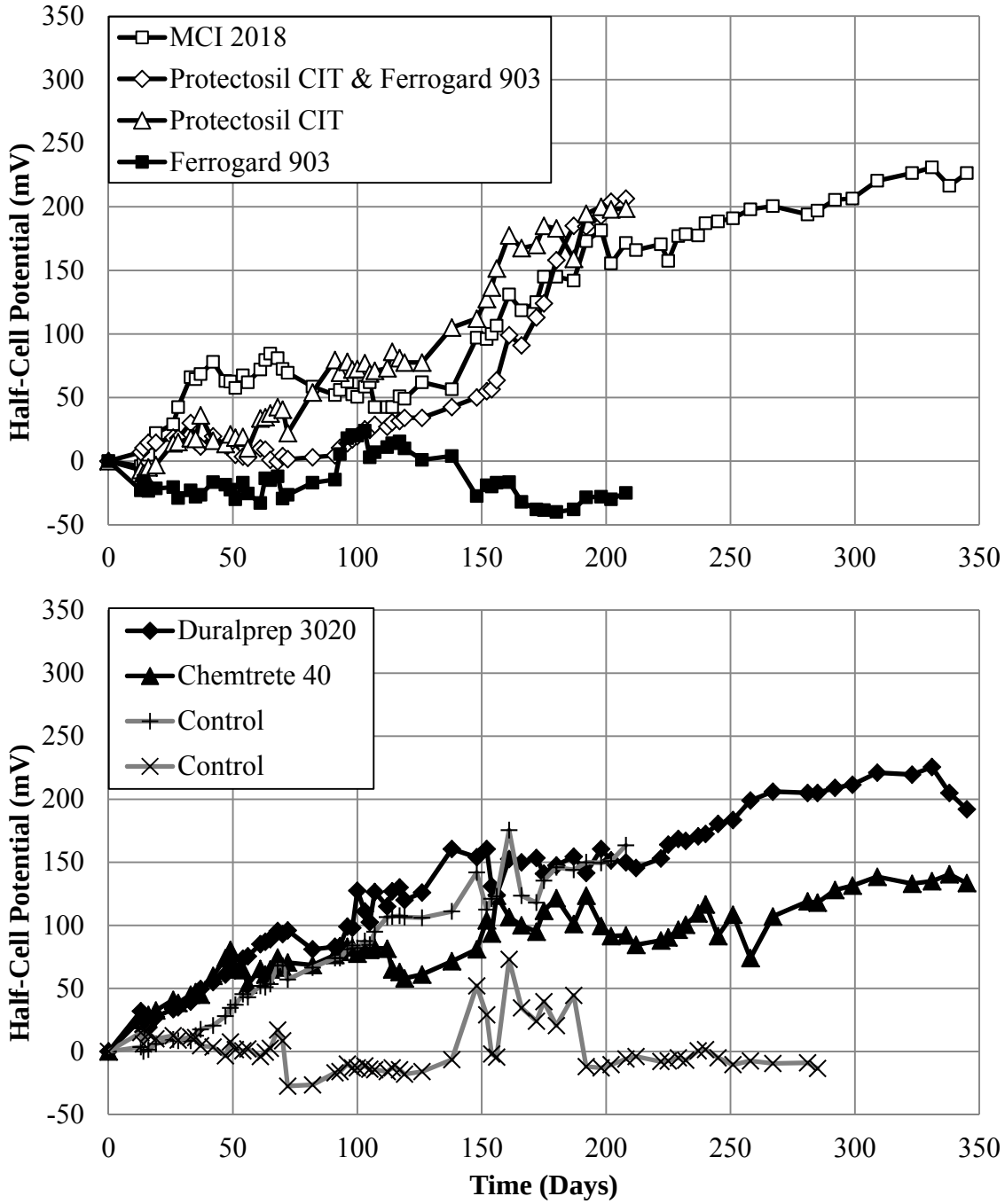

Figure 7-19: Wet specimens – change in half-cell potential after initial product application

Figure 7-20 shows the change in half-cell potential for each dry, cracked specimen from the time that the products were initially applied. It has been split into two plots for ease of viewing. As shown in Figure 7-20, the MCI-2018 specimen had the largest increase on half-cell potential of the cracked, dry specimens.

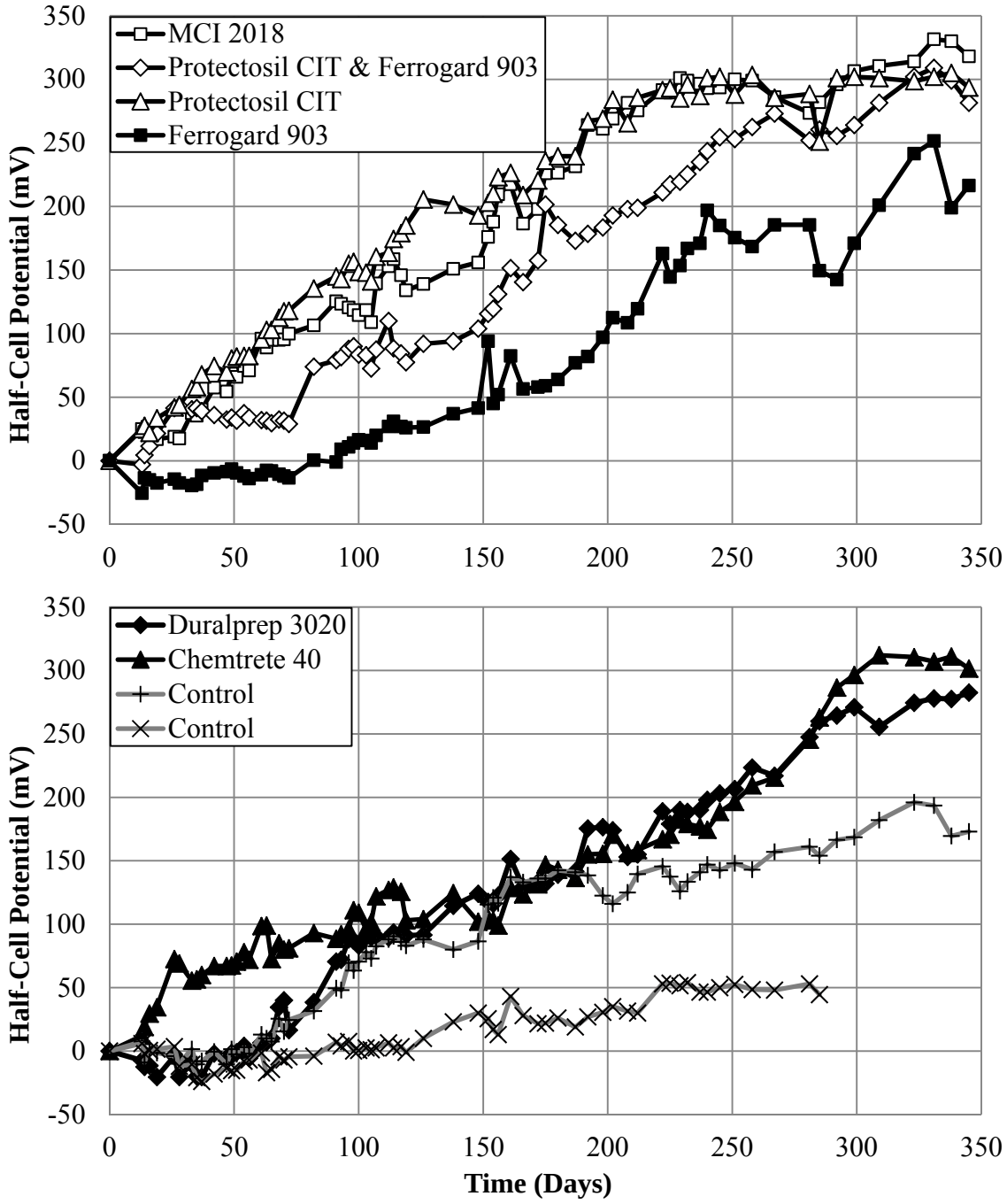

Figure 7-20: dry Specimens – change in half-cell potential after initial product application

Figure 7-21 shows the half-cell potentials of the uncracked specimens when salt was added to the mix. It has also been split into two plots for ease of viewing. Figure 7-22 shows the half-cell potentials of the uncracked specimens when no salt was added to the mix and no products applied.

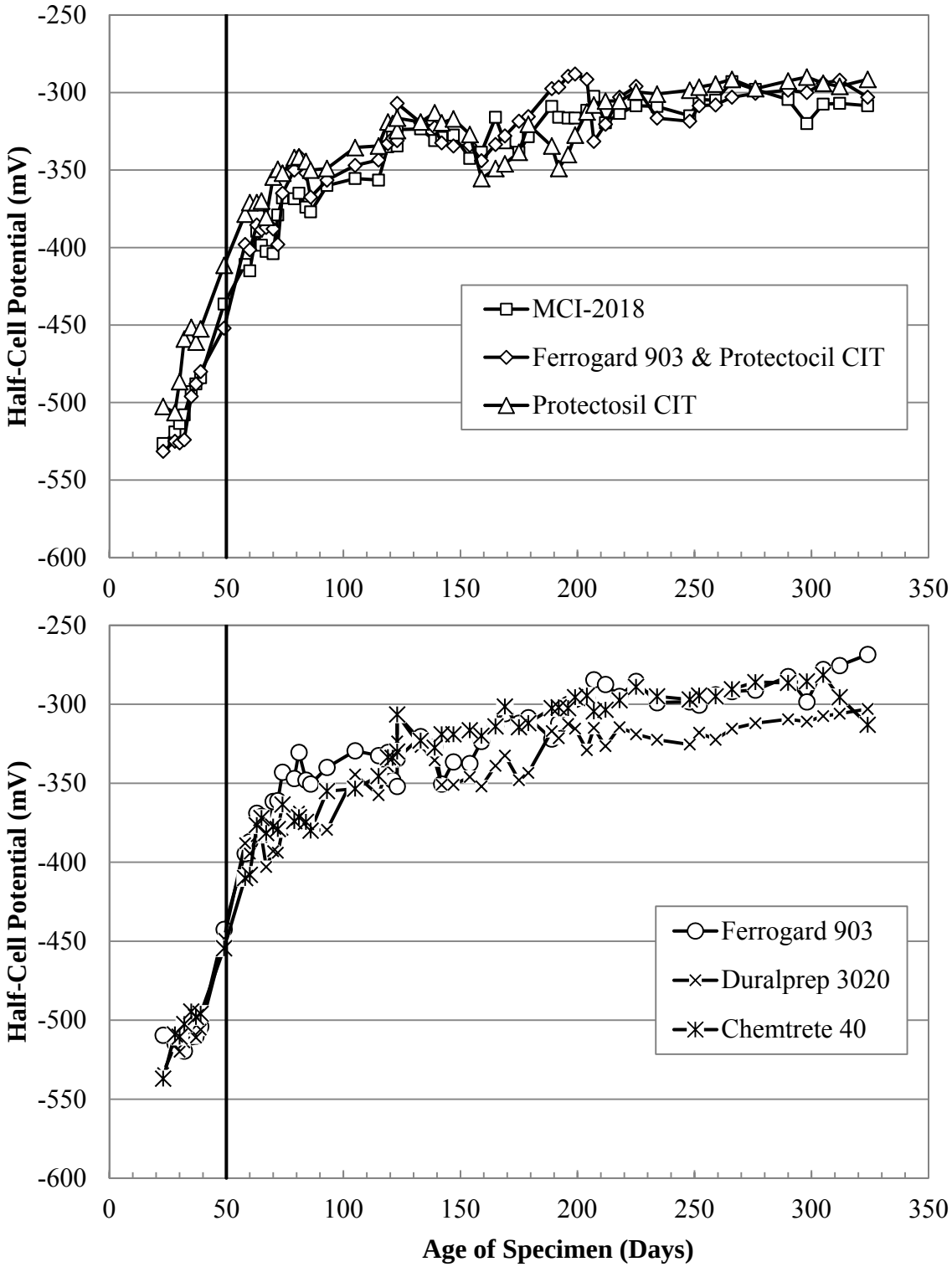

Figure 7-21: Half-cell potential of uncracked specimens with salt in mix

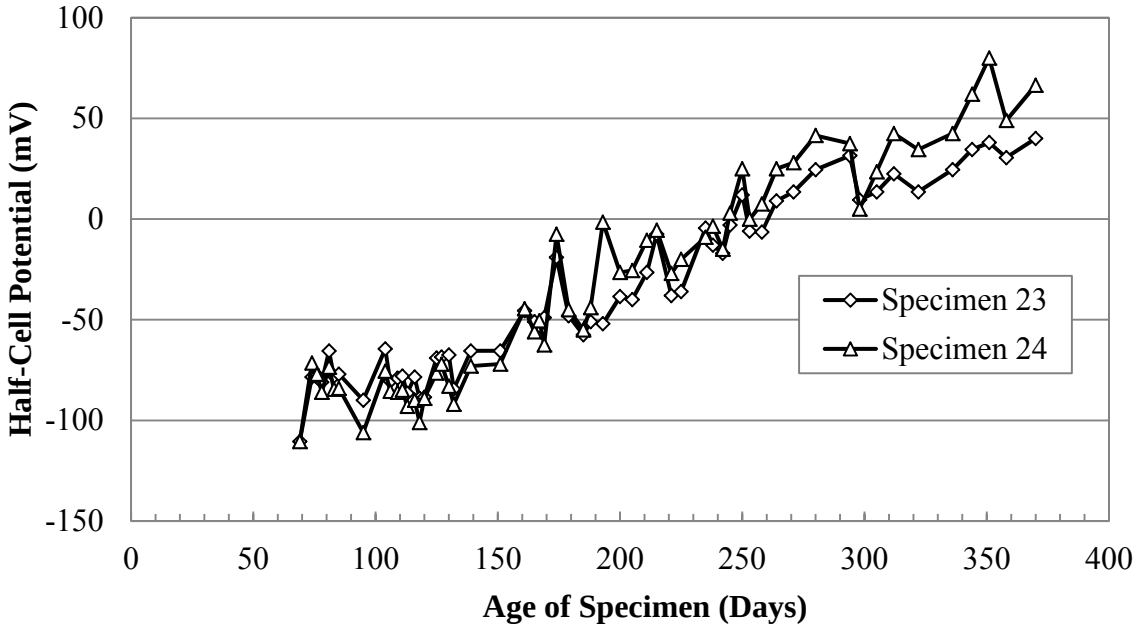

Figure 7-22: Half-cell potential of uncracked control specimens

7.2.4.1 Numeric Magnitude Technique for Laboratory Data

Although the numeric magnitude technique was determined in be unreliable for analyzing half-cell potentials in the field, a laboratory provides more stable conditions. For example, the temperatures for all specimens were kept at 72 degrees Fahrenheit; the wet, cracked specimens were ponded throughout half-cell potential testing; and all other specimens kept dry once the corrosion was initiated. This greatly reduced the fluctuation in temperature and moisture content of the concrete within a specimen type.

The basic principles behind the numeric magnitude technique should apply, but the ranges specified by ASTM C876-09 are likely incompatible because they were obtained by testing structures that were uncracked and had less than three inches of cover. Also the ranges for the wet specimens and the dry specimens are likely different, and the ranges for the cracked specimens may be different than the ranges for the uncracked specimens.

7.2.4.2 Further Analysis of the Half-Cell Potential for Laboratory Specimens

A potential alternative method to analyze the laboratory specimens would be to compare the magnitude of the increase in half-cell potential of the product specimens to the increase in half-cell potential of the corresponding control specimen over the same period of time as shown in Figure 7-19 and Figure 7-20. This method may not account for any changes in concrete properties caused by the application of the products. However, changes should occur relatively quickly after product application which would lead to a significant change in half-cell potential shortly after application, and this change in half-cell potential would be expected to occur in both the cracked and uncracked specimens. None of the uncracked specimens showed any noticeable changes in half-cell potential after product application, therefore the affect corrosion inhibitors have on the half-cell potential measurement was thought to be considerably less than the effect that the change in corrosion rate would have on half-cell potential measurement.

The only expected difference in half-cell potential measurements was the differences caused by the effect of the products on concrete properties, and the change in half-cell potential caused by differing amounts

of corrosion. However, for the wet, cracked, control specimens, one control specimen had a half-cell potential change of approximately +150 mV over the first 200 days after the initial product application date, and over the same time period, the other wet, cracked control specimen had a change in half-cell potential of approximately -10 mV as shown in Figure 7-19. These show that even between two identical specimens that were exposed to the same conditions, the half-cell potential can greatly vary. Also, the change in half-cell potential for the more positive control specimen was within 50 mV of the two product specimens with the highest increase in half-cell potential, as seen in Figure 7-20. This likely means that mitigation products did not perform more effectively than the controls.

The cracked, dry, control specimens also exhibited a large difference in half-cell potentials throughout the testing period as shown in Figure 7-21. For the dry, cracked specimens after 345 days, the half-cell potentials for all of the specimens with products applied, except for Ferrogard 903, experienced shifts of +275 to +325 mV. In comparison, Ferrogard 903 shifted approximately +220 mV, and the control specimens shifted approximately +175 mV and +50 mV.

The specimens with MCI-2018, Protectosil CIT & Ferrogard 903, Protectosil CIT, Duralprep 3020, and Chemtrete 40 had changes in half-cell potential that were more than 100 mV or 57 percent greater than the control specimen with the most positive relative change in half-cell potential. This indicates that for the dry, cracked specimen case, some of the products were at least partially effective in increasing the half-cell potentials which can be correlated to the probability of corrosion; however, because this comparison is using half-cell potentials, no reduction in corrosion rates or increased life expectancy can be directly calculated.

The uncracked specimens with salt in the mix had half-cell potentials within 50 mV of each other throughout the entire study. These specimens also did not exhibit any changes in the half-cell potential trend after the corrosion inhibitors were applied even though the half-cell potentials were very negative. This indicates a high probability of corrosion when the products were applied. The half-cell potentials of these specimens stabilized approximately 200 days after they were cast, at -300 mV with a range of ± 25 mV as shown in Figure 7-22. In comparison, the uncracked control specimens with no salt in the mix, half-cell potentials gradually shifted in positive direction, from -38.5mV and -26.5mV at 200 days after casting to 40 mV and 66.5 mV at 370 days after casting respectively. This comparison shows that corroding pavements with high chloride contents can exhibit up to 300 mV more negative half-cell potentials than intact, non-corroding pavements with no chlorides in it.

7.2.4.3 Chloride Ion Concentration Results of the Laboratory Specimens

As presented in Chapter 5 and 6, four wet, cracked specimens were tested for chloride ion concentrations. The chloride ion analysis results of the laboratory specimens showed that cracks can allow the rapid transport of chloride ions to the reinforcement. The chloride ion concentrations along the depth of the crack to the reinforcement for all specimens tested were above the threshold value of 1.244 lbs/yd^3. This means that sufficient chloride ions are reaching the reinforcement to disrupt the passive layer and initiate corrosion. This agrees with the half-cell potential analysis of the cracked specimens, which showed a large negative shift in half-cell potential within a few days after the specimens had been ponded with a chloride solution.

The chloride ion analysis away from the simulated crack showed that the top inch, measured from the bottom of the chloride well, had chloride ion concentrations up to 21 lbs/yd^3 which is much greater than

the chloride threshold. The chloride ion concentrations only decreased slightly away from the crack at the top one inch in the specimens. The chloride concentrations from depths of one inch to three and three-fourths inches were either slightly above or below the chloride threshold at one half inch and farther away from the crack. This shows that chloride ions did not penetrate into the intact portion of the concrete. However, the layer which contained the reinforcement had chloride ion concentrations above the threshold up to two inches away from the crack in three of the four specimens tested. The chloride solution traveled along the reinforcement, which could possibly be caused by incomplete consolidation of the concrete around the reinforcement. During chloride ponding, this was evident by salt crystals that formed around the concrete patches that were placed over the reinforcement after the specimens were cast. This is shown in Figure 7-23.

Figure 7-23: Salt crystals from the chloride solution migrating through the concrete.

7.2.4.4 SEM Results for the Laboratory Specimens

Localized or pitting corrosion up to 200 μm thick was detected in specimens that were tested. Also, a thin ring of corrosion approximately 15 – 25 μm thick was detected around the entire circumference of the reinforcement. These areas contained slightly less oxygen compared to the pitting corrosion. All specimens exhibited some minor, superficial corrosion, but no specimens lost a significant amount of cross-section.

The element maps for each of the specimens tested showed at least some chlorides at the site of the localized corrosion. The chloride concentrations at the energy dispersive X-ray spectroscopy testing locations varied from 0.43 percent chloride by weight (12 lbs/yd^3) to greater than 7 percent chloride by weight (265 lbs/yd^3). Only a small percentage of the corroded area of the reinforcement was tested, but it does show that chlorides were penetrating to the reinforcement and were concentrated in the areas where corrosion was observed.

8 CONCLUSIONS AND RECOMMENDATIONS

Conclusions and recommendations for this study are presented in this chapter. Topics discussed in the summary include the initial evaluation of CRCP, the statewide assessment of CRCP, and mitigation product evaluation. Conclusions regarding corrosion in CRCP are presented, as well as recommendations based on these conclusions.

8.1 CONCLUSIONS

Several conclusions were established from the general observations and crack data. First, corrosion was only observed at cracked or patched locations. Reinforcement corrosion was not evident at areas away from cracked or patched locations, except in the case of the longitudinal reinforcement placed near the longitudinal joint. However, there were areas of severe spalling and cracks that did not show signs of corrosion. This leads to the conclusion that observed pavement distresses are likely not the effect of corroded reinforcement. Also, the crack densities in the Sioux Falls area are greater than the crack densities at other South Dakota study sites by 44%. Furthermore, longitudinal cracking was observed on the sites near Sioux Falls, but not at the sites included in the statewide evaluation. This indicates that the performance of the Sioux Falls interstate sections is lower than the other CRCP interstates evaluated in South Dakota. Finally, the limited observed loss of cross-sectional area is only in limited sections of reinforcement; therefore, complete shear failure in these CRCP, leading to reduced pavement performance, would not be widespread.

The chloride analysis showed that chlorides have the ability to penetrate through cracks and patched locations of CRCP. Therefore, crack density is an appropriate means of determining a CRCP section's susceptibility to corrosion. The chloride analysis also showed that chloride contents were above the threshold level within the first lateral half inch of 11 of the 13 samples tested. Two out of three of the samples tested showed chloride levels above the threshold within the first lateral inch at the level of the reinforcement. This led to the conclusion that only localized reinforcement at cracked locations is susceptible to corrosion caused by deicing salts. The chloride analysis of the dust samples that were obtained away from crack locations showed that chlorides have not penetrated to the reinforcement through intact concrete during the lifetime of the pavements surveyed in this study. Thus, in general, an intact pavement section is not susceptible to corrosion caused by deicing salts.

The SEM analysis of the reinforcement in the cores of two of the three samples that were obtained at crack locations showed virtually no signs of corrosion. The reinforcement sample that was corroded showed evidence of chloride intrusion at the corroded location. The reinforcement of an additional core obtained from an intact section of pavement was analyzed with the SEM, and no signs of corrosion were found. This further confirmed the conclusions that pavement distresses observed are likely not the effect of corroded reinforcement and that reinforcement at cracked locations is susceptible to corrosion caused by deicing salts.

The half-cell potential measurements at all sites were determined to fall in either the high probability or uncertain range with respect to corrosion according to ASTM C876-09. Many unquantifiable factors affect the half-cell potential test including concrete resistance, moisture content, oxygen concentration at the steel interface, and concrete cover depth. Although the half-cell potential method has been a valid indicator of corrosion for concrete buildings and bridge decks, by itself it was inconclusive in determining the probability of corrosion in CRCP during this study. It was also shown that there was a strong

correlation between crack density and elevated half-cell potential measurements. Therefore, crack density can be used as an indicator to the susceptibility of a CRCP site to corrosion. The crack density was recorded for discrete locations within a 100 foot long section of CRCP, whereas the surface condition index (SCI) is obtained by evaluating a pavement section anywhere from several hundred feet to several miles. Therefore, the SCI cannot be used to evaluate a CRCP site's susceptibility to corrosion.

Several conclusions were also produced from this study pertaining to penetrating sealers and MCI's for corrosion mitigation. As with assessing corrosion of CRCP, many environmental factors affected half-cell potential measurements. This limited the analysis to using the potential difference technique of the corrosion mitigation methods, because this is the only analysis method technique that was not affected when the concrete properties change due to changing environmental conditions. Based on analyzing the field data using the potential difference technique, none of the sealers or MCI's appeared to be effective at reducing corrosion in cracked CRCP with chloride concentrations that were already higher than the chloride threshold.

For the laboratory specimens treated with corrosion mitigation products, the only expected differences in half-cell potential measurements were the differences caused by the effect of the products on the concrete properties, and the change in half-cell potential caused by changing rates of corrosion. However, the wet, cracked, control specimens had a large difference in change in half-cell potential, and the dry, cracked control specimens also exhibited a large difference in the change of half-cell potential between them. This shows that even for two similar specimens exposed to the same conditions, the half-cell potential can vary greatly.

For the wet cracked specimens treated with corrosion mitigation products, some of the specimens did show up to 50 mV more positive shift in half-cell potential at 200 days from product application than either control specimen, but this difference was much smaller than the difference between the two control specimens. Therefore, the effectiveness for the penetrating sealers and MCI's when subjected to continuous ponding is inconclusive. For the dry, cracked specimens, after 350 days, the half-cell potentials for all of the specimens with products applied to them, except for Ferrogard 903 had experienced positive shifts that were more than 57 percent more positive than the control specimen with the most positive shift. Therefore, the conclusion is that for the dry, cracked specimens, several of the products were at least partially effective in increasing the half-cell potentials (decreasing corrosion potential).

The overall conclusion about the topically applied corrosion mitigation products tested was that they did not appear to be effective in the field. The results were inconclusive on effectiveness of the products at reducing corrosion in a laboratory setting when a high concentration of chlorides was introduced after the products were applied, as shown in the wet, cracked specimens. However, when no chlorides were applied after the product application, several of the products did appear to be effective at reducing half-cell potentials in comparison to the control specimens.

The chloride analysis of the laboratory specimens confirmed the assessment part of the study that showed chlorides can readily penetrate through cracks in concrete. There were chloride concentrations greater than the chloride threshold at the bottom surface of the specimen well, along the crack, and along the reinforcement for all the specimens tested. This shows that chlorides dissolved in water can partially travel down the crack to the reinforcement, and then migrate along the reinforcement and concrete interface. This could result in corroded areas up to two or three inches away from of the crack. The

chloride analysis results showed that in the intact concrete that was away from the crack, chlorides had not penetrated deeper than one inch, in concentrations higher than the chloride threshold, even though the specimens had been ponded for approximately 300 days. Therefore, if there is sufficient concrete cover, the likely area of the pavement that is susceptible to corrosion initiated by deicing salts is the area of the pavement that is within a few inches of cracks. This also confirms similar conclusions from the assessment part of the study.

The SEM analysis also showed high concentrations of chlorides at the corroded areas of the reinforcement. This confirms the results of the chloride ion concentration testing by showing that the chlorides penetrated to the reinforcement in high concentrations. It also reaffirms that localized high concentrations of chlorides leads to pitting corrosion of the reinforcement.

8.2 RECOMMENDATIONS AND IMPLEMENTATION

The conclusions resulting from this research produce several recommendations regarding the evaluation and construction of CRCP. The severely corroded reinforcement observed near the longitudinal reinforcement led to the recommendation that more care should be taken during the construction of CRCP. The longitudinal reinforcement should be placed at least three inches away from the center longitudinal joint in newly constructed CRCP. The placement of the longitudinal reinforcement during construction and maintenance of CRCP should be monitored closely to ensure that the reinforcement will not be placed within the recommended three inches of the center joint.

The analysis methods of half-cell potential measurements using the ASTM C876 guidelines were deemed inconclusive for this research study. Although the half-cell measurements were successfully correlated to the crack mapping results to indicate areas of corrosion in CRCP, a separate method to test corrosion that does not require additional pavement information would be more efficient. Therefore, it is recommended that other non-destructive test methods to evaluate corrosion be considered. It is recommended that these methods allow for the measurement of corrosion on reinforcement that has concrete cover depths of at least 6 inches, as some of the CRCP sections in this study had cover depths of 5.5 inches. Other considerations for this additional research include the cost effectiveness of the test method and the possible implementation of the test method by SDDOT personnel for pavement management purposes.

Crack density was determined to be an indicator of corrosion susceptibility in CRCP. The relationship between crack width and corrosion susceptibility was not examined in this study. The interaction of crack density and crack width were also not examined with respect to corrosion. These relationships, if deemed of interest to the SDDOT, should be investigated as part of a separate research study. Also, at the time of this study, the SDDOT had not been obtaining crack density measurements as part of the pavement management program. Individual indices used by the SDDOT to rate pavement performance include D-cracking/ASR, joint spalling, corner cracking, faulting, joint seal damage, and punchouts. These indices are combined to develop the surface condition index. Since these indices are already being used by the SDDOT, it is recommended that one or several of these indices be related to crack density in order to determine the corrosion susceptibility of CRCP that has previously been evaluated by the SDDOT. Also, the use of the SDDOT pavement profiler and videolog to determine crack density should be considered.

Further research may be necessary to determine the principal causes of the distresses (besides corrosion) observed in the CRCP in South Dakota. Although the original SDDOT study made several recommendations for future construction of CRCP with such distresses in mind, the implementation of

these recommendations has been limited. It is recommended that a separate research study begin which analyzes the effectiveness of the recommendations of the original study.

The sealers and MCI's were likely not effective at reducing the variation in corrosion potentials when applied to CRCP pavement in the field. The laboratory testing was inconclusive with products appearing to show no benefit in the wet, cracked specimens or the uncracked specimen with salt in the mix; however, the dry, cracked specimens showed a notably greater reduction in half-cell potential than the control specimens for some products. Because, the products did not appear to be effective in the field, it is not recommended to apply these products to large sections of CRCP without further research. However, because some of the products showed effectiveness in reducing the corrosion potentials in the dry, cracked specimens, and because the half-cell potentials of each the product sections in the field all had a slight positive shift half-cell potentials in comparison to the control section, it may be beneficial to perform additional testing (using alternate methods recommended above), both in the field and on the laboratory specimens. This would help to determine if there are any beneficial long-term effects of the products that have not yet been observed.

The laboratory part of this study further confirmed the half-cell potential device coupled with the numeric magnitude technique as defined by ASTM C876-09 is likely inappropriate for CRCP. Modifying the ranges to the match half-cell potential values of CRCP may allow it to be used as a guideline; however, because of the large effects that environmental factors can have on half-cell potential measurements, the numeric magnitude technique would still not be applicable for all pavements and conditions. The use of the potential difference method coupled with contour maps was consistent throughout the testing period, as long as a good electrical connection was established. Therefore, the potential difference may be an appropriate technique for corrosion evaluation of CRCP. However, this method does not provide any specific probabilities of corrosion so experience and personal judgment is required to interpret the results.

9 REFERENCES

Ali, M. (1990). Reference half cells for monitoring corrosion condition of steel in reinforced concrete structures. *Anti-Corrosion Methods and Materials*, pp 10-11.

American Association of State Highway and Transportation Officials (AASHTO) (2004). "T 260-97 (2001), Standard Method of Test for Sampling and Testing for Chloride Ion in Concrete and Concrete Raw Materials," *Standard Specifications for Transportation Materials and Methods of Sampling and Testing*, *24th Edition.* AASHTO, pp. T 260-1 – T 260-15.

American Concrete Institute (ACI) (2001). Protection of Metals in Concrete Against Corrosion. ACI 222R-01. ACI. pp. 1– 41.

American Society for Testing and Materials (ASTM) (2004). "ASTM C1152, Standard Test Method for Acid-Soluble Chloride in Mortar and Concrete." ASTM. pp. 1– 4.

American Society for Testing and Materials (ASTM) (2009). "ASTM C 876 – 09, Standard Test Method for corrosion Potentials of uncoated Reinforcing Steel in Concrete." ASTM. pp. 1– 7.

Arya, C., & Ofori-Darko, F. (1996). Influence of Crack Frequency on Reinforcement Corrosion in Concrete. *Cement and Concrete Research , Volume 26,* Issue 3, pp. 345– 353.

Assouli, B., Ballivy, G., & Rivard, P. (2008). "Influence of Environmental Parameters on Application of Standard ASTM C876-91: Half Cell Potental Measurements." *Corrosion Engineering, Science and Technology,* 43(1), pp. 93-96.

ASTM (2009). "ASTM C 876 – 09, Standard Test Method for corrosion Potentials of uncoated Reinforcing Steel in Concrete." ASTM. pp. 1– 7.

Balzoni, F., Goidanich, S., Lazzari, L., and Ormellese, M. (2006). "Corrosion Inhibitors in Reinforced Concrete Structures Part 2 – Repair System." *Institute of Materials, Minerals and Mining.* pp. 1-9.

Bavarian, B. & Reiner, L. (2004). Improving Durability fo Reinforced Concrete Structures Using Migrating Corrosion Inhibitors. *Corrosion 2004,* Paper 04323. NACE International. pp. 1– 11.

Bjegovic, D., & Miksic, B. (1999). Migrating Corrosion Inhibitor Protection of Concrete. *Materials Performance* , November Issue, pp. 52– 56.

Böhni, H. (2005). "Corrosion in Reinforced Concrete Structures." Woodhead Publishing, Cambridge, England, pp. 1– 253.

Browne, R. (1980). Concrete in the Oceans: Marine Durability of the Tongue Sands Tower, CIRIA UEG Technical Report No. 5, Cement and Concrete Research.

Clear, K. (1976). Time-to-Corrosion of Reinforcing Steel in Concrete Slabs. FHWA-RD-76-70, FHWA.

Clemeña, G., Apusen, C. (2002). An Alternative Potentiometric Method for Determining Chloride Content in Concrete Samples from Reinforced-Concrete Bridges, Virginia Transportation Research Council, Charlottesville, Virginia. pp. 1– 18.

Concrete Reinforcing Steel Institute (CRSI). (2001). *CRCP - The Illinois Experience.* Case History Report 55, CRSI. pp. 1– 3.

Cortec Corporation. (2011). *MCI-2018 Sealer, Patented: Product Data Sheet.* Cortec Corporation. pp. 1-3.

Duke, E. (2010a, August 13). Telephone interview.

Duke, E. (2010b, August 03). E-mail interview.

El-Hacha, R., Mirman, A., Cook, A., and Rizkalla, S. (2011). "Effectiveness of Surface-Applied Corrosion Inhibitors for Concrete Bridges." *Journal of Materials in Civil Engineering,* 23(3), pp. 271-280.

Elsener, B. (2001). Half-cell potential mapping to assess repair work on RC structures. *Construction and Building Materials, 15,* pp. 133– 139.

Elsener, B., & Böhni, H. (1990). Potential Mapping and Corrosion of Steel in Concrete. In Berke, Chaker, & Whiting, *Corrosion Rates of Steel in Concrete, ASTM 1065*. Philadelphia: American Society for Testing and Materials (ASTM). pp. 143– 156.

Elsener, B., Andrade, C., Gulikers, J., Polder, R., & Raupach, M. (2003). Hall-cell potential measurements—Potential mapping on reinforced concrete structures. *Materials and Structures, Volume 36,* Issue 7, pp. 461– 471.

Everett, L. & Treadway, K. (1980). Deterioration due to corrosion in reinforced concrete, Information Paper 12/80. Building Research Establishment.

Evonik Industries. (2012a). *Protectosil CHEM-TRETE 40 VOC: Water Repellent Product Data and Test Information.* Evonik Industries. pp. 1-2.

Evonik Industries. (2012b). *Protectosil CIT: Corrosion Inhibitor Treatment Data and Test Information.* Evonik Industries. pp. 1-4.

FSD Webmaster. (2008) "Historical Records and Past Events." *National Weather Service Forcast Office: Sioux Falls, SD,* <http://www.crh.noaa.gov/fsd/climate/archive.php> (10/3/2012)

Gu, P., Beaudoin, J. (1998). Obtaining Effective Half-Cell Potential Measurements in Reinforced Concrete Structures. *Construction Technology Update, No. 18.* National Research Council Canada. pp. 1– 6.

Hansson, C. M., Mammoliti, L., & Hope, B. B. (1998). Corrosion Inhibitors in Concrete - Part I: The Principles. *Cement and Concrete Research* , *Volume 28*, Issue 12, pp. 1775– 1781.

Hope, B. B. (1987). *Corrosion Inhibitors for Use in New Concrete Construction.* The Research and Development Branch, Ontario Ministry of Transportation. pp. 1– 2.

Hou, X., Ostergaard, L., Nielsen, S. (2007). "Determination of Cl in nuclear waste from reactor decommissioning." *Analytical Chemistry*., 79(8), pp. 3126– 3134.

Ibrahim, M. and Al-Gahtani, A. S. (1999). "Use of Surface Treatment Materials to Improve Concrete Durability." *Journal of Materials in Civil Engineering,* 11(1), pp. 36-40

Islam, M., Sohanghpurwala, A., & Scannell, W. (2002). Long-Term Performance of Corrosion Inhibitors Used in Repair of Reinforced Concrete Bridges. FHWA-RD-01-097. FHWA. pp. viii– ix.

Jaggi, S., Bohni, H., and Elsener, B. (2001). "Macrocell Corrosion of Steel in Concrete – Experiments and Numerical Modelling." *Eurocorr,* Associazione Italiana Metallurgia (AIM), Milan, Italy, pp. 1-12.

Johnston, D. (2009). *Impact, Cause, and Remedies for Excessive Cracking in CRC Pavement.* SD2004-07-F, South Dakota Department of Transportation (SDDDOT). pp. 1– 63.

Leibrock, C. (2011, May – June). Telephone and e-mail communication.

Leibrock, C. (2012, November 16). E-mail communication.

Liang, M.-T., Huang, R., & Jheng, H.-Y. (2010). Revisited to the relationship between the free and total chloride diffusivity in concrete. *Journal of Marine Science and Technology , 18* (3), pp. 442– 448.

Malhotra, V., Carino, N. (2004). "Handbook on Nondestructive Testing of Concrete." *Methods to Evaluate Corrosion of Reinforcement,* CRC Press, West Conshohocken, PA, p. 11-9.

Mammoliti, L., Hansson, C. M., & Hope, B. B. (1999). "Corrosion Inhibitors in Concrete - Part II: Effect on Chloride Threshold Values for Corrosion of Steel in Synthetic Pore Solutions." *Cement and Concrete Research* , Volume 29, pp. 1583-1589.

Materials Evaluation and Engineering, Inc. (MEE) (2010). "Handbook of Analytical Methods for Materials." Plymouth, MN. pp. 15– 16.

Morris, W., Vico, A., and Vazquez, M. (2003). "The Performance of a Migrating Corrosion Inhibitor Suitable for Reinforced Concrete." *Journal of Applied Electrochemistry.* Volume 33, pp. 1183-1189.

Muench, S., Mahoney, J., Pierce, L. (2011). Washington State Department of Transportation (WSDOT) Pavement Guide. (WSDOT). pp. 1– 275.

Ormellese, M., Bolzoni, F., Goidanich, S., Pedeferri, M. P., and Brenna, A. (2011). "Corrosion Inhibitors in Reinforced concrete Structures Part 3 – Migration of Inhibitors into Concrete." *Institute of Materials, Minerals, and Mining, Volume 46,* Issue 4, pp. 334-339.

Otieno, M., Alexander, M., & Beushausen, H. (2010). Corrosion in cracked and uncracked concrete – influence of crack width, concrete quality and crack reopening. *Magazine of Concrete Research,Volume 62* (6), pp. 393– 404.

Pour-Ghaz, M., Isgor, O. B., and Ghods, Pouria. (2009). "Quantitative Interpretation of Half-Cell Measurements in Concrete Structures." *Journal of Materials in Civil Engineering,* Volume 21, Issue 9*,* pp. 467-475.

Rens, L., Caestecker, C., Decramer, H., *Sustainable Road Building with Low-Noise CRCP on Belgian Motorways*. pp. 32– 35.

Richardson, M. (2002). "Fundamentals of durable reinforced concrete." Taylor & Francis, New York, NY, pp. 1– 260.

Roesler, J., Popovics, J. , Ranchero, J., Mueller, M., & Lippert, D. (2005). Longitudinal Cracking Distress on Continuously reinforced Concrete Pavements in Illinois. *ASCE Journal of Performance of Constructed Facilities, Volume 19*, Issue 4*,* pp. 331– 338. ASCE.

Sanchez, M., Alonso, C., Fullea, J., Granizo, L., and Izquierdo, J. D. (2011). "Protection of Reinforcements Using mixed Corrosion Inhibitors. Dependence of Inhibition Mechanism on

Interaction Between Rebar and Corrosion Inhibitor." *Corrosion Engineering, Science and Technology,* 46(4), pp. 445-452.

Sika Ltd. (2008). *Ferrogard 903: Penetrating, corrosion inhibiting, impregnation coating for hardened concrete.* Sika Ltd. pp. 1-2.

Smith, W., Hashemi, J. (2005). "Foundations of Materials Science and Engineering." *Corrosion,* McGraw-Hill Science, New York, NY. pp. 669– 671.

Stanish, K. D., Hooton, R. D., & Thomas, M. A. (1997). *Testing the Chloride Penetration Resistance of Concrete: A Literature Review.* FHWA. p. 3.

Stark, D. (1989). *Influence of Design and Materials on Corrosion Resistance of Steel in Concrete,* Portland Cement Association, Research and Development Bulletin RD098, Skokie, Illinois. p. 2.

Stratfull, R. (1973). Half-Cell Potentials and the Corrosion of Steel in Concrete. *Transportation Research Record, 433,* pp. 12– 35.

Suh, Y-C., McCullough, B. (1994). Factors affecting crack width of continuously reinforced concrete pavement. *Transportation Research Record ,1449*, pp. 134– 140.

Tayabi, S., Zollinger, D., Korovesis, G., Stephanos, P., Gagnon, J. (1998). Performance of Continuously Reinforced Concrete Pavements: Volume I – Summary of Practice and Annotated Bibliography. FHWA-RD-94-178. FHWA. pp. 1– 229.

The Euclid Chemical Company (2000). *Duralprep 3020: Penetrating, Migratory Corrosion Inhibitor for Concrete.* The Euclid Chemical Company. pp. 1-2.

Tutti, K. (1977). Corrosion of steel in concrete. *EUROCOR '77, 6th European Congress on Metallic Corrosion*. London: Society of Chemical Industry. pp. 655– 661.

Virmani, Y. and Clemeña, G. (1998). *Corrosion Protection – Concrete Bridges.* FHWA-RD-98-088. FHWA.

Virmani, Y., Clemeña, G. (1998). *Corrosion Protection – Concrete Bridges.* FHWA-RD-98-088. FHWA.

Wolf, R., (2005). "What is ICP-MS…and more importantly, what can it do?" *ICP-MS Facilities in the USGS Geologic Discipline.* USGS.

SD2009-05-A

South Dakota
Department of Transportation
Office of Research

U.S. Department
of Transportation
Federal Highway
Administration

Mitigation of Corrosion in Continuously Reinforced Concrete Pavement

Study SD2009-05
Appendices
Volume 2

Prepared by
Allen L. Jones and Nadim I. Wehbe
South Dakota State University
Department of Civil and Environmental Engineering

TABLE OF CONTENTS

Table of Contents ii
List of Tables iii
List of Figures iv
Appendix A. Site Selection Matrix for Statewide Evaluation 1
Appendix B. equipotential contour maps for initial and Statewide Assessments 7
Appendix C. Chloride Profiles for Initial and Statewide Assessments 79
Appendix D. Pavement Distress Definitions 101
Appendix E. Equipotential Contour Maps for Mitigation Product Assessment 102
Appendix F. Plots of Half-Cell Potential Measurements for Field Testing of Mitigation products ... 168

LIST OF TABLES

Table A-1: Site selection matrix for statewide evaluation 2

LIST OF FIGURES

Figure B-1: Equipotential contour map legend 8
Figure B-2: MRM 87 fall 2010 from 80 to 100 feet 9
Figure B-3: MRM 87 fall 2010 from 60 to 80 feet 10
Figure B-4: MRM 87 fall 2010 from 40 to 60 feet 11
Figure B-5: MRM 87 fall 2010 from 20 to 40 feet 12
Figure B-6: MRM 87 fall 2010 from 0 to 20 feet 13
Figure B-7: MRM 87 spring 2011 from 80 to 100 feet 14
Figure B-8: MRM 87 spring 2011 from 60 to 80 feet 15
Figure B-9: MRM 87 spring 2011 from 40 to 60 feet 16
Figure B-10: MRM 87 spring 2011 from 20 to 40 feet 17
Figure B-11: MRM 87 spring 2011 from 0 to 20 feet 18
Figure B-12: MRM 68 fall 2010 from 80 to 100 feet 19
Figure B-13: MRM 68 fall 2010 from 60 to 80 feet 20
Figure B-14: MRM 68 fall 2010 from 40 to 60 feet 21
Figure B-15: MRM 68 fall 2010 from 20 to 40 feet 22
Figure B-16: MRM 68 fall 2010 from 0 to 20 feet 23
Figure B-17: MRM 68 spring 2011 from 80 to 100 feet 24
Figure B-18: MRM 68 spring 2011 from 60 to 80 feet 25
Figure B-19: MRM 68 spring 2011 from 40 to 60 feet 26
Figure B-20: MRM 68 spring 2011 from 20 to 40 feet 27
Figure B-21: MRM 68 spring 2011 from 0 to 20 feet 28
Figure B-22: MRM 411 fall 2010 from 80 to 100 feet 29
Figure B-23: MRM 411 fall 2010 from 60 to 80 feet 30
Figure B-24: MRM 411 fall 2010 from 40 to 60 feet 31
Figure B-25: MRM 411 fall 2010 from 20 to 40 feet 32
Figure B-26: MRM 411 fall 2010 from 0 to 20 feet 33
Figure B-27: MRM 411 spring 2011 from 80 to 100 feet 34
Figure B-28: MRM 411 spring 2011 from 60 to 80 feet 35
Figure B-29: MRM 411 spring 2011 from 40 to 60 feet 36
Figure B-30: MRM 411 spring 2011 from 20 to 40 feet 37
Figure B-31: MRM 411 spring 2011 from 0 to 20 feet 38

Figure B-32: MRM 33 from 80 to 100 feet....39
Figure B-33: MRM 33 from 60 to 80 feet....40
Figure B-34: MRM 33 from 40 to 60 feet....41
Figure B-35: MRM 33 from 20 to 40 feet....42
Figure B-36: MRM 33 from 0 to 20 feet....43
Figure B-37: MRM 44 from 80 to 100 feet....44
Figure B-38: MRM 44 from 60 to 80 feet....45
Figure B-39: MRM 44 from 40 to 60 feet....46
Figure B-40: MRM 44 from 20 to 40 feet....47
Figure B-41: MRM 44 from 0 to 20 feet....48
Figure B-42: MRM 25 from 80 to 100 feet....49
Figure B-43: MRM 25 from 60 to 80 feet....50
Figure B-44: MRM 25 from 40 to 60 feet....51
Figure B-45: MRM 25 from 20 to 40 feet....52
Figure B-46: MRM 25 from 0 to 20 feet....53
Figure B-47: MRM 54 from 80 to 100 feet....54
Figure B-48: MRM 54 from 60 to 80 feet....55
Figure B-49: MRM 54 from 40 for 60 feet....56
Figure B-50: MRM 54 from 20 to 40 feet....57
Figure B-51: MRM 54 from 0 to 20 feet....58
Figure B-52: MRM 222 from 80 to 100 feet....59
Figure B-53: MRM 222 from 60 to 80 feet....60
Figure B-54: MRM 222 from 40 to 60 feet....61
Figure B-55: MRM 222 from 20 to 40 feet....62
Figure B-56: MRM 222 from 0 to 20 feet....63
Figure B-57: MRM 246 from 80 to 100 feet....64
Figure B-58: MRM 246 from 60 to 80 feet....65
Figure B-59: MRM 246 from 40 to 60 feet....66
Figure B-60: MRM 246 from 20 to 40 feet....67
Figure B-61: MRM 246 from 0 to 20 feet....68
Figure B-62: MRM 168 NB from 80 to 100 feet....69
Figure B-63: MRM 168 NB from 60 to 80 feet....70

Figure B-64: MRM 168 NB from 40 to 60 feet 71
Figure B-65: MRM 168 NB from 20 to 40 feet 72
Figure B-66: MRM 168 NB from 0 to 20 feet 73
Figure B-67: MRM 168 SB from 80 to 100 feet 74
Figure B-68: MRM 168 SB from 60 to 80 feet 75
Figure B-69: MRM 168 SB from 40 to 60 feet 76
Figure B-70: MRM 168 SB from 20 to 40 feet 77
Figure B-71: MRM 168 SB from 0 to 20 feet 78
Figure C-1: Vertical chloride profile of dust sample 1 at MRM 87 80
Figure C-2: Vertical chloride profile of dust sample 2 at MRM 87 80
Figure C-3: Vertical chloride profile of dust sample 3 at MRM 87 81
Figure C-4: Vertical chloride profile of dust sample 4 at MRM 87 81
Figure C-5: Vertical chloride profile of dust sample 1 at MRM 68 82
Figure C-6: Vertical chloride profile of dust sample 2 at MRM 68 82
Figure C-7: Vertical chloride profile of dust sample 3 at MRM 68 83
Figure C-8: Vertical chloride profile of dust sample 4 at MRM 68 83
Figure C-9: Vertical chloride profile of dust sample 1 at MRM 411 84
Figure C-10: Vertical chloride profile of dust sample 2 at MRM 411 84
Figure C-11: Vertical chloride profile of dust sample 3 at MRM 411 85
Figure C-12: Vertical chloride profile of dust sample 4 at MRM 411 85
Figure C-13: Vertical chloride profile of dust sample 1 at MRM 33 86
Figure C-14: Vertical chloride profile of dust sample 2 at MRM 33 86
Figure C-15: Vertical chloride profile of dust sample 1 at MRM 44 87
Figure C-16: Vertical chloride profile of dust sample 2 at MRM 44 87
Figure C-17: Vertical chloride profile of dust sample 1 at MRM 25 88
Figure C-18: Vertical chloride profile of dust sample 2 at MRM 25 88
Figure C-19: Vertical chloride profile of dust sample 1 at MRM 54 89
Figure C-20: Vertical chloride profile of dust sample 2 at MRM 54 89
Figure C-21: Vertical chloride profile of dust sample 1 at MRM 222 90
Figure C-22: Vertical chloride profile of dust sample 2 at MRM 222 90
Figure C-23: Vertical chloride profile of dust sample 1 at MRM 246 91
Figure C-24: Vertical chloride profile of dust sample 2 at MRM 246 91

Figure C-25: Vertical chloride profile of dust sample 1 at MRM 168 NB 92
Figure C-26: Vertical chloride profile of dust sample 2 at MRM 168 NB 92
Figure C-27: Vertical chloride profile of dust sample 1 at MRM 168SB 93
Figure C-28: Vertical chloride profile of dust sample 2 at MRM 168SB 93
Figure C-29: Horizontal chloride profile of core MRM 87-3 at depth 0.5 inches.....94
Figure C-30: Horizontal chloride profile of core MRM 87-3 at depth 1.5 inches.....94
Figure C-31: Horizontal chloride profile of core MRM 87-3 at depth 2.5 inches.....95
Figure C-32: Horizontal chloride profile of core MRM 87-3 at depth 3.5 inches.....95
Figure C-33: Horizontal chloride profile of core MRM 68-3 at depth 0.5 inches.....96
Figure C-34: Horizontal chloride profile of core MRM 68-3 at depth 1.5 inches.....96
Figure C-35: Horizontal chloride profile of core MRM 68-3 at depth 2.5 inches.....97
Figure C-36: Horizontal chloride profile of core MRM 68-3 at depth 3.5 inches.....97
Figure C-37: Horizontal chloride profile of core MRM 68-3 at depth 4.5 inches.....98
Figure C-38: Horizontal chloride profile of core MRM 411-1 at depth 0.5 inches.....98
Figure C-39: Horizontal chloride profile of core MRM 411-1 at depth 1.5 inches.....99
Figure C-40: Horizontal chloride profile of core MRM 411-1 at depth 2.5 inches.....99
Figure C-41: Horizontal chloride profile of core MRM 411-1 at depth 3.5 inches.....100
Figure E-1: Legend for half-cell potential contour maps 103
Figure E-2: Section A – 8/25/2011.....104
Figure E-3: Section A – 10/6/2011.....105
Figure E-4: Section A – 10/27/2012.....106
Figure E-5: Section A – 4/10/2012.....107
Figure E-6: Section A – 5/9/2012.....108
Figure E-7: Section B – 8/25/2011.....109
Figure E-8: Section B – 10/6/2011.....110
Figure E-9: Section B – 10/27/2012.....111
Figure E-10: Section B – 4/10/2012.....112
Figure E-11: Section B – 5/9/2012.....113
Figure E-12: Section C – 8/25/2011.....114
Figure E-13: Section C – 10/6/2011.....115
Figure E-14: Section C – 10/27/2012.....116
Figure E-15: Section C – 4/10/2012.....117

Figure E-16: Section C – 5/9/2012 118
Figure E-17: Section D – 8/25/2011 119
Figure E-18: Section D – 10/6/2011 120
Figure E-19: Section D – 10/27/2012 121
Figure E-20: Section D – 4/10/2012 122
Figure E-21: Section D – 5/9/2012 123
Figure E-22: Section E – 8/25/2011 124
Figure E-23: Section E – 10/6/2011 125
Figure E-24: Section E – 10/27/2011 126
Figure E-25: Section E – 4/10/2012 127
Figure E-26: Section E – 5/9/2012 128
Figure E-27: Section F – 8/25/2011 129
Figure E-28: Section F – 10/6/2011 130
Figure E-29: Section F – 10/27/2011 131
Figure E-30: Section F – 4/10/2012 132
Figure E-31: Section F – 5/9/2012 133
Figure E-32: Section G – 8/25/2011 134
Figure E-33: Section G – 10/6/2011 135
Figure E-34: Section G – 10/27/2011 136
Figure E-35: Section G – 4/10/2012 137
Figure E-36: Section G – 5/9/2012 138
Figure E-37: Legend for the difference in half-cell potential contour maps 139
Figure E-38: Section A – Difference between 8/25/2011 and 10/6/2011 140
Figure E-39: Section A – Difference between 10/6/2011 and 10/27/2011 141
Figure E-40: Section A – Difference between 10/27/2011 and 4/10/2012 142
Figure E-41: Section A – Difference between 4/10/2012 and 5/9/2012 143
Figure E-42: Section B – Difference between 8/25/2011 and 10/6/2011 144
Figure E-43: Section B – Difference between 10/6/2011 and 10/27/2011 145
Figure E-44: Section B – Difference between 10/27/2011 and 4/10/2012 146
Figure E-45: Section B – Difference between 4/10/2012 and 5/9/2012 147
Figure E-46: Section C – Difference between 8/25/2011 and 10/6/2011 148
Figure E-47: Section C – Difference between 10/6/2011 and 10/27/2011 149

Figure E-48: Section C – Difference between 10/27/2011 and 4/10/2012 150
Figure E-49: Section C – Difference between 4/10/2012 and 5/9/2012 151
Figure E-50: Section D – Difference between 8/25/2011 and 10/6/2011 152
Figure E-51: Section D – Difference between 10/6/2011 and 10/27/2011 153
Figure E-52: Section D – Difference between 10/27/2011 and 4/10/2012 154
Figure E-53: Section D – Difference between 4/10/2012 and 5/9/2012 155
Figure E-54: Section E – Difference between 8/25/2011 and 10/6/2011 156
Figure E-55: Section E – Difference between 10/6/2011 and 10/27/2011 157
Figure E-56: Section E – Difference between 10/27/2011 and 4/10/2012 158
Figure E-57: Section E – Difference between 4/10/2012 and 5/9/2012 159
Figure E-58: Section F – Difference between 8/25/2011 and 10/6/2011 160
Figure E-59: Section F – Difference between 10/6/2011 and 10/27/2011 161
Figure E-60: Section F – Difference between 10/27/2011 and 4/10/2012 162
Figure E-61: Section F – Difference between 4/10/2012 and 5/9/2012 163
Figure E-62: Section G – Difference between 8/25/2011 and 10/6/2011 164
Figure E-63: Section G – Difference between 10/6/2011 and 10/27/2011 165
Figure E-64: Section G – Difference between 10/27/2011 and 4/10/2012 166
Figure E-65: Section G – Difference between 4/10/2012 and 5/9/2012 167
Figure F-1: Section A – Half-cell potential on 8/25/11 169
Figure F-2: Section A – Half-cell potential on 10/6/11 169
Figure F-3: Section A – Half-cell potential on 10/27/11 170
Figure F-4: Section A – Half-cell potential on 4/10/12 170
Figure F-5: Section A – Half-cell potential on 5/9/12 171
Figure F-6: Section B – Half-cell potential on 8/25/11 171
Figure F-7: Section B – Half-cell potential on 10/6/11 172
Figure F-8: Section B – Half-cell potential in 10/27/11 172
Figure F-9: Section B – Half-cell potential on 4/10/12 173
Figure F-10: Section B – Half-cell potential on 5/9/12 173
Figure F-11: Section C – Half-cell potential on 8/25/11 174
Figure F-12: Section C – Half-cell potential on 10/6/11 174
Figure F-13: Section C – Half-cell potential in 10/27/11 175
Figure F-14: Section C – Half-cell potential on 4/10/12 175

Figure F-15: Section C – Half-cell potential on 5/9/12 176
Figure F-16: Section D – Half-cell potential on 8/25/11 176
Figure F-17: Section D – Half-cell potential on 10/6/11 177
Figure F-18: Section D – Half-cell potential in 10/27/11 177
Figure F-19: Section D – Half-cell potential on 4/10/12 178
Figure F-20: Section D – Half-cell potential on 5/9/12 178
Figure F-21: Section E – Half-cell potential on 8/25/11 179
Figure F-22: Section E – Half-cell potential on 10/6/11 179
Figure F-23: Section E – Half-cell potential on 10/27/11 180
Figure F-24: Section E – Half-cell potential on 4/10/12 180
Figure F-25: Section E – Half-cell potential on 5/9/12 181
Figure F-26: Section F – Half-cell potential on 8/25/11 181
Figure F-27: Section F – Half-cell potential on 10/6/11 182
Figure F-28: Section F – Half-cell potential on 10/27/11 182
Figure F-29: Section F – Half-cell potential on 4/10/12 183
Figure F-30: Section F – Half-cell potential on 5/9/12 183
Figure F-31: Section G – Half-cell potential on 8/25/11 184
Figure F-32: Section G – Half-cell potential on 10/6/11 184
Figure F-33: Section G – Half-cell potential on 10/27/11 185
Figure F-34: Section G – Half-cell potential on 4/10/12 185
Figure F-35: Section G – Half-cell potential on 5/9/12 186
Figure F-36: Section A – Change in Half-cell potential from 8/25/11 to 10/6/11 186
Figure F-37: Section A – Change in Half-cell potential from 10/6/11 to 10/27/11 187
Figure F-38: Section A – Change in Half-cell potential from 10/27/11 to 4/10/12 187
Figure F-39: Section A – Change in Half-cell potential from 4/10/12 to 5/9/12 188
Figure F-40: Section A – Change in Half-cell potential from 8/25/11 to 5/9/12 188
Figure F-41: Section B – Change in Half-cell potential from 8/25/11 to 10/6/11 189
Figure F-42: Section B – Change in Half-cell potential from 10/6/11 to 10/27/11 189
Figure F-43: Section B – Change in Half-cell potential from 10/27/11 to 4/10/12 190
Figure F-44: Section B – Change in Half-cell potential from 4/10/12 to 5/9/12 190
Figure F-45: Section B – Change in Half-cell potential from 8/25/11 to 5/9/12 191
Figure F-46: Section C – Change in Half-cell potential from 8/25/11 to 10/6/11 191

Figure F-47: Section C – Change in Half-cell potential from 10/6/11 to 10/27/11.....192
Figure F-48: Section C – Change in Half-cell potential from 10/27/11 to 4/10/12.....192
Figure F-49: Section C – Change in Half-cell potential from 4/10/12 to 5/9/12.....193
Figure F-50: Section C – Change in Half-cell potential from 8/25/11 to 5/9/12.....193
Figure F-51: Section D – Change in Half-cell potential from 8/25/11 to 10/6/11 194
Figure F-52: Section D – Change in Half-cell potential from 10/6/11 to 10/27/11 194
Figure F-53: Section D – Change in Half-cell potential from 10/27/11 to 4/10/12 195
Figure F-54: Section D – Change in Half-cell potential from 4/10/12 to 5/9/12 195
Figure F-55: Section D – Change in Half-cell potential from 8/25/11 to 5/9/12 196
Figure F-56: Section E – Change in Half-cell potential from 8/25/11 to 10/6/11.....196
Figure F-57: Section E – Change in Half-cell potential from 10/6/11 to 10/27/11.....197
Figure F-58: Section E – Change in Half-cell potential from 10/27/11 to 4/10/12.....197
Figure F-59: Section E – Change in Half-cell potential from 4/10/12 to 5/9/12.....198
Figure F-60: Section E – Change in Half-cell potential from 8/25/11 to 5/9/12.....198
Figure F-61: Section F – Change in Half-cell potential from 8/25/11 to 10/6/11 199
Figure F-62: Section F – Change in Half-cell potential from 10/6/11 to 10/27/11 199
Figure F-63: Section F – Change in Half-cell potential from 10/27/11 to 4/10/12 200
Figure F-64: Section F – Change in Half-cell potential from 4/10/12 to 5/9/12 200
Figure F-65: Section F – Change in Half-cell potential from 8/25/11 to 5/9/12 201
Figure F-66: Section G – Change in Half-cell potential from 8/25/11 to 10/6/11 201
Figure F-67: Section G – Change in Half-cell potential from 10/6/11 to 10/27/11 202
Figure F-68: Section G – Change in Half-cell potential from 10/27/11 to 4/10/12 202
Figure F-69: Section G – Change in Half-cell potential from 4/10/12 to 5/9/12 203
Figure F-70: Section G – Change in Half-cell potential from 8/25/11 to 5/9/12 203

APPENDIX A. SITE SELECTION MATRIX FOR STATEWIDE EVALUATION

Table A-1: Site selection matrix for statewide evaluation

Project Rank (1)	Project Rating (5) ,(6)	Segment Rank (2)	Segment Rating (5), (6)	Interstate	Beginning MRM	Ending MRM	Length (miles)	Lane	Project Number(3)	Region/ Reporting Unit (1),(4)	Surface Condition Index (4)	Year Built (4)	Precipitation Region(5)	Average 3-year Maintenance Cost (per mile)(4)	Estimated Deicer Applied per mile (lbs) (3),(5)	Indices(5)				
																Condition Value	Age Value	Precipitation Value	Maintenance Activities Value	Deicer Application Value
1	1.429	12	1.422	I-29	65.00	72.00	7.00	NB	IM 29-2(9)61	271	4.02	2001	Wet	1807	459,127	0.804	0.500	0.5	0.334	0.059	(a), (b)
		13	1.440	I-29	61.00	64.57	3.57	NB	IM 29-2(9)61	271	4.11	2001	Wet	1807	459,127	0.822	0.500	0.5	0.334	0.059	(a)
		16	1.458	I-29	64.57	65.00	0.43	NB	IM 29-2(9)61	271	4.20	2001	Wet	1807	459,127	0.840	0.500	0.5	0.334	0.059	(a)
2	1.442	1	1.118	I-229	5.70	8.28	2.58	NB	IM 229-2(50)2	271	4.17	2001	Wet	2712	459,127	0.834	0.500	0.5	0.000	0.059	(a)
		3	1.418	I-229	2.08	2.89	0.81	NB	IM 229-2(50)2	271	4.20	2001	Wet	1914	459,127	0.840	0.500	0.5	0.294	0.059	(a)
		3	1.418	I-229	2.89	3.12	0.23	NB	IM 229-2(50)2	271	4.20	2001	Wet	1914	459,127	0.840	0.500	0.5	0.294	0.059	(a)
		3	1.418	I-229	3.93	4.16	0.23	NB	IM 229-2(50)2	271	4.20	2001	Wet	1914	459,127	0.840	0.500	0.5	0.294	0.059	(a)
		3	1.418	I-229	4.95	5.00	0.05	NB	IM 229-2(50)2	271	4.20	2001	Wet	1914	459,127	0.840	0.500	0.5	0.294	0.059	(a)
		7	1.418	I-229	2.07	2.08	0.01	NB	IM 229-2(50)2	271	4.20	2001	Wet	1913	459,127	0.840	0.500	0.5	0.295	0.059	(a)
		7	1.418	I-229	3.12	3.93	0.81	NB	IM 229-2(50)2	271	4.20	2001	Wet	1913	459,127	0.840	0.500	0.5	0.295	0.059	(a)
		7	1.418	I-229	4.16	4.95	0.79	NB	IM 229-2(50)2	271	4.20	2001	Wet	1913	459,127	0.840	0.500	0.5	0.295	0.059	(a)
		7	1.419	I-229	5.00	5.32	0.32	NB	IM 229-2(50)2	271	4.20	2001	Wet	1912	459,127	0.840	0.500	0.5	0.295	0.059	(a)
		19	1.578	I-229	2.94	3.12	0.18	SB	IM 229-2(50)2	271	4.05	2001	Wet	1399	459,127	0.810	0.500	0.5	0.484	0.059	(a)
		20	1.594	I-229	3.12	3.97	0.85	SB	IM 229-2(50)2	271	4.13	2001	Wet	1398	459,127	0.826	0.500	0.5	0.485	0.059	(a)
		20	1.595	I-229	5.70	8.28	2.58	SB	IM 229-2(50)2	271	4.24	2001	Wet	1455	459,127	0.848	0.500	0.5	0.463	0.059	(a)
		23	1.603	I-229	3.97	4.16	0.19	SB	IM 229-2(50)2	271	4.17	2001	Wet	1397	459,127	0.834	0.500	0.5	0.485	0.059	(a)
		24	1.608	I-229	4.16	5.32	1.16	SB	IM 229-2(50)2	271	4.20	2001	Wet	1398	459,127	0.840	0.500	0.5	0.485	0.059	(a)
		24	1.609	I-229	2.08	2.94	0.86	SB	IM 229-2(50)2	271	4.20	2001	Wet	1397	459,127	0.840	0.500	0.5	0.485	0.059	(a)
		26	1.609	I-229	2.07	2.08	0.01	SB	IM 229-2(50)2	271	4.20	2001	Wet	1395	459,127	0.840	0.500	0.5	0.486	0.059	(a)

																Indices[5]				
Project Rank (1)	**Project Rating** (5) ,(6)	**Segment Rank** (2)	**Segment Rating** (5), (6)	**Interstate**	**Beginning MRM**	**Ending MRM**	**Length (miles)**	**Lane**	**Project Number**[3]	**Region/ Reporting Unit** (1),(4)	**Surface Condition Index** (4)	**Year Built** (4)	**Precipitation Region**[5]	**Average 3-year Maintenance Cost (per mile)**[4]	**Estimated Deicer Applied per mile (lbs)** (3),(5)	**Condition Value**	**Age Value**	**Precipitation Value**	**Maintenance Activities Value**	**Deicer Application Value**	
3	1.461	2	1.344	I-29	83.00	83.70	0.70	NB	IM 29-3(68)80	271	4.12	2003	Wet	2047	487,828	0.824	0.667	0.5	0.245	0.000	(a)
		11	1.361	I-29	80.29	83.00	2.71	NB	IM 29-3(68)80	271	4.20	2003	Wet	2046	487,828	0.840	0.667	0.5	0.246	0.000	(a)
		28	1.573	I-29	83.00	83.38	0.38	SB	IM 29-3(68)80	271	4.20	2003	Wet	1470	487,828	0.840	0.667	0.5	0.458	0.000	(a)
		29	1.577	I-29	80.29	83.00	2.71	SB	IM 29-3(68)80	271	4.22	2003	Wet	1470	487,828	0.844	0.667	0.5	0.458	0.000	(a)
4	1.492	14	1.385	I-29	79.98	80.29	0.31	NB	IM 29-3(38)79 & P 1298(2)	271	4.20	2004	Wet	2047	487,828	0.840	0.750	0.5	0.245	0.000	(a)
		15	1.386	I-29	79.26	79.98	0.72	NB	IM 29-3(38)79 & P 1298(2)	271	4.20	2004	Wet	2046	487,828	0.840	0.750	0.5	0.246	0.000	(a)
		31	1.598	I-29	79.26	79.98	0.72	SB	IM 29-3(38)79 & P 1298(2)	271	4.20	2004	Wet	1470	487,828	0.840	0.750	0.5	0.458	0.000	(a)
		31	1.598	I-29	79.98	80.29	0.31	SB	IM 29-3(38)79 & P 1298(2)	271	4.20	2004	Wet	1470	487,828	0.840	0.750	0.5	0.458	0.000	(a)
5	1.551	26	1.551	I-29	85.35	97.00	11.65	NB	IM 29-3(82)84	271	3.68	1999	Wet	975	487,828	0.736	0.333	0.5	0.640	0.000	(a), (b)
6	1.597	17	1.498	I-29	83.38	84.21	0.83	SB	IM 29-3(83)84	271	4.20	2000	Wet	1469	487,828	0.840	0.417	0.5	0.458	0.000	(a)
		33	1.604	I-29	85.00	97.00	12.00	SB	IM 29-3(83)84	271	4.02	2000	Wet	1085	487,828	0.804	0.417	0.5	0.600	0.000	(a)
7	1.602	22	1.602	I-29	61.00	72.00	11.00	SB	IM 29-2(10)62	271	4.18	2000	Wet	1336	459,127	0.836	0.417	0.5	0.507	0.059	(a)
8	1.641	18	1.558	I-29	72.00	73.78	1.78	NB	IM 29-2(52)72	271	4.20	2005	Wet	1807	459,127	0.840	0.833	0.5	0.334	0.059	(a)
		36	1.731	I-29	72.00	73.66	1.66	SB	IM 29-2(52)72	271	4.20	2005	Wet	1336	459,127	0.840	0.833	0.5	0.507	0.059	(a)
9	1.649	30	1.649	I-90	401.61	412.00	10.39	WB	IM 90-9(63)401	271	4.01	1997	Wet	913	459,127	0.802	0.167	0.5	0.663	0.059	(a), (b)
10	1.707	34	1.707	I-90	401.61	412.00	10.39	EB	IMID 90-9(70)401	271	3.89	1998	Wet	758	459,127	0.778	0.250	0.5	0.721	0.059	(a)
11	1.719	35	1.719	I-29	97.00	110.10	13.10	NB	IM 29-3(92)97	272	3.66	1998	Wet	975	392,085	0.732	0.250	0.5	0.640	0.196	(a)
12	1.753	37	1.753	I-29	97.00	110.11	13.11	SB	IM29-3(89)97	272	4.16	1997	Wet	1085	392,085	0.832	0.167	0.5	0.600	0.196	(a)

13	2.262	38	2.262	I-29	110.10	110.10	0.00	NB	IM 29-4(58)	272	5.00	2009	Wet	974	392,085	1.000	1.167	0.5	0.641	0.196

(c)

Project Rank (1)	Project Rating (5),(6)	Segment Rank (2)	Segment Rating (5), (6)	Interstate	Beginning MRM	Ending MRM	Length (miles)	Lane	Project Number(3)	Region/ Reporting Unit(1),(4)	Surface Condition Index(4)	Year Built(4)	Precipitation Region(5)	Average 3-year Maintenance Cost (per mile)(4)	Estimated Deicer Applied per mile (lbs)(3),(5)	Condition Value	Age Value	Precipitation Value	Maintenance Activities Value	Deicer Application Value
14	**2.526**	**40**	**2.526**	**I-90**	**213.10**	**226.68**	**13.58**	**EB**	**IM 90-5(66)187**	**391**	**4.01**	**2000**	**Dry**	**688**	**144,958**	**0.802**	**0.417**	**1**	**0.746**	**0.703**
		41	**2.533**	**I-90**	**226.68**	**227.00**	**0.32**	**EB**	**IM 90-5(66)187**	**391**	**4.04**	**2000**	**Dry**	**685**	**144,958**	**0.808**	**0.417**	**1**	**0.747**	**0.703**
15	2.539	39	2.515	I-90	18.48	19.42	0.94	EB	IM 90-1(45)18	451	4.06	2001	Dry	657	173,100	0.812	0.500	1	0.758	0.645
		43	2.541	I-90	19.42	28.34	8.92	EB	IM 90-1(45)18	451	4.19	2001	Dry	656	173,100	0.838	0.500	1	0.758	0.645
16	2.567	44	2.567	I-90	10.08	18.48	8.40	EB		451	3.82	2005	Dry	656	173,100	0.764	0.833	1	0.758	0.645
17	**2.579**	**45**	**2.579**	**I-29**	**27.00**	**37.32**	**10.32**	**SB**	**IM 29-1(44)27**	**291**	**4.33**	**2001**	**Wet**	**764**	**112,280**	**0.866**	**0.500**	**0.5**	**0.718**	**0.770**
118	2.638	442	2.535	I-90	210.14	213.10	2.96	EB	IM 90-5(52)210	391	4.18	1999	Dry	688	144,958	0.836	0.333	1	0.746	0.703
		52	2.739	I-90	210.14	213.15	3.01	WB	IM 90-5(52)210	391	4.42	1999	Dry	265	144,958	0.884	0.333	1	0.902	0.703
19	2.643	46	2.636	I-90	264.68	265.00	0.32	EB	IM 90-5(80)262	253	4.20	1995	Wet	523	41,895	0.840	0.000	0.5	0.807	0.914
		46	2.637	I-90	263.34	264.68	1.34	EB	IM 90-5(80)262	253	4.20	1995	Wet	522	41,895	0.840	0.000	0.5	0.808	0.914
		48	2.651	I-90	263.39	265.00	1.61	WB	IM 90-5(80)262	253	4.29	1995	Wet	533	41,895	0.858	0.000	0.5	0.803	0.914
20	2.681	49	2.681	I-90	10.08	18.58	8.50	WB		451	3.46	2005	Dry	152	173,100	0.692	0.833	1	0.944	0.645
21	2.693	50	2.684	I-90	18.58	19.42	0.84	WB	IM 90-1(25)19	451	4.10	2000	Dry	152	173,100	0.820	0.417	1	0.944	0.645
		51	2.694	I-90	19.42	28.34	8.92	WB	IM 90-1(25)19	451	4.15	2000	Dry	152	173,100	0.830	0.417	1	0.944	0.645
22	2.742	53	2.742	I-90	213.15	227.00	13.85	WB	IM 90-5(53)213	391	4.18	2001	Dry	264	144,958	0.836	0.500	1	0.903	0.703
23	2.747	54	2.747	I-90	251.60	259.90	8.30	EB	IM-IDR 90-5(73)251	253	4.08	1996	Dry	429	41,895	0.816	0.083	1	0.842	0.914
24	2.814	55	2.814	I-29	27.00	37.32	10.32	NB	IM 29-1(63)	291	4.49	2002	Wet	282	112,280	0.898	0.583	0.5	0.896	0.770
25	2.824	56	2.824	I-29	37.32	46.31	8.99	SB	IM 29-1(84)	291	4.93	2006	Wet	764	112,280	0.986	0.917	0.5	0.718	0.770
26	2.826	57	2.822	I-90	251.60	259.52	7.92	WB	IM 90-5(86)251	253	4.07	1997	Dry	289	41,895	0.814	0.167	1	0.893	0.914
		73	2.954	I-90	259.60	259.88	0.28	WB	IM 90-5(86)251	253	4.20	1997	Dry	0	41,895	0.840	0.167	1	1.000	0.914

Project Rank [1]	Project Rating [5],[6]	Segment Rank [2]	Segment Rating [5], [6]	Interstate	Beginning MRM	Ending MRM	Length (miles)	Lane	Project Number[3]	Region/ Reporting Unit[1],[4]	Surface Condition Index[4]	Year Built[4]	Precipitation Region[5]	Average 3-year Maintenance Cost (per mile)[4]	Estimated Deicer Applied per mile (lbs)[3],[5]	Condition Value	Age Value	Precipitation Value	Maintenance Activities Value	Deicer Application Value
27	**2.853**	**58**	**2.853**	**I-29**	**4.64**	**17.00**	**12.36**	**NB**	**IM 29-1(72)4**	**291**	**4.25**	**2006**	**Wet**	**316**	**112,280**	**0.850**	**0.917**	**0.5**	**0.883**	**0.770**
28	**2.866**	**59**	**2.864**	**I-90**	**335.00**	**344.34**	**9.34**	**EB**	**IM-BRF 90-8(40)334**	**252**	**3.99**	**2003**	**Wet**	**85**	**86,853**	**0.798**	**0.667**	**0.5**	**0.969**	**0.822**
		69	**2.906**	**I-90**	**334.54**	**335.00**	**0.46**	**EB**	**IM-BRF 90-8(40)334**	**252**	**4.20**	**2003**	**Wet**	**84**	**86,853**	**0.840**	**0.667**	**0.5**	**0.969**	**0.822**
29	2.877	60	2.877	I-90	353.07	362.00	8.93	EB	IM 90-8(79)353	252	4.18	2002	Wet	85	86,853	0.836	0.583	0.5	0.969	0.822
30	2.882	63	2.882	I-90	353.07	362.00	8.93	WB	IM 90-8-(33)353	252	4.30	2001	Wet	68	86,853	0.860	0.500	0.5	0.975	0.822
31	2.883	61	2.881	I-90	338.42	343.73	5.31	WB	IM 90-8(83)334	252	4.17	2002	Wet	68	86,853	0.834	0.583	0.5	0.975	0.822
		61	2.881	I-90	343.73	344.34	0.61	WB	IM 90-8(83)334	252	4.17	2002	Wet	68	86,853	0.834	0.583	0.5	0.975	0.822
		64	2.887	I-90	335.00	338.00	3.00	WB	IM 90-8(83)334	252	4.20	2002	Wet	68	86,853	0.840	0.583	0.5	0.975	0.822
		64	2.887	I-90	334.54	335.00	0.46	WB	IM 90-8(83)334	252	4.20	2002	Wet	67	86,853	0.840	0.583	0.5	0.975	0.822
		64	2.887	I-90	338.00	338.42	0.42	WB	IM 90-8(83)334	252	4.20	2002	Wet	67	86,853	0.840	0.583	0.5	0.975	0.822
32	2.915	71	2.915	I-90	344.34	353.07	8.73	WB	IM-BRF 90-8(41)344	252	4.09	2004	Wet	67	86,853	0.818	0.750	0.5	0.975	0.822
33 (tie)	**2.916**	**67**	**2.907**	**I-90**	**247.00**	**251.60**	**4.60**	**EB**	**IM 90-5(61)236**	**391**	**4.56**	**2007**	**Dry**	**429**	**144,958**	**0.912**	**1.000**	**1**	**0.842**	**0.703**
		68	**2.912**	**I-90**	**246.00**	**247.00**	**1.00**	**EB**	**IM 90-5(61)236**	**391**	**4.59**	**2007**	**Dry**	**430**	**144,958**	**0.918**	**1.000**	**1**	**0.841**	**0.703**
		70	**2.921**	**I-90**	**236.00**	**246.00**	**10.00**	**EB**	**IM 90-5(61)236**	**391**	**4.63**	**2007**	**Dry**	**429**	**144,958**	**0.926**	**1.000**	**1**	**0.842**	**0.703**
33 (tie)	**2.916**	**71**	**2.916**	**I-90**	**344.34**	**353.07**	**8.73**	**EB**	**IM 90-8(43)344**	**252**	**4.00**	**2005**	**Wet**	**85**	**86,853**	**0.800**	**0.833**	**0.5**	**0.969**	**0.822**
35	**2.967**	**74**	**2.967**	**I-29**	**165.00**	**179.00**	**14.00**	**SB**	**IMBR29-6(23)164**	**171**	**4.02**	**2004**	**Dry**	**449**	**22,729**	**0.804**	**0.750**	**1**	**0.834**	**0.953**
36	3.008	75	3.008	I-29	151.22	165.00	13.78	SB	IM29-6(21)	171	4.35	2003	Dry	449	22,729	0.870	0.667	1	0.834	0.953
37	3.114	77	3.114	I-29	139.30	151.22	11.92	SB	IM29-5(22)141	171	4.38	2007	Dry	449	22,729	0.876	1.000	1	0.834	0.953
38	3.120	76	3.079	I-90	52.44	56.00	3.56	EB	IMBF 90-1(10)6	452	4.47	2005	Dry	122	83,170	0.894	0.833	1	0.955	0.830
		79	3.161	I-90	52.44	56.00	3.56	WB	IMBF 90-1(10)6	452	4.80	2005	Dry	78	83,170	0.960	0.833	1	0.971	0.830
39	3.136	78	3.136	I-29	151.31	165.00	13.69	NB	IMBF29-6(15)151	171	4.21	2005	Dry	162	22,729	0.842	0.833	1	0.940	0.953
40	**3.173**	**80**	**3.173**	**I-29**	**165.00**	**179.00**	**14.00**	**NB**	**IM29-6(26)164**	**171**	**4.27**	**2006**	**Dry**	**162**	**22,729**	**0.854**	**0.917**	**1**	**0.940**	**0.953**

Notes:

Recommended projects in bold print.

(1) Projects are ranked from 1 to 40, with 1 being the lowest quality and 40 being the highest quality

(2) Pavement Segments are ranked from 1 to 80, with 1 being the lowest quality and 80 being the highest quality

(3) Information provided by SDDOT

(4) Information provided by SDDOT Highway Needs and Project Analysis Report

(5) See attached discussion

(6)

Category	**Weighting Factor**
Condition	1.00
Age	0.30
Precipitation	0.15
Maintenance	1.00
Deicer Application	1.00

(a) Project within 20 miles of Sioux Falls

(b) Tested previously, exclude

(c) Maintenance site, exclude

APPENDIX B. EQUIPOTENTIAL CONTOUR MAPS FOR INITIAL AND STATEWIDE ASSESSMENTS

Crack and Equipotential Maps

MRM 87 Fall 2010

MRM 87 Spring 2011

MRM 68 Fall 2010

MRM 68 Spring 2011

MRM 411 Fall 2010

MRM 411 Spring 2011

MRM 33

MRM 44

MRM 25

MRM 54

MRM 222

MRM 246

MRM 168NB

MRM 168SB

Minimum Reading (mV)	Maximum Reading (mV)	Color
−750.00	−720.00	
−720.00	−690.00	
−690.00	−660.00	
−660.00	−630.00	
−630.00	−600.00	
−600.00	−570.00	
−570.00	−540.00	
−540.00	−510.00	
−510.00	−480.00	
−480.00	−450.00	
−450.00	−420.00	
−420.00	−390.00	
−390.00	−360.00	
−360.00	−330.00	
−330.00	−300.00	
−300.00	−270.00	
−270.00	−240.00	
−240.00	−210.00	
−210.00	−180.00	
−180.00	−150.00	

Figure B-1: Equipotential contour map legend

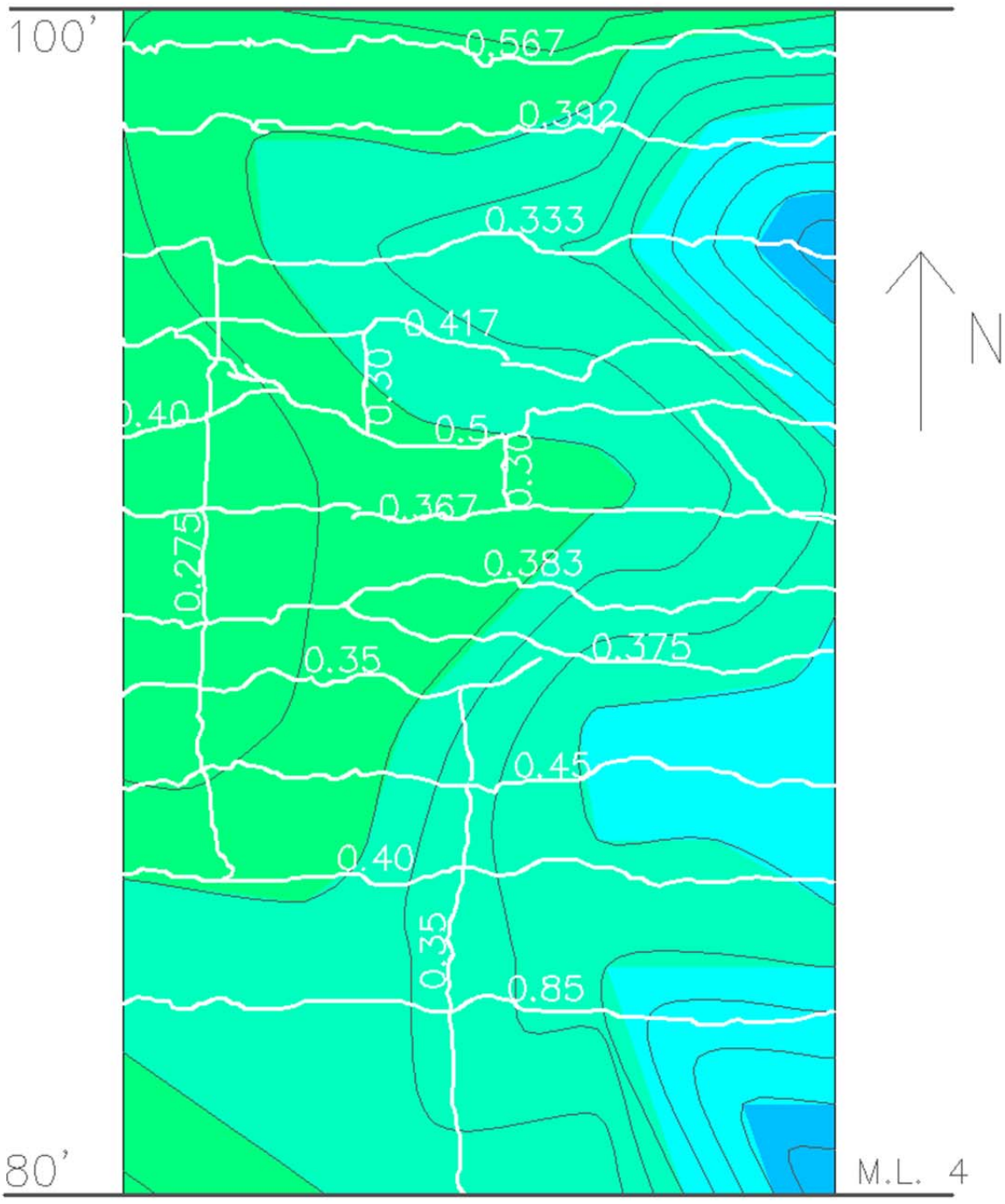

Figure B-2: MRM 87 fall 2010 from 80 to 100 feet

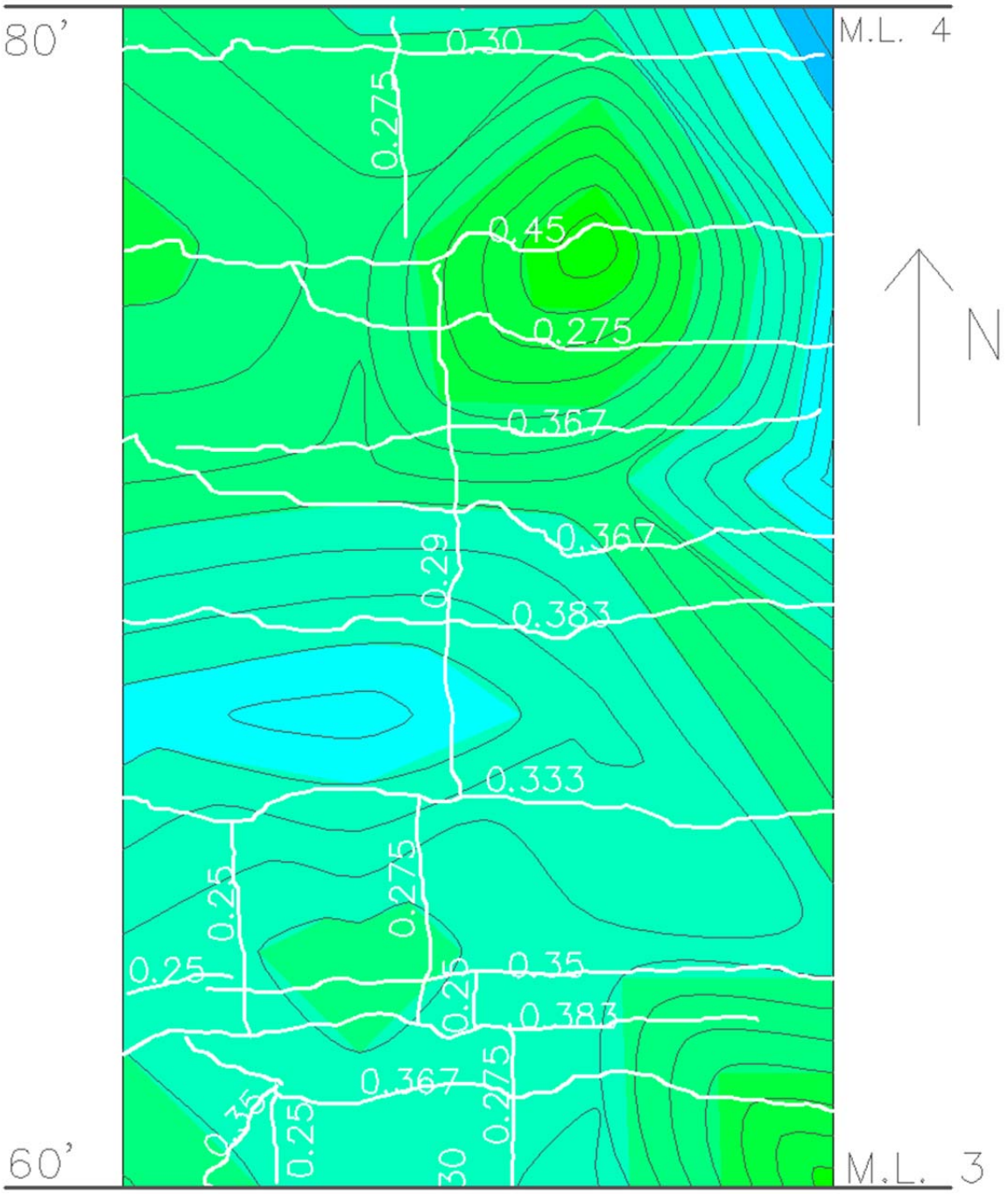

Figure B-3: MRM 87 fall 2010 from 60 to 80 feet

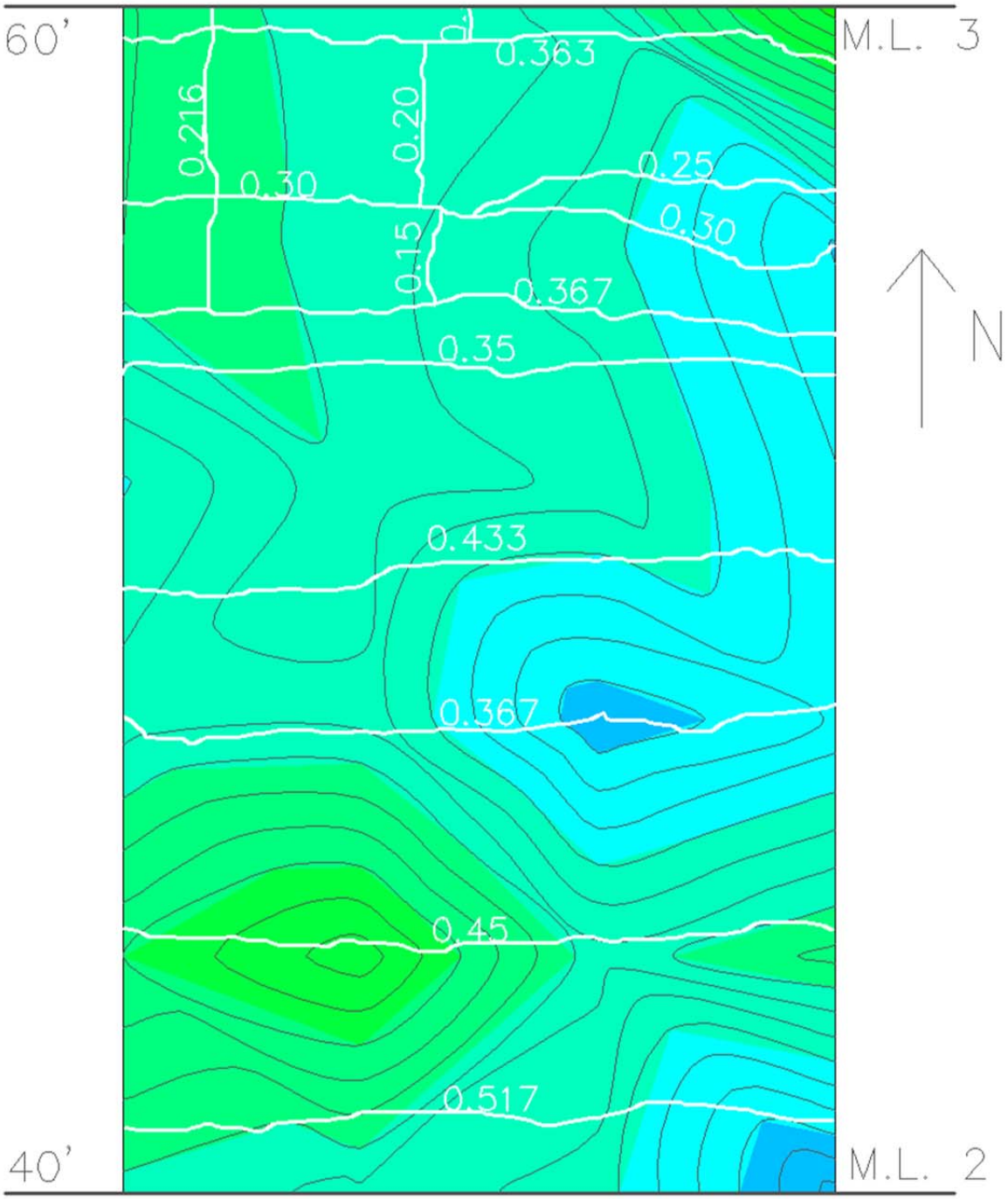

Figure B-4: MRM 87 fall 2010 from 40 to 60 feet

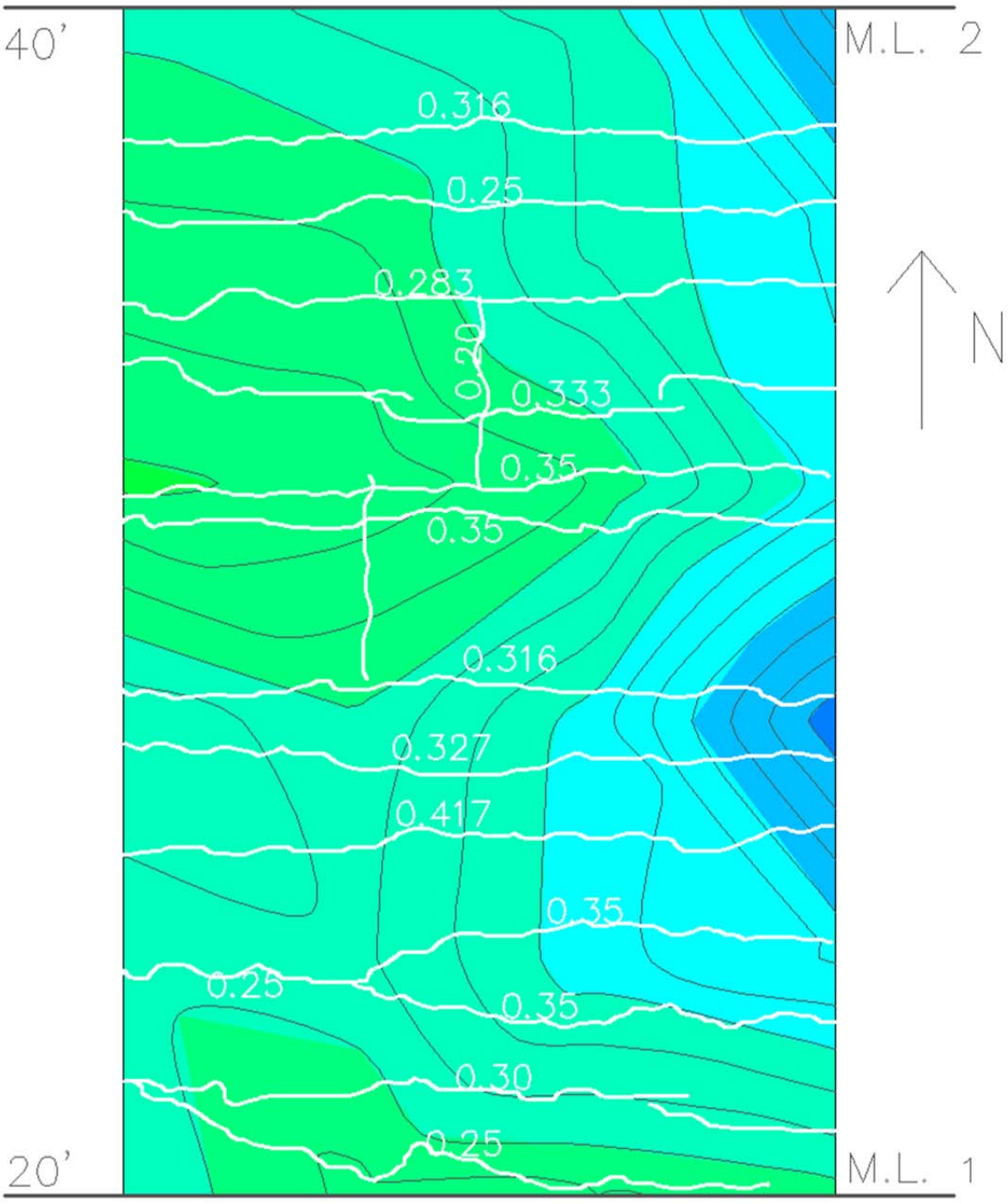

Figure B-5: MRM 87 fall 2010 from 20 to 40 feet

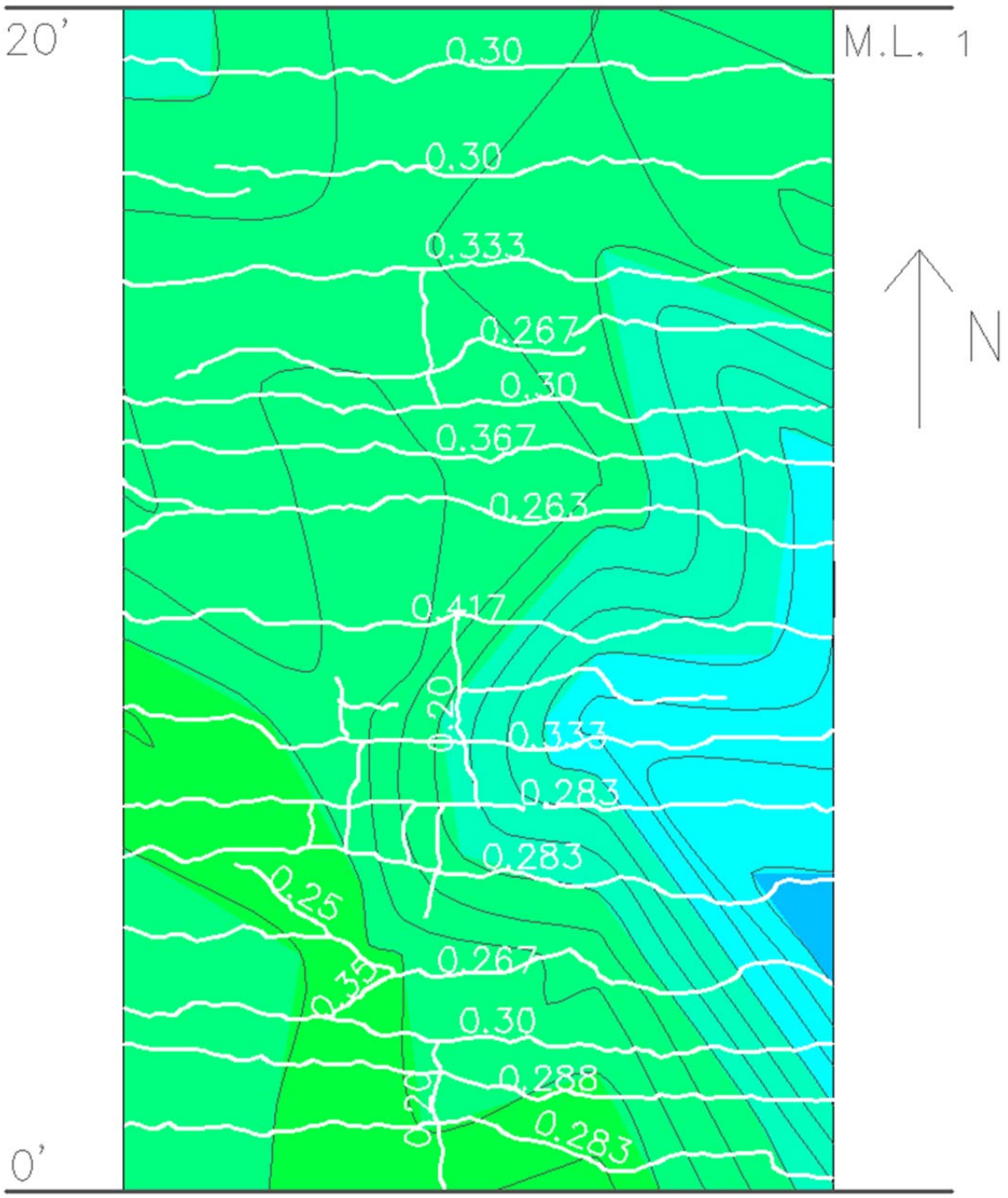

Figure B-6: MRM 87 fall 2010 from 0 to 20 feet

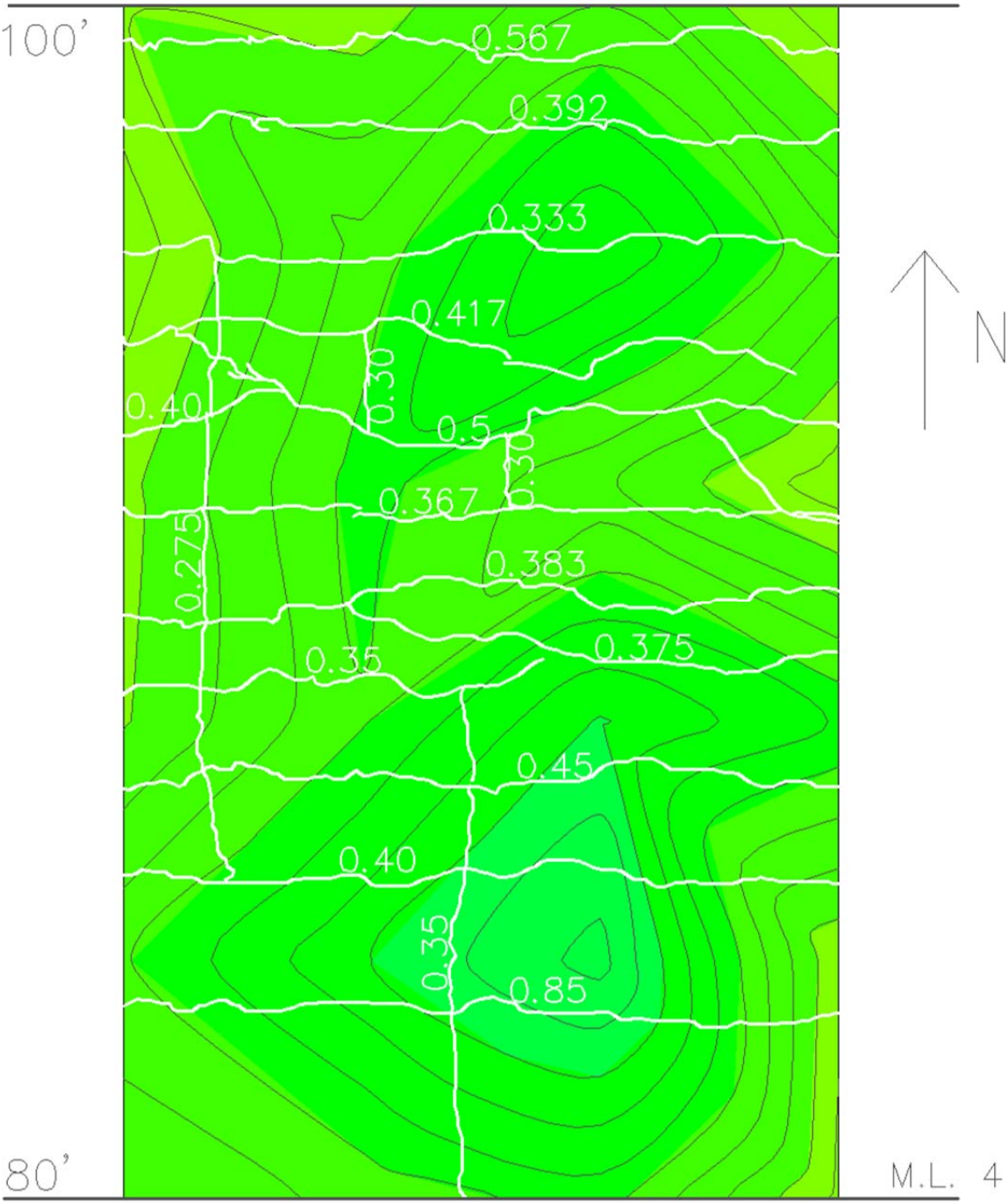

Figure B-7: MRM 87 spring 2011 from 80 to 100 feet

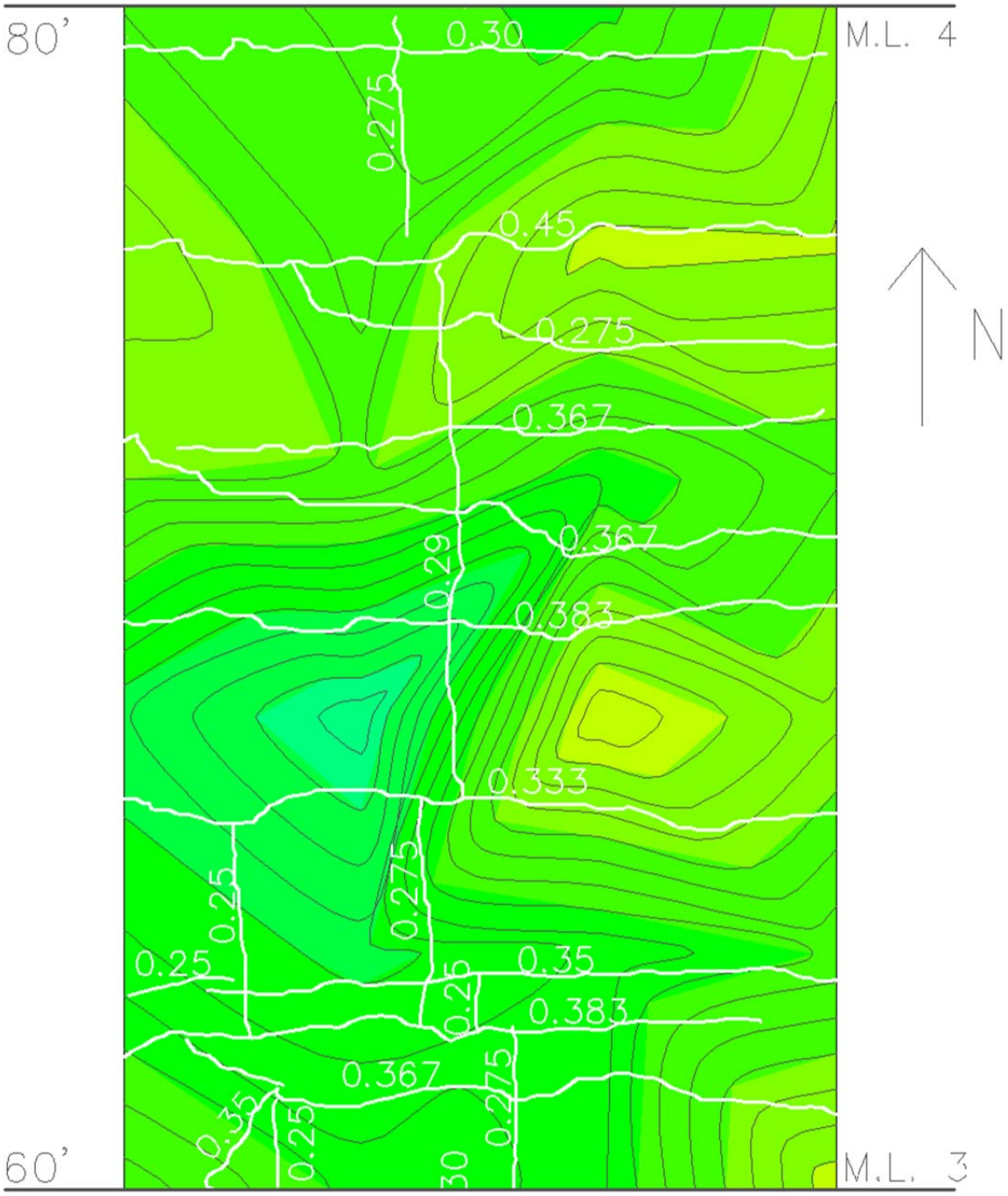

Figure B-8: MRM 87 spring 2011 from 60 to 80 feet

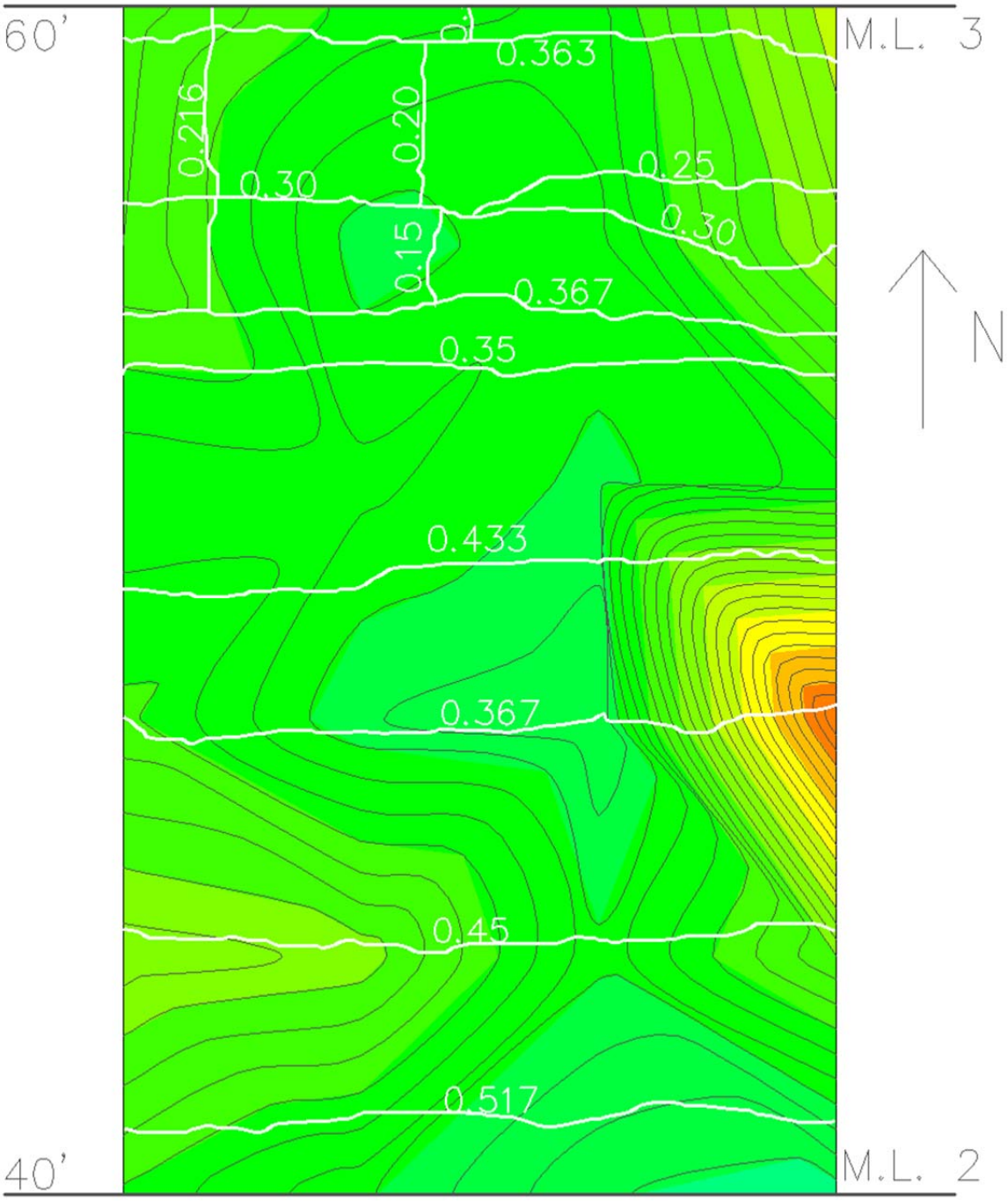

Figure B-9: MRM 87 spring 2011 from 40 to 60 feet

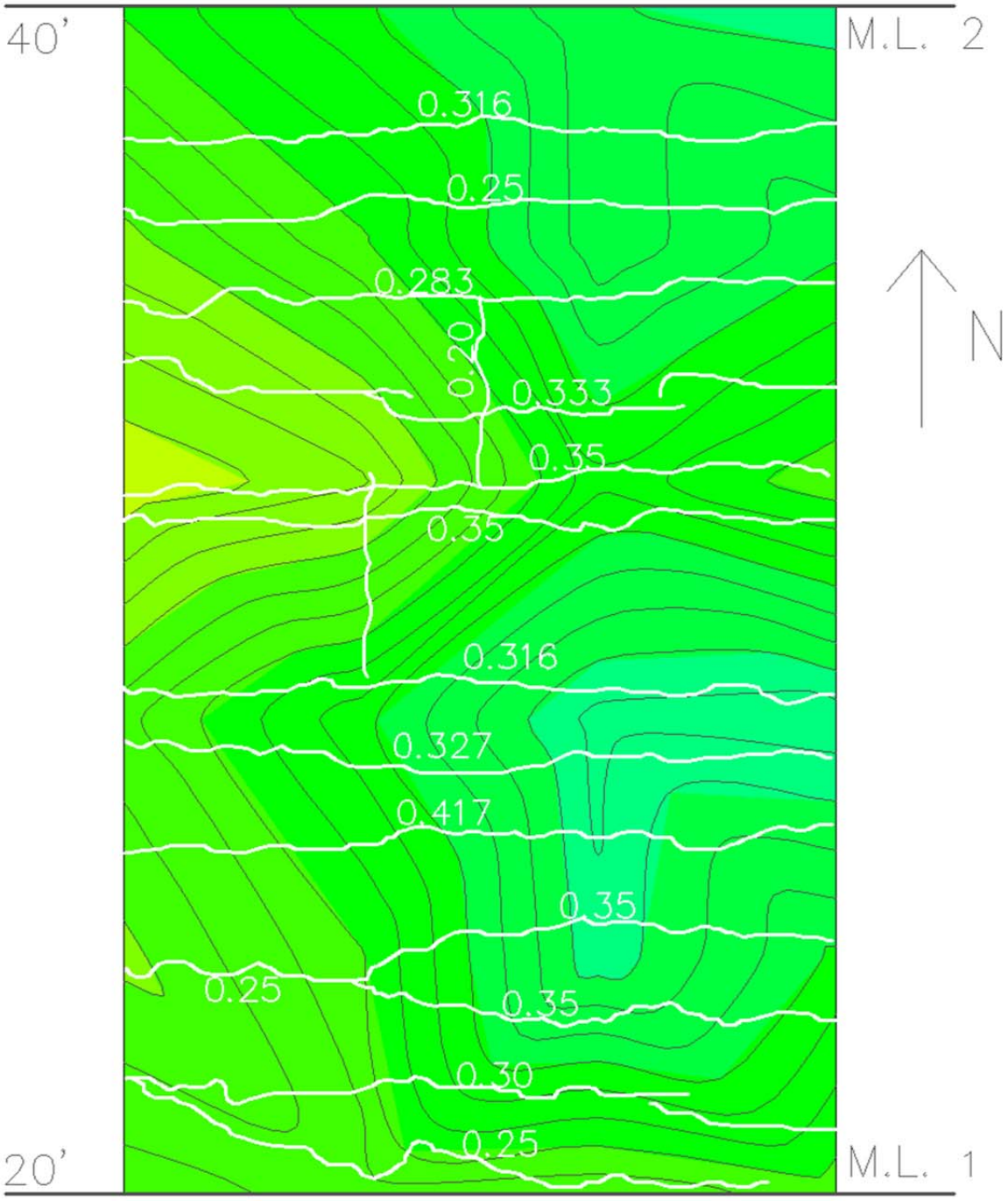

Figure B-10: MRM 87 spring 2011 from 20 to 40 feet

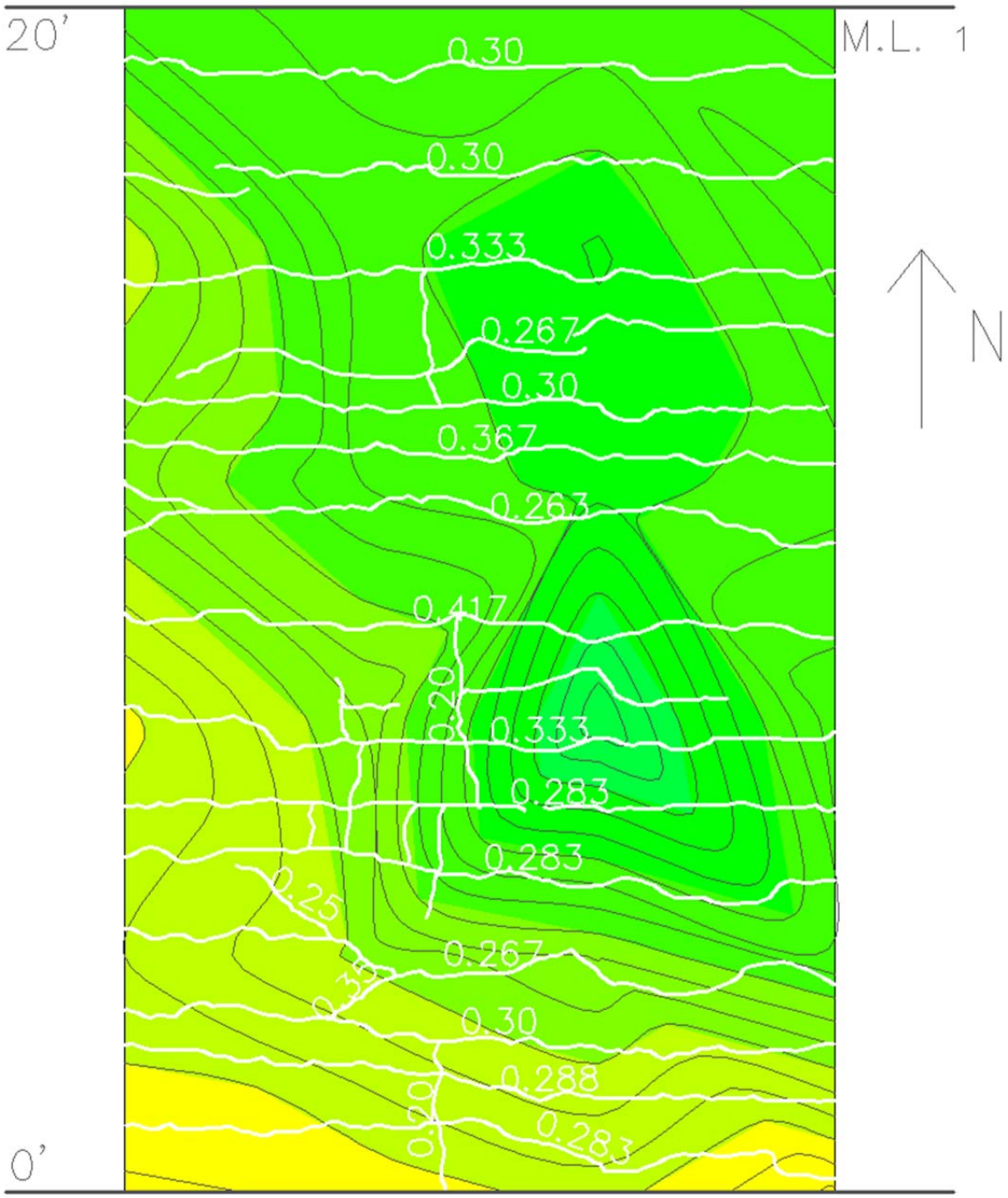

Figure B-11: MRM 87 spring 2011 from 0 to 20 feet

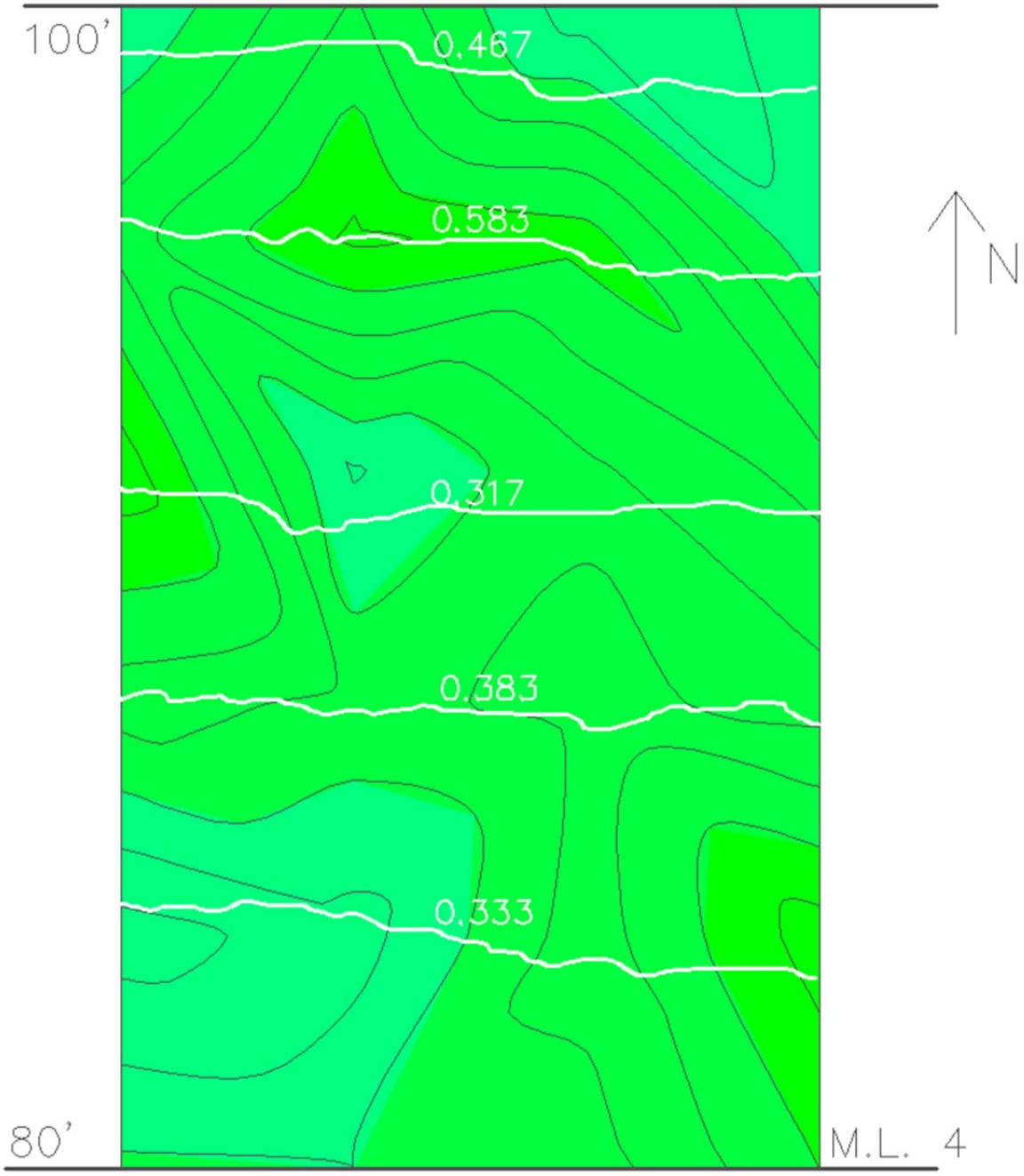

Figure B-12: MRM 68 fall 2010 from 80 to 100 feet

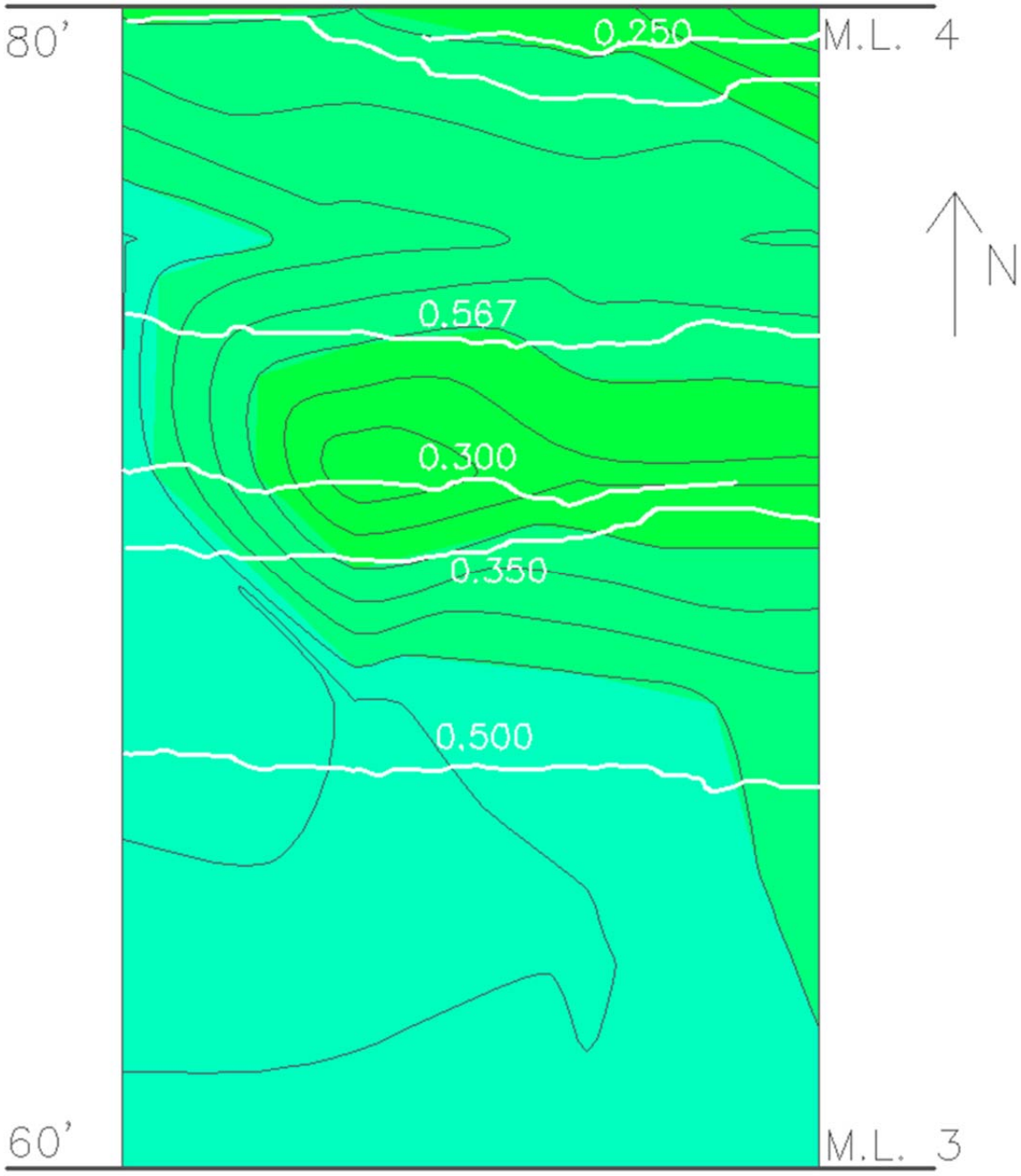

Figure B-13: MRM 68 fall 2010 from 60 to 80 feet

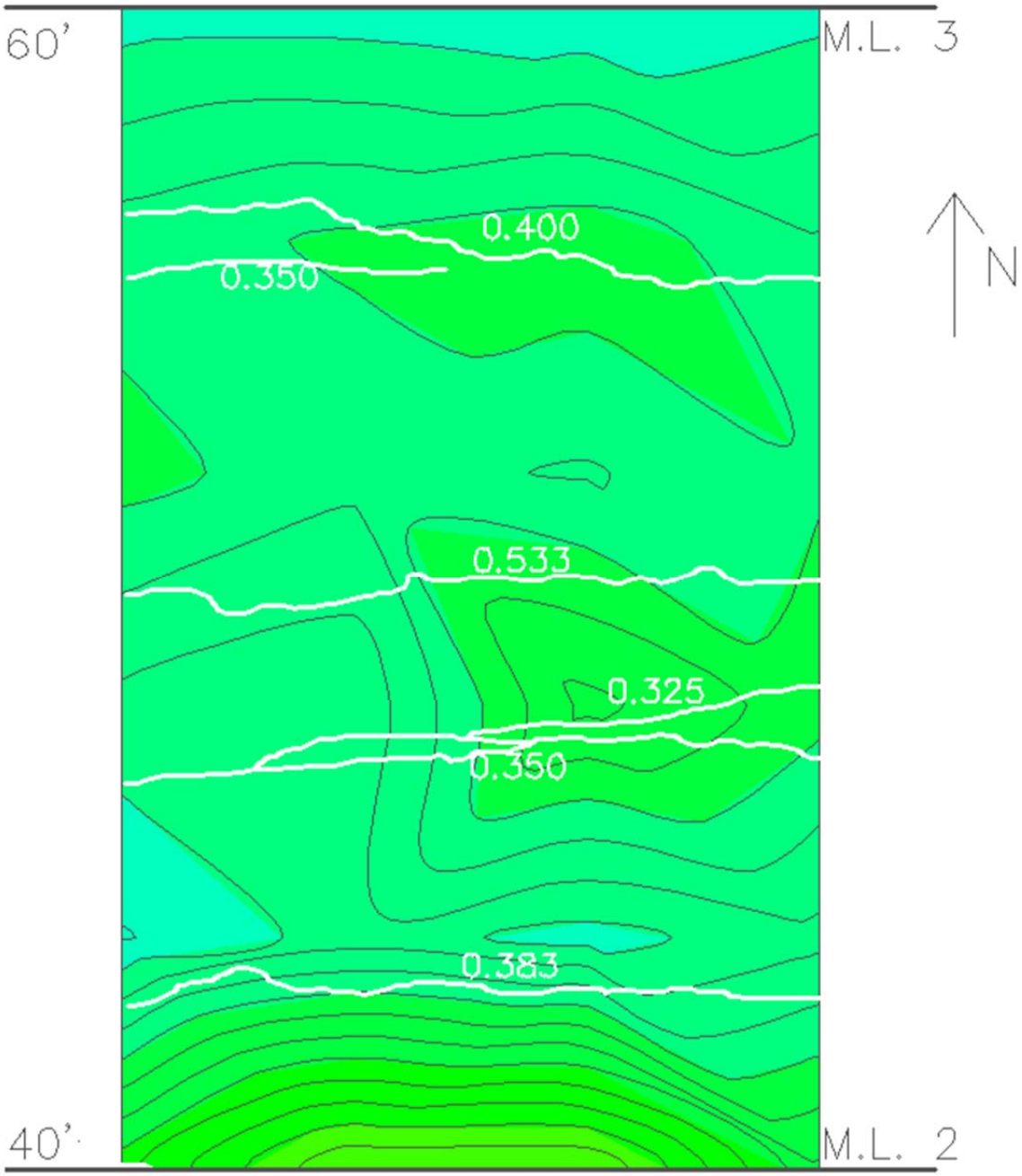

Figure B-14: MRM 68 fall 2010 from 40 to 60 feet

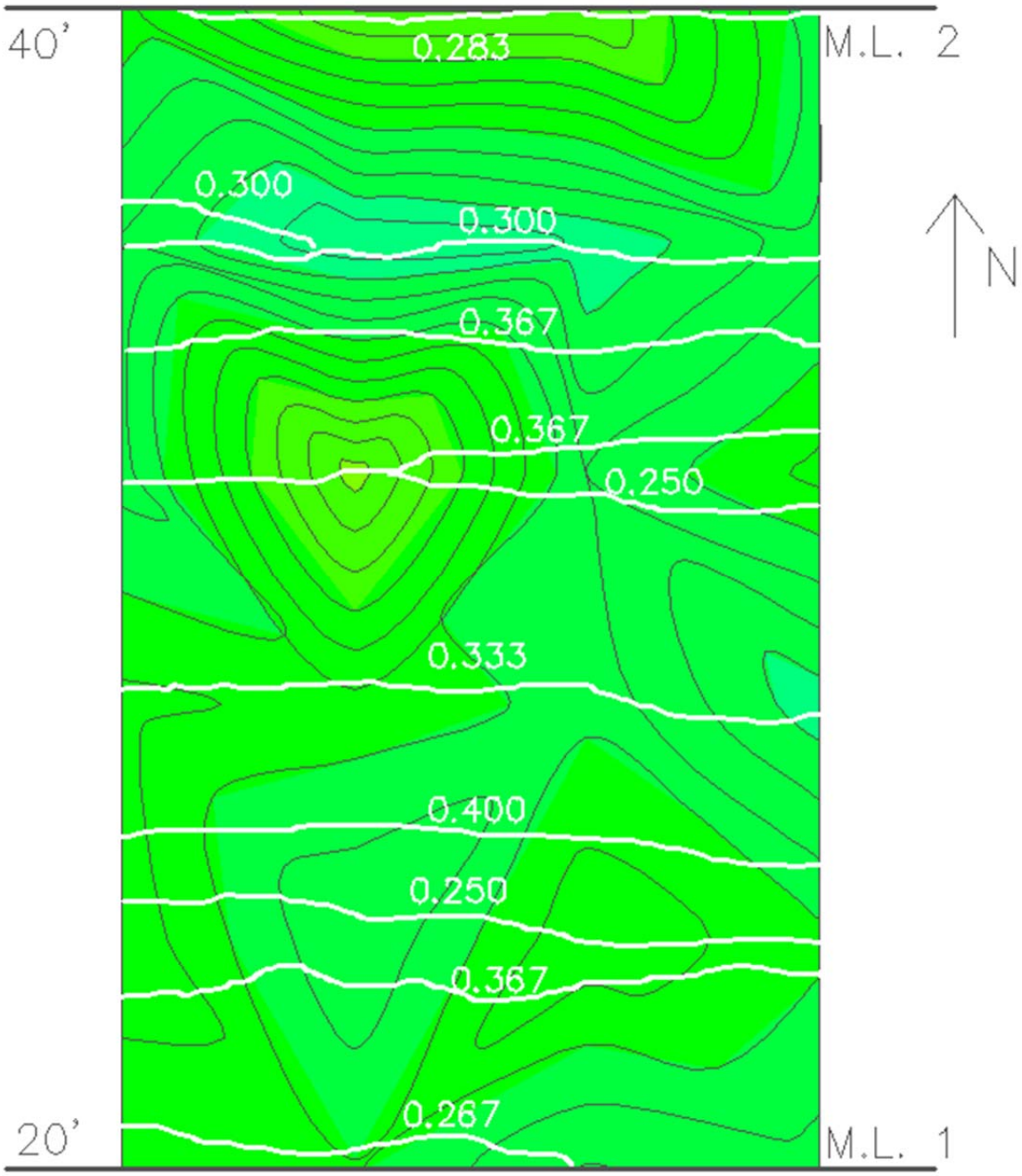

Figure B-15: MRM 68 fall 2010 from 20 to 40 feet

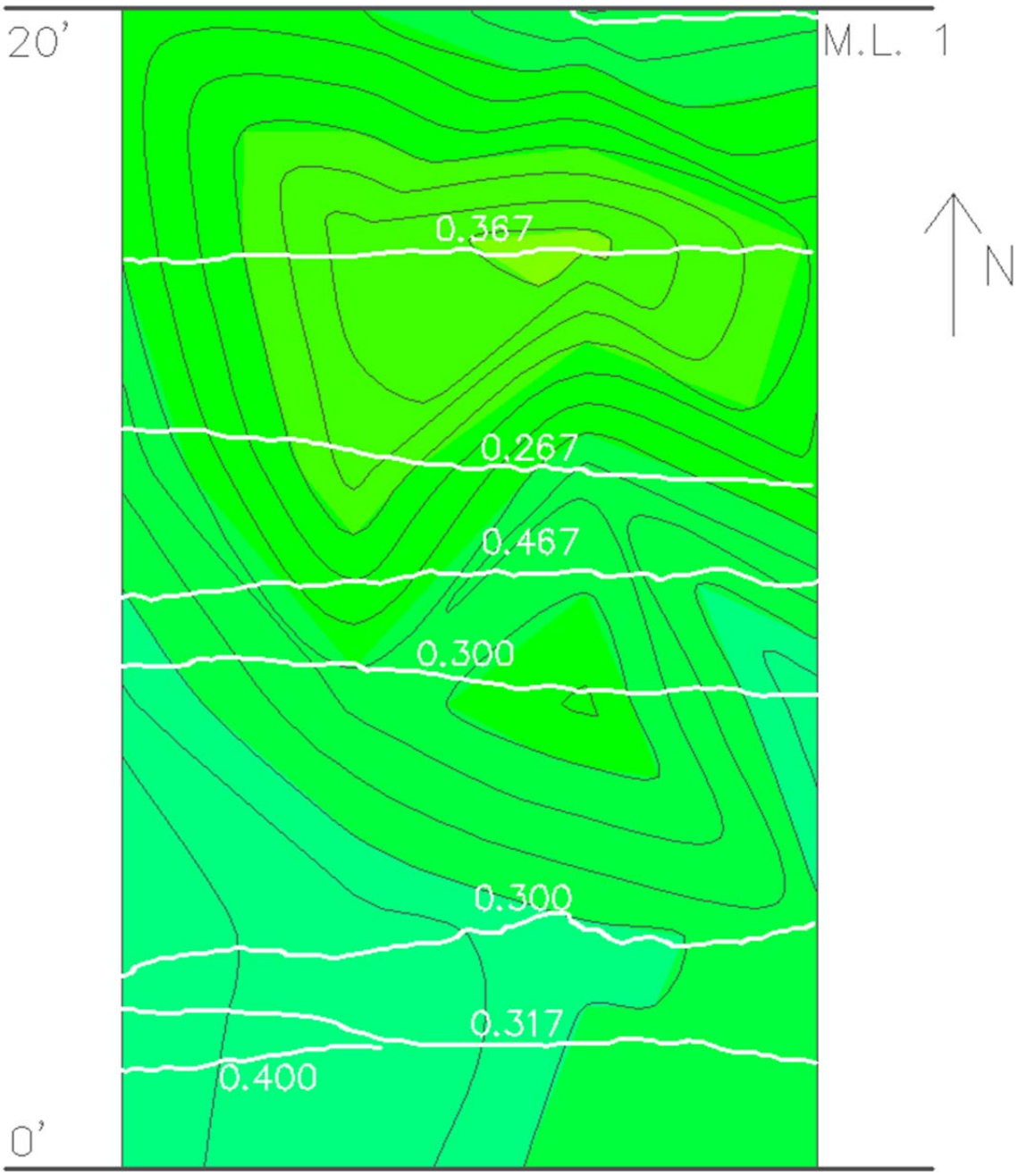

Figure B-16: MRM 68 fall 2010 from 0 to 20 feet

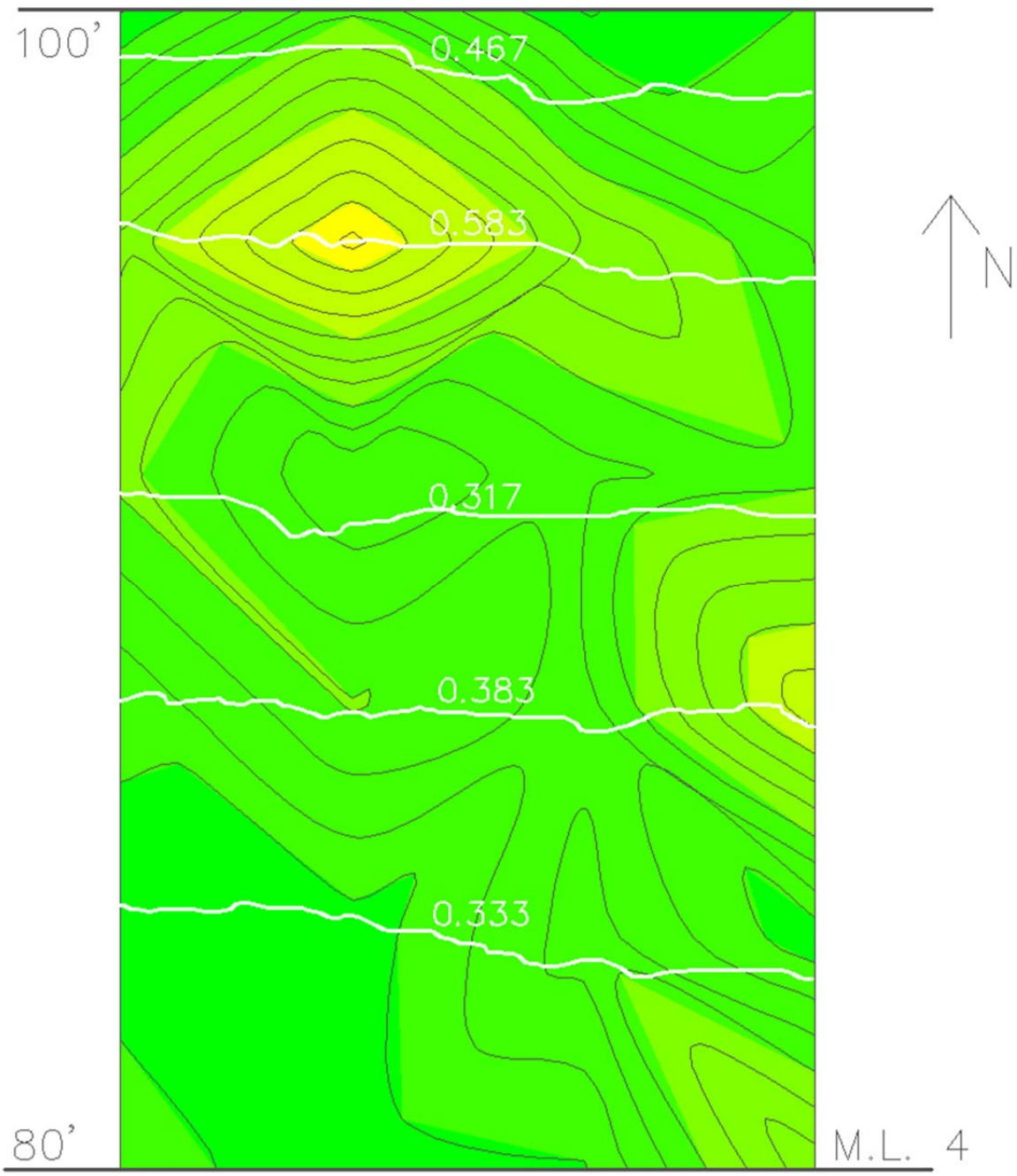

Figure B-17: MRM 68 spring 2011 from 80 to 100 feet

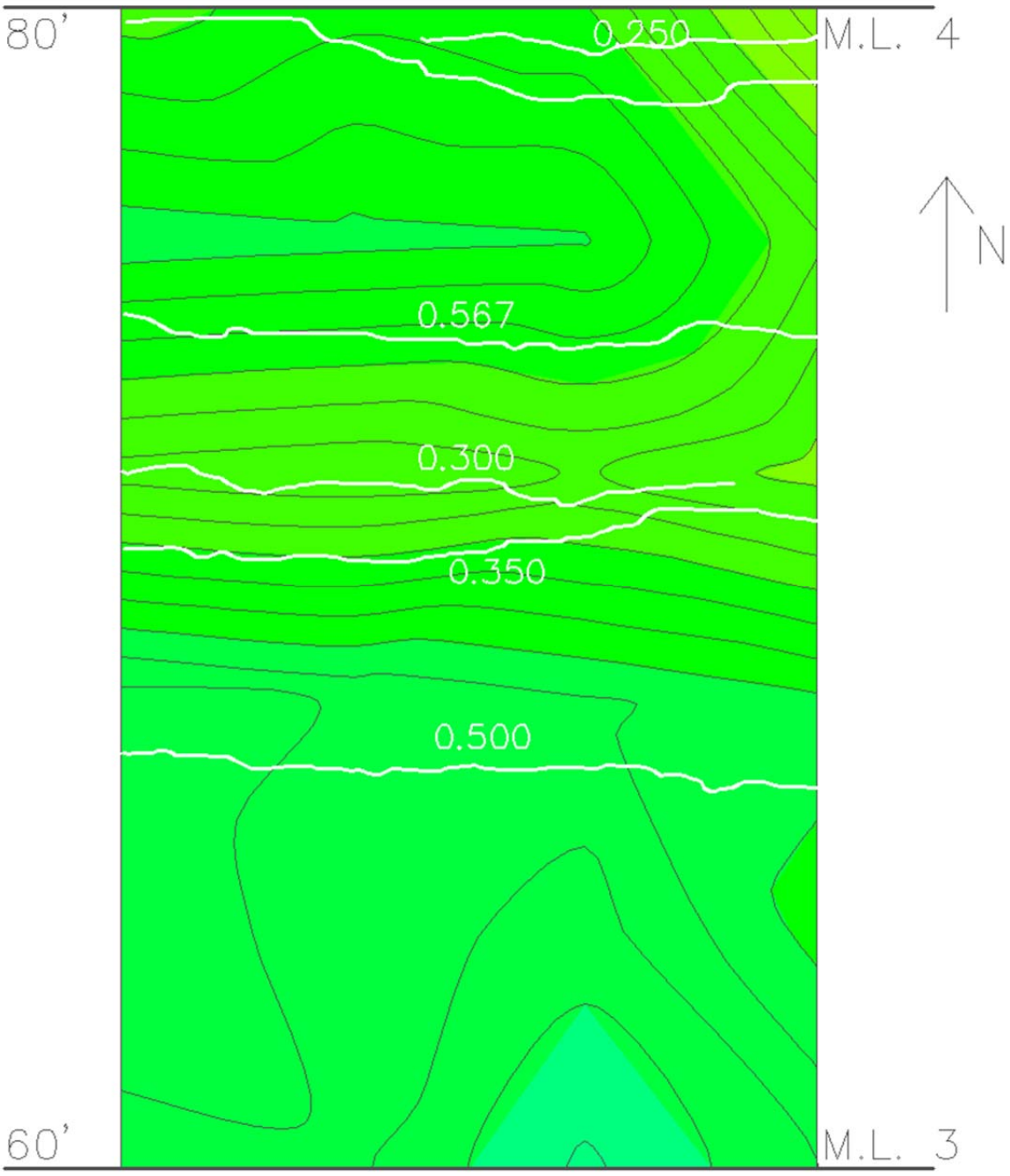

Figure B-18: MRM 68 spring 2011 from 60 to 80 feet

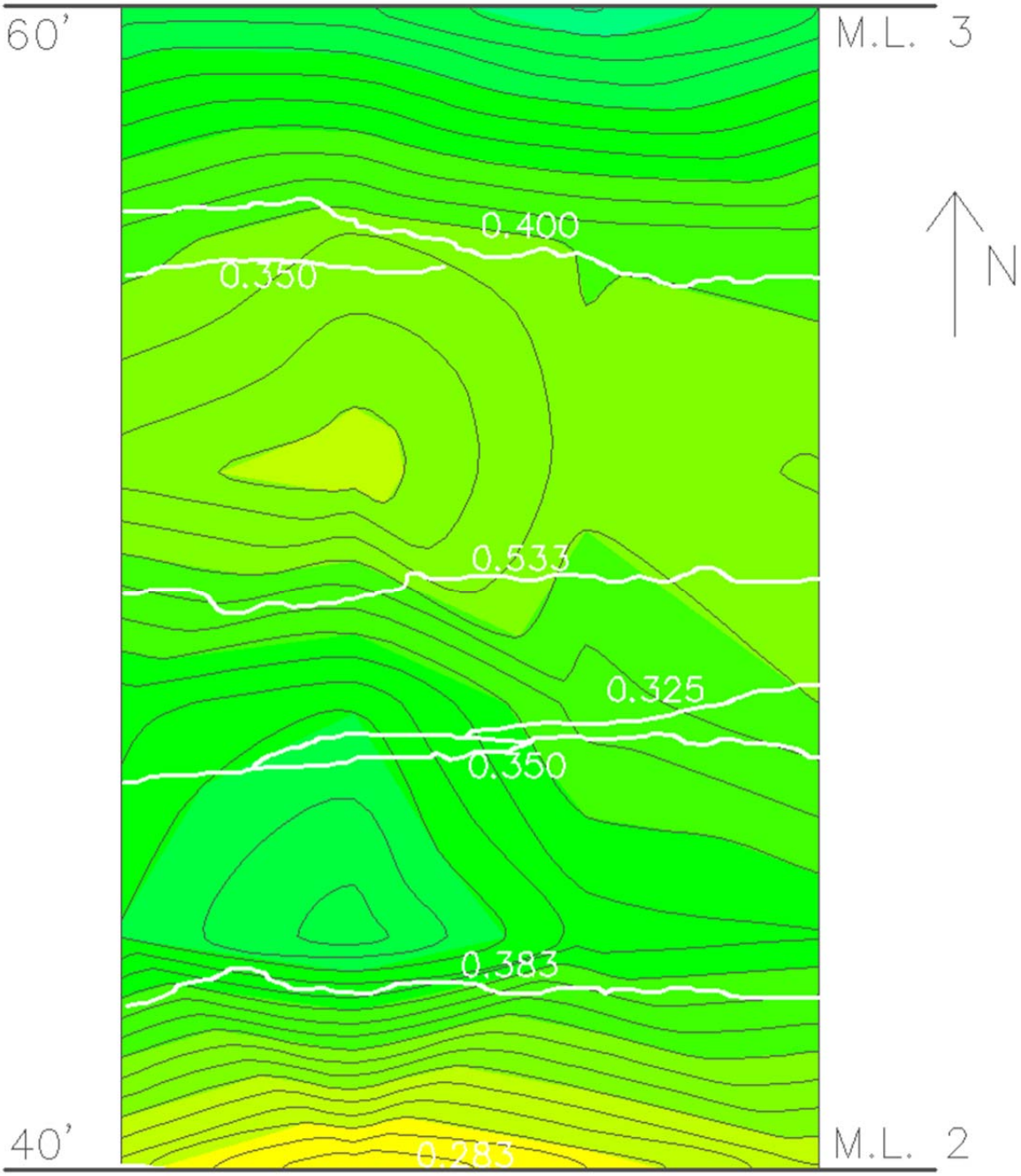

Figure B-19: MRM 68 spring 2011 from 40 to 60 feet

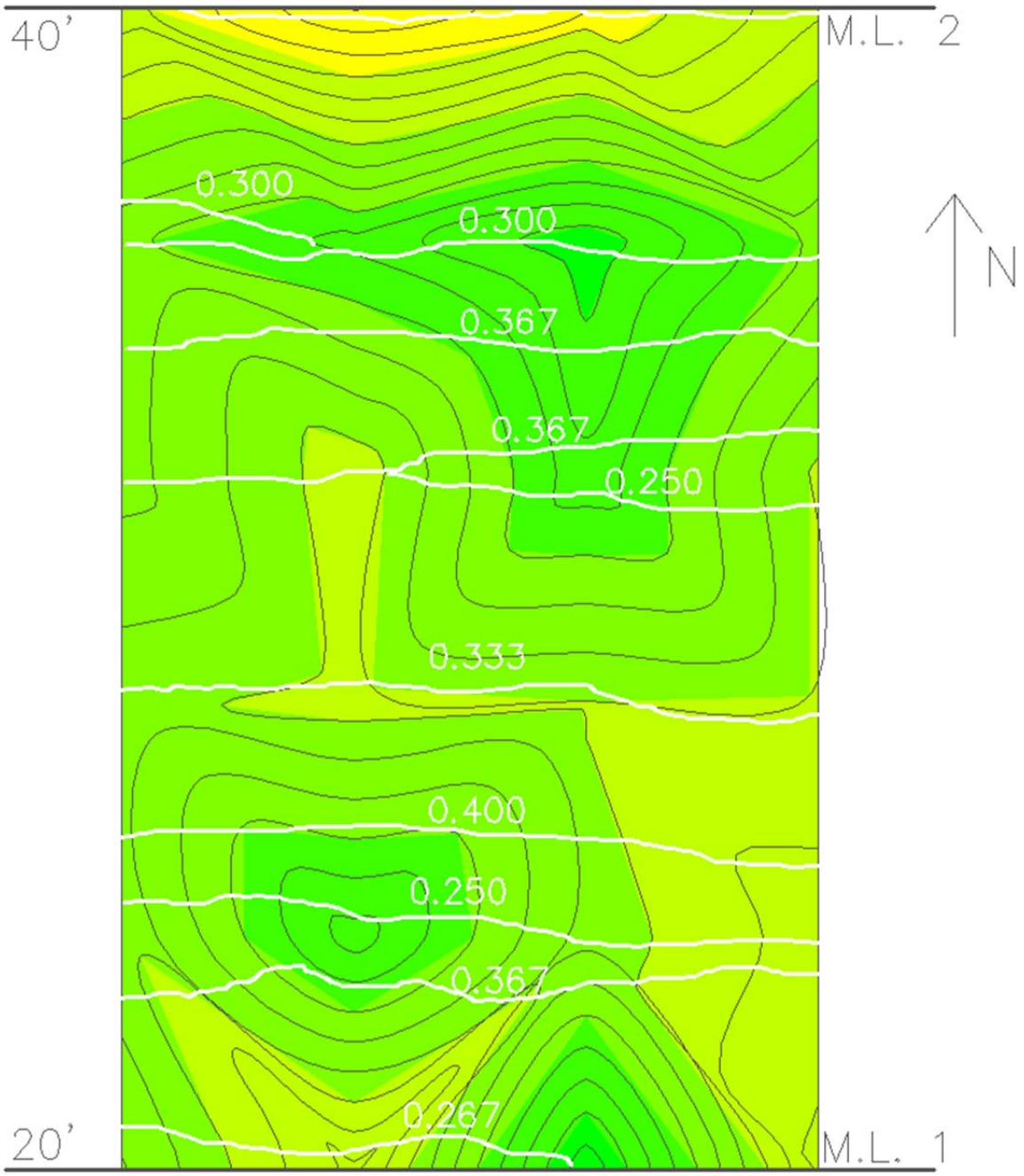

Figure B-20: MRM 68 spring 2011 from 20 to 40 feet

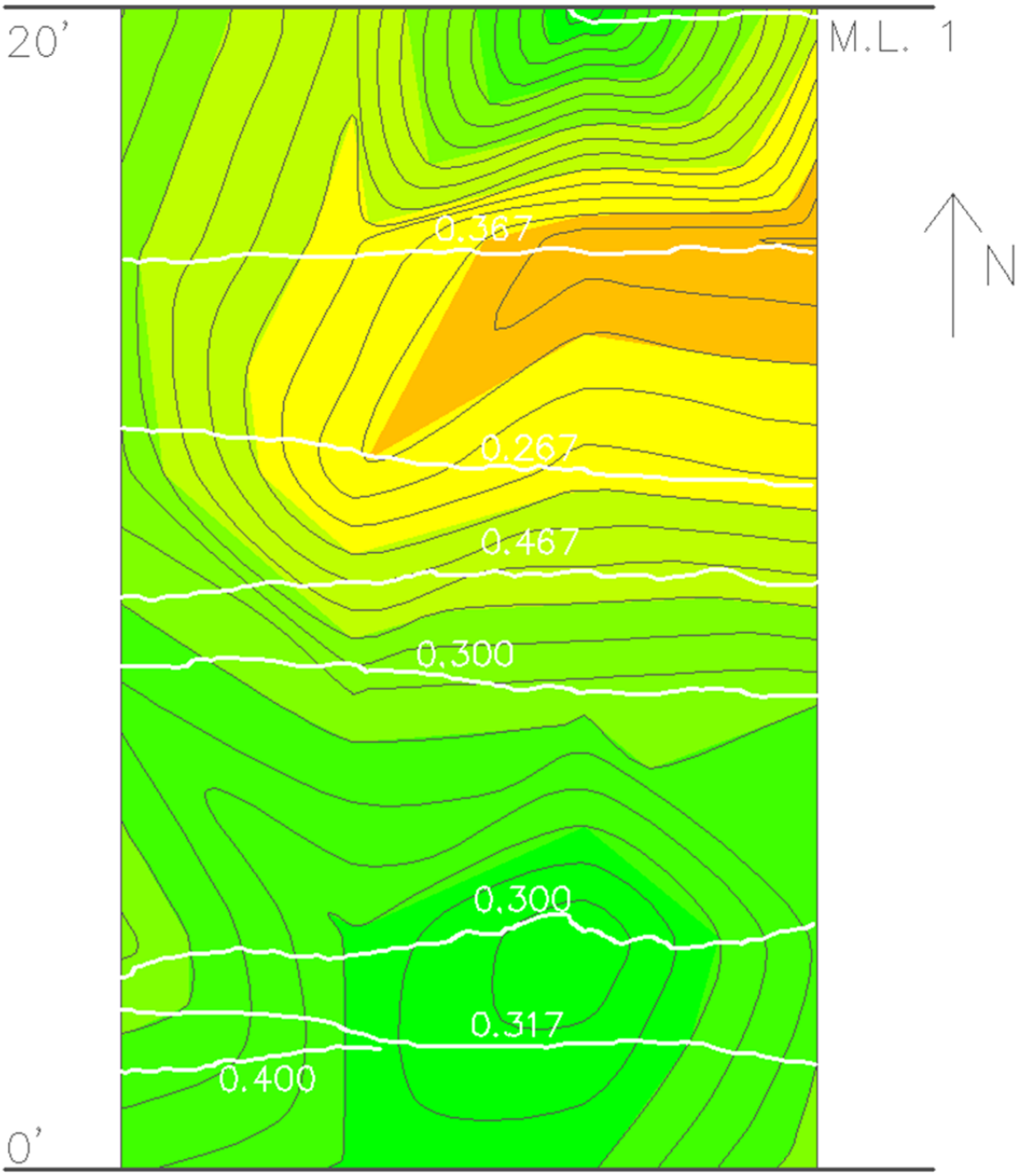

Figure B-21: MRM 68 spring 2011 from 0 to 20 feet

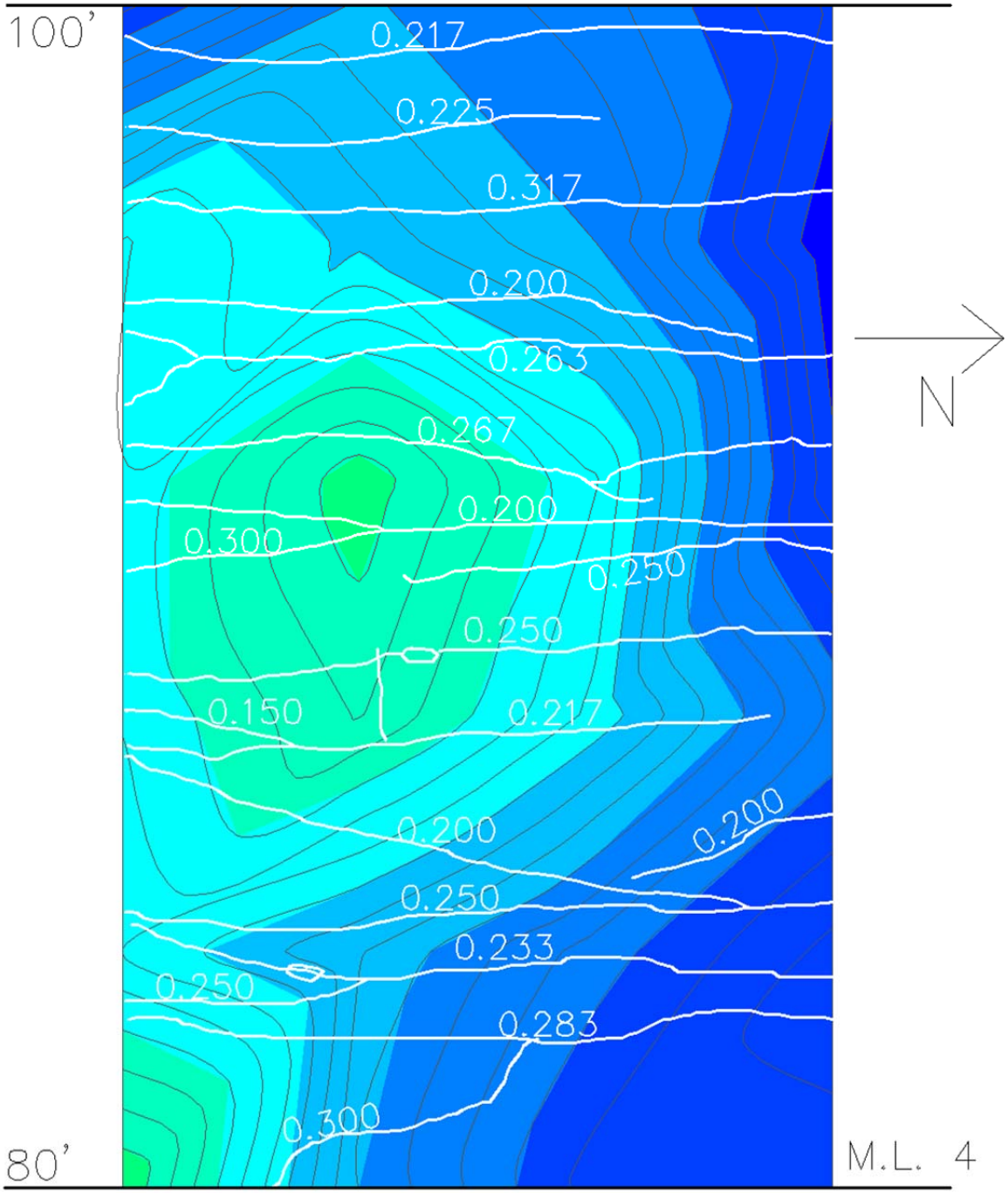

Figure B-22: MRM 411 fall 2010 from 80 to 100 feet

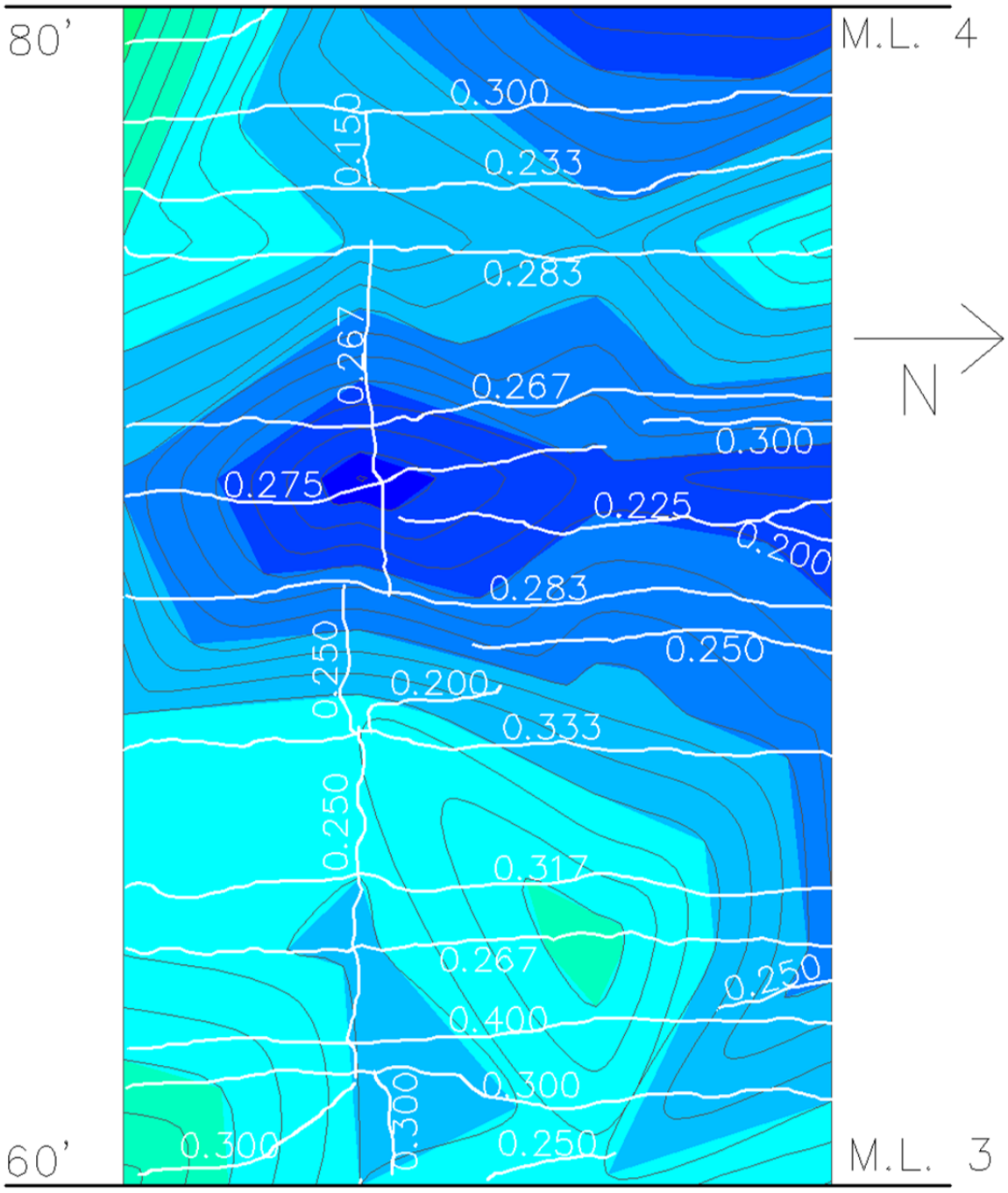

Figure B-23: MRM 411 fall 2010 from 60 to 80 feet

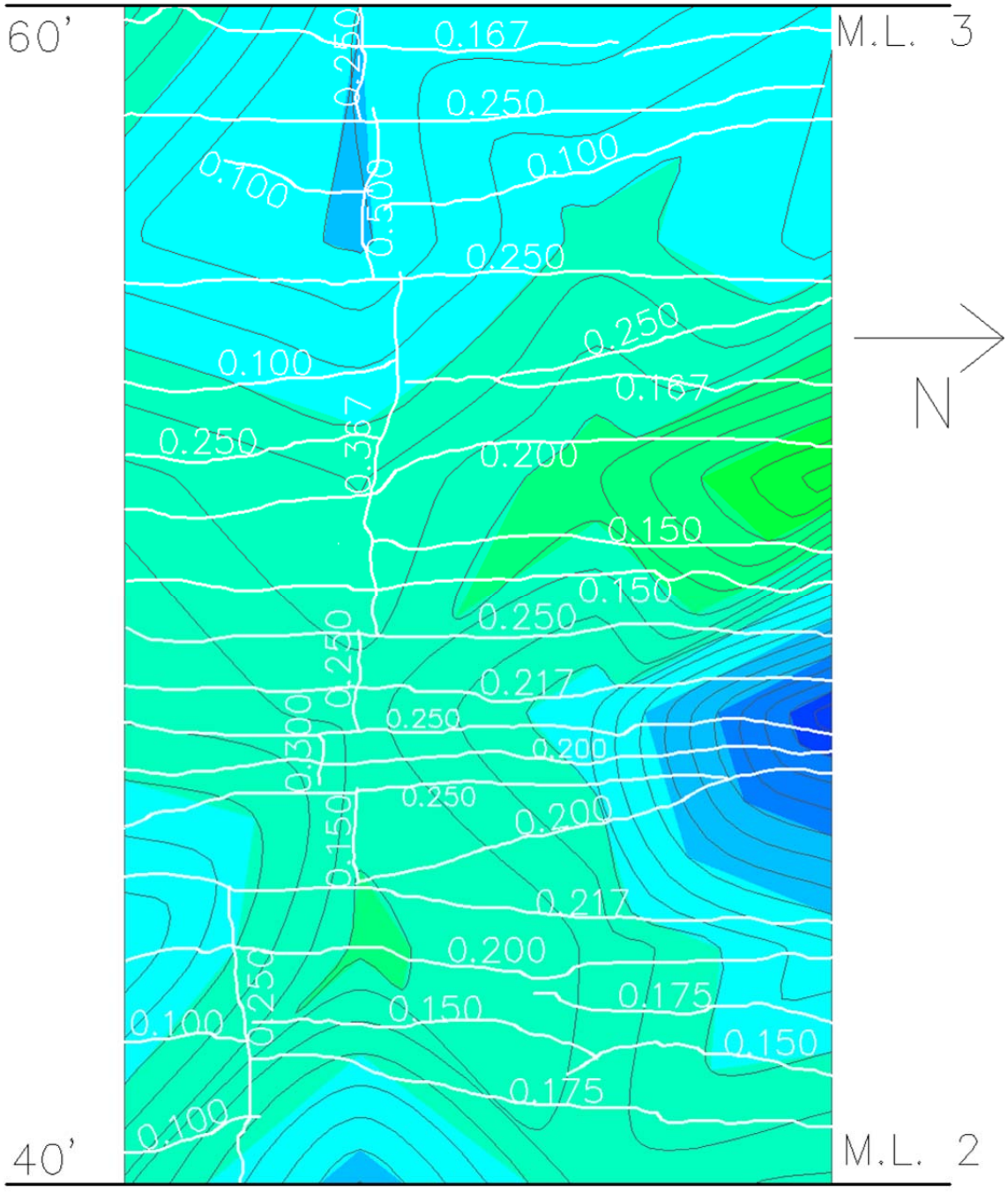

Figure B-24: MRM 411 fall 2010 from 40 to 60 feet

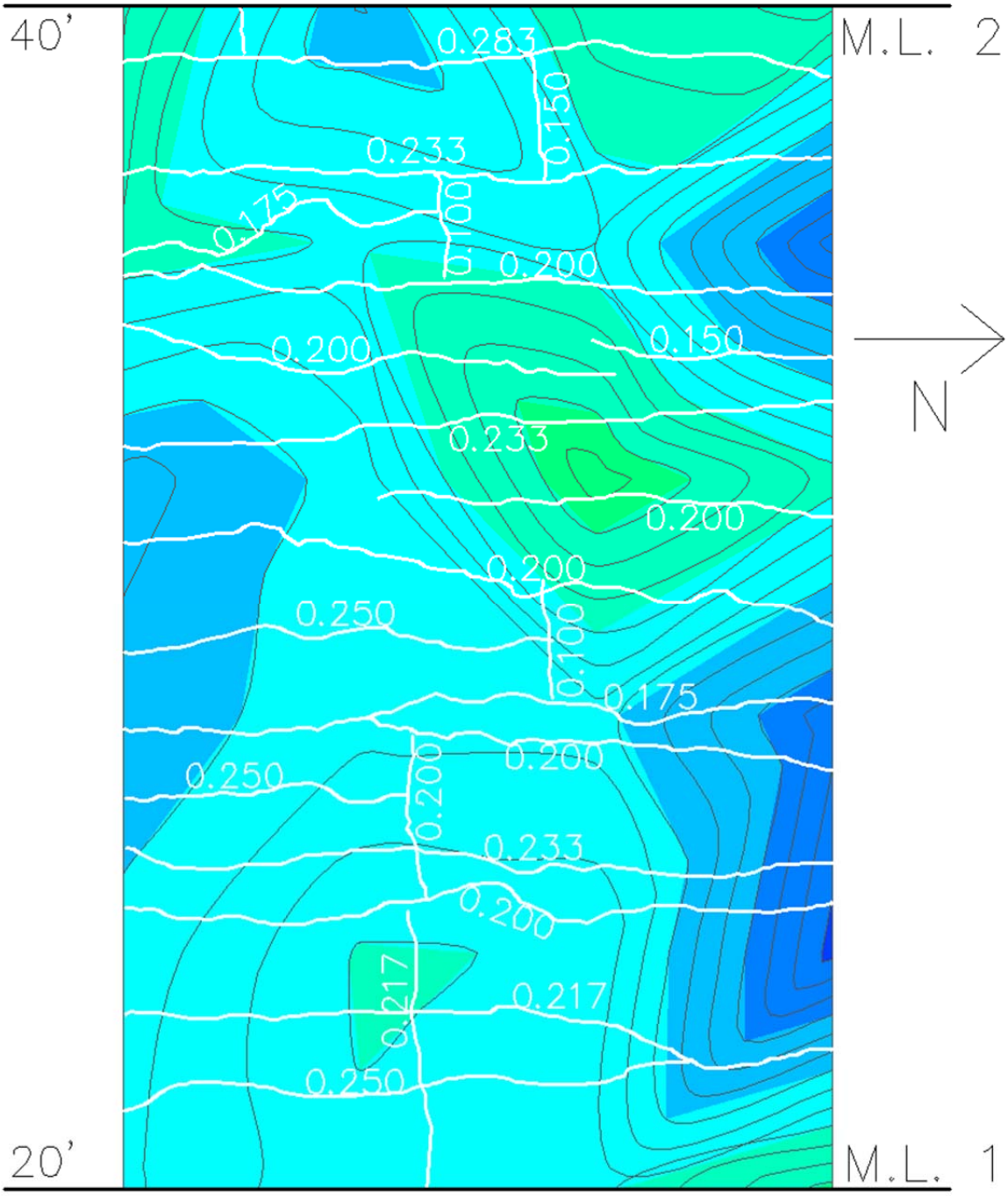

Figure B-25: MRM 411 fall 2010 from 20 to 40 feet

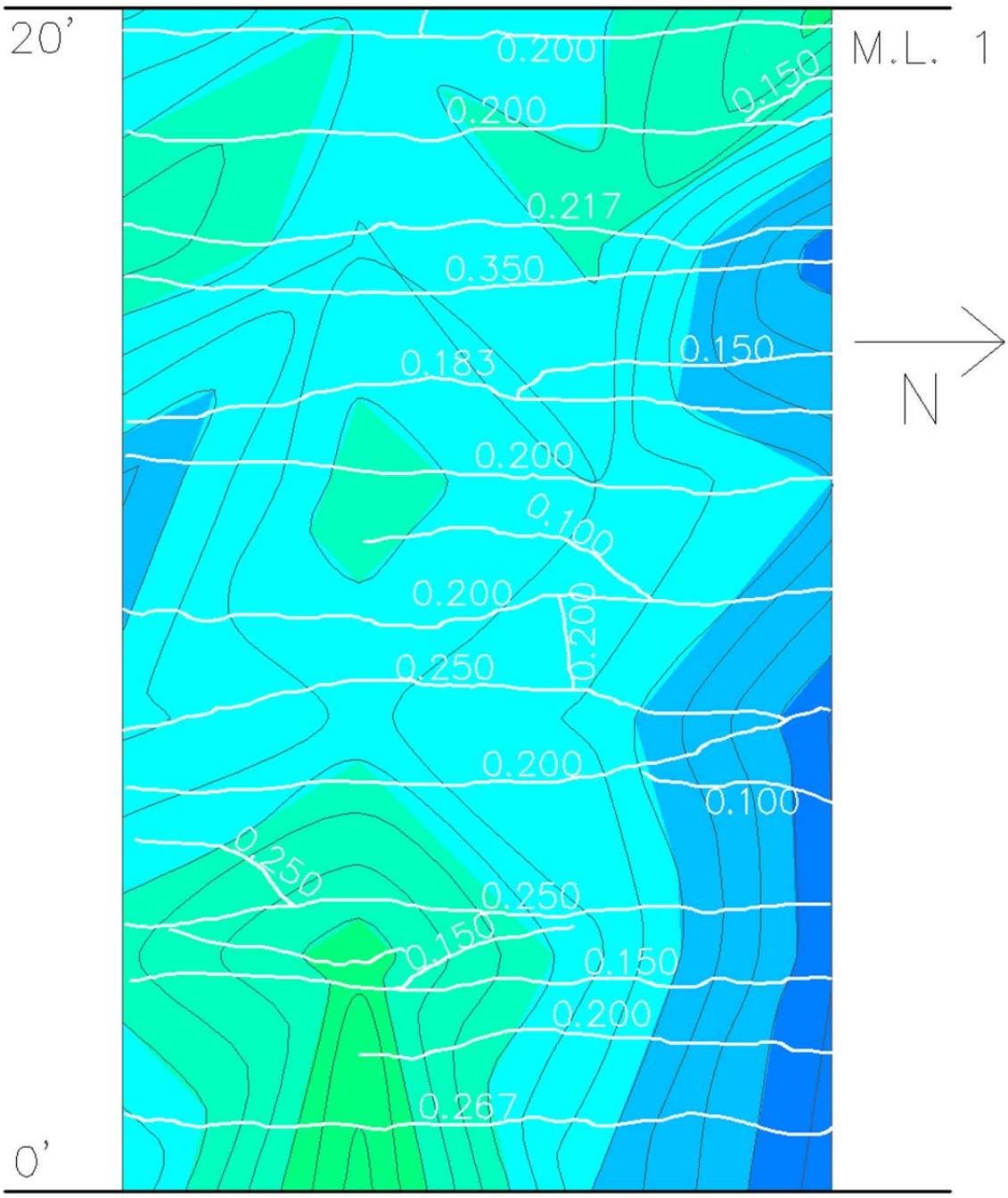

Figure B-26: MRM 411 fall 2010 from 0 to 20 feet

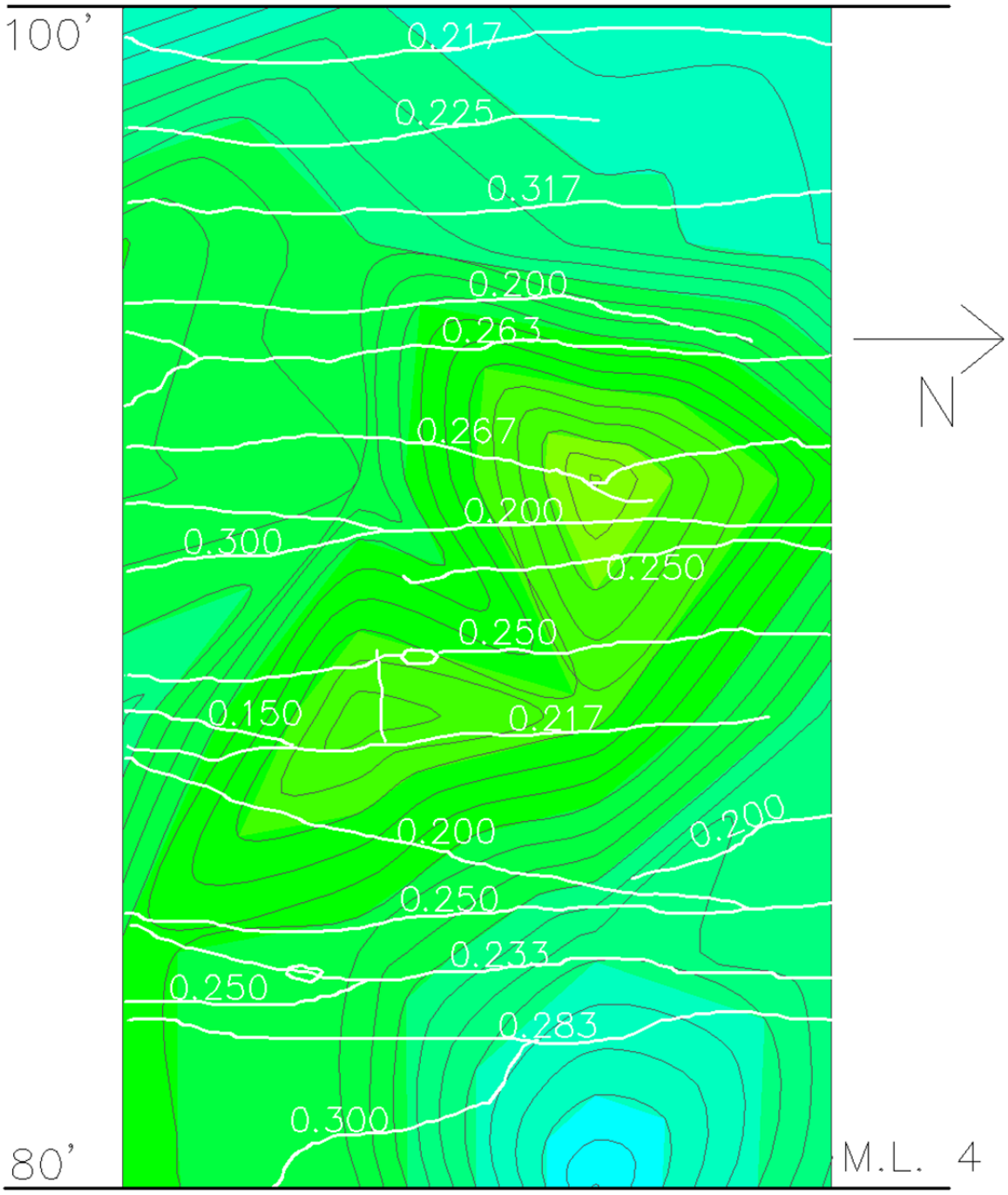

Figure B-27: MRM 411 spring 2011 from 80 to 100 feet

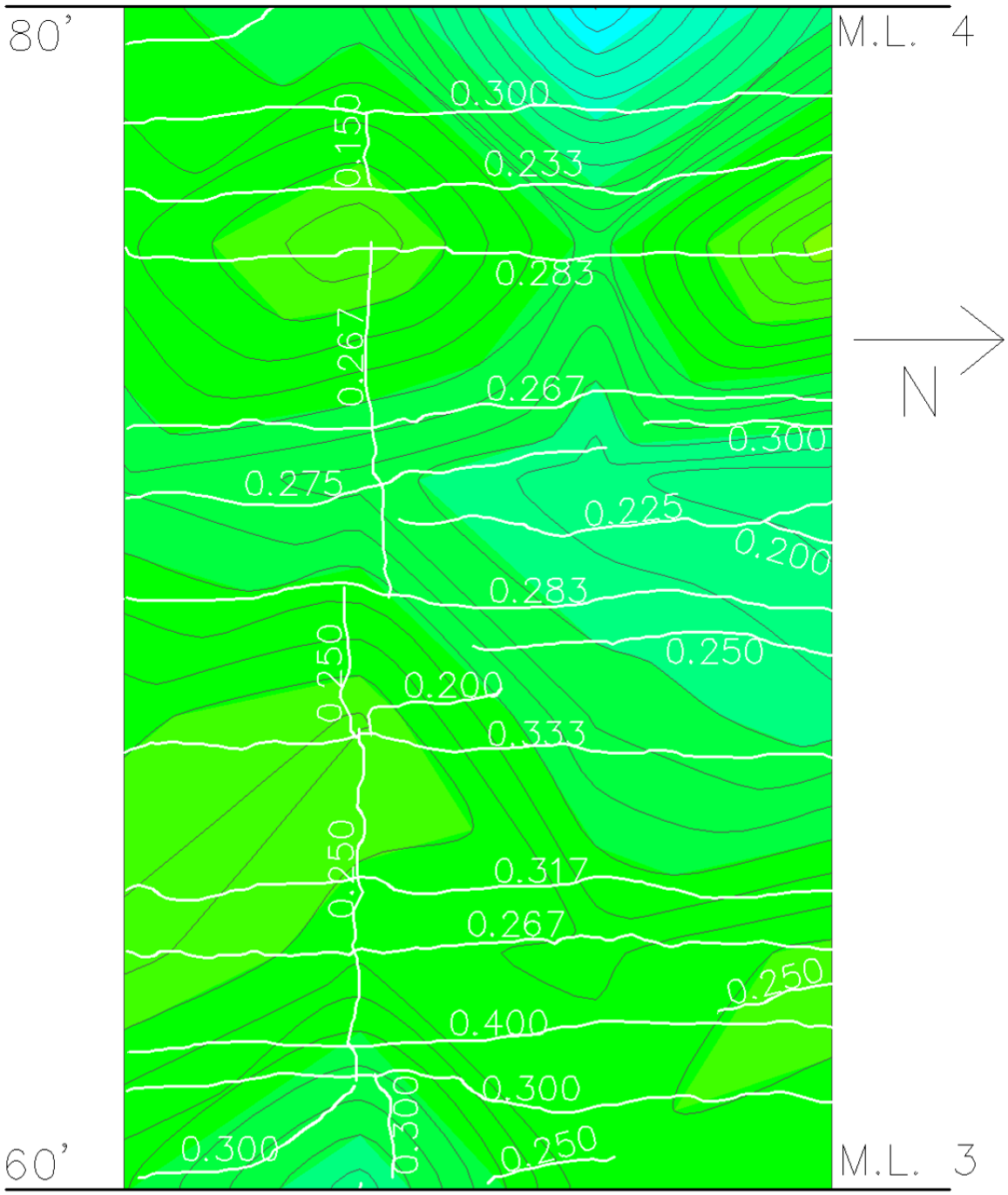

Figure B-28: MRM 411 spring 2011 from 60 to 80 feet

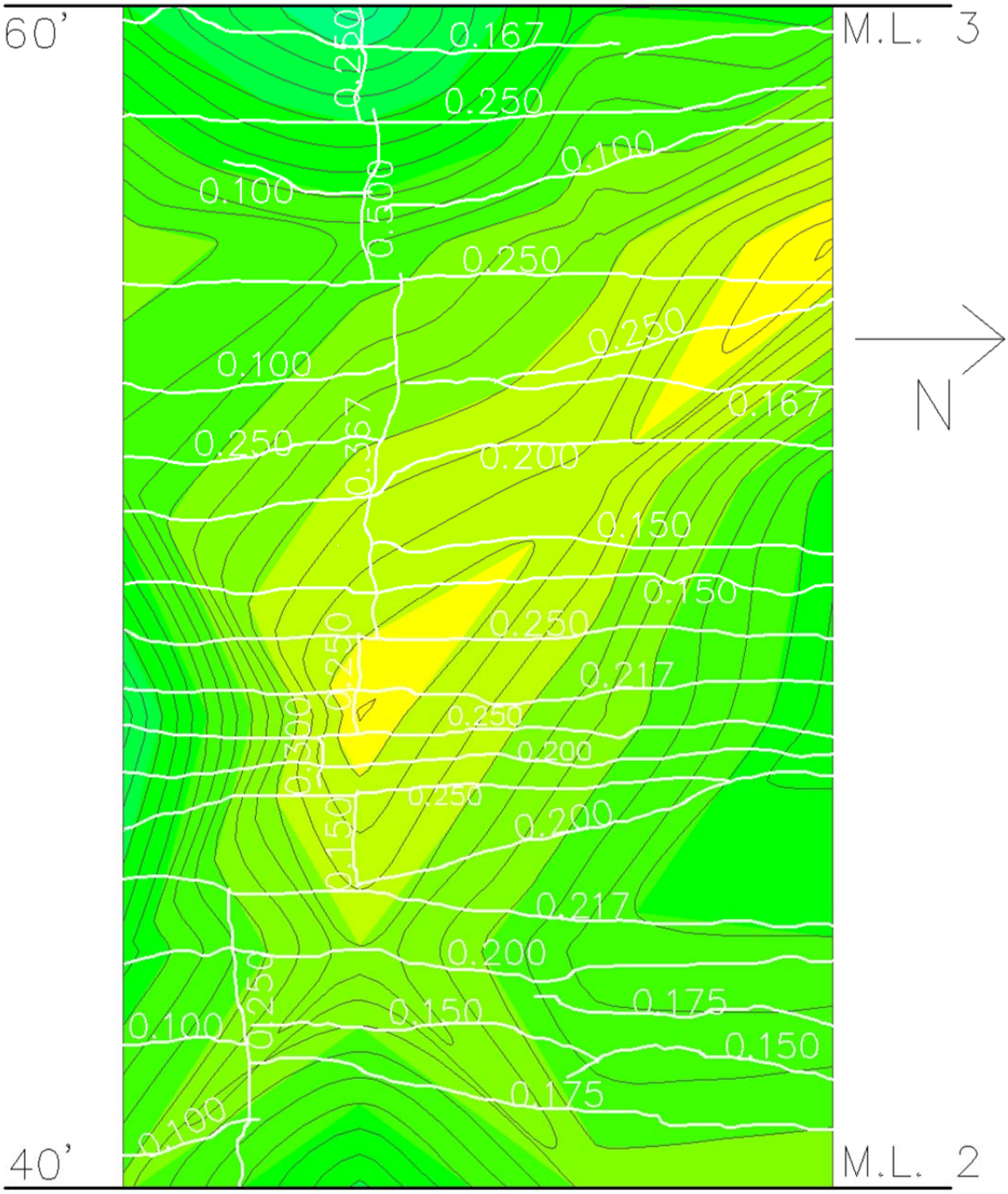

Figure B-29: MRM 411 spring 2011 from 40 to 60 feet

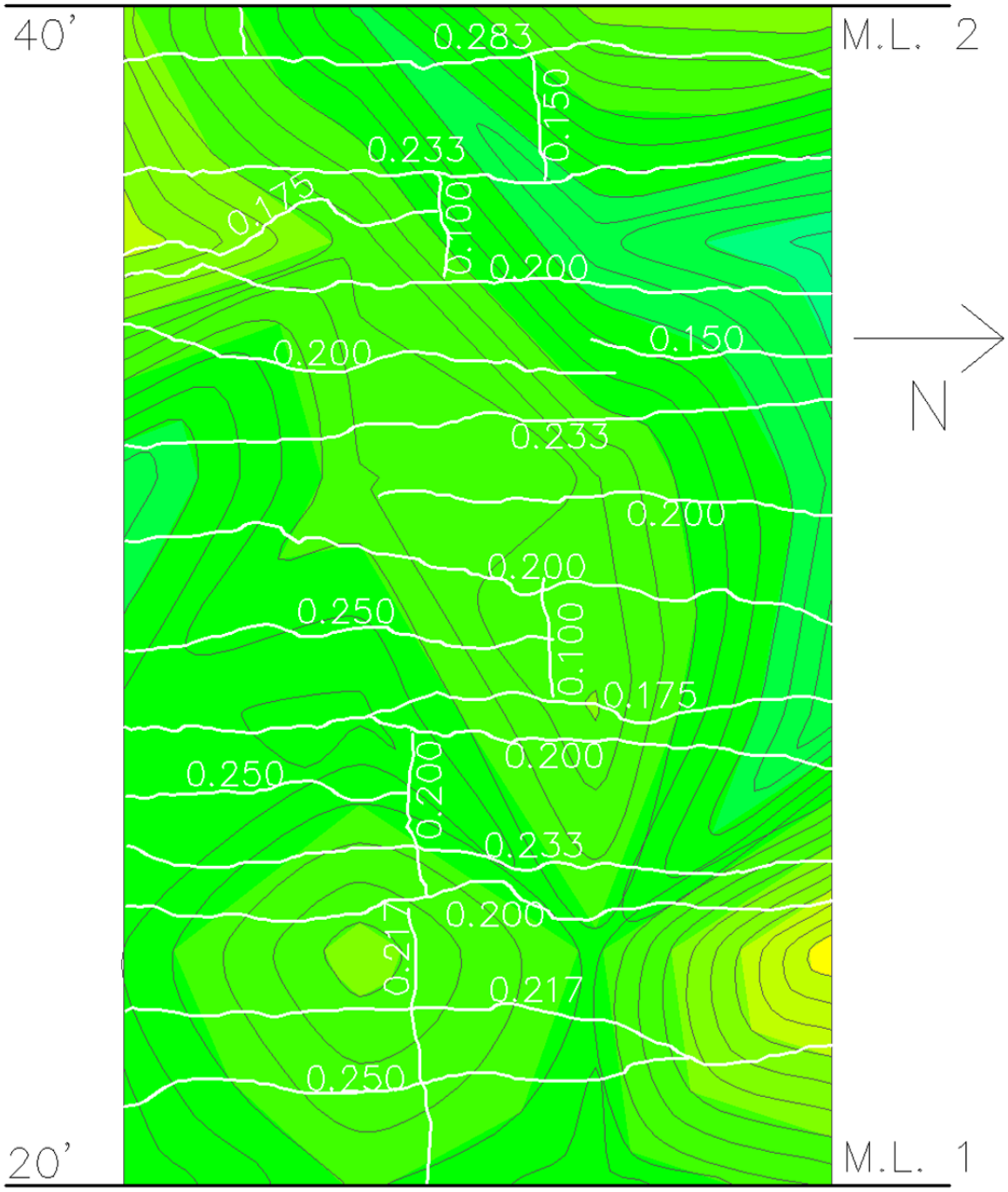

Figure B-30: MRM 411 spring 2011 from 20 to 40 feet

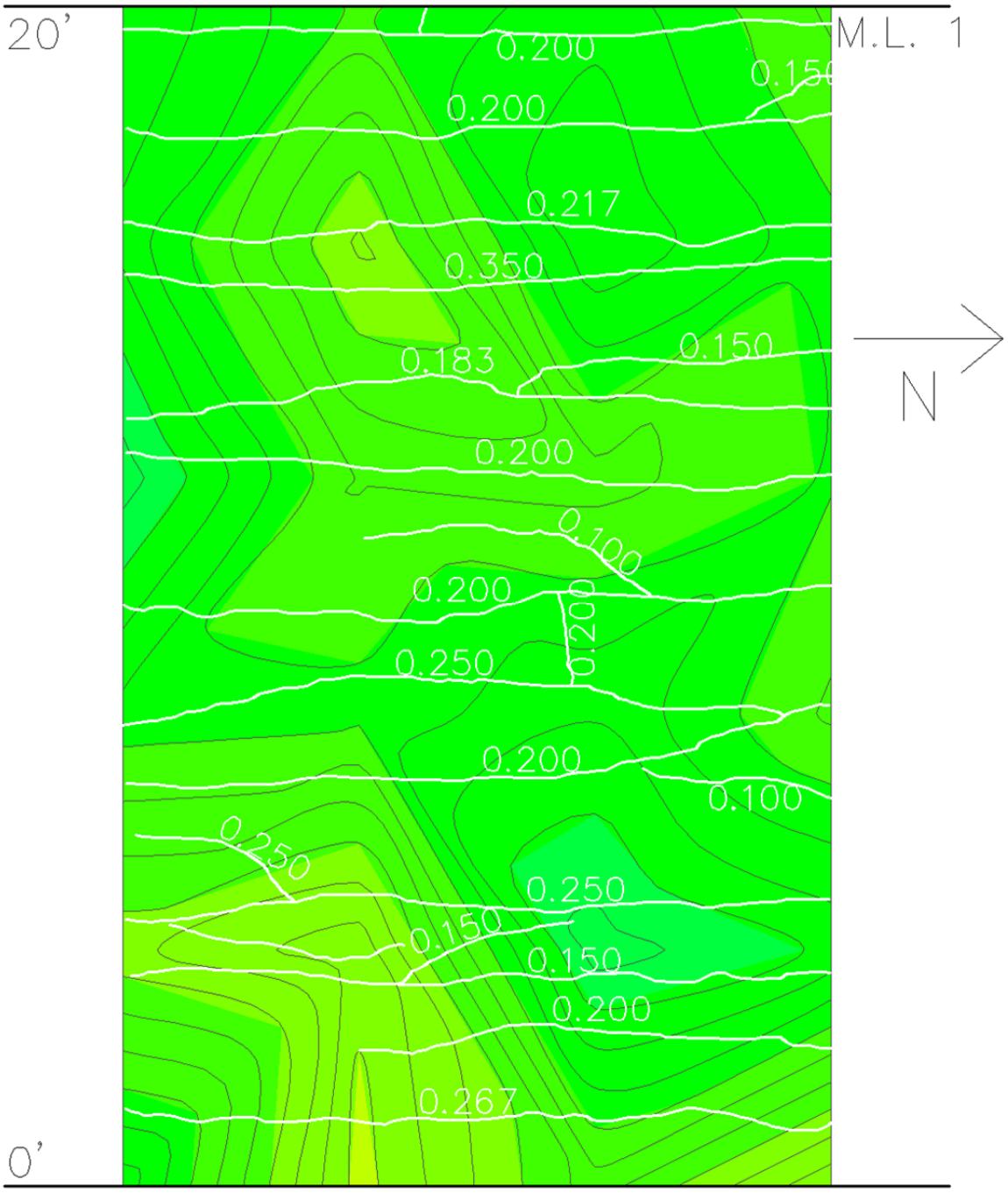

Figure B-31: MRM 411 spring 2011 from 0 to 20 feet

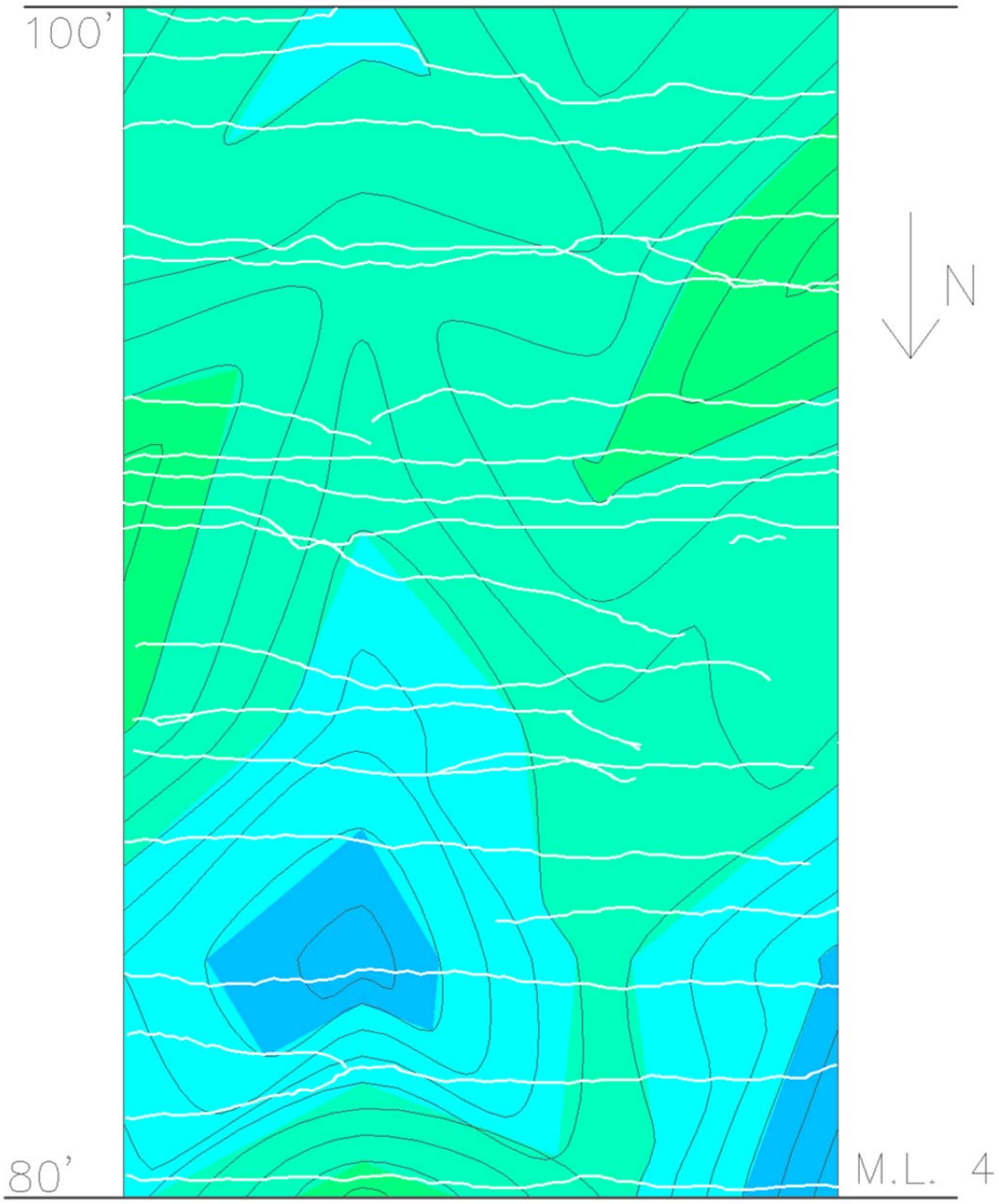

Figure B-32: MRM 33 from 80 to 100 feet

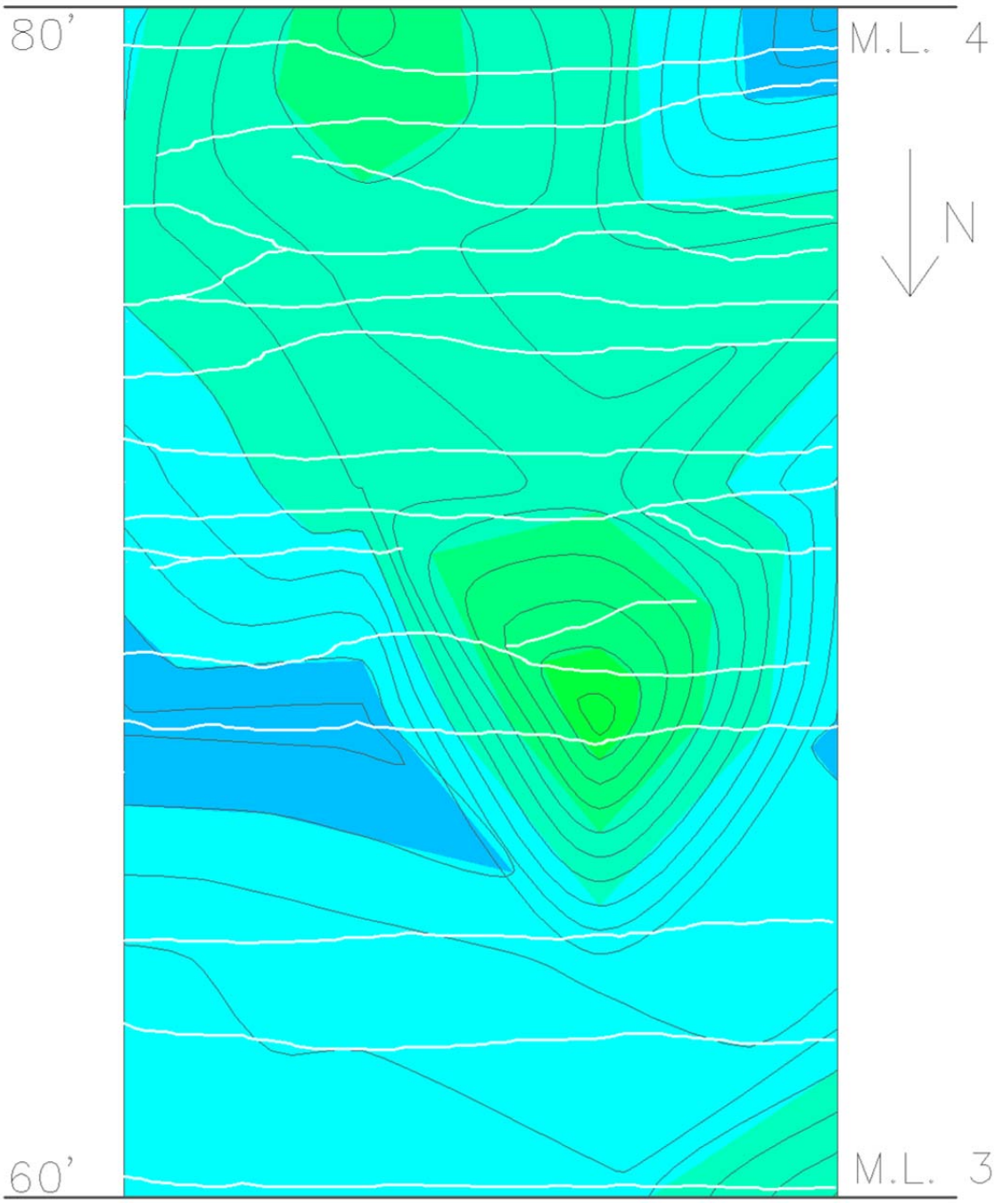

Figure B-33: MRM 33 from 60 to 80 feet

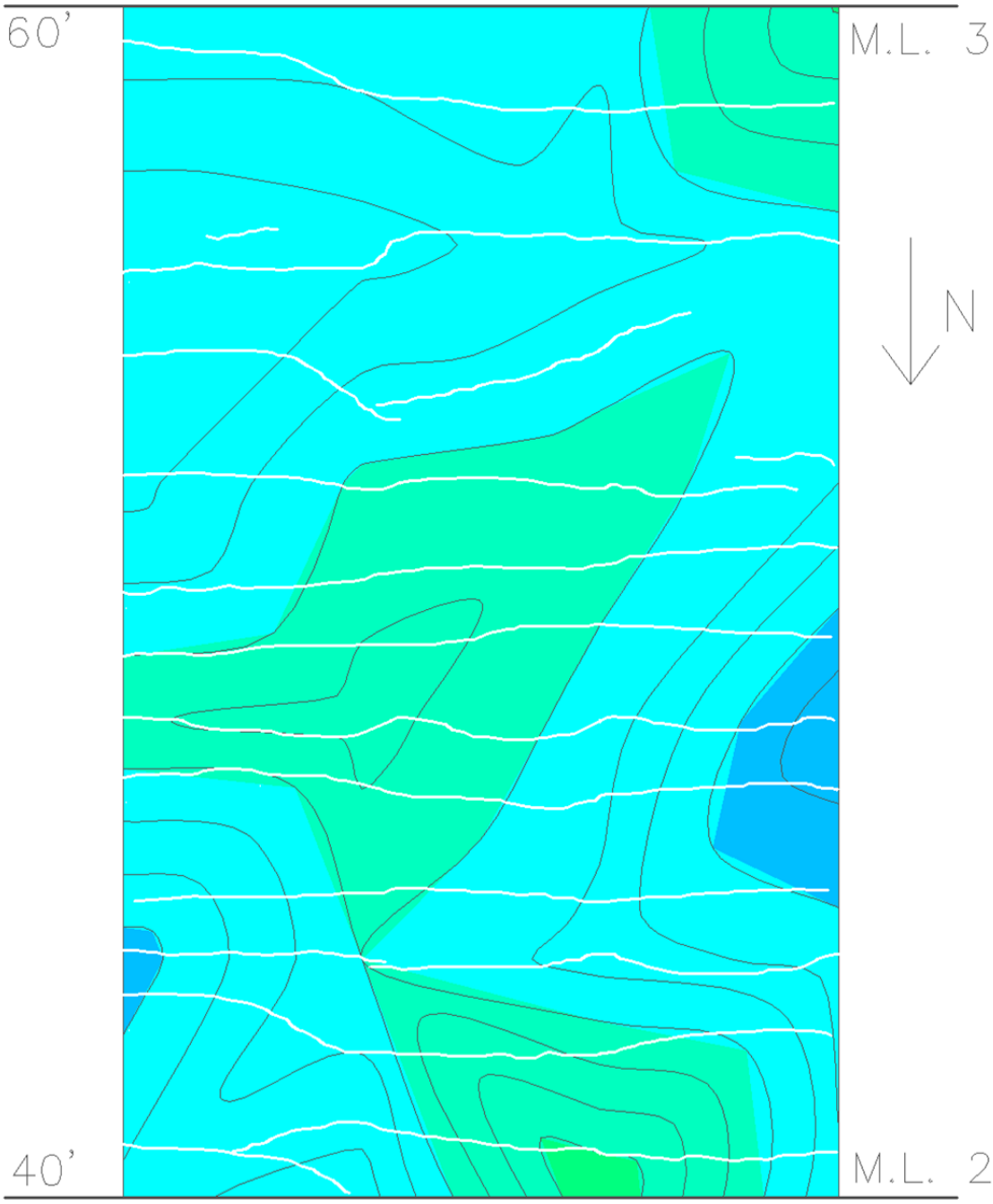

Figure B-34: MRM 33 from 40 to 60 feet

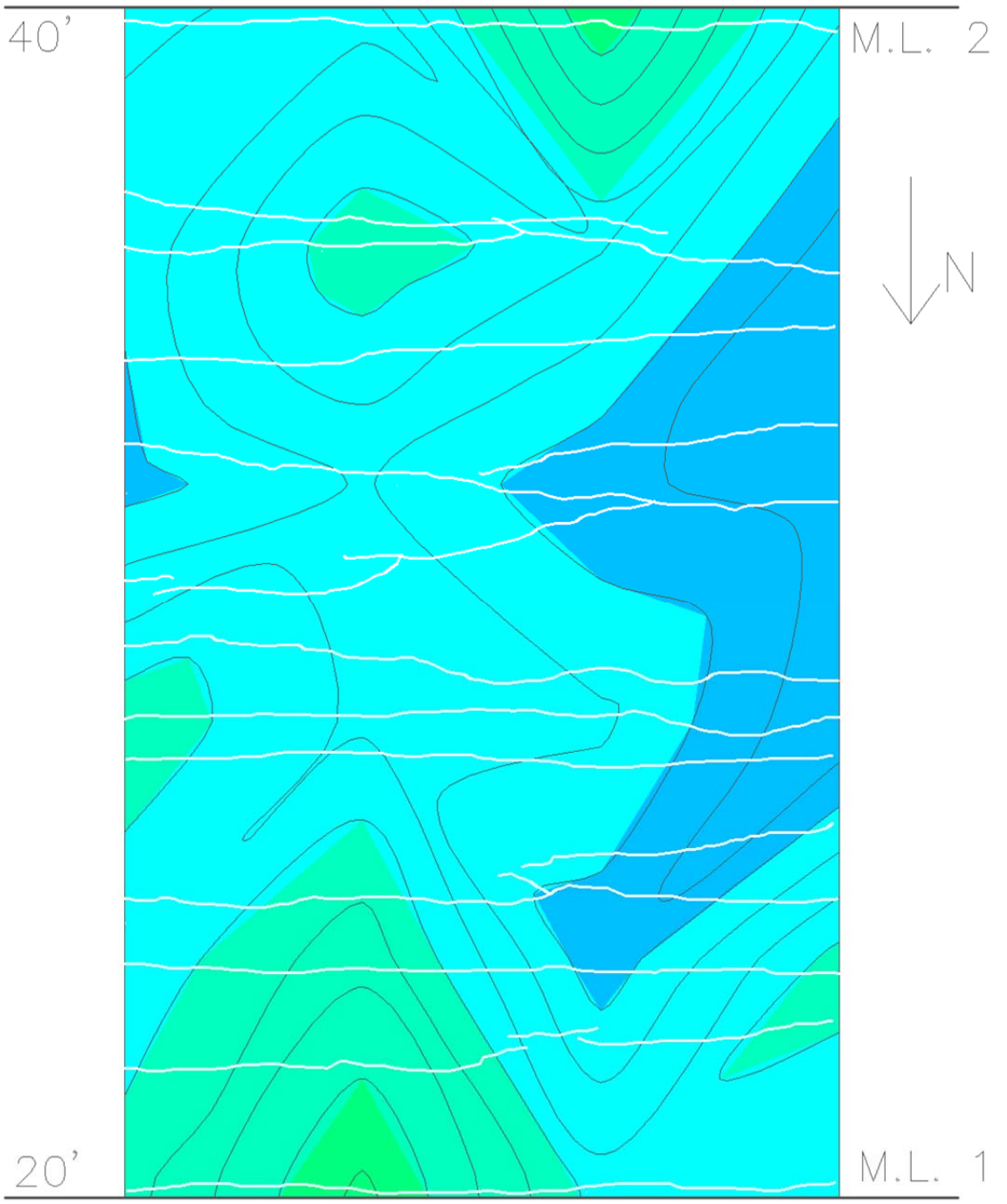

Figure B-35: MRM 33 from 20 to 40 feet

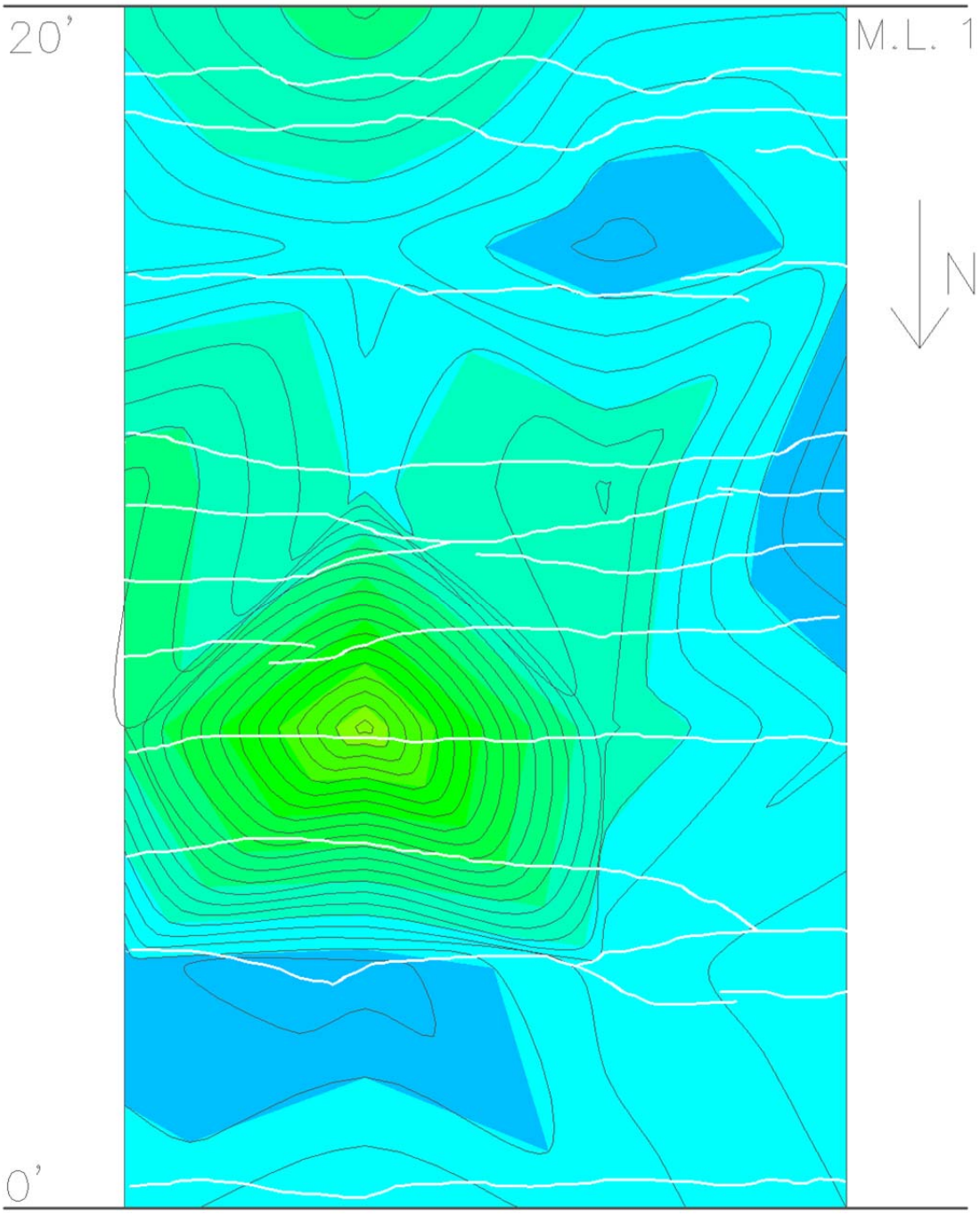

Figure B-36: MRM 33 from 0 to 20 feet

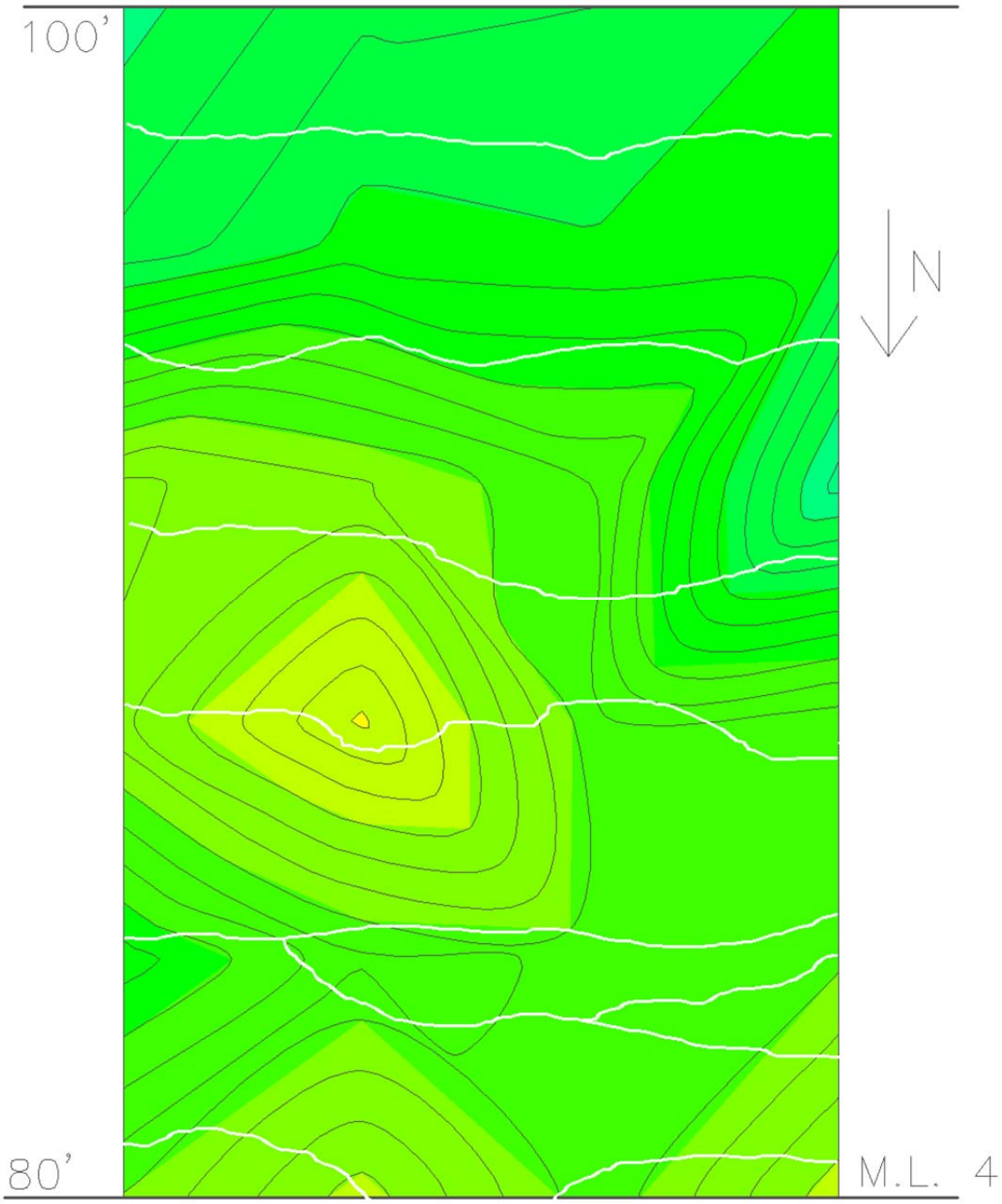

Figure B-37: MRM 44 from 80 to 100 feet

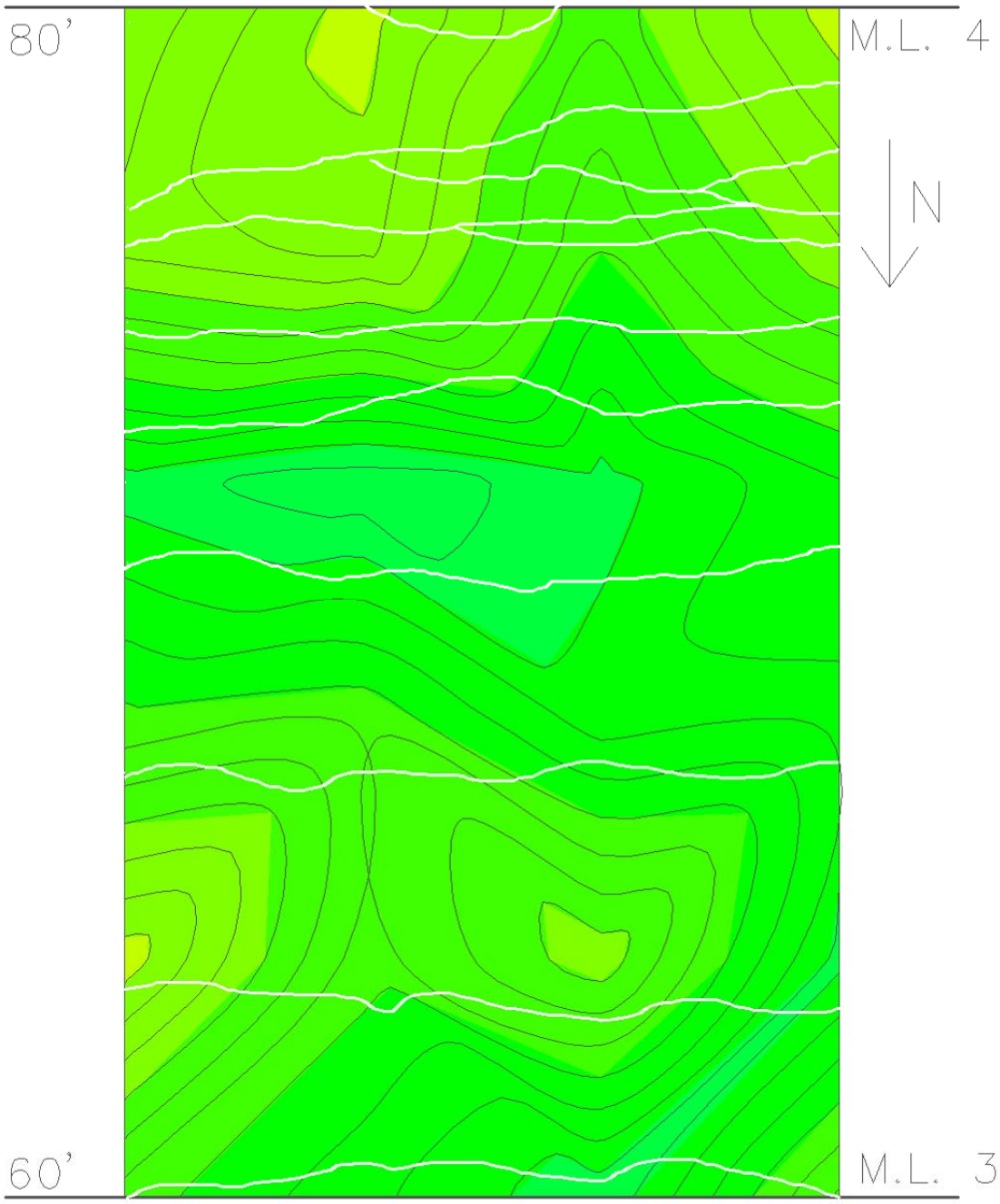

Figure B-38: MRM 44 from 60 to 80 feet

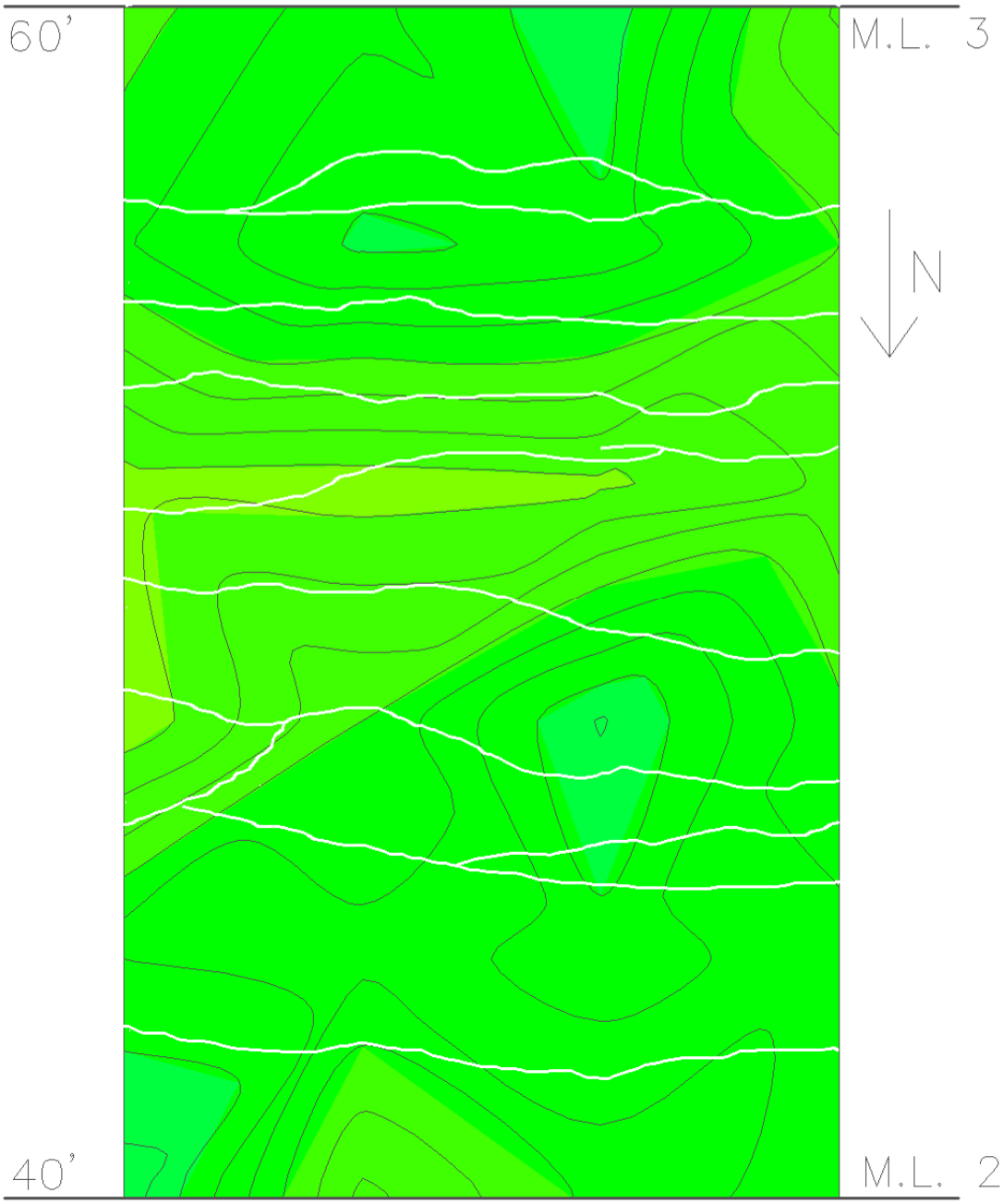

Figure B-39: MRM 44 from 40 to 60 feet

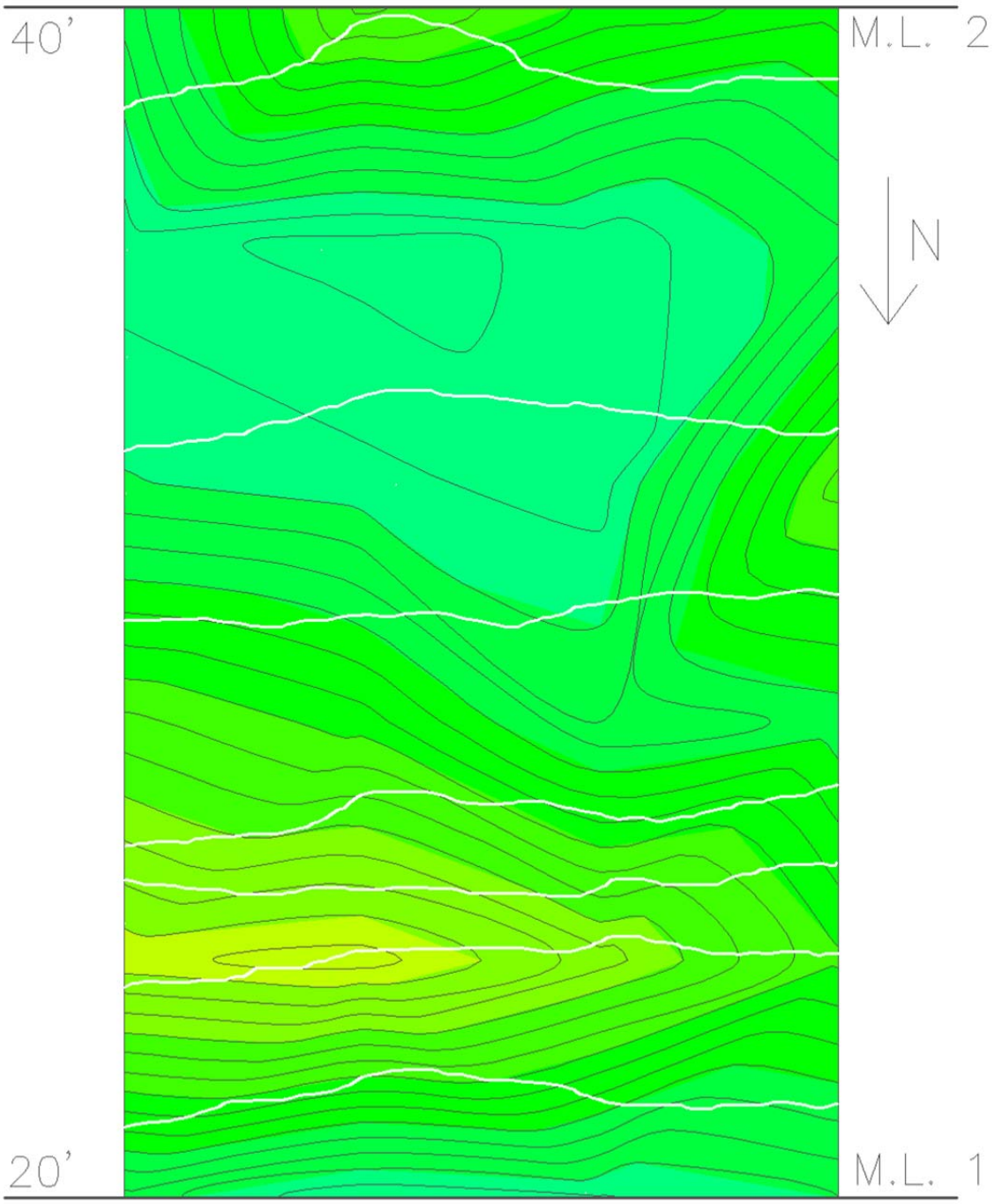

Figure B-40: MRM 44 from 20 to 40 feet

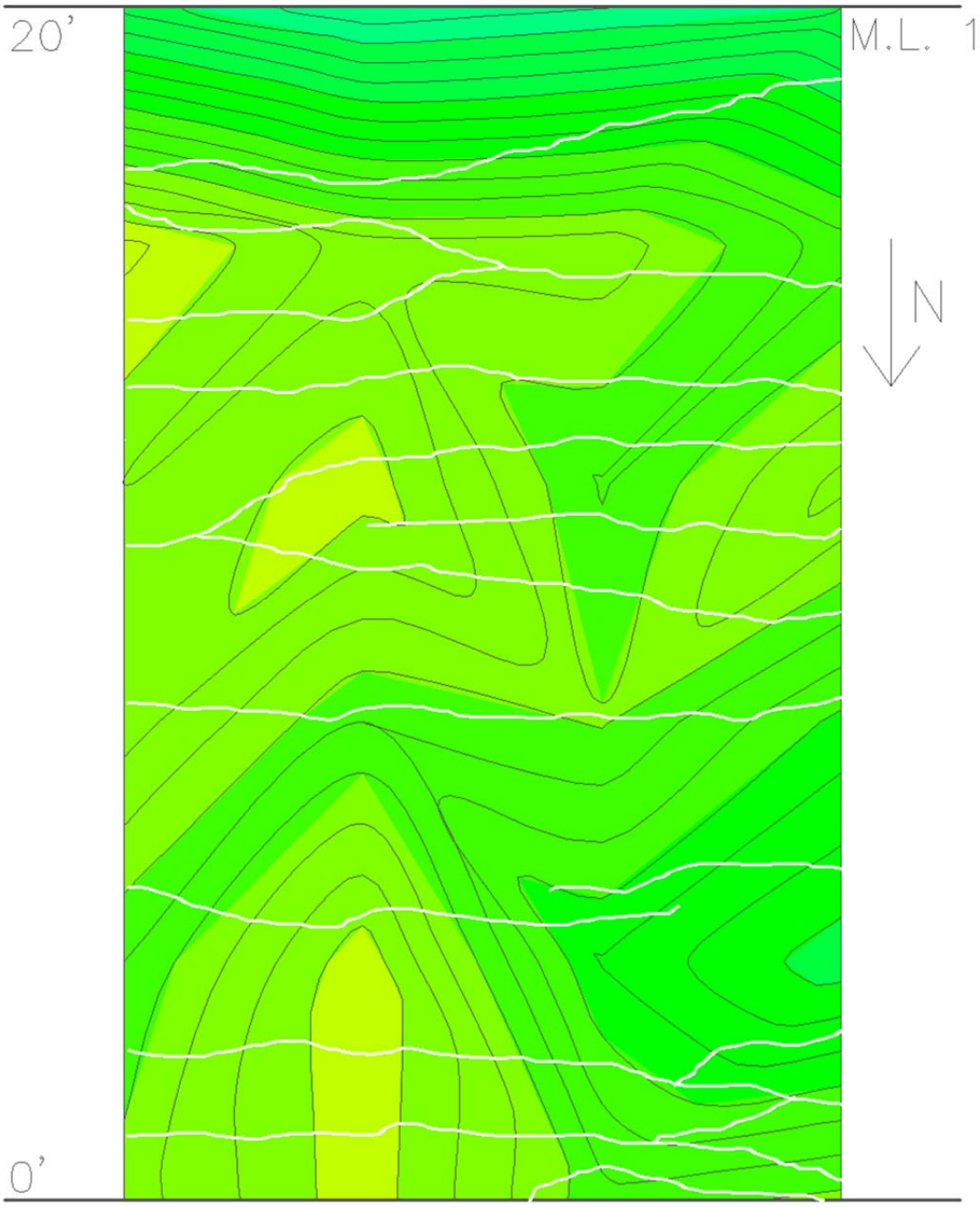

Figure B-41: MRM 44 from 0 to 20 feet

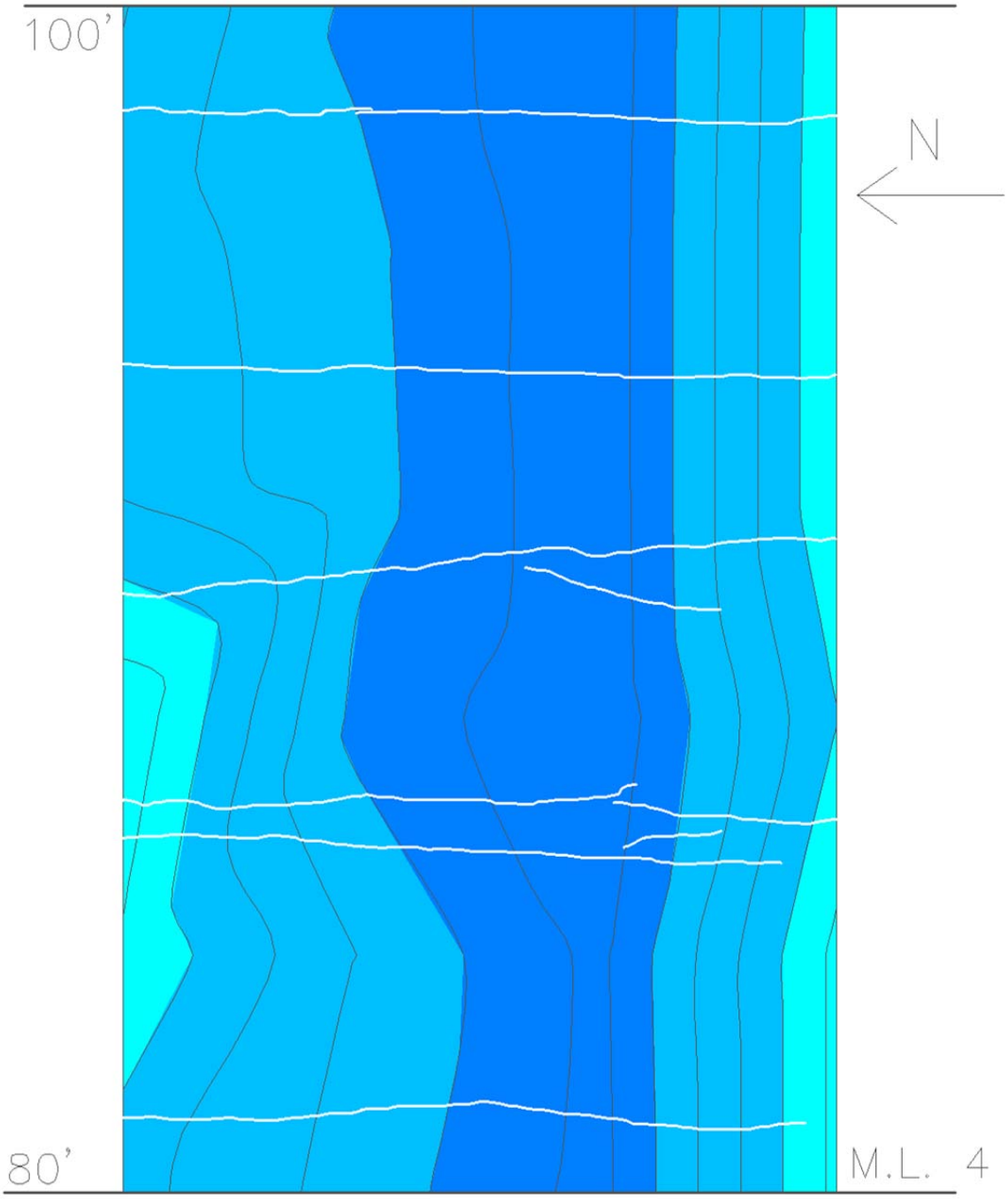

Figure B-42: MRM 25 from 80 to 100 feet

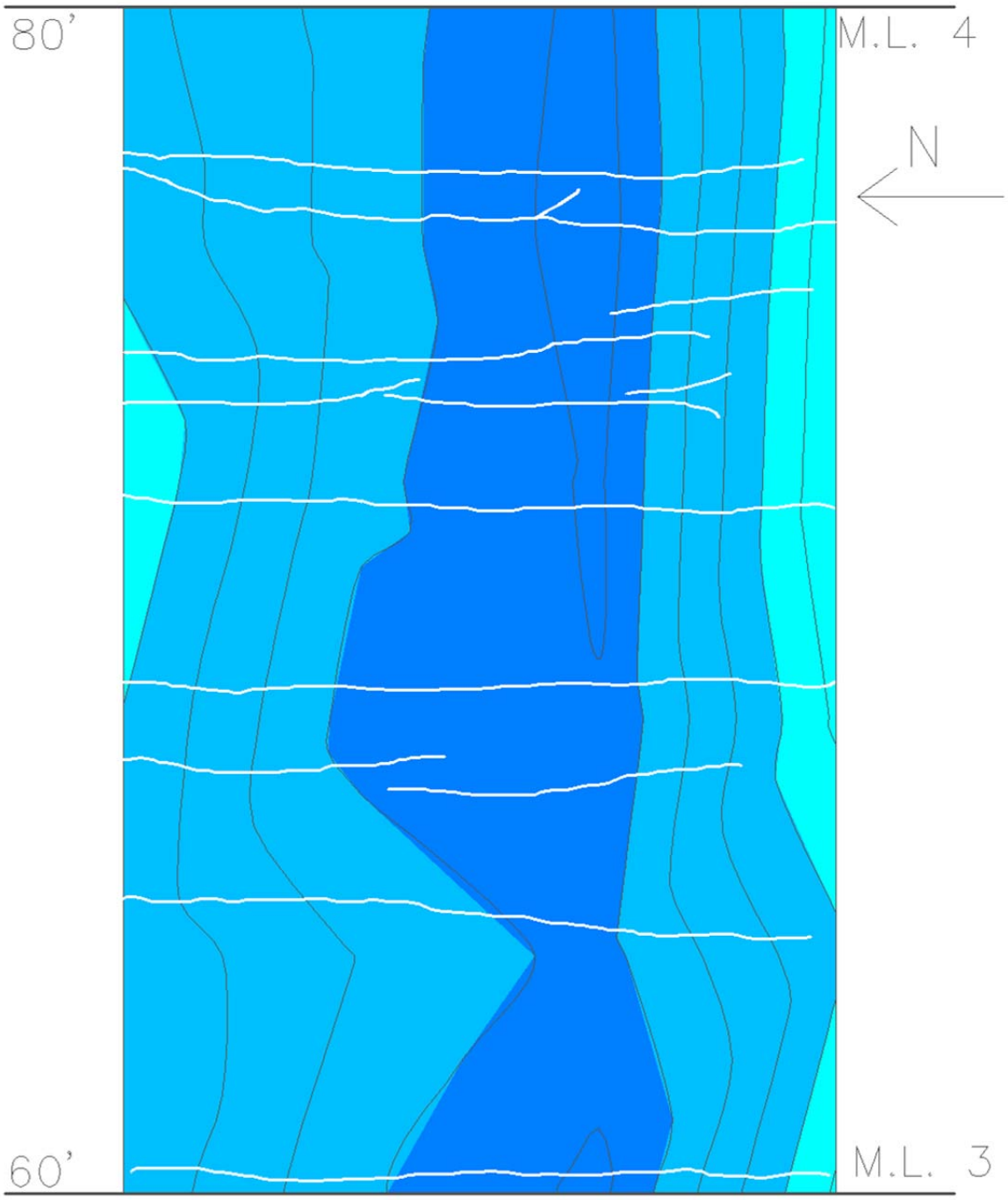

Figure B-43: MRM 25 from 60 to 80 feet

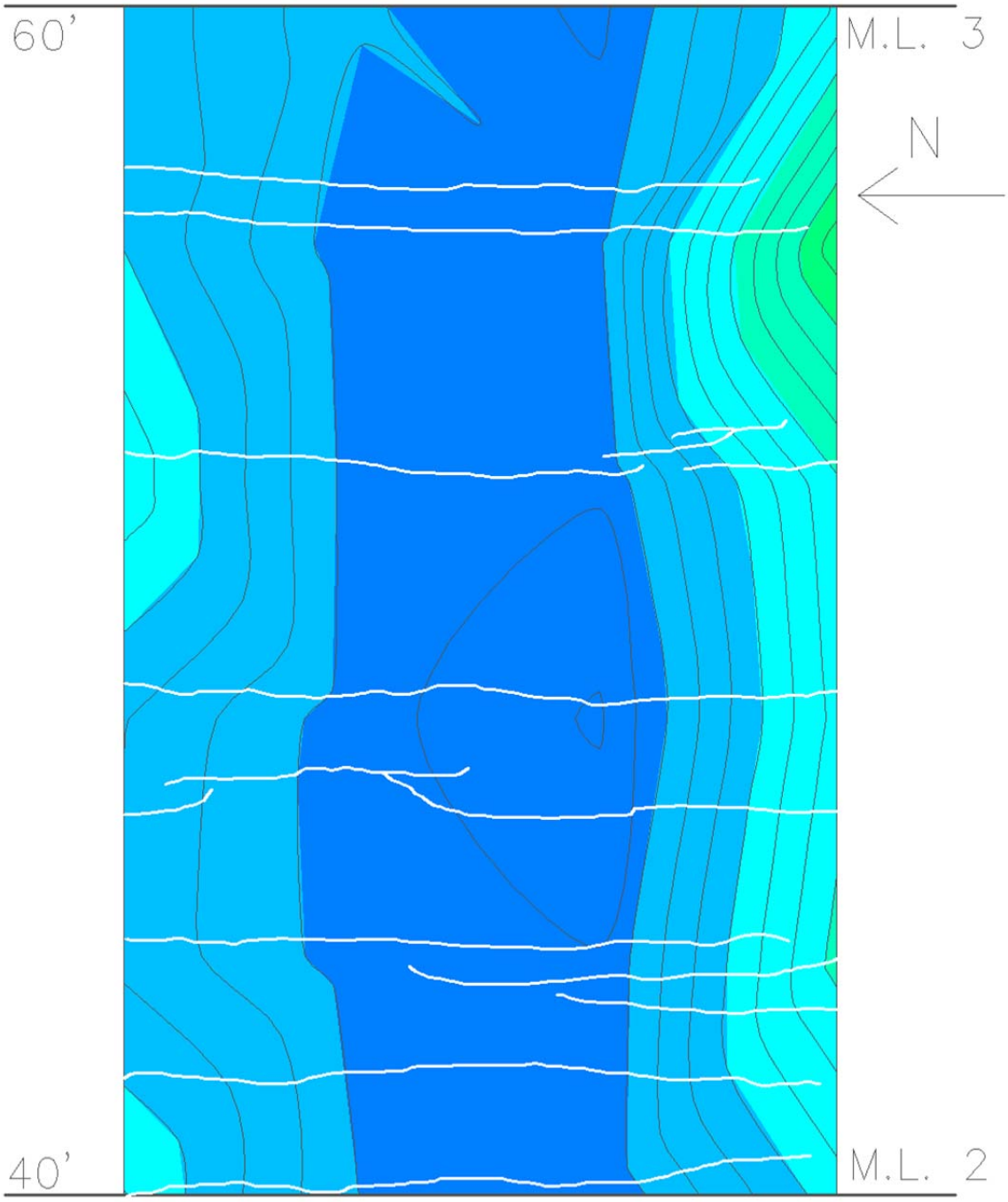

Figure B-44: MRM 25 from 40 to 60 feet

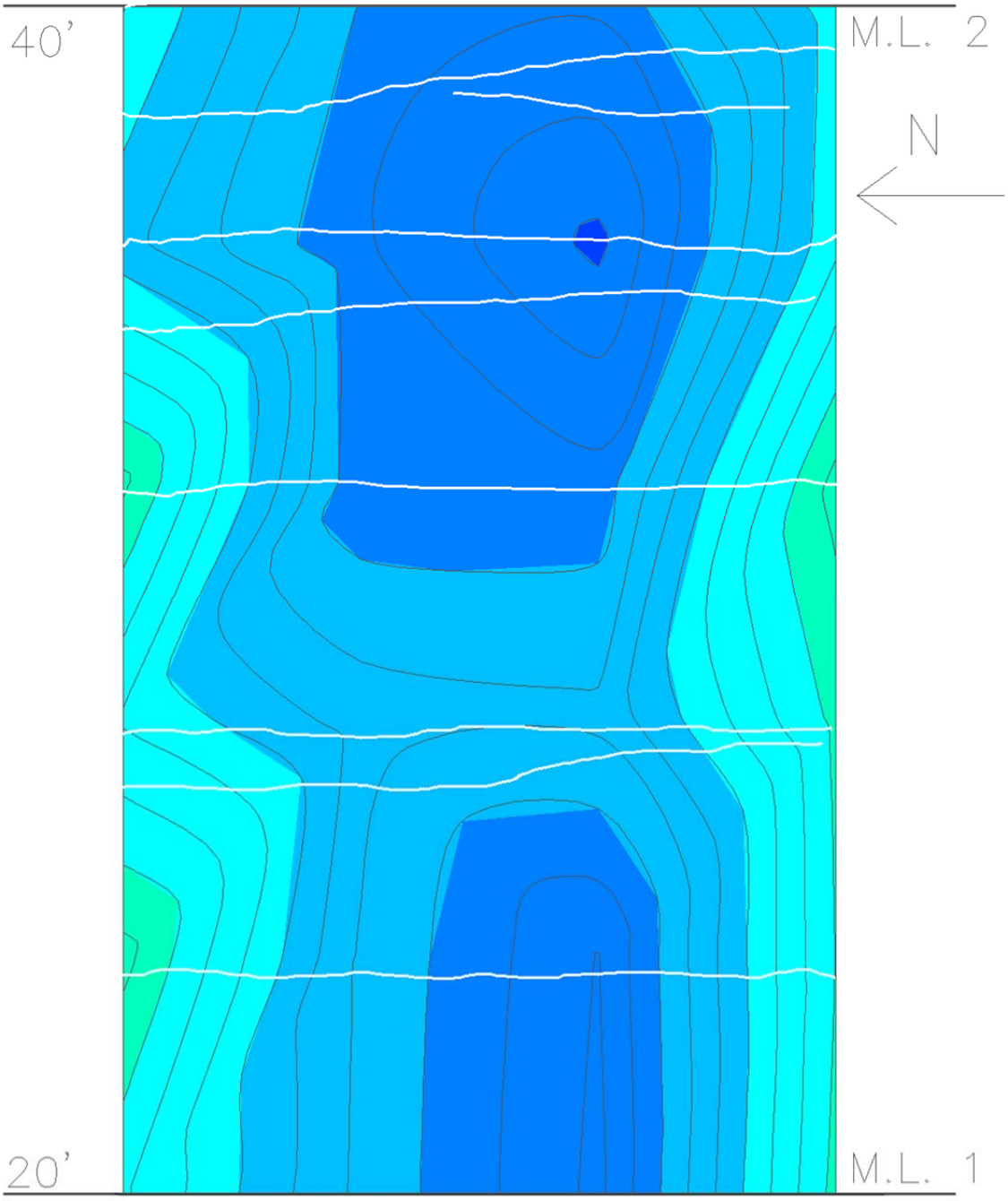

Figure B-45: MRM 25 from 20 to 40 feet

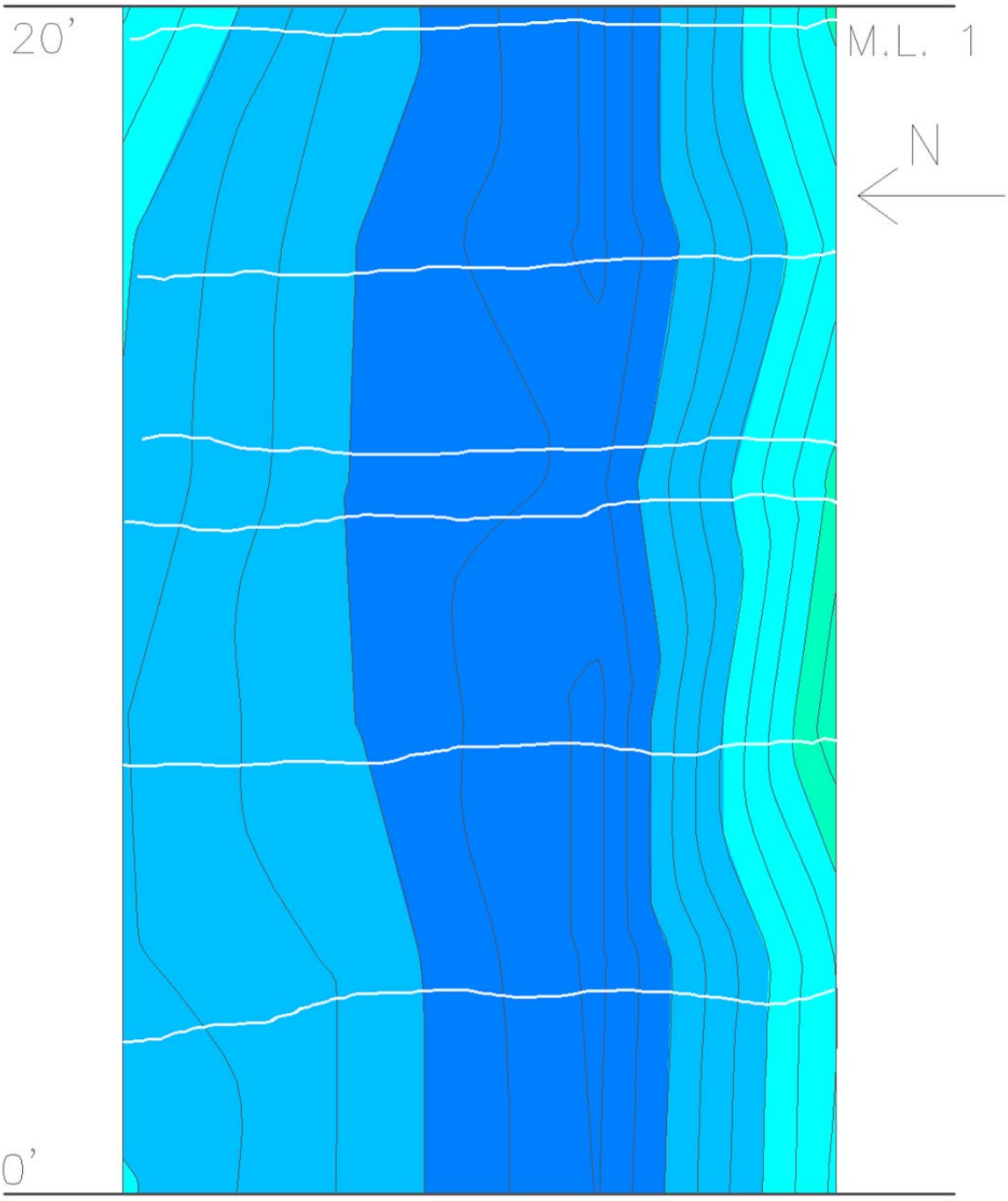

Figure B-46: MRM 25 from 0 to 20 feet

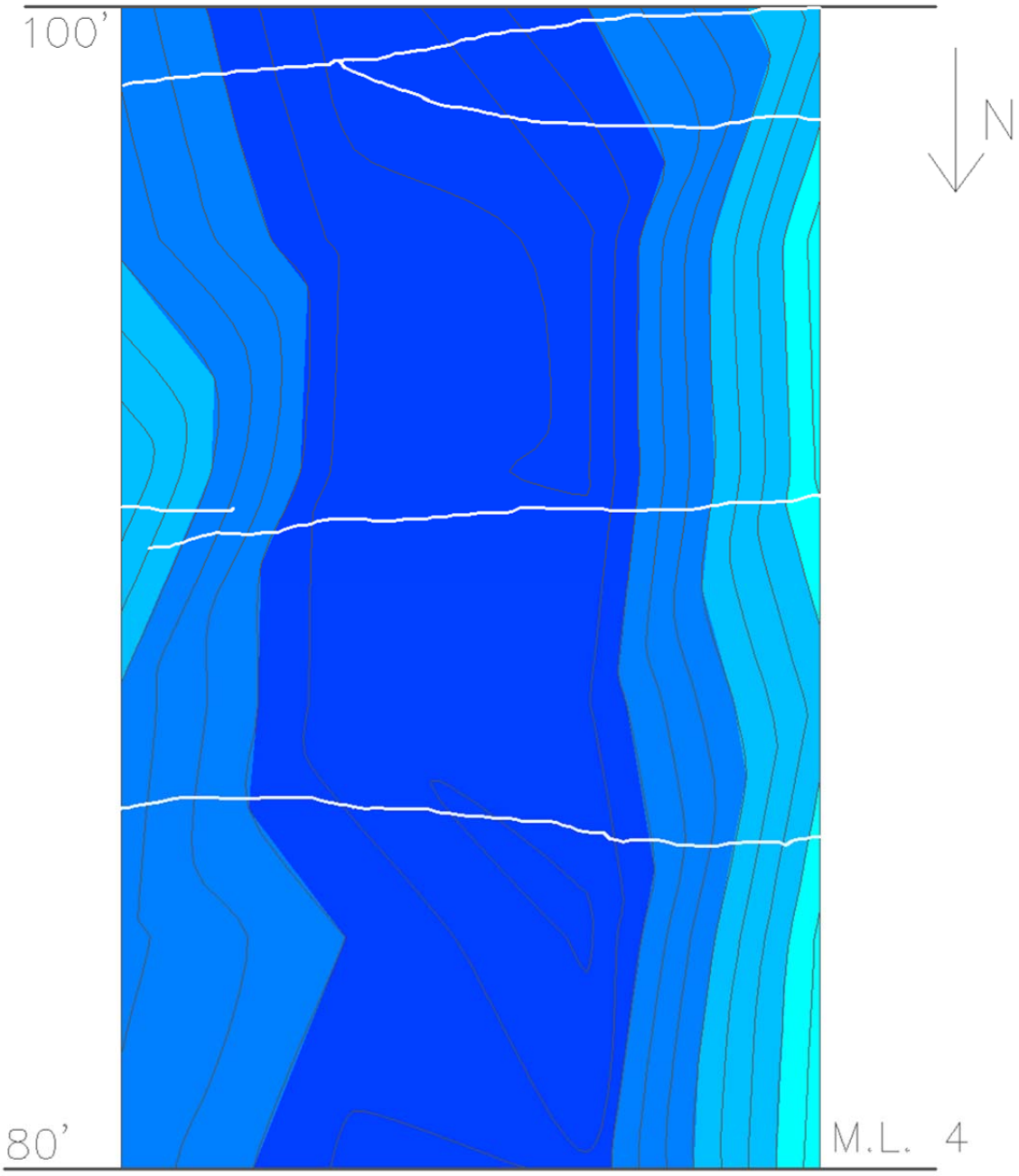

Figure B-47: MRM 54 from 80 to 100 feet

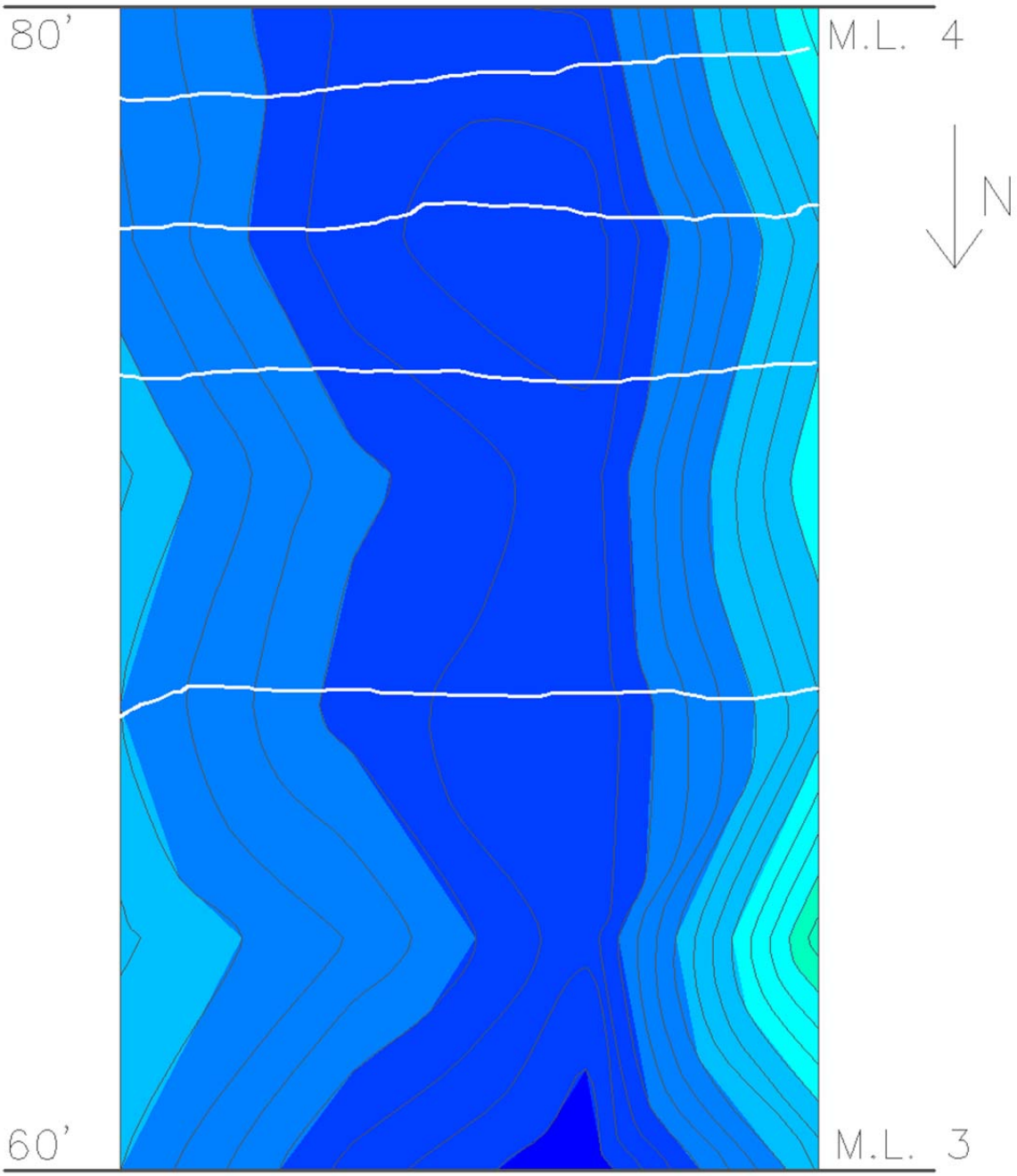

Figure B-48: MRM 54 from 60 to 80 feet

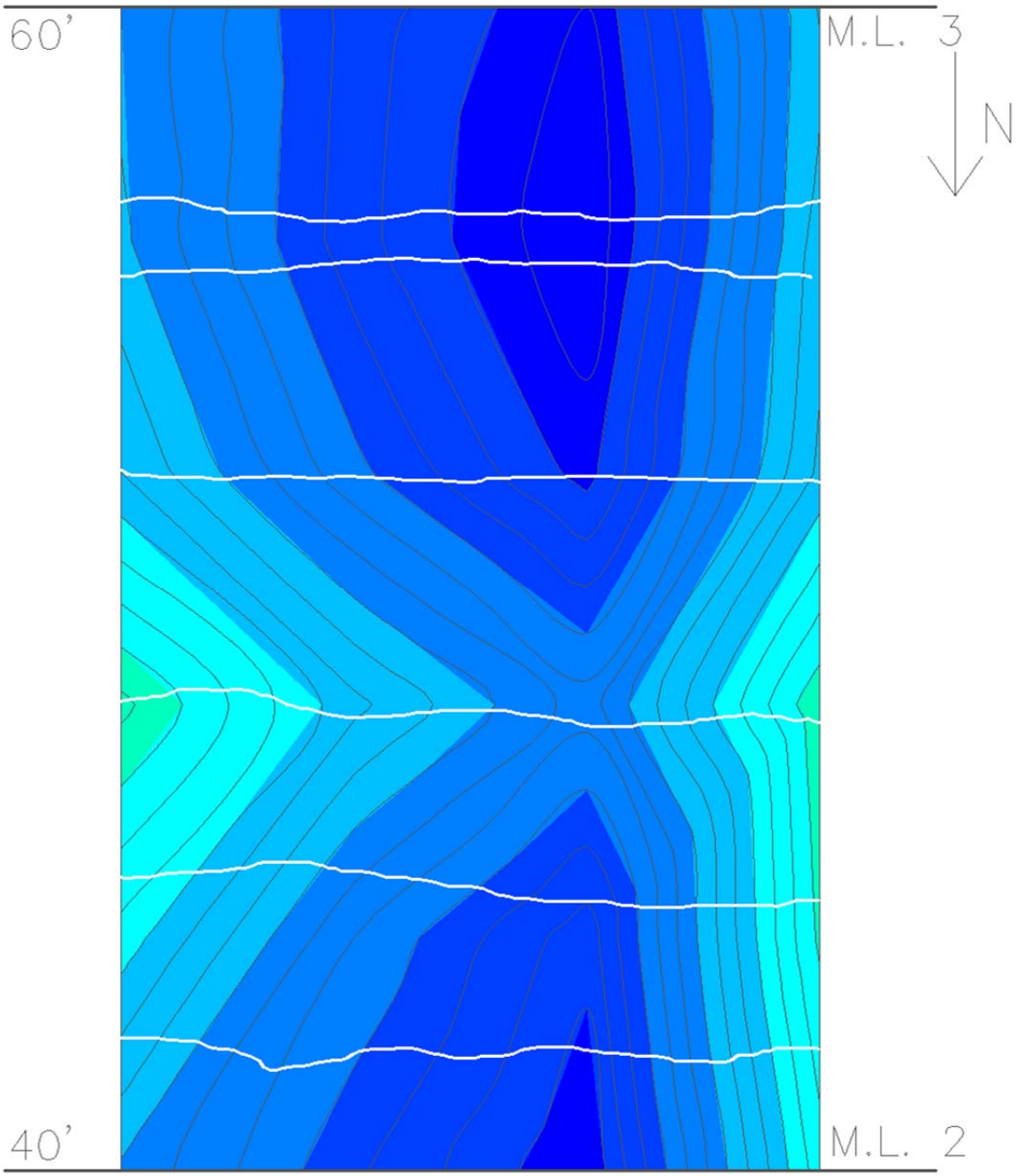

Figure B-49: MRM 54 from 40 for 60 feet

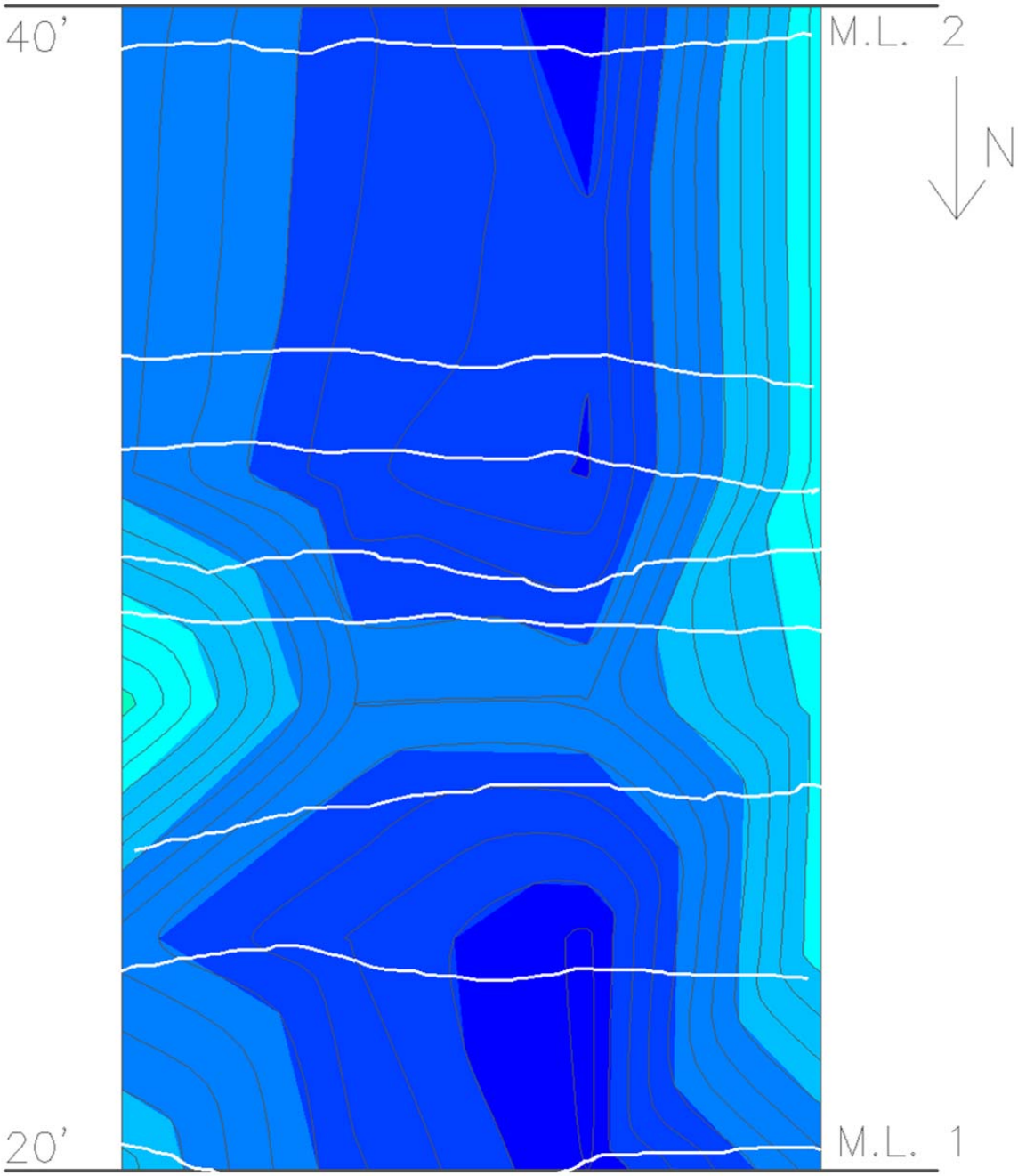

Figure B-50: MRM 54 from 20 to 40 feet

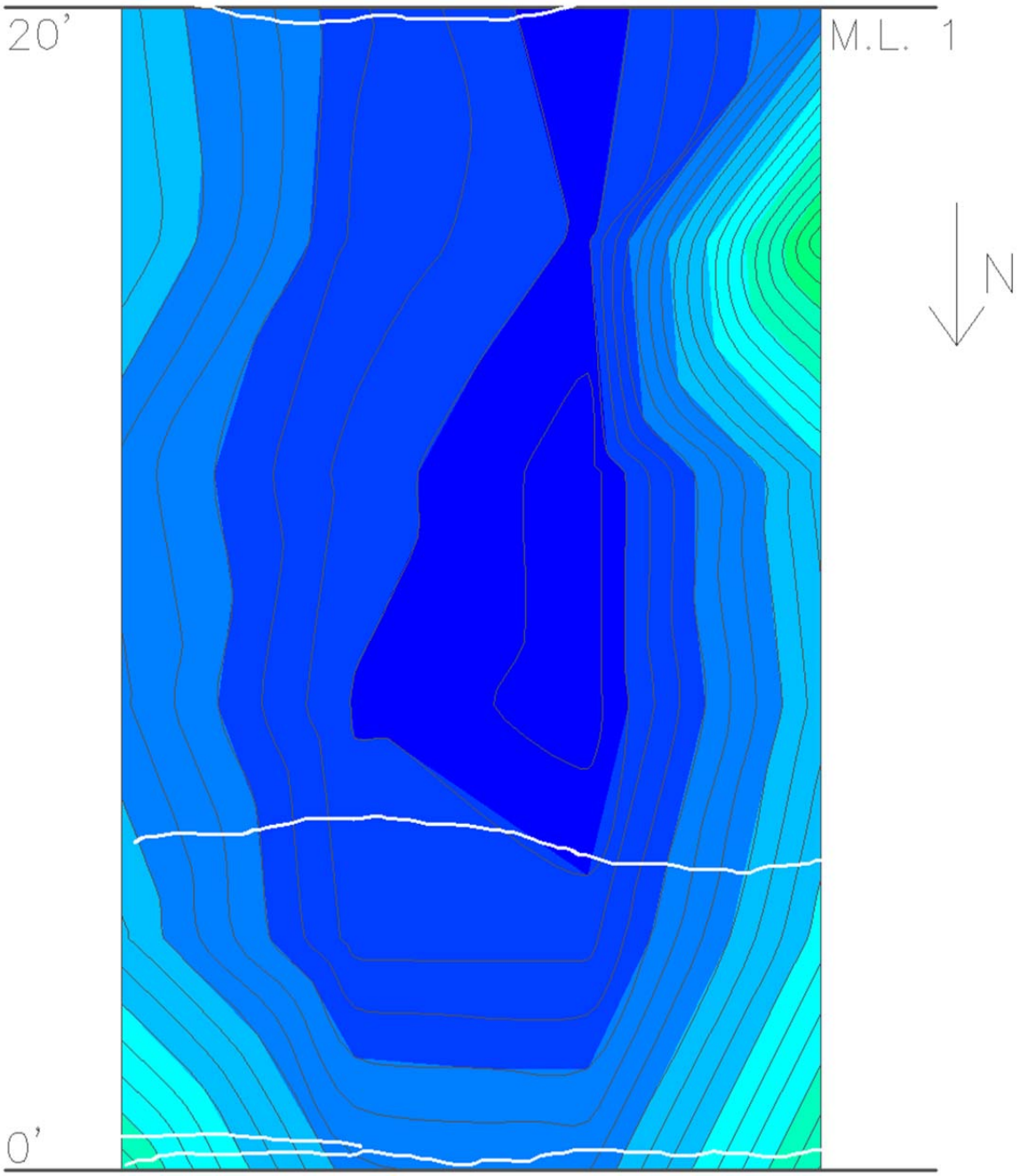

Figure B-51: MRM 54 from 0 to 20 feet

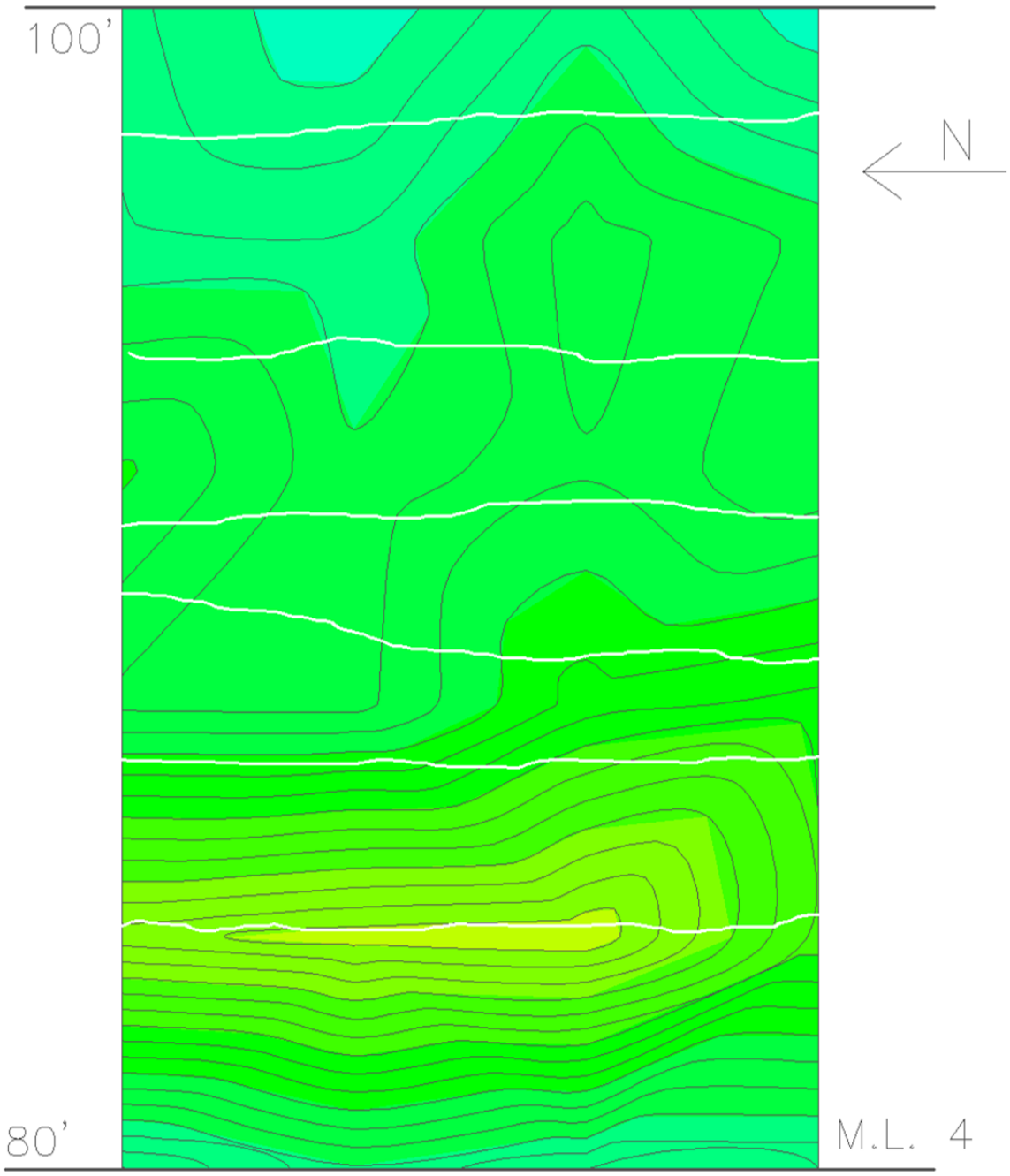

Figure B-52: MRM 222 from 80 to 100 feet

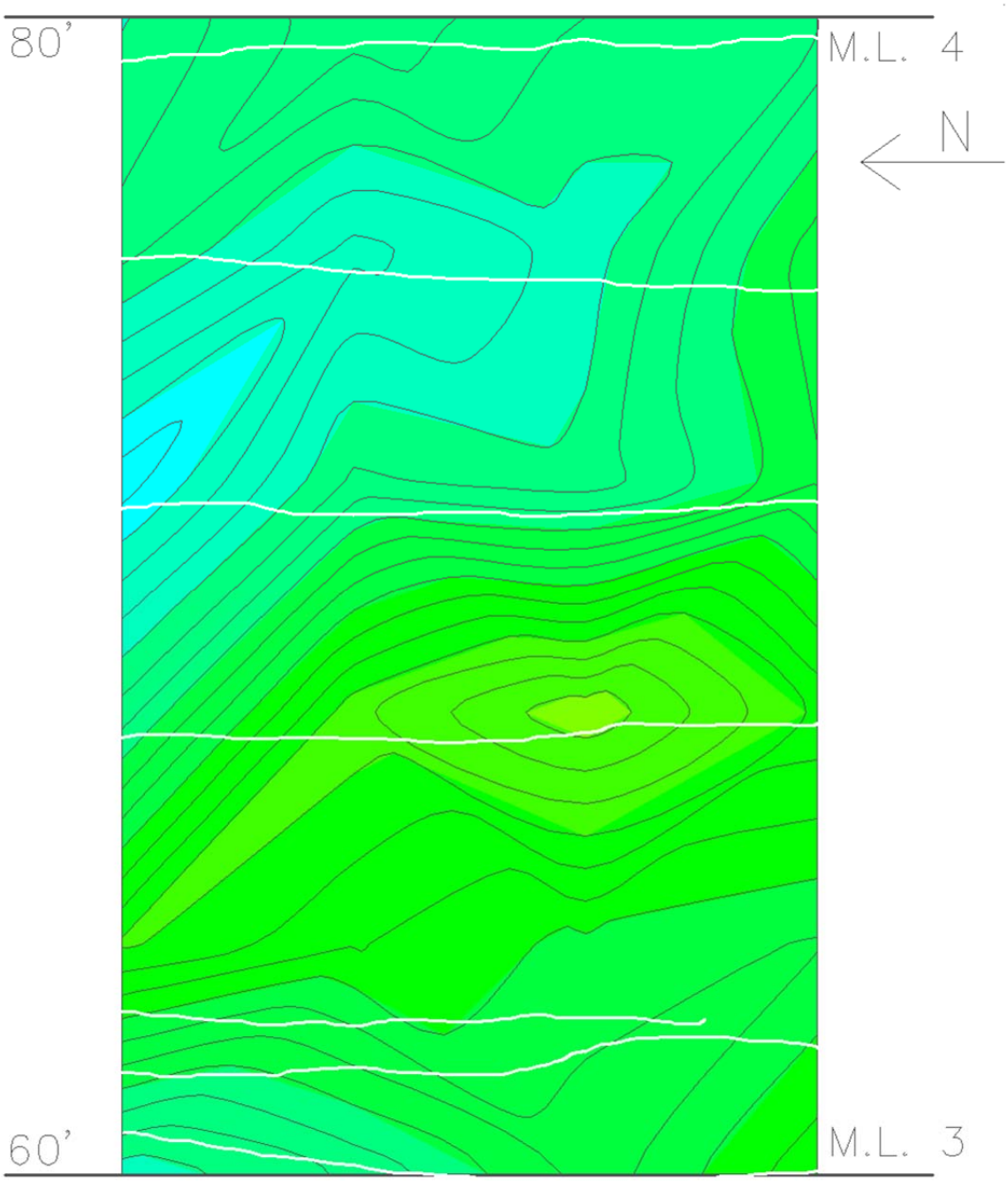

Figure B-53: MRM 222 from 60 to 80 feet

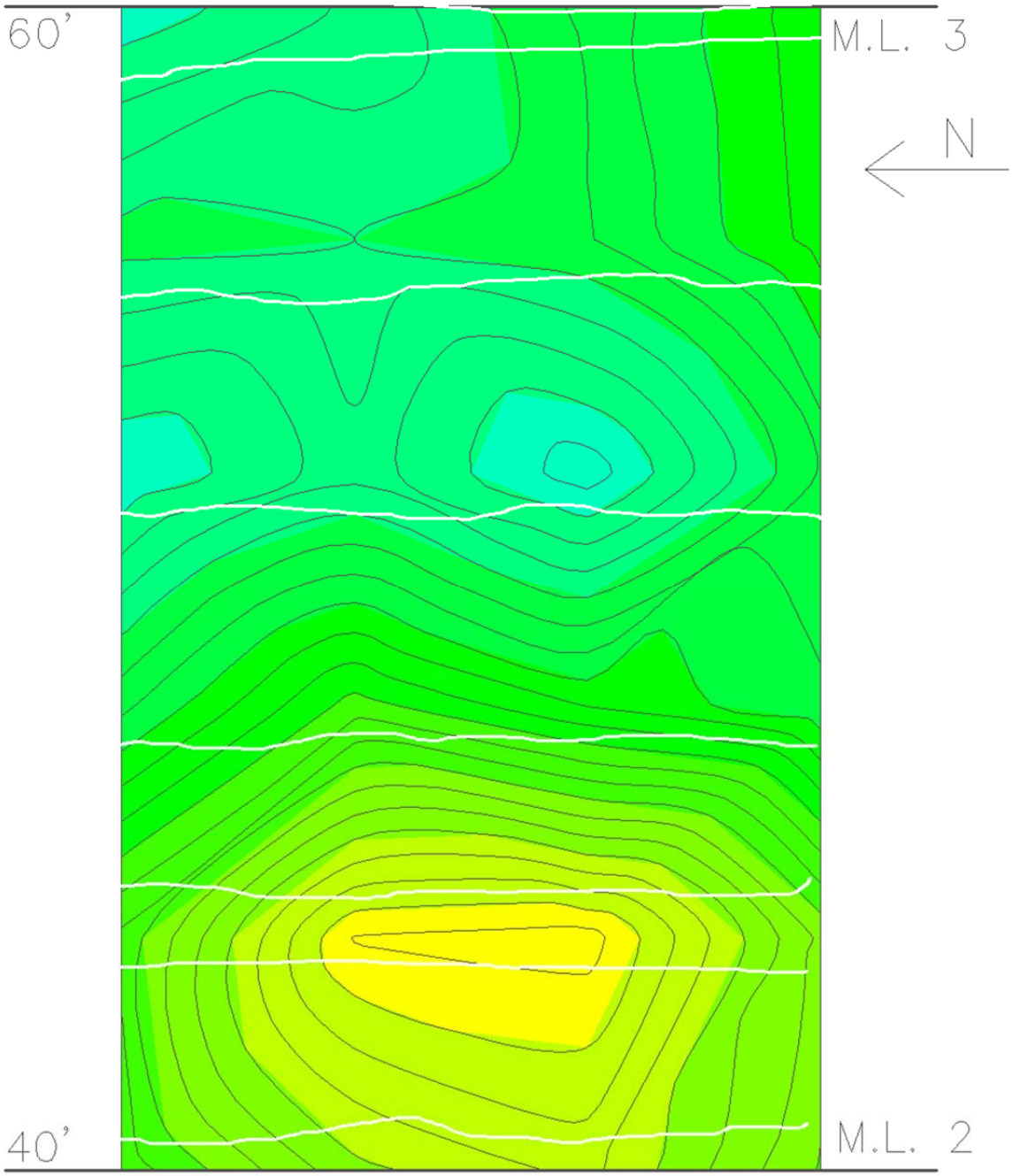

Figure B-54: MRM 222 from 40 to 60 feet

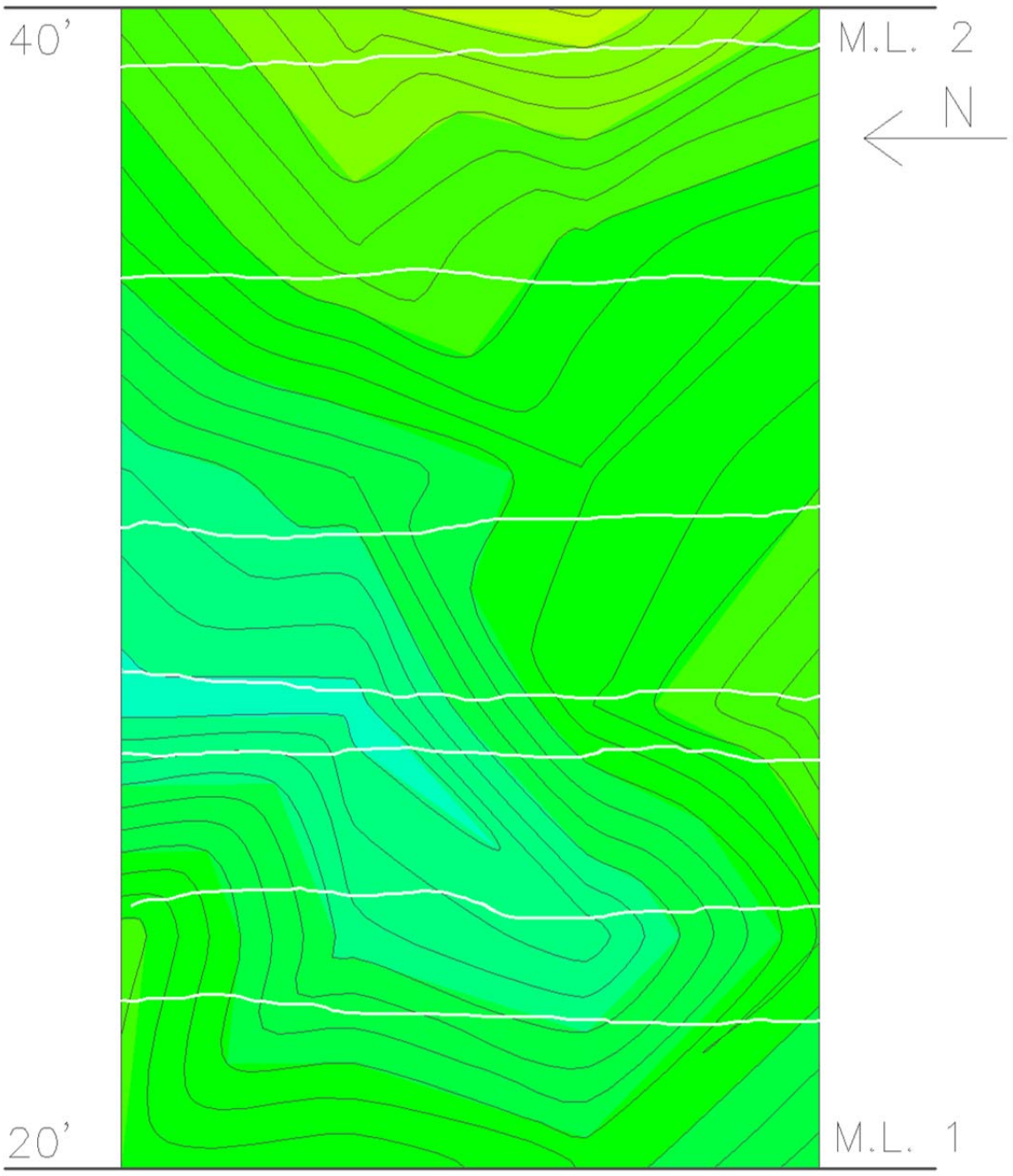

Figure B-55: MRM 222 from 20 to 40 feet

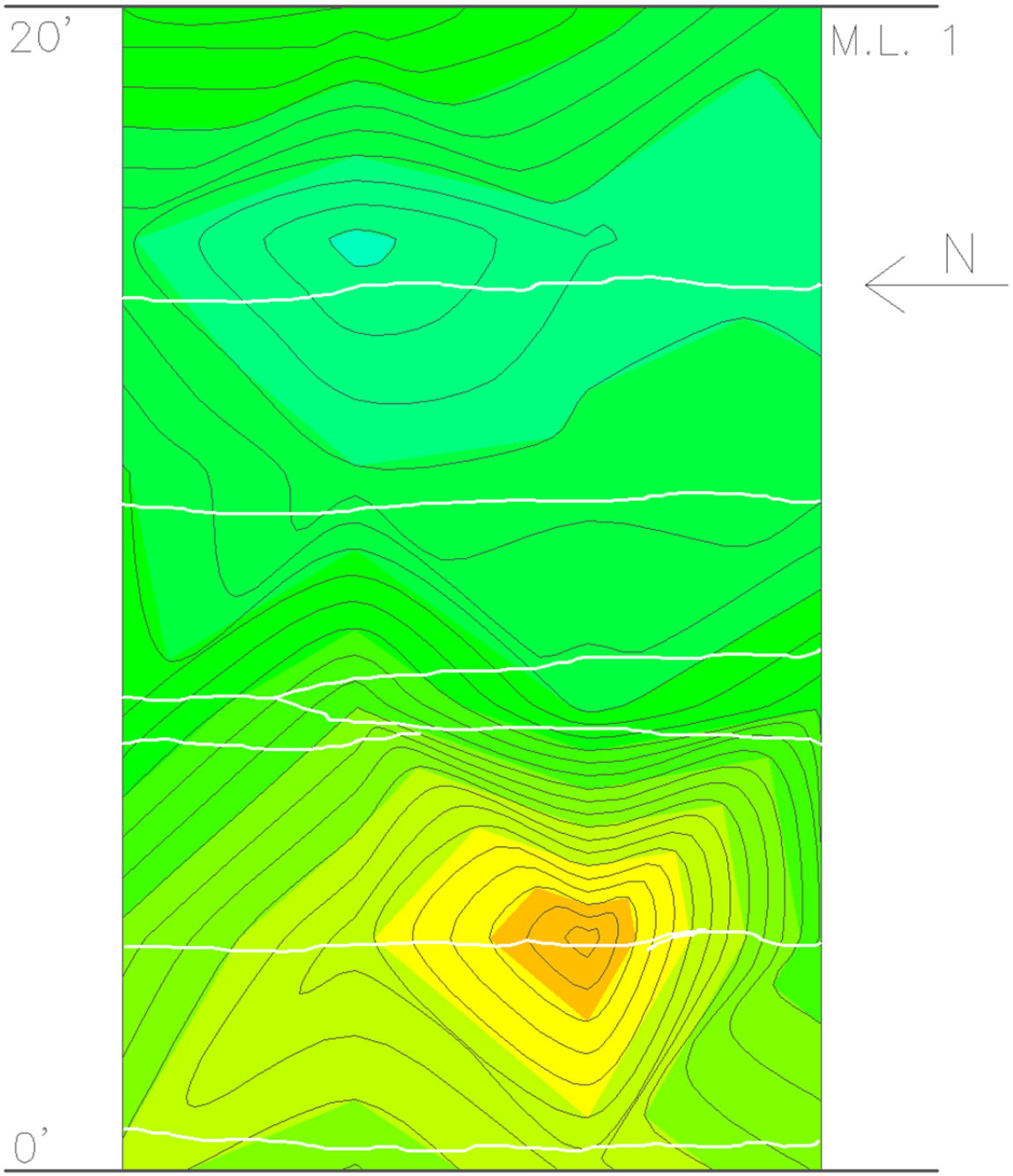

Figure B-56: MRM 222 from 0 to 20 feet

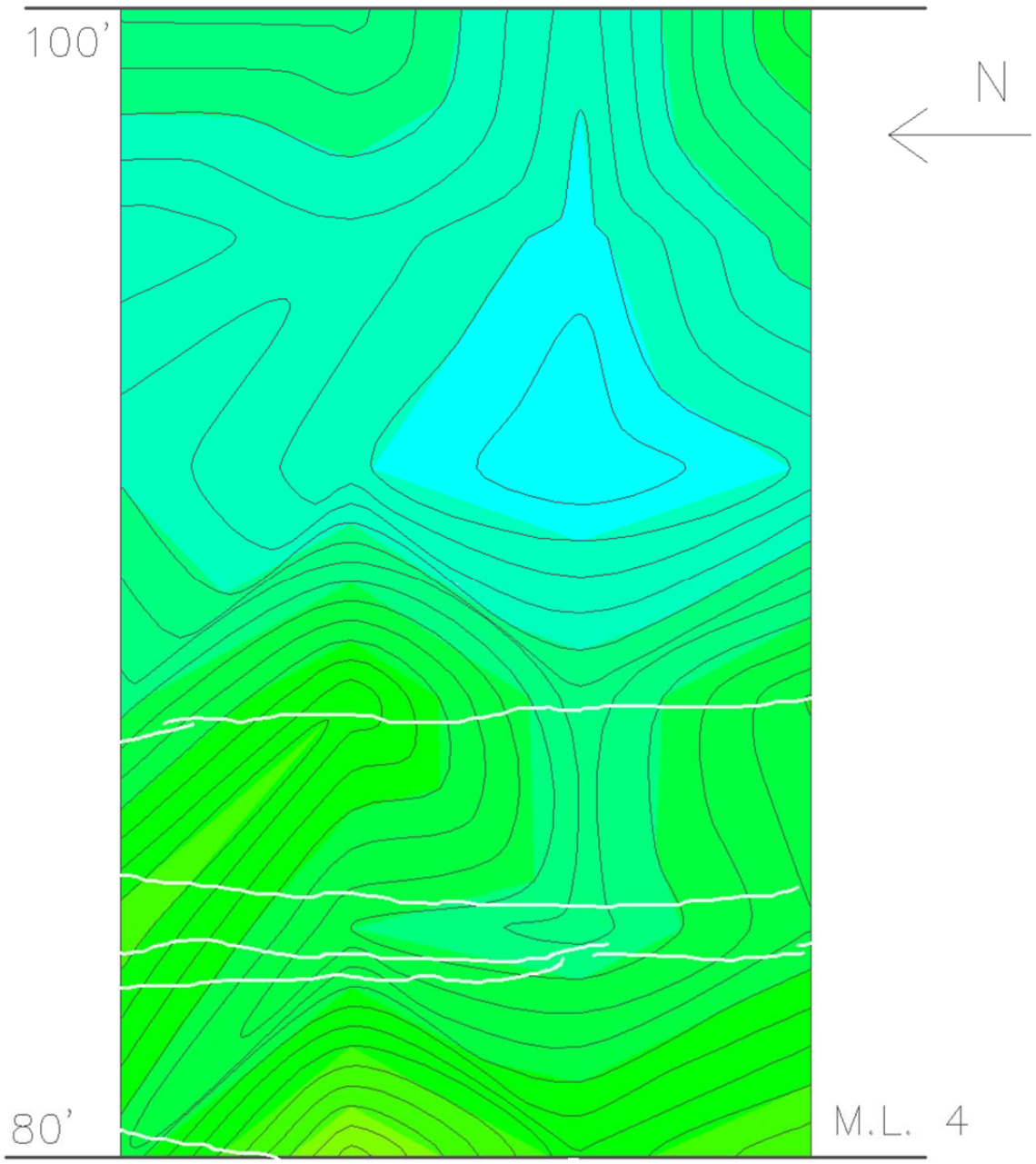

Figure B-57: MRM 246 from 80 to 100 feet

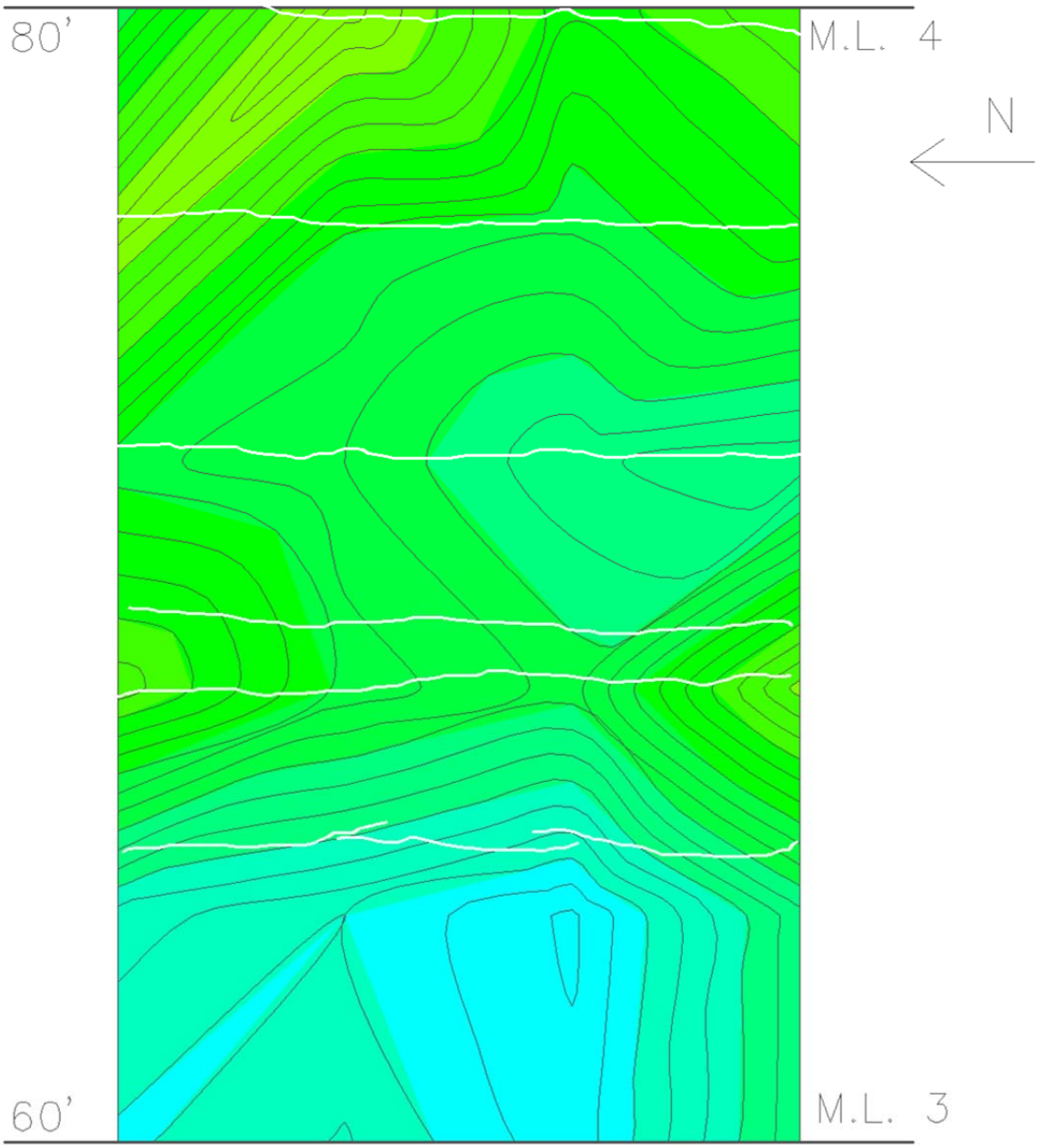

Figure B-58: MRM 246 from 60 to 80 feet

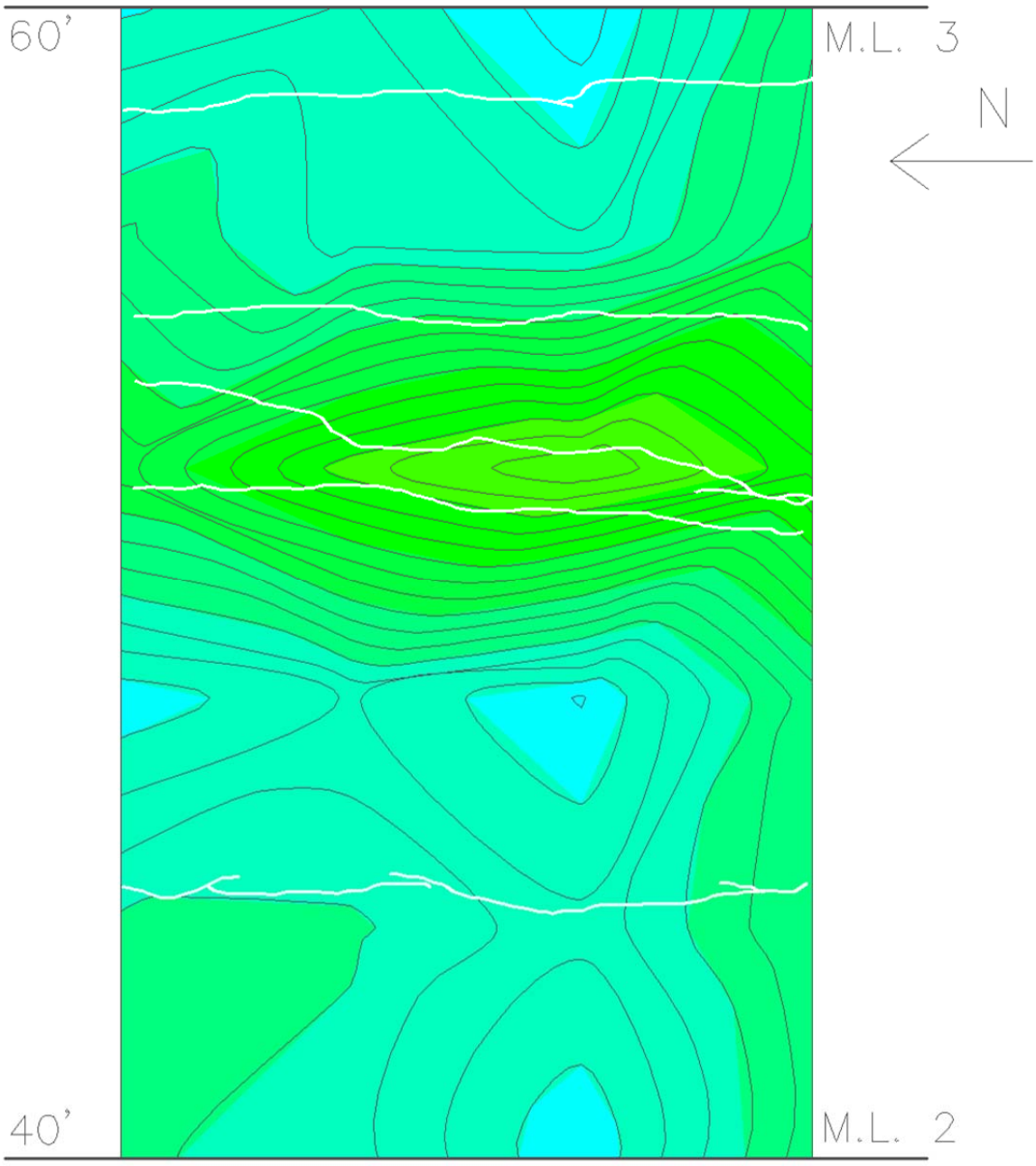

Figure B-59: MRM 246 from 40 to 60 feet

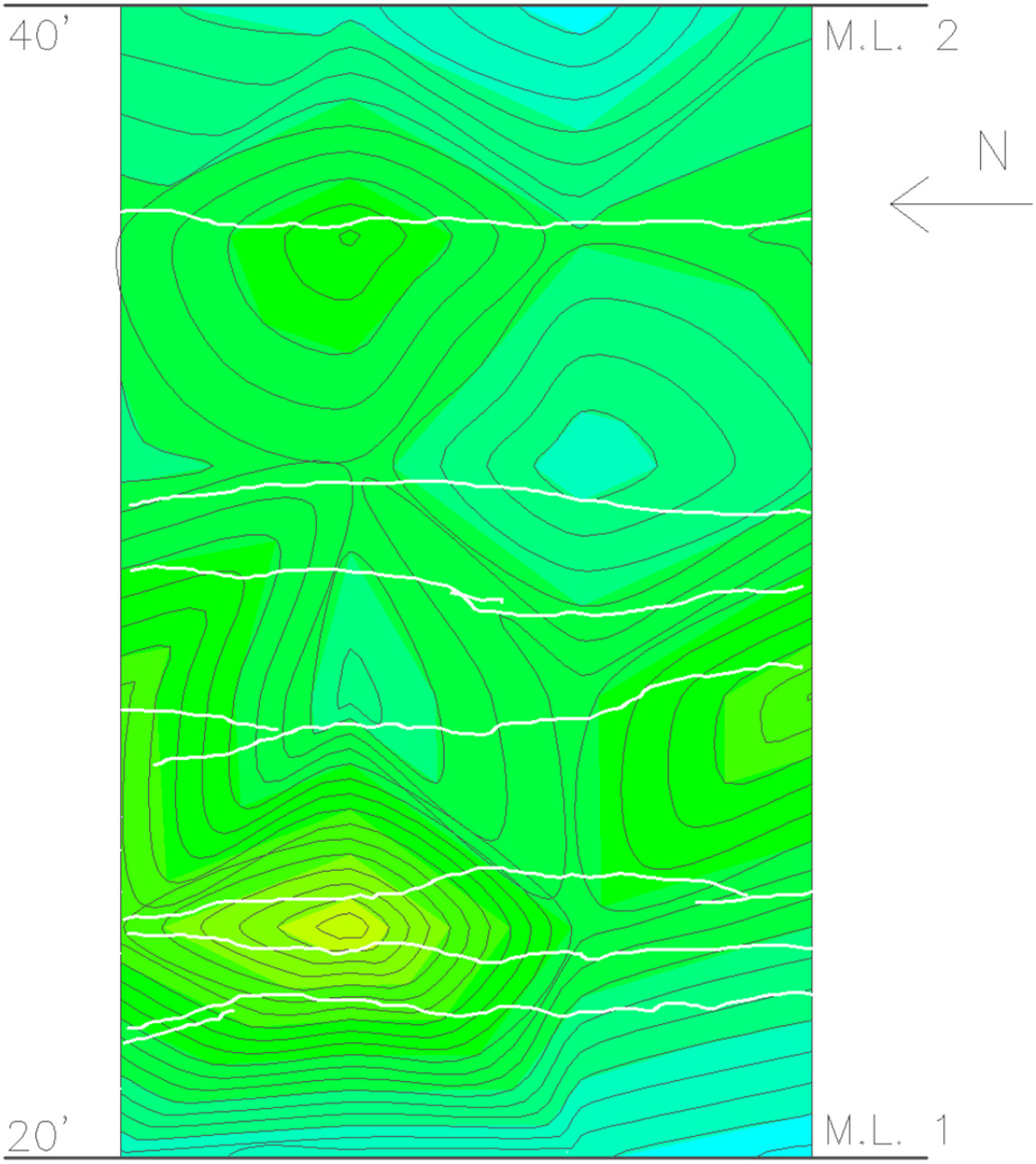

Figure B-60: MRM 246 from 20 to 40 feet

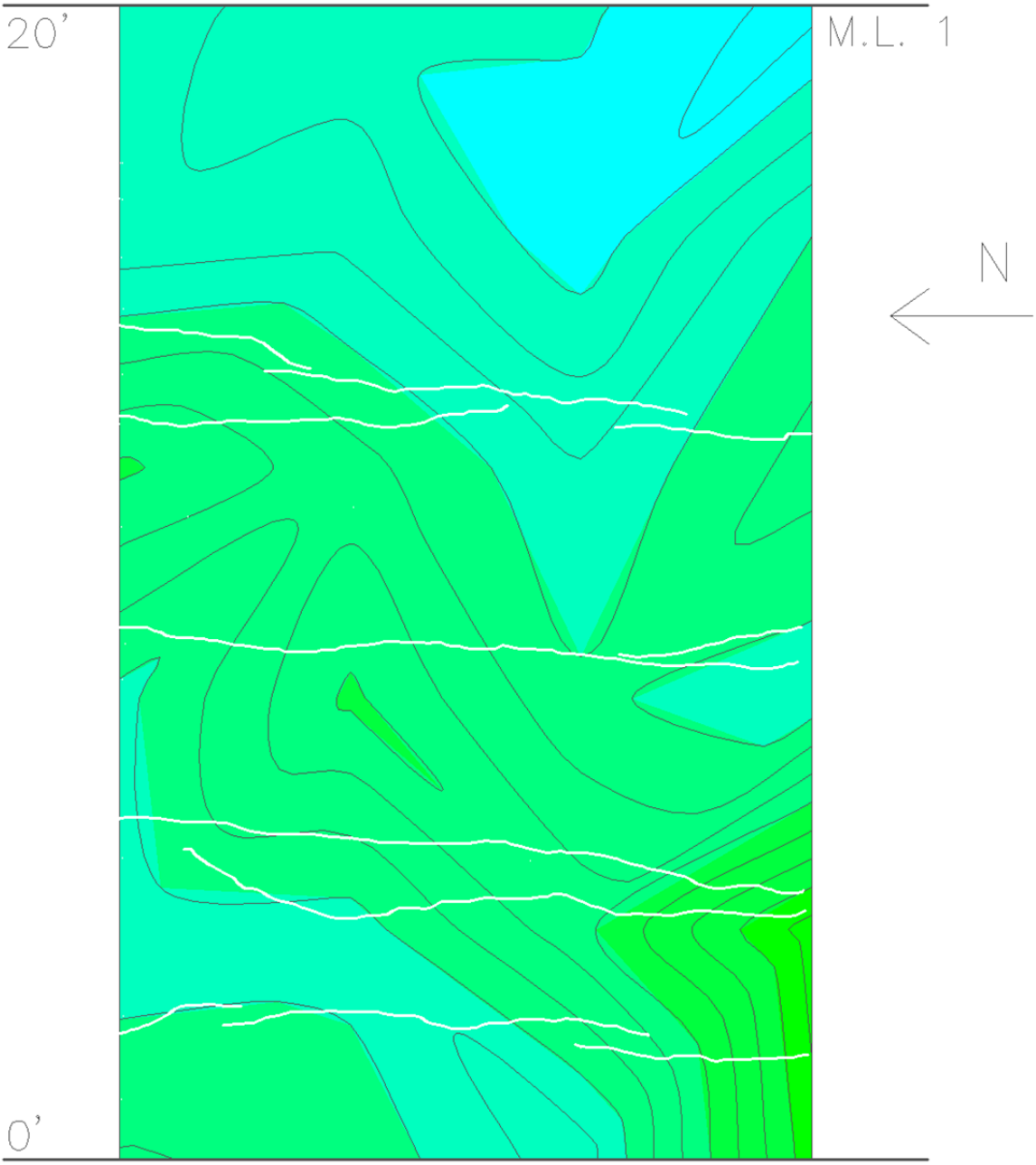

Figure B-61: MRM 246 from 0 to 20 feet

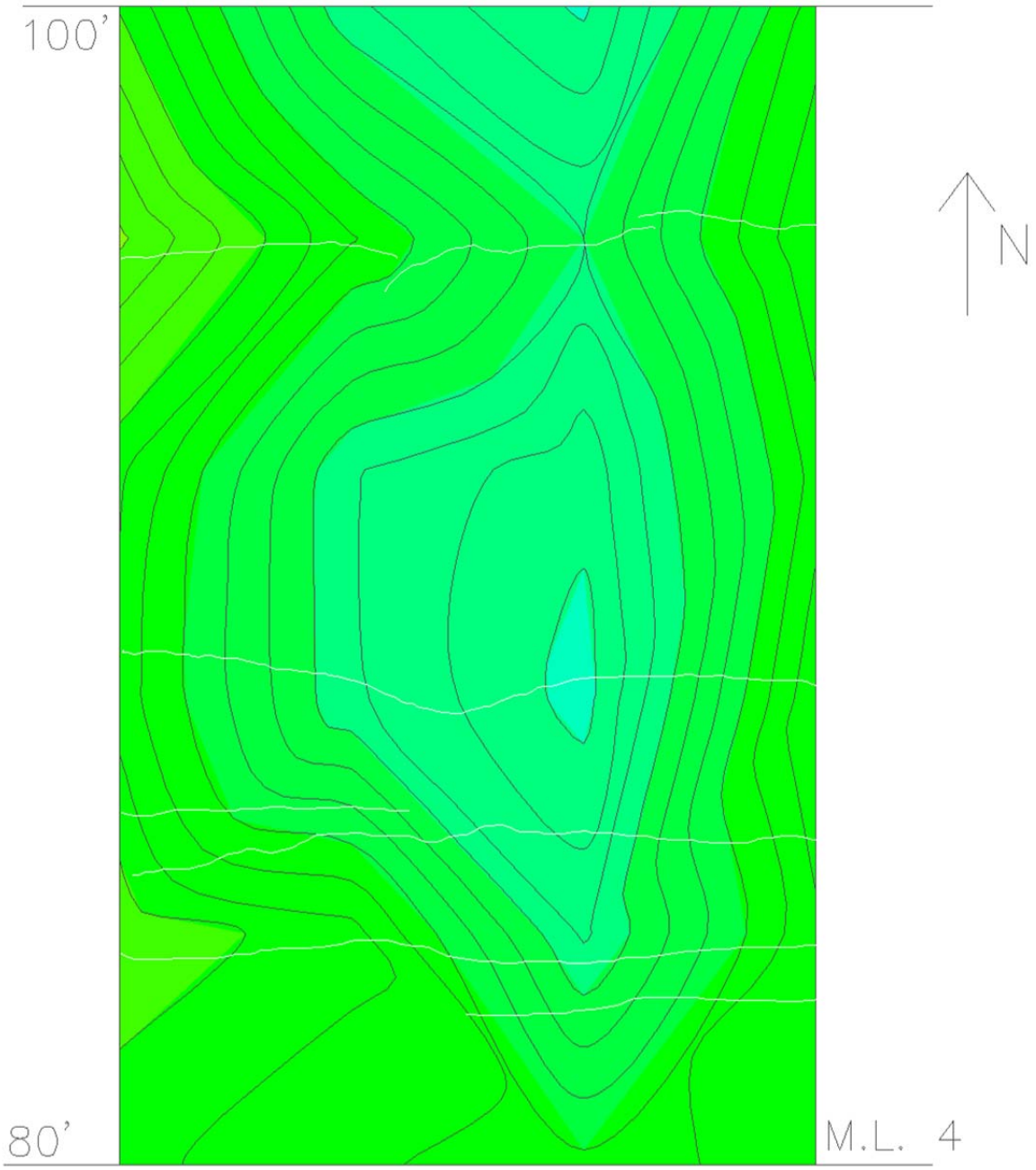

Figure B-62: MRM 168 NB from 80 to 100 feet

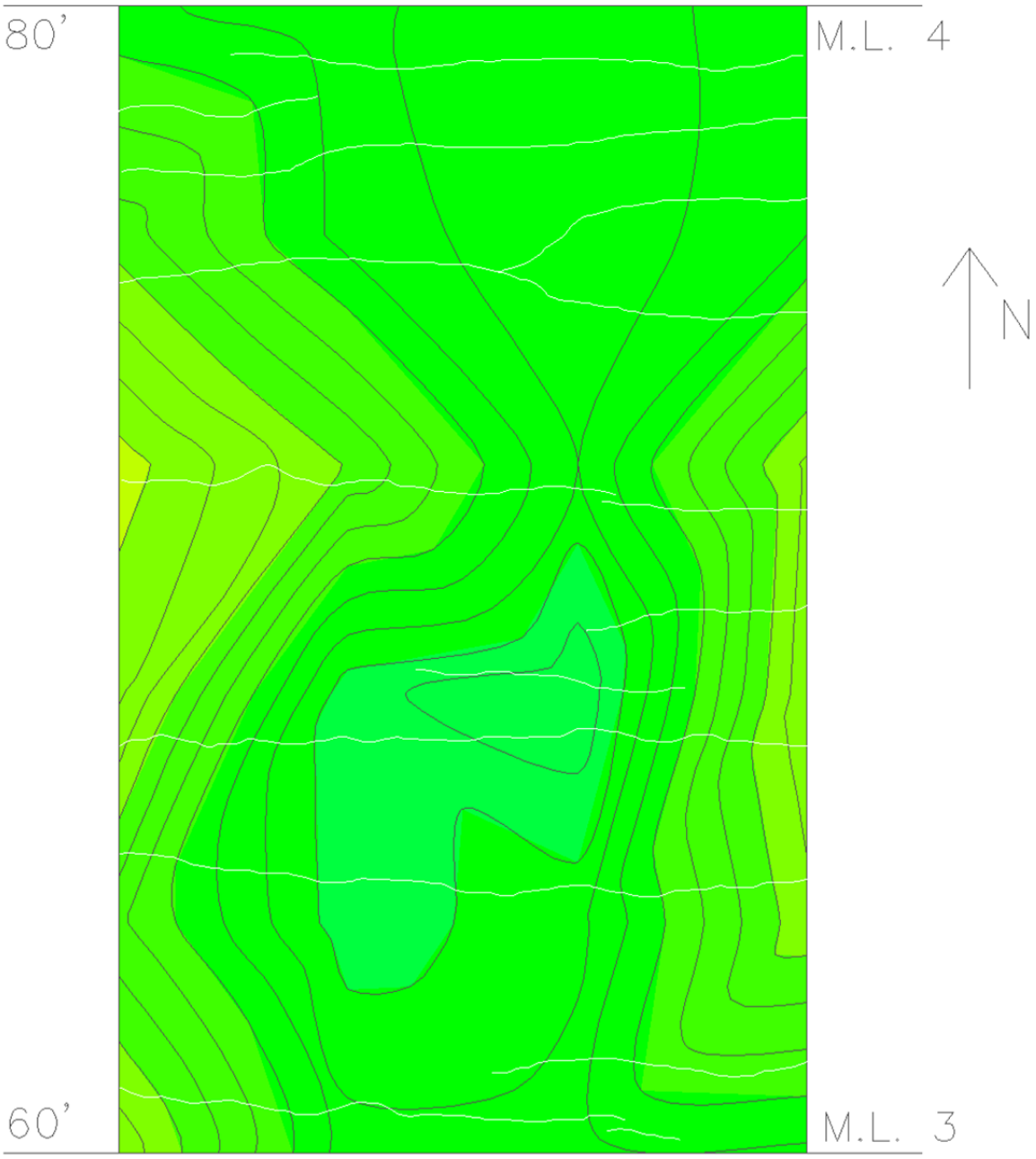

Figure B-63: MRM 168 NB from 60 to 80 feet

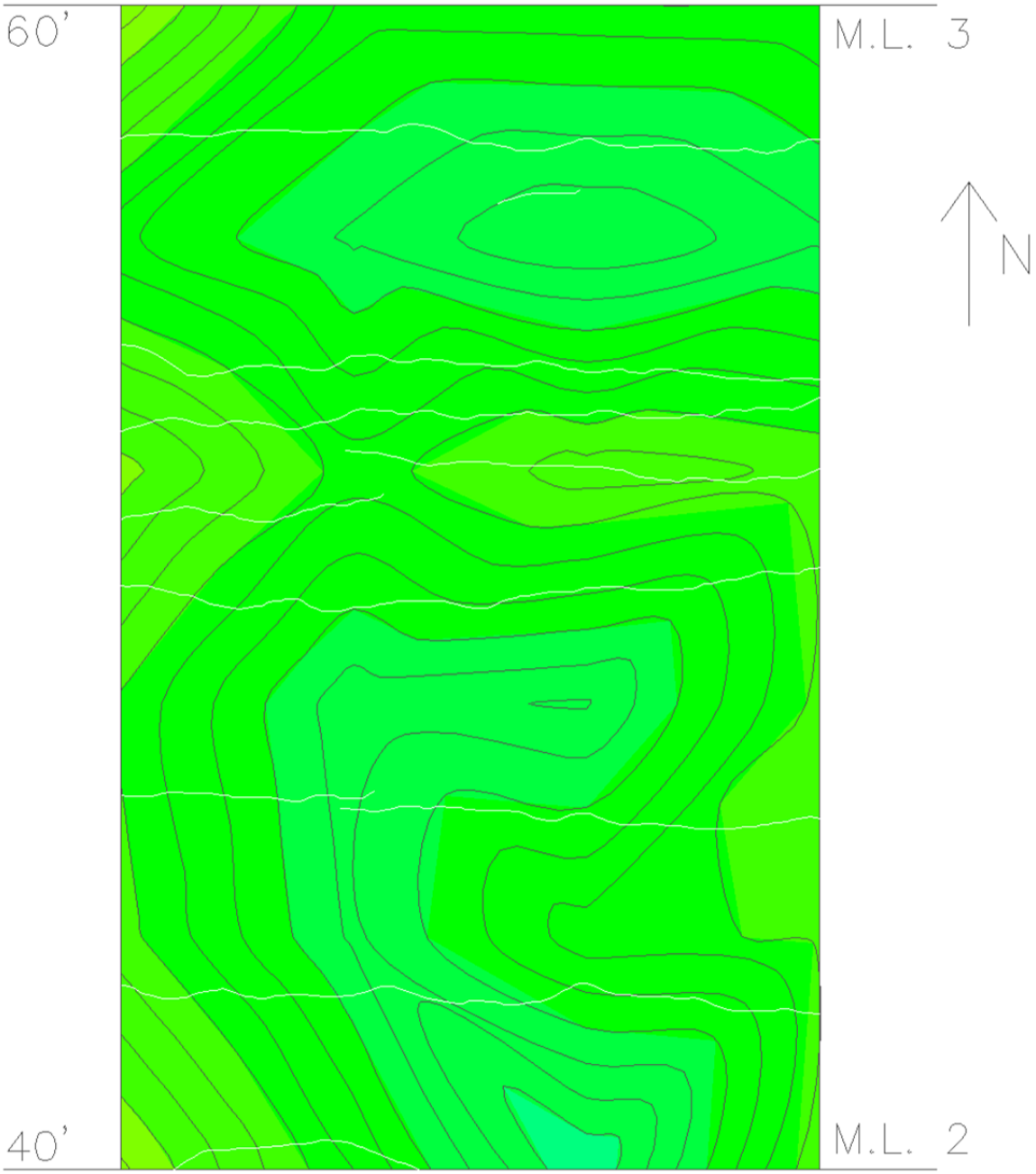

Figure B-64: MRM 168 NB from 40 to 60 feet

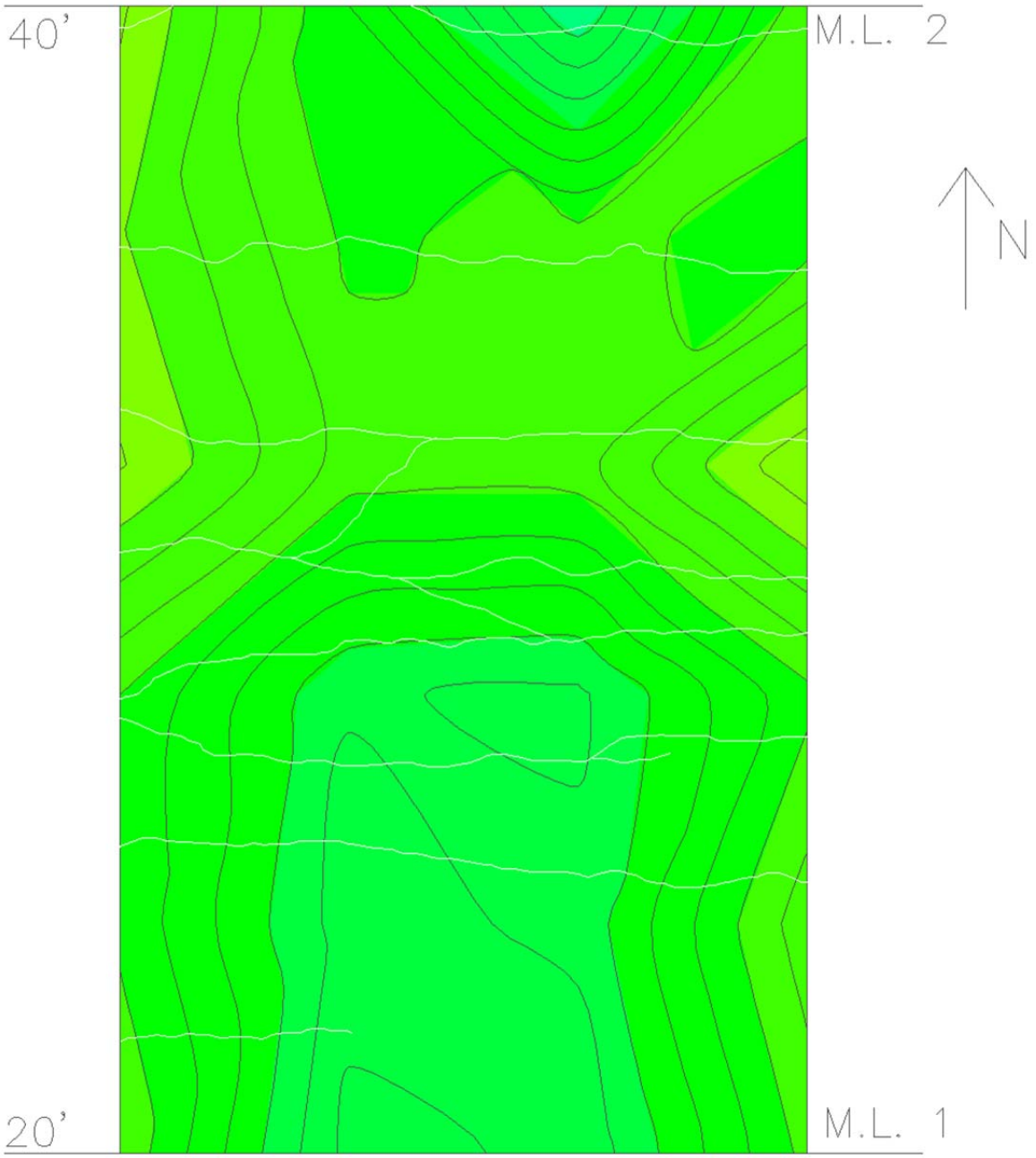

Figure B-65: MRM 168 NB from 20 to 40 feet

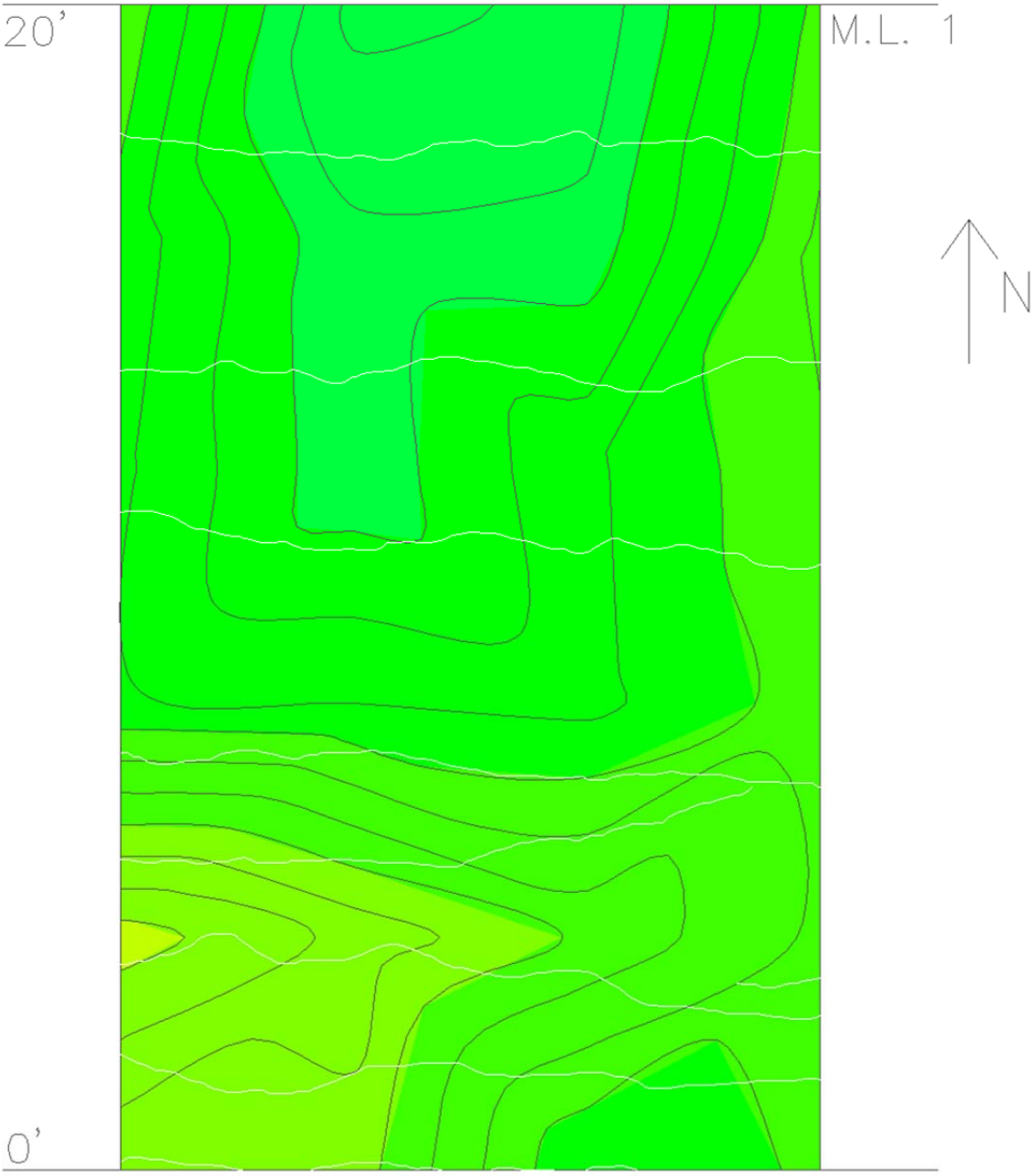

Figure B-66: MRM 168 NB from 0 to 20 feet

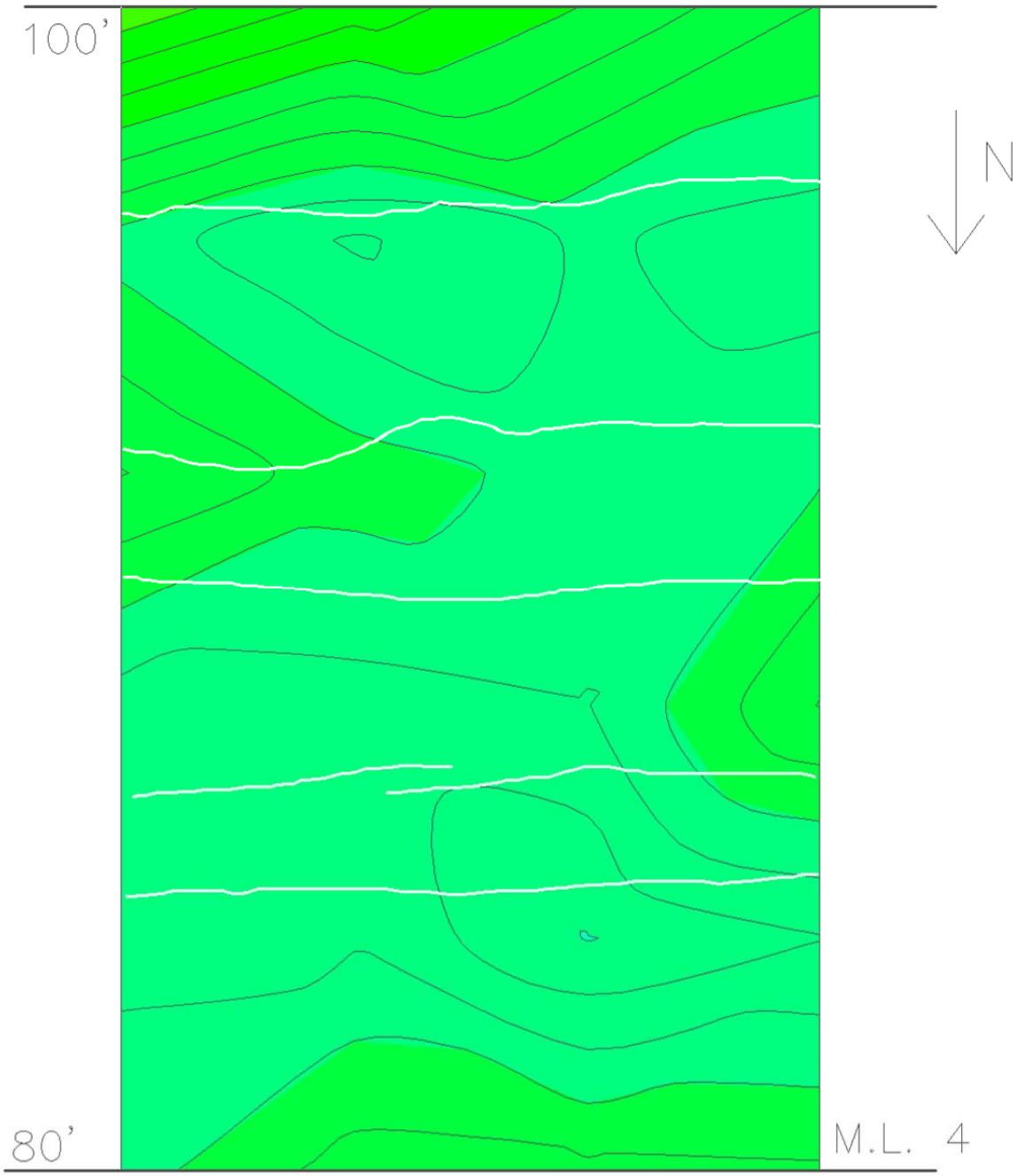

Figure B-67: MRM 168 SB from 80 to 100 feet

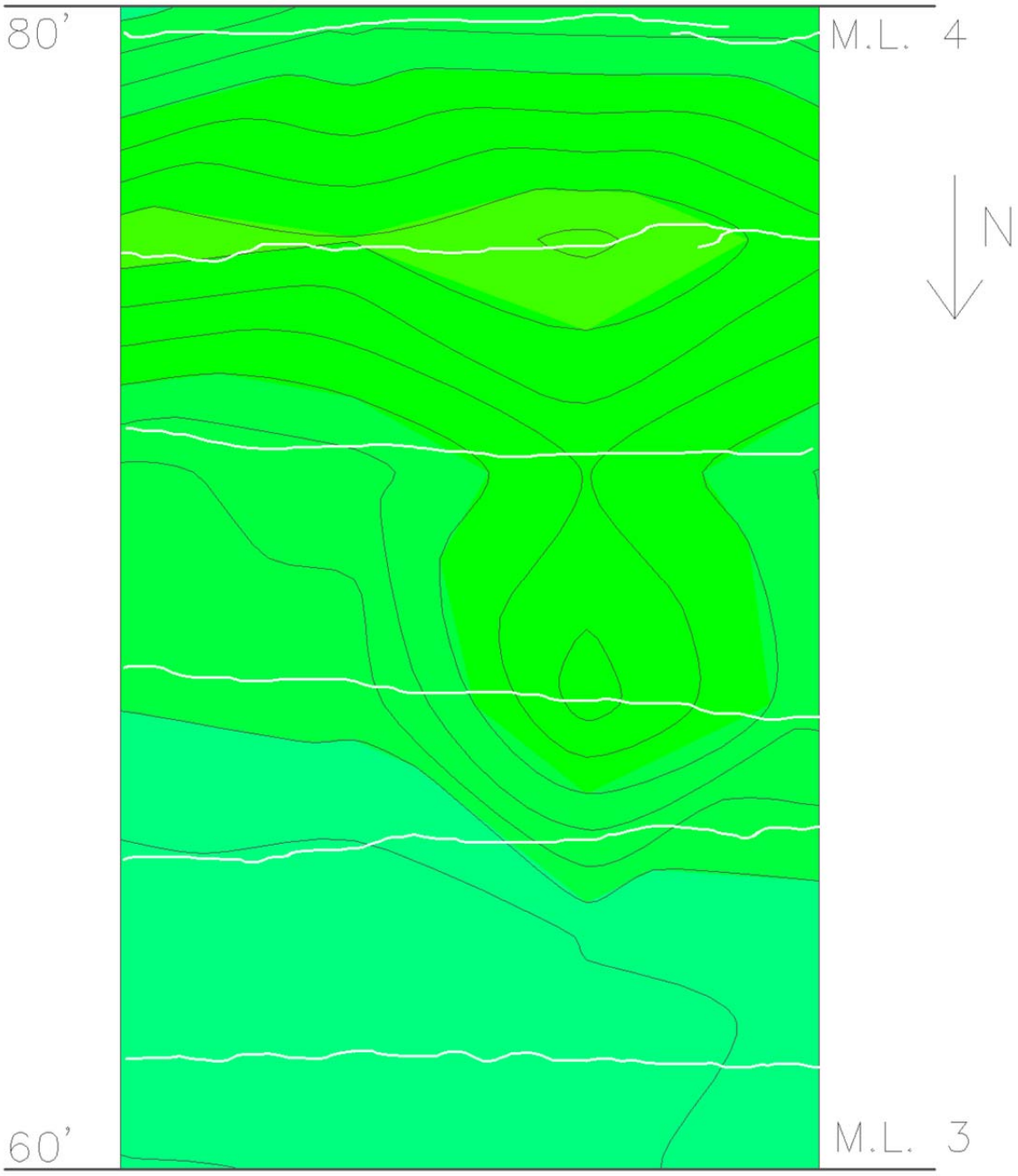

Figure B-68: MRM 168 SB from 60 to 80 feet

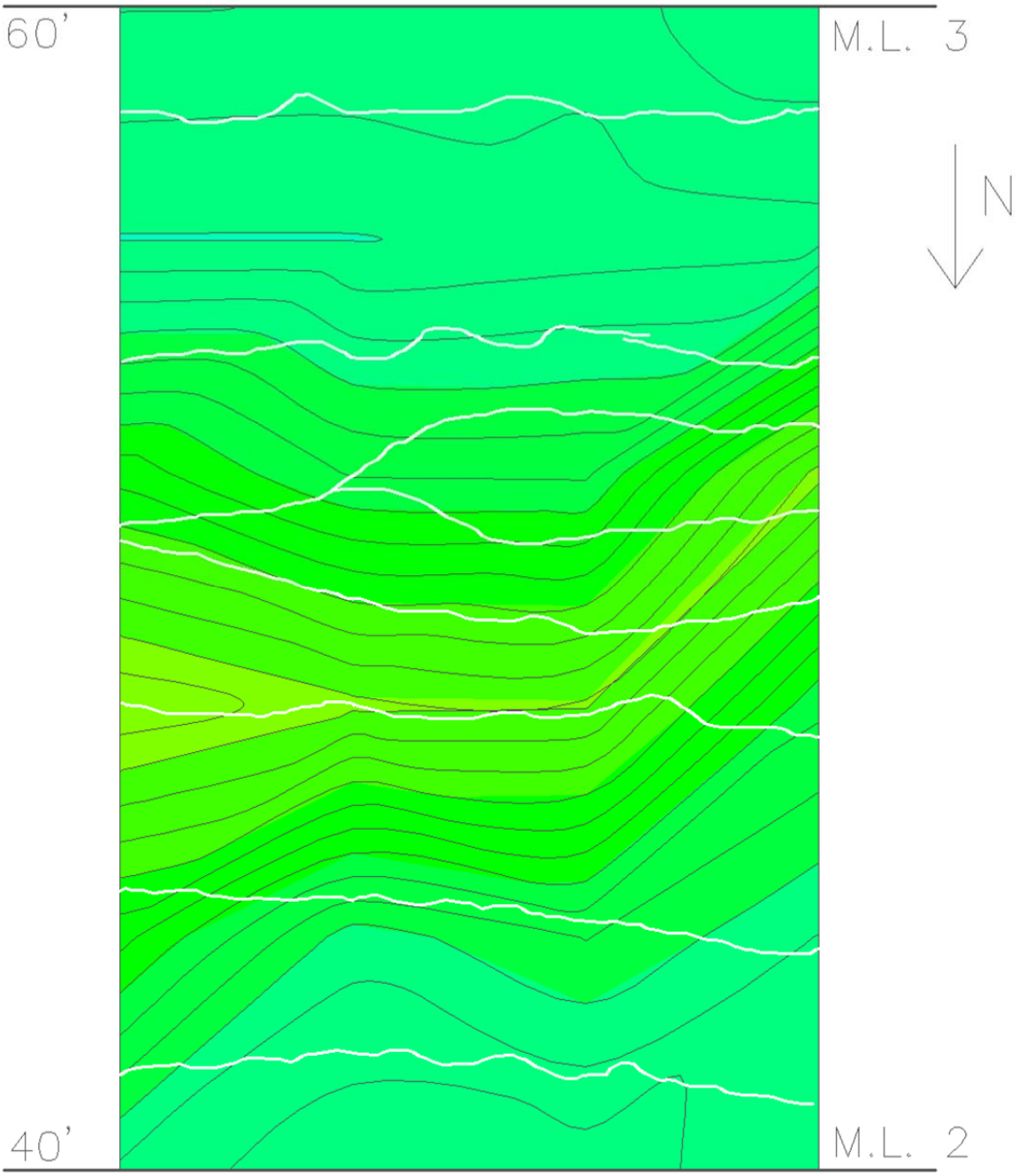

Figure B-69: MRM 168 SB from 40 to 60 feet

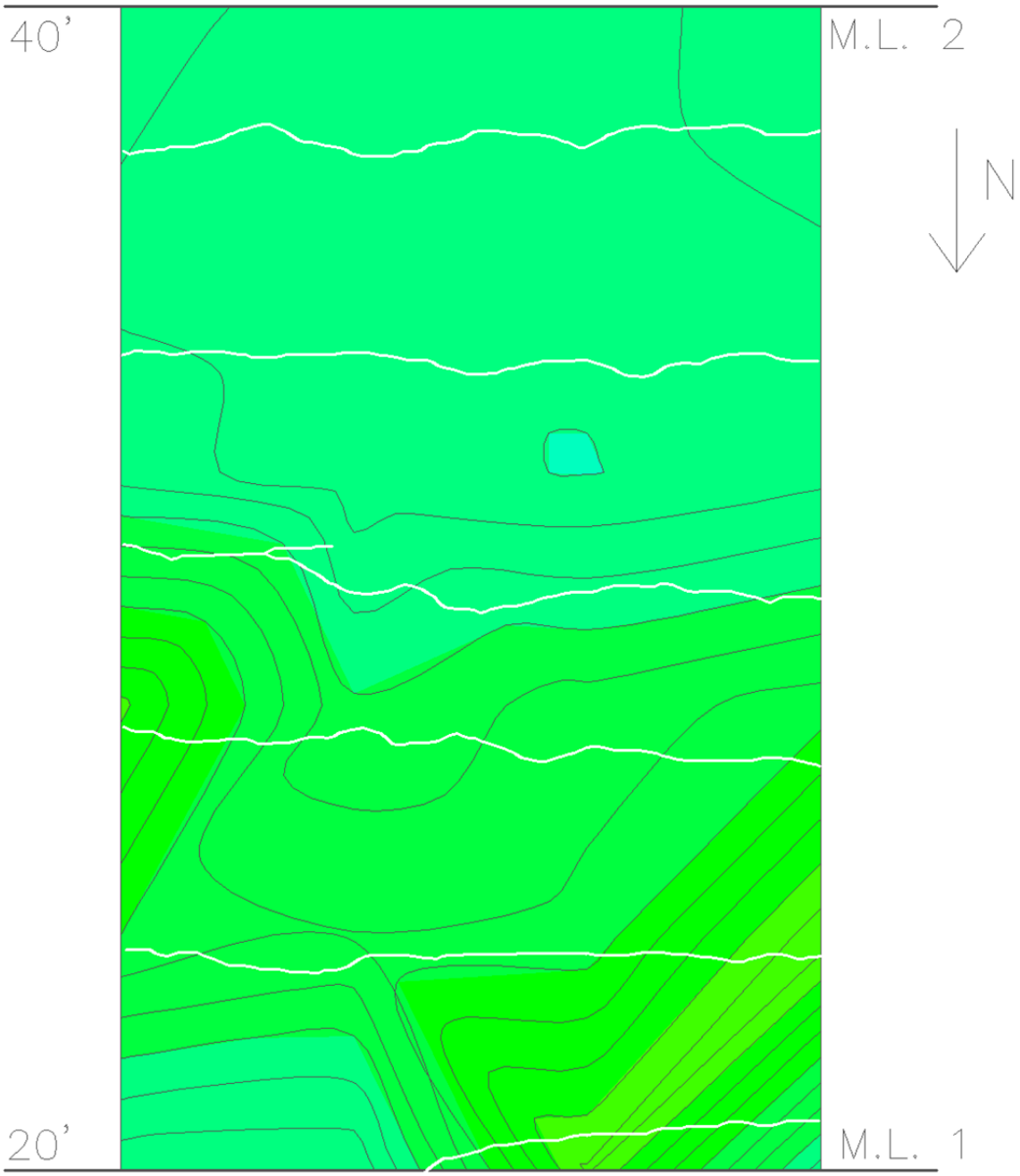

Figure B-70: MRM 168 SB from 20 to 40 feet

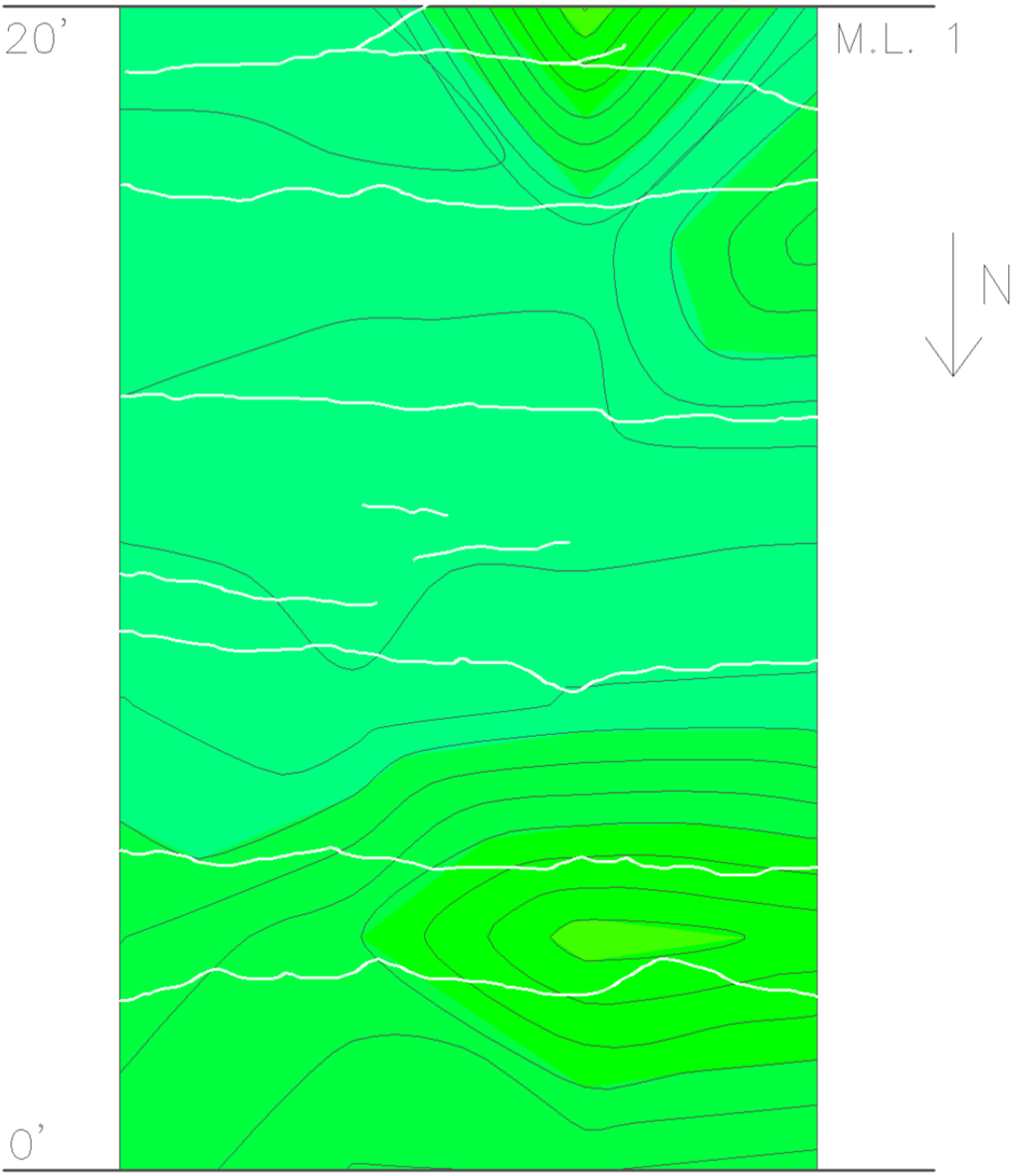

Figure B-71: MRM 168 SB from 0 to 20 feet

APPENDIX C. CHLORIDE PROFILES FOR INITIAL AND STATEWIDE ASSESSMENTS

Vertical chloride profiles

- MRM 87
- MRM 68
- MRM 411
- MRM 33
- MRM 44
- MRM 25
- MRM 54
- MRM 222
- MRM 246
- MRM 168NB
- MRM 168SB

Horizontal chloride profiles

- MRM 87
- MRM 68
- MRM 411

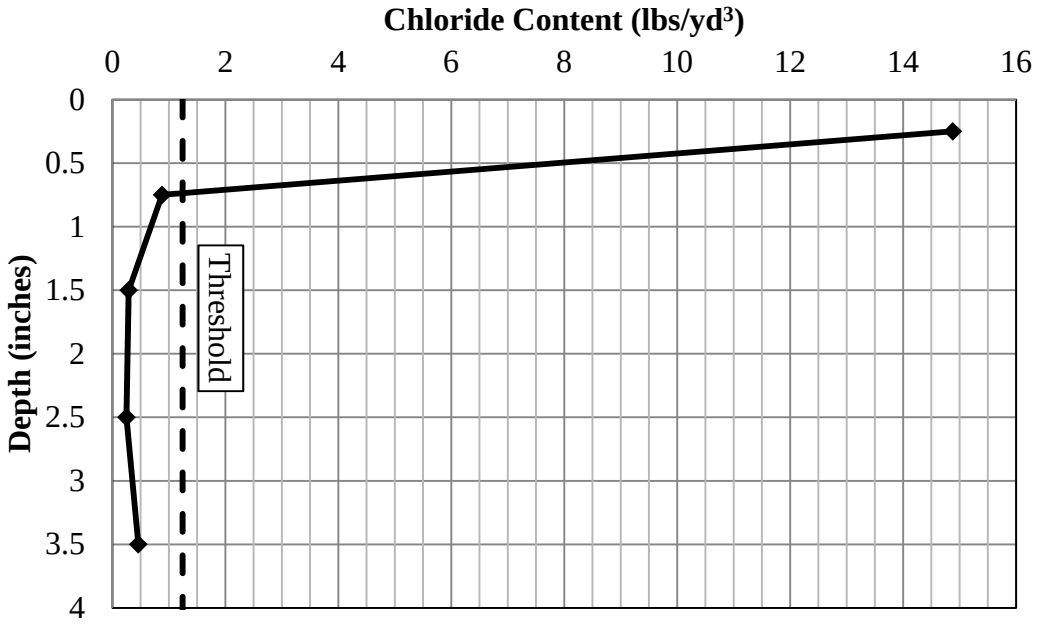

Figure C-1: Vertical chloride profile of dust sample 1 at MRM 87

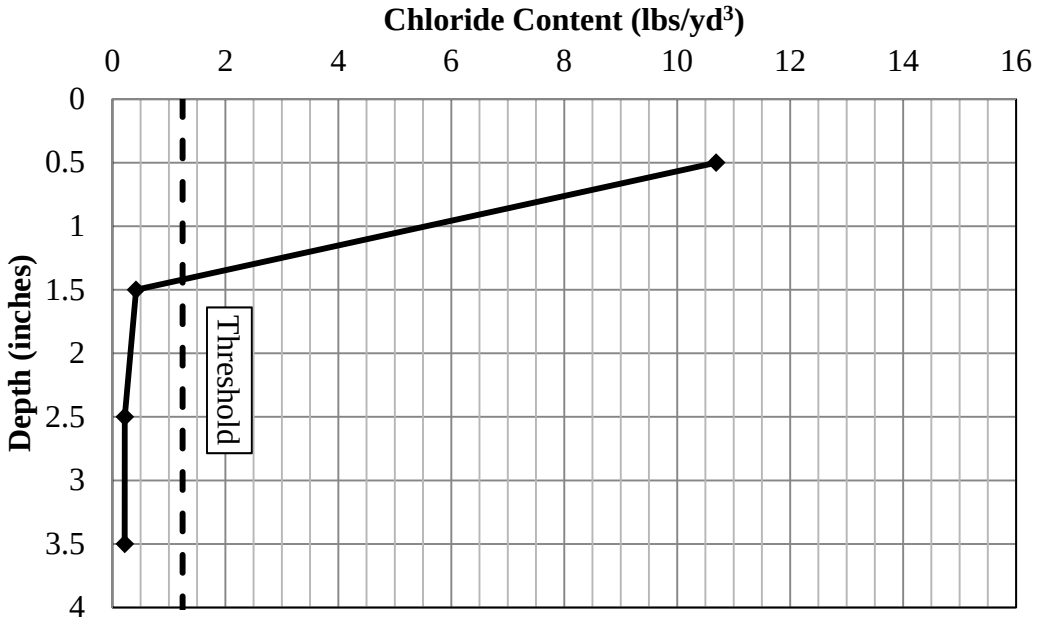

Figure C-2: Vertical chloride profile of dust sample 2 at MRM 87

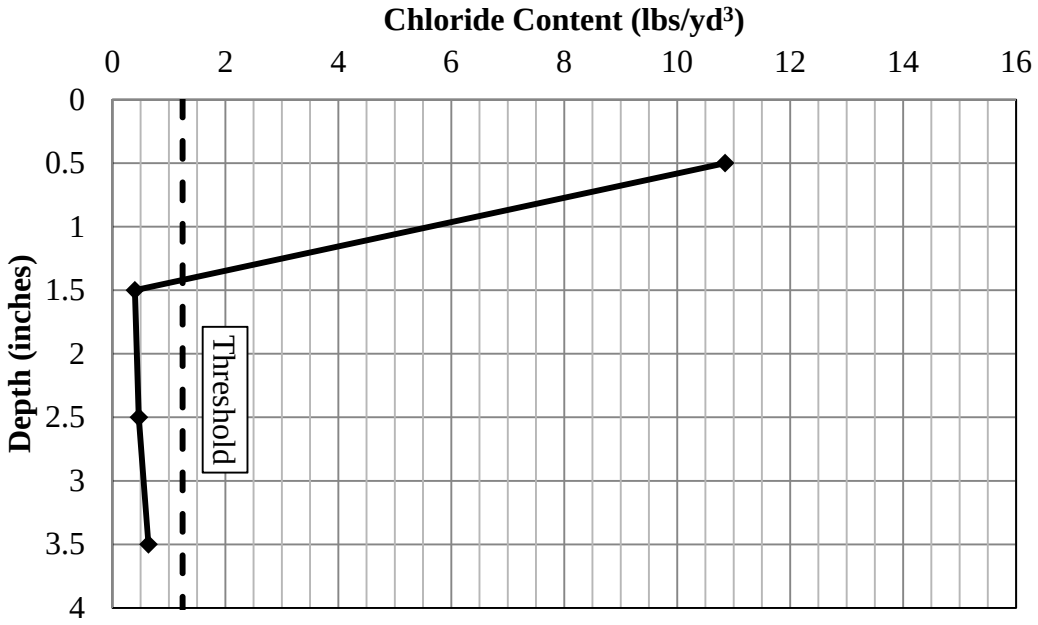

Figure C-3: Vertical chloride profile of dust sample 3 at MRM 87

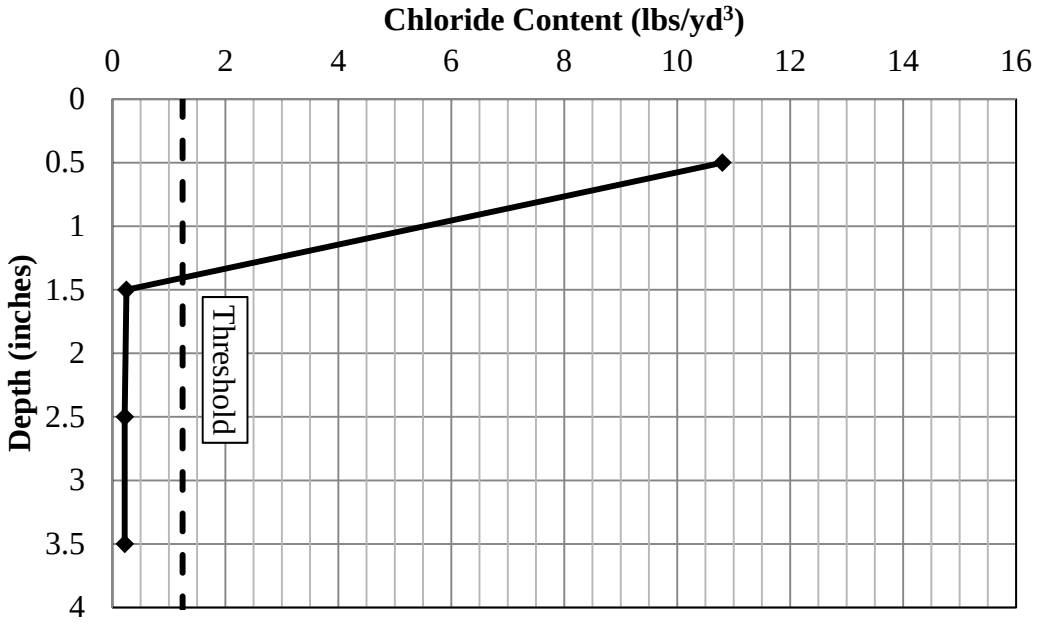

Figure C-4: Vertical chloride profile of dust sample 4 at MRM 87

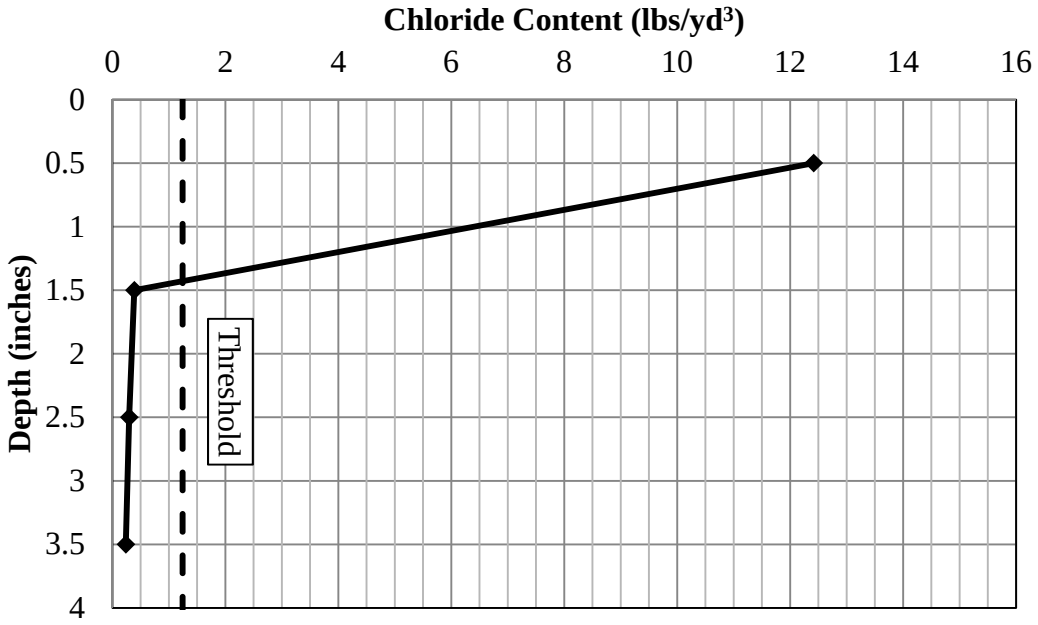

Figure C-5: Vertical chloride profile of dust sample 1 at MRM 68

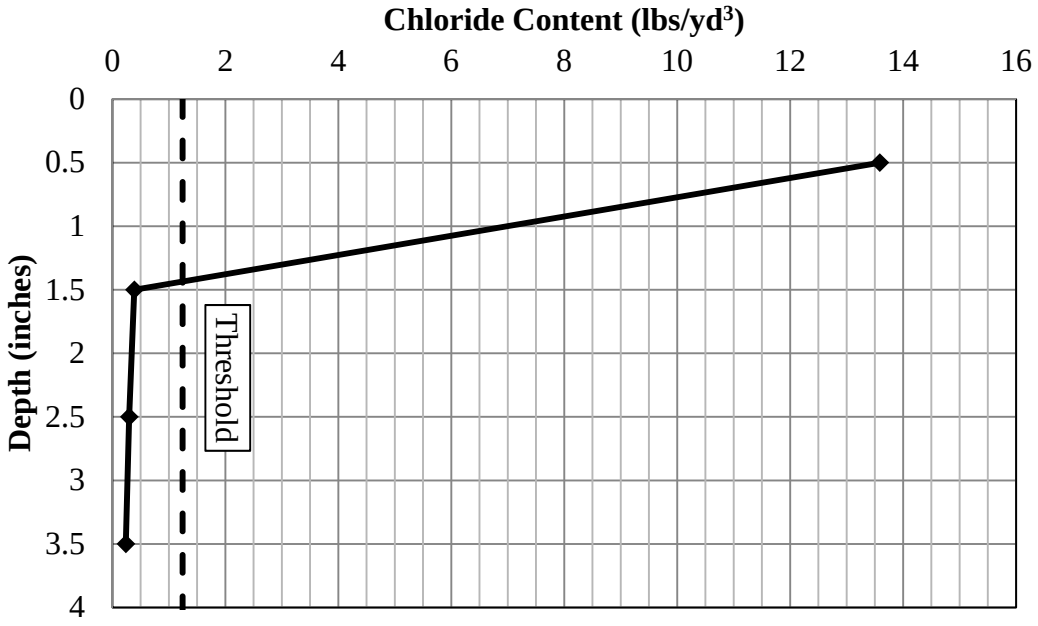

Figure C-6: Vertical chloride profile of dust sample 2 at MRM 68

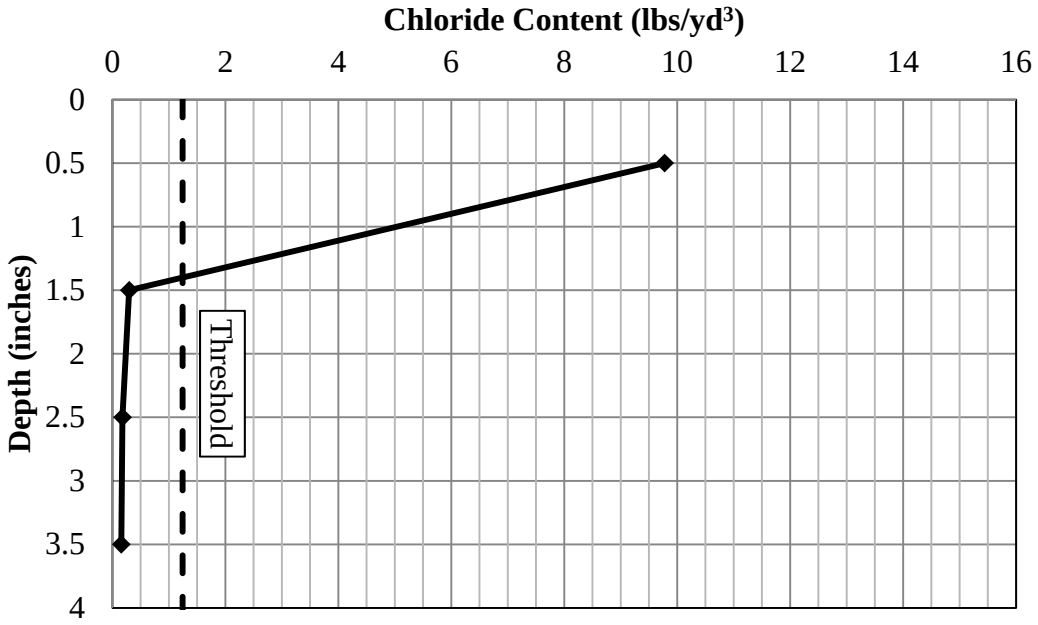

Figure C-7: Vertical chloride profile of dust sample 3 at MRM 68

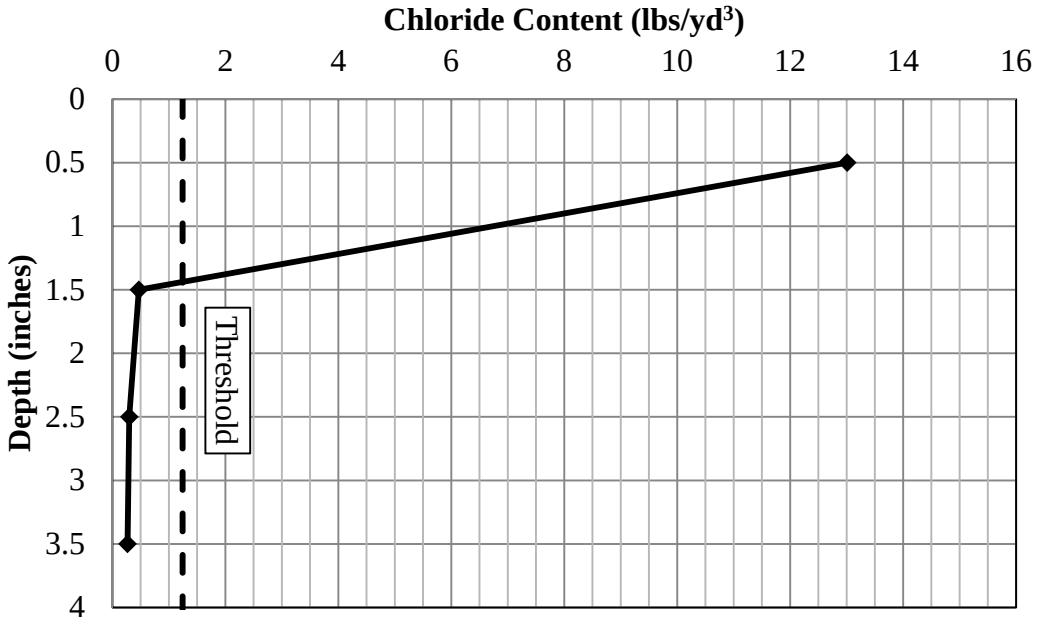

Figure C-8: Vertical chloride profile of dust sample 4 at MRM 68

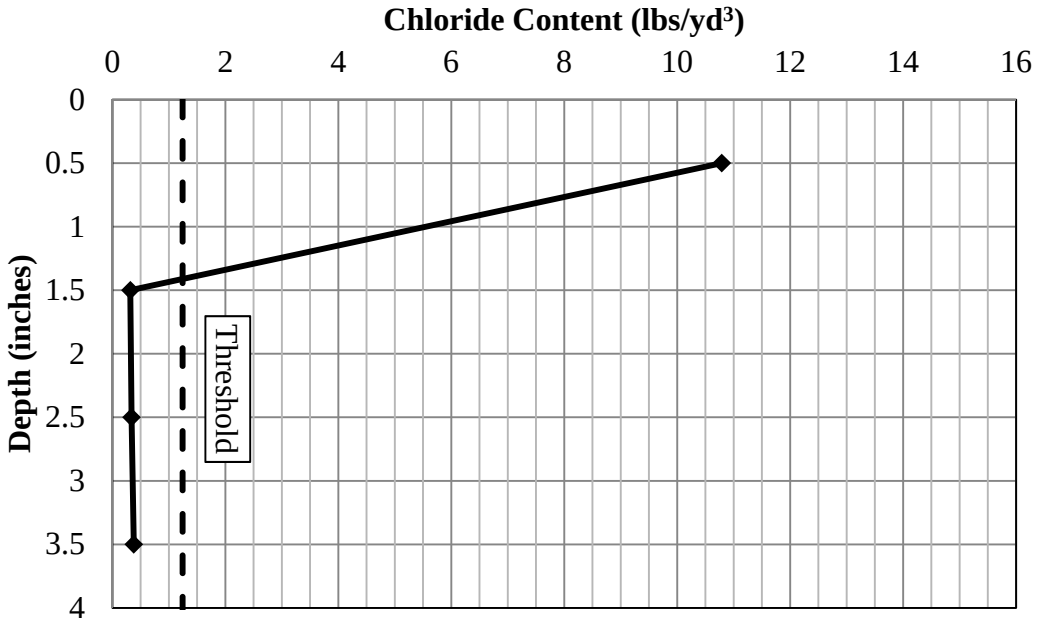

Figure C-9: Vertical chloride profile of dust sample 1 at MRM 411

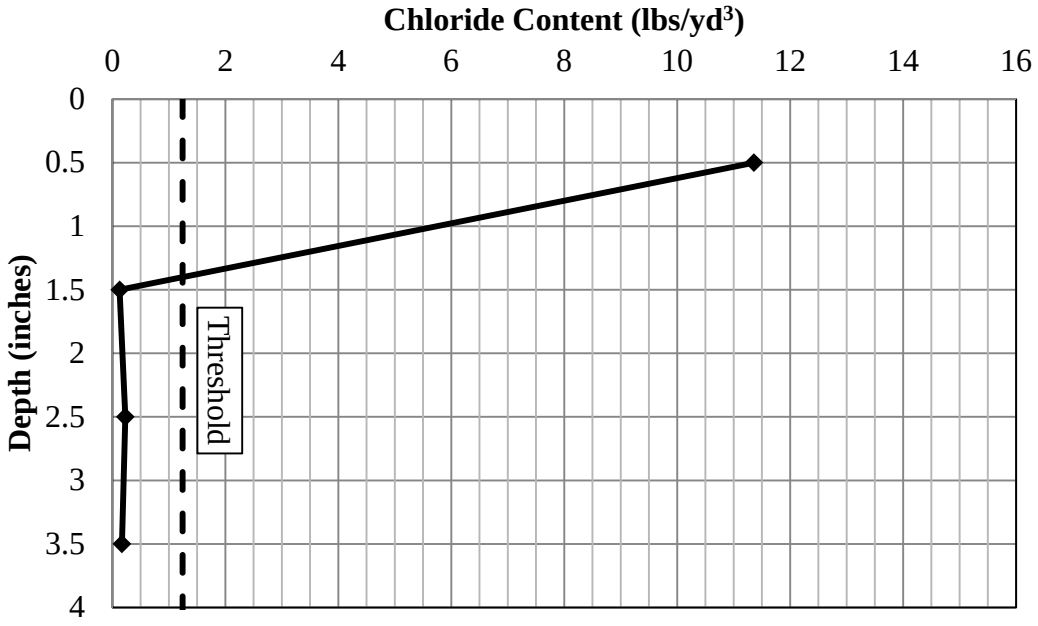

Figure C-10: Vertical chloride profile of dust sample 2 at MRM 411

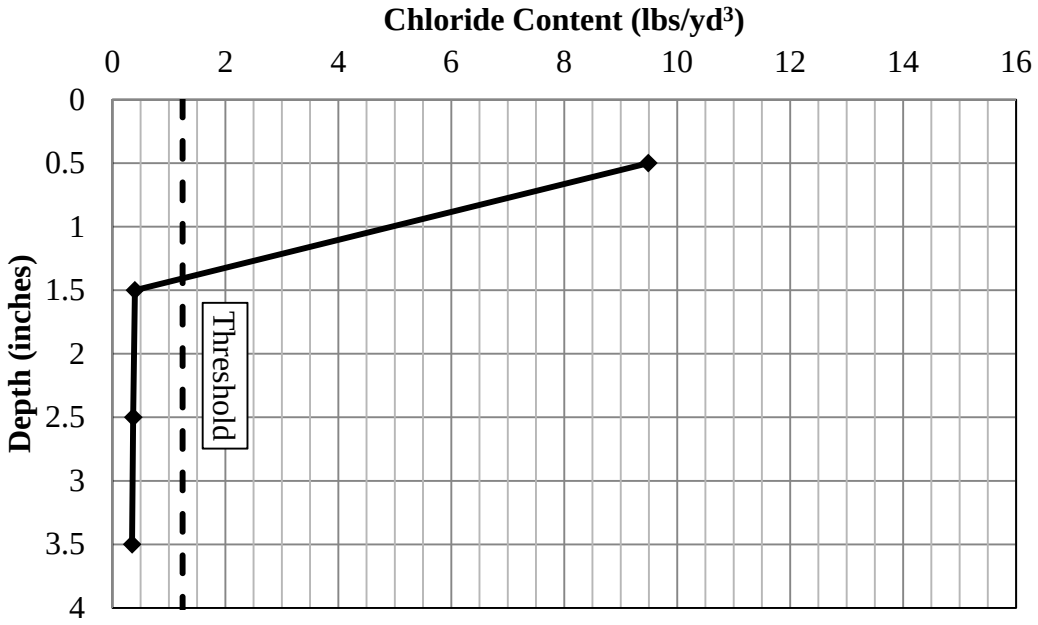

Figure C-11: Vertical chloride profile of dust sample 3 at MRM 411

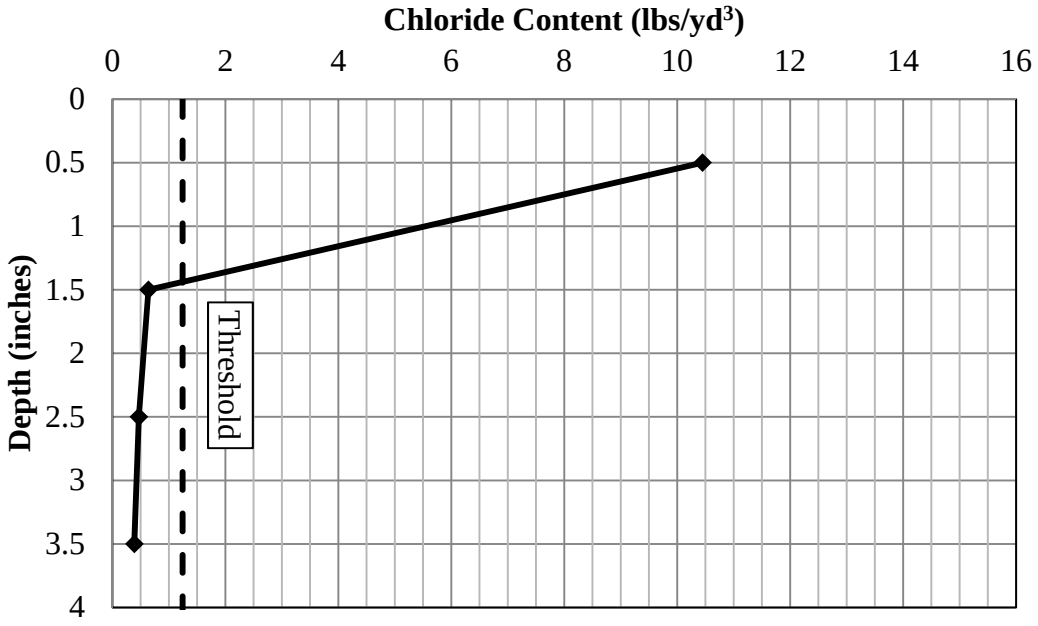

Figure C-12: Vertical chloride profile of dust sample 4 at MRM 411

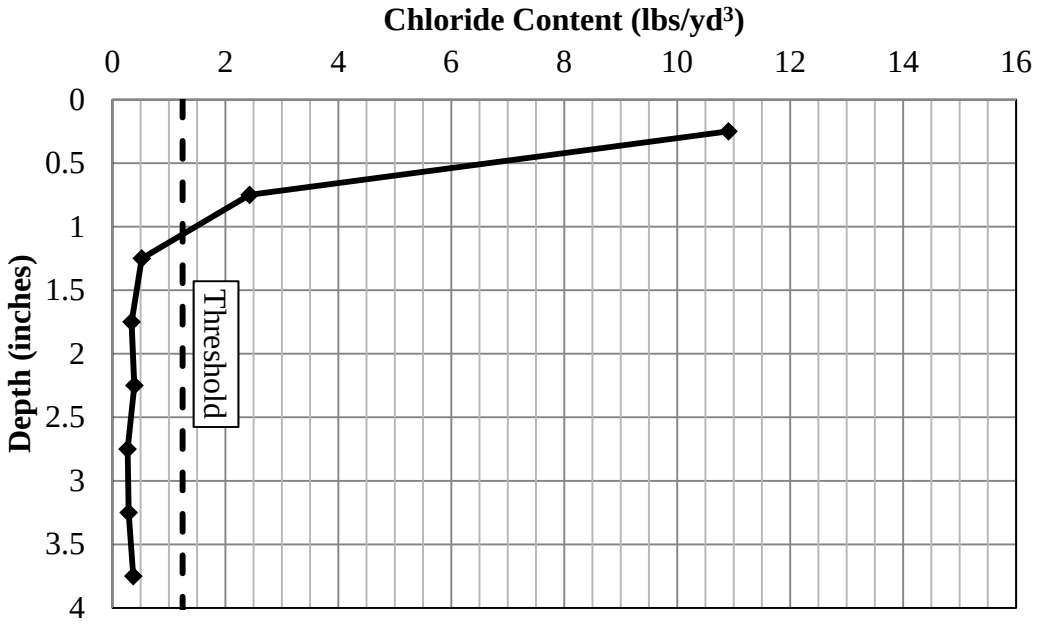

Figure C-13: Vertical chloride profile of dust sample 1 at MRM 33

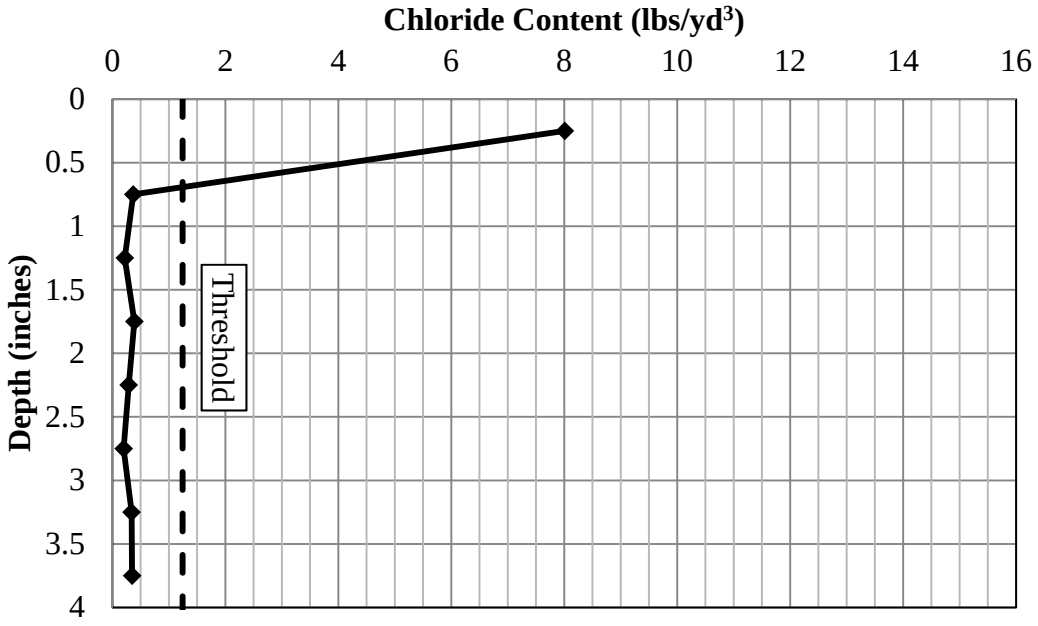

Figure C-14: Vertical chloride profile of dust sample 2 at MRM 33

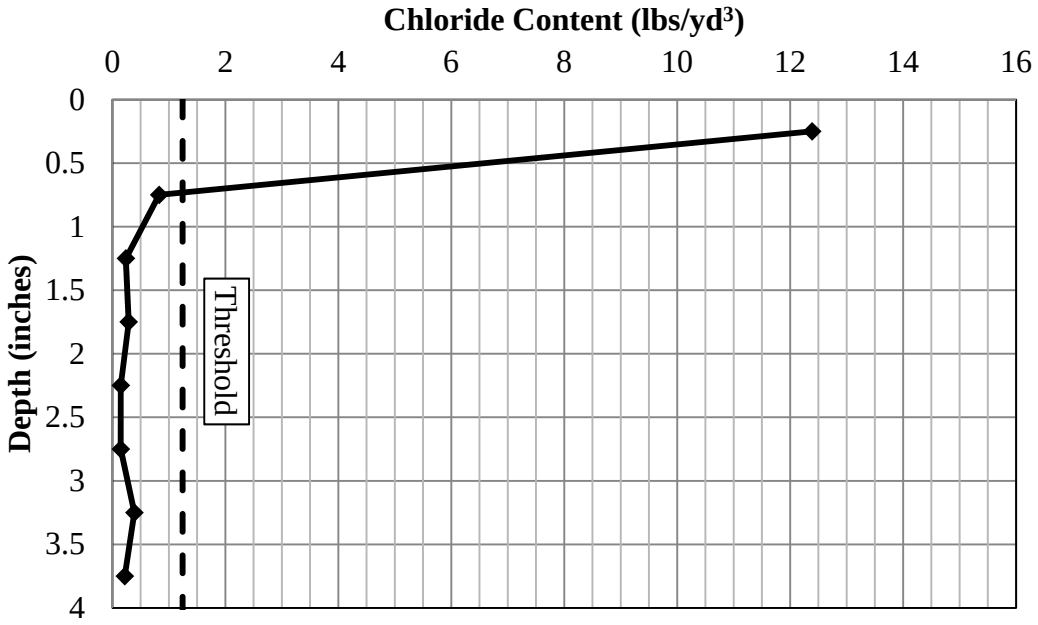

Figure C-15: Vertical chloride profile of dust sample 1 at MRM 44

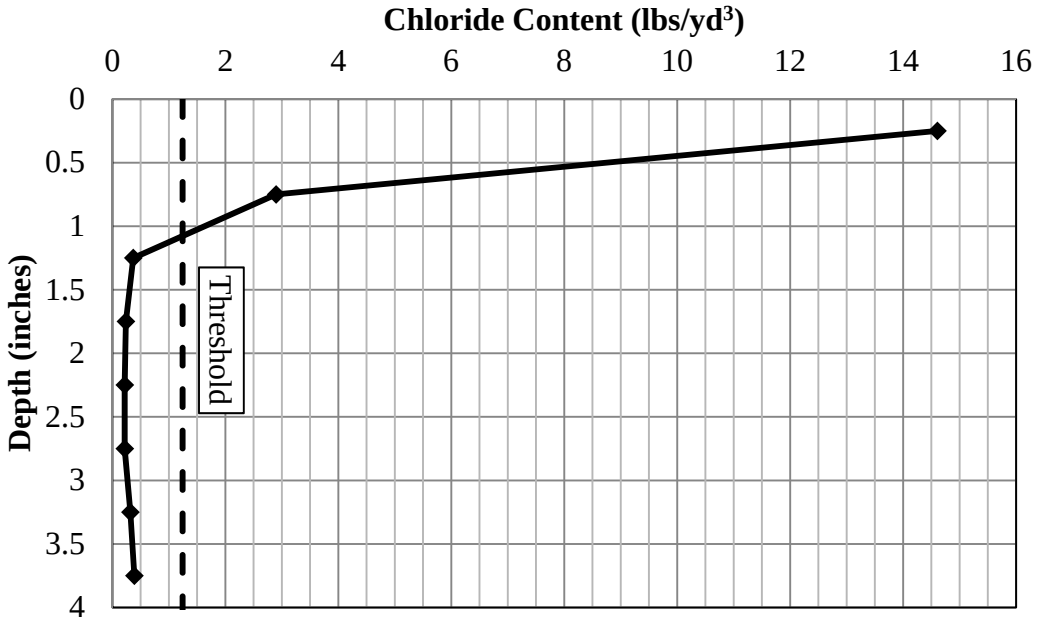

Figure C-16: Vertical chloride profile of dust sample 2 at MRM 44

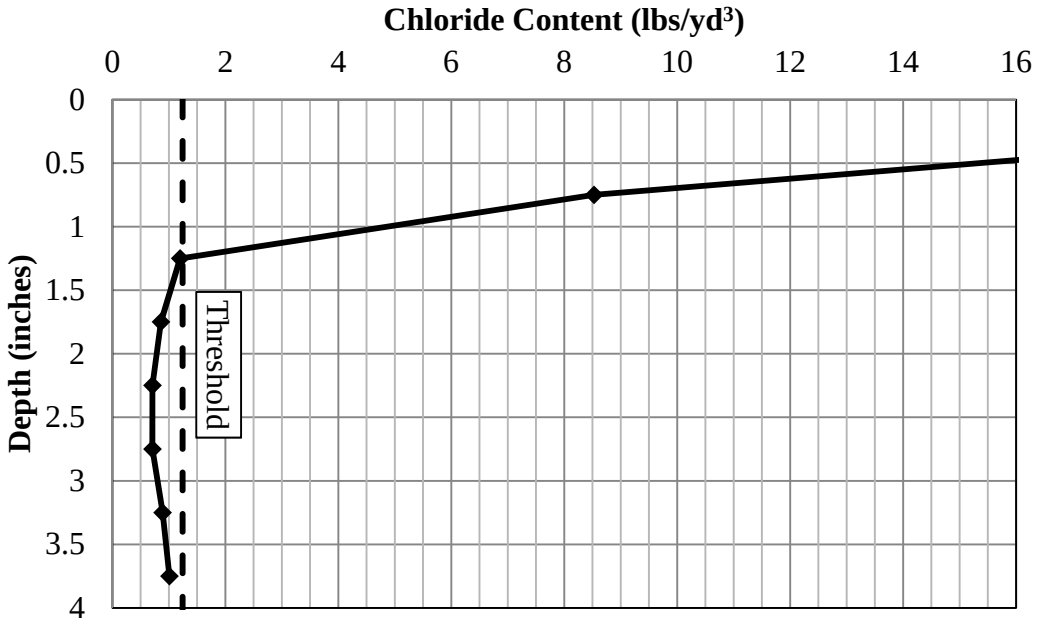

Figure C-17: Vertical chloride profile of dust sample 1 at MRM 25

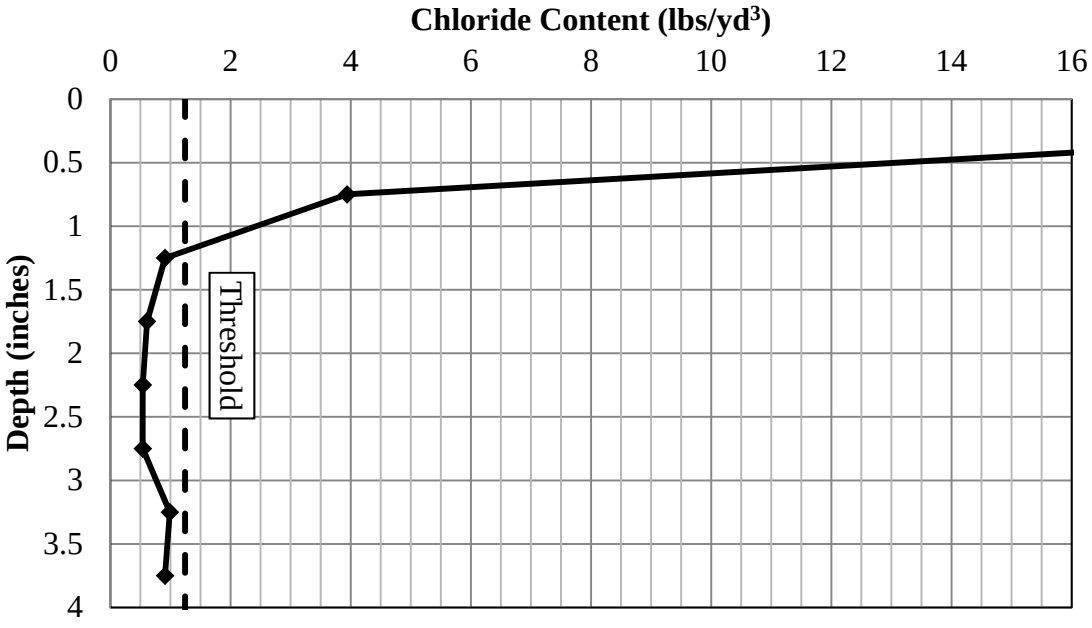

Figure C-18: Vertical chloride profile of dust sample 2 at MRM 25

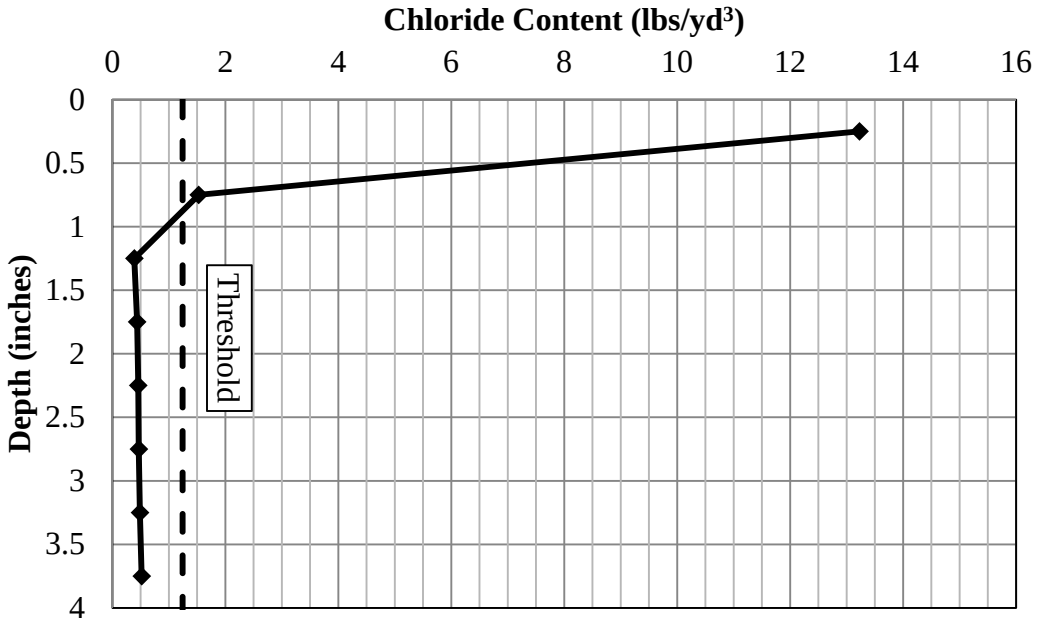

Figure C-19: Vertical chloride profile of dust sample 1 at MRM 54

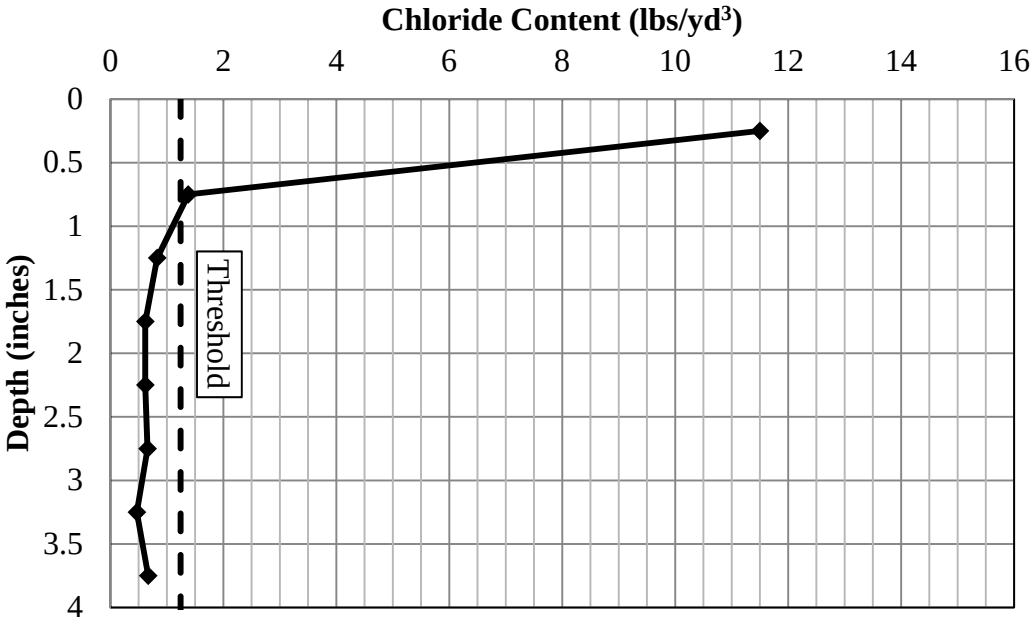

Figure C-20: Vertical chloride profile of dust sample 2 at MRM 54

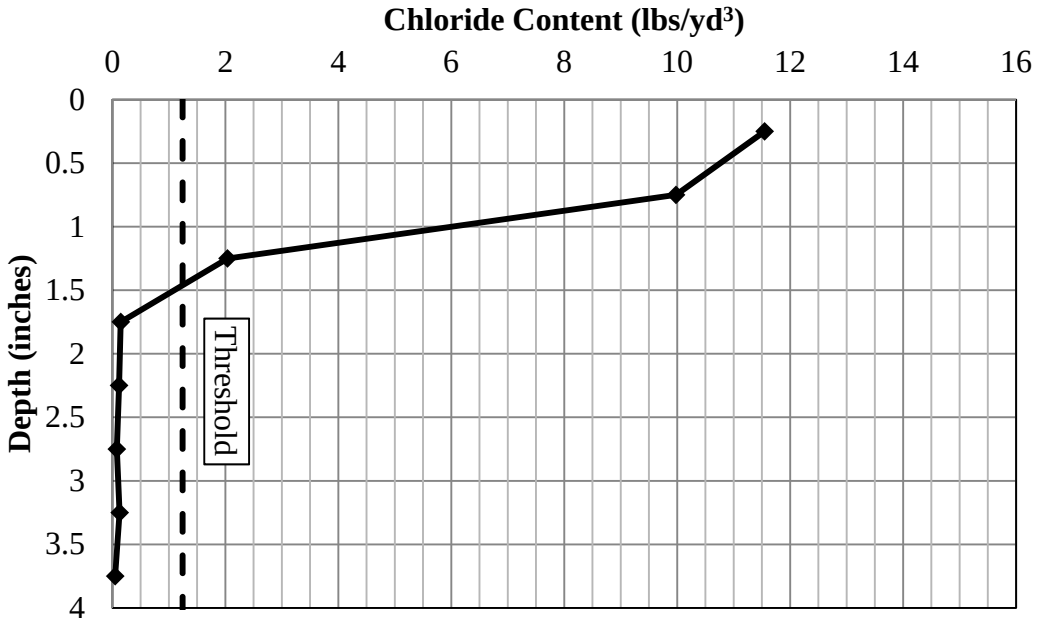

Figure C-21: Vertical chloride profile of dust sample 1 at MRM 222

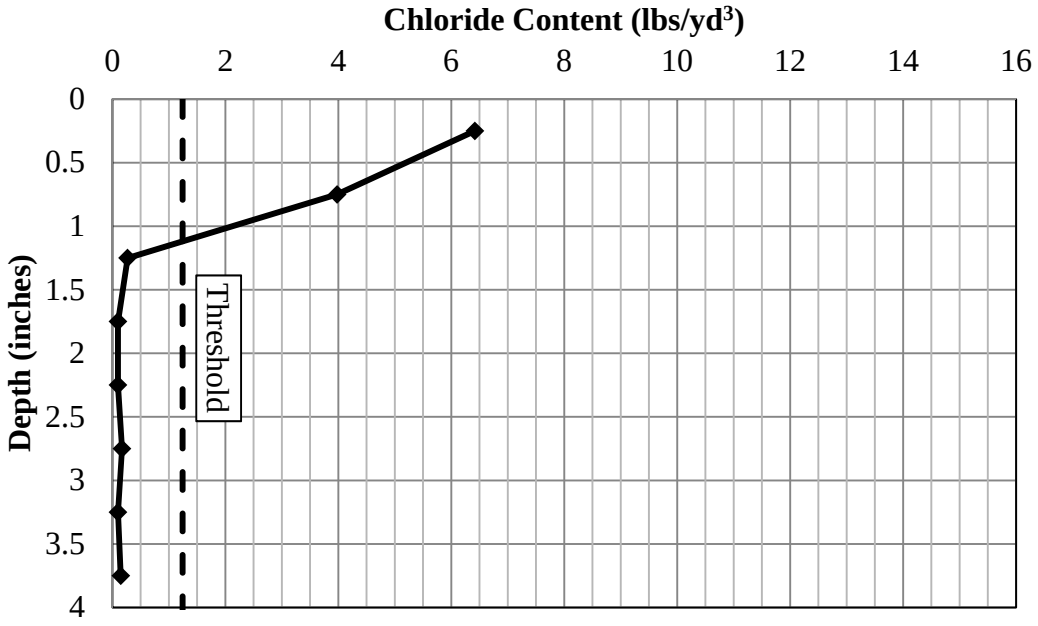

Figure C-22: Vertical chloride profile of dust sample 2 at MRM 222

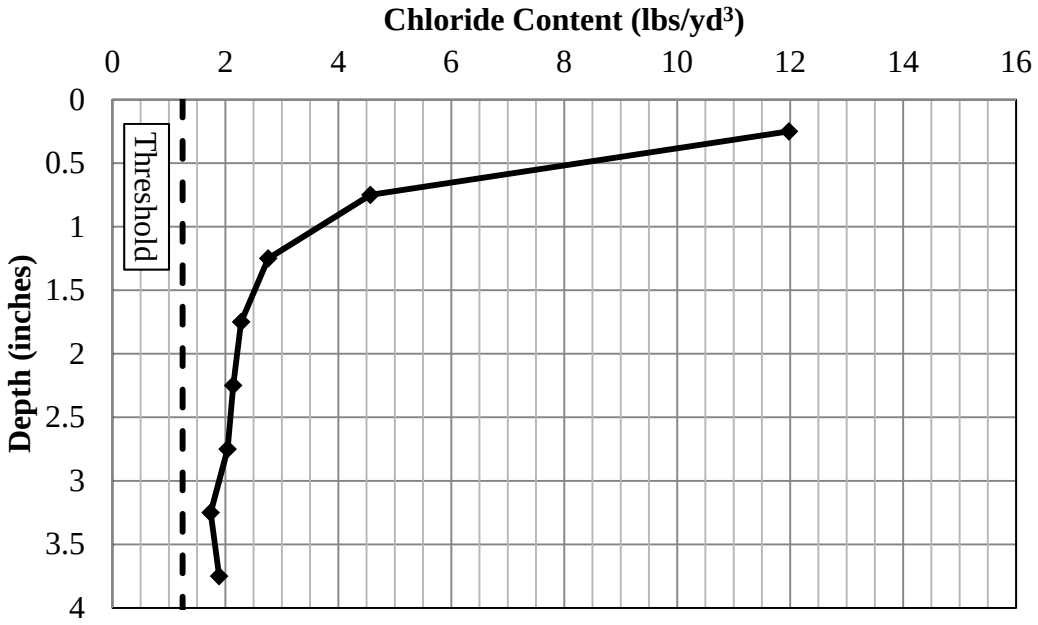

Figure C-23: Vertical chloride profile of dust sample 1 at MRM 246

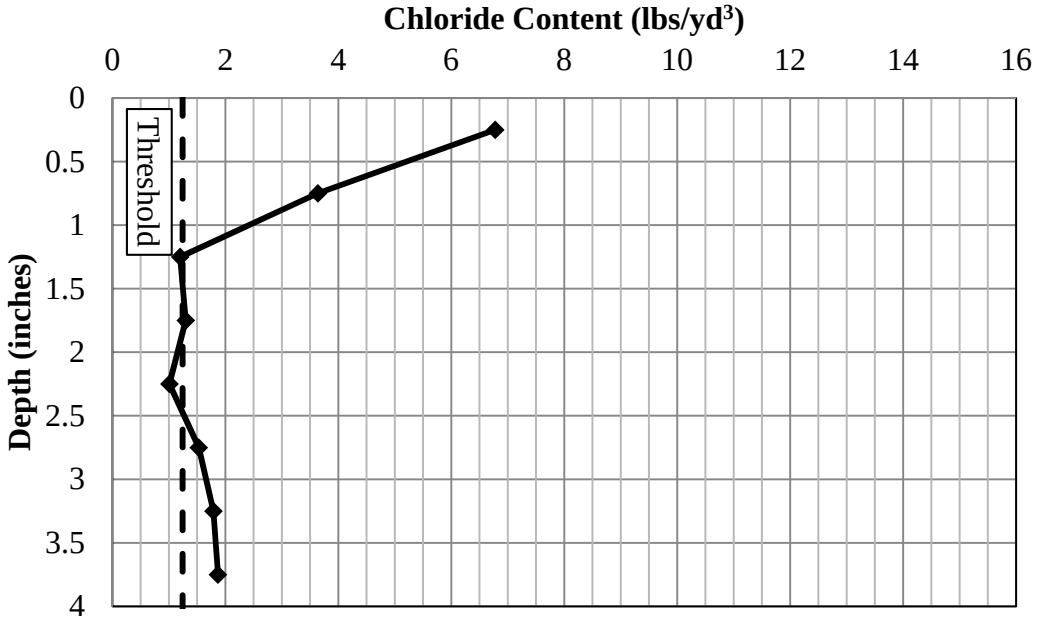

Figure C-24: Vertical chloride profile of dust sample 2 at MRM 246

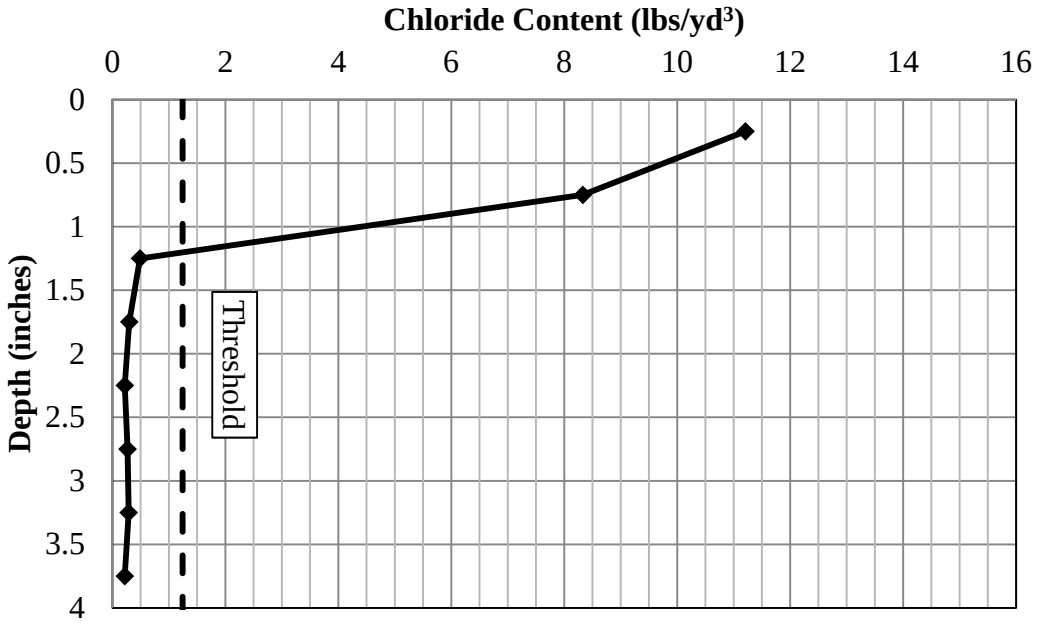

Figure C-25: Vertical chloride profile of dust sample 1 at MRM 168 NB

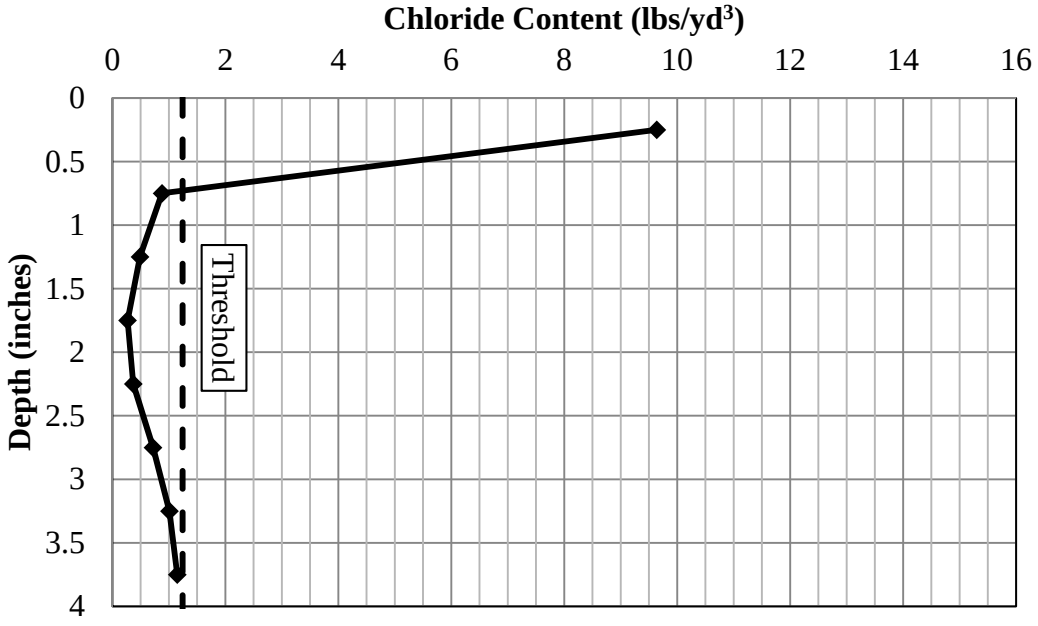

Figure C-26: Vertical chloride profile of dust sample 2 at MRM 168 NB

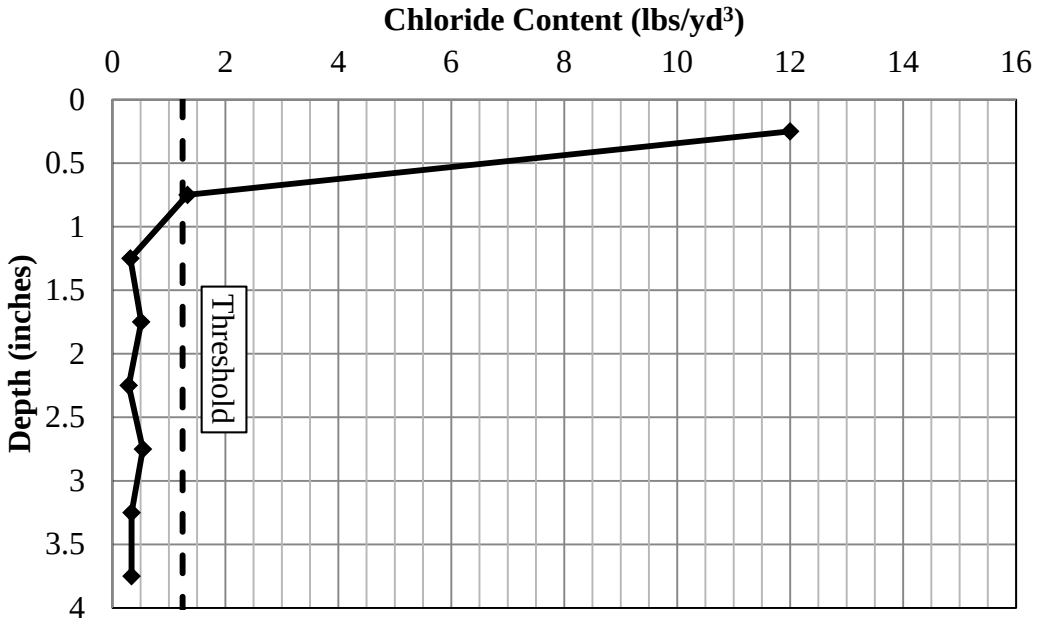

Figure C-27: Vertical chloride profile of dust sample 1 at MRM 168SB

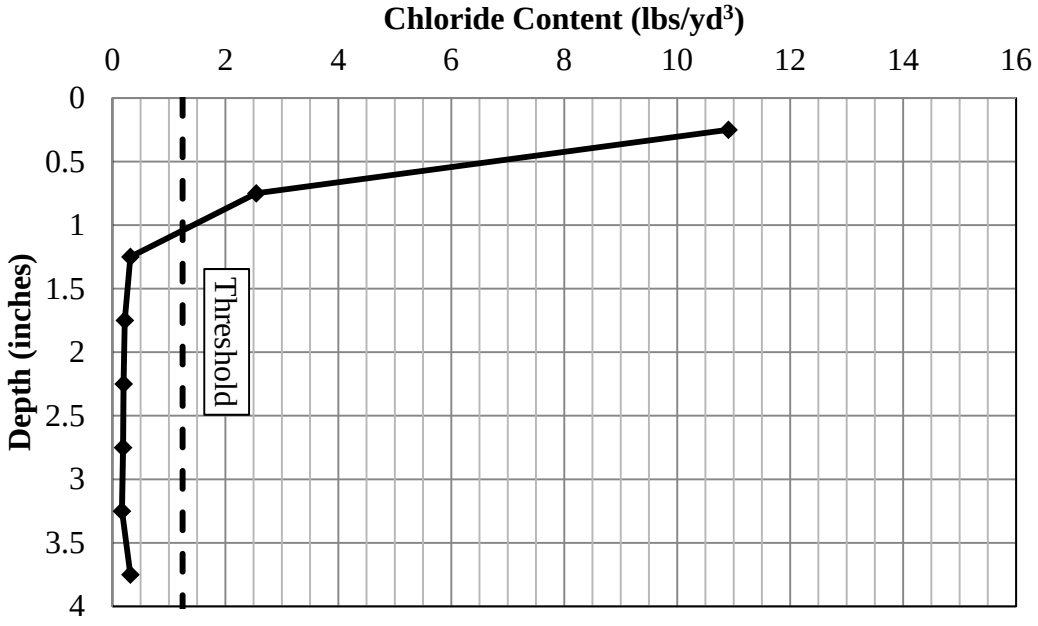

Figure C-28: Vertical chloride profile of dust sample 2 at MRM 168SB

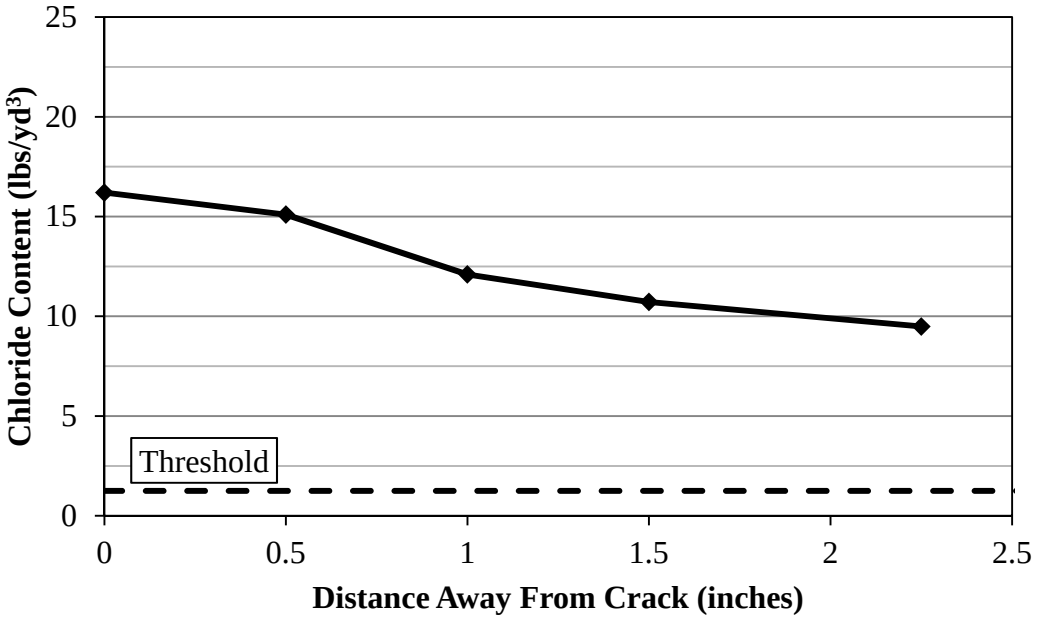

Figure C-29: Horizontal chloride profile of core MRM 87-3 at depth 0.5 inches

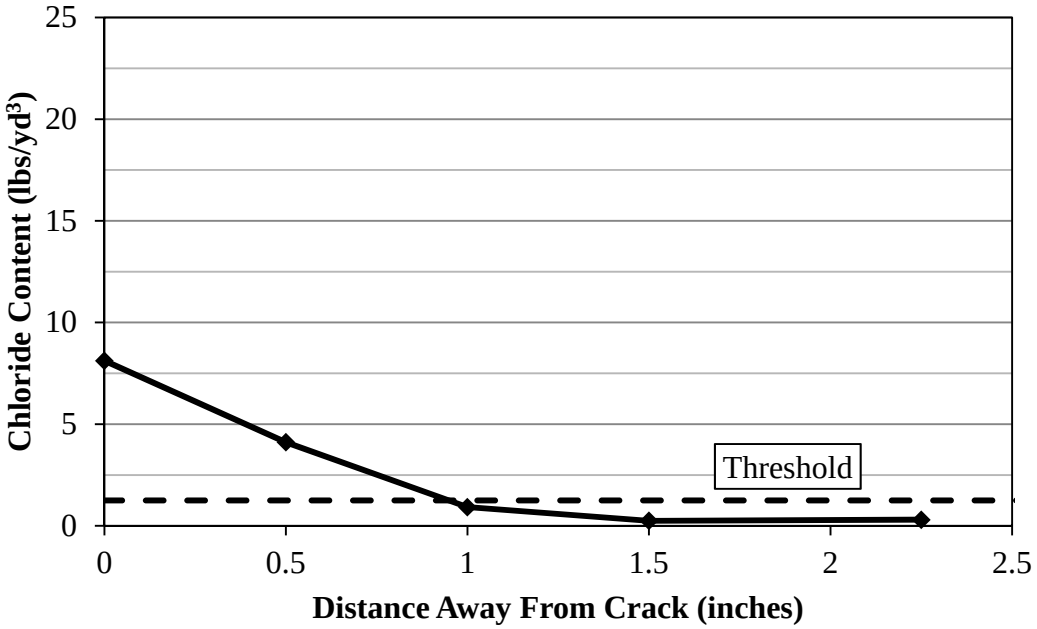

Figure C-30: Horizontal chloride profile of core MRM 87-3 at depth 1.5 inches

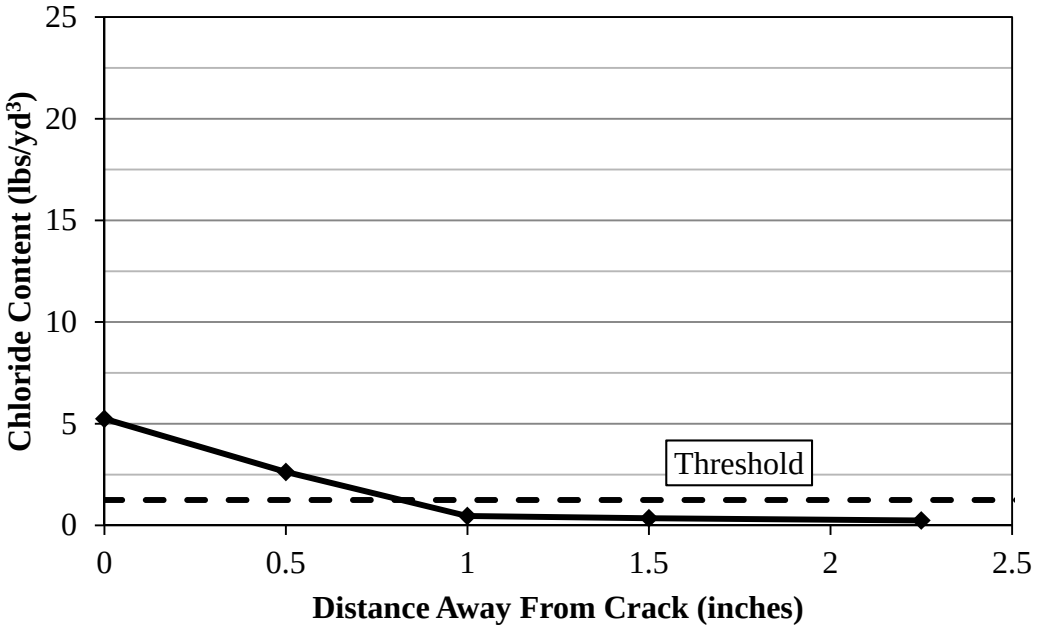

Figure C-31: Horizontal chloride profile of core MRM 87-3 at depth 2.5 inches

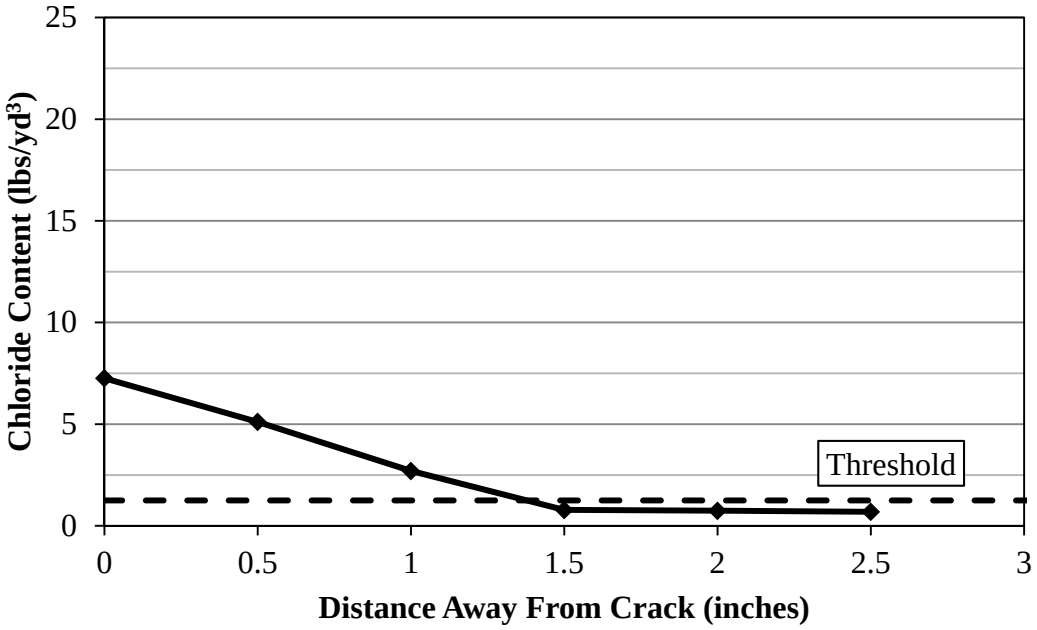

Figure C-32: Horizontal chloride profile of core MRM 87-3 at depth 3.5 inches

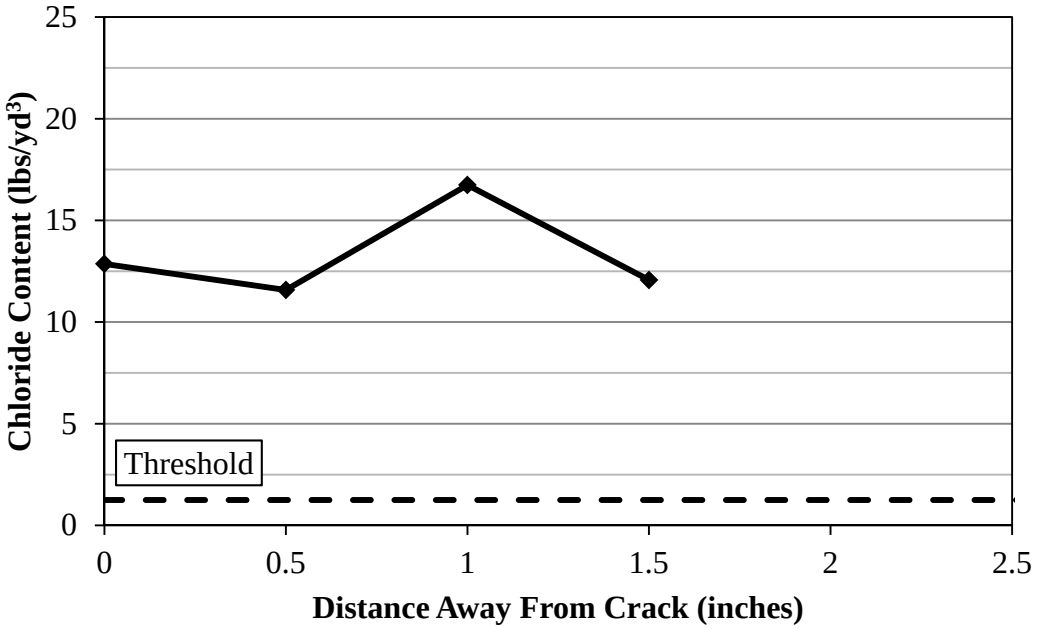

Figure C-33: Horizontal chloride profile of core MRM 68-3 at depth 0.5 inches

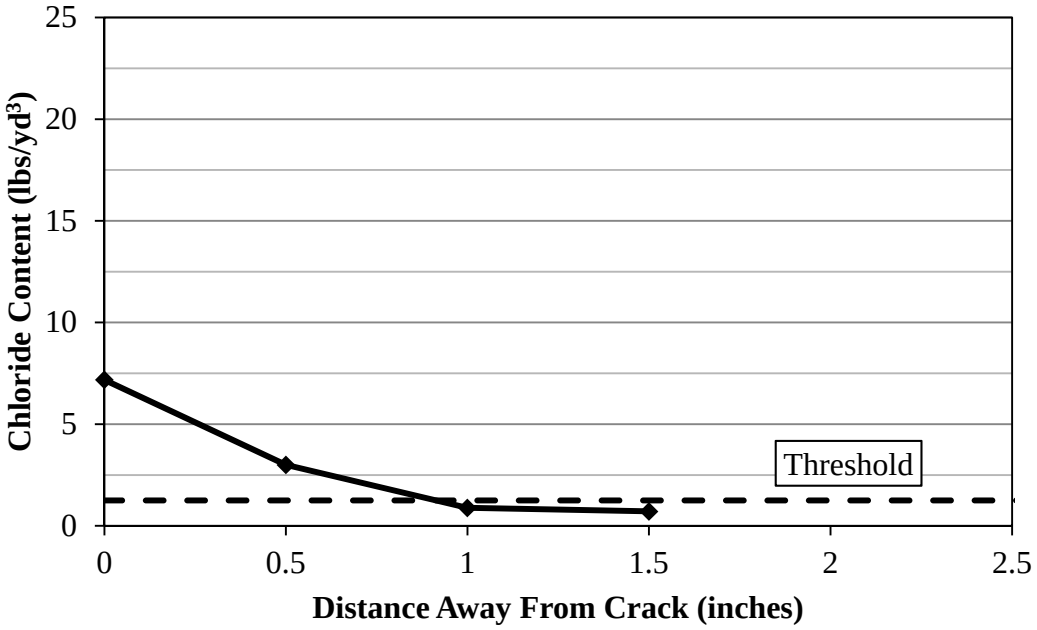

Figure C-34: Horizontal chloride profile of core MRM 68-3 at depth 1.5 inches

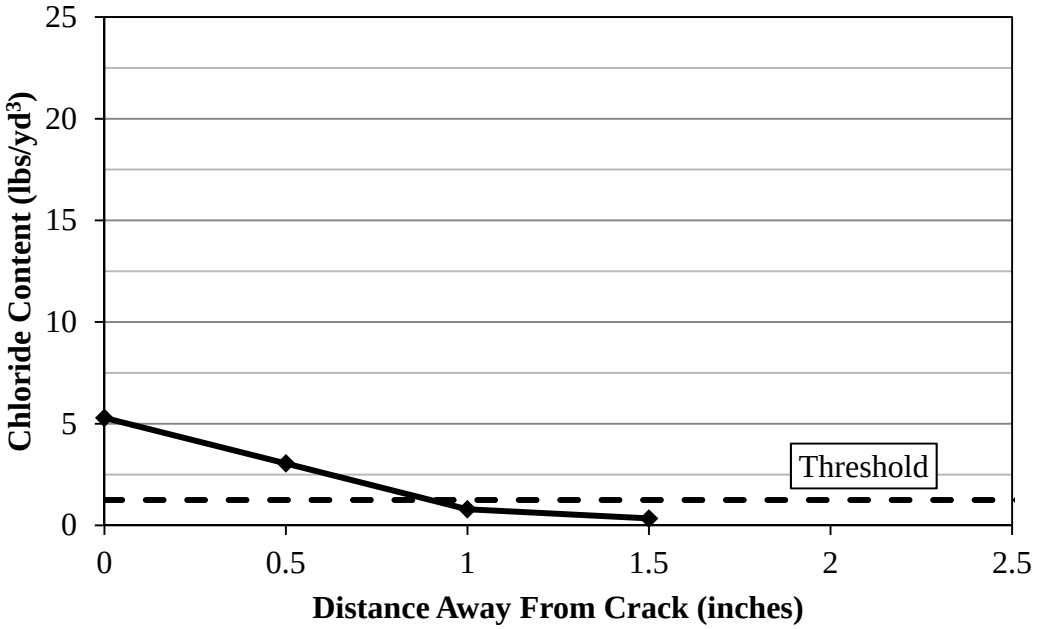

Figure C-35: Horizontal chloride profile of core MRM 68-3 at depth 2.5 inches

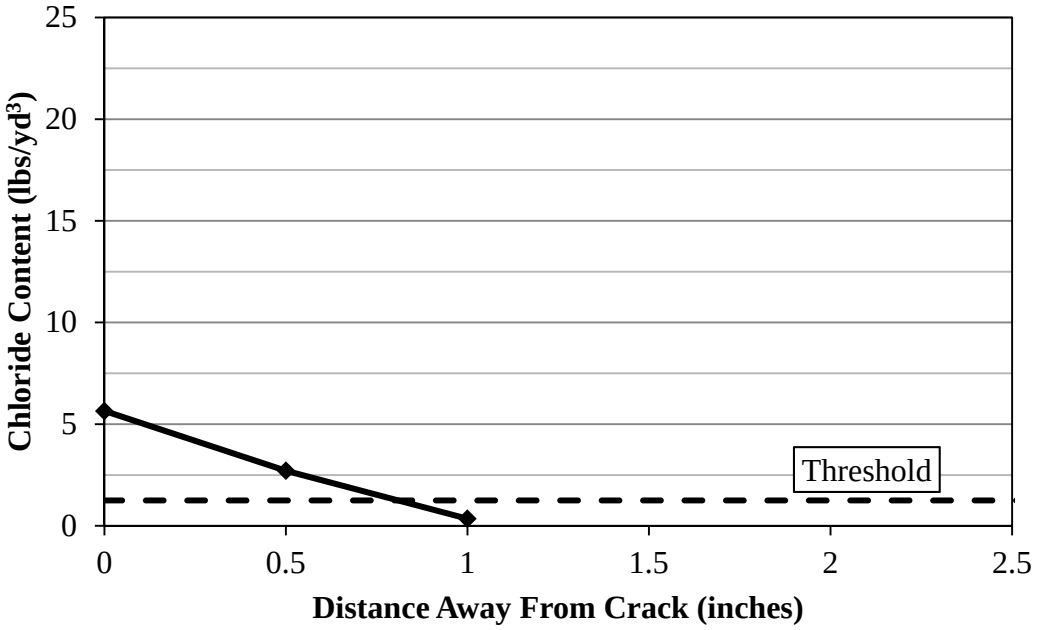

Figure C-36: Horizontal chloride profile of core MRM 68-3 at depth 3.5 inches

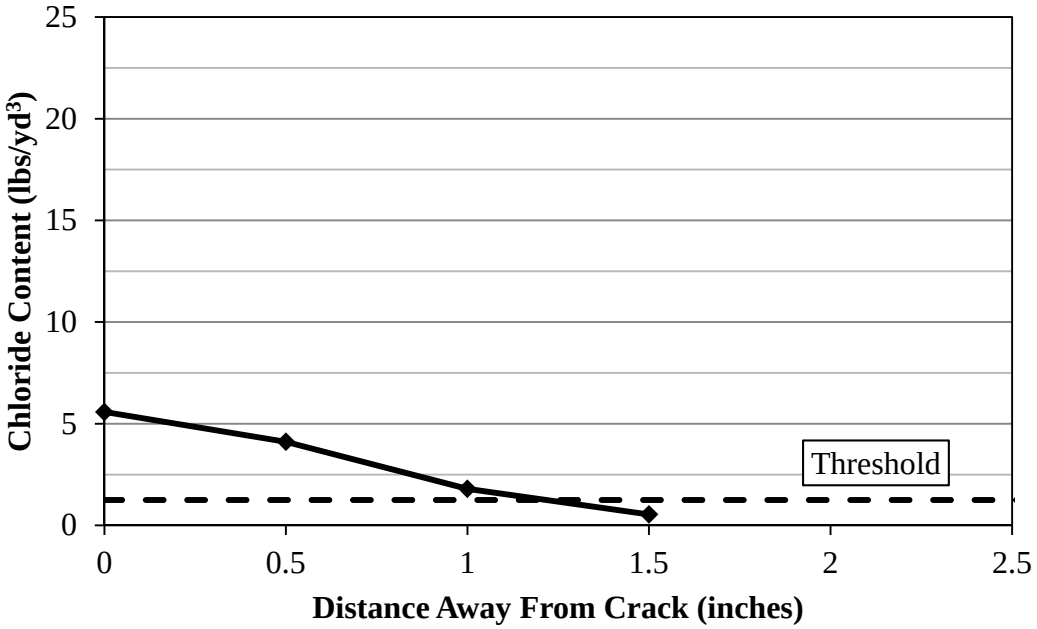

Figure C-37: Horizontal chloride profile of core MRM 68-3 at depth 4.5 inches

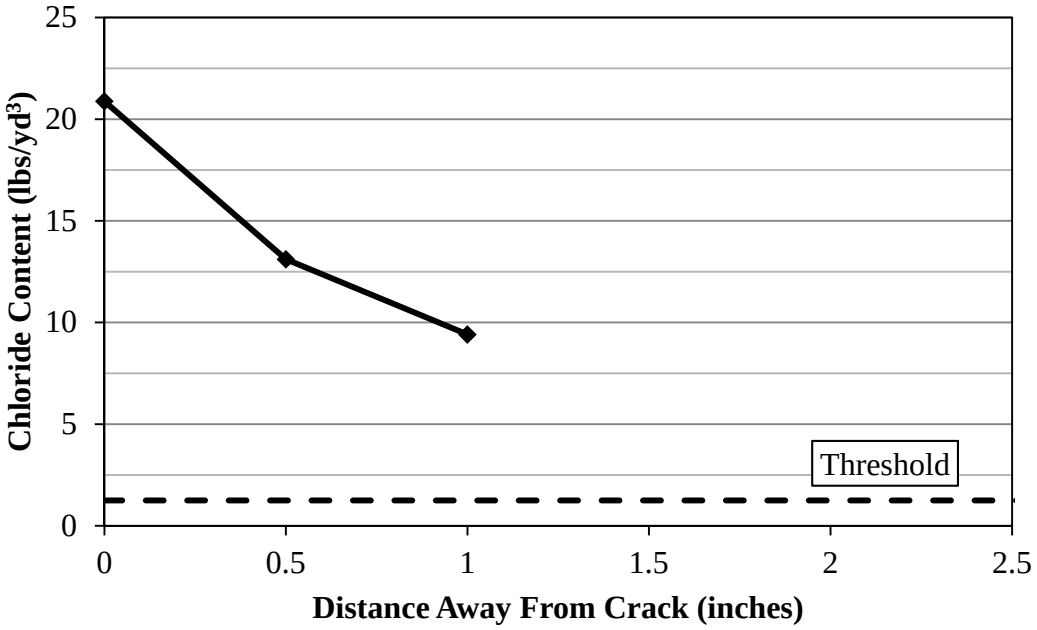

Figure C-38: Horizontal chloride profile of core MRM 411-1 at depth 0.5 inches

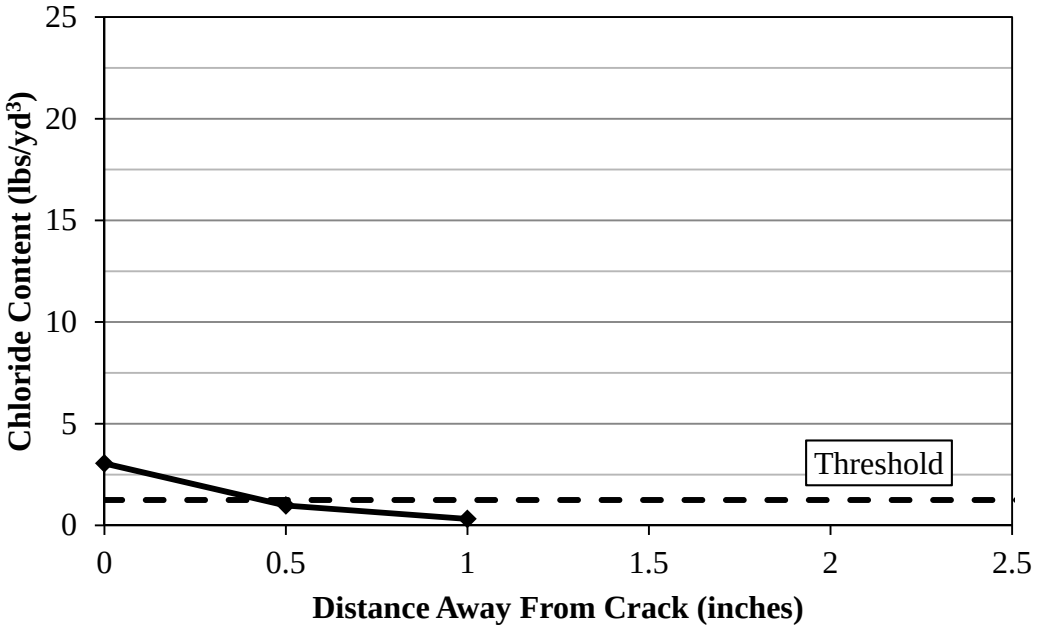

Figure C-39: Horizontal chloride profile of core MRM 411-1 at depth 1.5 inches

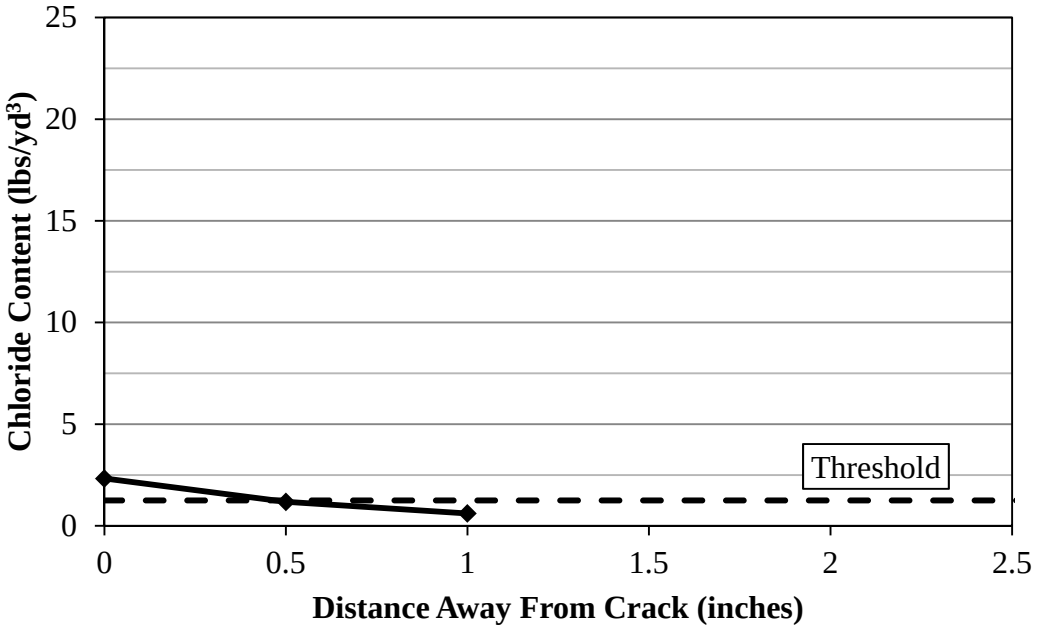

Figure C-40: Horizontal chloride profile of core MRM 411-1 at depth 2.5 inches

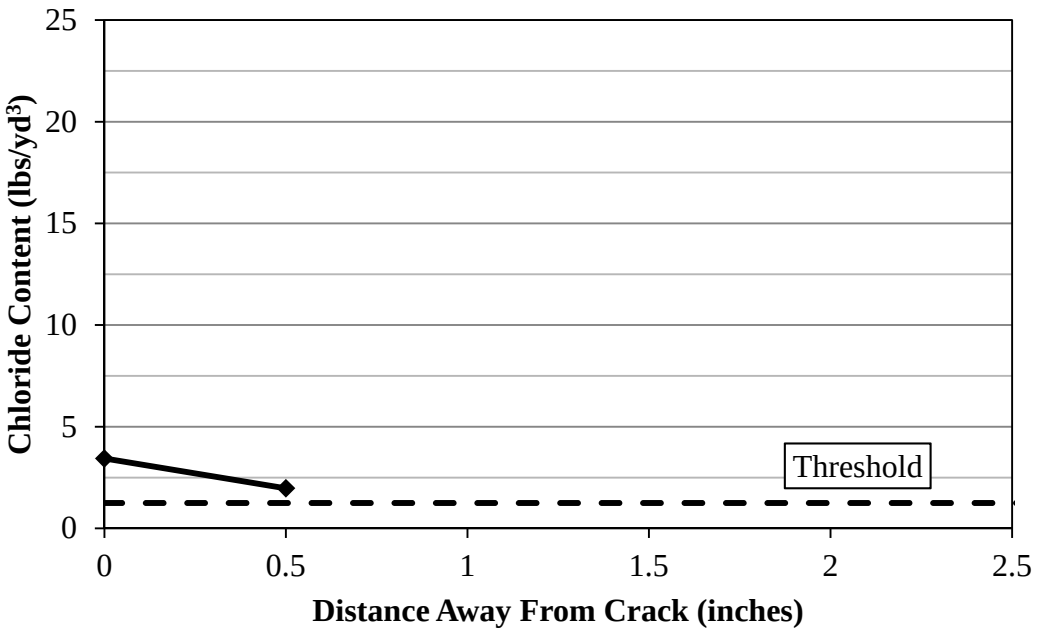

Figure C-41: Horizontal chloride profile of core MRM 411-1 at depth 3.5 inches

APPENDIX D. PAVEMENT DISTRESS DEFINITIONS

The definitions presented in this appendix were obtained from the Distress Identification Manual for the Long-Term Pavement Performance Program.

Longitudinal Cracking: Cracks that are predominately parallel to the pavement centerline.

Transverse Cracking: Cracks that are predominantly perpendicular to the pavement centerline.

Polished Aggregate: Surface mortar and texturing worn away to expose coarse aggregate.

Popouts: Small pieces of pavement broken loose from the surface, normally ranging in diameter from 25 mm to 100 mm and depth from 13 mm to 50 mm.

Patch/Patch Deterioration: A portion, greater than 0.1 m^2, or all of the original concrete slab that has been removed and replaced, or additional material applied to the pavement after original construction.

Punchouts: The area enclosed by two closely spaced (usually < 0.6 m) transverse cracks, a short longitudinal crack, and the edge of the pavement or a longitudinal joint. Also includes "Y" cracks that exhibit spalling, breakup, or faulting.

Spalling of Longitudinal Joints: Cracking, breaking, chipping, or fraying of slab edges within 0.3 m from the face of the longitudinal joint.

APPENDIX E. EQUIPOTENTIAL CONTOUR MAPS FOR MITIGATION PRODUCT ASSESSMENT

The grid shown on the equipotential contour maps (Figure E-2 through Figure E-65) is 4 feet by 4 feet. However, the half-cell potential measurements were obtained on a 2 feet by 2 feet grid.

Figure E-2 through Figure E-36 show contour maps of the half-cell potential measurements at the date indicated.

Figure E-38 through Figure E-65 show contour maps of the differences between half-cell measurements at the dates indicated.

Section A – MCI-2018

Section B – Protectosil CIT and Ferrogard 903

Section C – Protectosil CIT

Section D – Ferrogard 903

Section E – Duralprep 3020

Section F – Chemtrete 40

Section G – Control

Minimum Reading (mV)	Maximum Reading (mV)	Color
−750.00	−720.00	
−720.00	−690.00	
−690.00	−660.00	
−660.00	−630.00	
−630.00	−600.00	
−600.00	−570.00	
−570.00	−540.00	
−540.00	−510.00	
−510.00	−480.00	
−480.00	−450.00	
−450.00	−420.00	
−420.00	−390.00	
−390.00	−360.00	
−360.00	−330.00	
−330.00	−300.00	
−300.00	−270.00	
−270.00	−240.00	
−240.00	−210.00	
−210.00	−180.00	
−180.00	−150.00	

Figure E-1: Legend for half-cell potential contour maps

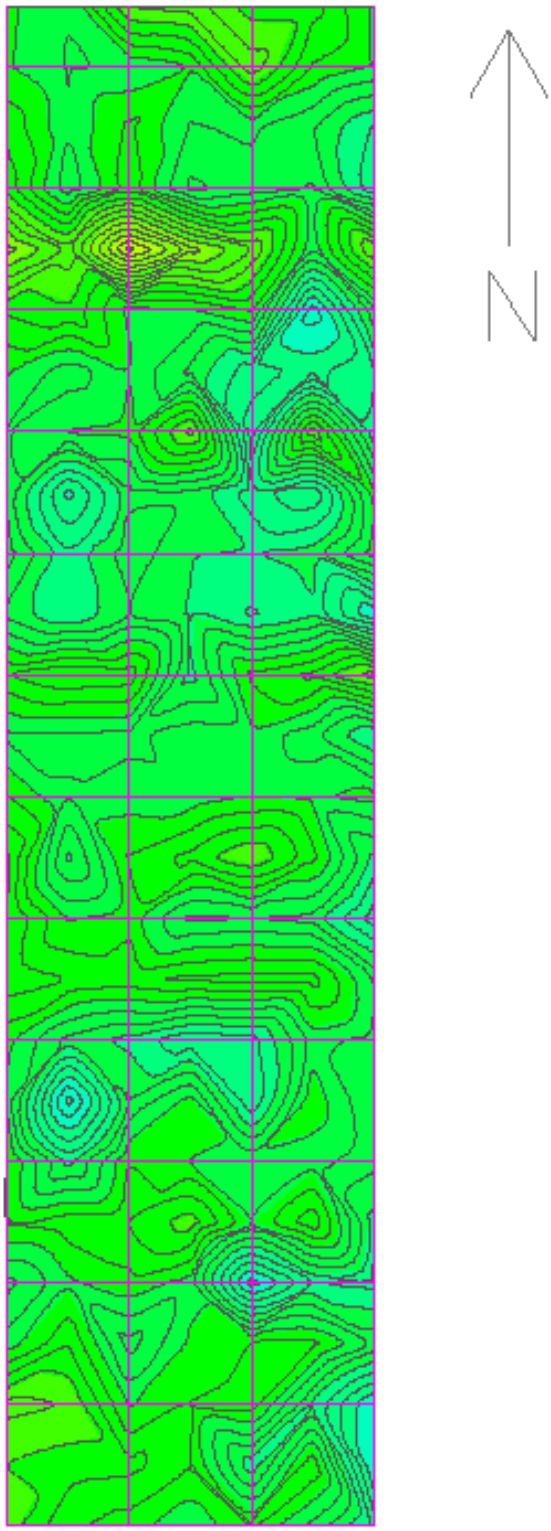

Figure E-2: Section A – 8/25/2011

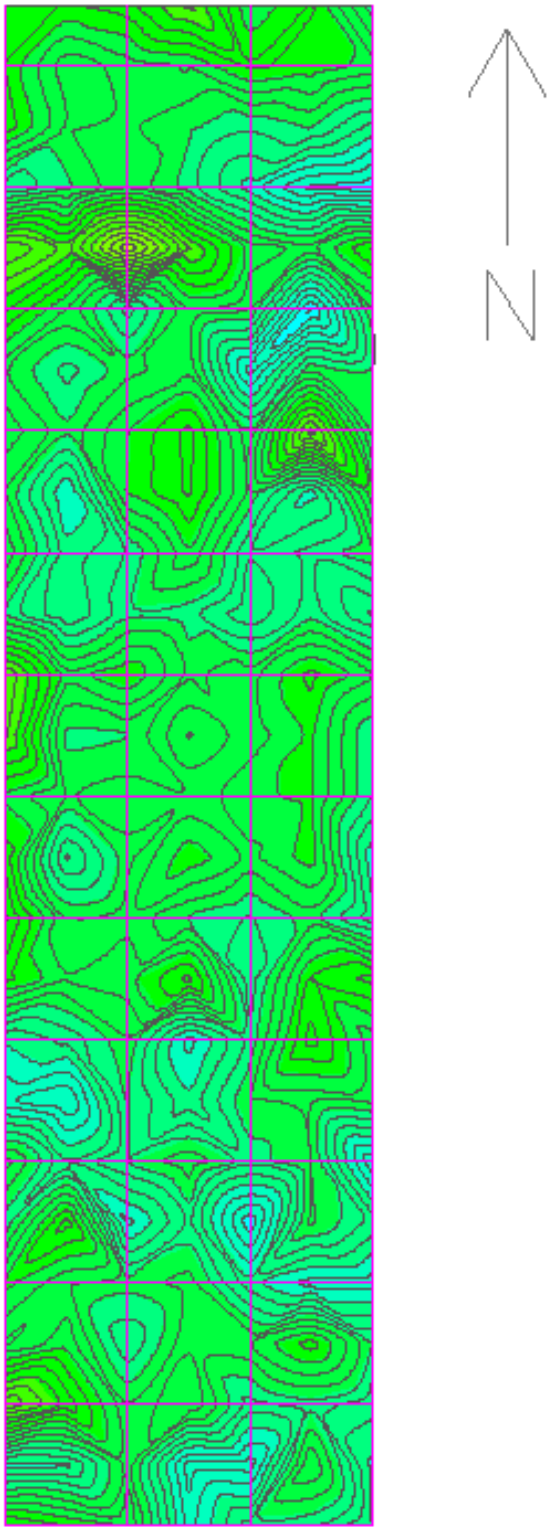

Figure E-3: Section A – 10/6/2011

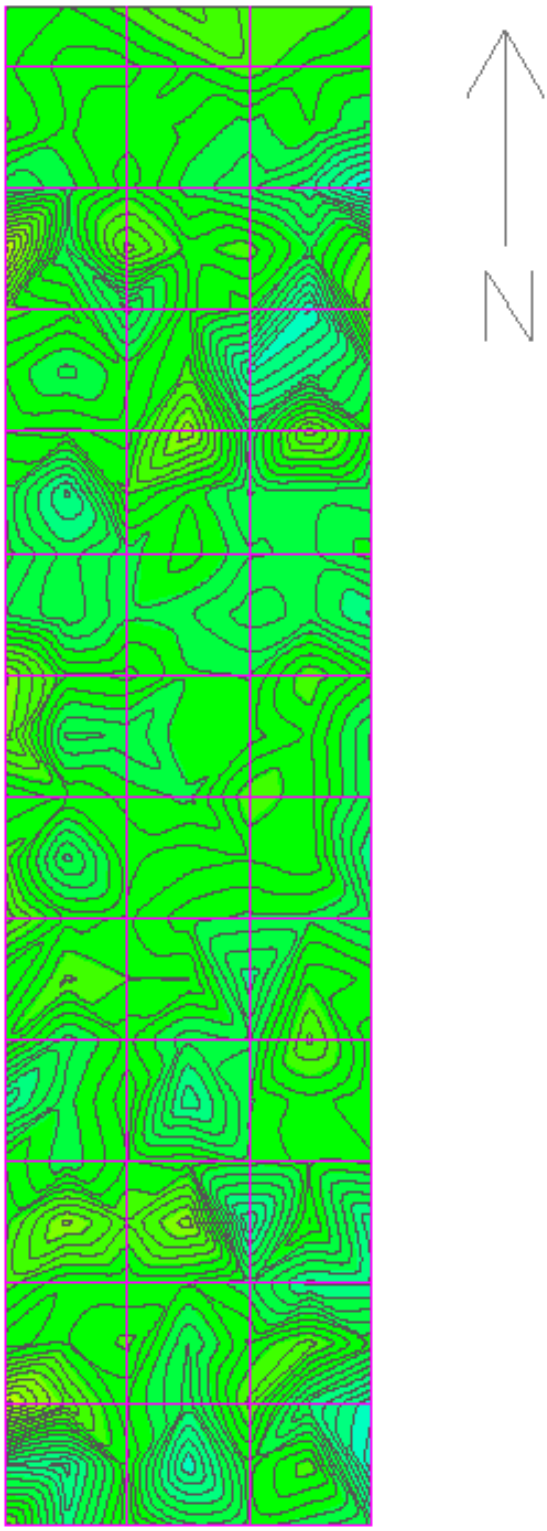

Figure E-4: Section A – 10/27/2012

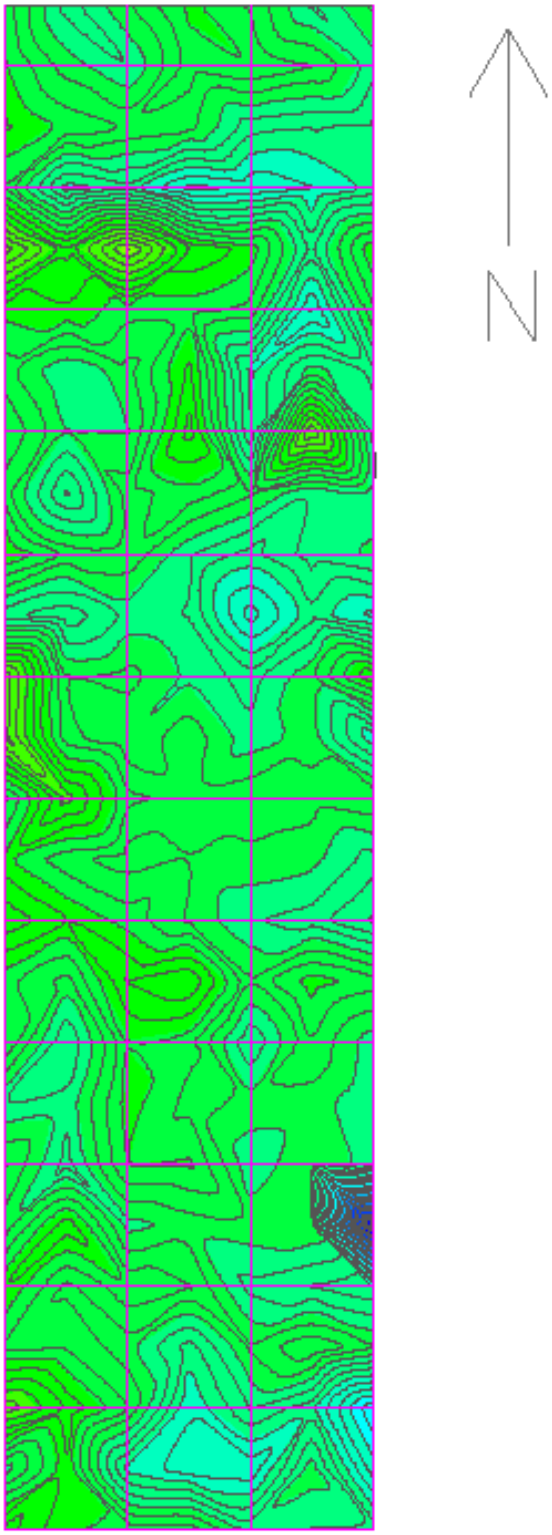

Figure E-5: Section A – 4/10/2012

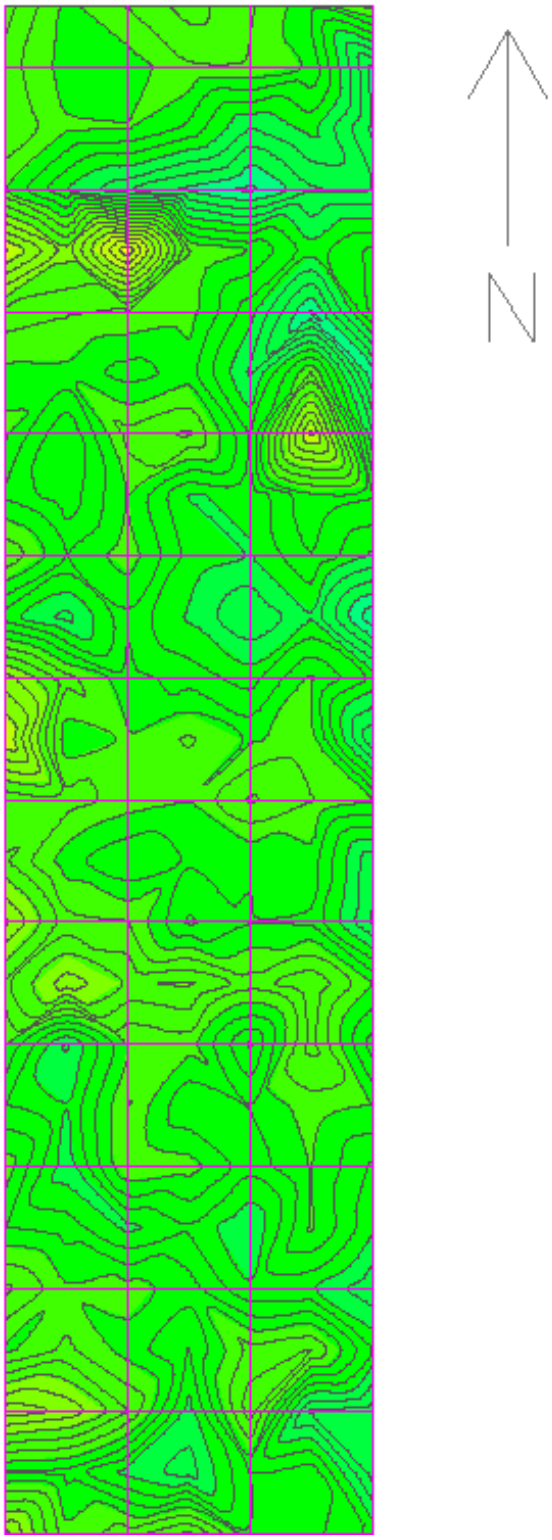

Figure E-6: Section A – 5/9/2012

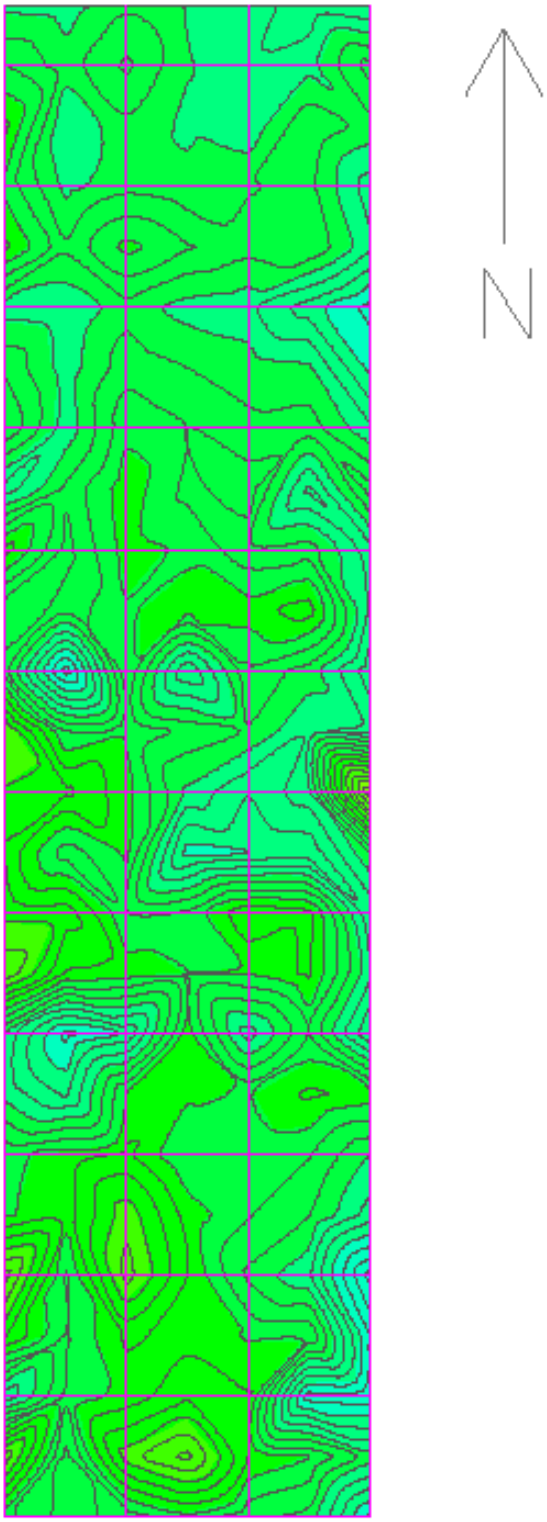

Figure E-7: Section B – 8/25/2011

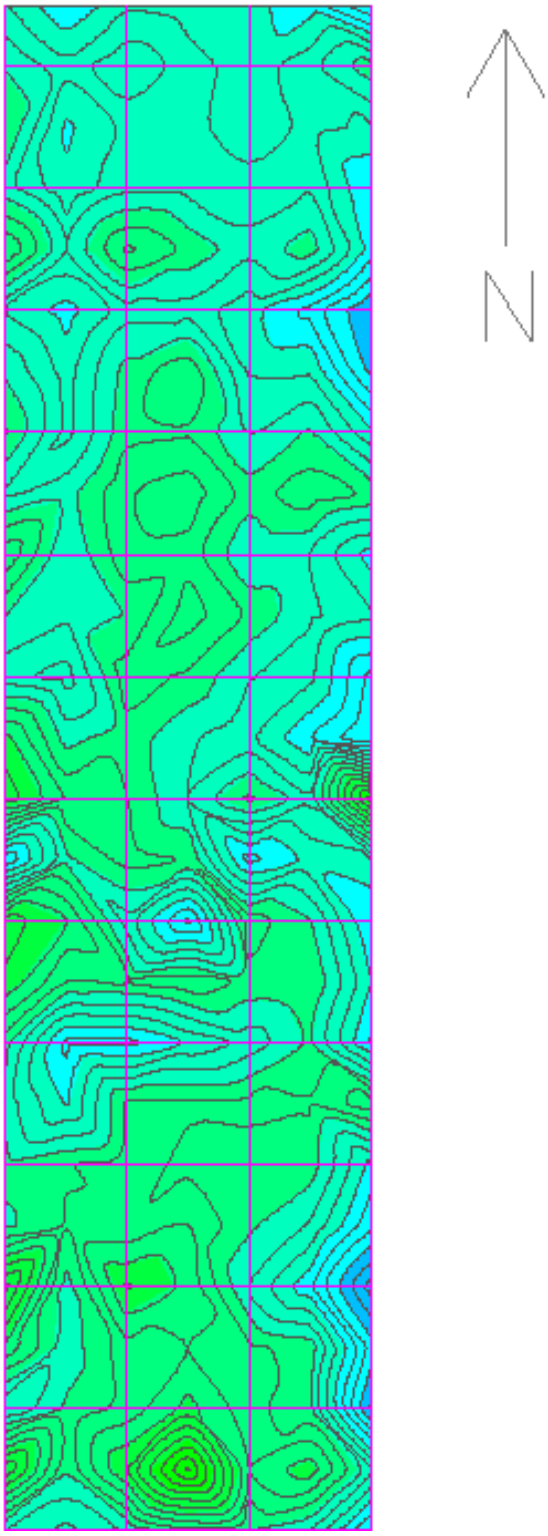

Figure E-8: Section B – 10/6/2011

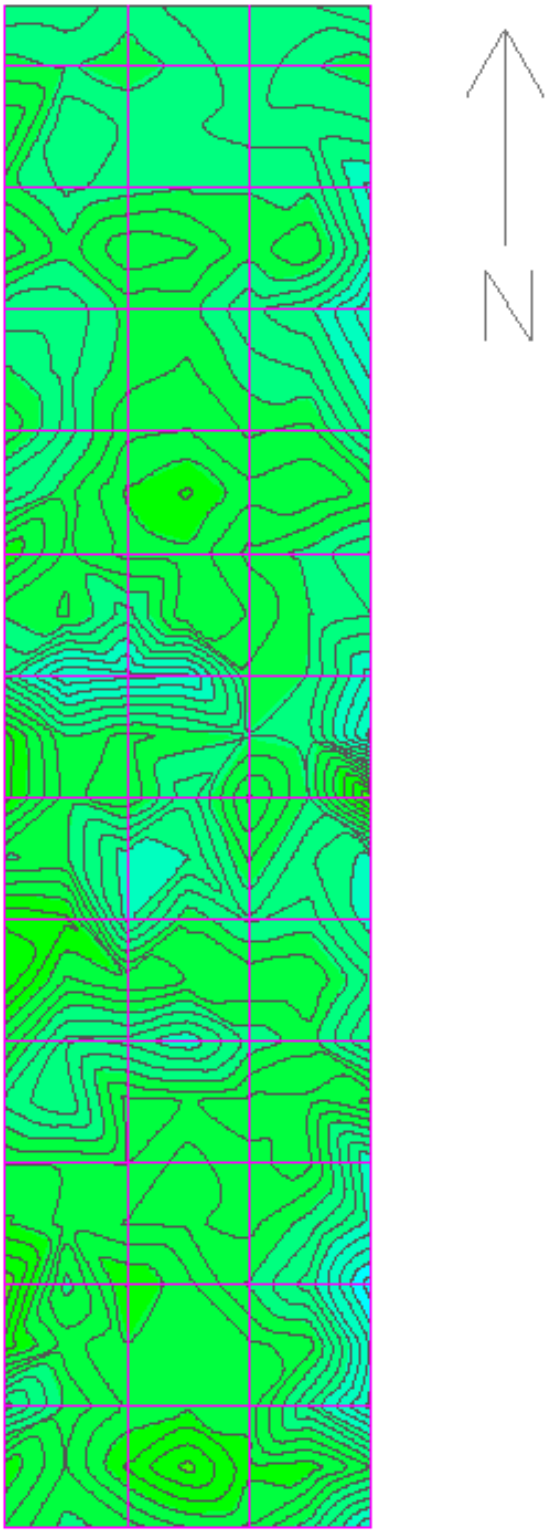

Figure E-9: Section B – 10/27/2012

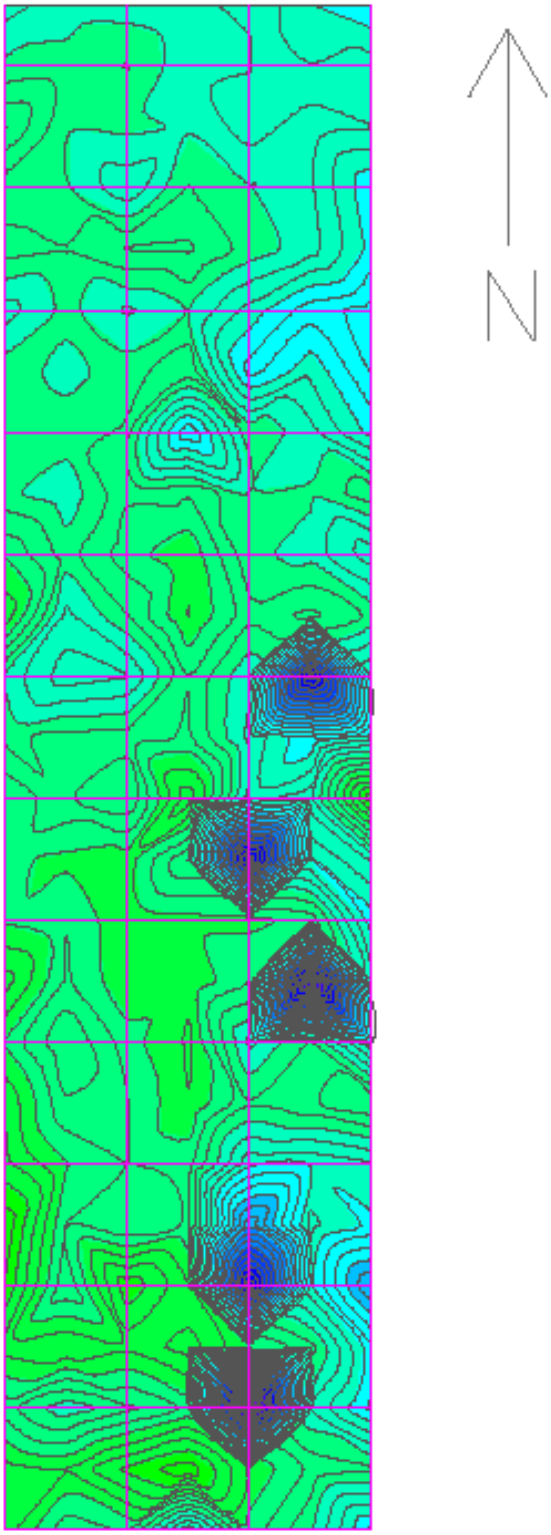

Figure E-10: Section B – 4/10/2012

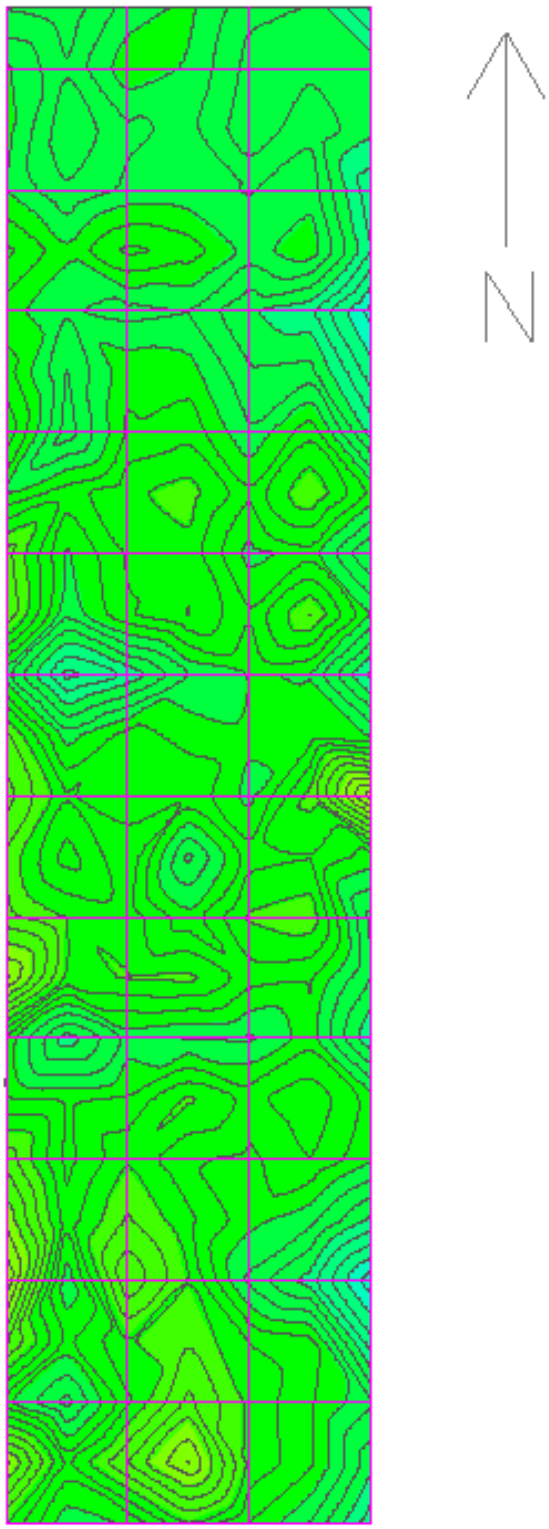

Figure E-11: Section B – 5/9/2012

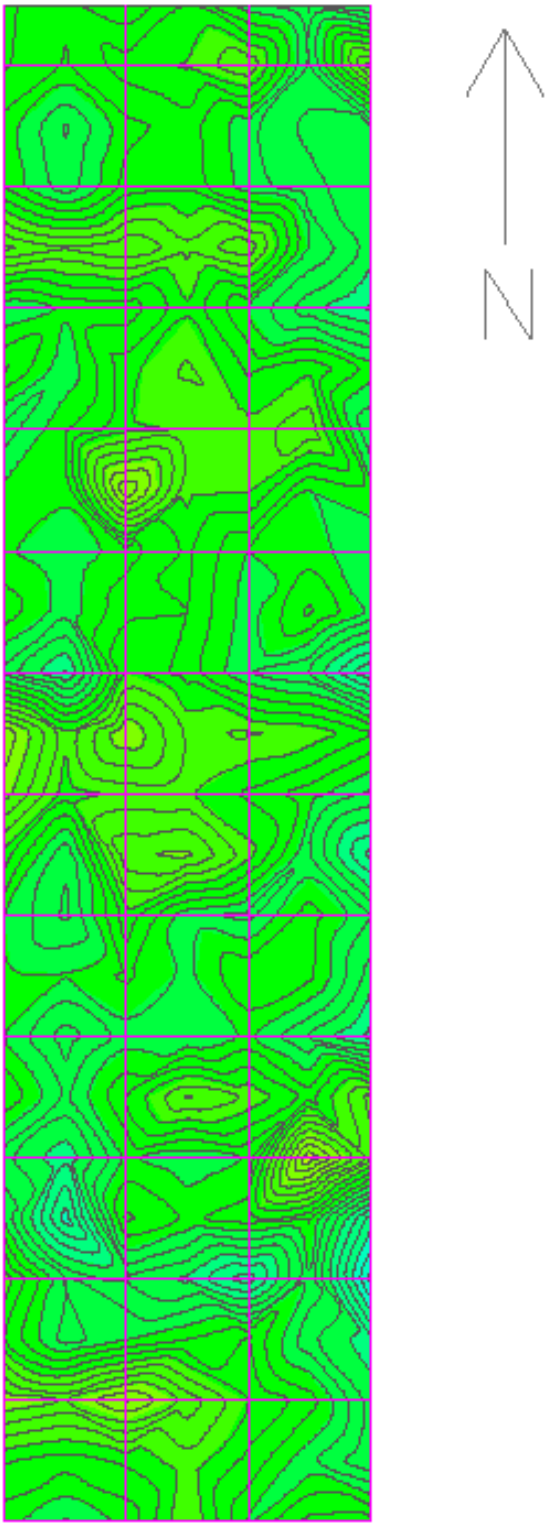

Figure E-12: Section C – 8/25/2011

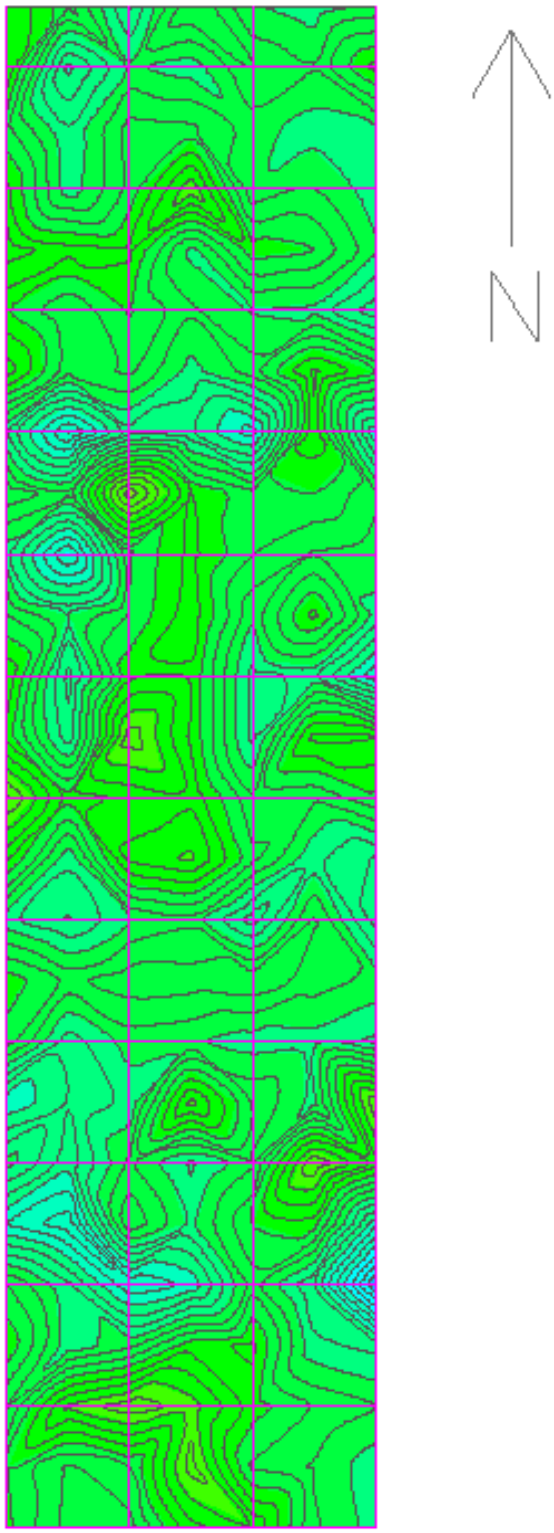

Figure E-13: Section C – 10/6/2011

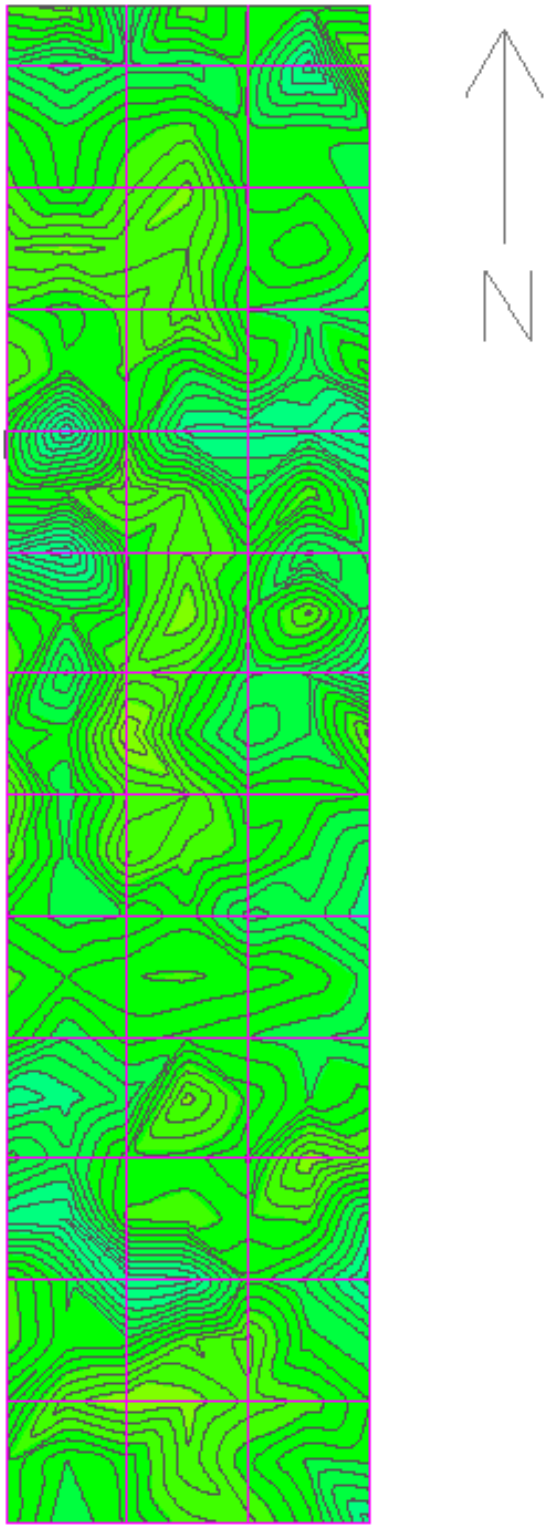

Figure E-14: Section C – 10/27/2012

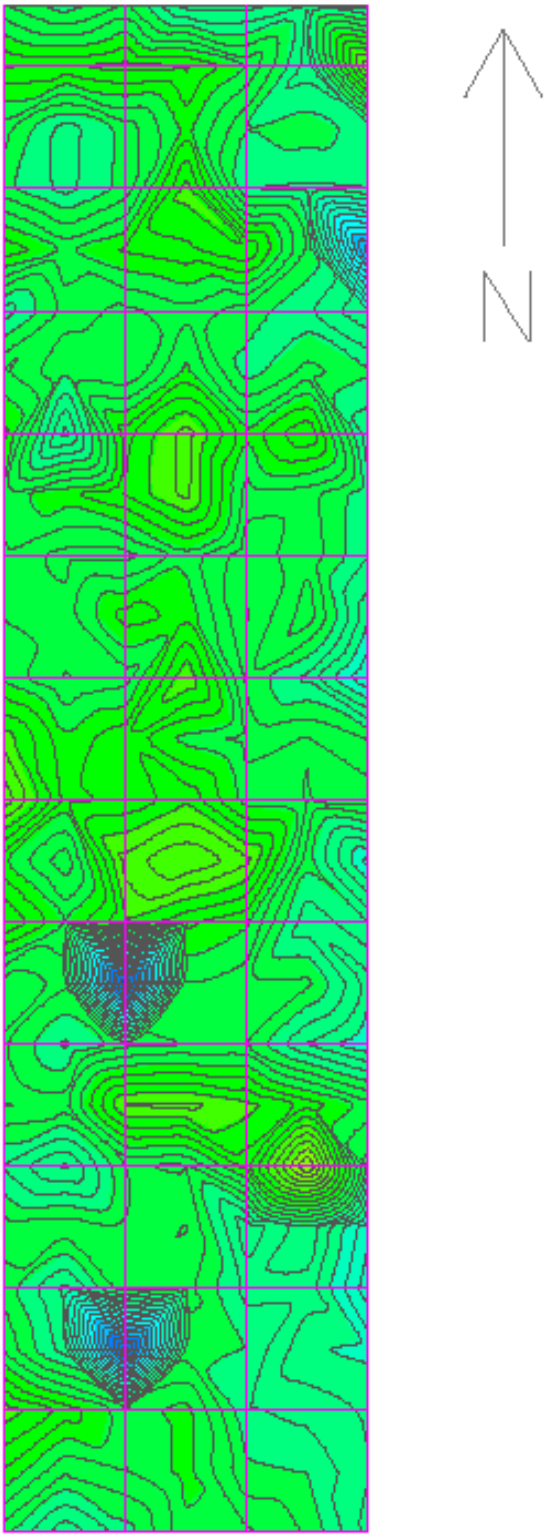

Figure E-15: Section C – 4/10/2012

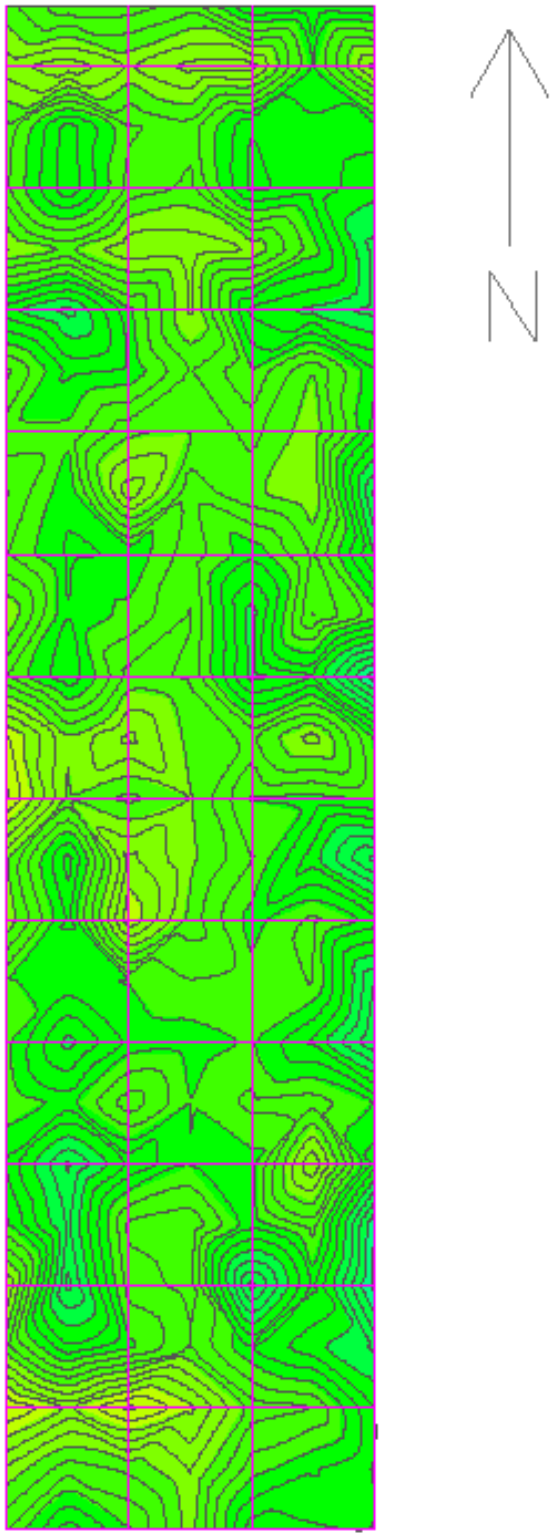

Figure E-16: Section C – 5/9/2012

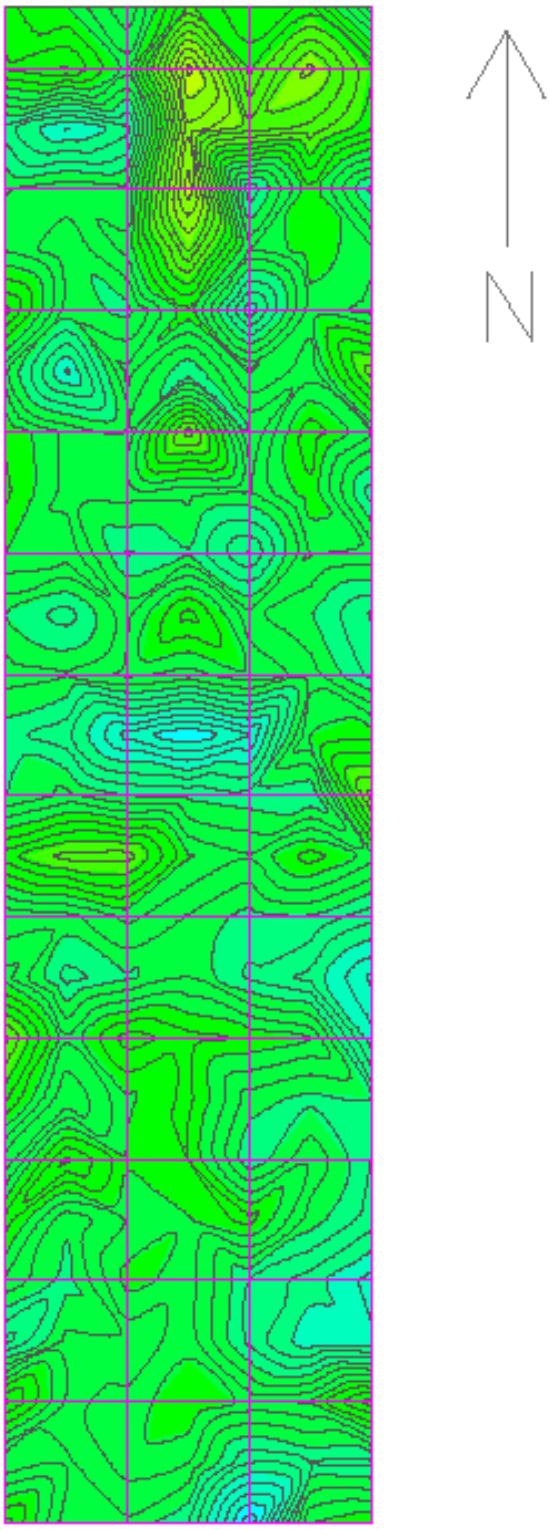

Figure E-17: Section D – 8/25/2011

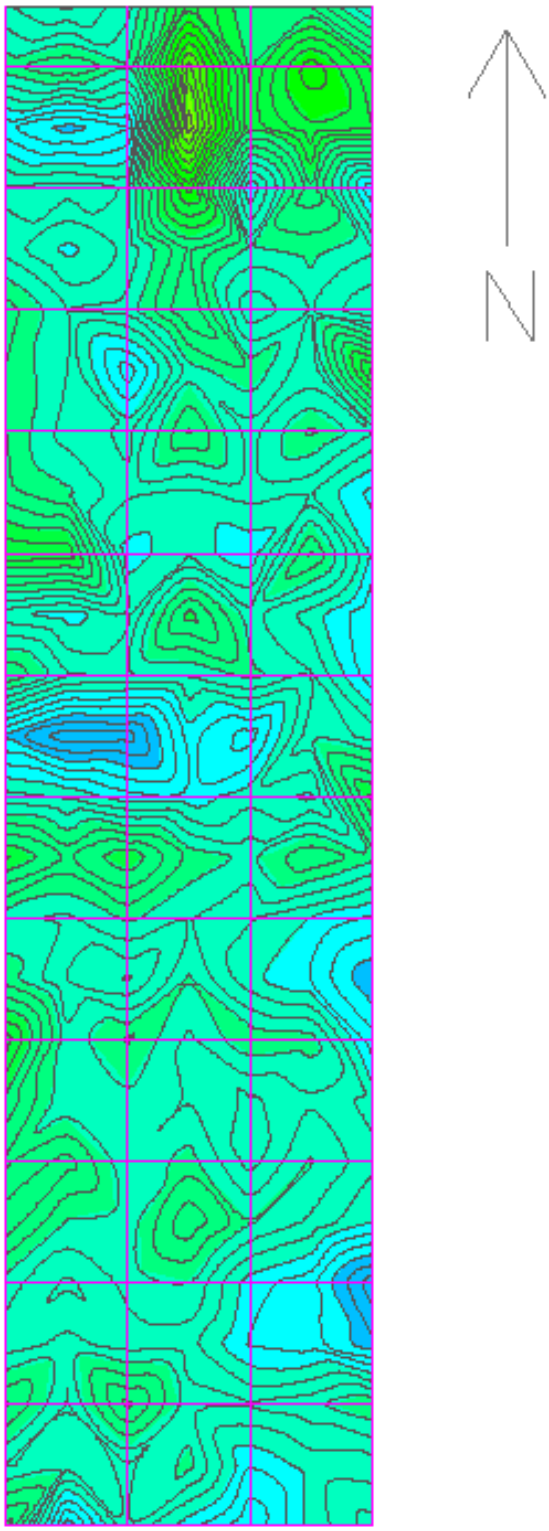

Figure E-18: Section D – 10/6/2011

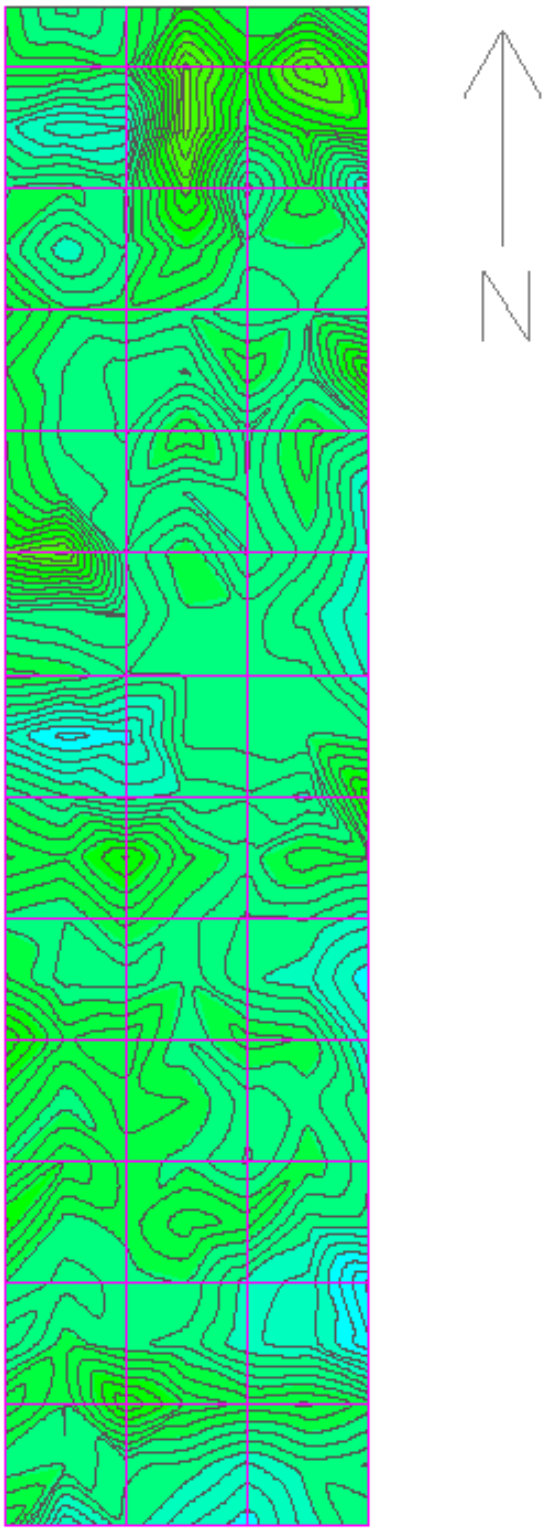

Figure E-19: Section D – 10/27/2012

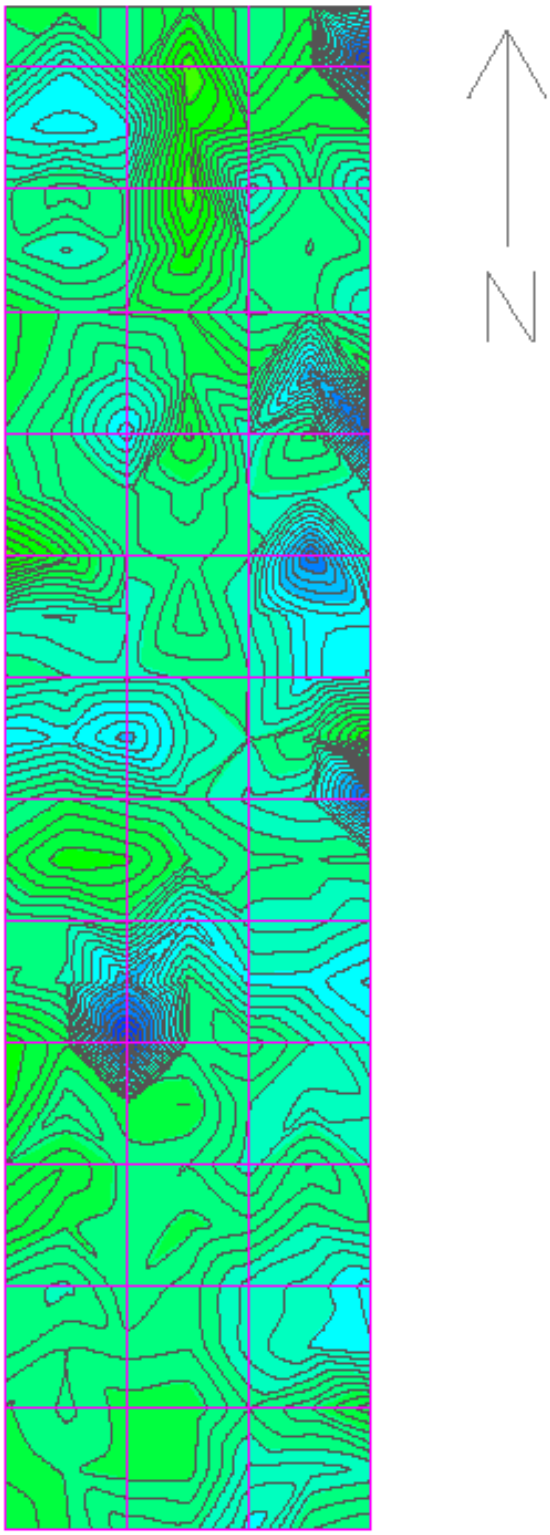

Figure E-20: Section D – 4/10/2012

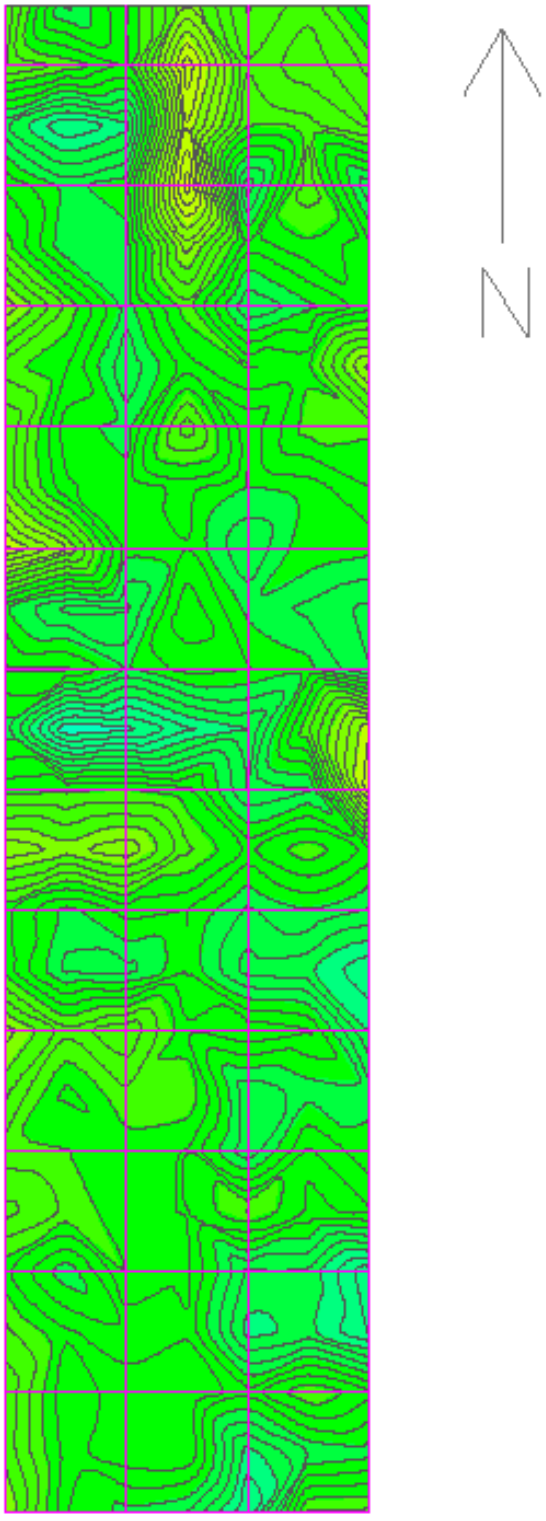

Figure E-21: Section D – 5/9/2012

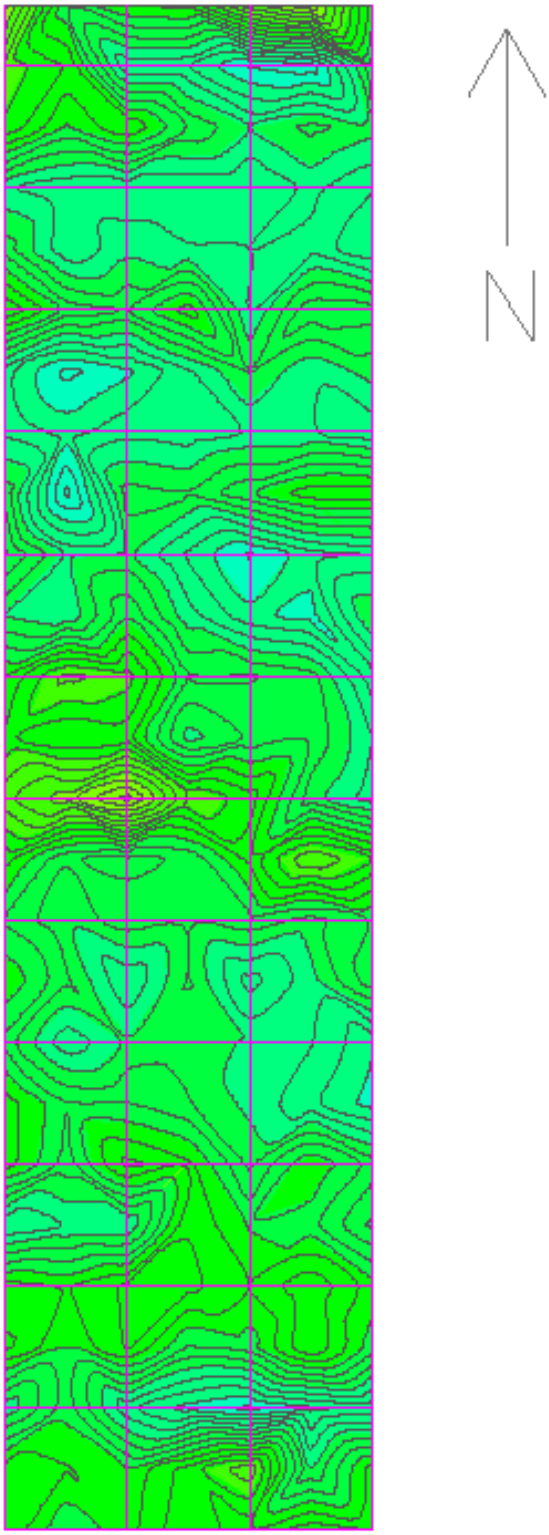

Figure E-22: Section E – 8/25/2011

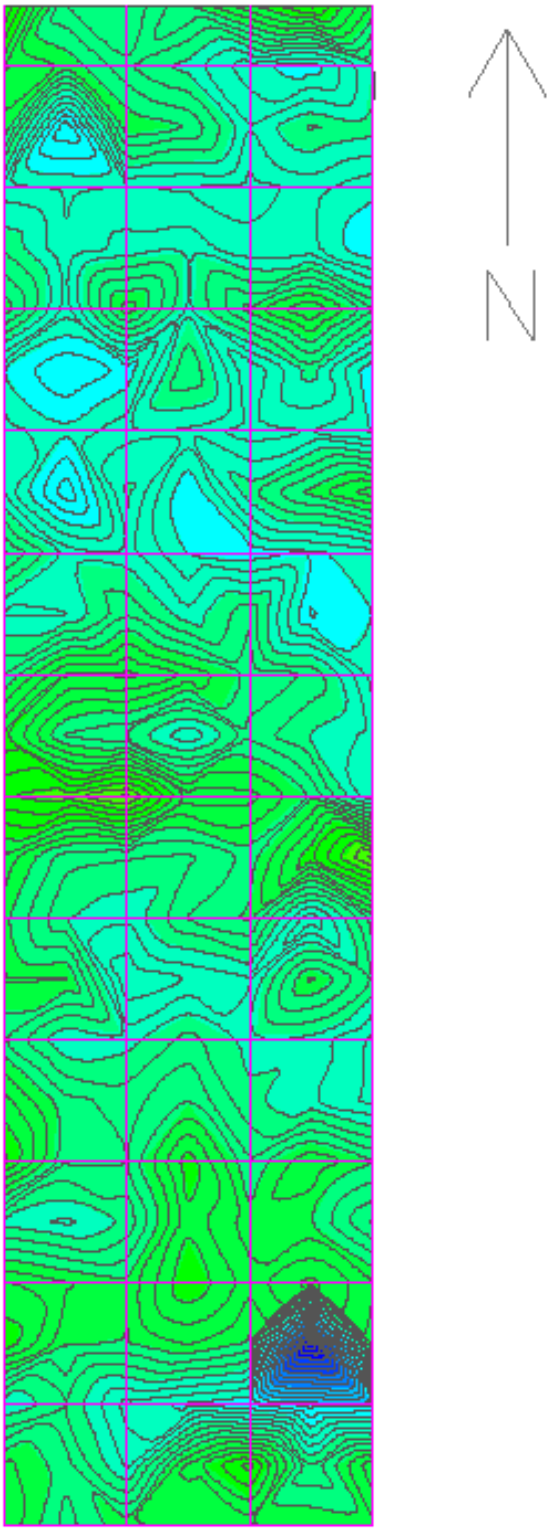

Figure E-23: Section E – 10/6/2011

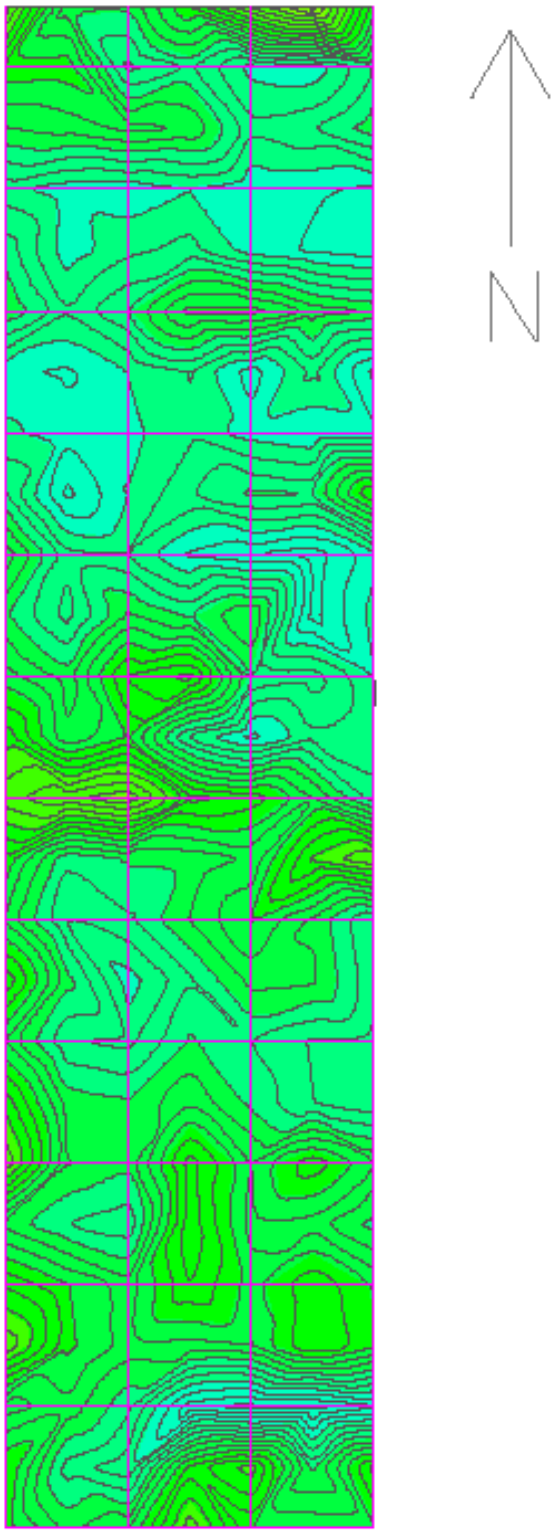

Figure E-24: Section E – 10/27/2011

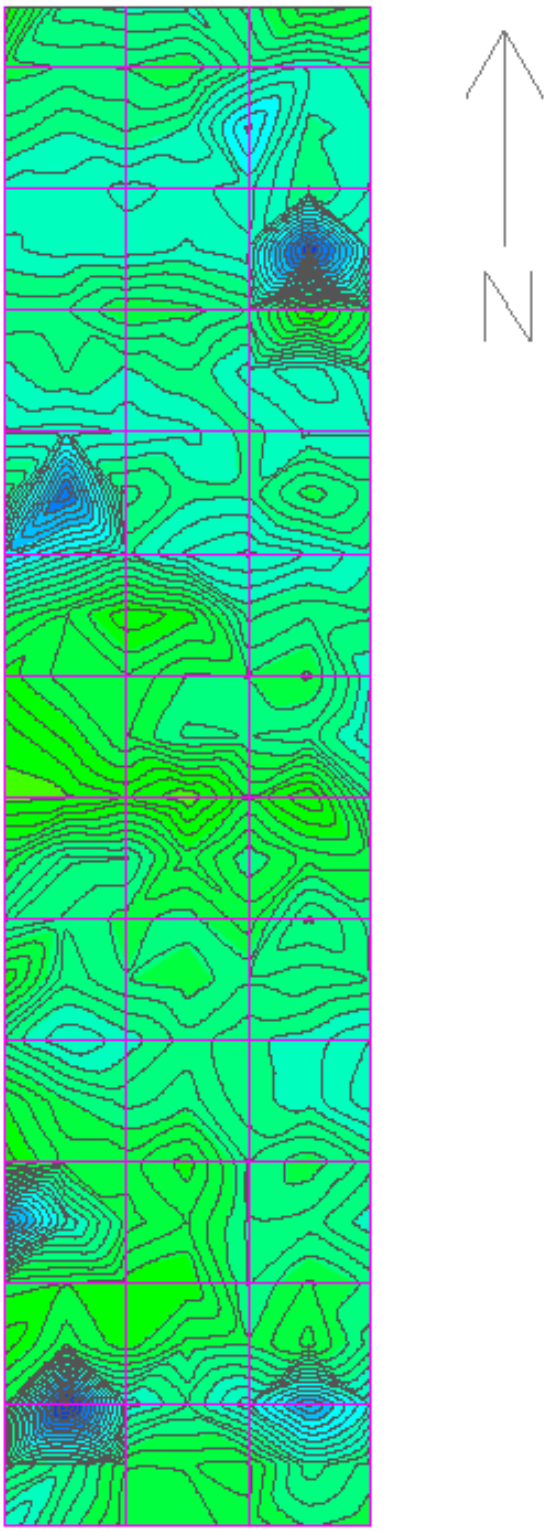

Figure E-25: Section E – 4/10/2012

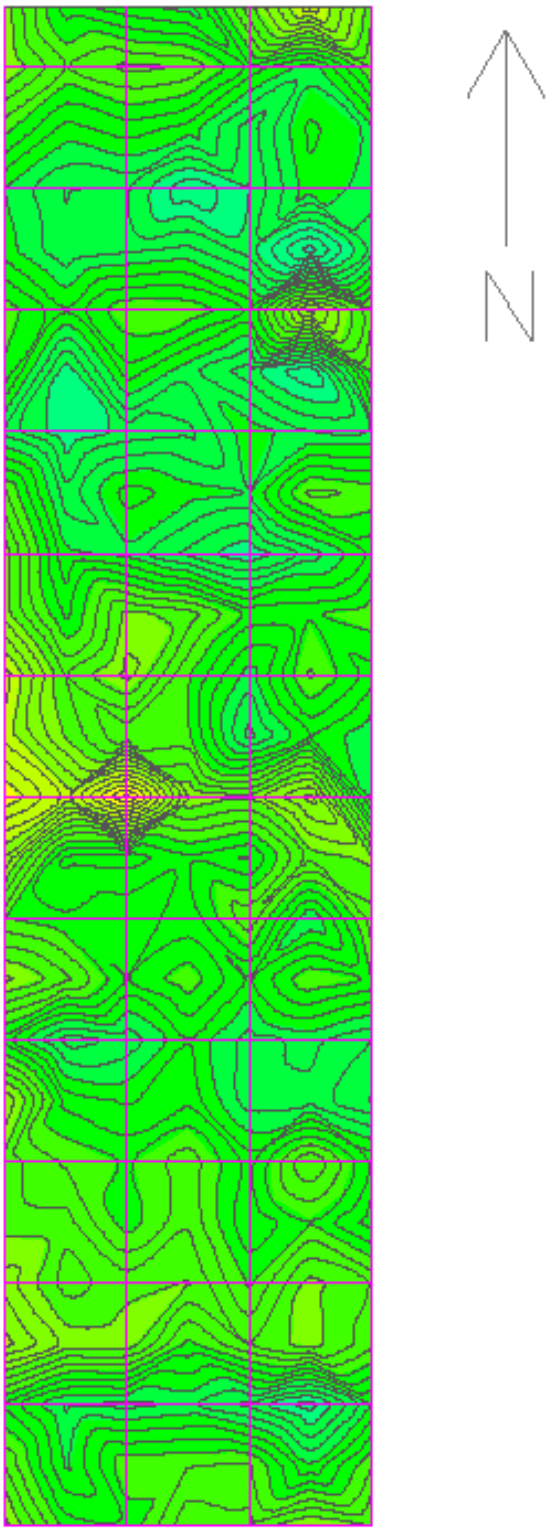

Figure E-26: Section E – 5/9/2012

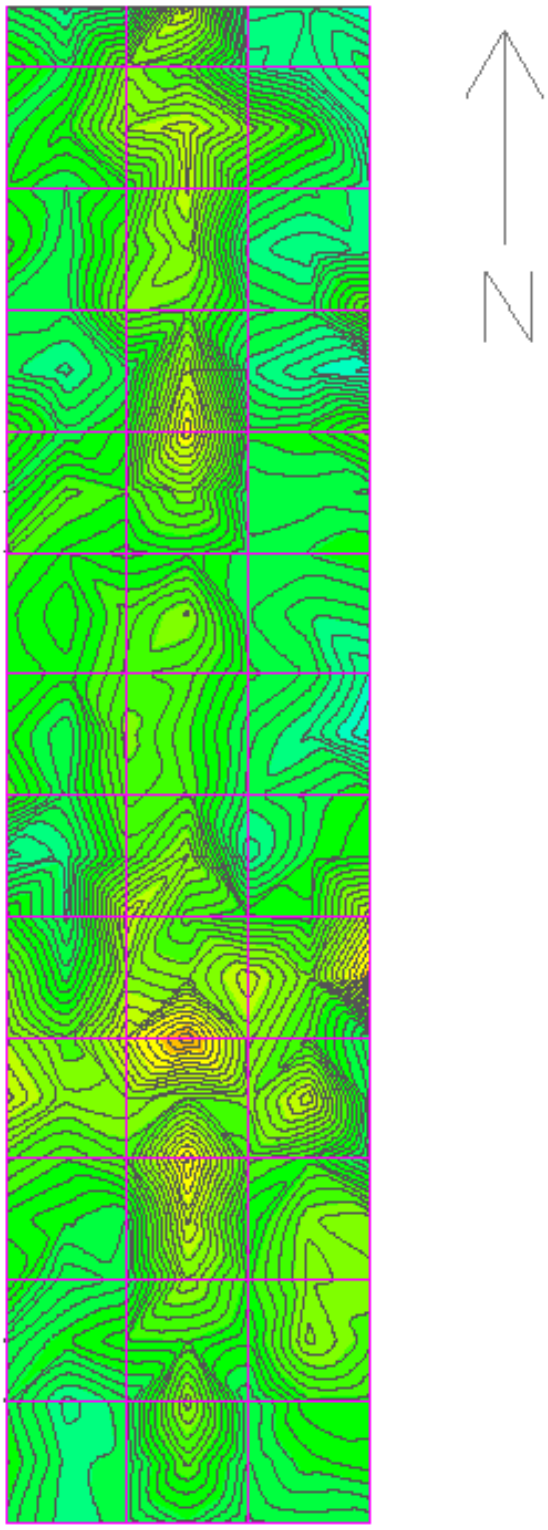

Figure E-27: Section F – 8/25/2011

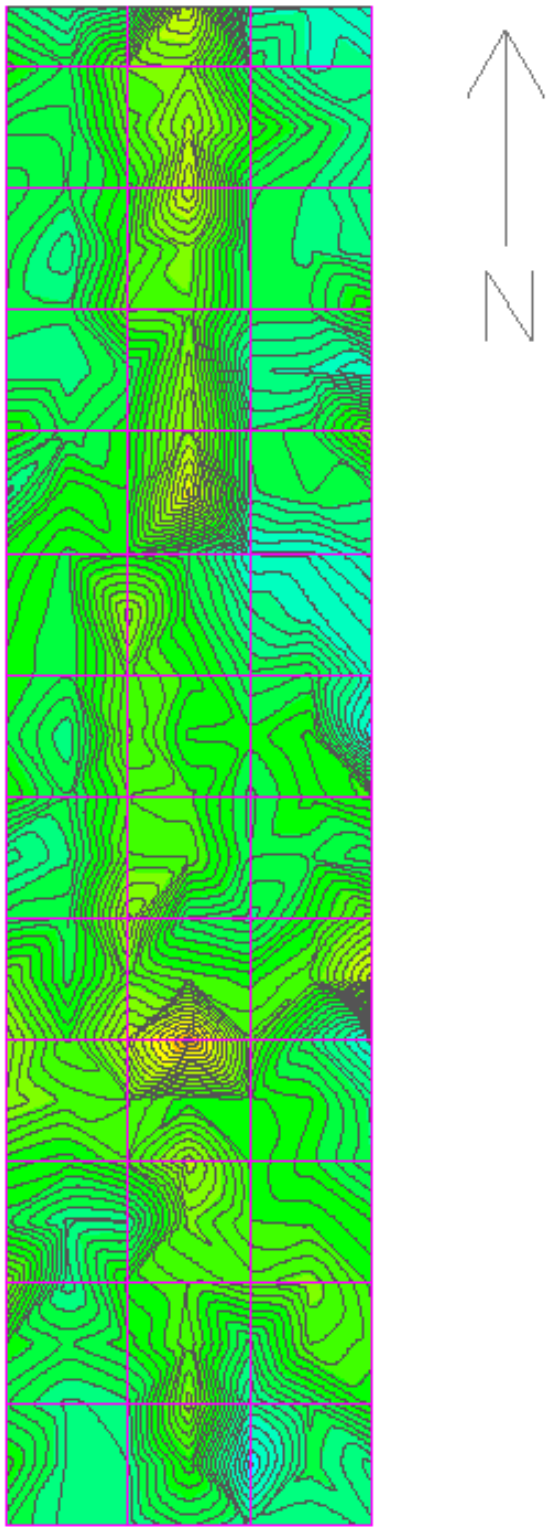

Figure E-28: Section F – 10/6/2011

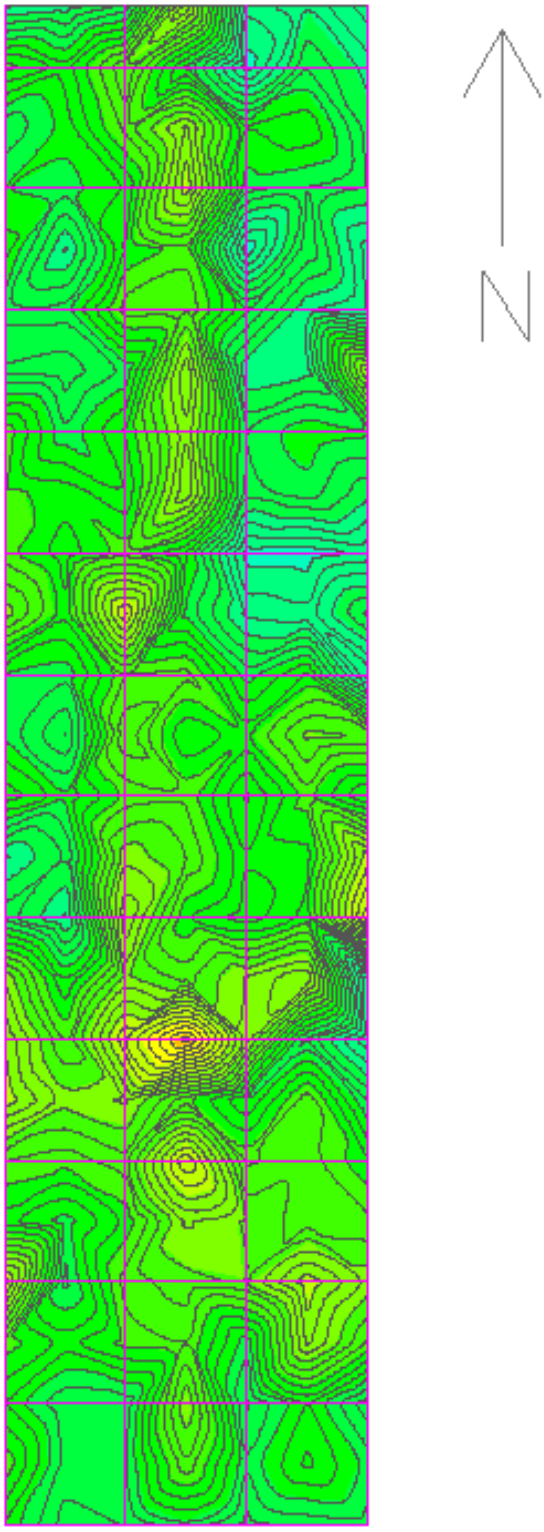

Figure E-29: Section F – 10/27/2011

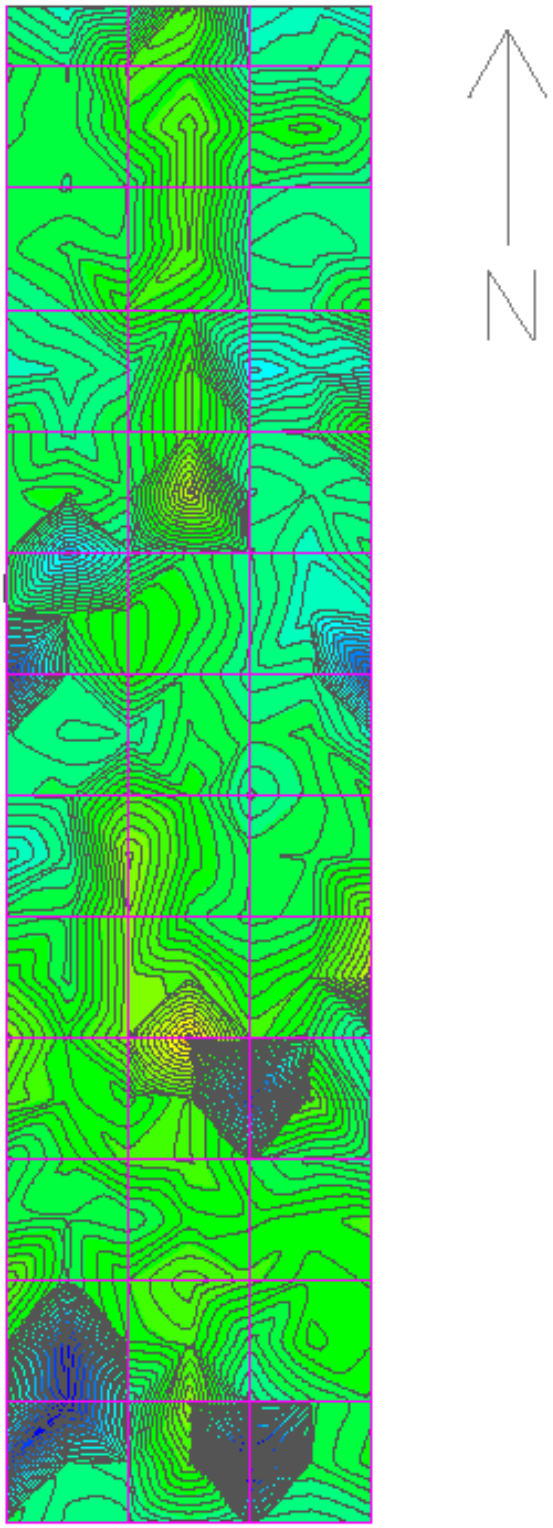

Figure E-30: Section F – 4/10/2012

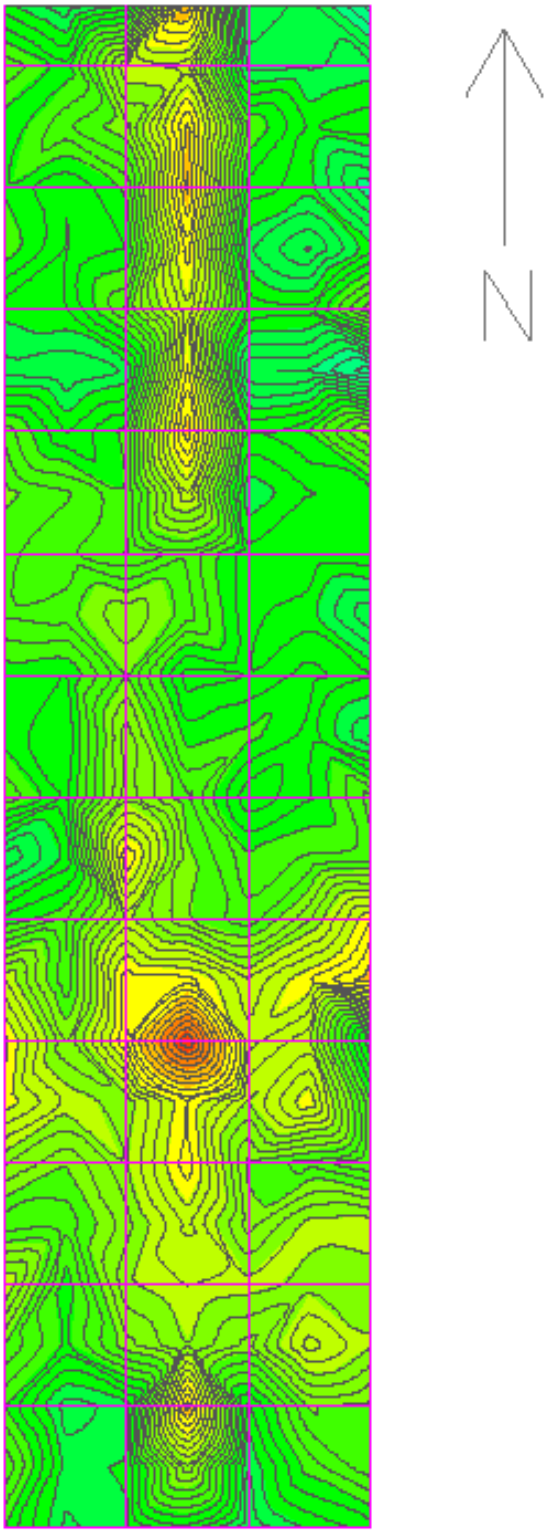

Figure E-31: Section F – 5/9/2012

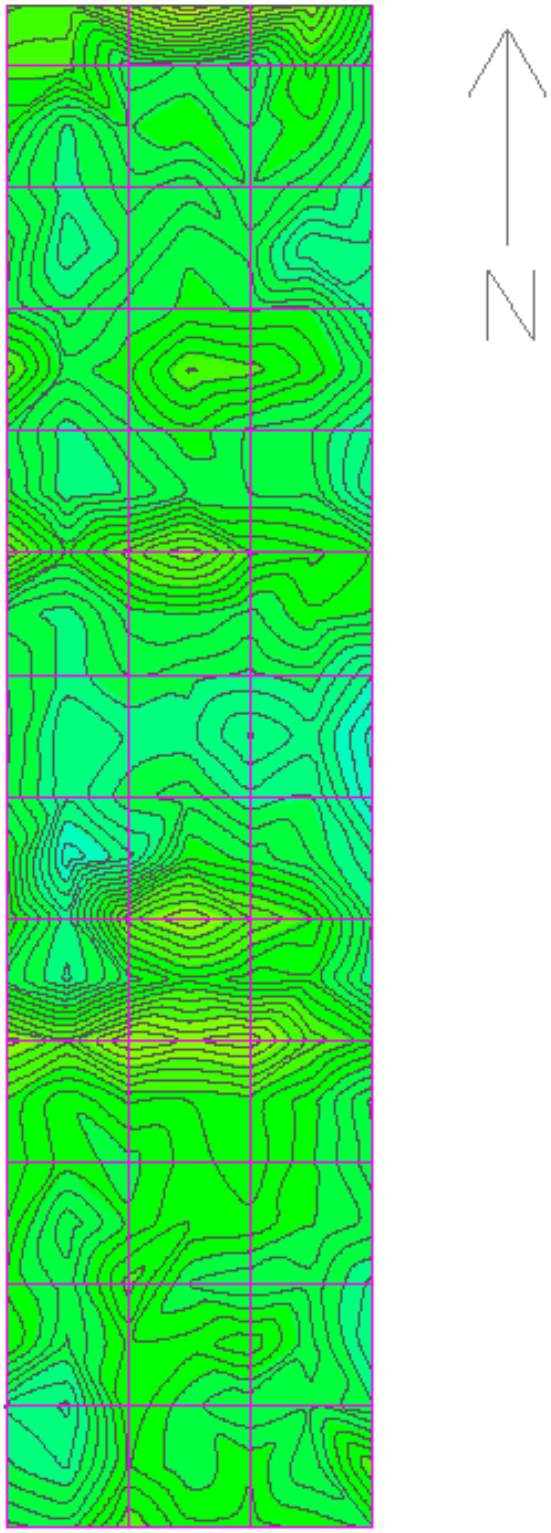

Figure E-32: Section G – 8/25/2011

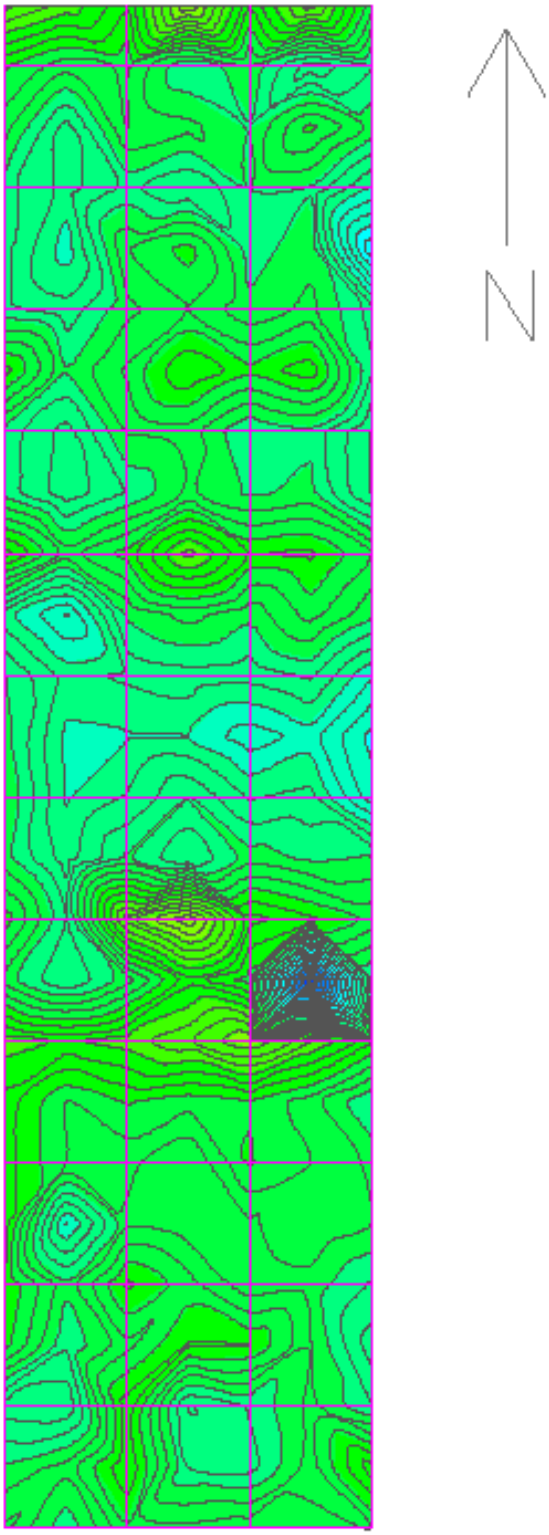

Figure E-33: Section G – 10/6/2011

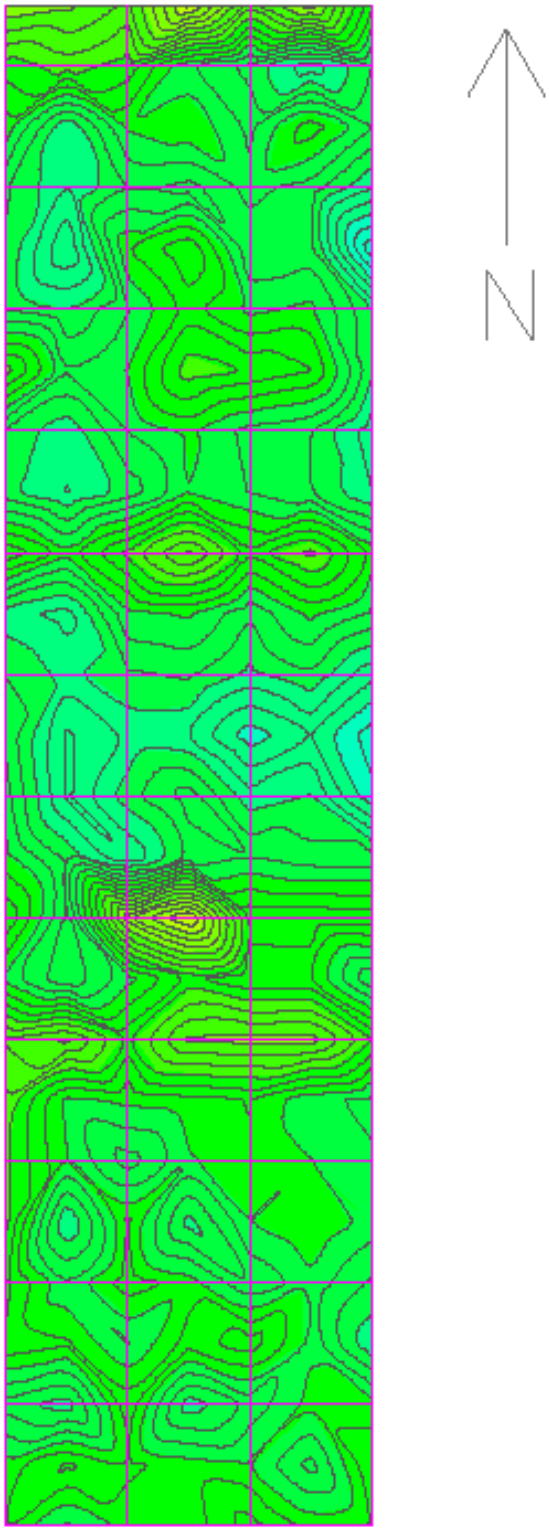

Figure E-34: Section G – 10/27/2011

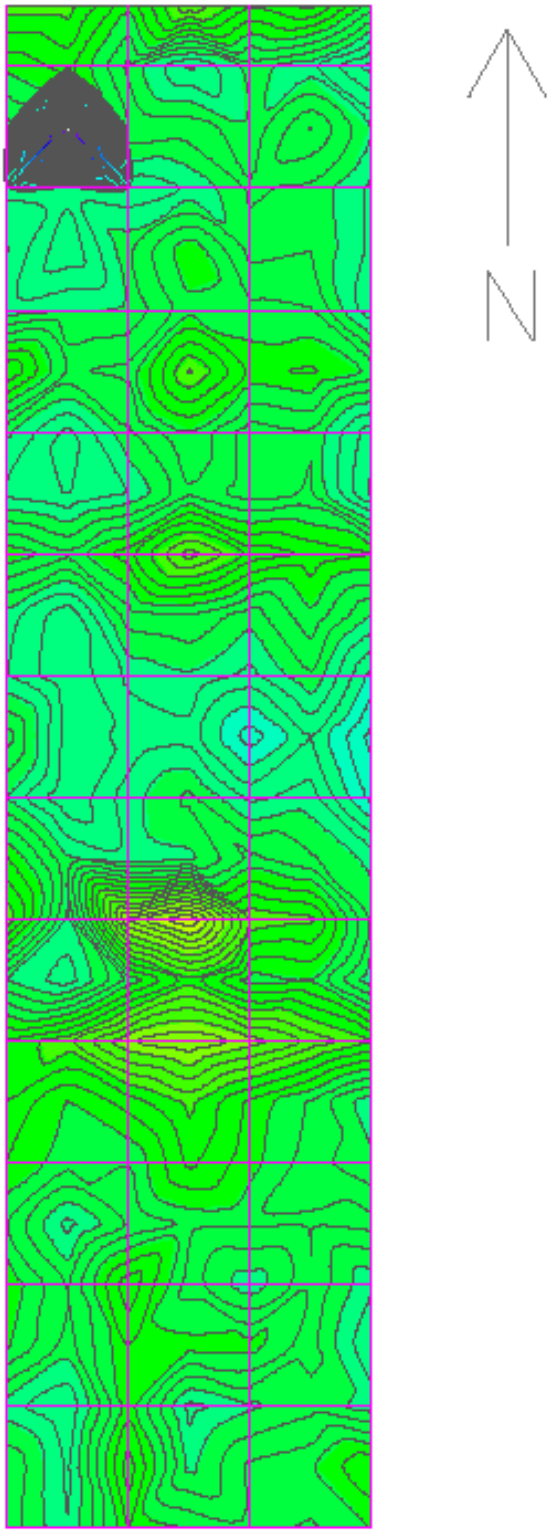

Figure E-35: Section G – 4/10/2012

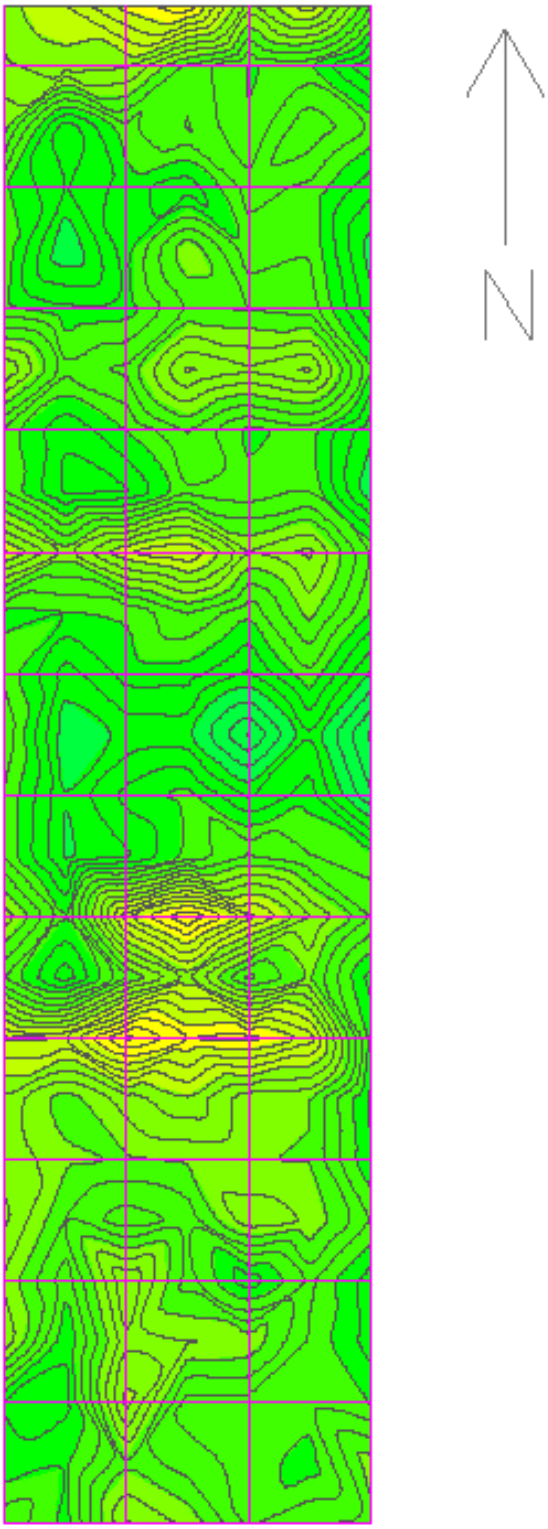

Figure E-36: Section G – 5/9/2012

Minimum Elevation	Maximum Elevation	Color
−150.00	−120.00	
−120.00	−90.00	
−90.00	−60.00	
−60.00	−30.00	
−30.00	0.00	
0.00	30.00	
30.00	60.00	
60.00	90.00	
90.00	120.00	
120.00	150.00	
150.00	180.00	
180.00	210.00	
210.00	240.00	
240.00	270.00	

Figure E-37: Legend for the difference in half-cell potential contour maps

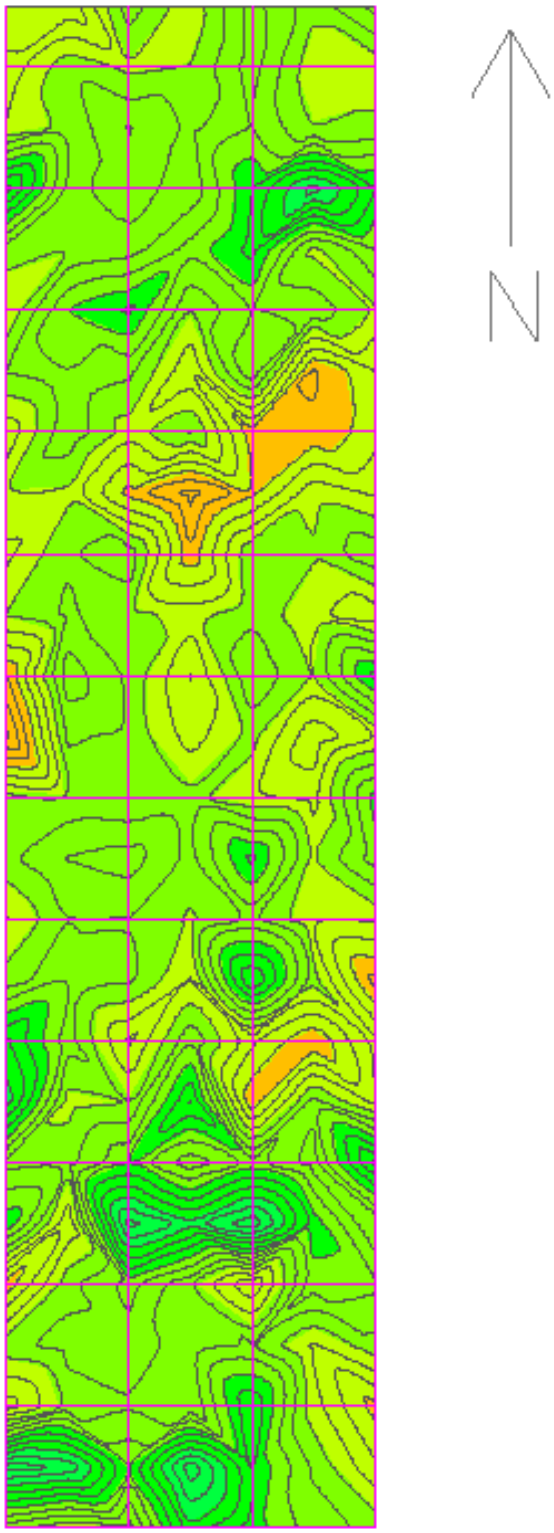

Figure E-38: Section A – Difference between 8/25/2011 and 10/6/2011

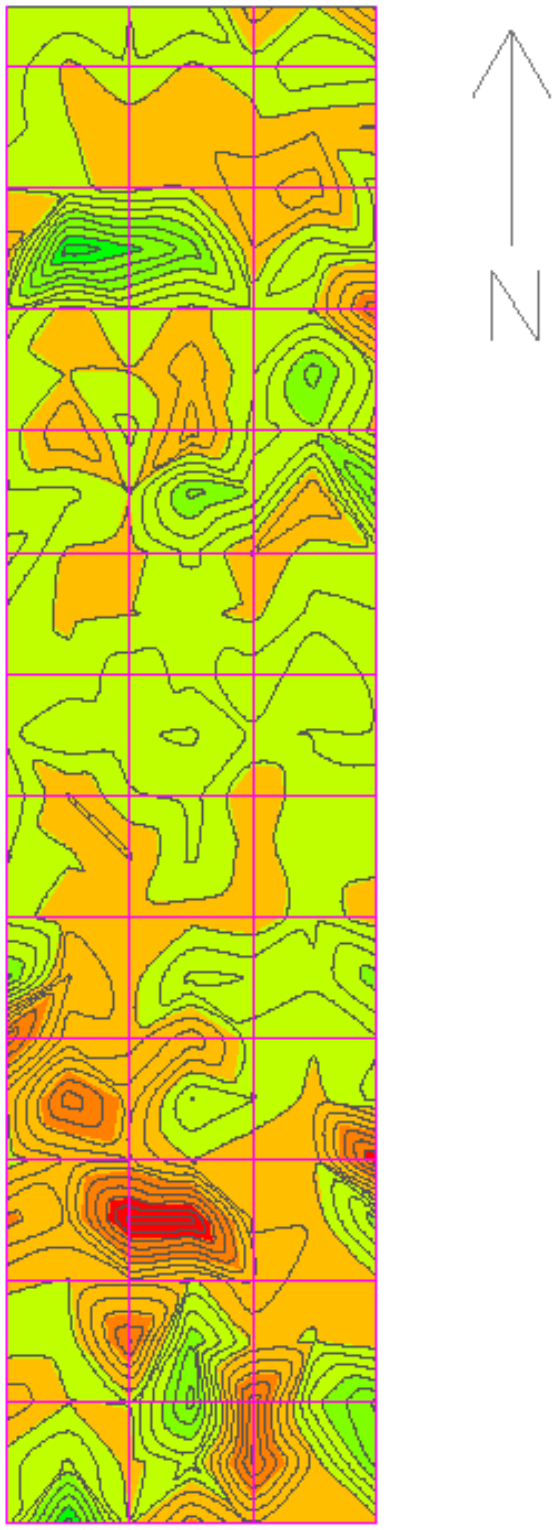

Figure E-39: Section A – Difference between 10/6/2011 and 10/27/2011

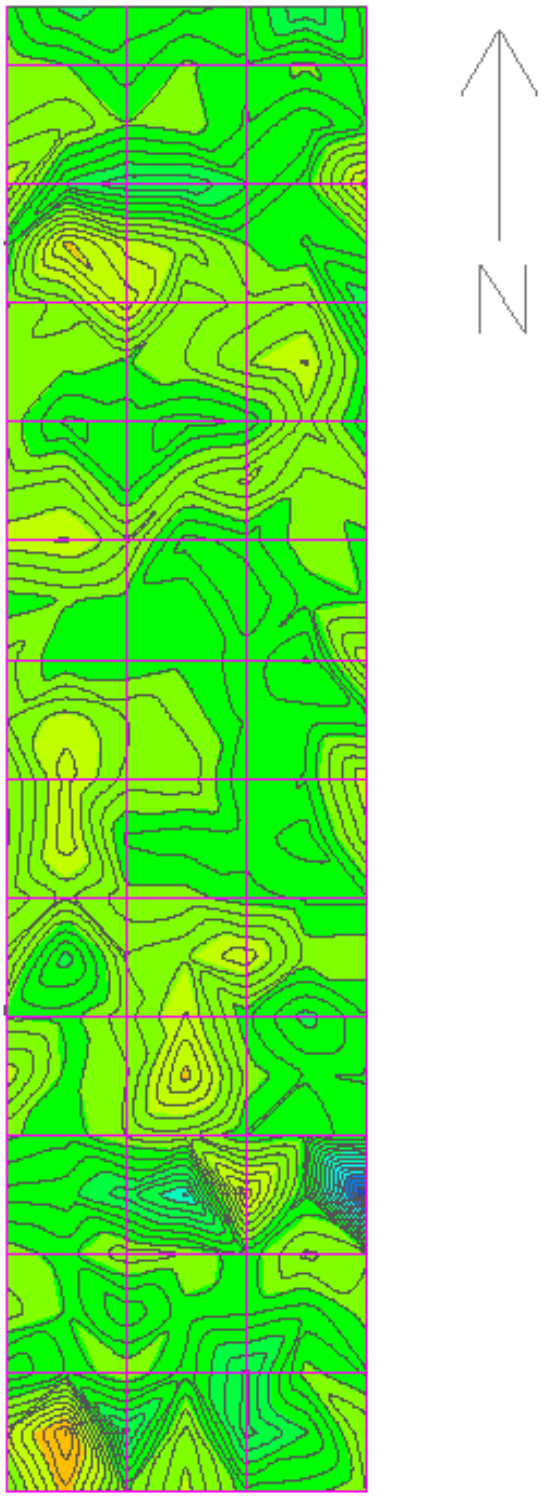

Figure E-40: Section A – Difference between 10/27/2011 and 4/10/2012

Figure E-41: Section A – Difference between 4/10/2012 and 5/9/2012

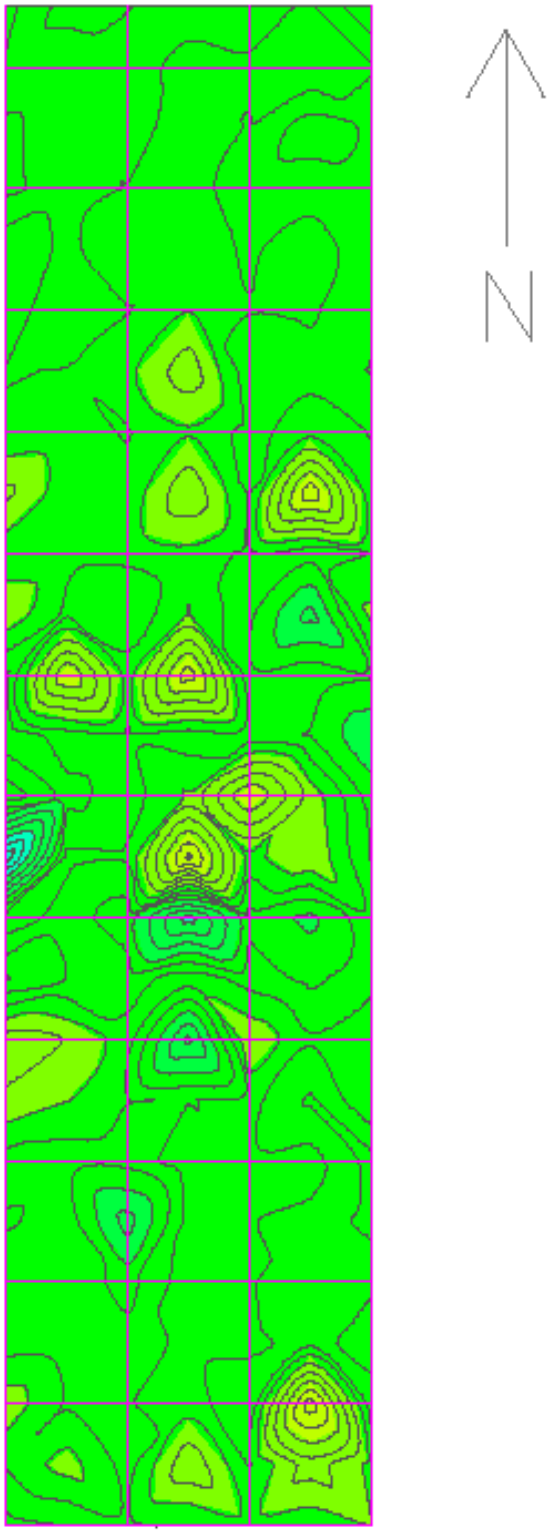

Figure E-42: Section B – Difference between 8/25/2011 and 10/6/2011

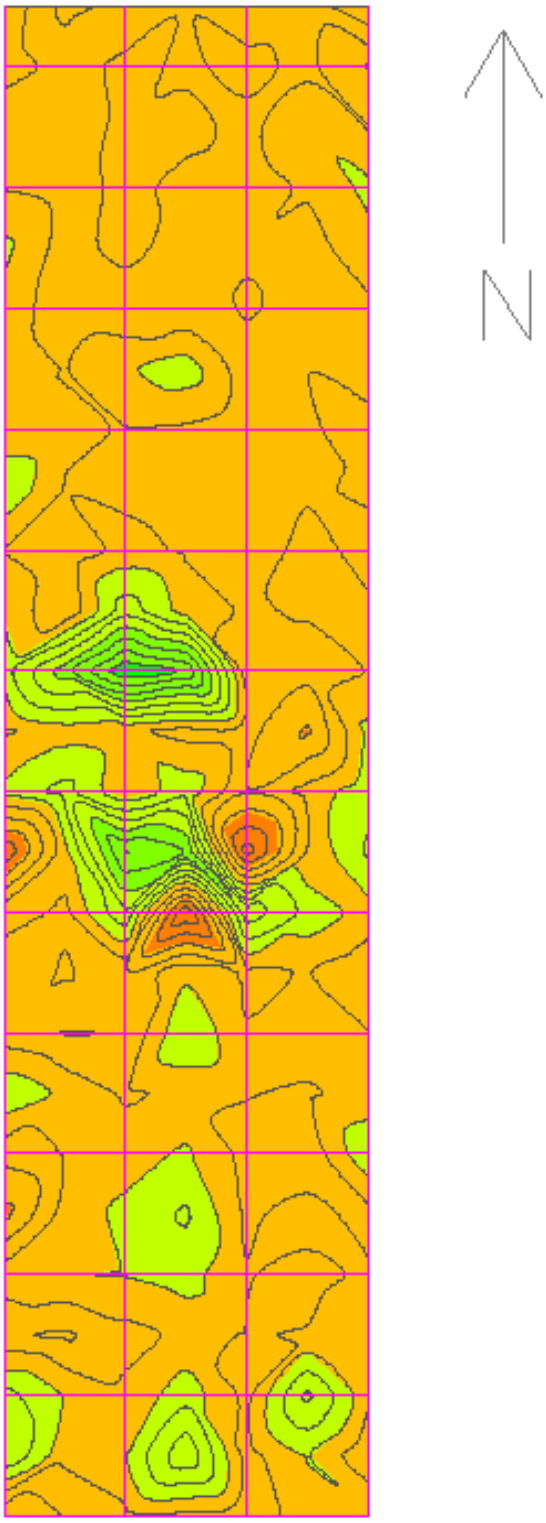

Figure E-43: Section B – Difference between 10/6/2011 and 10/27/2011

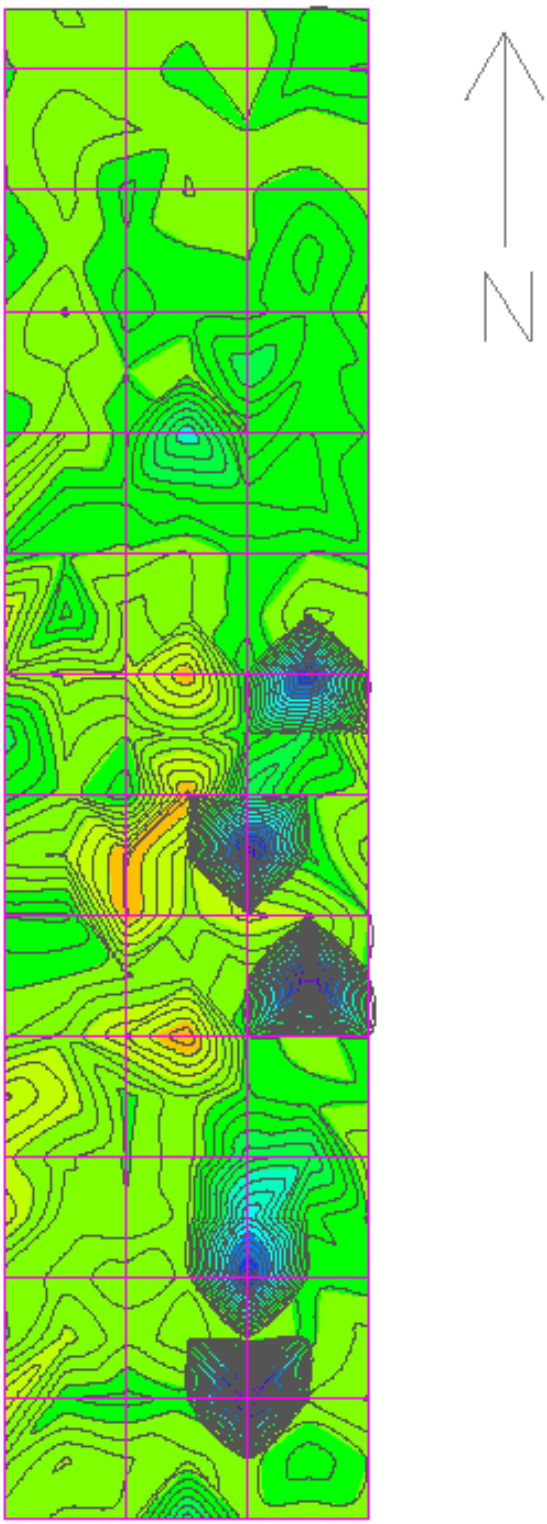

Figure E-44: Section B – Difference between 10/27/2011 and 4/10/2012

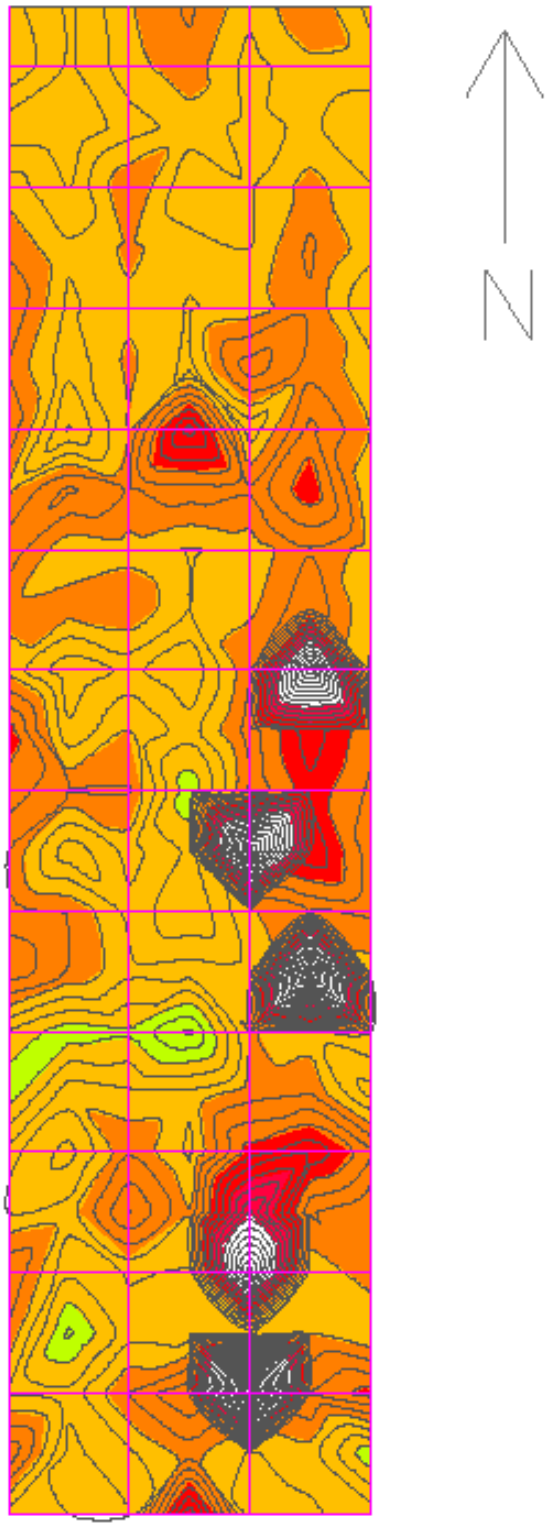

Figure E-45: Section B – Difference between 4/10/2012 and 5/9/2012

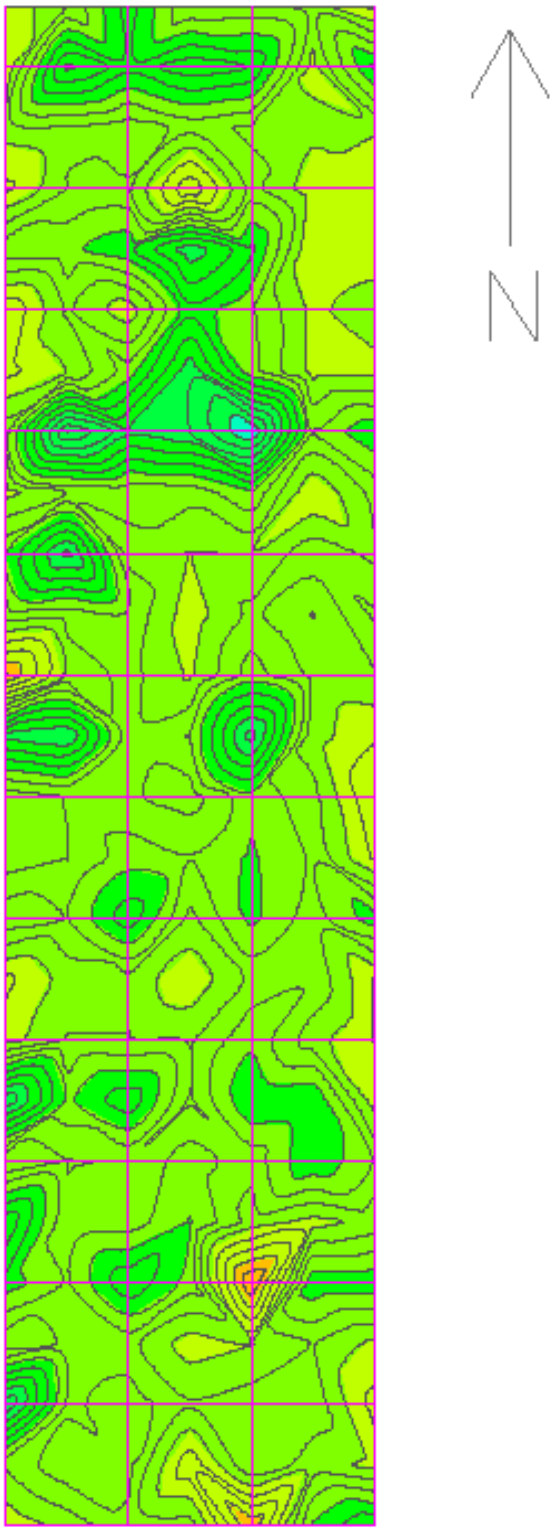

Figure E-46: Section C – Difference between 8/25/2011 and 10/6/2011

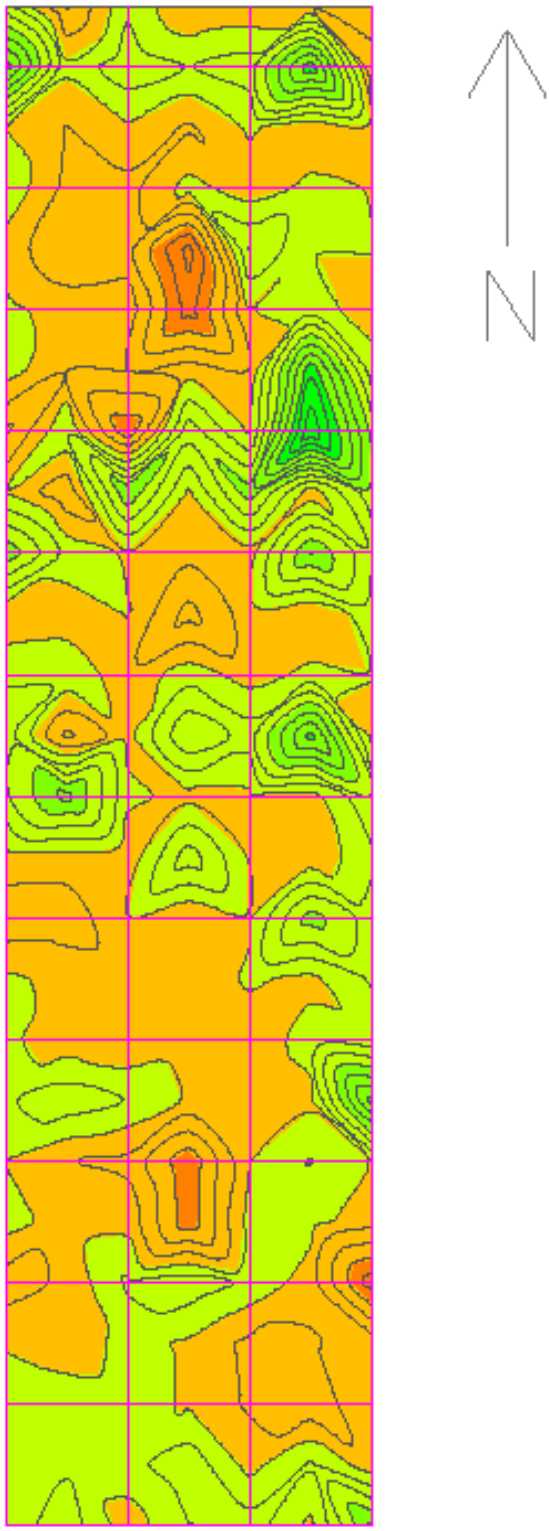

Figure E-47: Section C – Difference between 10/6/2011 and 10/27/2011

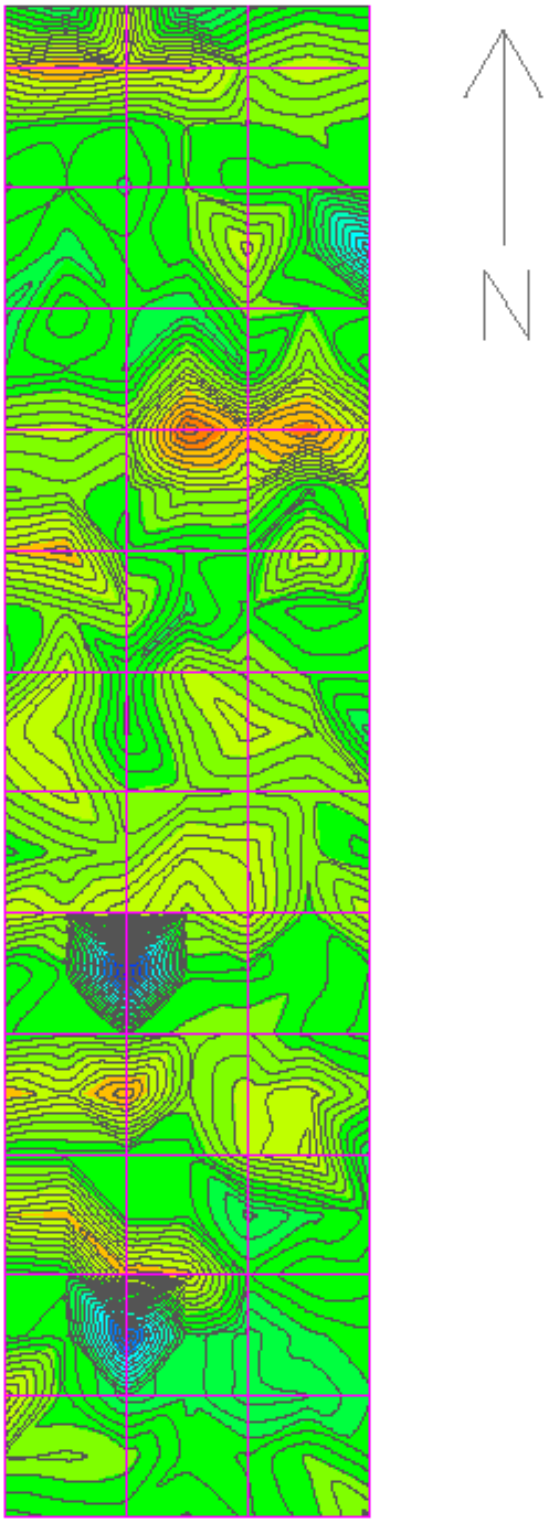

Figure E-48: Section C – Difference between 10/27/2011 and 4/10/2012

Figure E-49: Section C – Difference between 4/10/2012 and 5/9/2012

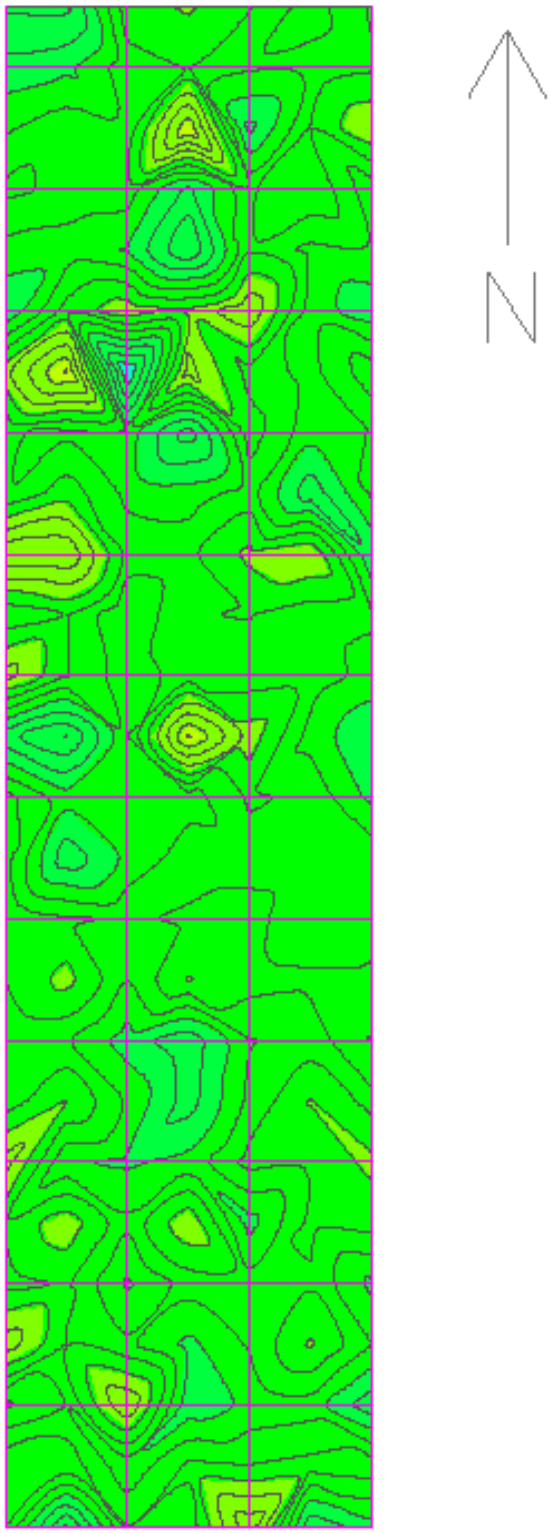

Figure E-50: Section D – Difference between 8/25/2011 and 10/6/2011

Figure E-51: Section D – Difference between 10/6/2011 and 10/27/2011

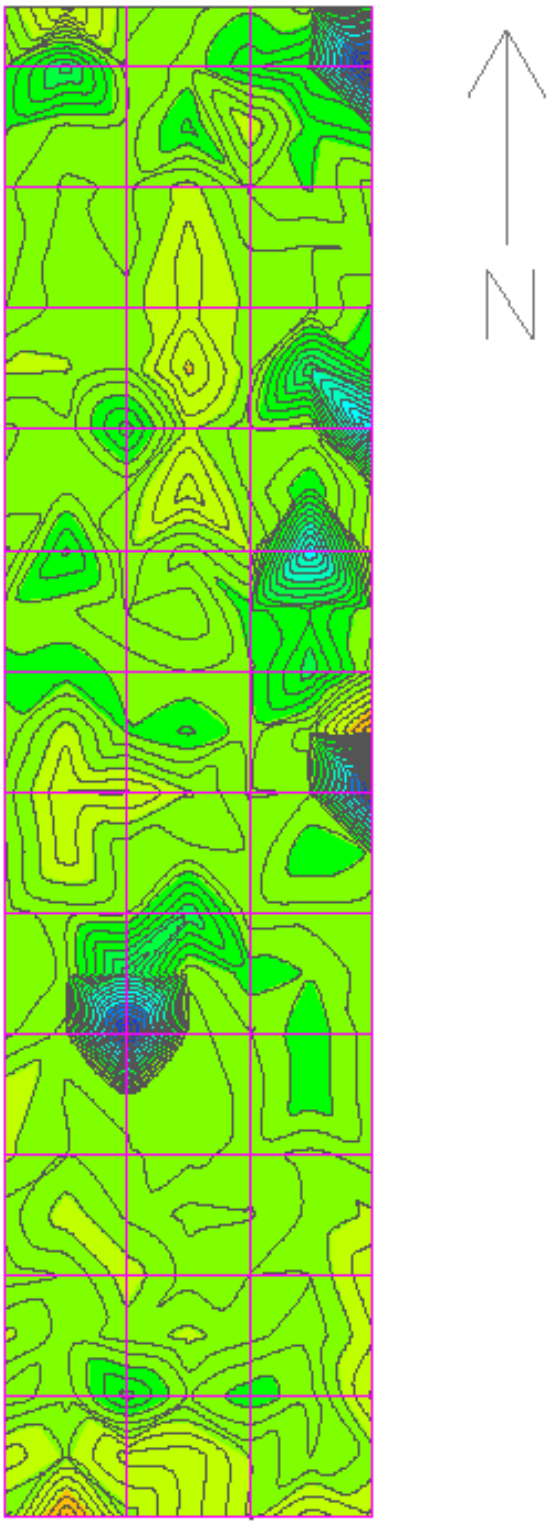

Figure E-52: Section D – Difference between 10/27/2011 and 4/10/2012

Figure E-53: Section D – Difference between 4/10/2012 and 5/9/2012

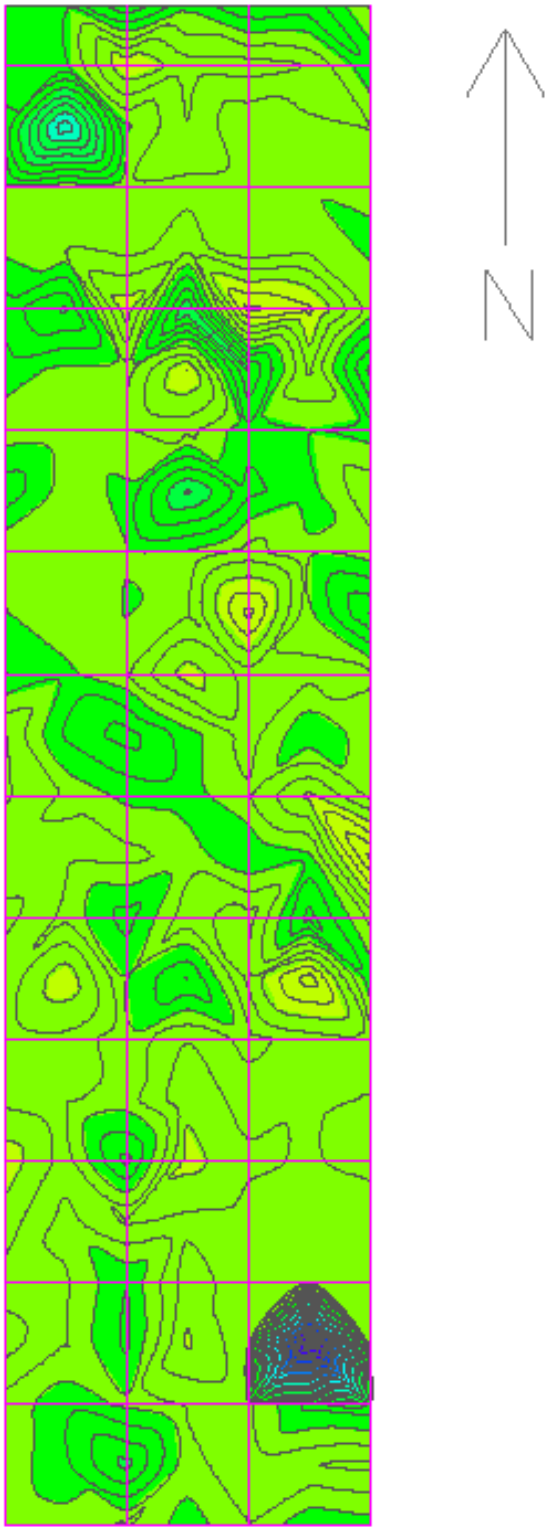

Figure E-54: Section E – Difference between 8/25/2011 and 10/6/2011

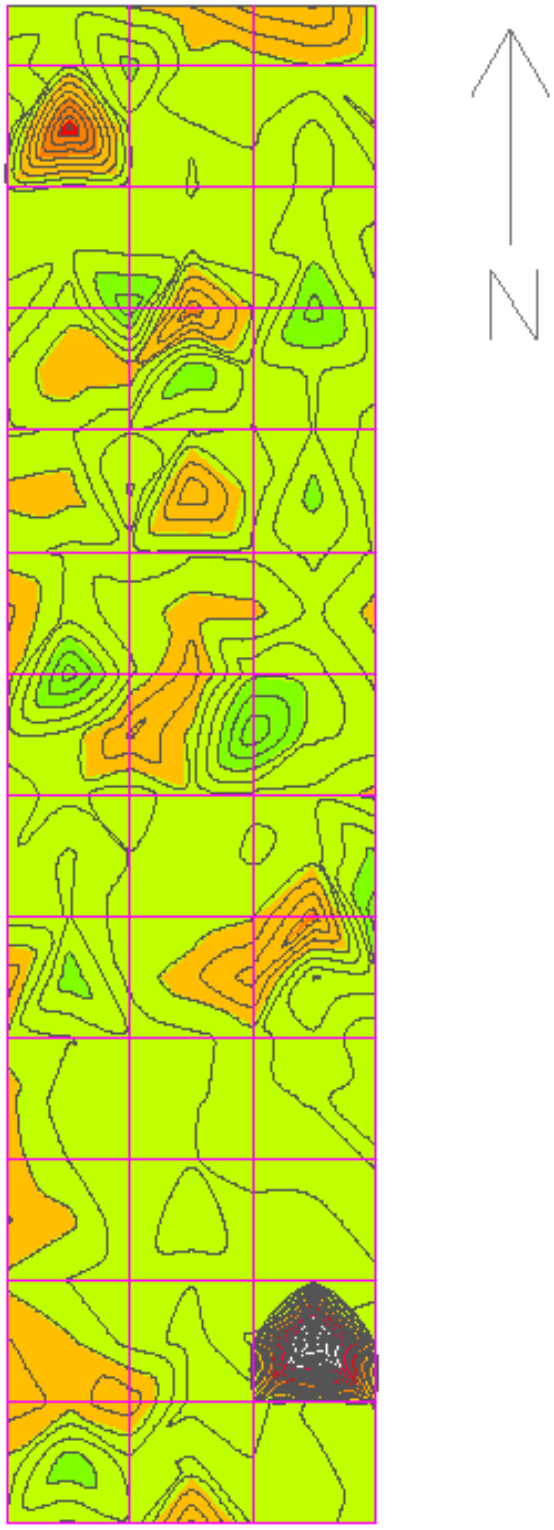

Figure E-55: Section E – Difference between 10/6/2011 and 10/27/2011

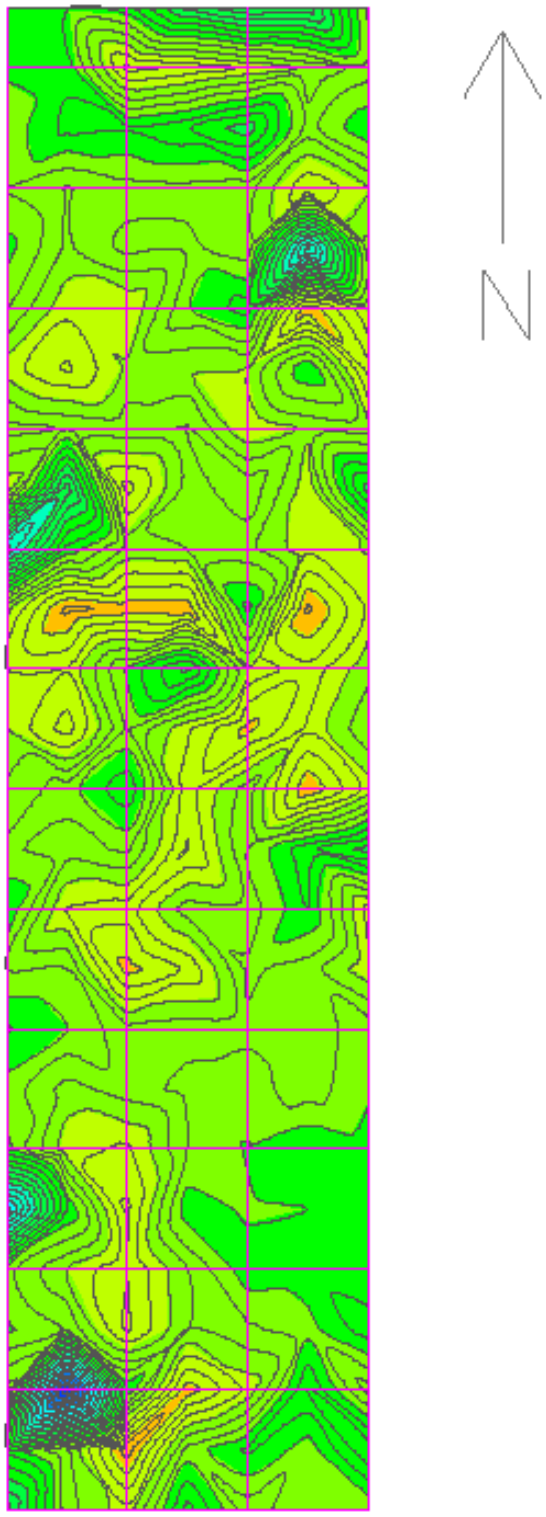

Figure E-56: Section E – Difference between 10/27/2011 and 4/10/2012

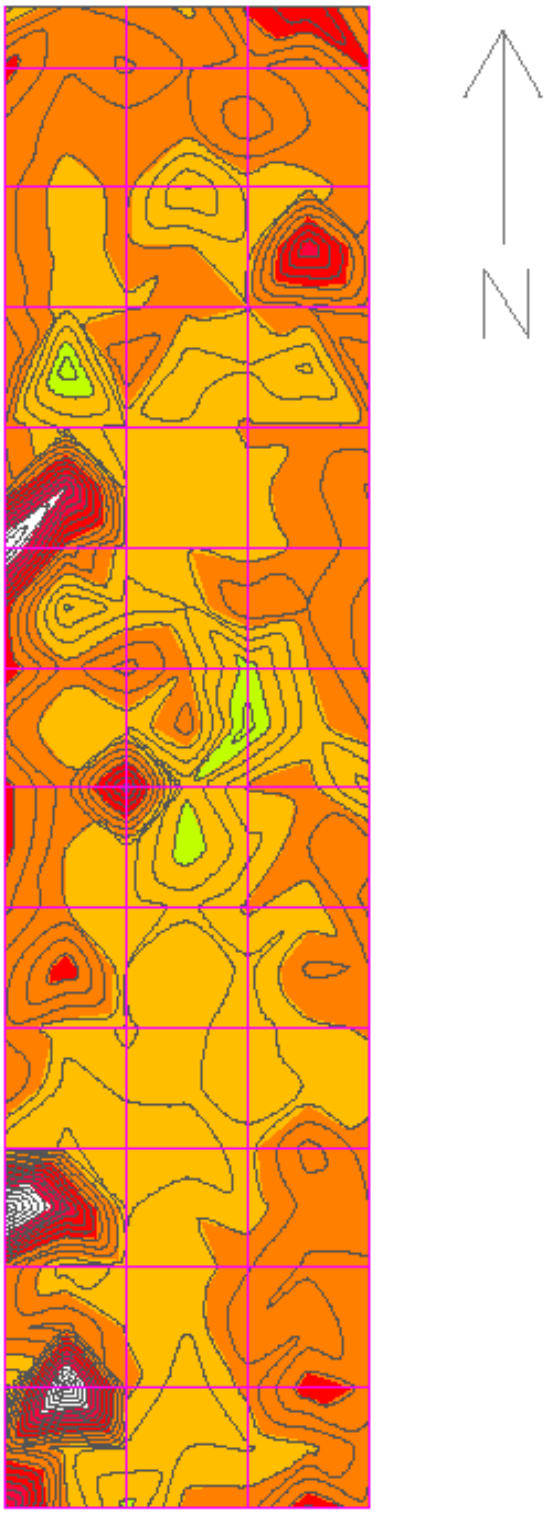

Figure E-57: Section E – Difference between 4/10/2012 and 5/9/2012

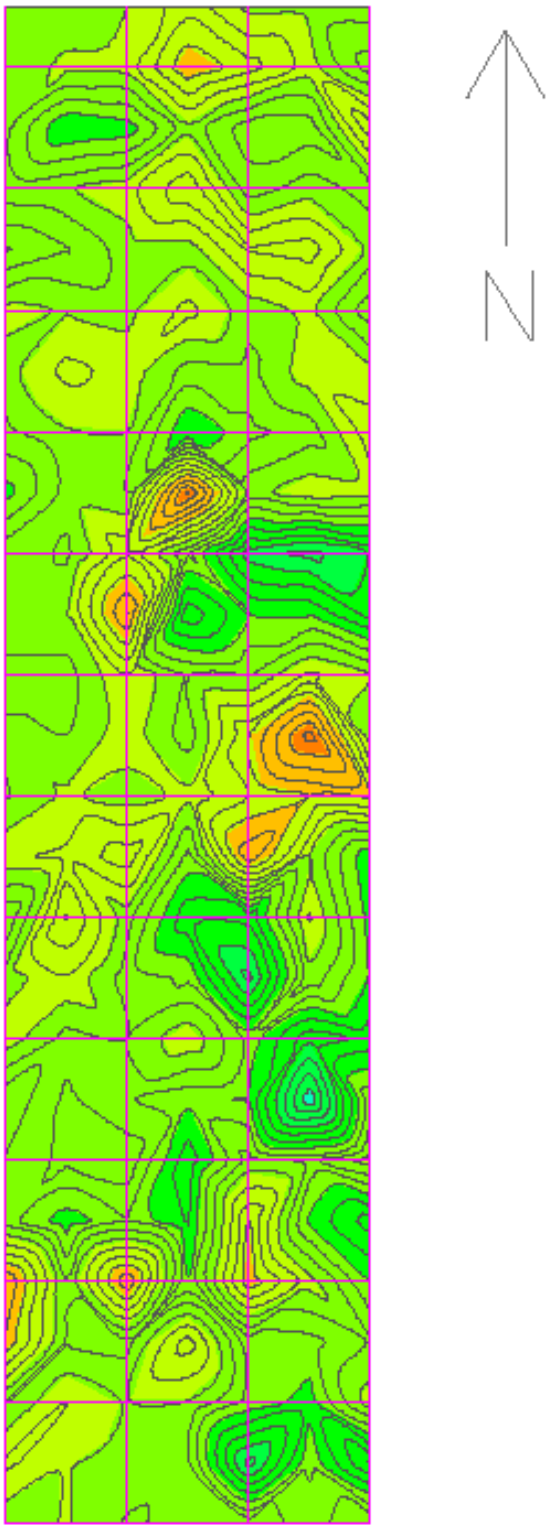

Figure E-58: Section F – Difference between 8/25/2011 and 10/6/2011

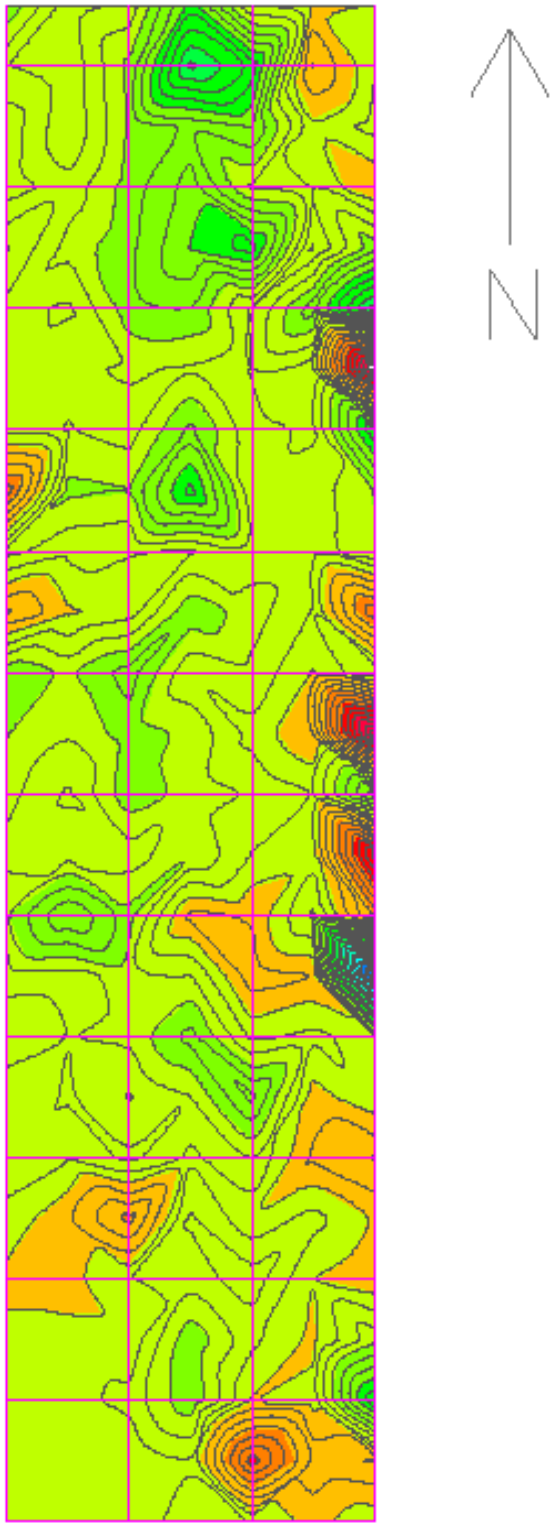

Figure E-59: Section F – Difference between 10/6/2011 and 10/27/2011

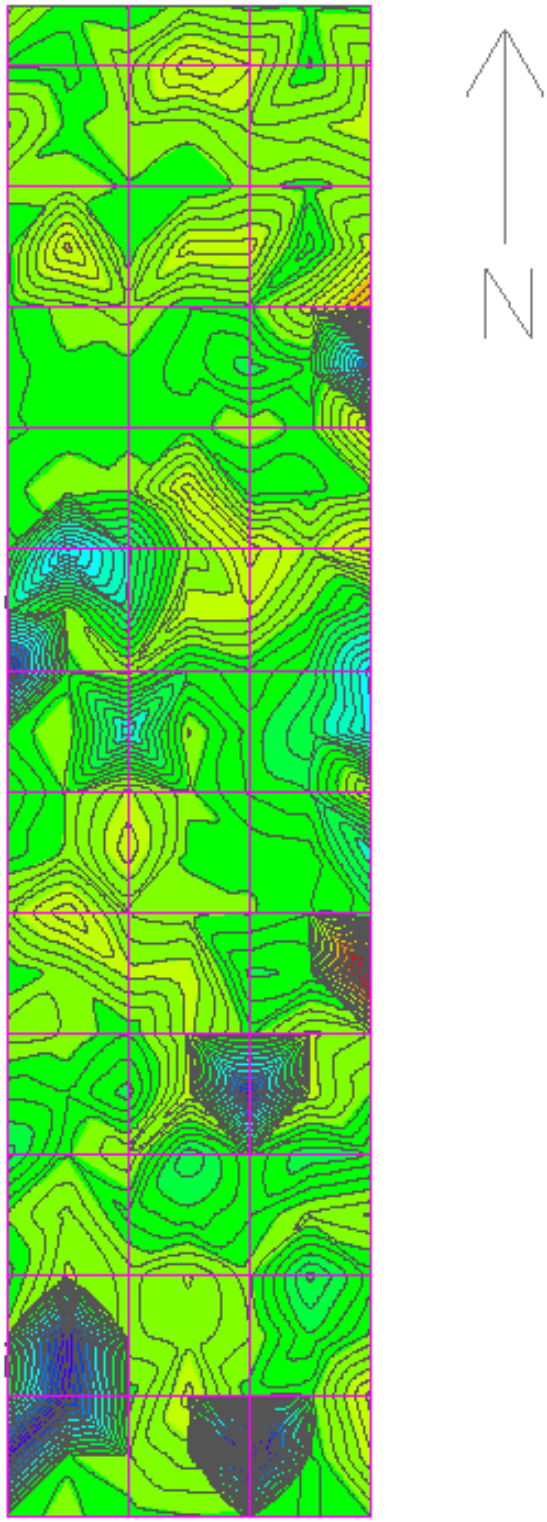

Figure E-60: Section F – Difference between 10/27/2011 and 4/10/2012

Figure E-61: Section F – Difference between 4/10/2012 and 5/9/2012

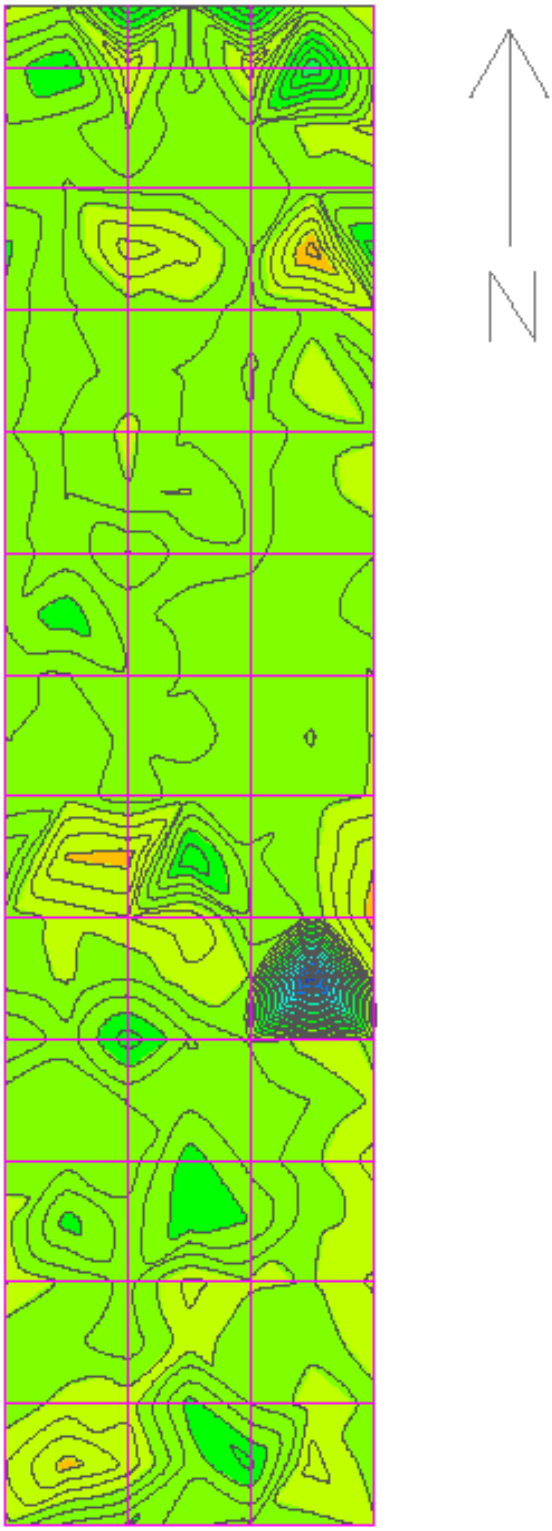

Figure E-62: Section G – Difference between 8/25/2011 and 10/6/2011

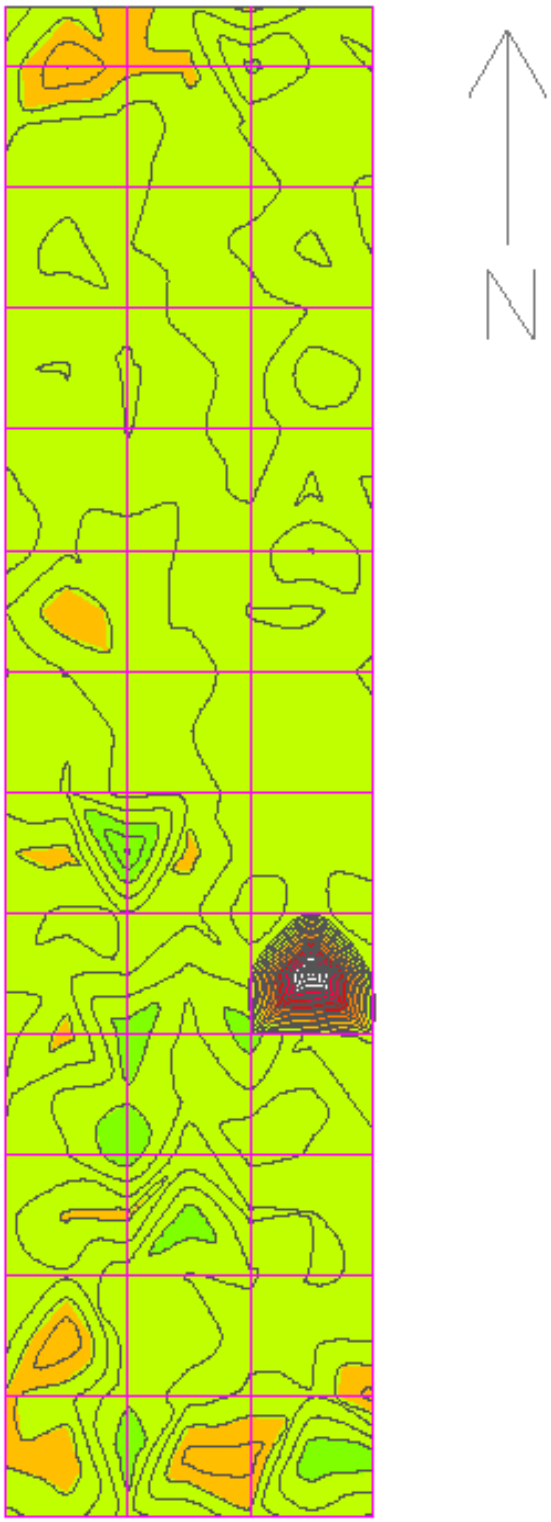

Figure E-63: Section G – Difference between 10/6/2011 and 10/27/2011

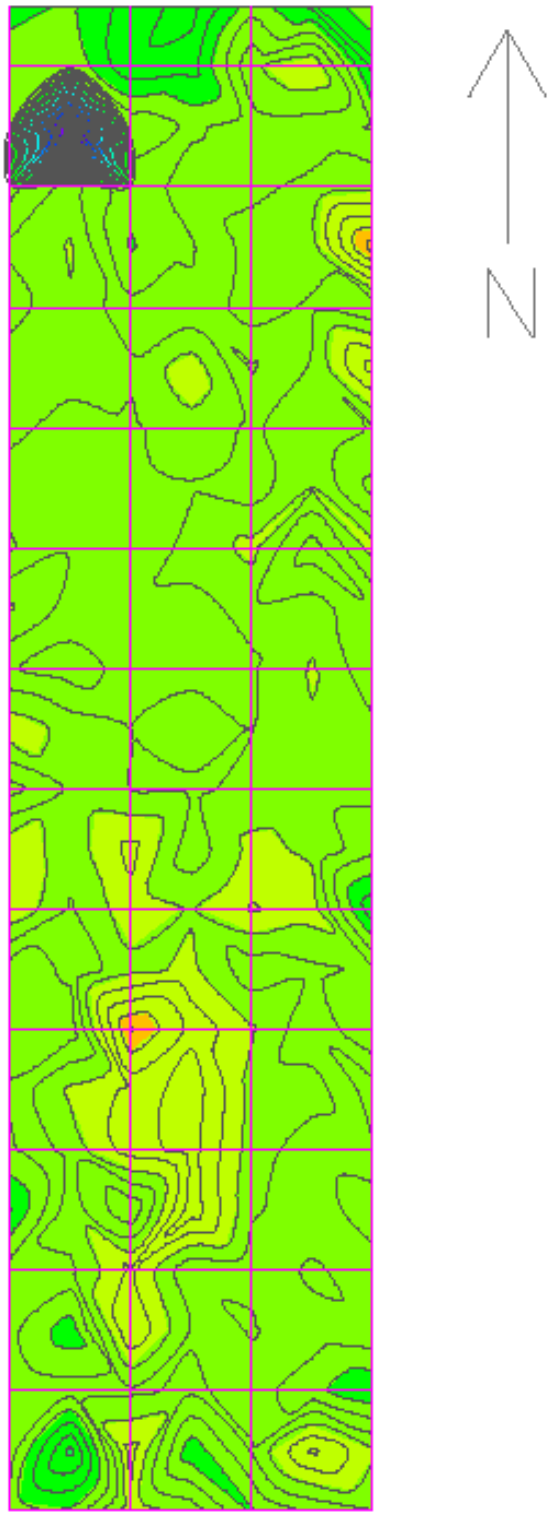

Figure E-64: Section G – Difference between 10/27/2011 and 4/10/2012

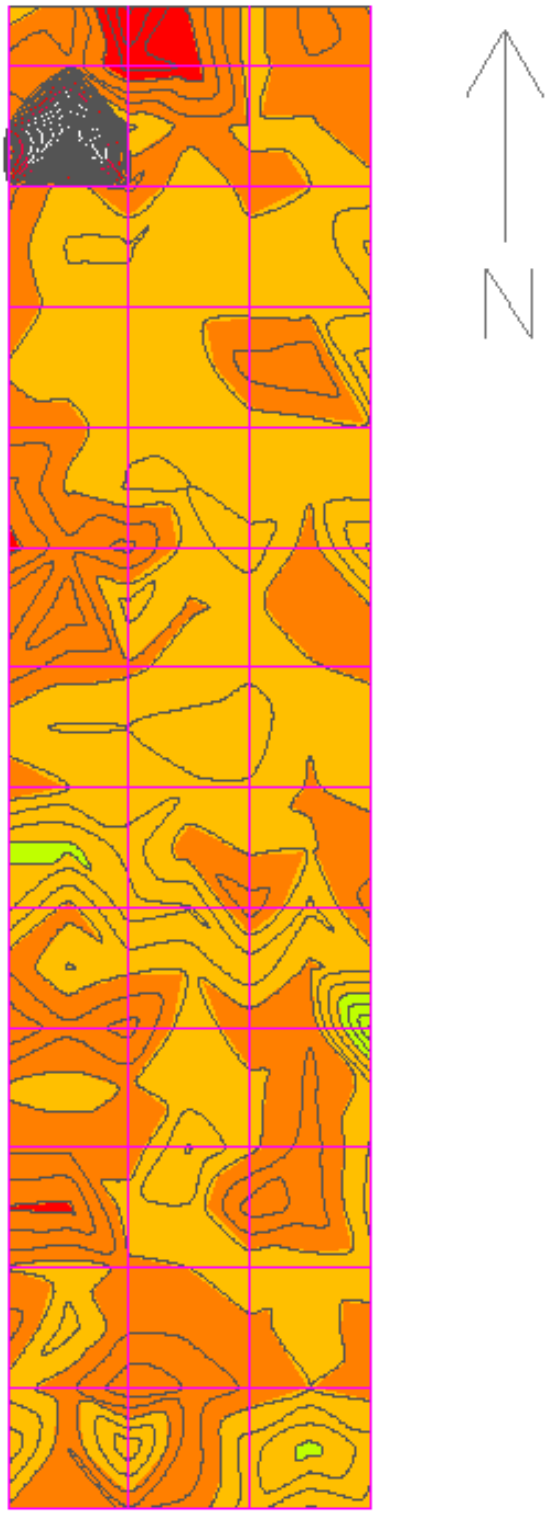

Figure E-65: Section G – Difference between 4/10/2012 and 5/9/2012

APPENDIX F. PLOTS OF HALF-CELL POTENTIAL MEASUREMENTS FOR FIELD TESTING OF MITIGATION PRODUCTS

Figure F-1 through Figure F-35 show plots of the half-cell potential measurements at the date indicated.

Figure F-36 through Figure F-70 show plots of the differences between half-cell measurements at the dates indicated.

Section A – MCI-2018

Section B – Protectosil CIT and Ferrogard 903

Section C – Protectosil CIT

Section D – Ferrogard 903

Section E – Duralprep 3020

Section F – Chemtrete 40

Section G – Control

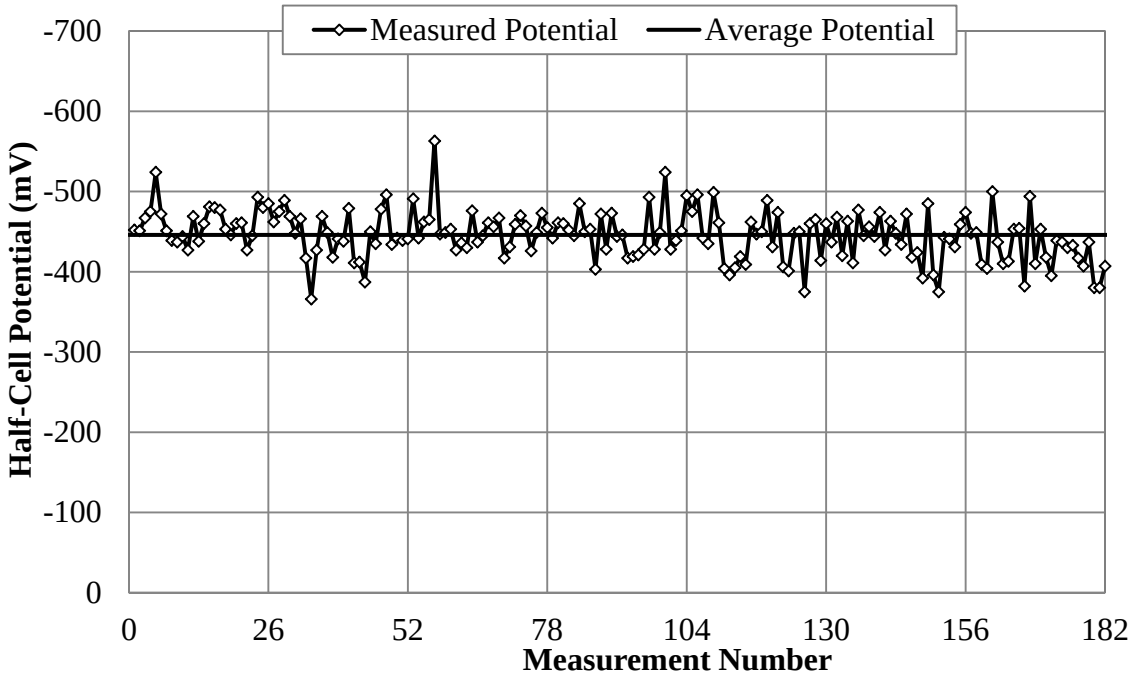

Figure F-1: Section A – Half-cell potential on 8/25/11

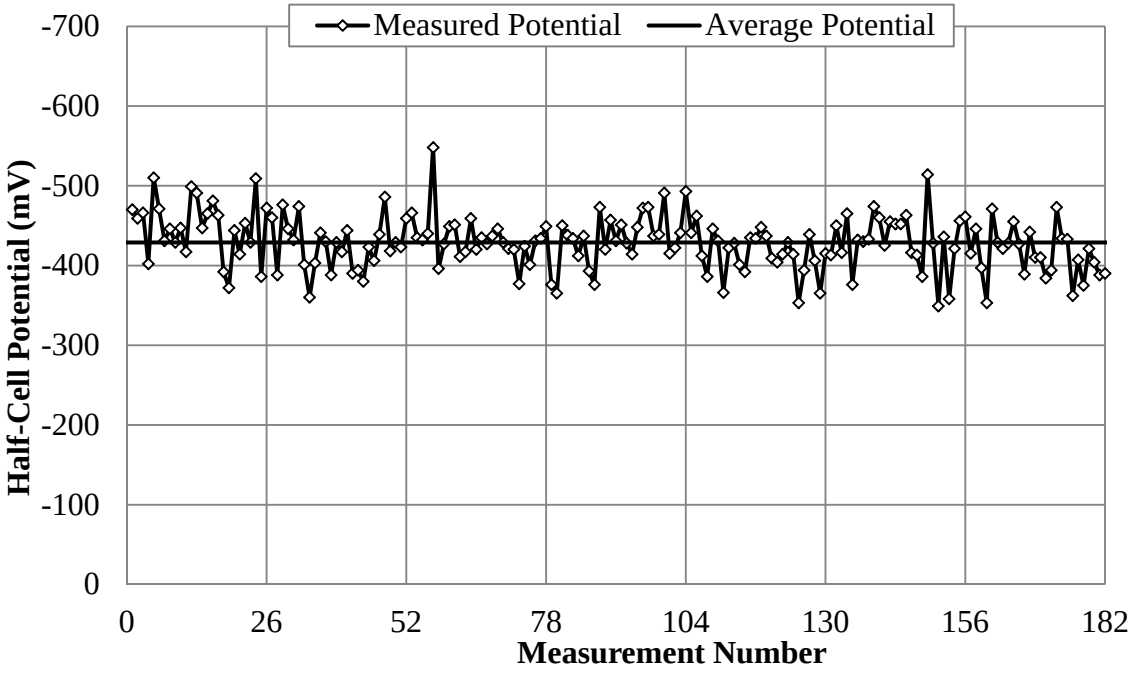

Figure F-2: Section A – Half-cell potential on 10/6/11

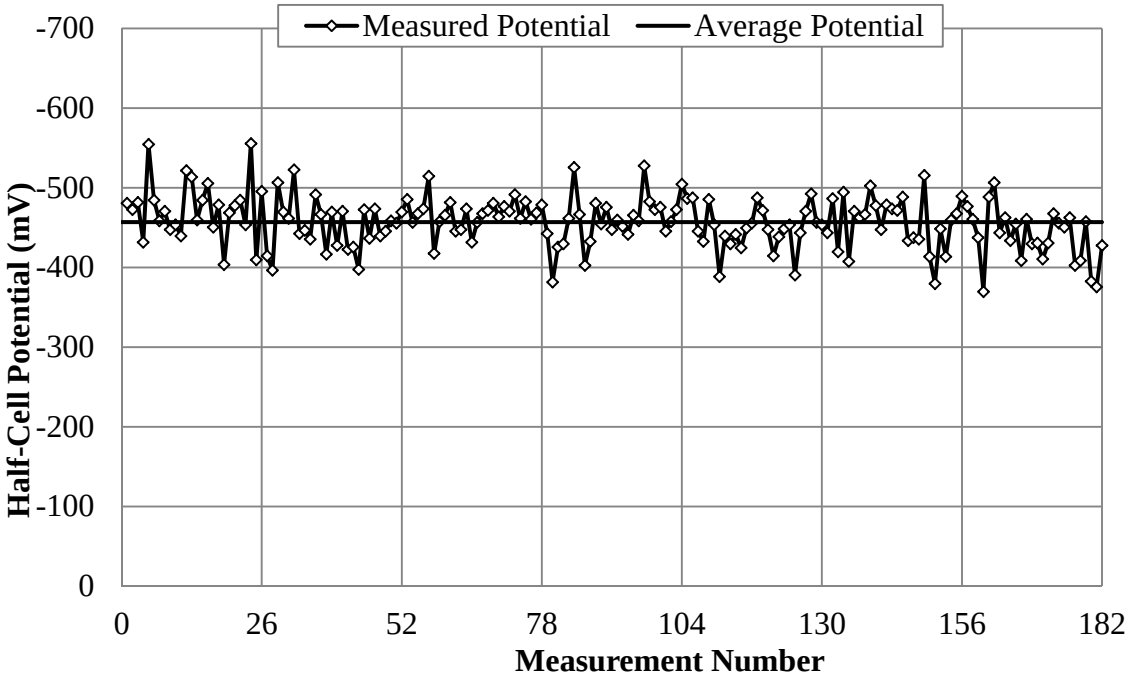

Figure F-3: Section A – Half-cell potential on 10/27/11

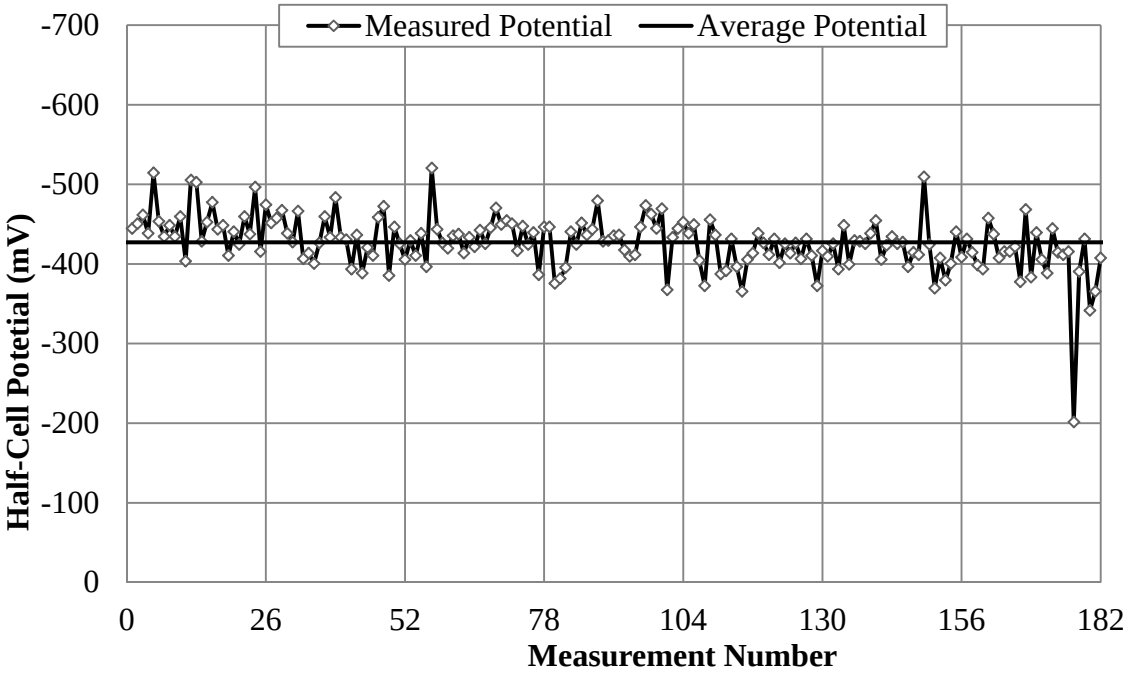

Figure F-4: Section A – Half-cell potential on 4/10/12

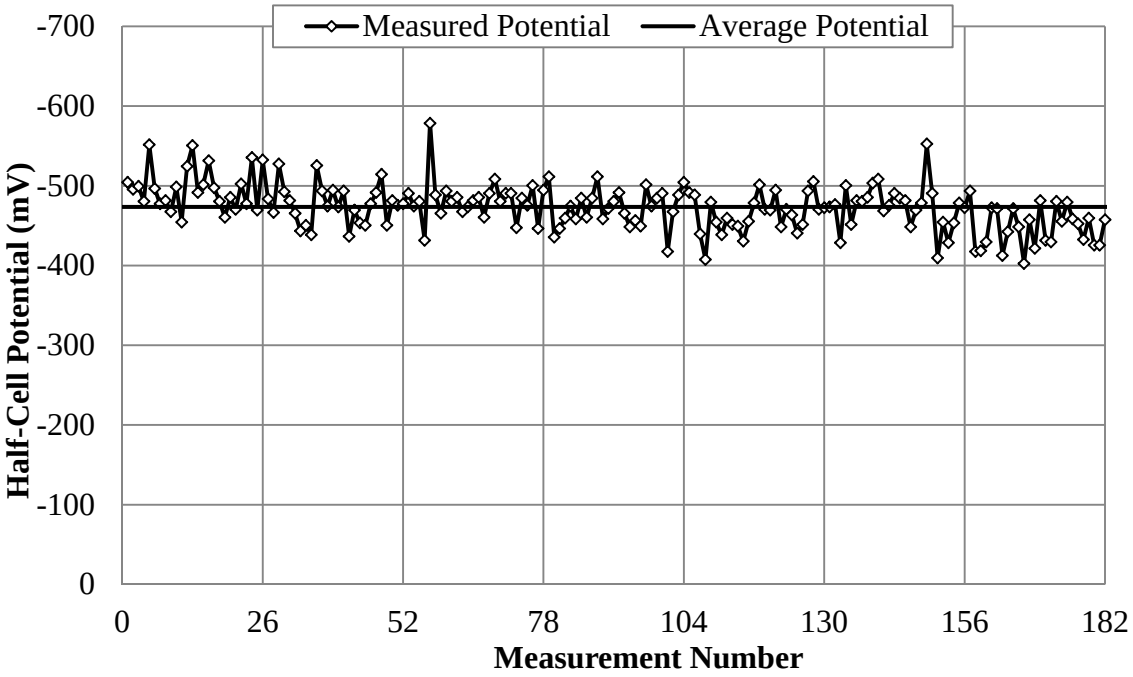

Figure F-5: Section A – Half-cell potential on 5/9/12

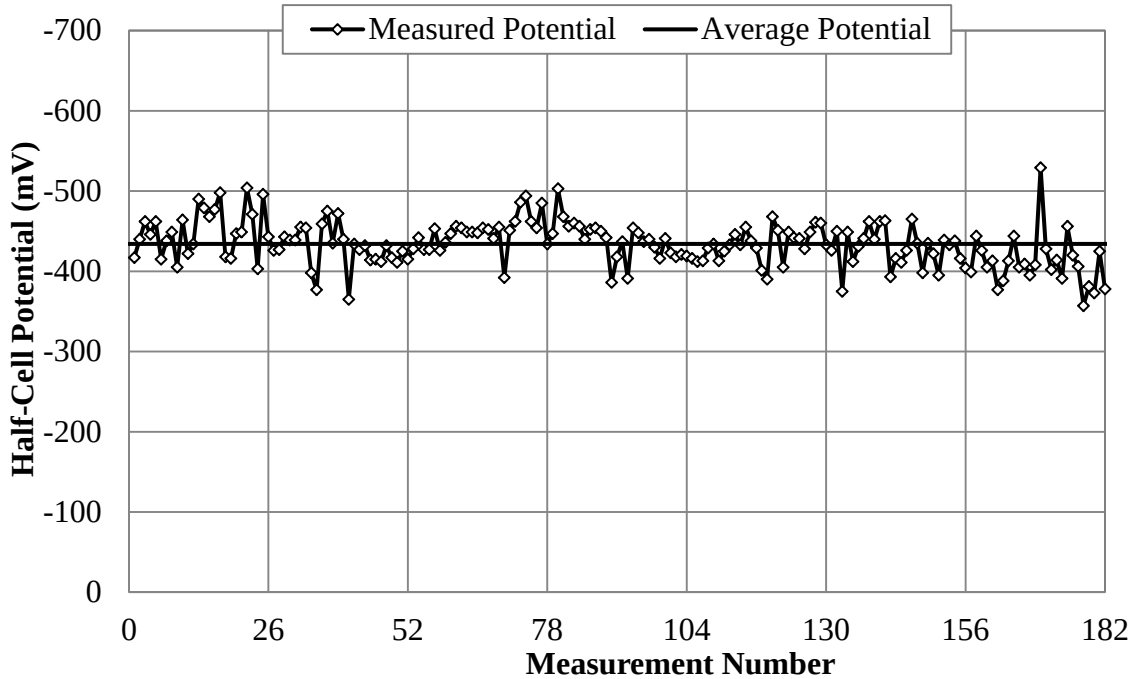

Figure F-6: Section B – Half-cell potential on 8/25/11

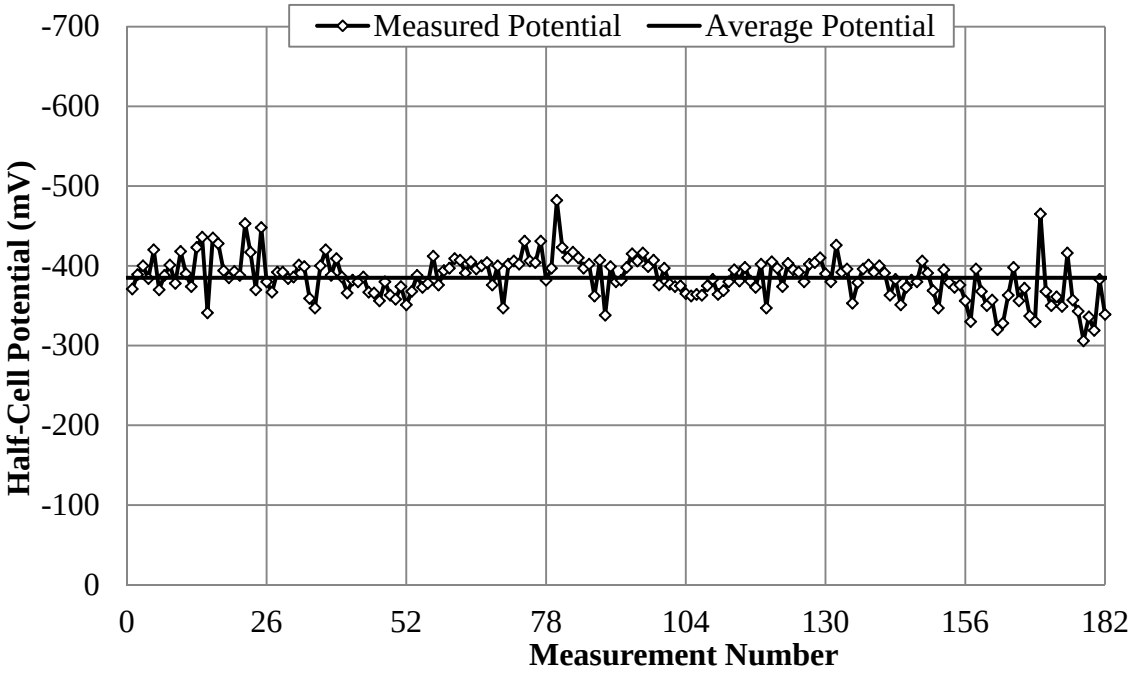

Figure F-7: Section B – Half-cell potential on 10/6/11

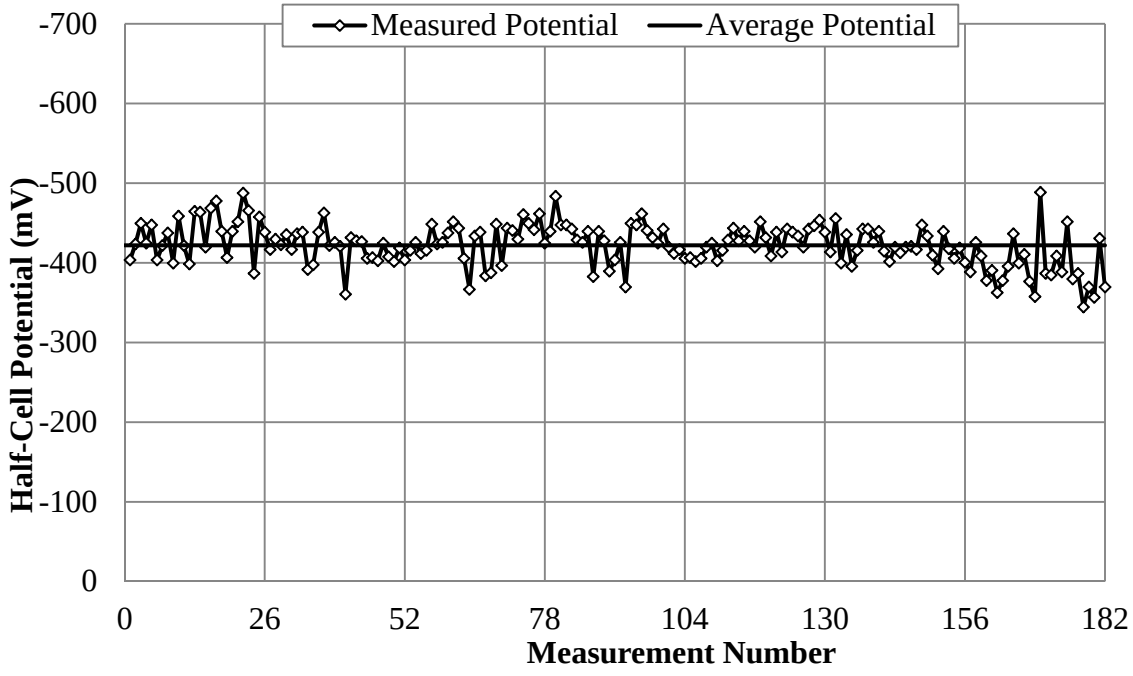

Figure F-8: Section B – Half-cell potential in 10/27/11

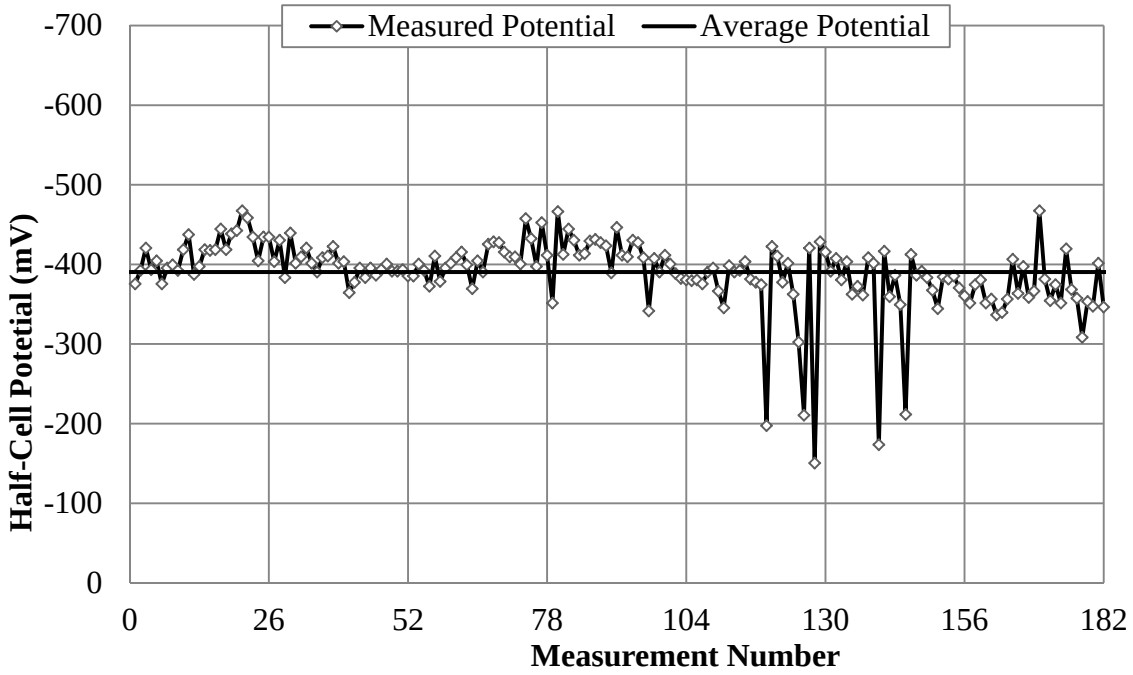

Figure F-9: Section B – Half-cell potential on 4/10/12

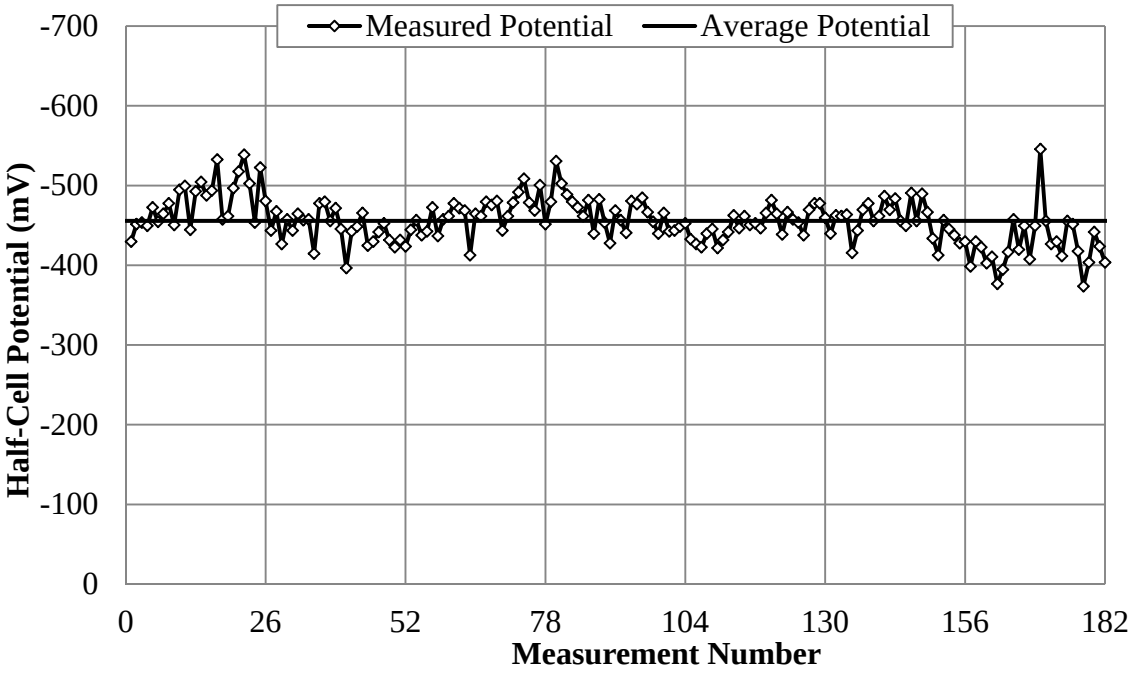

Figure F-10: Section B – Half-cell potential on 5/9/12

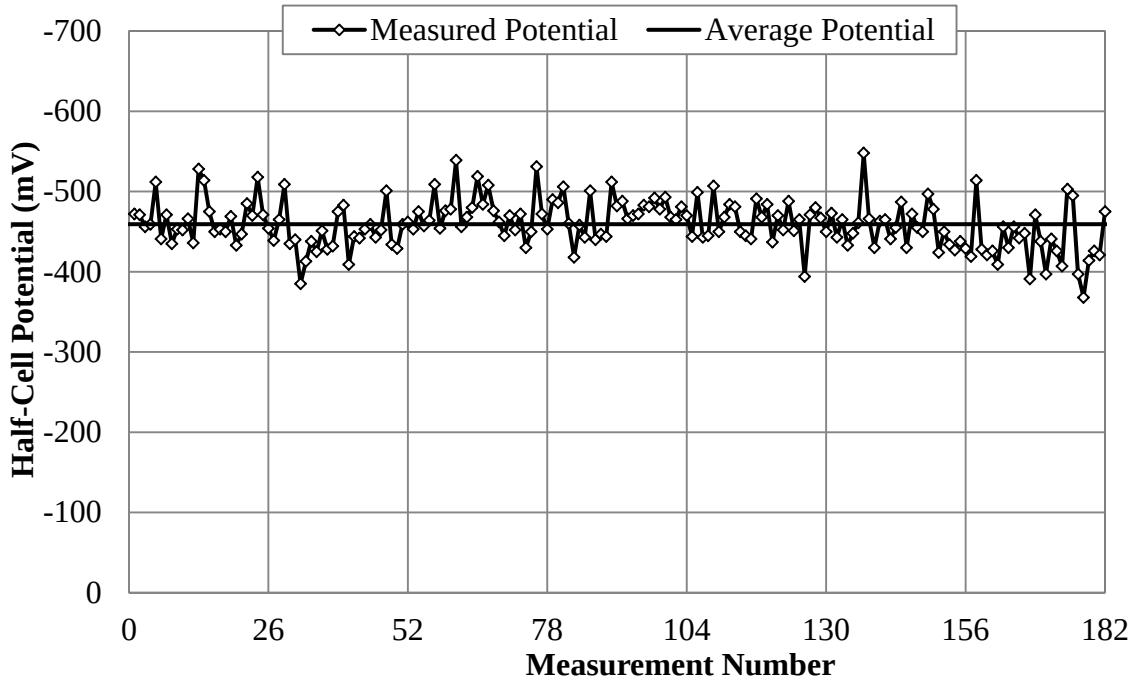

Figure F-11: Section C – Half-cell potential on 8/25/11

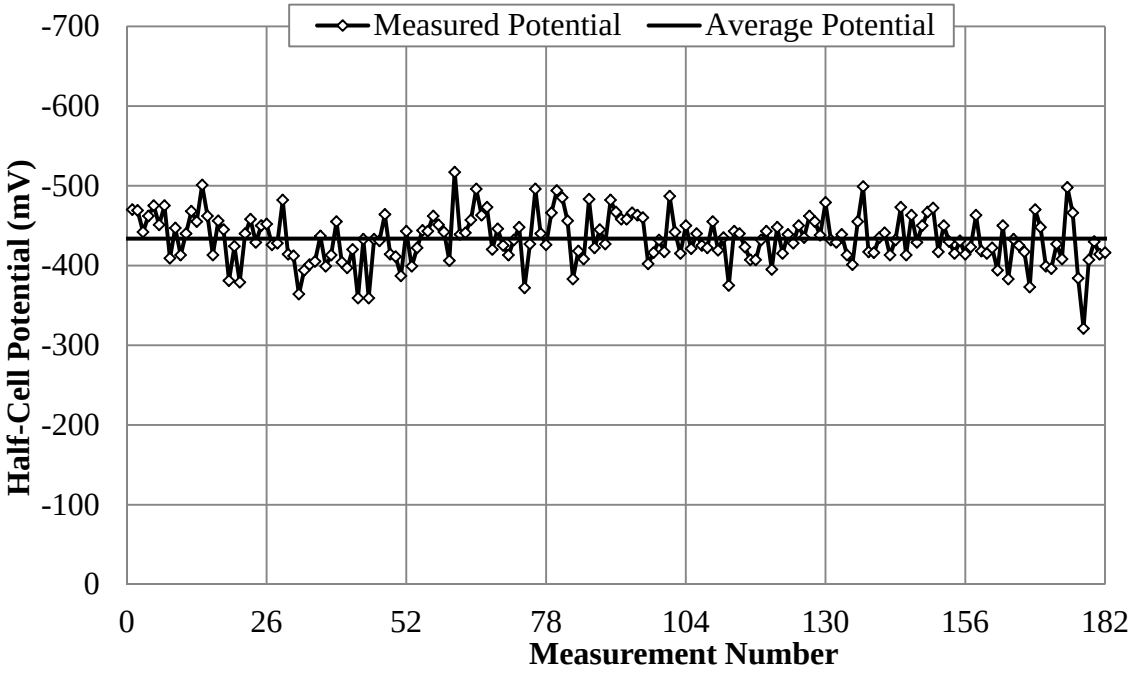

Figure F-12: Section C – Half-cell potential on 10/6/11

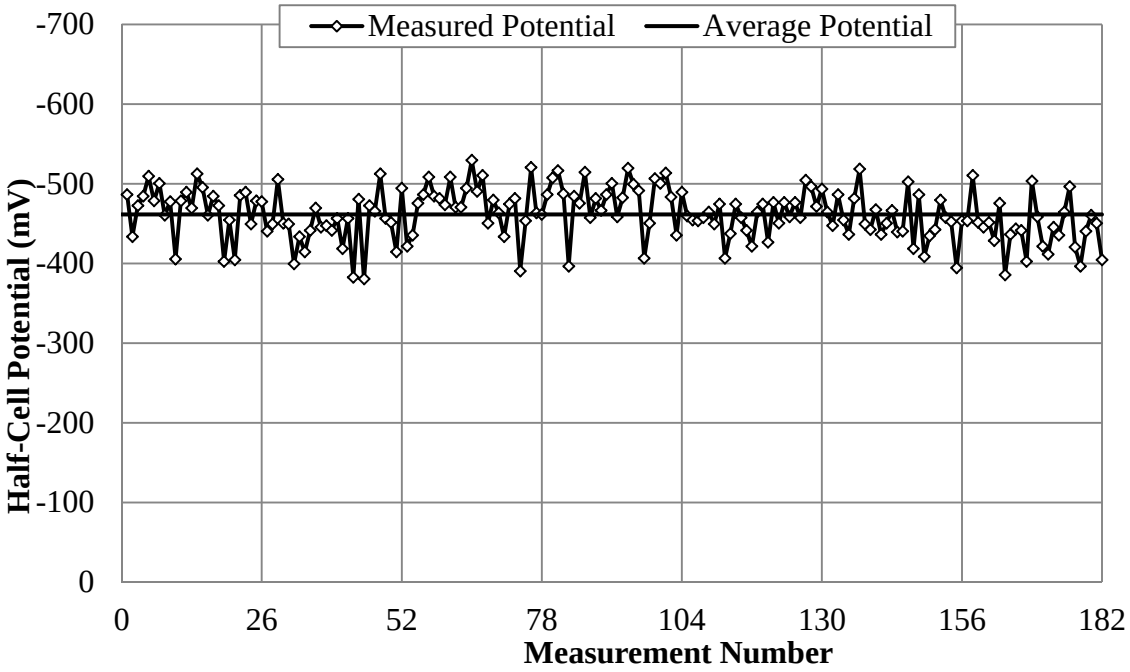

Figure F-13: Section C – Half-cell potential in 10/27/11

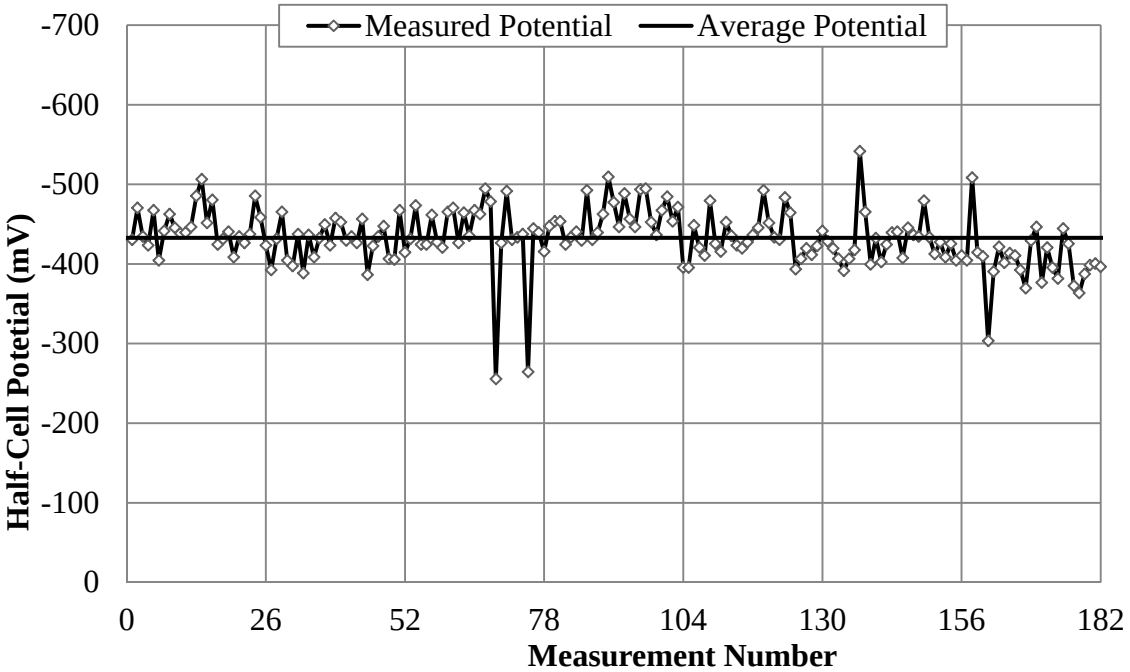

Figure F-14: Section C – Half-cell potential on 4/10/12

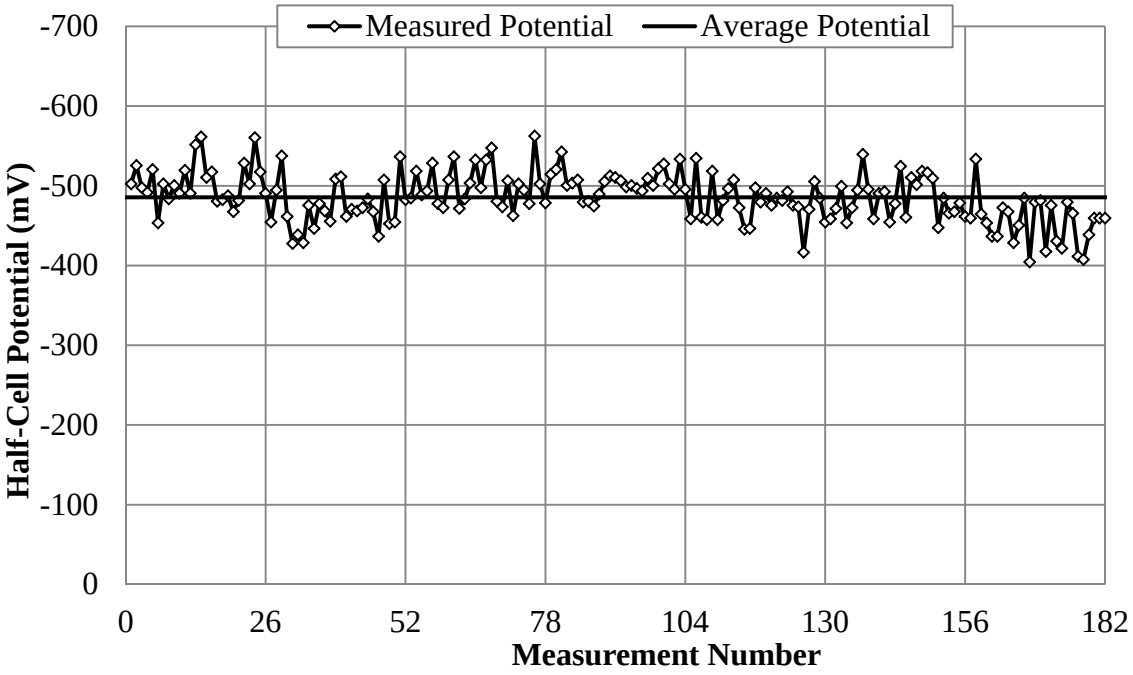

Figure F-15: Section C – Half-cell potential on 5/9/12

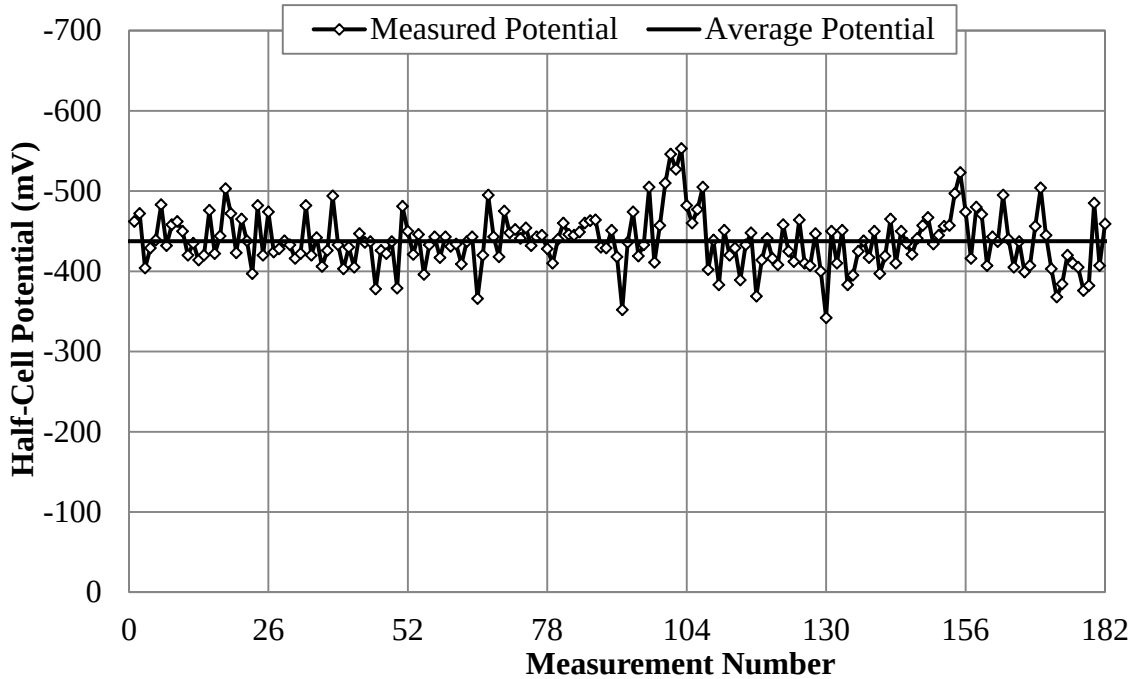

Figure F-16: Section D – Half-cell potential on 8/25/11

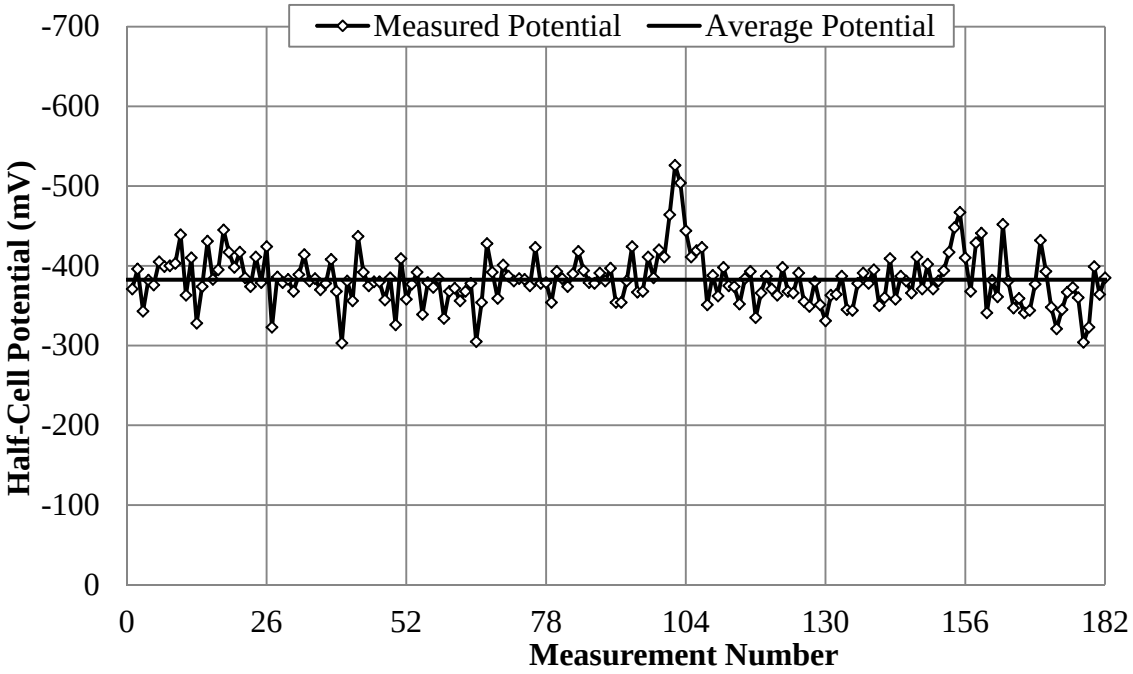

Figure F-17: Section D – Half-cell potential on 10/6/11

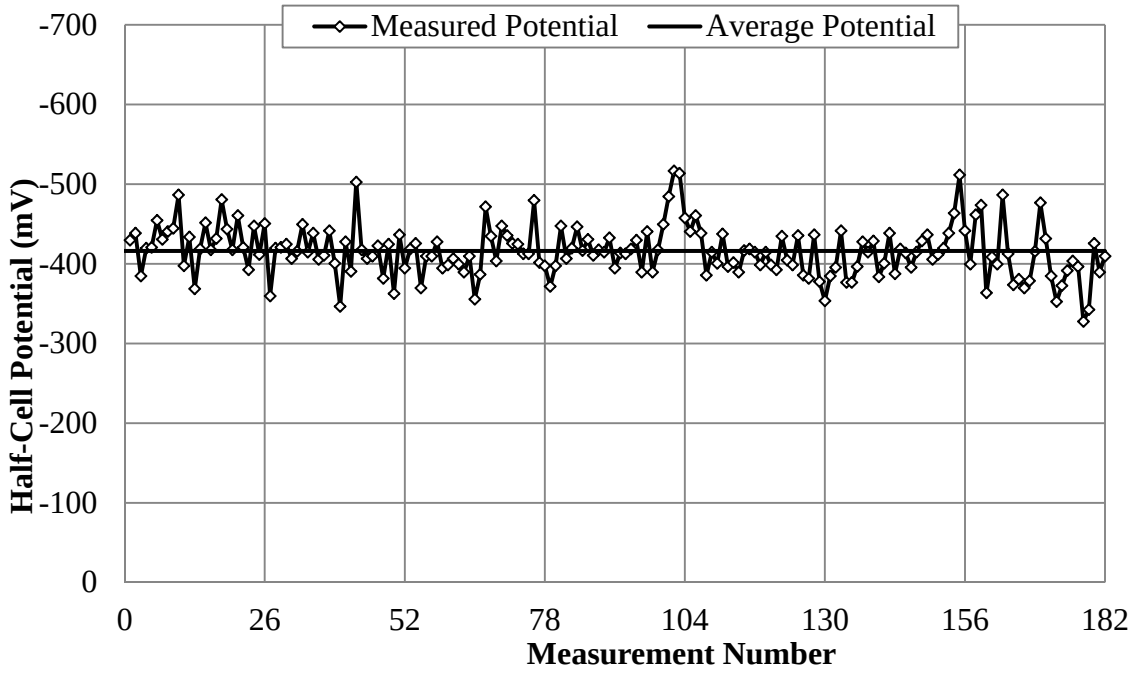

Figure F-18: Section D – Half-cell potential in 10/27/11

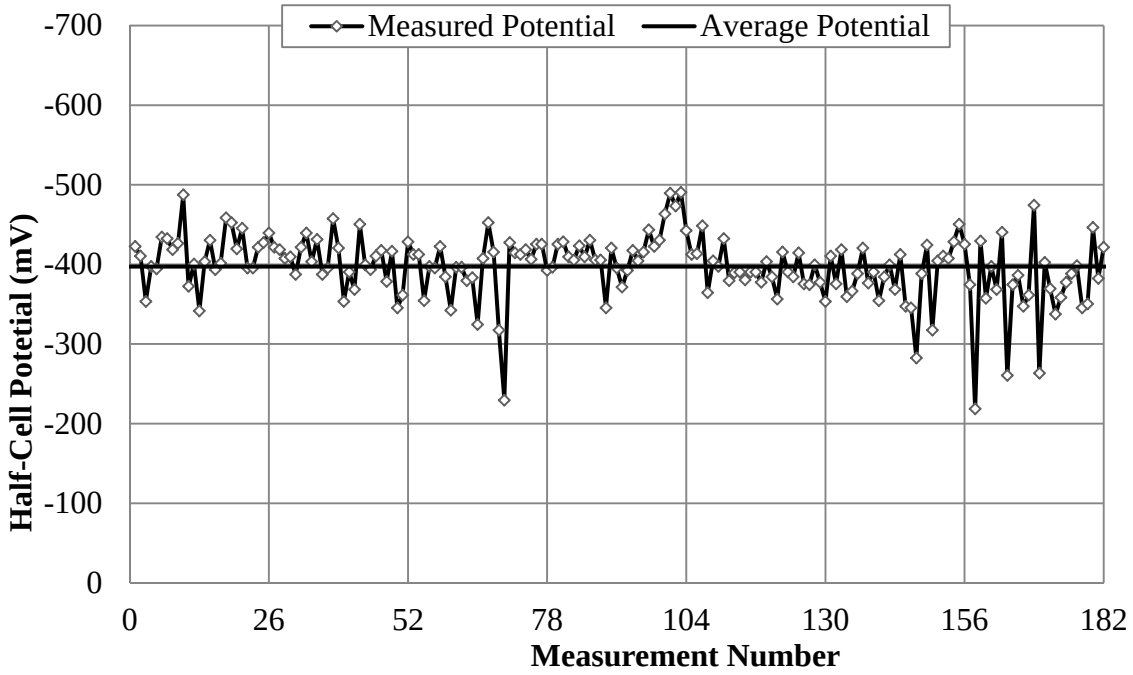

Figure F-19: Section D – Half-cell potential on 4/10/12

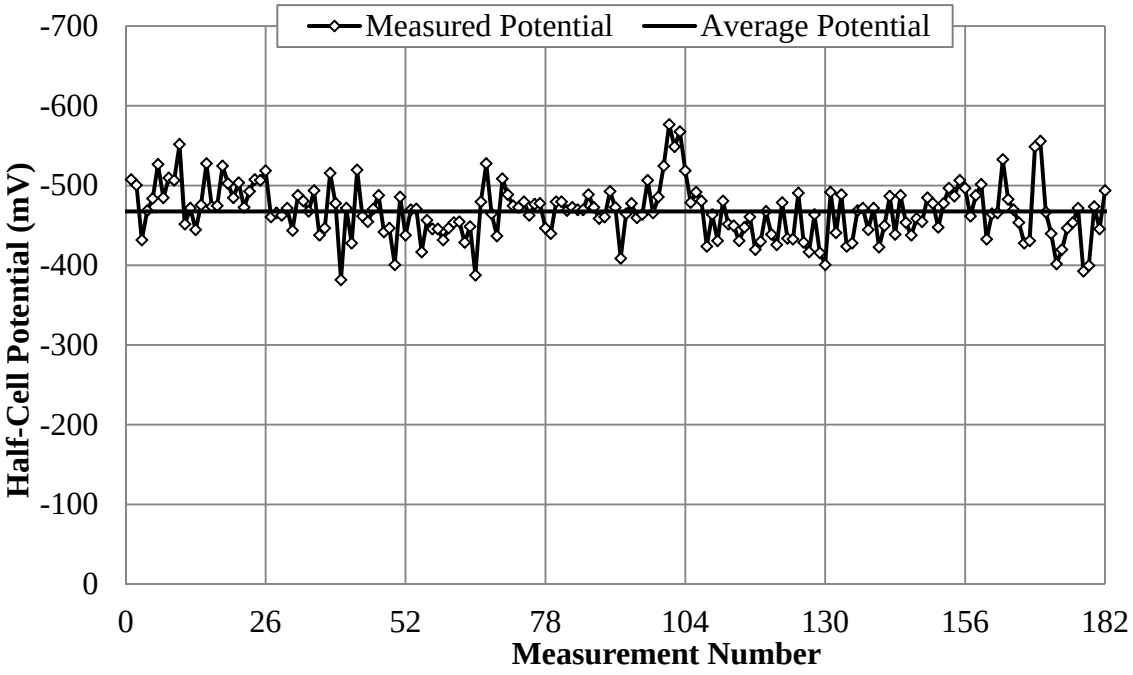

Figure F-20: Section D – Half-cell potential on 5/9/12

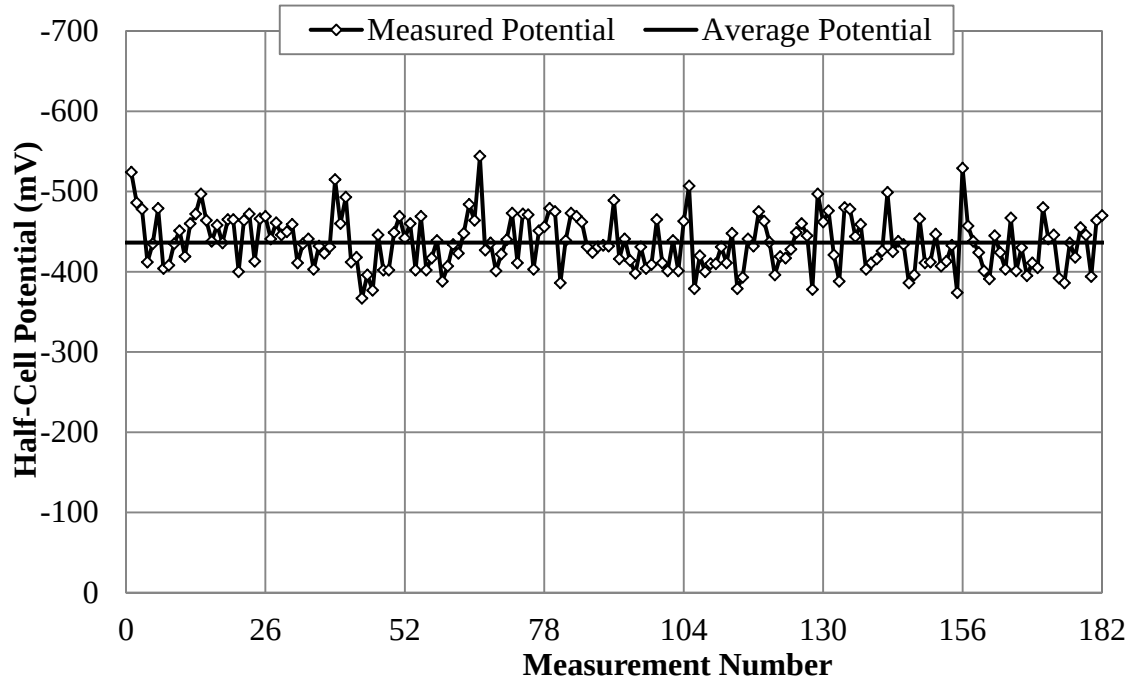

Figure F-21: Section E – Half-cell potential on 8/25/11

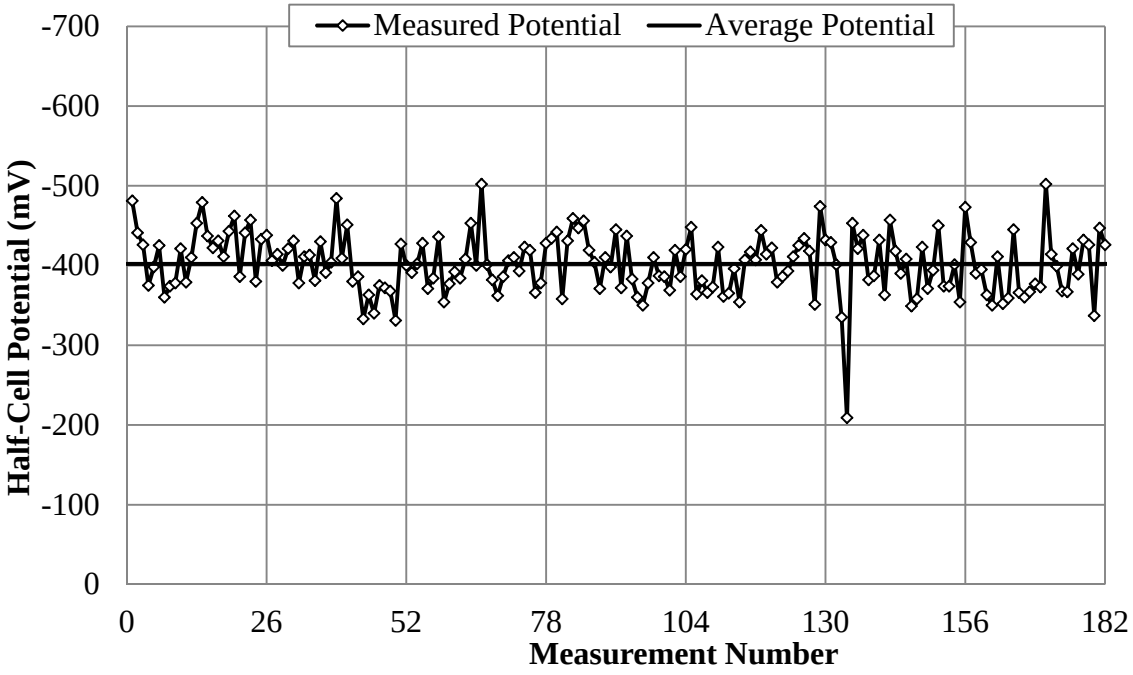

Figure F-22: Section E – Half-cell potential on 10/6/11

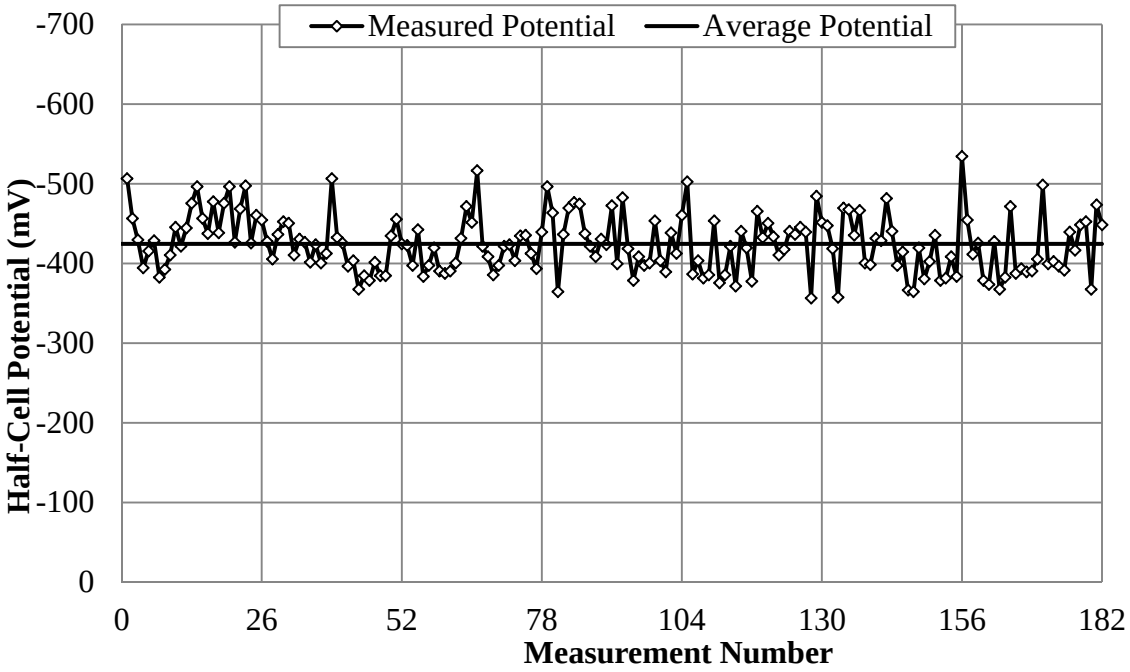

Figure F-23: Section E – Half-cell potential on 10/27/11

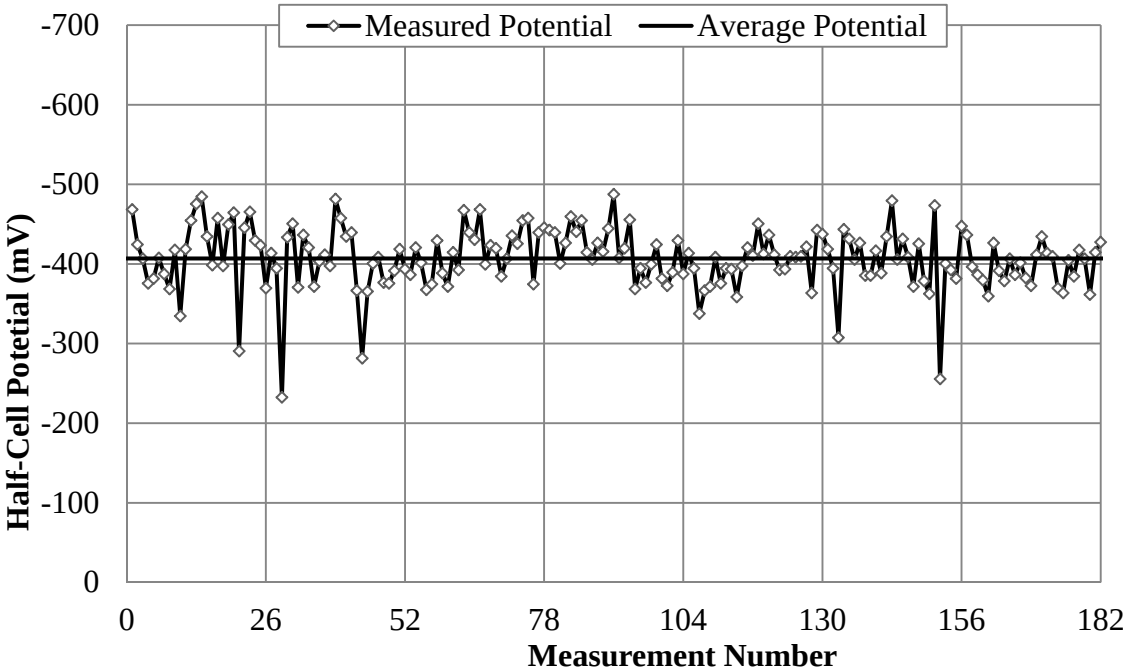

Figure F-24: Section E – Half-cell potential on 4/10/12

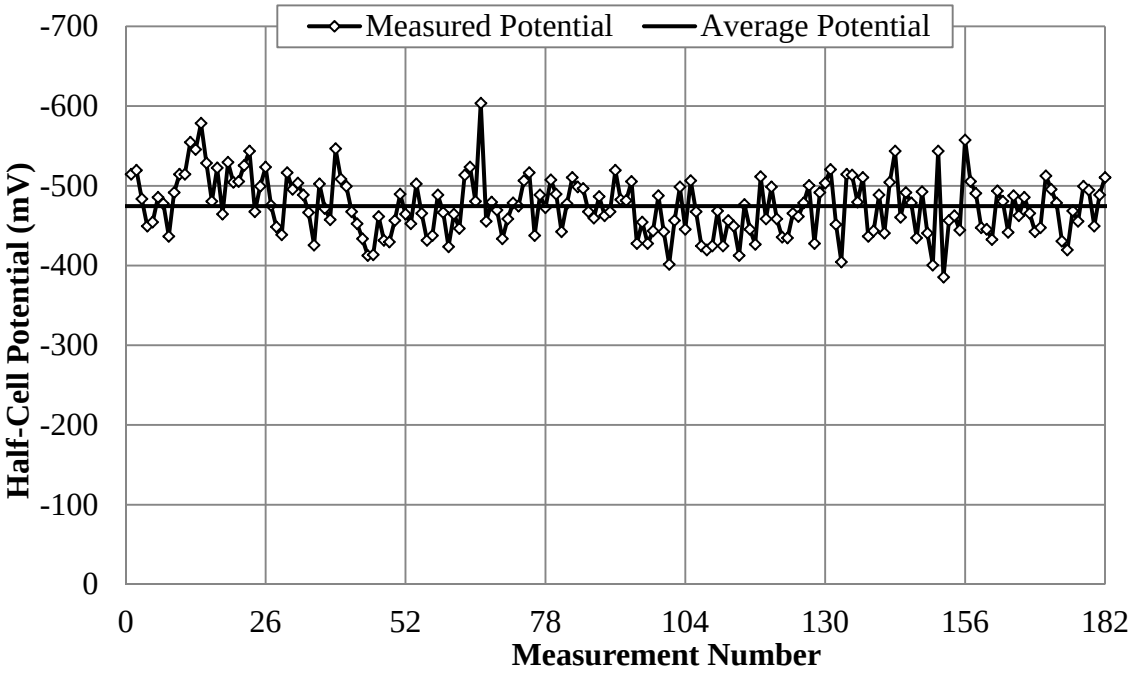

Figure F-25: Section E – Half-cell potential on 5/9/12

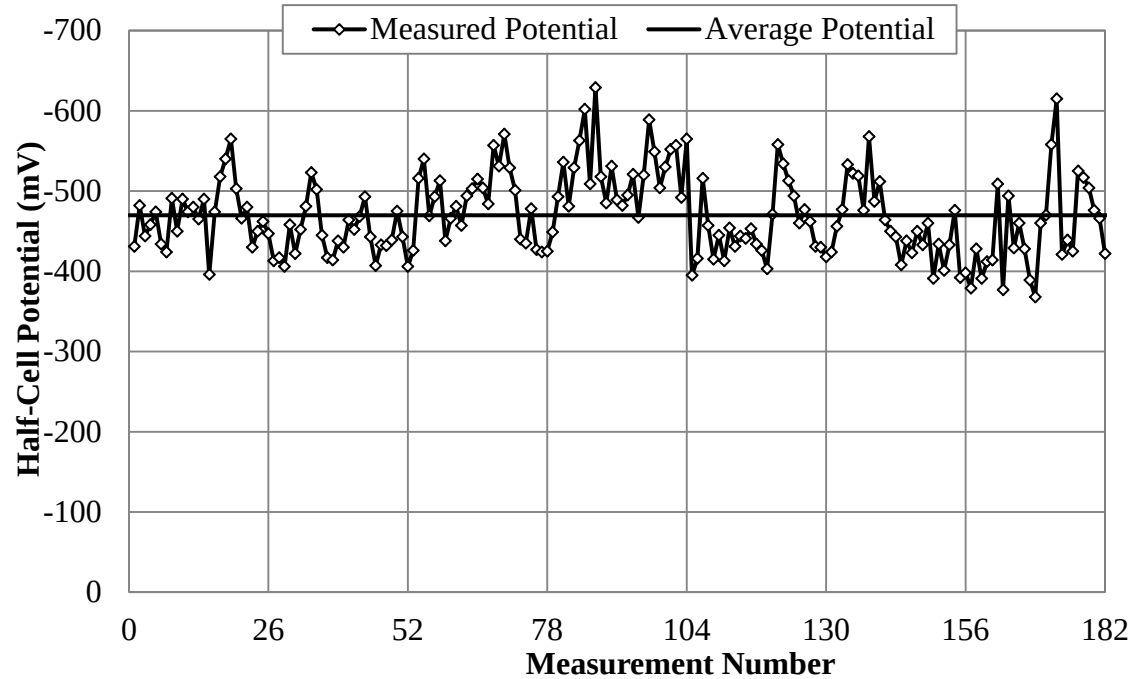

Figure F-26: Section F – Half-cell potential on 8/25/11

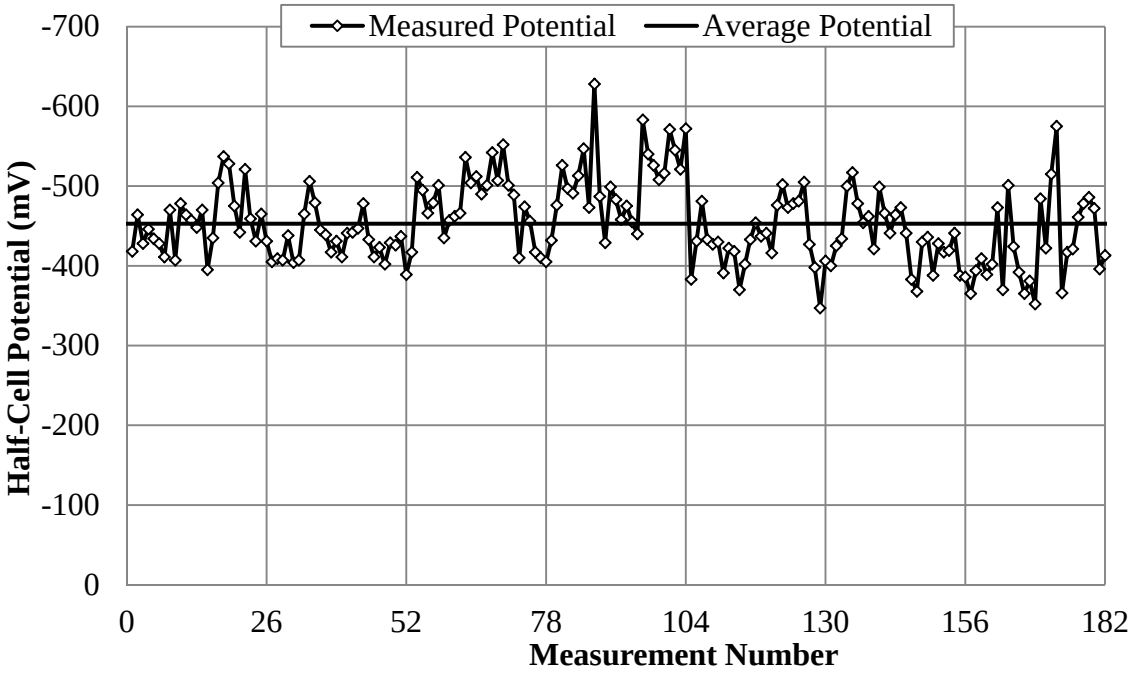

Figure F-27: Section F – Half-cell potential on 10/6/11

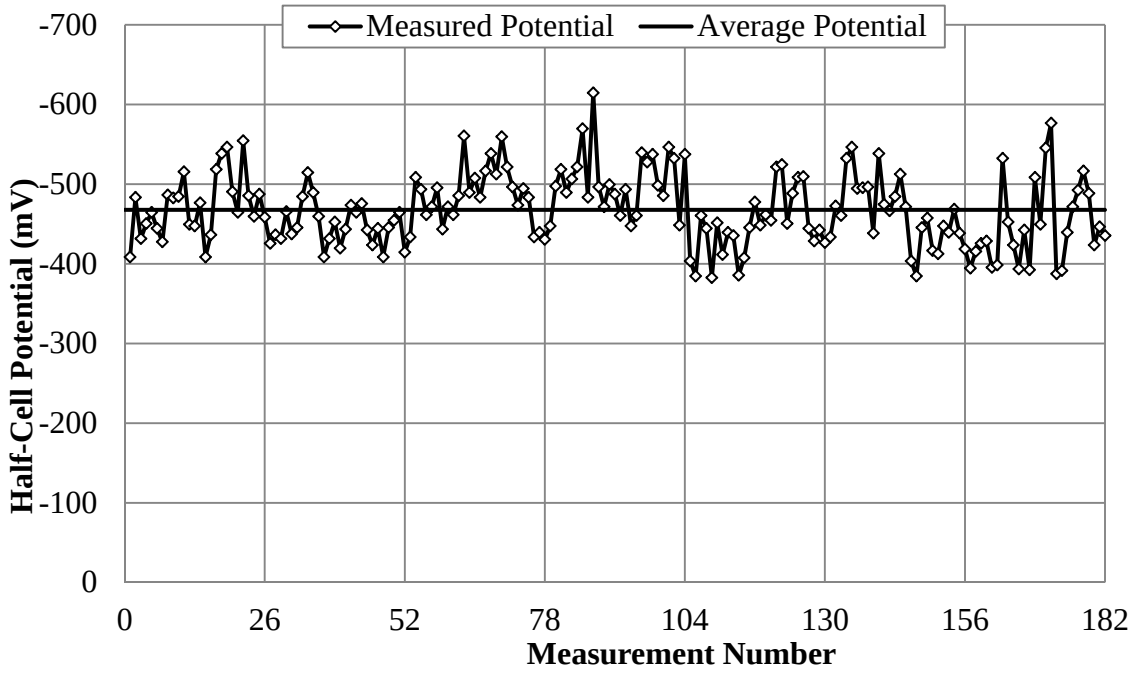

Figure F-28: Section F – Half-cell potential on 10/27/11

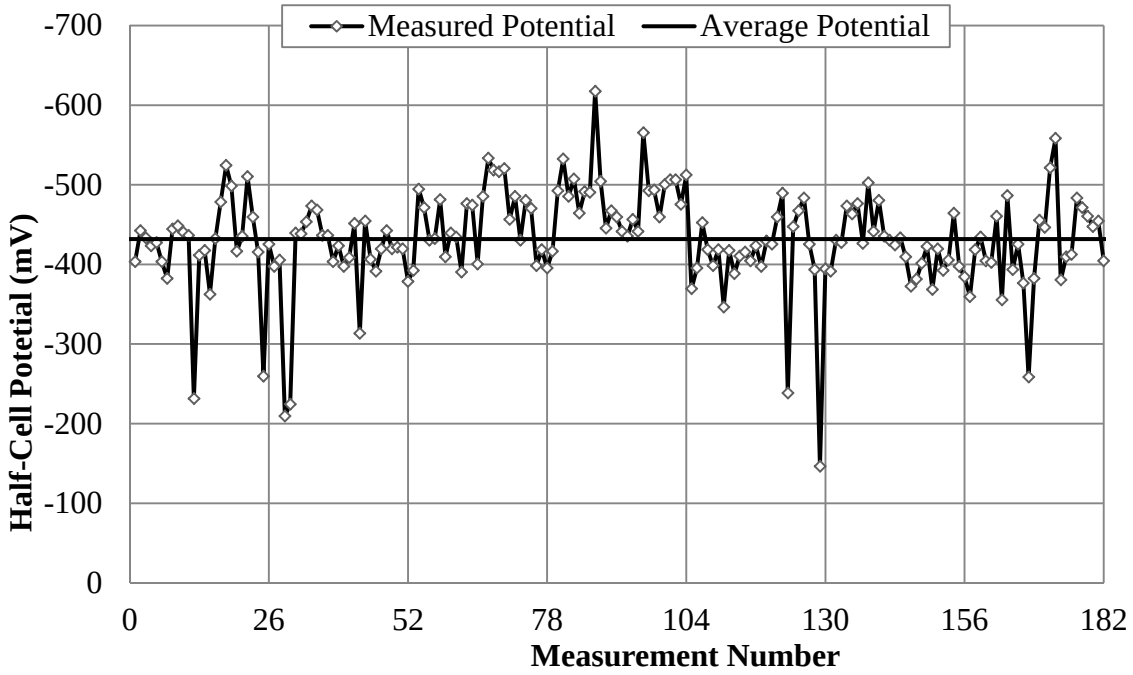

Figure F-29: Section F – Half-cell potential on 4/10/12

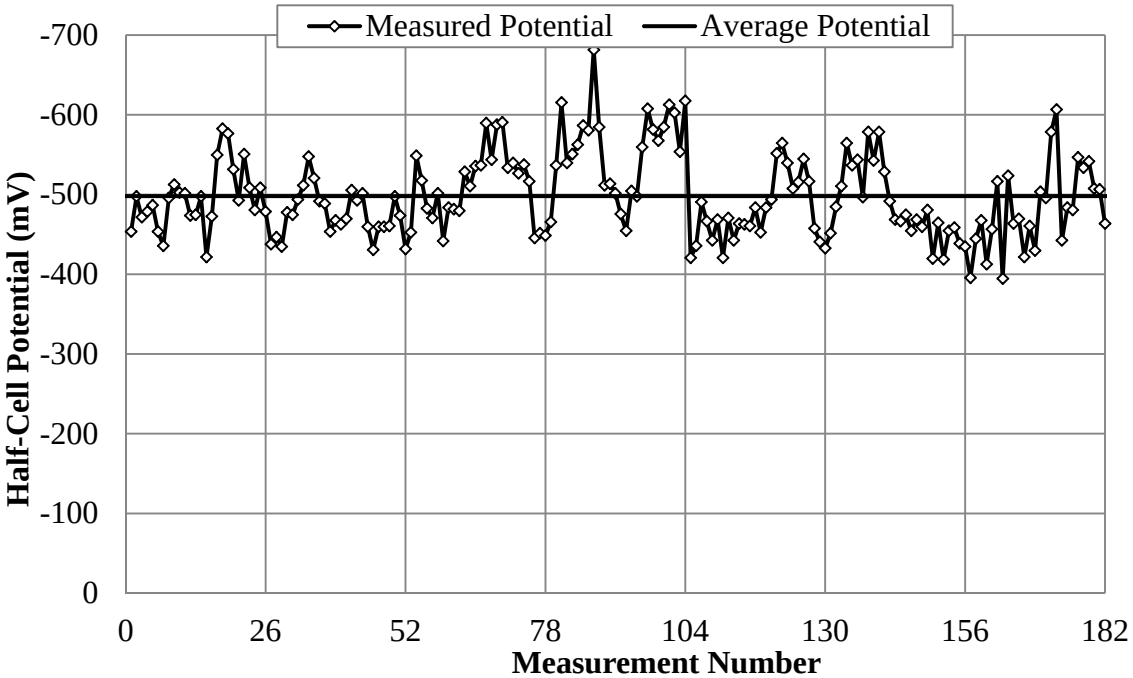

Figure F-30: Section F – Half-cell potential on 5/9/12

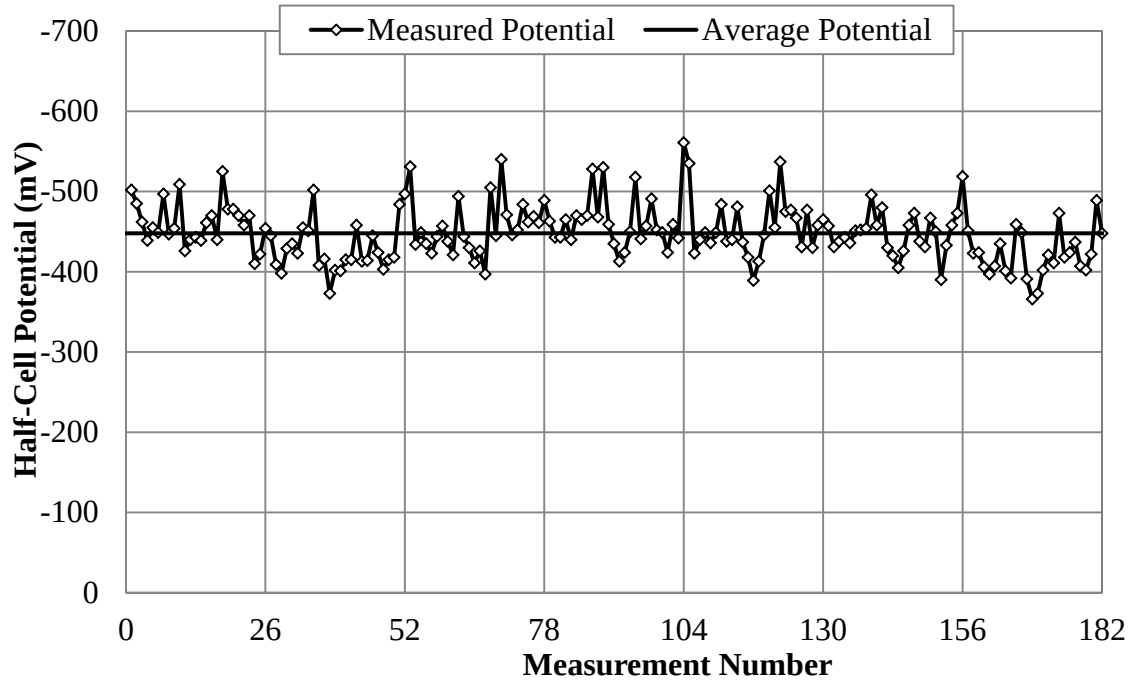

Figure F-31: Section G – Half-cell potential on 8/25/11

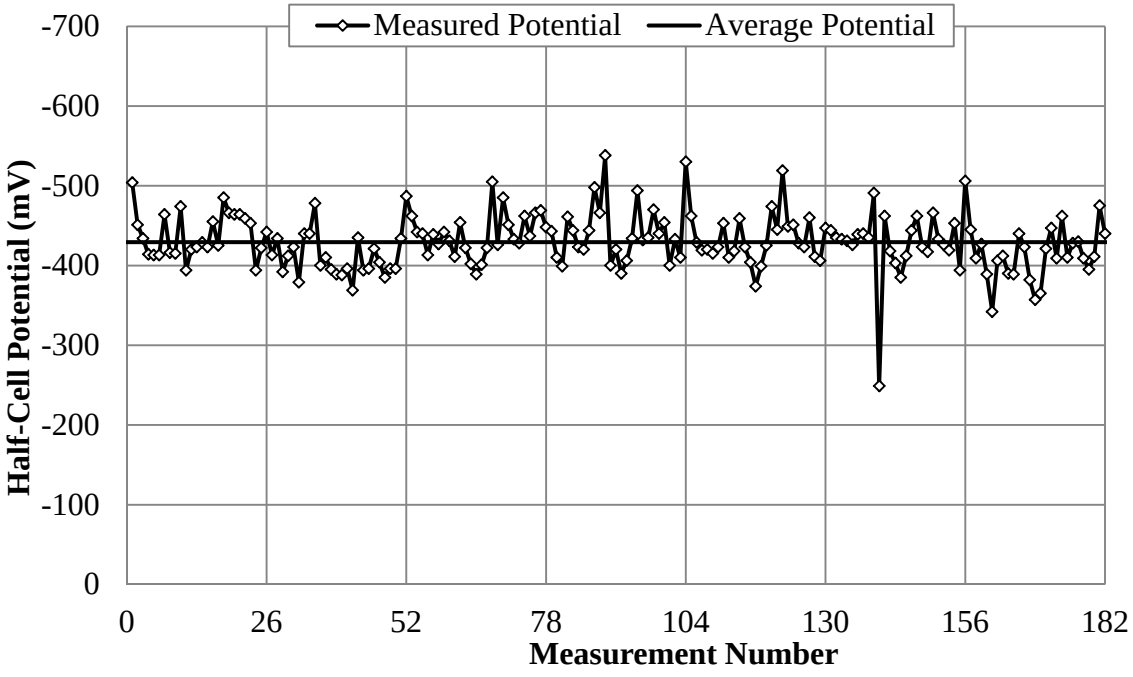

Figure F-32: Section G – Half-cell potential on 10/6/11

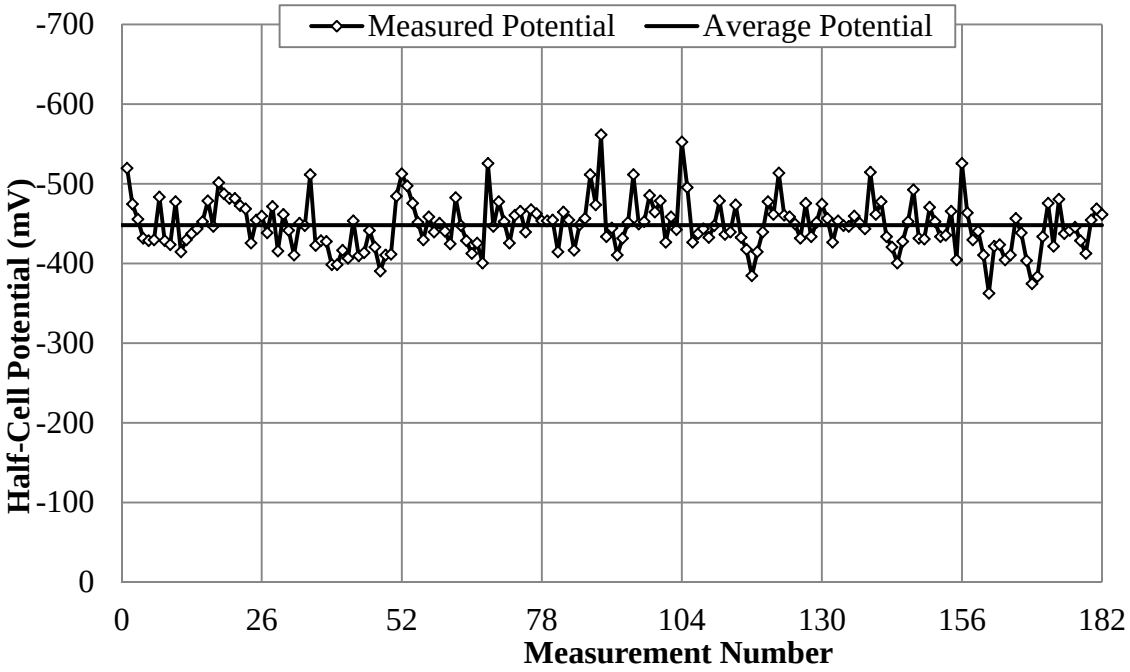

Figure F-33: Section G – Half-cell potential on 10/27/11

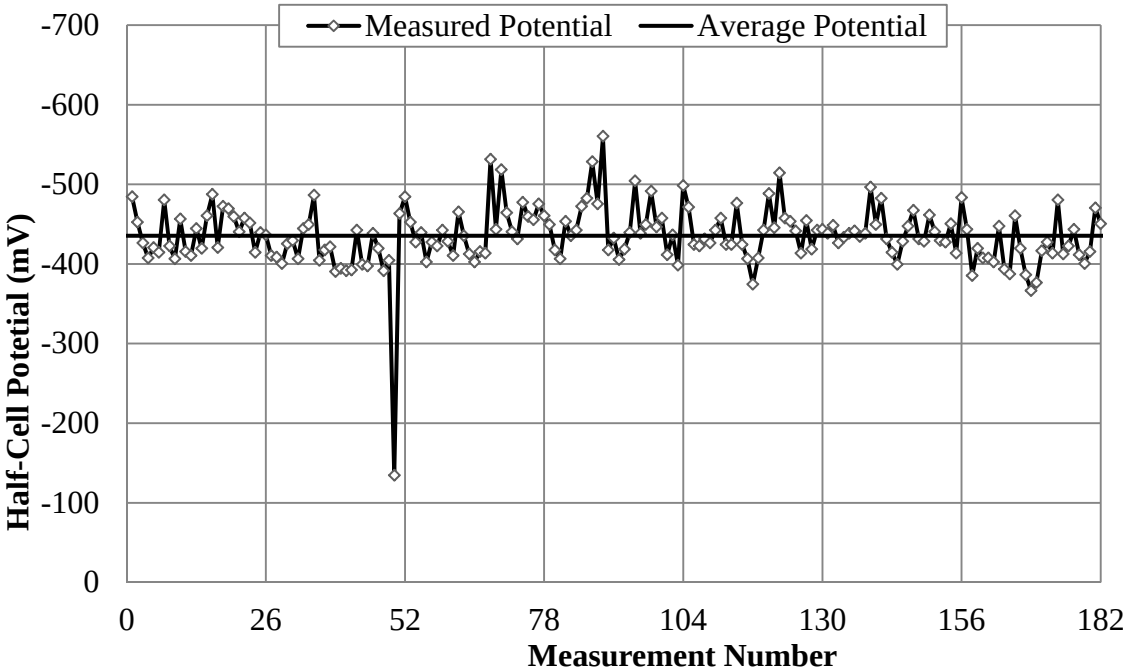

Figure F-34: Section G – Half-cell potential on 4/10/12

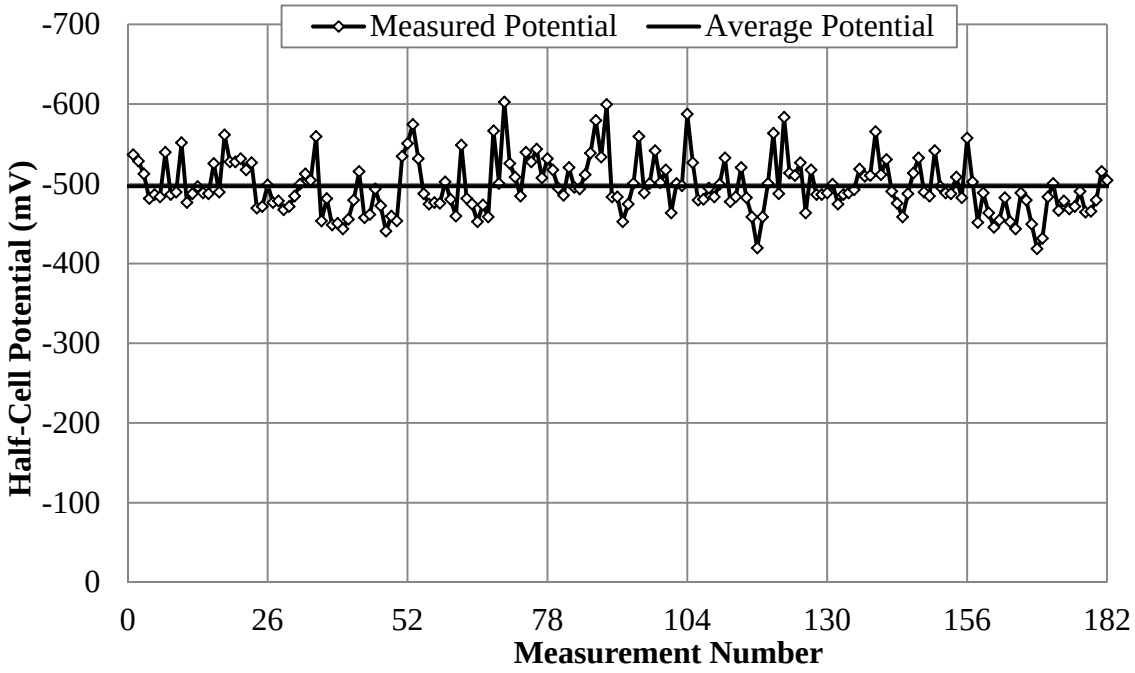

Figure F-35: Section G – Half-cell potential on 5/9/12

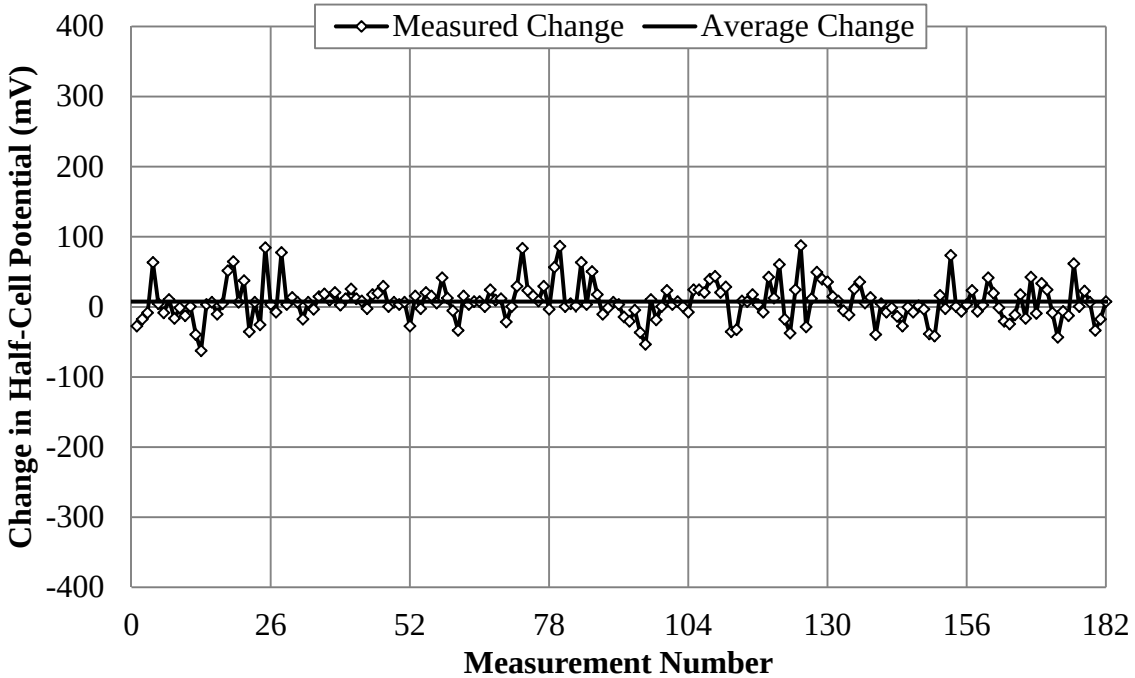

Figure F-36: Section A – Change in Half-cell potential from 8/25/11 to 10/6/11

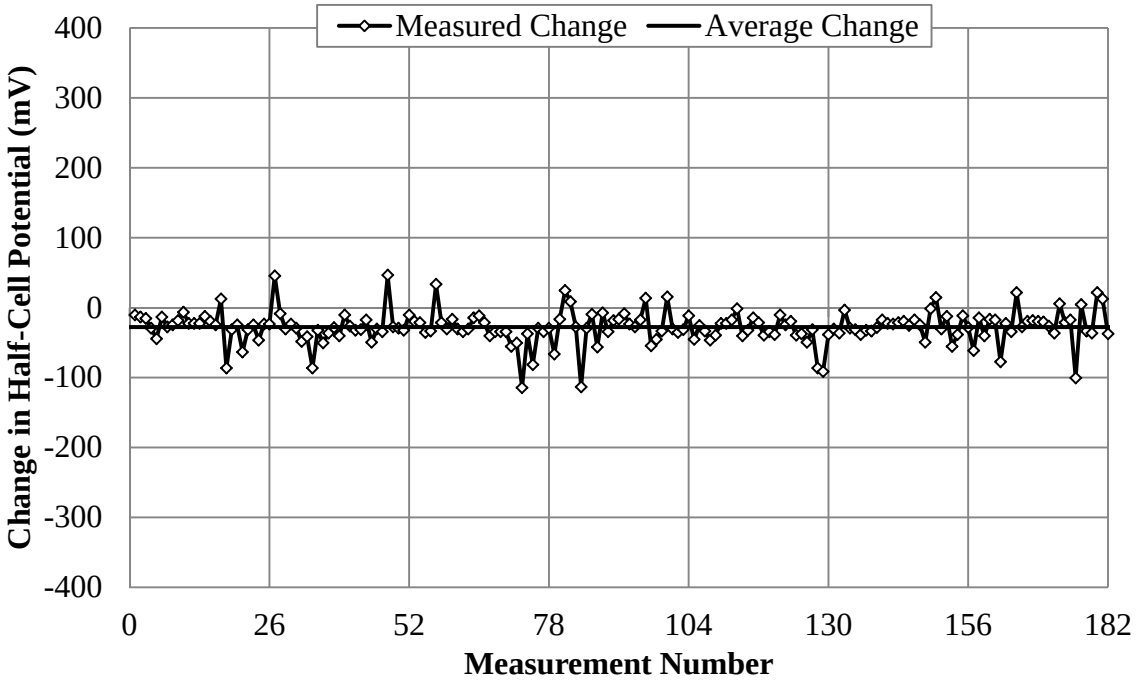

Figure F-37: Section A – Change in Half-cell potential from 10/6/11 to 10/27/11

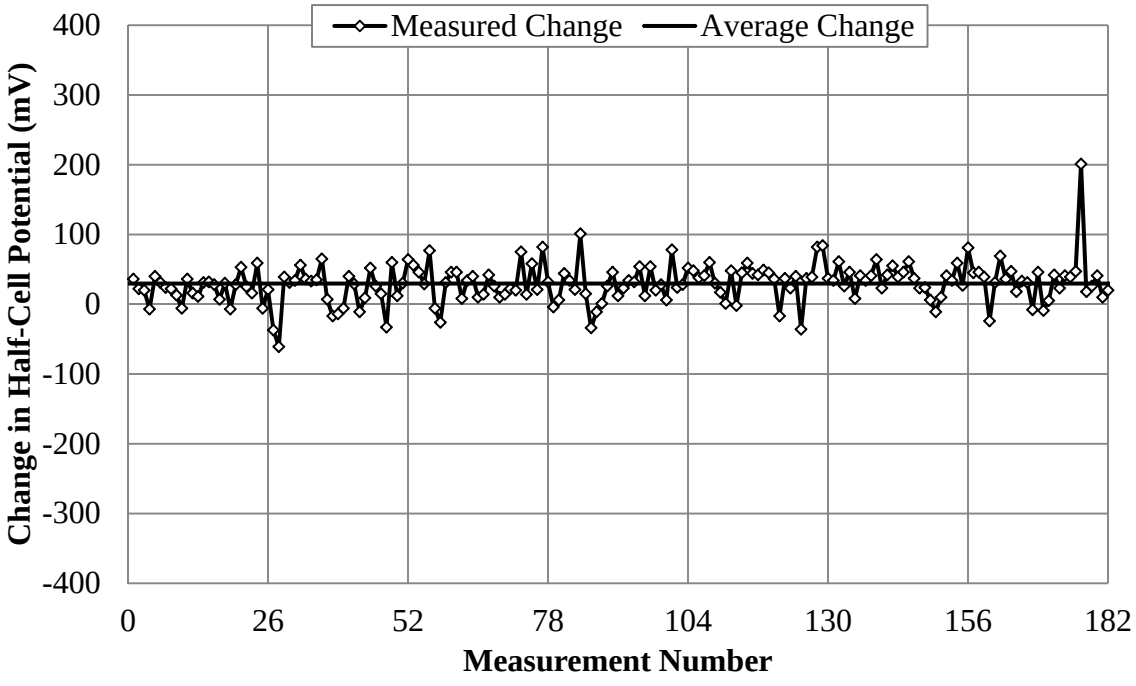

Figure F-38: Section A – Change in Half-cell potential from 10/27/11 to 4/10/12

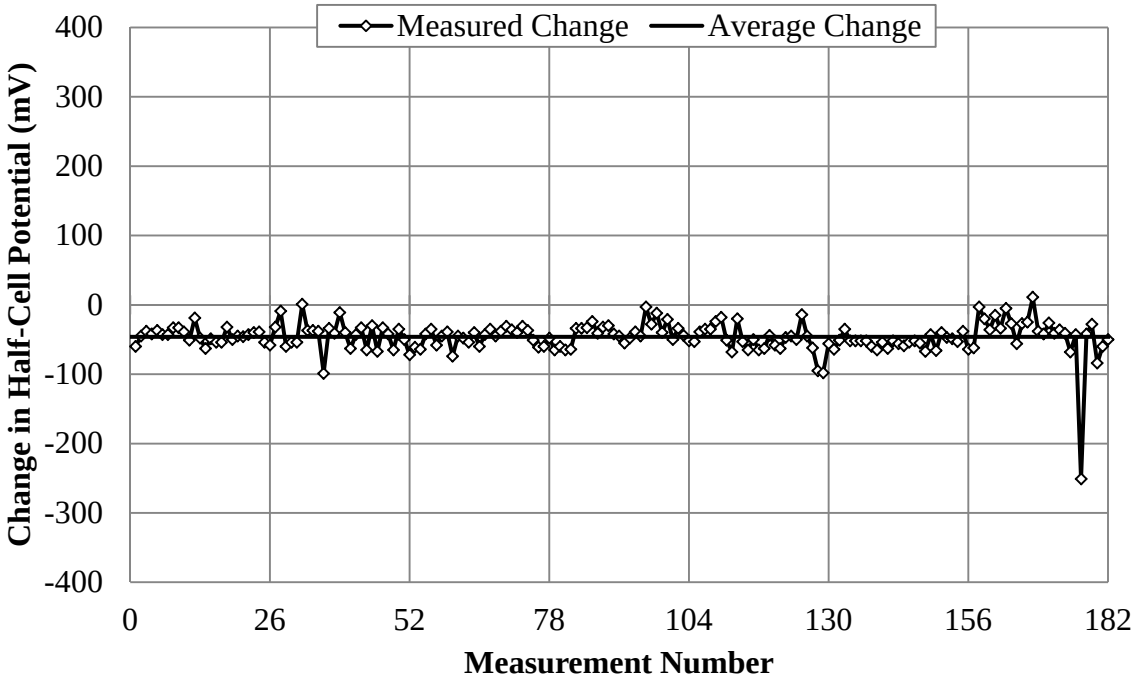

Figure F-39: Section A – Change in Half-cell potential from 4/10/12 to 5/9/12

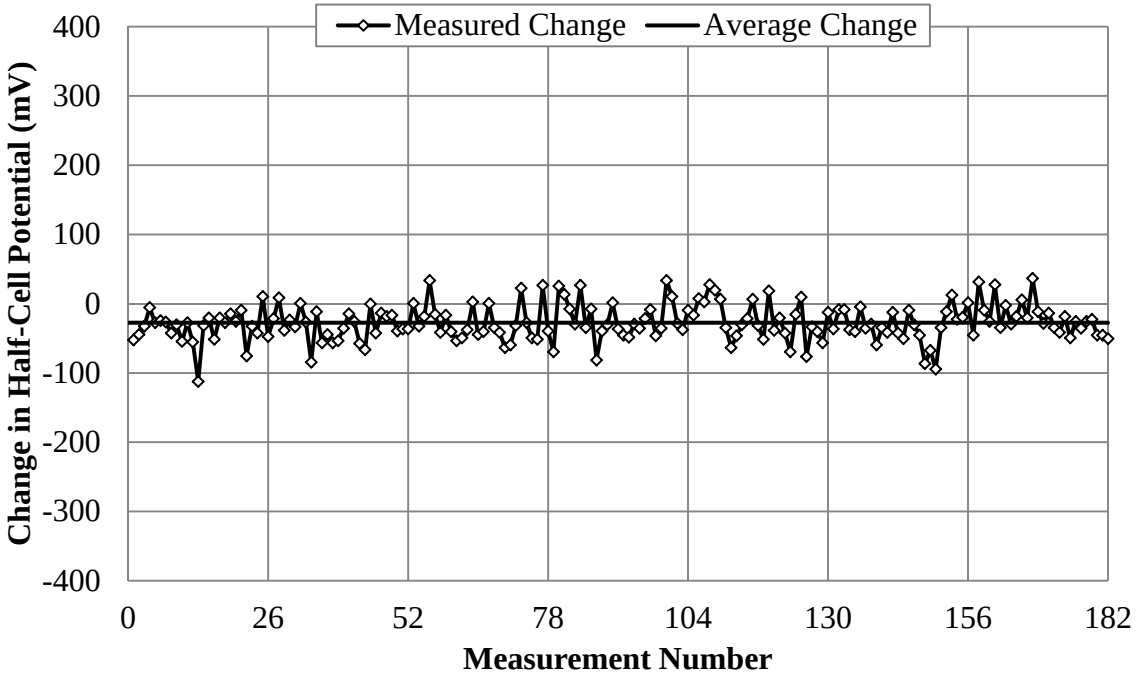

Figure F-40: Section A – Change in Half-cell potential from 8/25/11 to 5/9/12

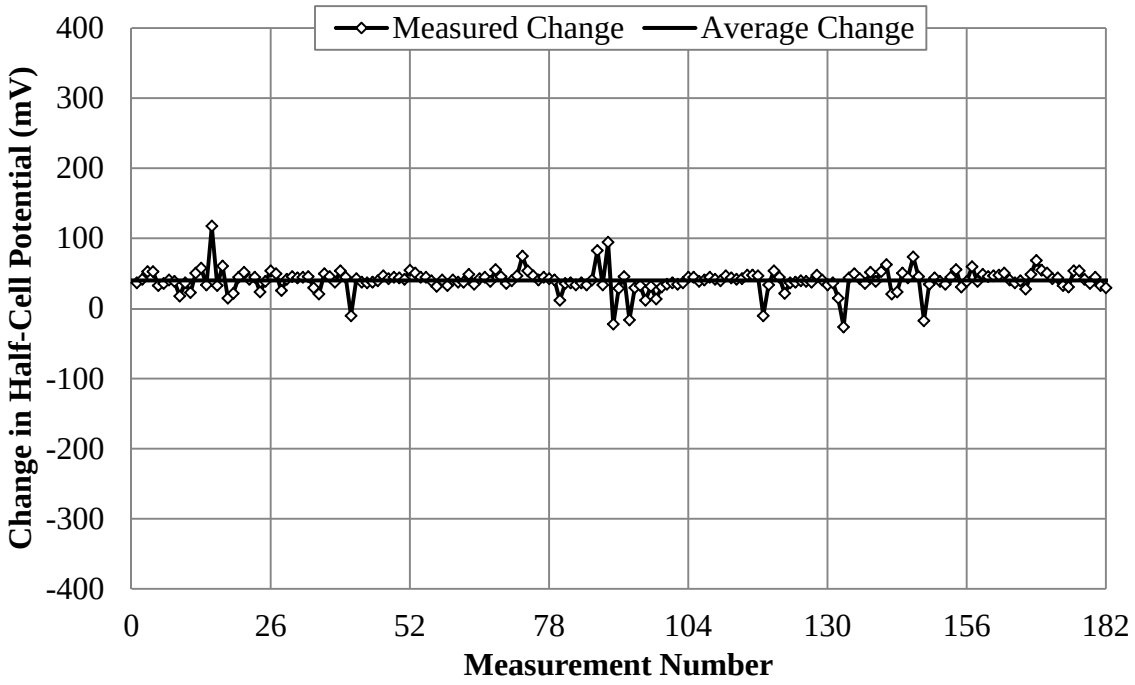

Figure F-41: Section B – Change in Half-cell potential from 8/25/11 to 10/6/11

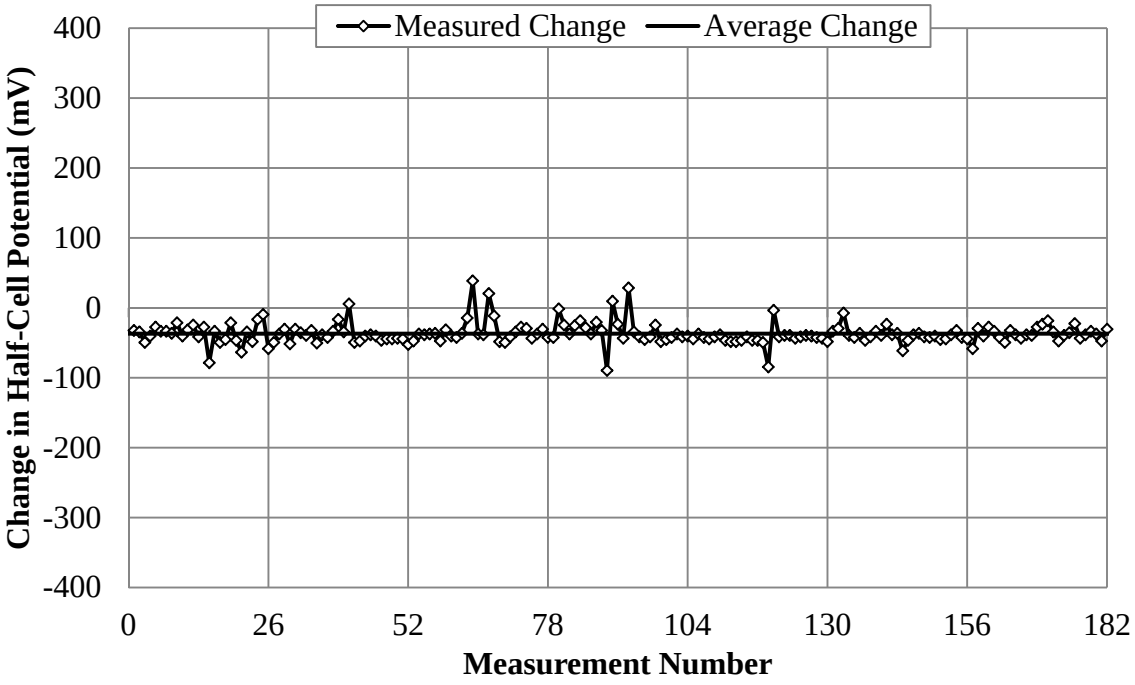

Figure F-42: Section B – Change in Half-cell potential from 10/6/11 to 10/27/11

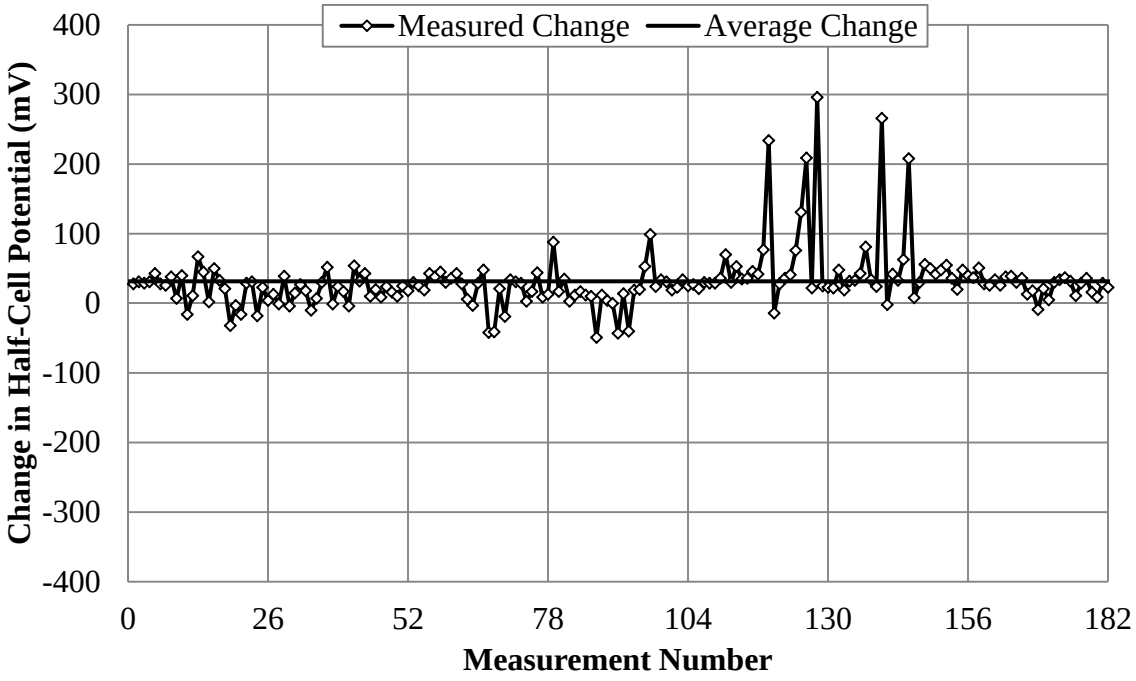

Figure F-43: Section B – Change in Half-cell potential from 10/27/11 to 4/10/12

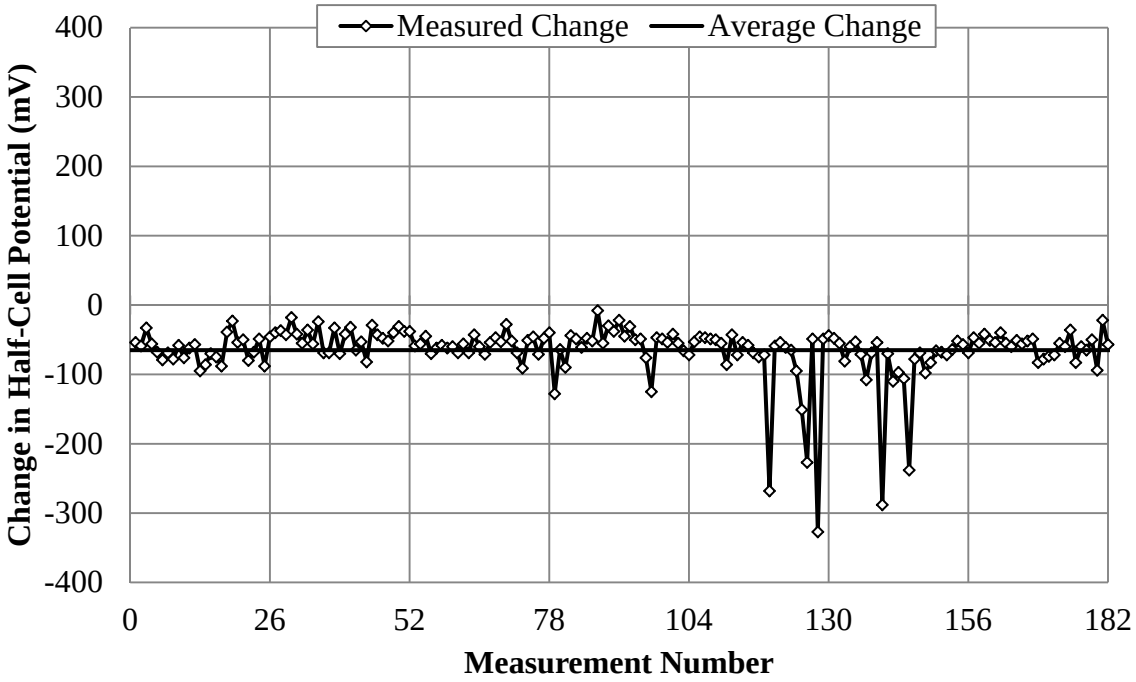

Figure F-44: Section B – Change in Half-cell potential from 4/10/12 to 5/9/12

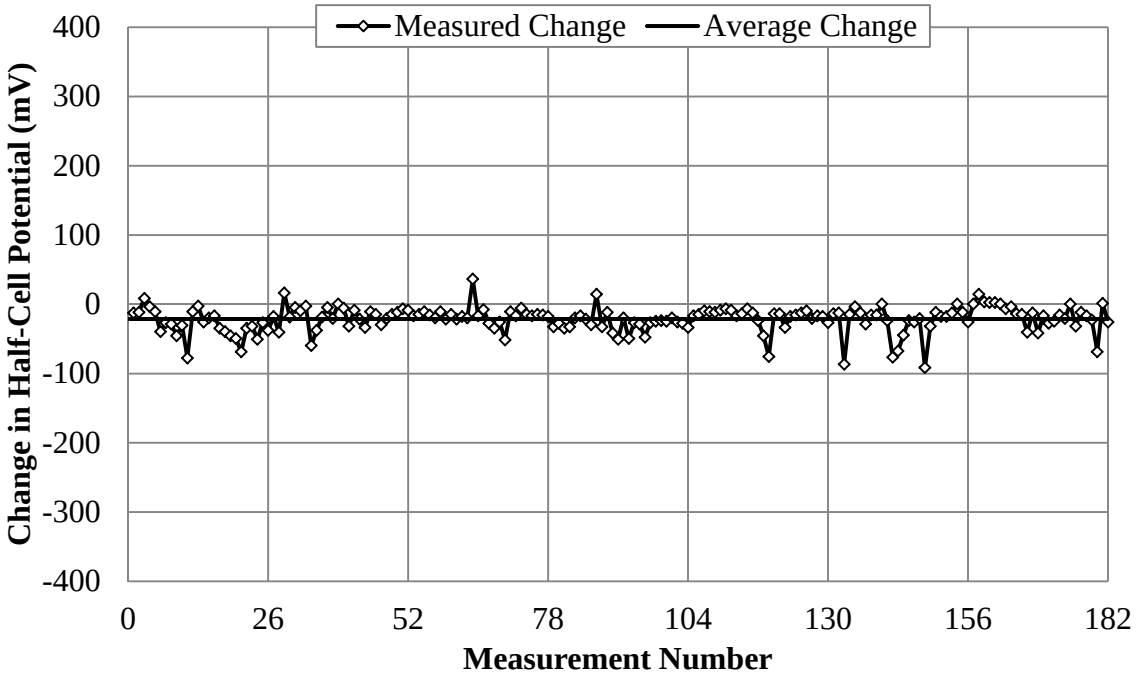

Figure F-45: Section B – Change in Half-cell potential from 8/25/11 to 5/9/12

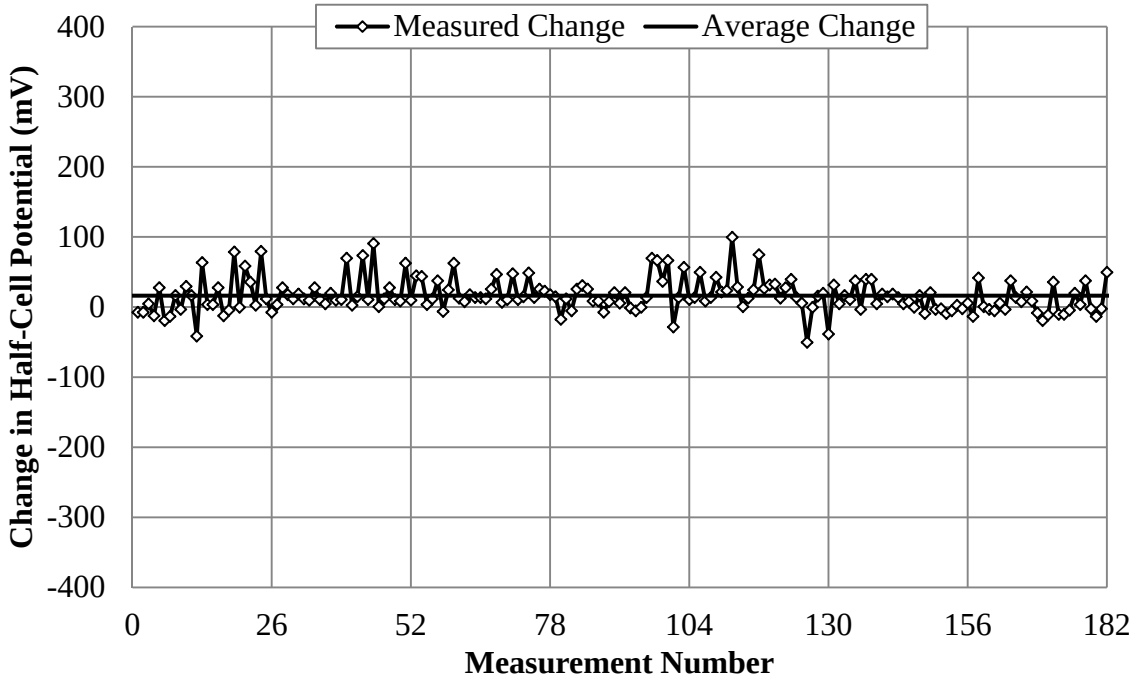

Figure F-46: Section C – Change in Half-cell potential from 8/25/11 to 10/6/11

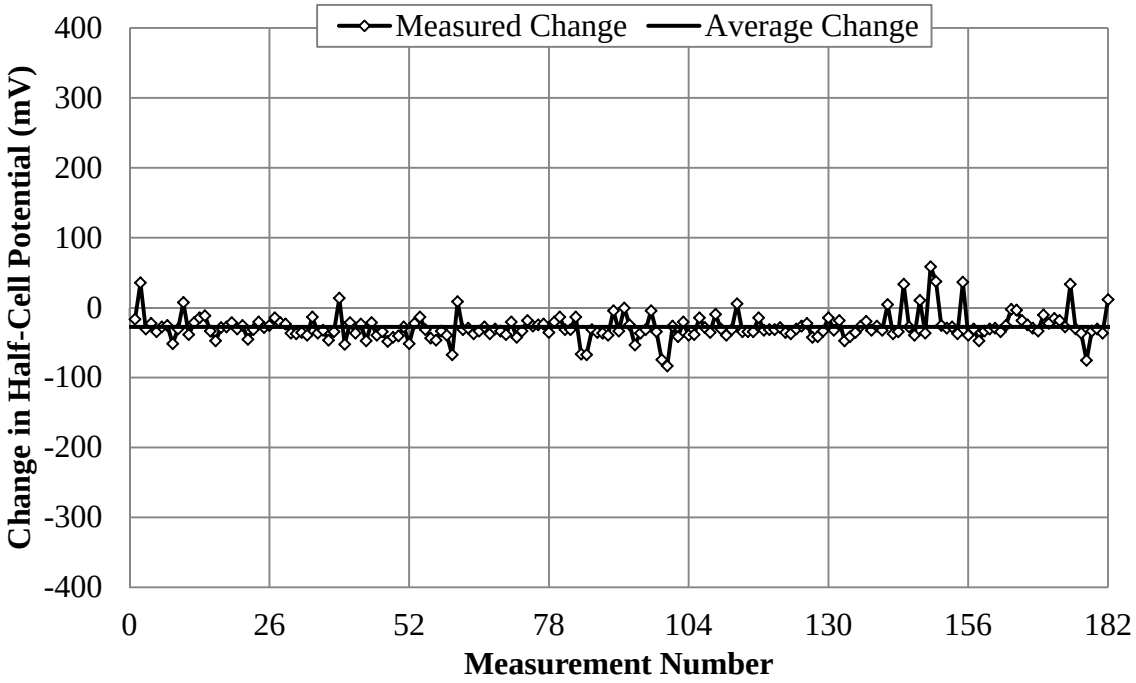

Figure F-47: Section C – Change in Half-cell potential from 10/6/11 to 10/27/11

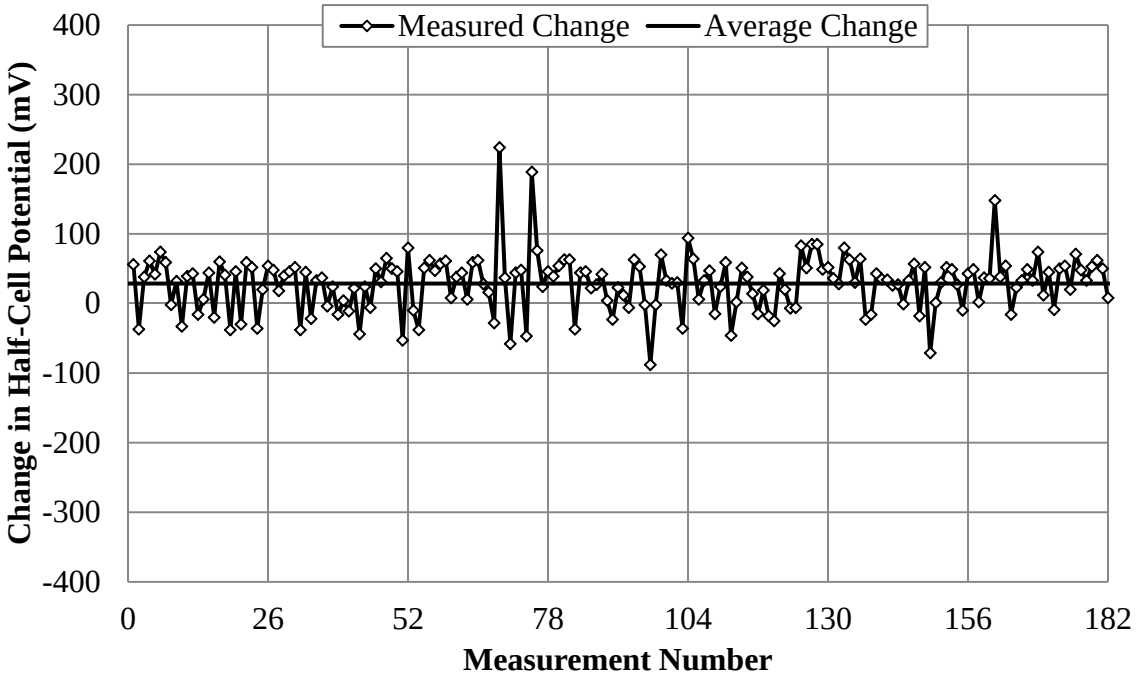

Figure F-48: Section C – Change in Half-cell potential from 10/27/11 to 4/10/12

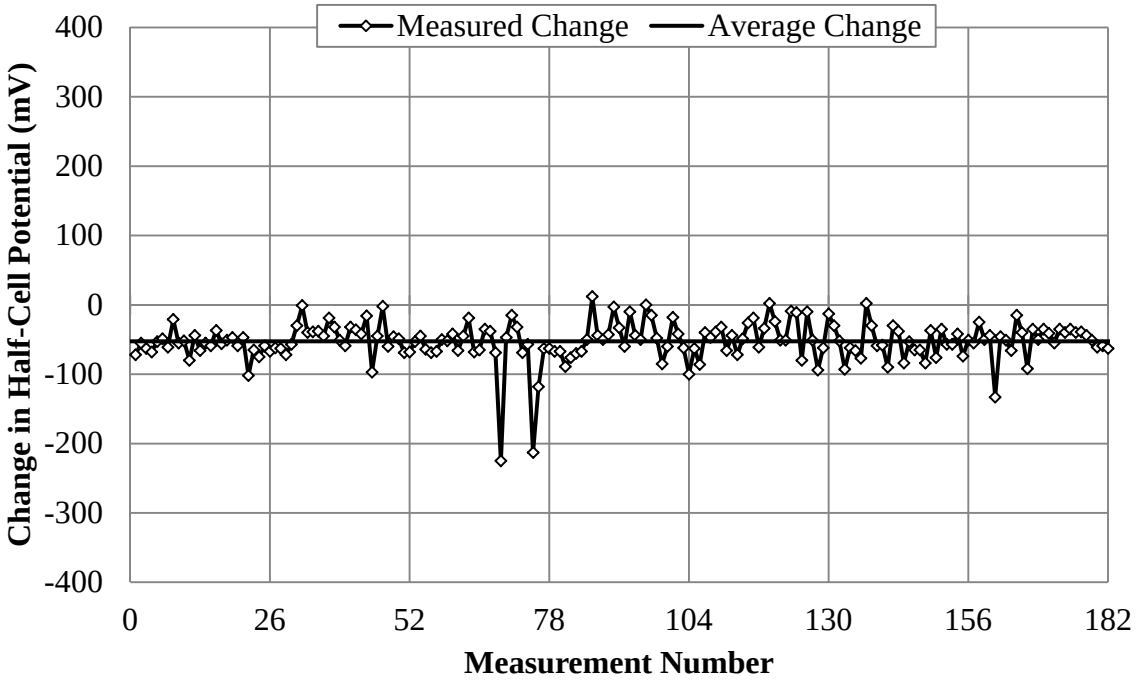

Figure F-49: Section C – Change in Half-cell potential from 4/10/12 to 5/9/12

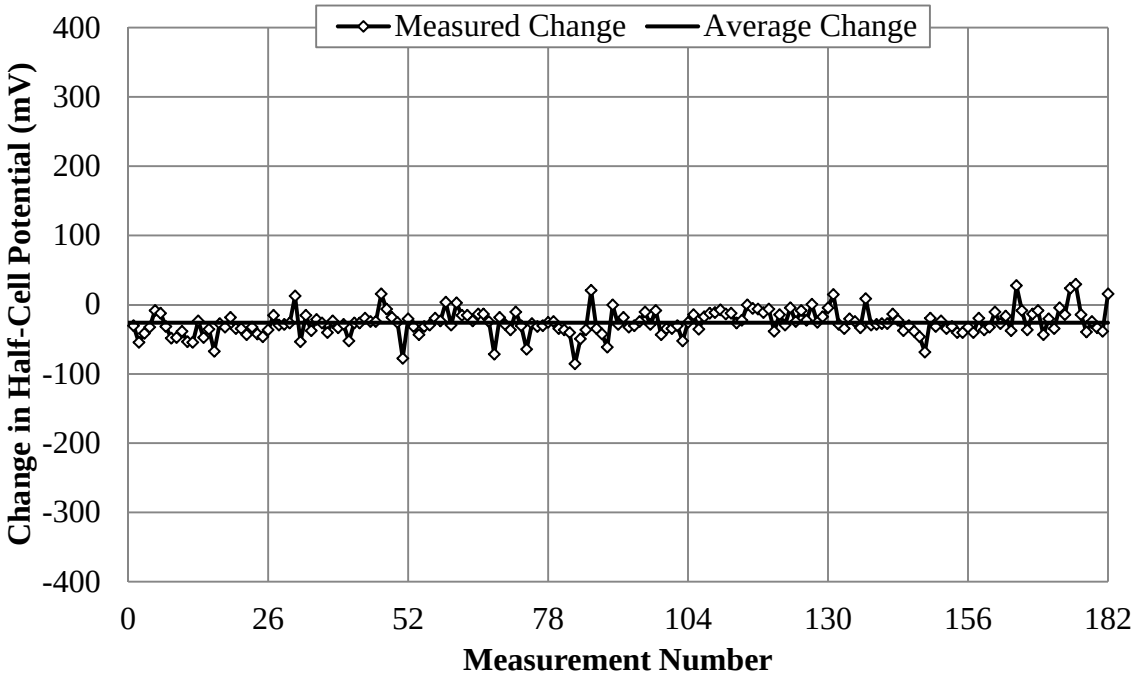

Figure F-50: Section C – Change in Half-cell potential from 8/25/11 to 5/9/12

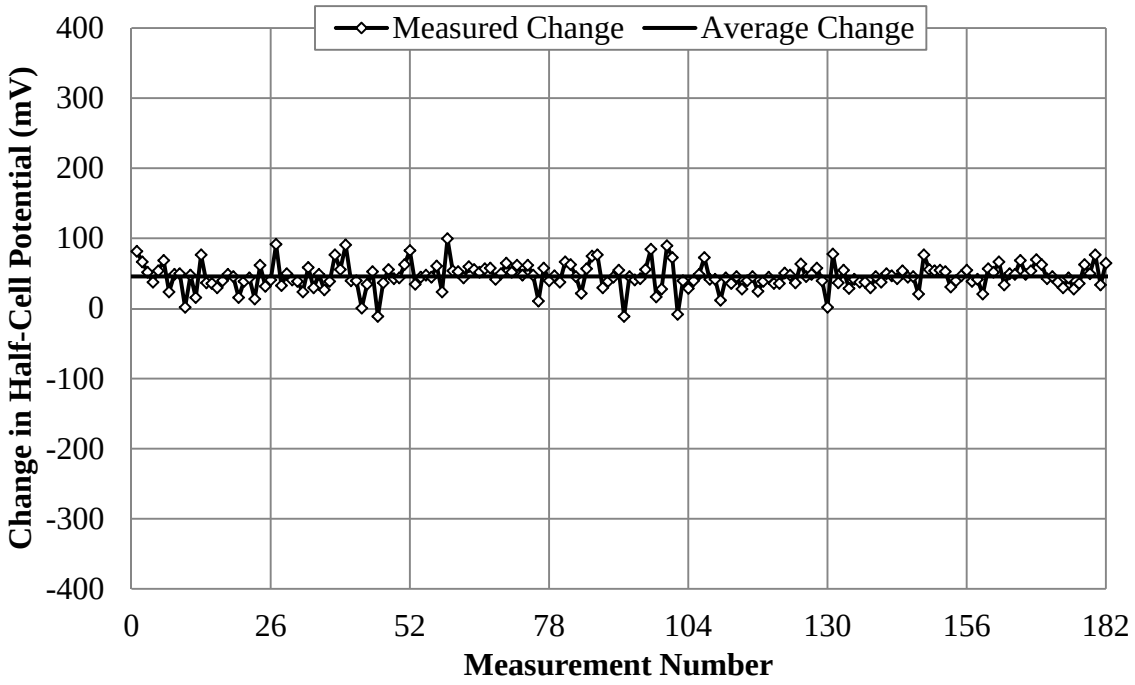

Figure F-51: Section D – Change in Half-cell potential from 8/25/11 to 10/6/11

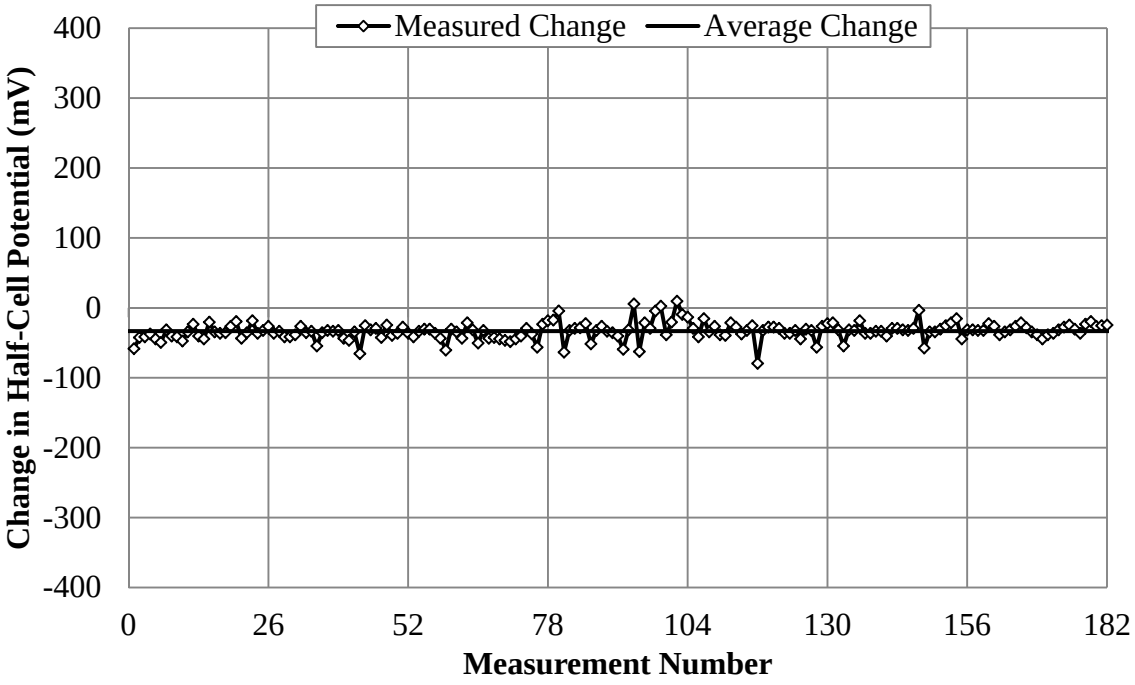

Figure F-52: Section D – Change in Half-cell potential from 10/6/11 to 10/27/11

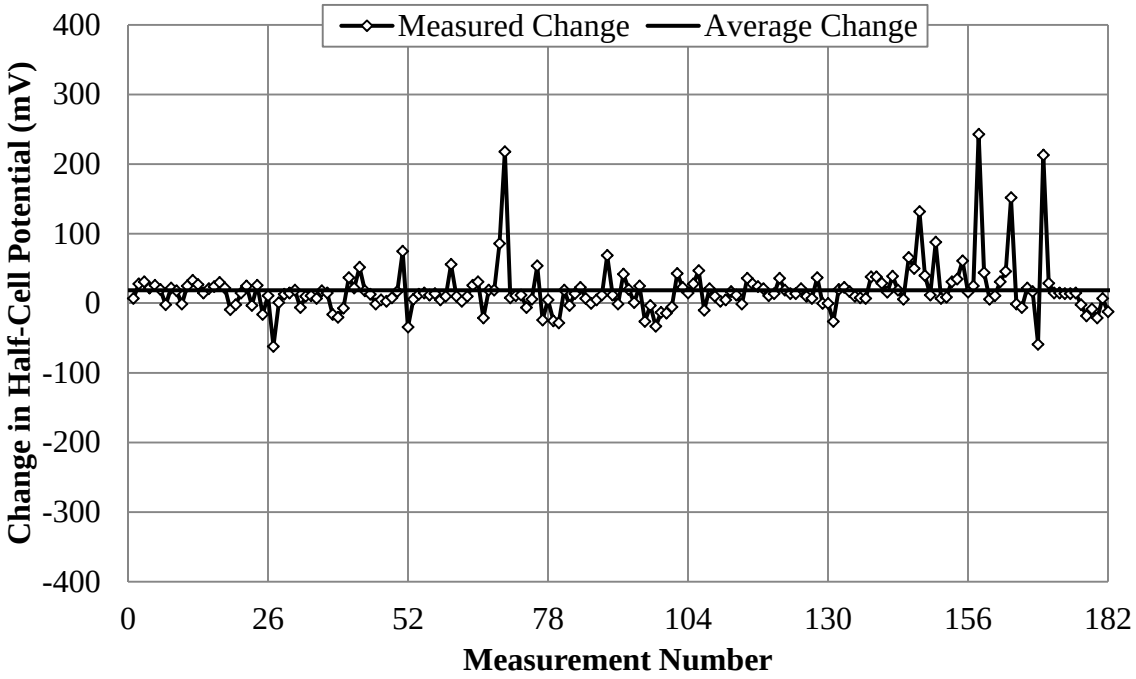

Figure F-53: Section D – Change in Half-cell potential from 10/27/11 to 4/10/12

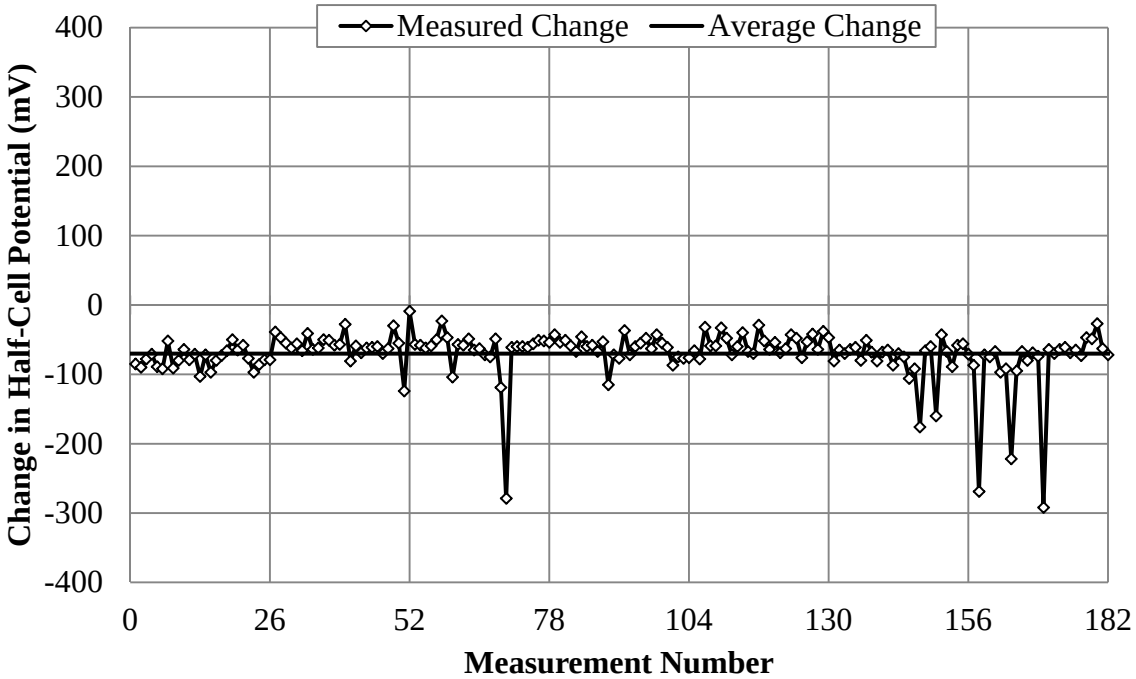

Figure F-54: Section D – Change in Half-cell potential from 4/10/12 to 5/9/12

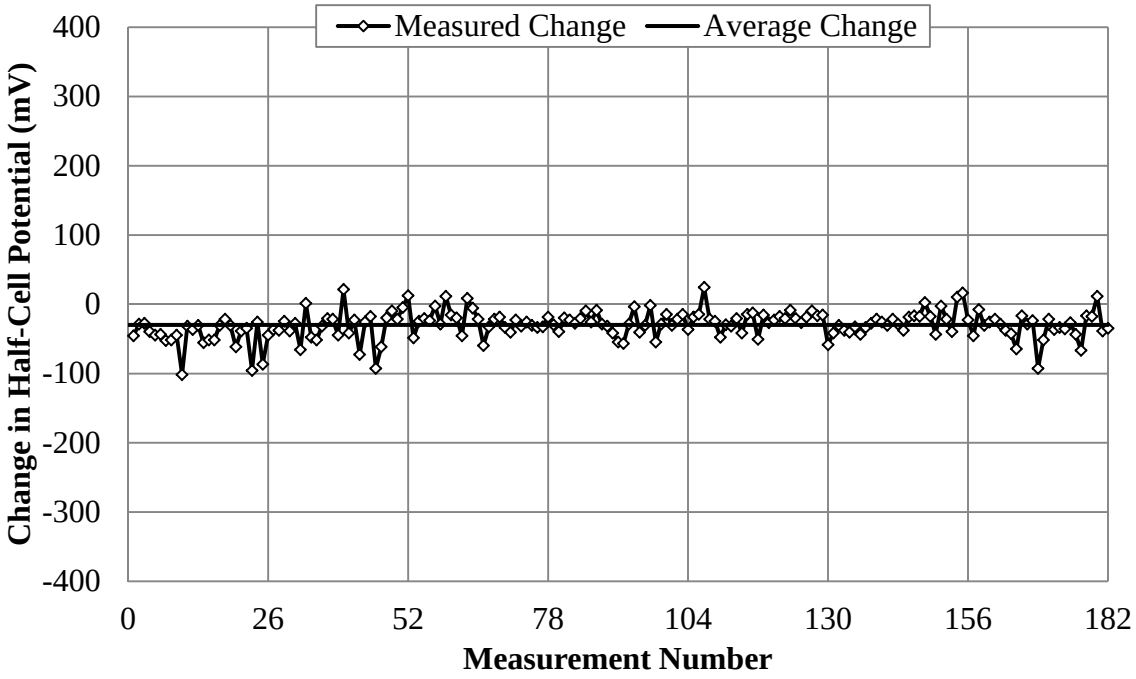

Figure F-55: Section D – Change in Half-cell potential from 8/25/11 to 5/9/12

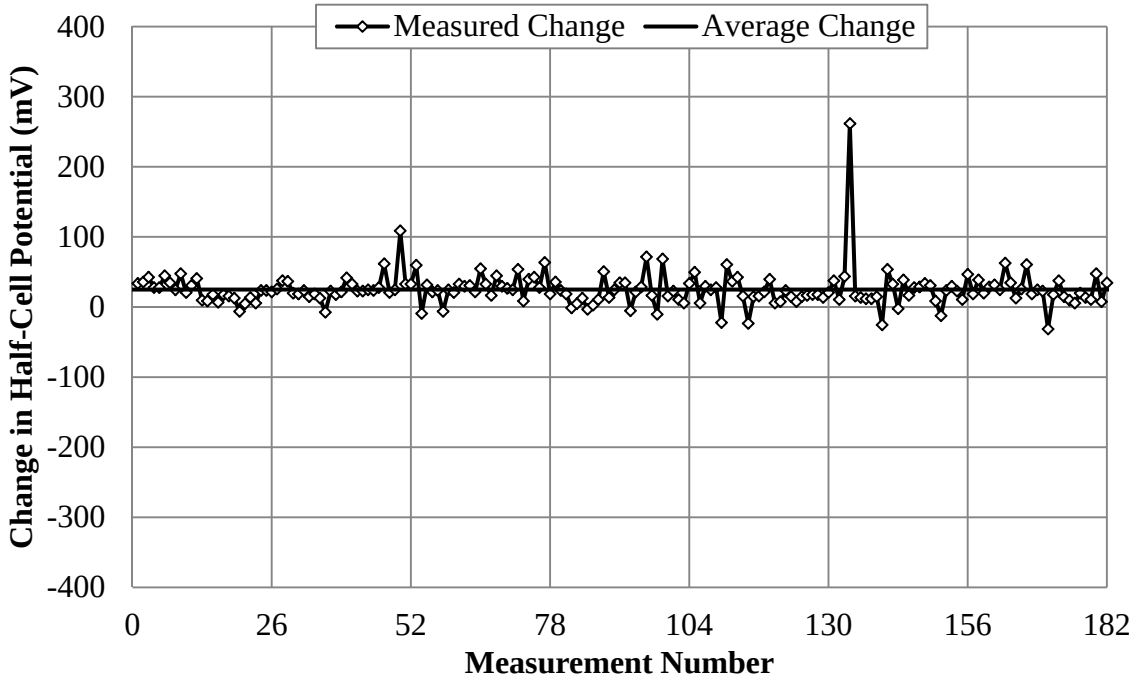

Figure F-56: Section E – Change in Half-cell potential from 8/25/11 to 10/6/11

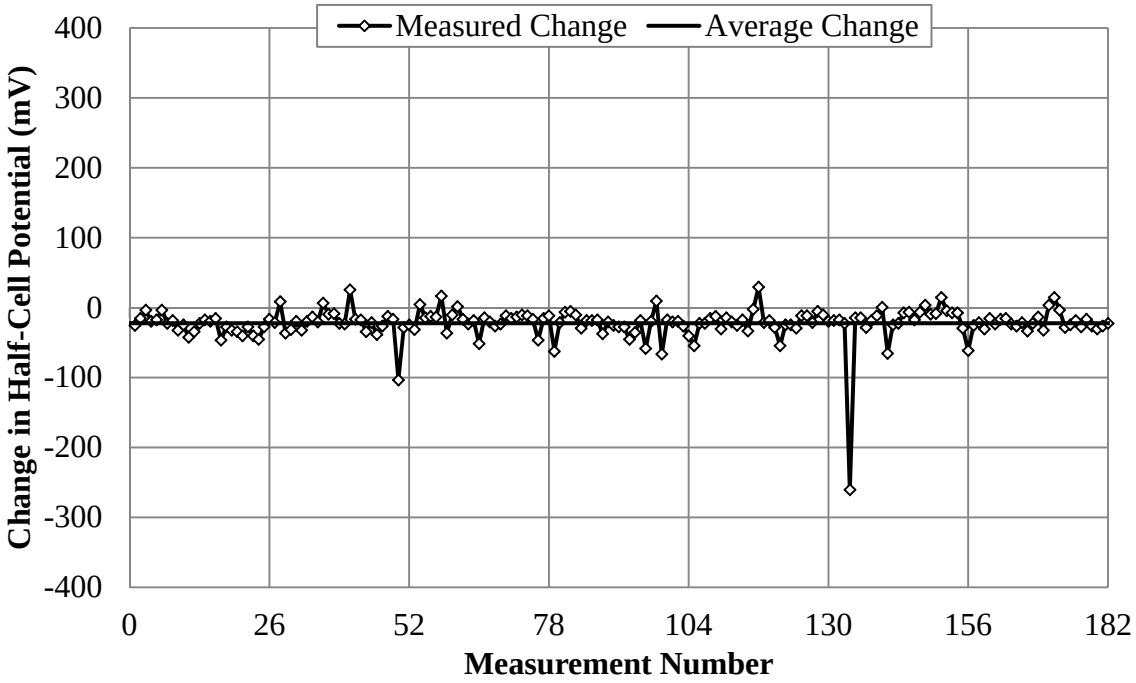

Figure F-57: Section E – Change in Half-cell potential from 10/6/11 to 10/27/11

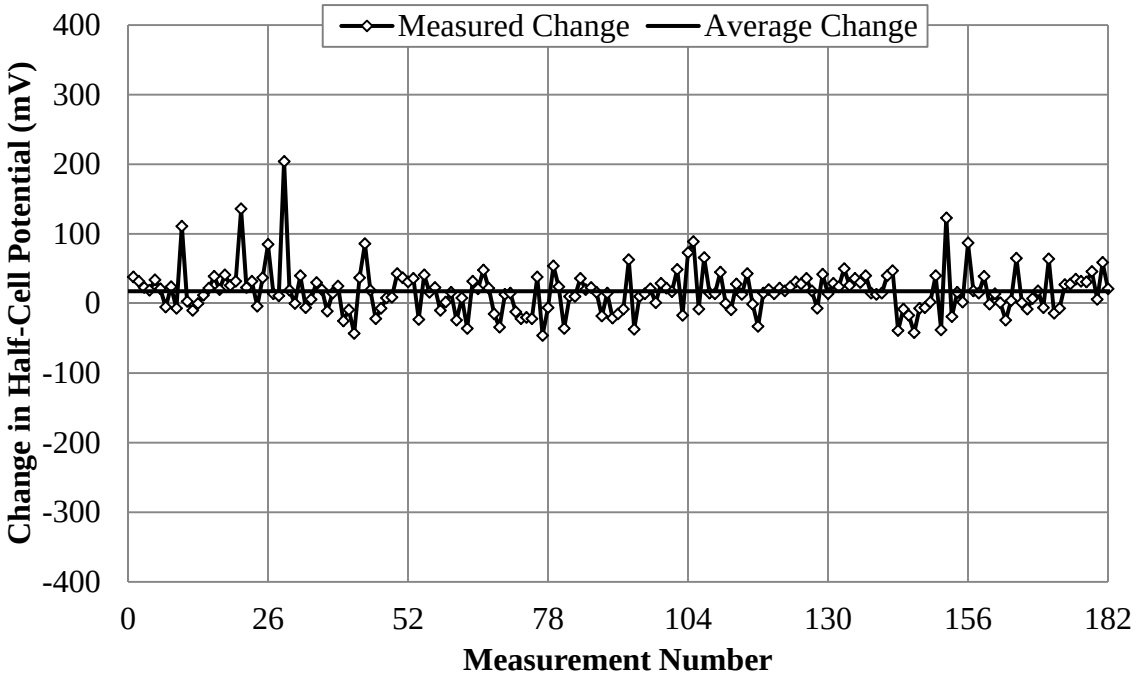

Figure F-58: Section E – Change in Half-cell potential from 10/27/11 to 4/10/12

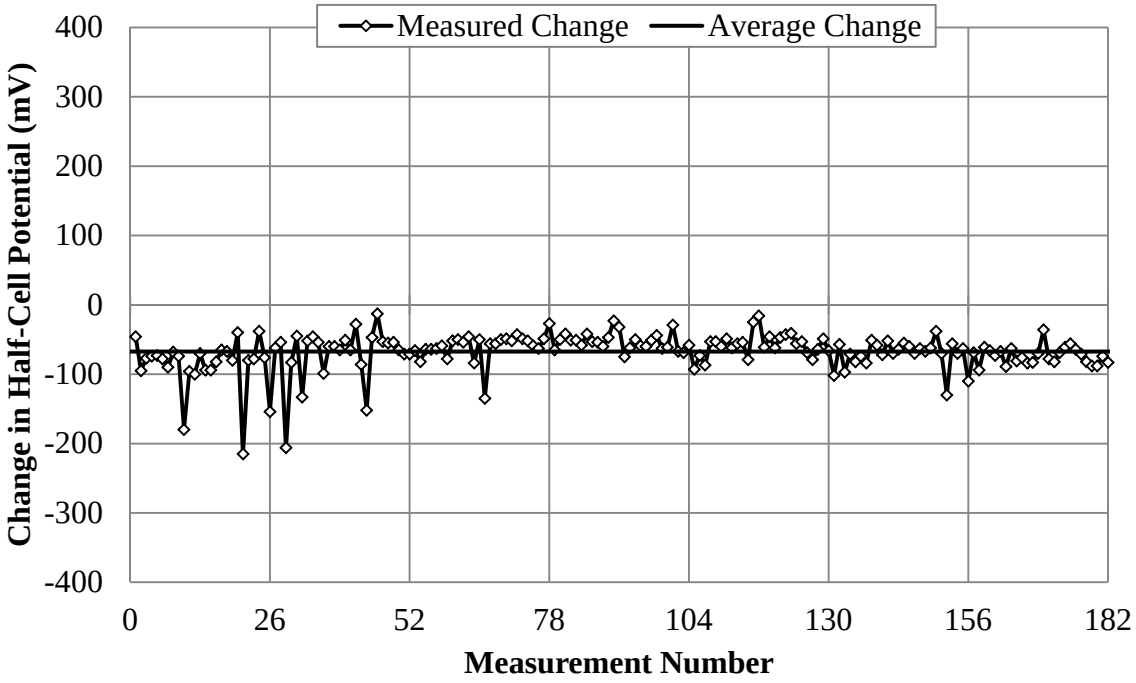

Figure F-59: Section E – Change in Half-cell potential from 4/10/12 to 5/9/12

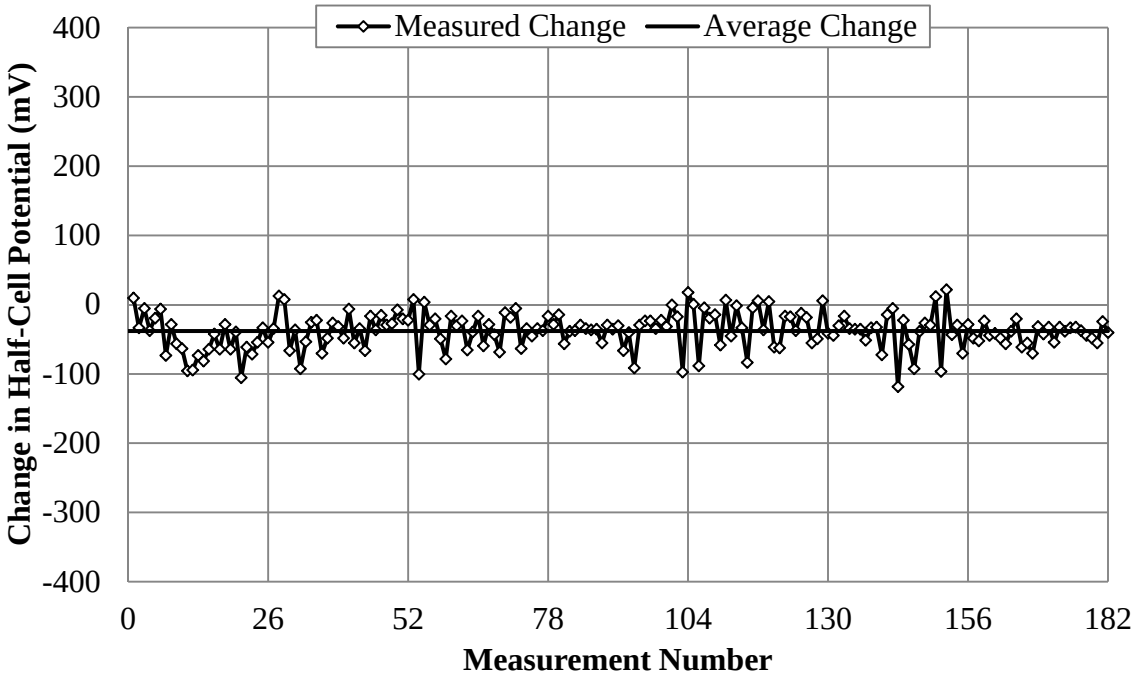

Figure F-60: Section E – Change in Half-cell potential from 8/25/11 to 5/9/12

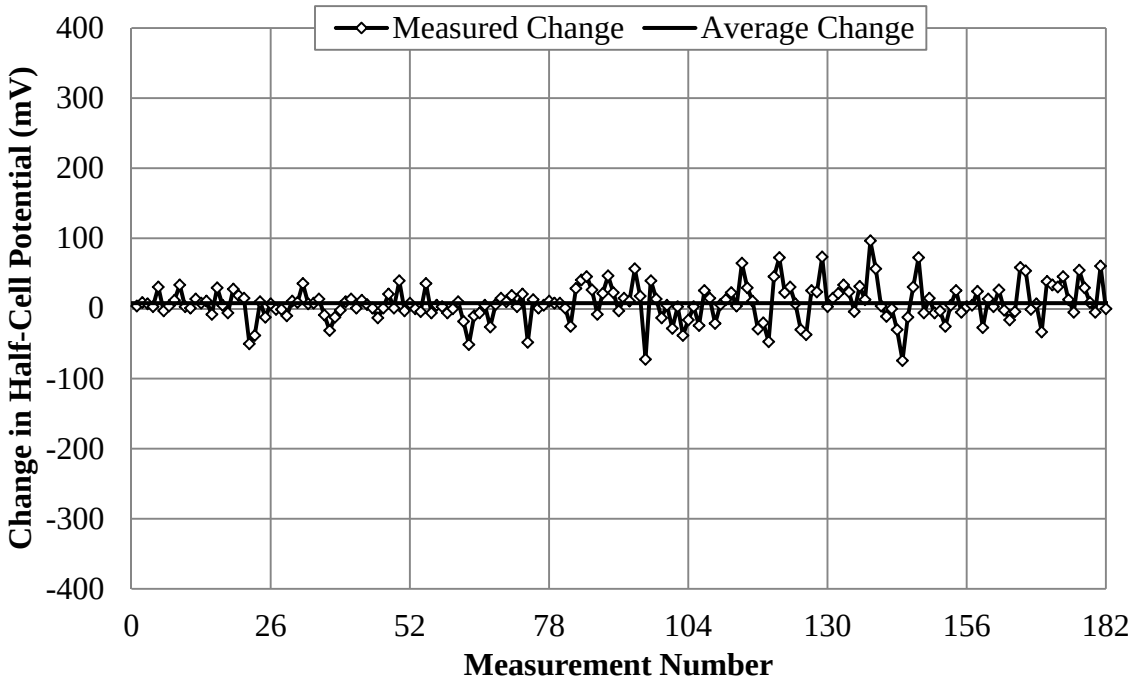

Figure F-61: Section F – Change in Half-cell potential from 8/25/11 to 10/6/11

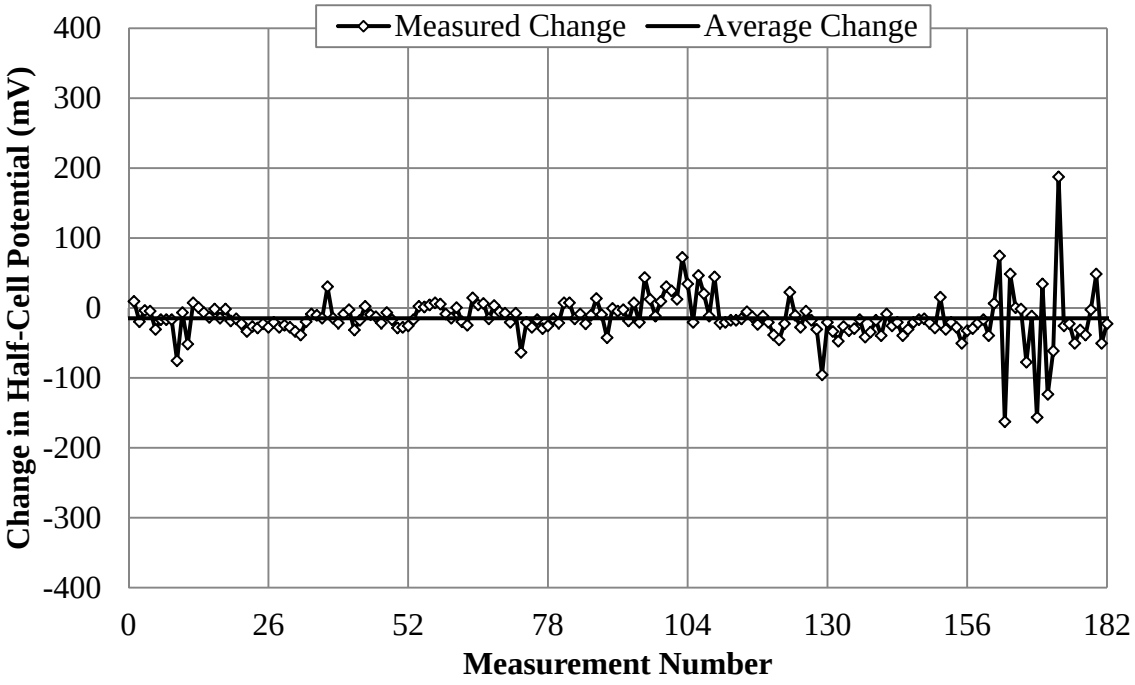

Figure F-62: Section F – Change in Half-cell potential from 10/6/11 to 10/27/11

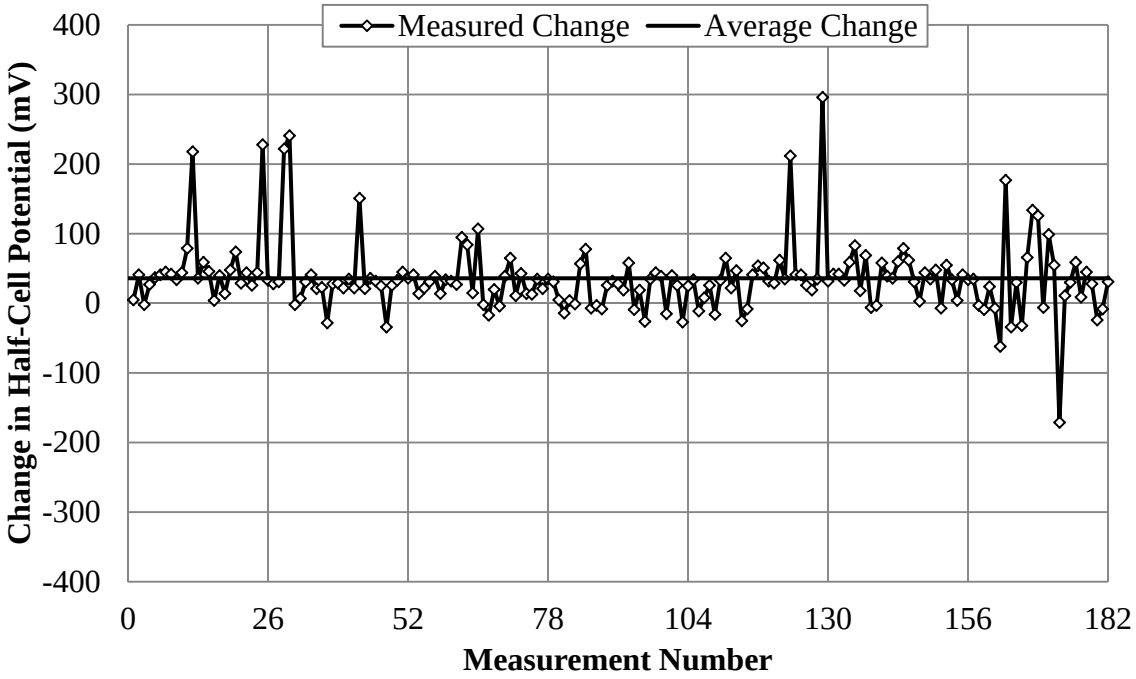

Figure F-63: Section F – Change in Half-cell potential from 10/27/11 to 4/10/12

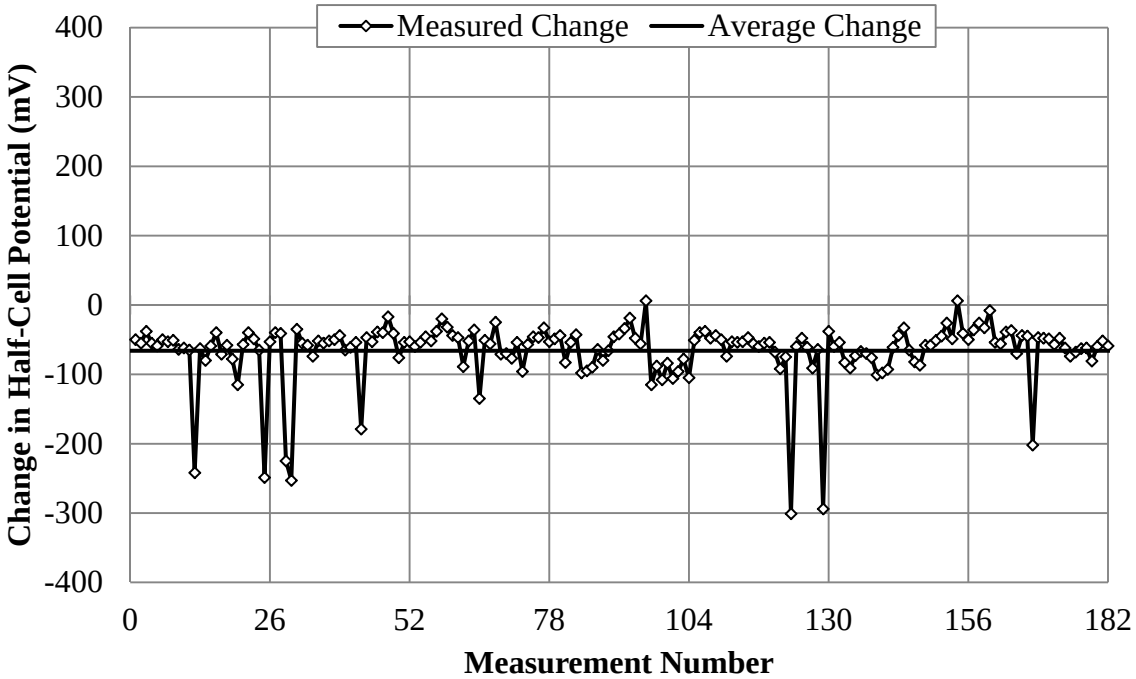

Figure F-64: Section F – Change in Half-cell potential from 4/10/12 to 5/9/12

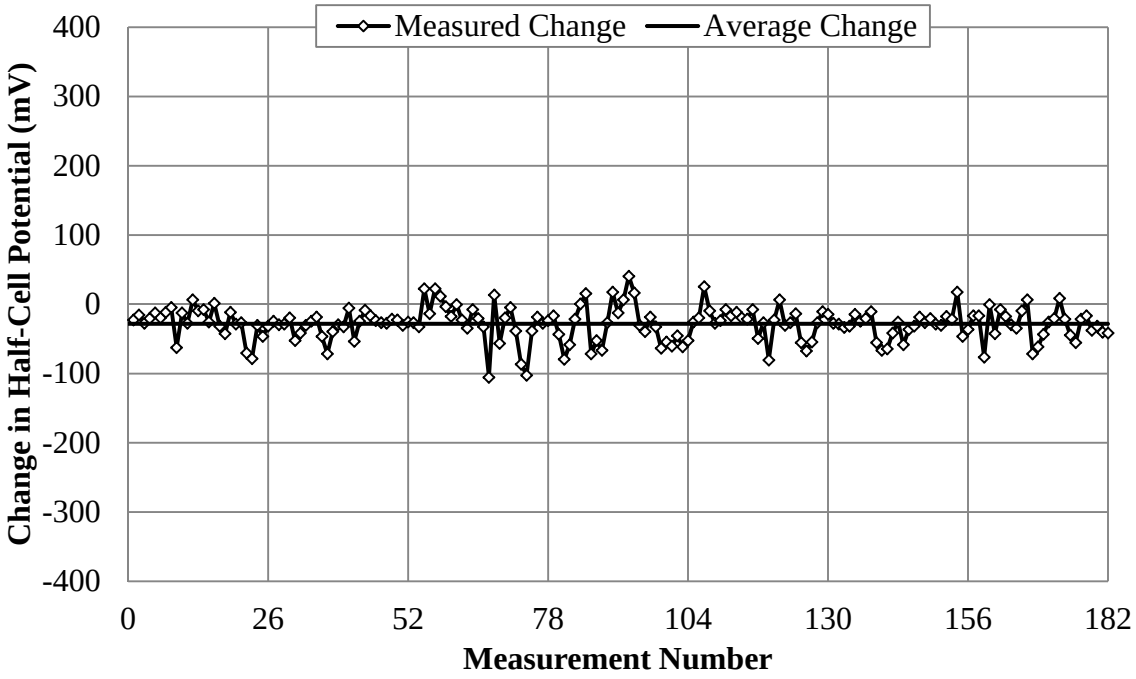

Figure F-65: Section F – Change in Half-cell potential from 8/25/11 to 5/9/12

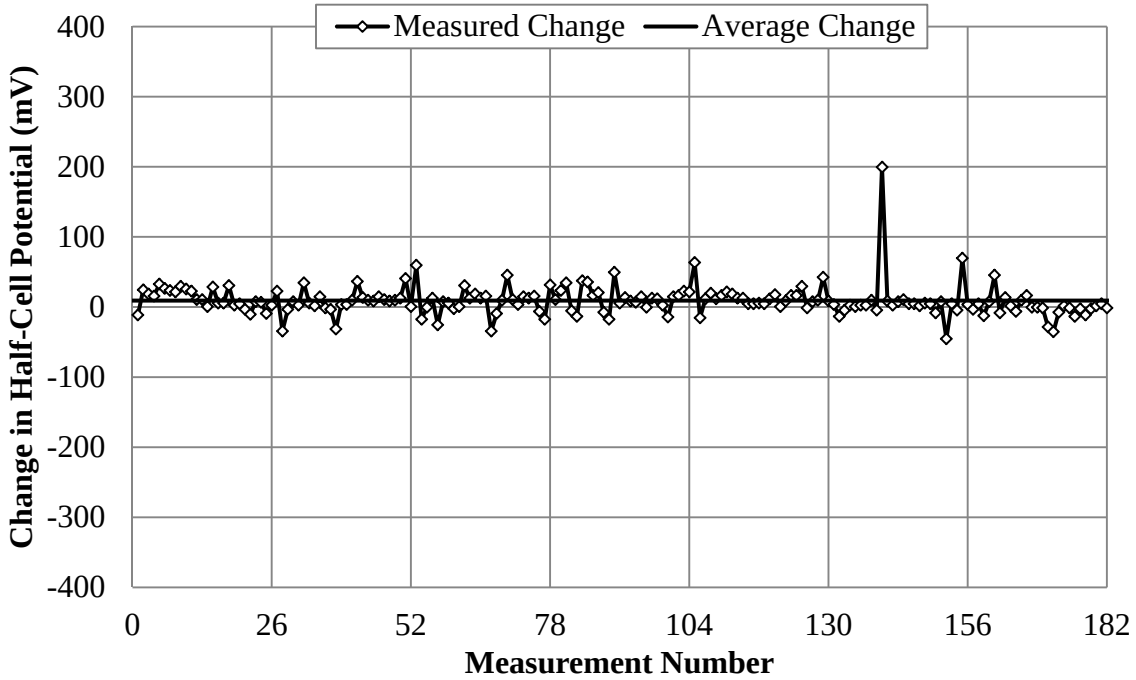

Figure F-66: Section G – Change in Half-cell potential from 8/25/11 to 10/6/11

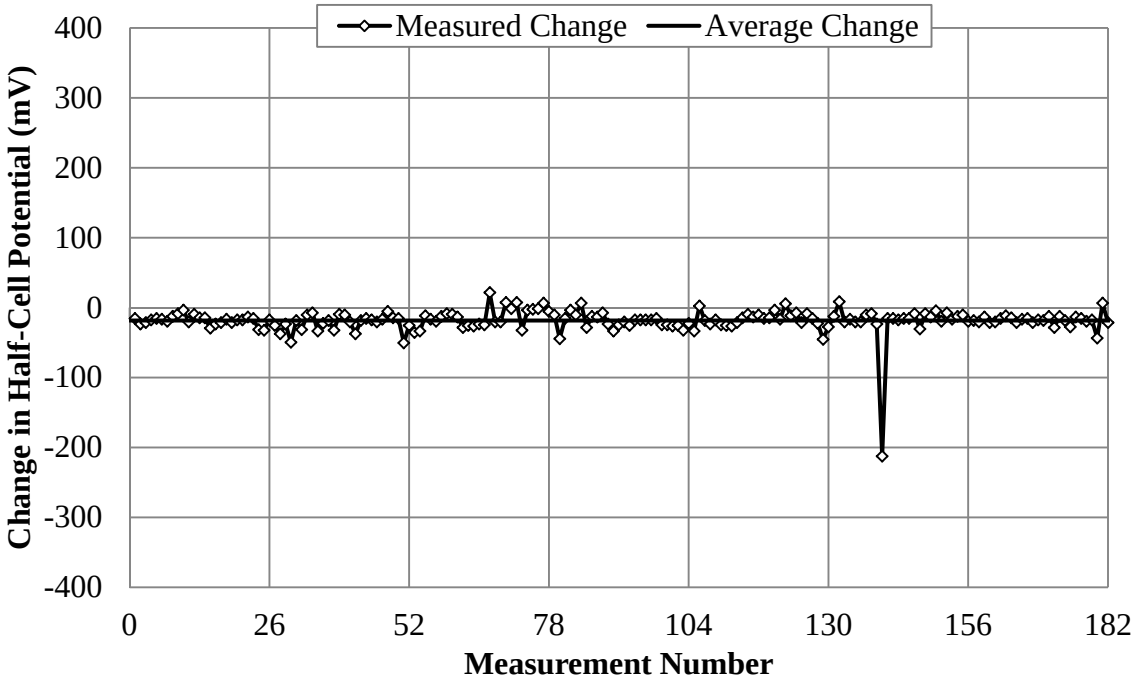

Figure F-67: Section G – Change in Half-cell potential from 10/6/11 to 10/27/11

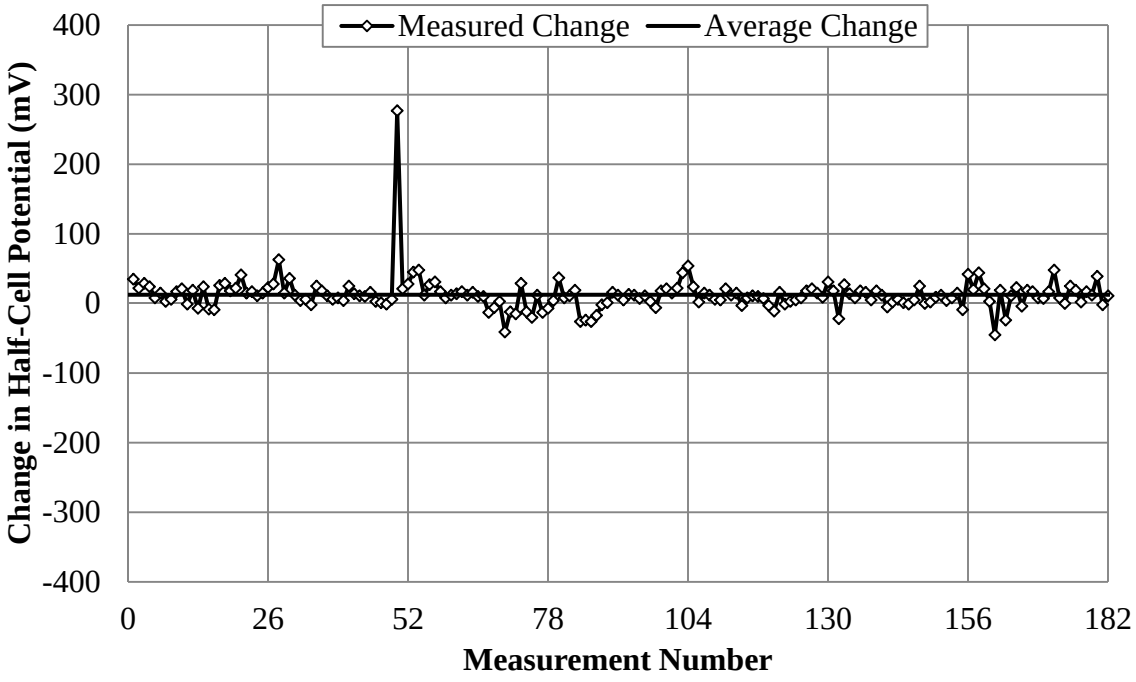

Figure F-68: Section G – Change in Half-cell potential from 10/27/11 to 4/10/12

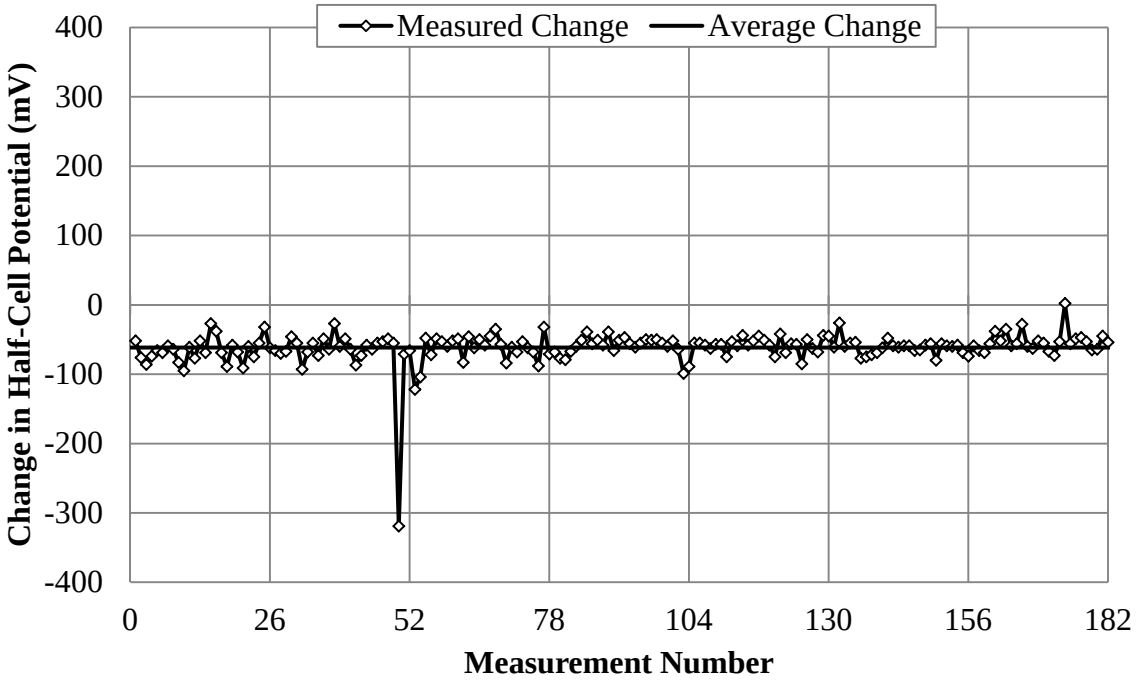

Figure F-69: Section G – Change in Half-cell potential from 4/10/12 to 5/9/12

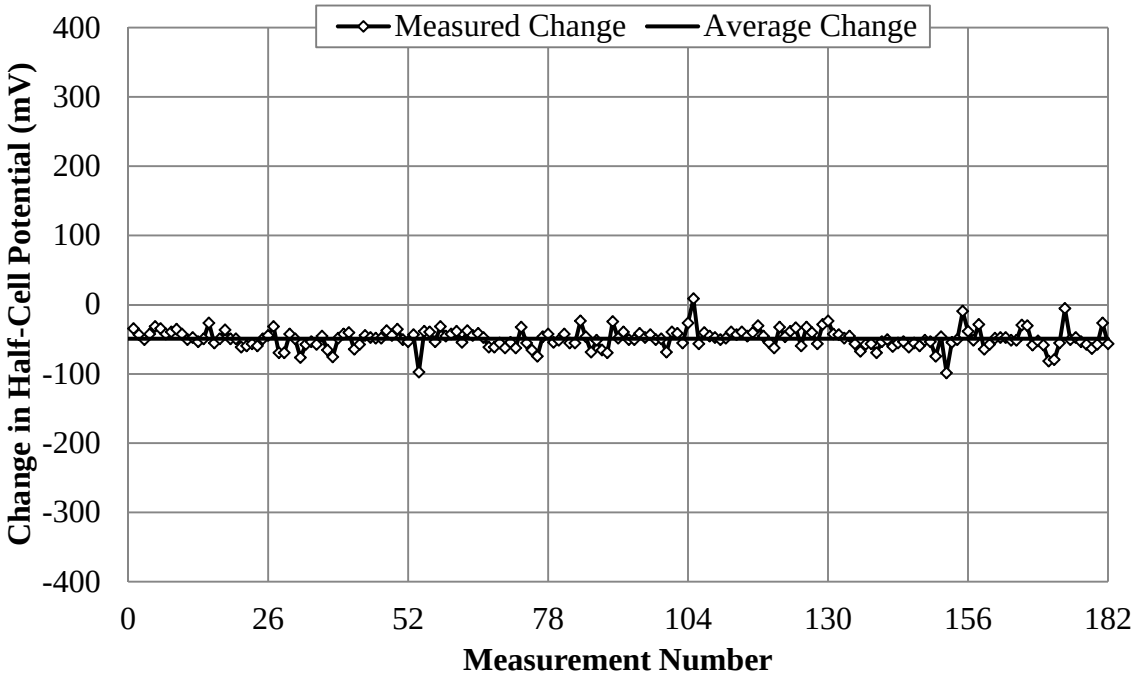

Figure F-70: Section G – Change in Half-cell potential from 8/25/11 to 5/9/12